

# Flow Rate Variability in Powder-Based Additive Manufacturing

Helen Chang, Yi Wei, Arnold Bangel PhD, Xuan Song PhD

Industrial Systems Engineering, University of Iowa

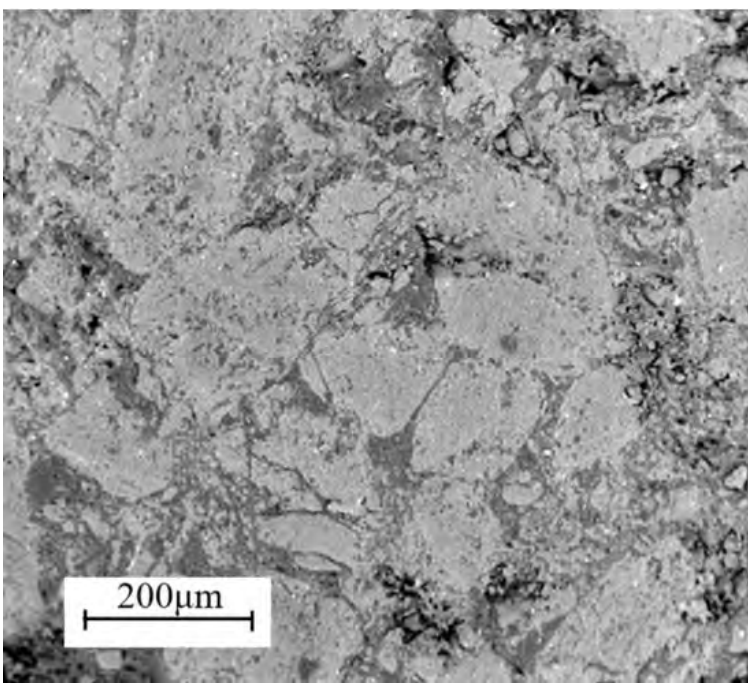


## Introduction

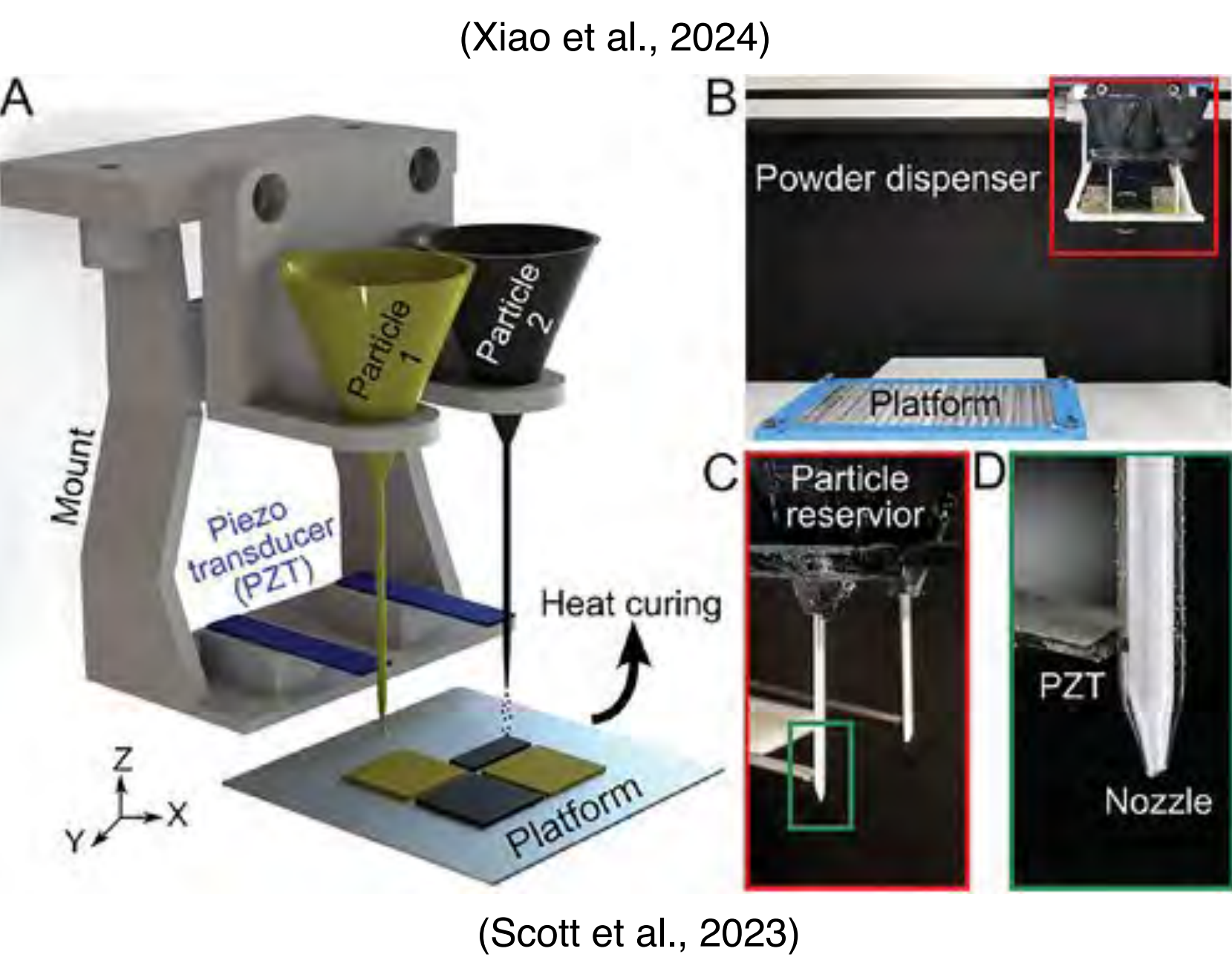
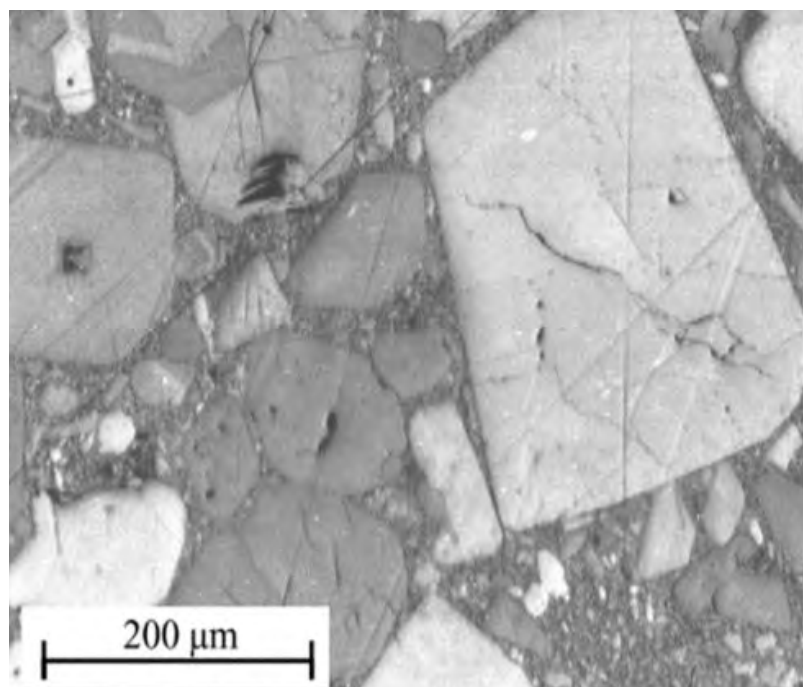
Acoustic-modulated deposition for multi manufacturing system for sugar particles:

- Vibrations through the piezo transducer hits the nozzle to dispense
- Dual material printer: two reservoirs and dispensers to allow for multiple materials (Scott et al., 2023)
- Different sized particles need different nozzles and vibration settings for optimal flow rate
- Powder-based additive manufacturing is a novel and intricate way to print that uses acoustic waves to deposit particles precisely
- **Polymer bonded sugar (PBS)** composites were used as a substitute for **polymer bonded explosive materials (PBX)**

PBS



PBX

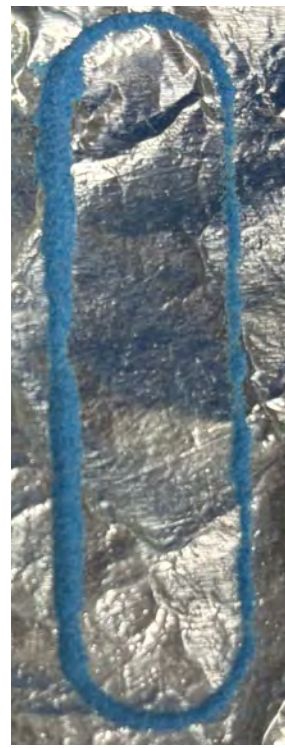


## Goals:

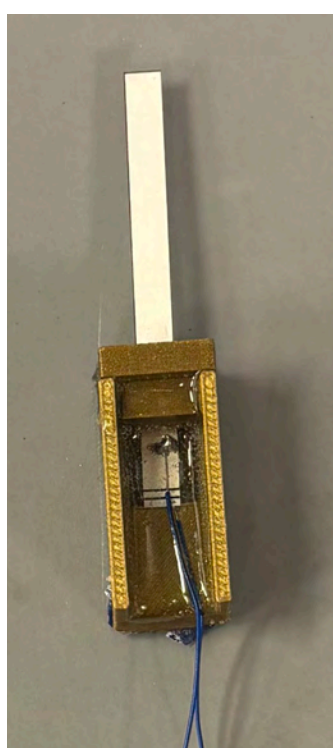
- To understand how particle size influences flow rate and print accuracy
- Be able to predict what print settings are best for each particle size
- Print small yet intricate designs accurately

## Methodology

- Sugar particles were dyed with pink or blue food dye and ball milled for 30-60 mins. They they were sifted using an automatic vibrating sieve
- 180µm, 106µm, and 75µm sized sugar particles were selected from their respective layers
- By pulling and trimming glass tubes, glass nozzles with diameters of 1.21mm and 1.06mm were used. The 180µm and 106µm sugar particles used the 1.21mm nozzle while the 75µm size used the 1.06mm nozzle
- Using CAD, designs were made and then translated to g-code using Slic3r
- Voltage and frequency were changed using a Tektronix Arbitrary Function Generator AFG31000 that sent a sinusoidal signal through the a ceramic piezo (60x5x0.4mm 28kHz). Speed was held constant at 4
- The piezo transducer was made by first soldering a wire on either side of the piezo, then inserting the piezo 2cm into the plastic container and filling the container with epoxy
- The wires connect the piezo to the function generator
- Speed was changed by manipulating the g-code. Speeds 1, 5, and 10 were tested for all three sizes. Speed 7 was tested for 106µm size as it seemed speed 5 was an outlier. The most accurate frequency and voltage were used and kept constant through three trials
- The printed results were measured in width using a caliber, and the uniformity was visually inspected
- Accurate = uniform flow → uniform print
- Only accurate prints were considered as “Did Print”



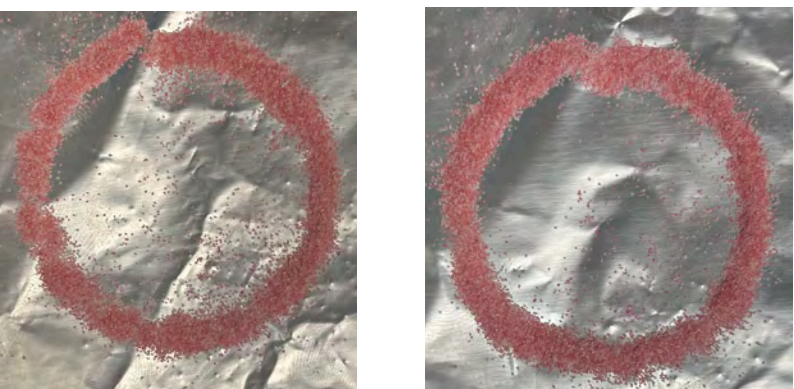
Uniform Print Non-uniform Print Did Not Print



Piezo Transducer

## Results—Frequency and Voltage

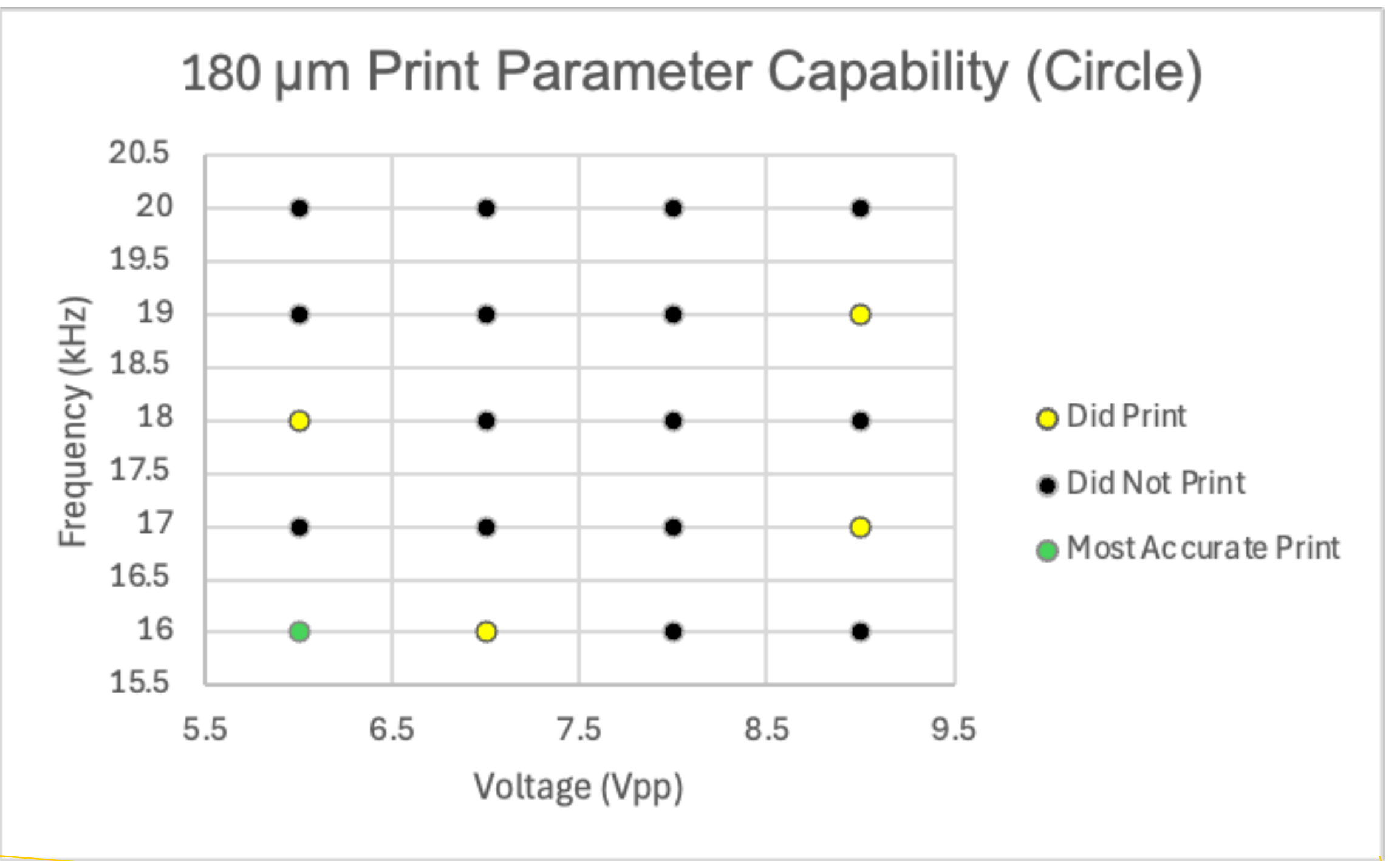
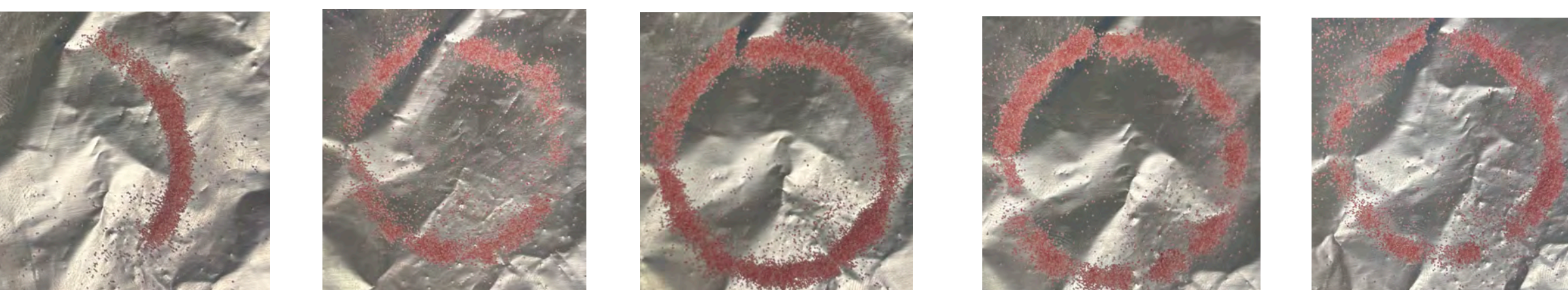
Did Print:



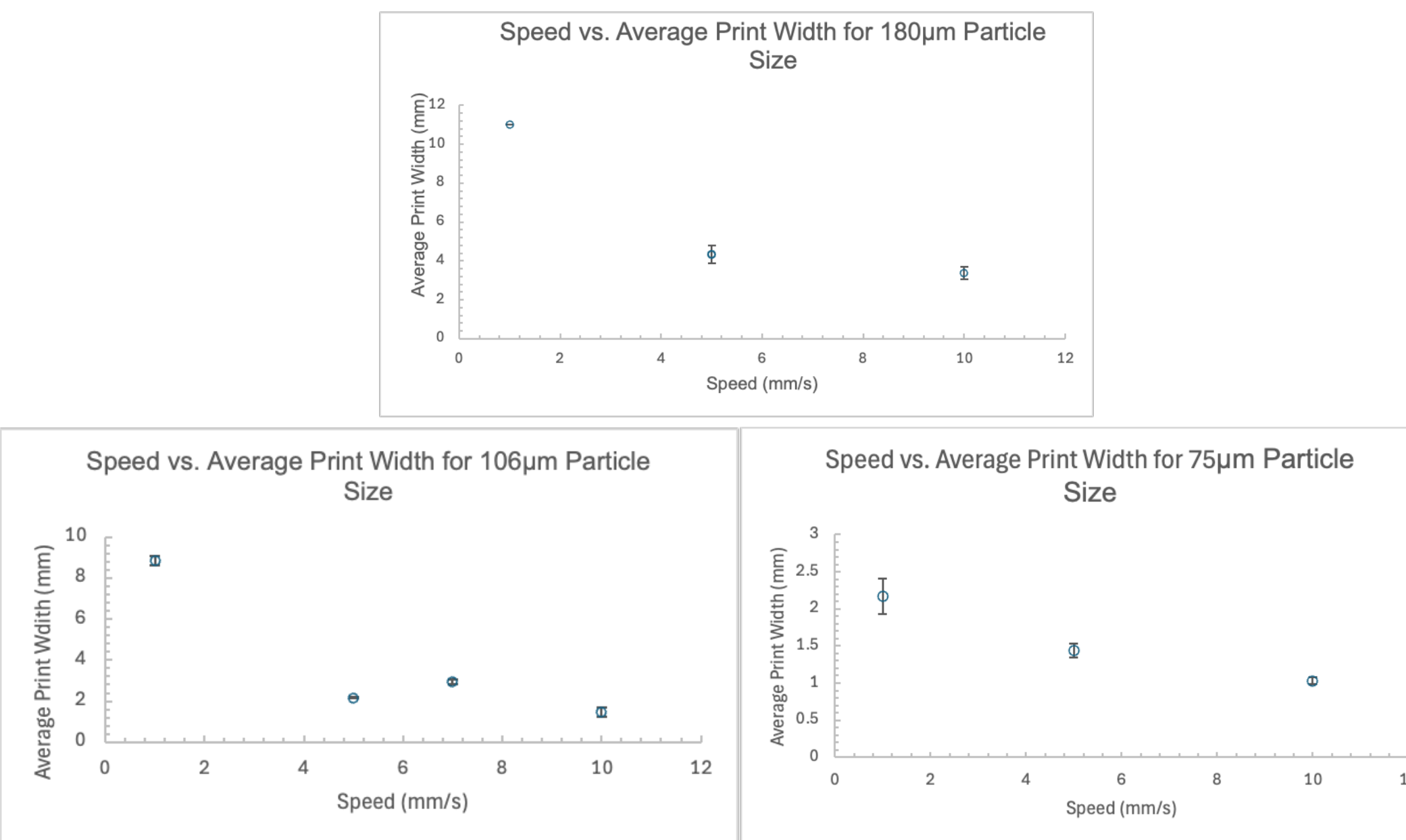
Most Accurate Print:



Did Not Print:



## Results—Speed



## Results—Print Results

Diameter: 4cm



Slic3r generated path



Print

## Conclusion

Large particle sizes are the most random, small particle sizes have the most narrow range of workable parameters, and middle particle sizes have the widest range of workable parameters. As speed increases, width decreases. The rate of change also decreases as the speed increases.

### Future Work

First, study how nozzle size influences print quality. Then, refine print quality when printing with different particle sizes and material.

## Acknowledgments

We thank the Air Force office of Scientific Research (Grant No. FA9550-24-1-0147) and the National Science Foundation (Grant No. 2236905).

## References

Kirby, L. et al. (2023). Additive Manufacturing.  
Scott, M. et al. (2023). Advanced Materials Technologies.  
Xiao, Y. et al. (2024). Polymers.



# 16p11.2 Microdeletion Associated with Neurodevelopmental Disorders Results in Sex-Specific Changes in Placental Glycogen Cell Prevalence in Mouse Embryos



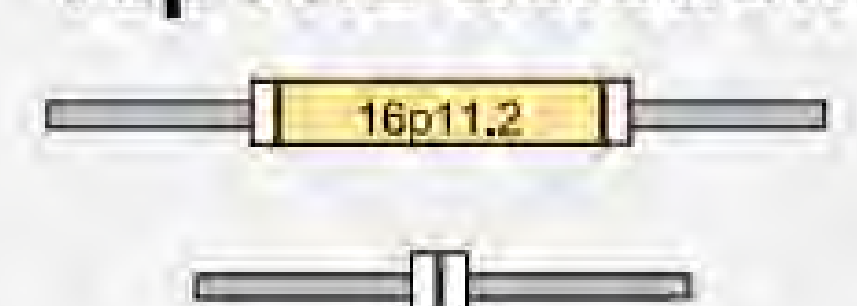
Madeline Cheng<sup>1,2</sup>, Annemarie Carver<sup>1,2</sup>, Faith Fairbairn<sup>1,2</sup>, Benjamin Kelvington<sup>2</sup>, Ted Abel<sup>2</sup>, Hanna Stevens<sup>1,2</sup>  
Department of Psychiatry<sup>1</sup>, Iowa Neuroscience Institute<sup>2</sup>, University of Iowa, Iowa City, Iowa

**IOWA**

## Introduction

- The **16p11.2** microdeletion of ~20 genes is strongly associated with neurodevelopmental disorders (NDDs), specifically **autism spectrum disorder (ASD)**<sup>1</sup>
- ASD is **four** times more common in **males** than females<sup>2</sup>
- In mouse models heterozygous for the microdeletion, social and cognitive phenotypes similar to those in humans with NDDs have been observed<sup>3,4</sup>

### 16p11.2 deletion

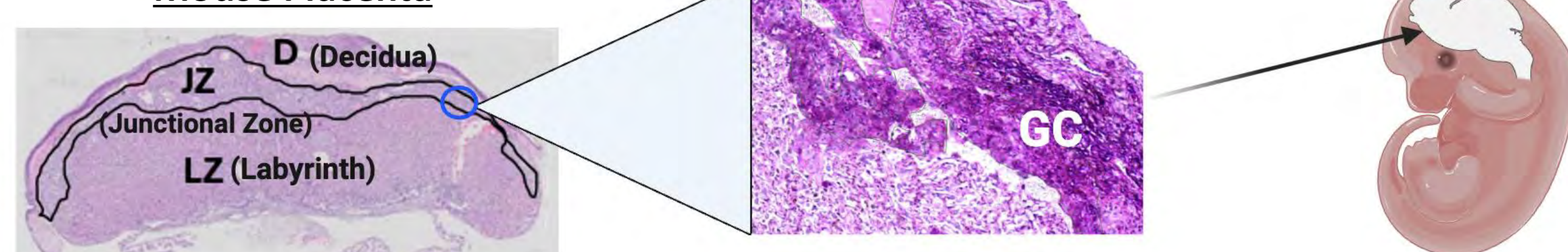


ASD (16.1-25.6%)  
ID (10.3%-28.1%)  
Epilepsy/seizures (21.8-26.8%)  
Macrocephaly (17.1-17.3%)  
Speech/language delay  
Motor/developmental delay  
Depression/anxiety  
ADHD

- 16p11.2 includes genes that function in fetal development expressed in the **placenta**, mainly *Mapk3*, *Mvp*, *Qprt*, and *Aldoa*<sup>1</sup>

- Aldoa* deficiency is linked to **glycogen accumulation/reduced blood flow**<sup>5</sup>
- Changes in placental morphology and cell populations may indicate mechanisms by which the deletion alters fetal neurodevelopment<sup>6,7</sup>
- The placenta is a temporary organ that connects the mother and fetus during pregnancy and supplies oxygen, nutrients, and hormones<sup>6,8</sup>

### Mouse Placenta



- Glycogen cells** (GCs) reside in the JZ and migrate into the DZ mid-gestation<sup>8</sup>
- Previous studies in the lab found changes in male placental structure with the deletion on embryonic day 16 (E16) which indicates an increase in GCs<sup>9</sup>

## Hypothesis

We hypothesized that the 16p11.2 microdeletion would **increase** glycogen accumulation in the placenta and at a greater degree in male mouse embryos compared to females.

## Methods

- Wildtype females and males heterozygous for the 16p11.2 microdeletion were bred, resulting embryos were labeled **WT** or **DEL** if heterozygous for the deletion
- qPCR** of 16p11.2 genes was conducted to validate the deletion in the placenta
- Embryos collected on **E16 & E18** as well as embryonic & placental mass



- Applied **periodic acid Schiff** staining to placental sections to mark glycogen
- Stained slides were analyzed under Axio Imager M.2 microscope (Zeiss)
- The DZ, JZ, and LZ of each placenta were outlined on a reference slide
- GC area** in each region was then quantified by contouring the PAS-stained portions and a percentage of GCs for each region and in total was calculated
- Graphs were created in **GraphPad Prism**, linear mixed effects model done in **R** to incorporate litter as a covariate
- p-values indicated by: # < 0.1, \* < 0.05, \*\* < 0.01, \*\*\* < 0.001, and \*\*\*\* < 0.0001

## Reduction in Placental Gene Expression in 16p11.2

### Males with 16p11.2 Deletion

	E16	E18
<i>Mapk3</i>	↓ **	↓ ***
<i>Mvp</i>	↓ ***	↓ ***
<i>Qprt</i>	↓ **	↓ **
<i>Aldoa</i>	↓ *	↓ ***

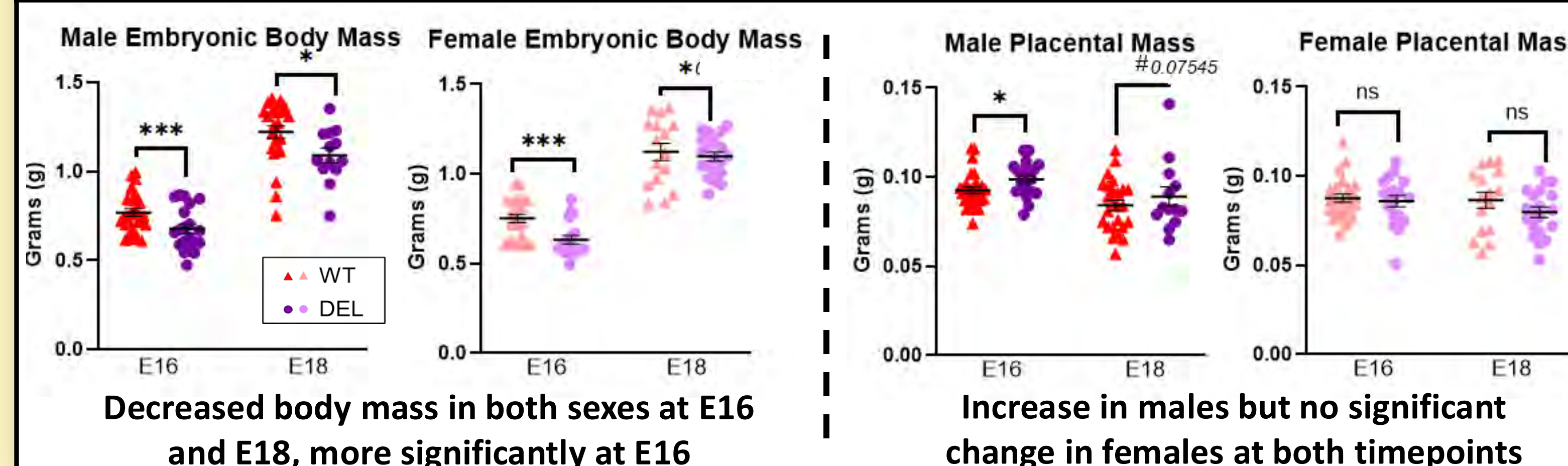
Decrease in all at both timepoints

### Females with 16p11.2 Deletion

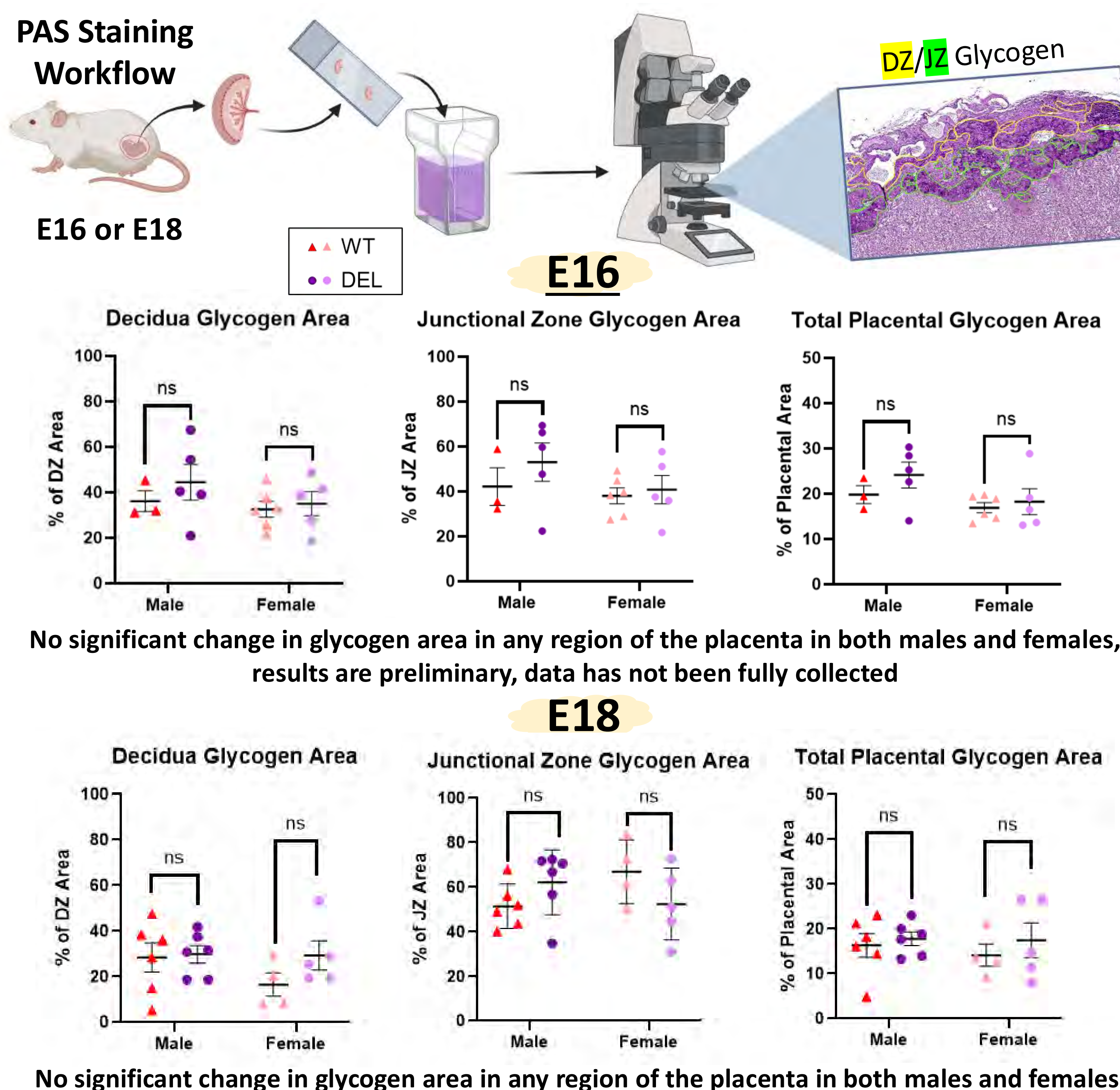
	E16	E18
<i>Mapk3</i>	ns	↓ *
<i>Mvp</i>	↓ p=0.07	↓ **
<i>Qprt</i>	↓ **	↓ **
<i>Aldoa</i>	↓ **	↓ *

Decrease in all except *Mapk3* in E16 females

## Sex-Specific Changes in Placental Mass



## Effect on Placental Glycogen Cell Area



## Conclusions

### Female 16p11.2 Deletion Placentas and Embryos

- Deletion of 16p11.2 results in expected 50% expression, except for *Mapk3* at E16 in females which is likely a compensatory mechanism
- No change in female placental mass may suggest normal functioning that could be linked to reduced susceptibility to ASD compared to males
- Deletion females show no gross change in placental mass or glycogen area. This suggests a female ability to compensate for 16p11.2 deletion, including through upregulation of *Mapk3*, may benefit neurodevelopment and lower ASD risk.

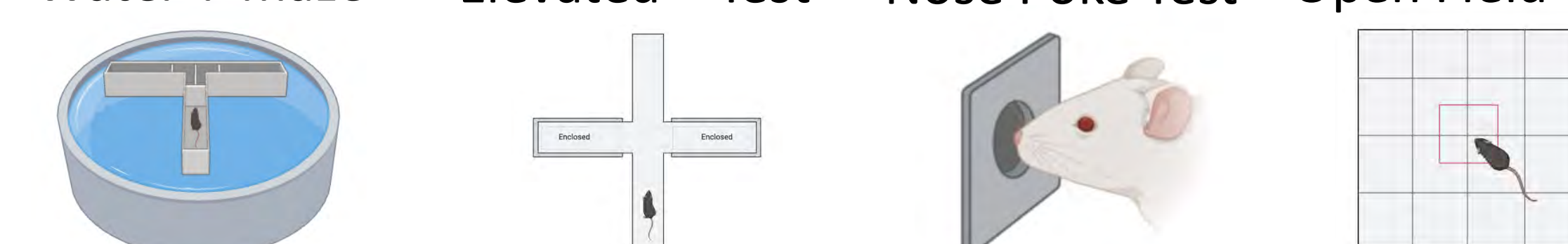
### Male 16p11.2 Deletion Placentas and Embryos

- Significant changes in male placental mass but not female may subsequently alter neurodevelopment in males and could be linked to the increased prevalence of ASD in males
- Previous results in the lab for E16 indicate impaired migration of GCs into the decidua in males, causing accumulation in the JZ, leading to poor placentation. However, the current preliminary results are unfinished for E16.
- Deletion males present with significantly decreased 16p11.2 placental gene expression and severe phenotypic defects in body and placental mass, aligning with their higher prevalence of ASD
- No change in glycogen area indicates GCs are likely not the driving factor in male mass changes

Decreased expression of 16p11.2 genes in the placenta likely impacts placental function, particularly in males, and may contribute to ASD risk.

## Future Directions

Water T-maze Elevated + Test Nose Poke Test Open Field Test



- Manipulation of 16p11.2 placental gene expression to rescue glycogen cell area changes and impacts on neurodevelopment and behavior through cognitive tests
- Investigate sex-specific differences in behavior postnatally

## Acknowledgements

I would like to extend my gratitude to Dr. Hanna Stevens for her invaluable mentorship and providing me the opportunity to contribute to this project as well as to Anna Carver, Faith Fairbairn, and Robert Taylor for supporting and guiding me through every step of the research process.

## References

- Rein, B., & Yan, Z. (2021). 16p11.2 copy number variations and neurodevelopmental disorders. *Trends in Neurosciences*, 43(11), 886–901. <https://doi.org/10.1016/j.tins.2020.09.001>
- Napolitano, A., Schiavi, S., La Rosa, P., Rossi-Espagnet, M. C., Petrillo, S., Bottino, F., Tagliente, E., Longo, D., Lupi, E., Casula, G., Piemonte, F., Trezza, V., & Vicari, S. (2022). Sex Differences in Autism Spectrum Disorder: Diagnostic, Neurobiological, and Behavioral Features. *Frontiers in psychiatry*, 13, 889636. <https://doi.org/10.3389/fpsyg.2022.889636>
- Hudon, C., Roy, J., Barber, S., Duzend, M., Wallace, A., Martin, C., Ledbetter, D., Hansen, E., Goin-Kochel, R., Green-Snyder, L., Chung, W., Eichler, E., & Bernier, R. (2020). Evaluating heterogeneity in ASD symptomatology, cognitive ability, and adaptive functioning among 16p11.2 CNV carriers. *Autism Research*, 13(8), 1300–1310. <https://doi.org/10.1002/aur.2332>
- Hanson, E., Bernier, R., Porsche, K., Jackson, F., Goin-Kochel, R., Green-Snyder, L., Snow, A., Wallace, A., Campe, K., Zhang, Y., Chen, Q., D'Angelo, D., Moreno-De-Luca, A., Orr, P., Boomer, K., Evans, D., Kanne, S., Berry, L., Miller, F., Olson, J. et al. (2015). The cognitive and behavioral phenotype of the 16p11.2 deletion in a clinically ascertained population. *Biological Psychiatry*, 77(9), 785–793. <https://doi.org/10.1016/j.biopsych.2014.04.021>
- Kara, E., Kor, D., Bulut, F. D., Hergüner, O., Ceylaner, S., Köşec, B., Burgaç, E., & Mungan, N. O. (2021). Glycogen storage disease type XII; an ultra rare cause of hemolytic anemia and rhabdomyolysis: one new case report. *Journal of Pediatric Endocrinology & Metabolism - JPEM*, 34(10), 1335–1339. <https://doi.org/10.1515/jpem-2021-0258>
- Kundu, S., Maurer, S., & Stevens, H. (2021). Future horizons for neurodevelopmental disorders: Placental mechanisms. *Frontiers*, 9. <https://www.frontiersin.org/journals/pediatrics/articles/10.3389/fped.2021.653230/full>
- Tunstall, S., Creech, H., John, R. (2016). The imprinted *Phf22* gene modulates a major endocrine compartment of the placenta to regulate placental demands for maternal resources. *Developmental Biology*, 409(1), 251–260. <https://doi.org/10.1016/j.ydbio.2015.10.015>
- Elmore, S., Cochran, R., Bolon, B., Lubeck, B., Mahler, B., Sabio, D., & Ward, J. (2022). Histology atlas of the developing mouse placenta. *Toxicologic Pathology*, 50(1), 60–117. <https://journals.sagepub.com/doi/full/10.1177/01926232211042270>
- Carver, A., Kelvington, B., Fairbairn, F., Abel, T., Stevens, H. (2024). 16p11.2 microdeletion induces sex-specific defects in placental development in mice. *Placenta (Eastbourne)*, 154, 16–17. <https://doi.org/10.1016/j.placenta.2024.07.011>



# Vegetative Flow Resistance as a Nature-Based Solution for Bridge Waterway Scour Mitigation



Aarush Dey<sup>1</sup>, Abhishek Ghimire<sup>2</sup>, Priscilla Williams<sup>3</sup>

<sup>1</sup>SSTP Research Assistant, Rye Country Day School, Rye, NY

<sup>2</sup>PhD Student, Department of Civil and Environmental Engineering, IIHR – Hydrosience & Engineering, University of Iowa, Iowa City, IA

<sup>3</sup>Assistant Professor, Department of Civil and Environmental Engineering, IIHR – Hydrosience & Engineering, University of Iowa, Iowa City, IA

IOWA

IIHR—Hydrosience  
and Engineering

## Introduction

### Background

Every year, scour weakens or destroys bridges throughout the world. Scour refers to the erosion of sediment around bridge piers and abutments caused by flowing water. Typical engineering solutions include concrete and steel which can be costly and environmentally damaging.<sup>1</sup>

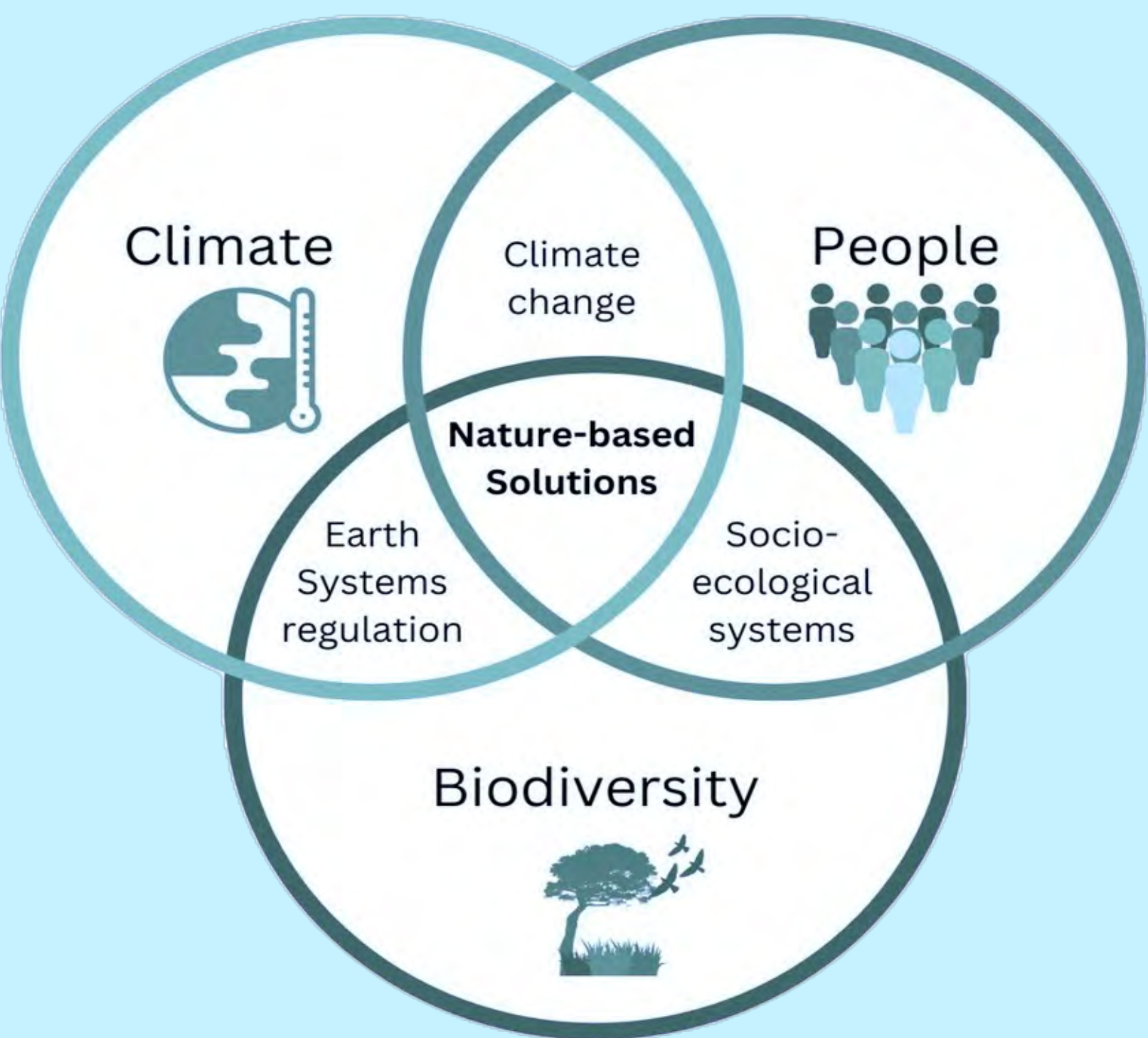


Figure 1: Venn diagram summarizing the three major purposes of Nature-Based Solutions

A new alternative is

**Nature-Based Solutions (NBS)**

NBS are design strategies that take advantage of natural processes, like vegetation growth, to mitigate environmental impacts<sup>2</sup>

The purpose of this project is to explore if vegetation can be effectively implemented to decrease flow velocity and subsequently, scour around bridge foundations. If any methods are successful, this will confirm the potential for a lower-cost, nature-based method for protecting our bridge infrastructure from scour-related damage.

## Purpose

### Research Question

How does in-stream vegetation influence flow velocity and sediment transport near bridge piers in a controlled flume environment?

### Why?

To explore NBS for infrastructure resilience by understanding how in-stream vegetation can reduce scour at critical points, ultimately contributing to a larger shift to sustainable and cost-effective hydraulic engineering.

## Methodology

My experiment was conducted in a 0.9 meter wide high-gradient flume, designed to simulate river flow conditions around bridge structures. We used Particle Image Velocimetry (PIV), a method that allows us to visualize and calculate fluid velocity by tracking seeding particles in the water.

### Flume and Structure Setup

We placed a small-scale model of a wingwall abutment and pier in the sediment bed of the flume and then leveled it completely using brushes, shovels, and trowels.

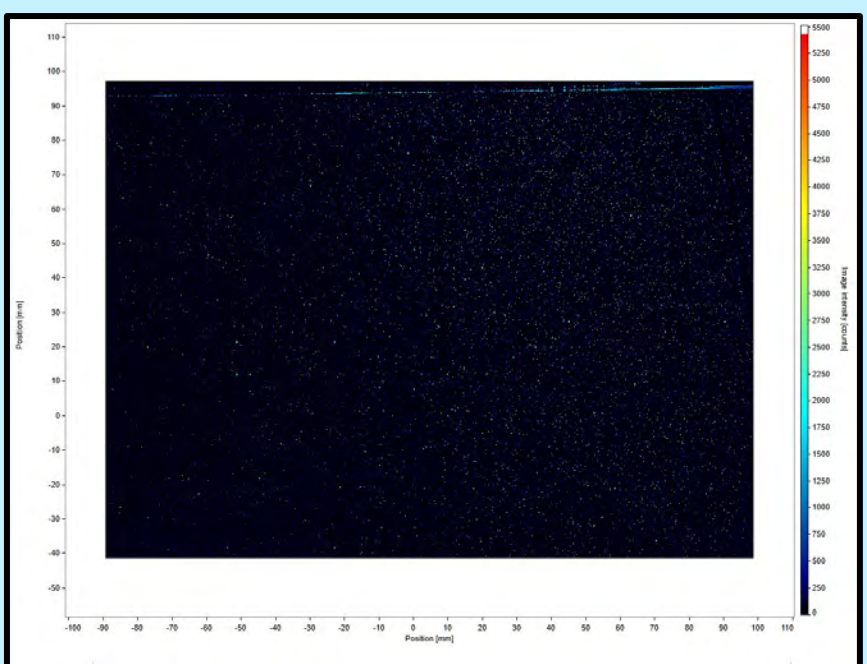
### Baseline Test (No Vegetation)

- The flume was filled to desired flow depth ( $h = 13$  cm) and the pump frequency was increased until desired flow conditions ( $Q = 35.3$  L/s) were reached
- We took photographs of the flow and bed
- We recorded variables including velocity, flow rate, pump frequency, the slope of the flume, and the flow depth to ensure that the flume was functioning correctly
- We used a laser sheet to illuminate the water seeded with particles
- Using the PIV system, we measured flow velocity and patterns at three key locations: the **pier nose** (where the deepest scour typically forms)<sup>3</sup>, **midway** between pier and abutment, and the **leading edge of the wingwall abutment**.

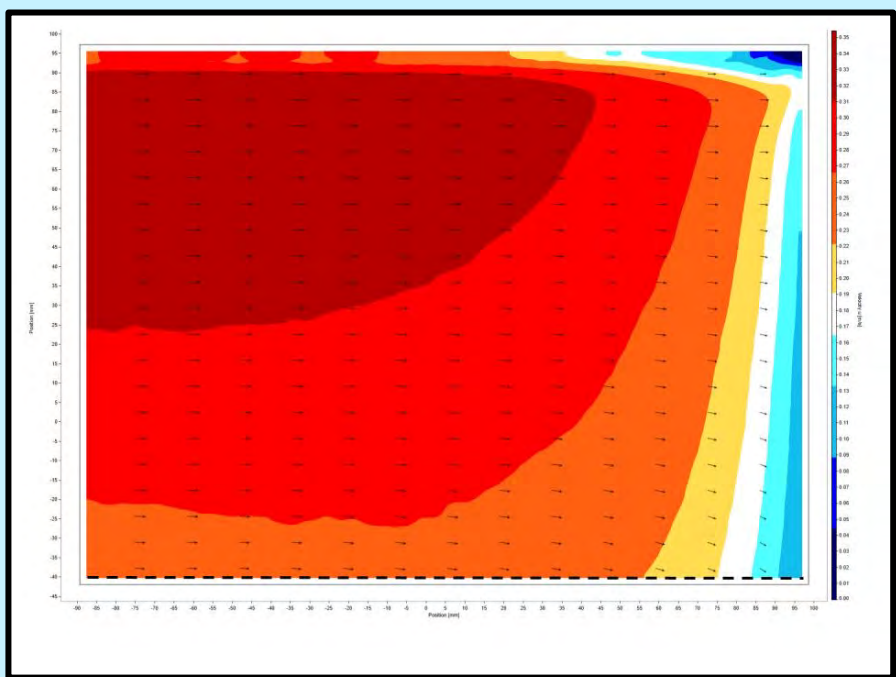
### NBS Evaluation Test (With Vegetation)

- For the next test we repeated the same procedure, but added a model of **Softstem Bullrush** (a native Iowan plant) at the point of deepest scour to explore how it impacts scour
- The vegetation model consisted of a 7 cm diameter cylindrical baseplate with 2.5 mm holes arranged on its top surface in which 2.5 mm diameter metal rods were inserted vertically to simulate stems

### Data Processing



Raw Image of Seeded Flow



Velocity Vector Maps

Lastly, after each trial, we scanned the sediment bed to identify the pattern of scour, as well as the depths of scour at pivotal points in and around the abutment and pier using a mobile 3D scanner app called **Scaniverse**. These depth and height measurements allowed us to create contour maps that display both erosion and deposition near the pier and abutment.

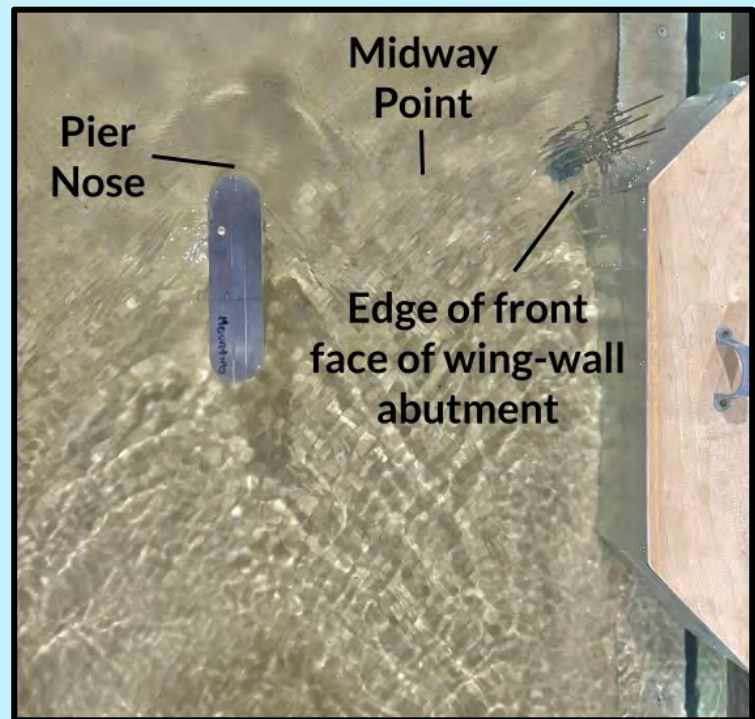


Figure 2: Top Perspective of Small-Scale Elongated Cylindrical Pier and Wing-wall Abutment in High Gradient Flume



Figure 3: Softstem Bullrush (*Schoenoplectus Tabernaemontani*)<sup>4</sup>

## Results

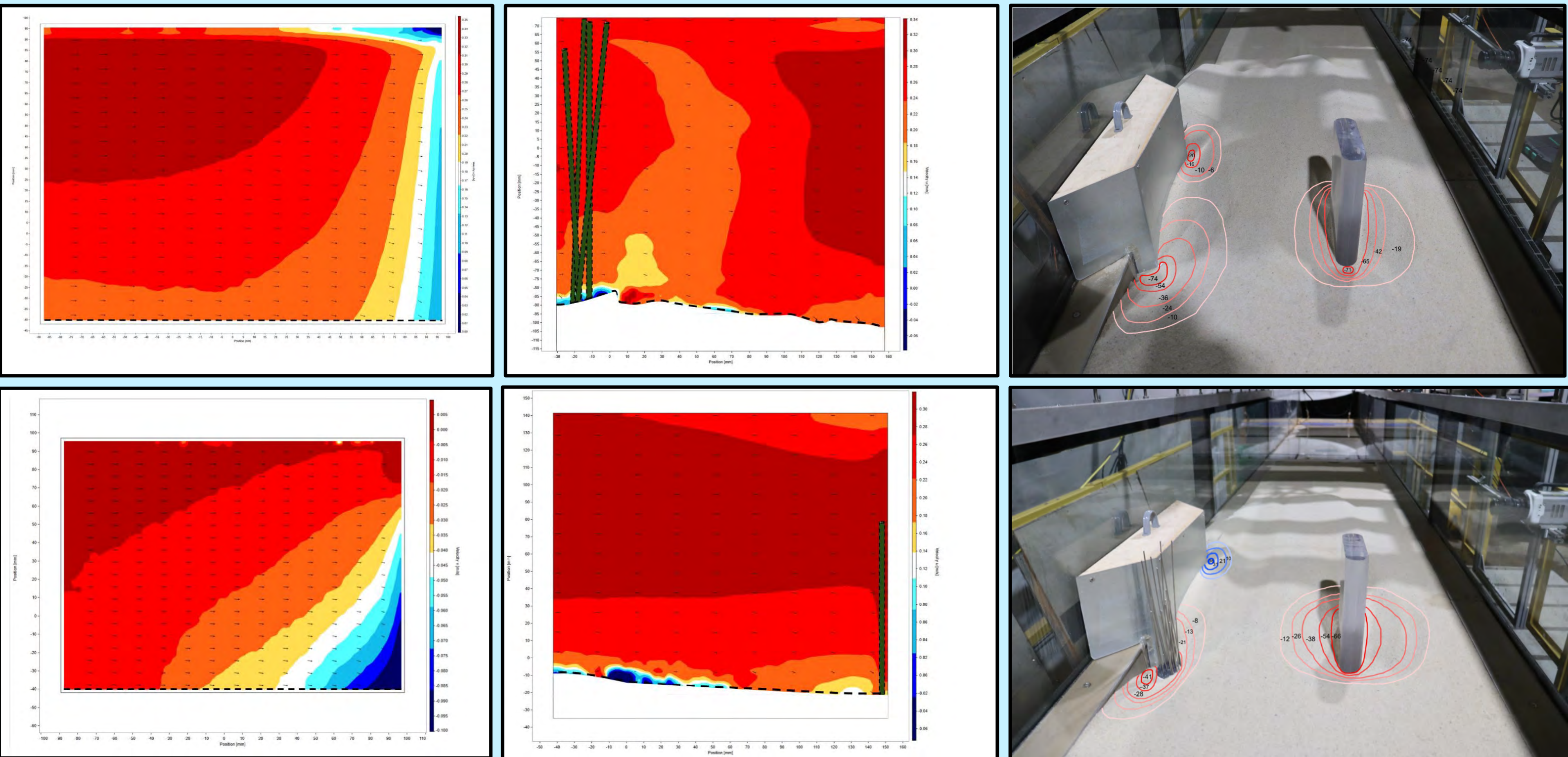


Figure 4: Velocity vector maps showing low vectors just before the pier (A), velocity becomes downward and stronger when reaching close to the pier (B), at toe of the abutment (start of abutment) with plants (C), flow field when the vegetation is slightly upstream from the deepest scour hole (D).

## Conclusion

Placing simulated vegetation at the upstream edge of the wing-wall abutment led to a substantial reduction in local scour. In the control (non-vegetated) trial, the maximum scour depth was approximately -74 mm. With vegetation present, this depth was instead -41 mm. Moreover, there was a maximum deposition height of +21 mm that was observed downstream of the abutment.

However, it is important to acknowledge that over time the sediment near the vegetation model eroded so much that the cylindrical baseplate became partially exposed, potentially introducing experimental error in the recorded scour depth. To address this, scour width was analyzed as a secondary metric, for better accuracy. The vegetation reduced the scour width from approximately 274 mm to 231 mm.

These results **support our initial hypothesis that vegetation can mitigate flow-induced sediment erosion**, particularly in critical areas such as abutments. As of now, the WEST Lab is experimenting with vegetation placement in front of pier. In the latest trial, we moved vegetation upstream of the deepest scour hole in pier, which resulted in a scour width reduction of 60 mm and a scour depth reduction of 30 mm.

Overall, these findings highlight the potential of vegetation as a NBS to reduce erosion around bridge foundation infrastructure. With refinement, the strategic placement of vegetation can serve as a low-cost and sustainable countermeasure against bridge scour.

## Acknowledgements

I'm deeply grateful to Dr. Williams, Abhishek Ghimire, Chukwudum Eluchie, and Anthony Lamoreux for their guidance and support throughout this project. Their mentorship made my time at the WEST Lab incredibly rewarding and educational.

## References





# Antioxidants and the antibiotic Tetracycline suppress seizures in a *Drosophila* model of epilepsy

Meher Garg<sup>1</sup>; Avery Yu<sup>2</sup>; Brady Williquett<sup>3</sup>; J. Robert Manak, PhD<sup>3,4</sup>

<sup>1</sup>Springfield High School, <sup>2</sup>Oak Park High School, <sup>3</sup>Department of Biology, University of Iowa, <sup>4</sup>Department of Pediatrics, University of Iowa

## INTRODUCTION

- Epilepsy affects over 50 million people worldwide.<sup>1</sup>
- About 1 in 3 patients are resistant to current medications, and 2 out of 3 patients suffer adverse side effects from their anti-seizure medications.<sup>1,2</sup>
- Mutations of the *prickle-spiny-legs* ( $pk^{sple}$ ) isoform of *Drosophila prickle* causes spontaneous seizures and ataxia, similar to the seizure syndrome observed in humans carrying *PRICKLE* mutations.<sup>3,4</sup>
- Since *PRICKLE* is evolutionarily conserved from flies to humans, *prickle* mutant flies can be used as a model for epilepsy research.
- Previous work in the Manak Lab identified a direct genetic link between oxidative stress, neuronal death, and increased frequency of seizures.<sup>4</sup>

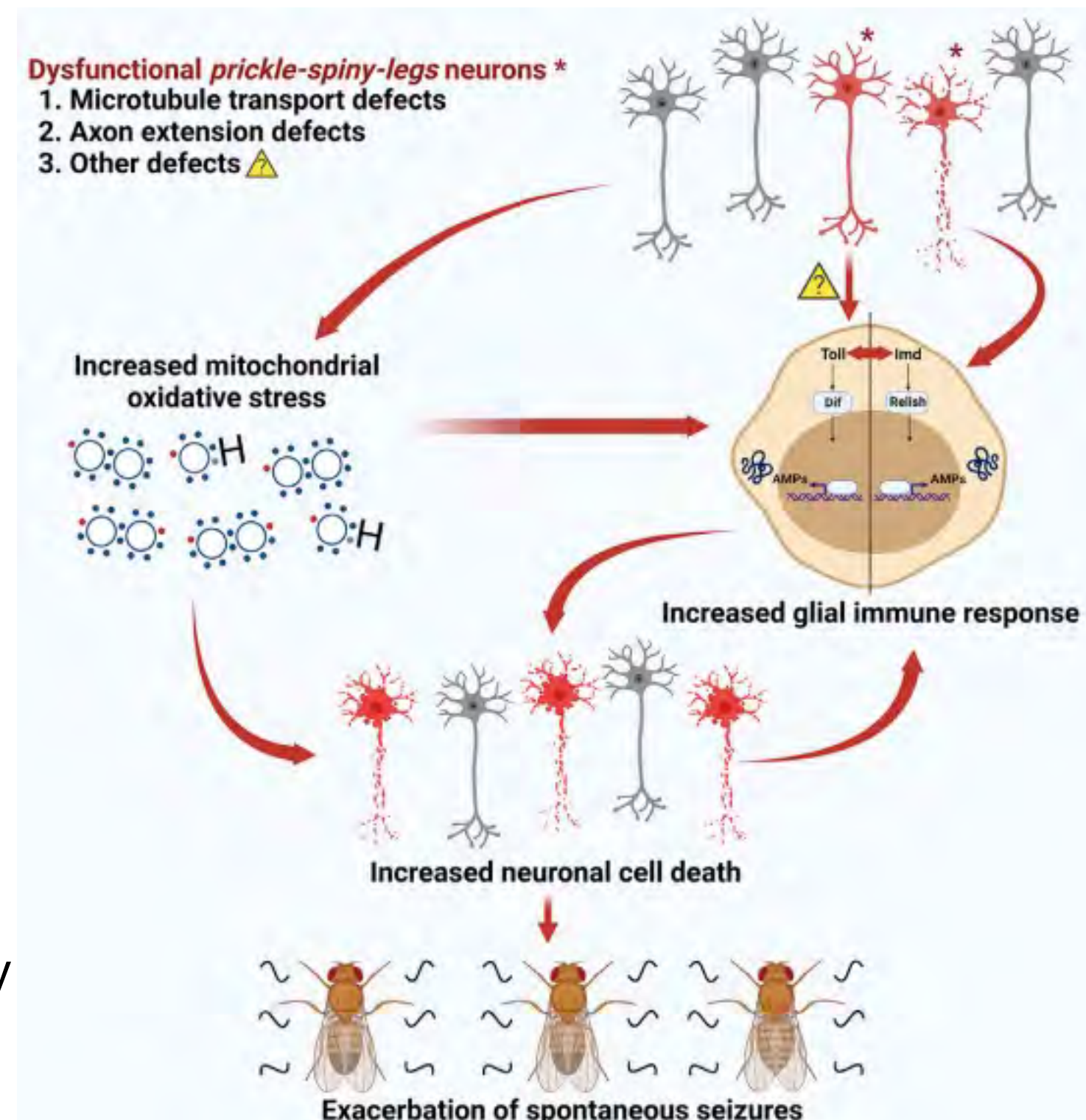
Specifically, oxidative stress creates reactive oxygen species (ROS) which damage cell structures including mitochondria and trigger the glial-mediated innate immune response (IIR). This response ultimately leads to increased neuronal death and seizure frequency. Notably, oxidative stress precedes IIR activation in this cascade.<sup>4</sup>

### Antioxidants in epilepsy

- Antioxidants (AOs) can neutralize reactive oxygen species, thereby reducing oxidative stress to potentially hinder the progression of epilepsy.<sup>5,6</sup>

### Antibiotics in epilepsy

- Antibiotics show promising signs of decreasing epilepsy progression since they mildly disrupt mitochondrial function, triggering a beneficial cellular stress response called mitohormesis.<sup>7</sup>
- Mitohormesis can reduce inflammation and oxidative stress, potentially reducing seizures.<sup>7</sup>



## RESEARCH OBJECTIVES

- Systematically test 9 AOs to determine which work best at suppressing seizures
  - First comprehensive study to systematically screen a large number (9) of antioxidants in an *in vivo* genetic model of epilepsy.
- Determine the effectiveness of NAC in suppressing *prickle* mutant seizures over the course of different stages of *Drosophila* development.
  - Oxidative stress in *prickle* mutants was found to be most pronounced in larval stages<sup>4</sup>; we will thus treat three developmental groups of mutants to assess which treatment is most effective in suppressing adult seizures: larval, adult, larval+adult.
- Determine the effectiveness of the antibiotic tetracycline in suppressing *prickle*-mediated seizures
  - Could have a possible mitohormesis effect by slightly stressing the mitochondria, thereby upregulating the antioxidant response and mitigating the IIR.

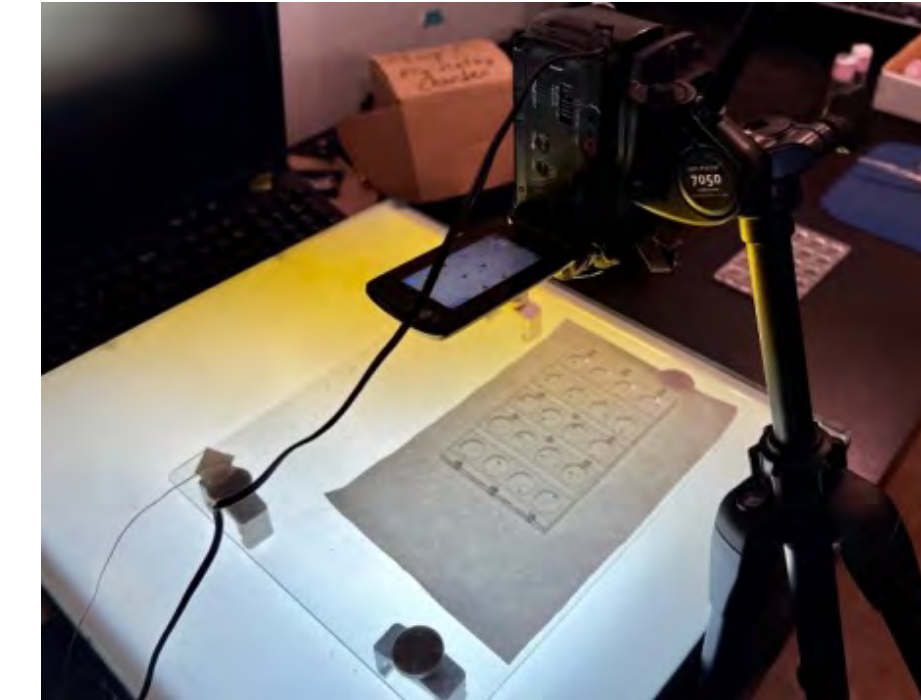
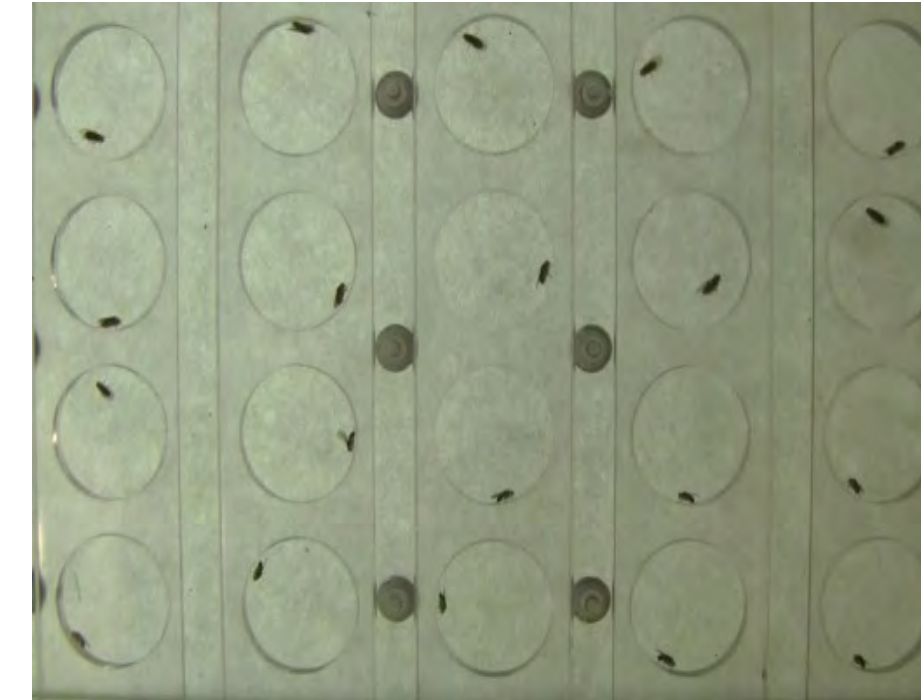
## MATERIALS AND METHODS

*prickle spiny legs* ( $pk^{sple}$  or *sple*) flies were fed standard cornmeal molasses medium containing an antioxidant or the antibiotic tetracycline from embryo until 15 days post eclosion with the exception of NAC (see list of drugs below):

- |                                 |                               |   |
|---------------------------------|-------------------------------|---|
| Tetracycline (0.05 mg/mL)       | Valdecobix (1 $\mu$ M)        | N-acetyl cysteine (NAC) (1 mM): Administered during larval, adult or laval+adult stages |
| Trans-resveratrol (100 $\mu$ M) | Allyl Disulfide (200 $\mu$ M) |   |
| Ibuprofen (10 $\mu$ M)          | Genistein (400 $\mu$ M)       |   |
| Licofelone (1 $\mu$ M)          | Curcumin (1 mM)               |   |
| Gallic Acid (1 mM)              |                               |   |

Spontaneous Seizure Assay: Flies were individually mouth-pipetted into chambers.

- Behavior was recorded using high-resolution videography.
- Videos were analyzed by eye for spontaneous seizure events in a blinded manner.



## RESULTS

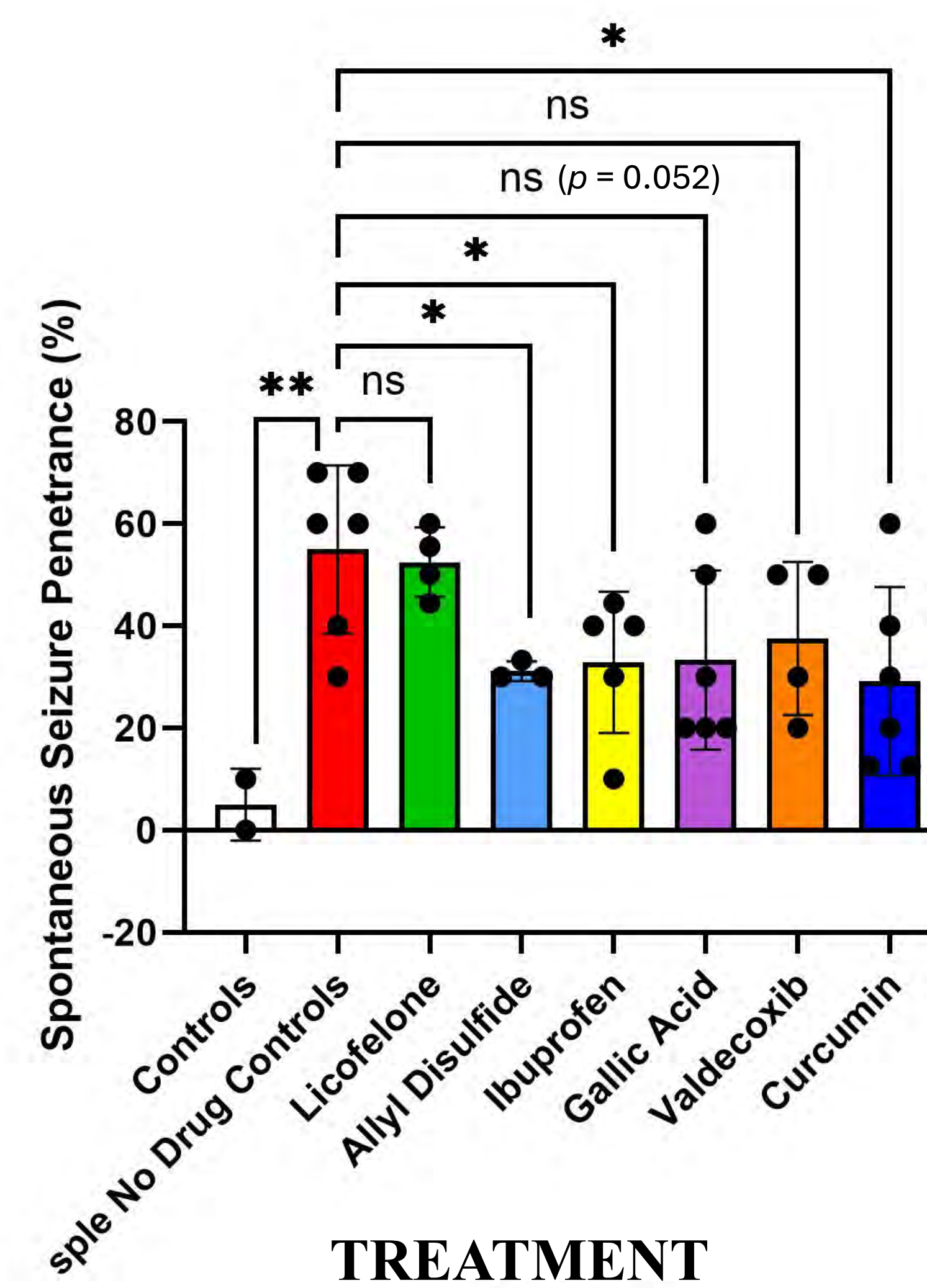


**Figure 1: Allyl disulfide, ibuprofen, and curcumin suppress seizures in  $pk^{sple}$  mutant flies.** Although not statistically significant, gallic acid treatment trended towards significance.

Spontaneous seizure assays performed on 14-16 dpe males. Student's t-test,  $N \geq 2$  biological replicates, 8-10 flies/replicate.

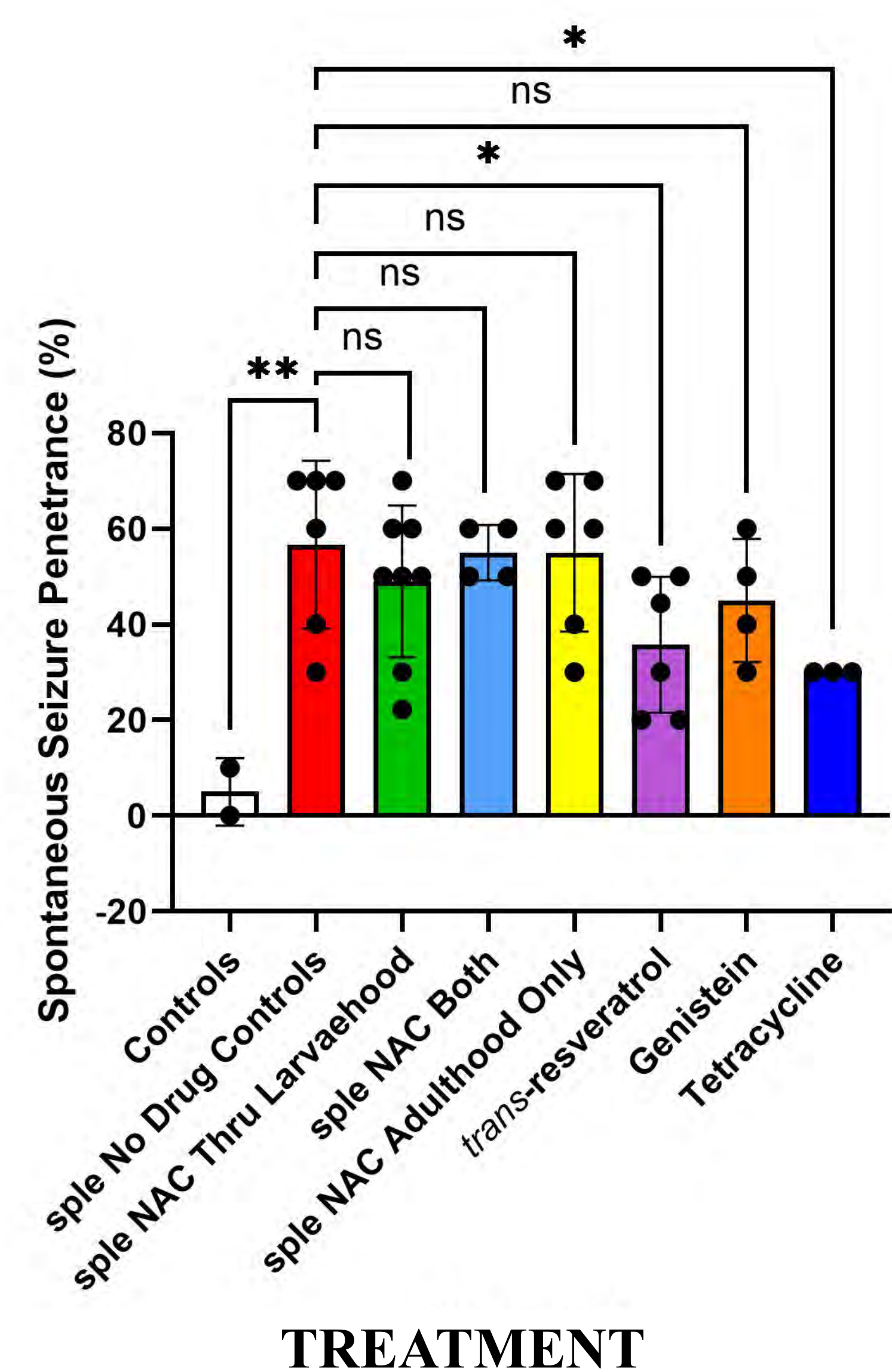


**Figure 2: Trans-resveratrol and tetracycline suppress seizures in  $pk^{sple}$  mutant flies.**

Spontaneous seizure assays performed on 14-16 dpe males. Student's t-test,  $N \geq 2$  biological replicates, 8-10 flies/replicate.

## CONCLUSIONS

### Antioxidants

- Allyl disulfide, ibuprofen, curcumin, and trans-resveratrol suppress seizure penetrance in a fly epilepsy model of a human epilepsy syndrome (*prickle*-associated seizures).
- Licofelone, valdecobix, N-acetylcysteine (NAC), and genistein were unable to reduce seizure penetrance.
- Gallic acid seizure suppression trended towards significance ( $p=0.0516$ )

### Antibiotic Tetracycline

- Tetracycline suppressed seizure penetrance in *prickle* mutant flies.
  - Supports the mitohormesis model of reducing oxidative stress.

### N-acetyl cysteine (NAC) feeding during developmental intervals

- During no developmental stage (larval, adult, larval+adult) did NAC administration significantly reduce seizures.

## DISCUSSION

Our results demonstrate that four antioxidants—allyl disulfide, ibuprofen, curcumin, and trans-resveratrol—significantly reduced seizure penetrance in the  $pk^{sple}$  mutant. These data are consistent with our work showing that oxidative stress leads to activation of the innate immune response to exacerbate seizures. Gallic acid showed a trend towards significance, warranting further investigation. Given the large percentage of epileptics that respond poorly to current anti-epileptic drugs, these data strongly suggest that antioxidants may be an effective treatment modality for epilepsy patients, perhaps in combination with other medications.

Licofelone, valdecobix, NAC, and genistein did not yield statistically significant results effects under the conditions tested, demonstrating that these compounds are less effective in seizure suppression. Despite the known antioxidant properties of NAC, this compound was unable to suppress seizures in this experiment. The four antioxidant compounds shown to suppress seizures could be tested to determine whether they might have differential effects when given during different developmental stages.

Interestingly, tetracycline, an antibiotic, also significantly reduced seizure penetrance. This finding supports a possible link between mitochondrial stress responses and seizure activity, aligning with the mitohormesis model. As tetracycline has known effects on mitochondrial translation, this result raises the possibility that mild mitochondrial inhibition may activate protective stress pathways.

Future directions will explore combinatorial AO treatments, identification of mitochondrial signaling markers, and assessment of transcriptomic responses after AO treatment to identify mechanisms and optimize therapeutic strategies.

## REFERENCES

- Kanner AM, Bicchi MM. Antiseizure medications for adults with epilepsy: a review. *JAMA*. 2022;327(13):1269-1281. doi:10.1001/jama.2022.3880
- Asadi-Pooya AA, Brigo F, Lattanzi S, Blümcke I. Adult epilepsy. *Lancet*. 2023;402(10399):412-424. doi:10.1016/S0140-6736(23)01048-6
- Bassuk AG, Wallace RH, Buhr A, et al. A homozygous mutation in human PRICKLE1 causes an autosomal-recessive progressive myoclonus epilepsy-ataxia syndrome. *Am J Hum Genet*. 2008;83(5):572-581. doi:10.1016/j.ajhg.2008.10.003
- Nukala KM, Lilienthal AJ, Lye SH, Bassuk AG, Chtarbanova S, Manak JR. Downregulation of oxidative stress-mediated glial innate immune response suppresses seizures in a fly epilepsy model. *Cell Rep*. 2023;42(1):112004. doi:10.1016/j.celrep.2023.112004
- Aguilar CC, Almeida AB, Araújo PV, et al. Oxidative stress and epilepsy: literature review. *Oxid Med Cell Longev*. 2012;2012:795259. doi:10.1155/2012/795259
- Lüthy K, Mei D, Fischer B, et al. TBC1D24-TLDC-related epilepsy exercise-induced dystonia: rescue by antioxidants in a disease model. *Brain*. 2019;142(8):2319-2335. doi:10.1093/brain/awz175
- Valero T. Mitochondrial biogenesis: pharmacological approaches. *Curr Pharm Des*. 2014;20(35):5507-5509. doi:10.2174/138161282035140911142118

## ACKNOWLEDGEMENTS

We would like to thank Dr. Manak, Brady Williquett, and the Manak Lab for their invaluable guidance and mentorship. We thank the Manak Lab, University of Iowa, and Belin-Blank Center for providing us this opportunity.



# Targeting DNA replication stress in Ewing sarcoma to trigger the rapid induction of CDK1 and caspase-dependent apoptosis

Stephanie A. Gearing<sup>1</sup>, Stacia L. Koppenhafer<sup>2</sup>, Mary V. Thomas<sup>2</sup>, David J. Gordon, PhD<sup>2</sup>

Vista Ridge High School, Cedar Park TX<sup>1</sup>; Division of Pediatric Hematology/Oncology, University of Iowa<sup>2</sup>

## Introduction

### Background

- Ewing sarcoma is a bone and soft tissue cancer that primarily affects children and young adults between the ages of 10-20 years old.<sup>3</sup> Despite only modest improvements in outcomes, the standard treatment for Ewing sarcoma has remained largely unchanged over the past three decades.
- Researchers have identified key checkpoint kinases such as ATR, CHK1, WEE1, and MYT1 that regulate DNA damage response and cell cycle progression.<sup>1</sup> Targeting these kinases with specific inhibitors disrupts the tumor's ability to manage replication stress. This study aims to target this pathway to inhibit unhealthy cell proliferation.

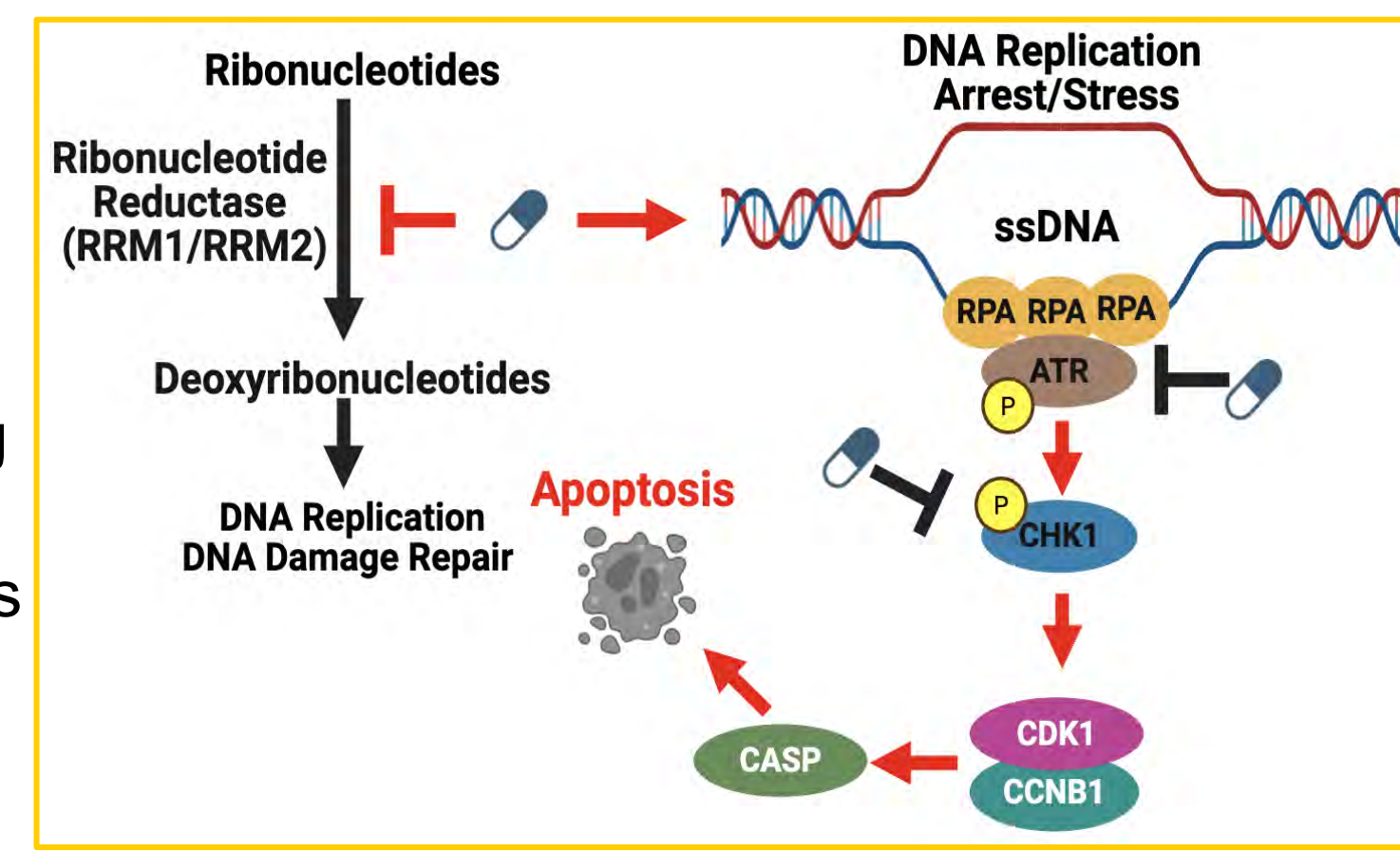


**Figure 1.** ATR CHK1 WEE1 DNA damage response pathway and how inhibitors induce apoptosis.

### Current Strategies

- Combining agents that increase DNA replication stress with ATR-CHK1-WEE1 pathway inhibitors, which disrupt the DNA damage response and cell cycle checkpoints, is a promising strategy now under clinical investigation in Ewing sarcoma and other cancers.<sup>1,3,5</sup>
- The mechanisms by which these drug combinations selectively kill cancer cells experiencing DNA replication stress remain poorly understood and are often attributed—without strong evidence in many tumor types—to replication catastrophe and/or forced mitotic entry.<sup>2</sup>

### Research Objectives

- To identify which drugs rescue apoptosis in Ewing sarcoma, how their effects differ between cell lines, and how this can aid in our understanding of cell cycle inhibition to predict drug synergy.

## Methods

### Cell Viability Assays

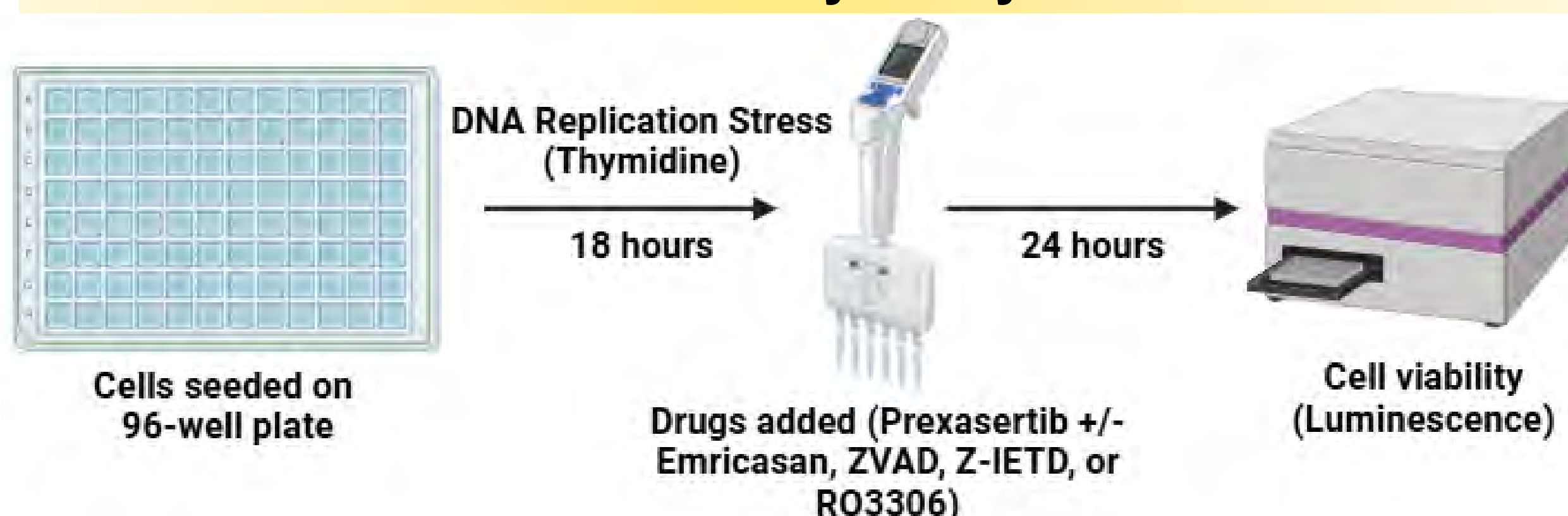


**Figure 2.** Visualization of a cell viability assay. Drug descriptions: Thymidine (RNR inhibitor), Prexasertib (CHK1 inhibitor), Emricasan (Pan-caspase inhibitor), ZVAD (Pan-caspase inhibitor), Z-IETD (Caspase-8 inhibitor), RO-3306 (CDK1 inhibitor).

### EVOS Imaging



**Figure 3.** Visualization of EVOS Imaging process. Parental and H2B Ewing sarcoma cells (EW8) were plated and Prexasertib, ZVAD, or RO3306 were added accordingly. Cells were stained with DAPI, imaged, and counted to calculate percentage mitotic. Zoom shows cells in anaphase stage of mitosis.

## Results

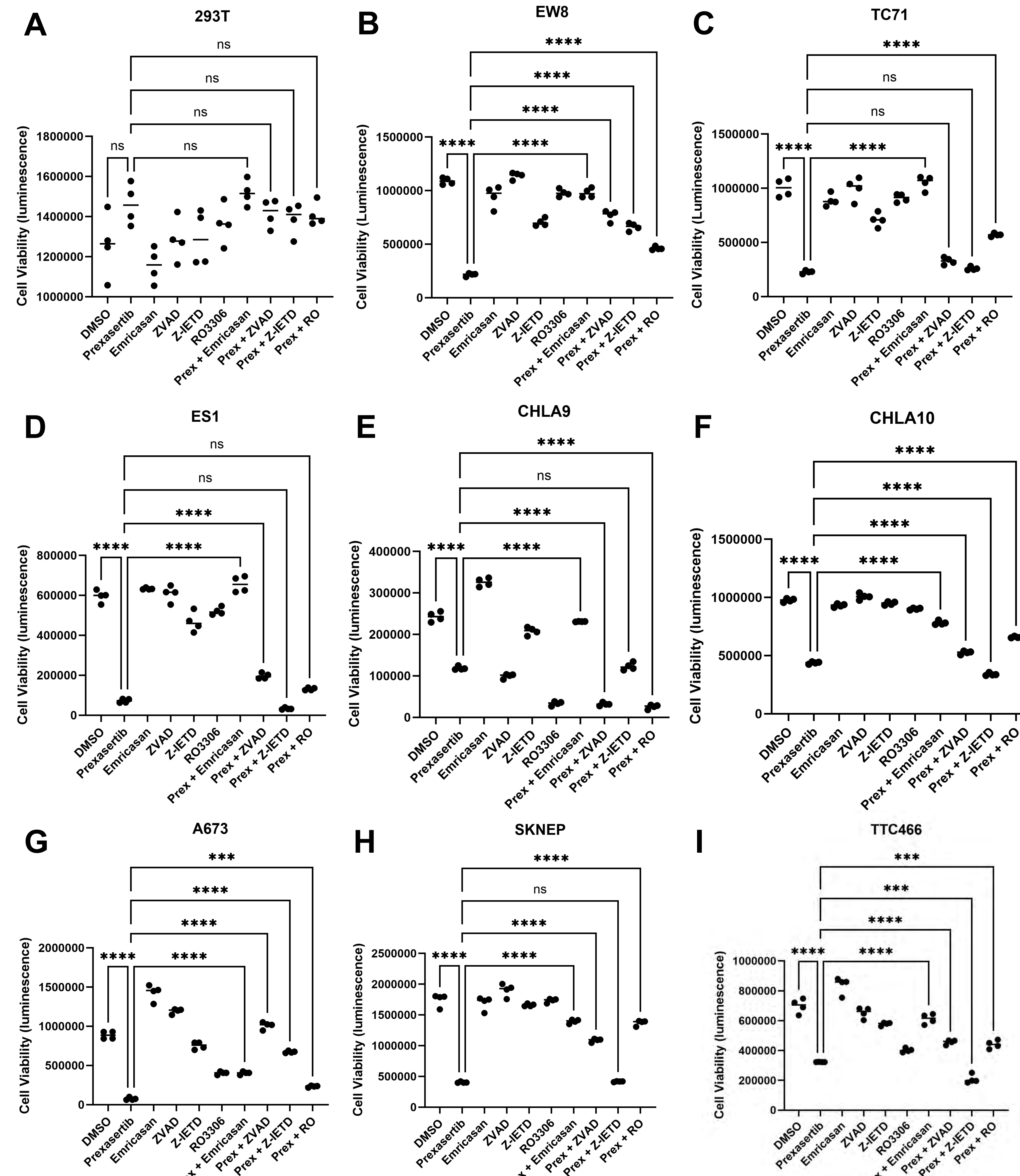


**Figure 4.** Multiple Comparison One Way ANOVA comparing cell viability for the control (DMSO) vs Prexasertib and Prexasertib alone vs Prexasertib in combination with Emricasan, ZVAD, Z-IETD, or RO3306. (A) Healthy cell line 293T. (B-D) Ewing sarcoma cell lines (E) Ewing sarcoma cell line CHLA9 (expresses p53) (F) Ewing sarcoma cell line CHLA10 (does not express p53) (G-I) Ewing sarcoma cell lines. Asterisks indicate a significant difference.

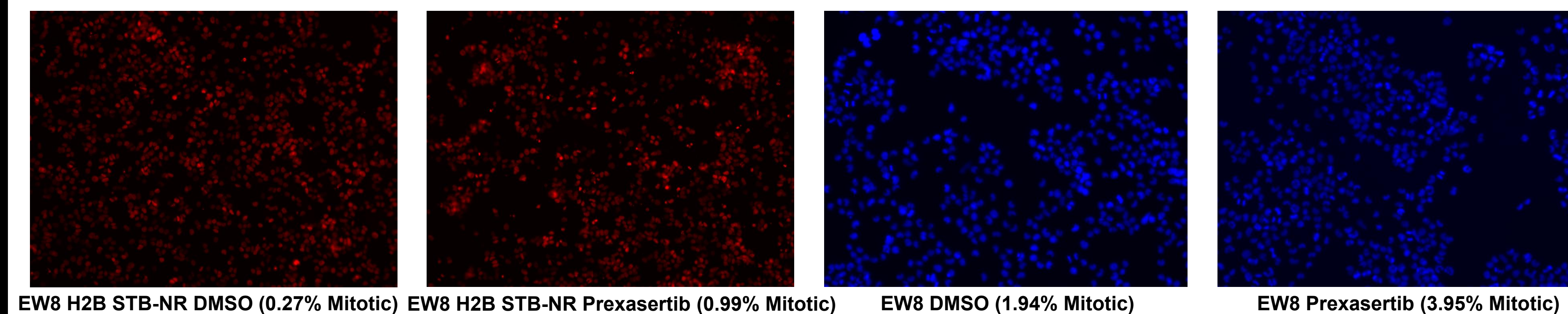


**Figure 5.** EVOS imaging of EW8 H2B and parental EW8 cells +/- Single Thymidine Block - No Release (STB-NR) + DMSO or Prexasertib. The total number of cells per window was counted using ImageJ and the percentage of mitotic cells was calculated. The percentage of mitotic cells was higher in cells that weren't treated with thymidine and those treated with Prexasertib.

## Discussion

This work identified that dual inhibition of DNA replication and the ATR-CHK1-WEE1 signaling axis induces apoptosis in Ewing sarcoma cells through a CDK1- and caspase-dependent mechanism.

- Figure 5 demonstrates the inhibition of DNA replication. Thymidine arrests cells in the G1/S phase transition creating replication stress and preventing cells from progressing through the cell cycle. This explains why the mitotic percentages for the STB-NR cells are lower than those without thymidine. Prexasertib is a CHK1 inhibitor and blocks a crucial part of the signaling pathway that manages replication stress and DNA damage repair.<sup>4</sup> When prexasertib was administered, it interrupted key cell cycle checkpoints and cells bypassed these checkpoints, entering mitosis prematurely. The differences between the DMSO and Prexasertib treated cells explains methods in Figure 4.
- Inhibition of the ATR-CHK1-WEE1 pathway in S-phase-arrested Ewing sarcoma cells rapidly induces apoptosis within 2-4 hours.<sup>4</sup> This apoptotic response is driven by activation of cyclin-dependent kinase 1 (CDK1) and the aberrant accumulation of cyclin B1 (CCNB1).
- Figure 4 shows the main experiments run using cell viability assays. This data shows a correlation between DNA replication and ATR-CHK1-WEE1 pathway inhibitors and induced apoptosis in Ewing sarcoma.
- Cell line 293T is a healthy adenovirus-immortalized human embryonic kidney cell line and serves as a control to highlight that Ewing sarcoma cells are more sensitive to regulatory inhibitors than normal cells. As the graph indicates, there was no significant difference between the DMSO treated cells and any of the Prexasertib drug combinations.
- Across multiple Ewing sarcoma cell lines (EW8, CHLA10, and TTC466), significant differences in cell viability were observed between Prexasertib monotherapy and its combination with other agents. Therefore, in these cell lines, Emricasan, ZVAD, and RO3306 rescue apoptosis to varying degrees. The expression of tumor suppressant p53 is the only difference between cell line CHLA9 and CHLA10. Interestingly, CHLA9 was affected differently than CHLA10 indicating that p53 plays a role in mitotic pathways and proliferation. This will lead to further analysis of the function of tumor suppressants within the cell cycle.
- This data highlights the importance of cell cycle context and caspase activation in mediating the antitumor effects of these agents and suggest that CDK1-CCNB1 dysregulation and caspase-8 level could serve as predictive biomarkers for drug response. Future studies will extend these experiments to additional cancer cell lines, with a focus on other sarcoma subtypes. The effects of protein synthesis inhibitors on apoptotic pathways and how these preclinical findings might inform clinical translation will also be investigated.

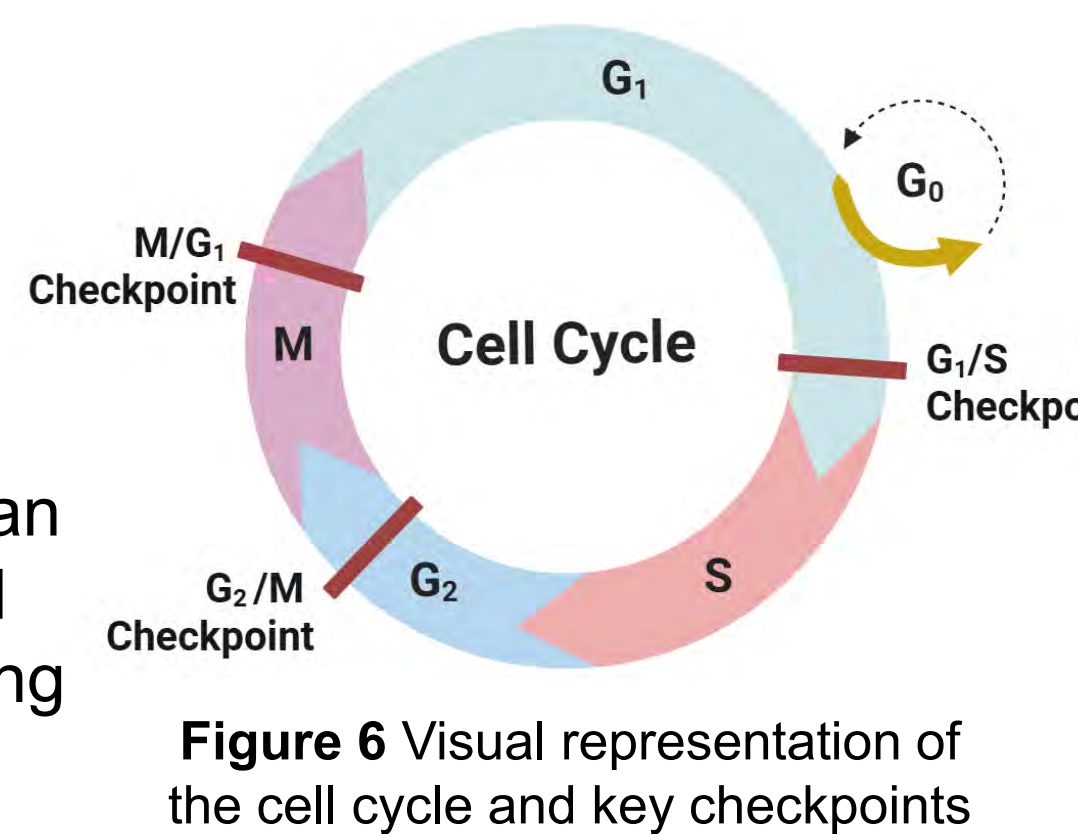


**Figure 6** Visual representation of the cell cycle and key checkpoints

### Cyclin Expression during Cell Cycle



**Figure 7** Graph showing cyclin activity throughout stages of the cell cycle

## Acknowledgements

Thank you to the entire Gordon Lab for supporting me throughout my research and giving me this opportunity. Thank you to SSTP for allowing me to showcase my work and providing me with insight into the research environment. Graphics created using BioRender and graphs created using GraphPad PRISM.

## References

- da Costa AABA, Chowdhury D, Shapiro GI, D'Andrea AD, Konstantinopoulos PA. Targeting replication stress in cancer therapy. *Nature Reviews Drug Discovery*. 2022;22(1):38-58. <https://doi.org/10.1038/s41573-022-00558-5>
- Naumann JA, Widen JC, Jonart LA, et al. SN-38 Conjugated Gold Nanoparticles Activated by Ewing Sarcoma Specific mRNAs Exhibit In Vitro and In Vivo Efficacy. *Bioconjugate Chemistry*. 2018;29(4):1111-1118. <https://doi.org/10.1021/acs.bioconjchem.7b00774>
- Goss KL, Koppenhafer SL, Harmoney KM, Terry VW, Gordon DJ. Inhibition of CHK1 sensitizes Ewing sarcoma cells to the ribonucleotide reductase inhibitor gemcitabine. *Oncotarget*. 2017;8(50). <https://doi.org/10.18632/oncotarget.18776>
- Heidler CL, Roth EK, Thiemann M, et al. Prexasertib (LY2606368) reduces clonogenic survival by inducing apoptosis in primary patient-derived osteosarcoma cells and synergizes with cisplatin and talazoparib. *International Journal of Cancer*. 2019;147(4):1059-1070. <https://doi.org/10.1002/ijc.32814>
- Crozier L, Foy R, Mouery BL, et al. CDK4/6 inhibitors induce replication stress to cause long-term cell cycle withdrawal. *The EMBO Journal*. 2022;41(6). <https://doi.org/10.15252/emj.2021108599>



# SETDB1 Gene's Role in Endometrial Cancer Progression in Lean and Obese Models

## Exploring SETDB1's pro-tumor properties through immune regulation

Nico Gong<sup>1</sup>; Kiarash Salari, PhD<sup>2</sup>; Shujie Yang, PhD<sup>2</sup>

<sup>1</sup>BASIS Independent Silicon Valley, CA; <sup>2</sup>Department of Pathology, University of Iowa



## Introduction

Endometrial Cancer is a lethal gynecological cancer, where cases have increased steadily; for example, 2003 to 2015, endometrial cancer rates saw a steady growth of 1% annually(Mullins & Cote, 2019) .

SETDB1 is an oncogene identified as overexpressed in endometrial cancer, being found to regulate cell death through mechanisms like immune evasion(Yang et al. 2024).

Figure 1: This Western Blot proves the knockout of SETDB1 in these MECPK cells for the tumor measurements below.

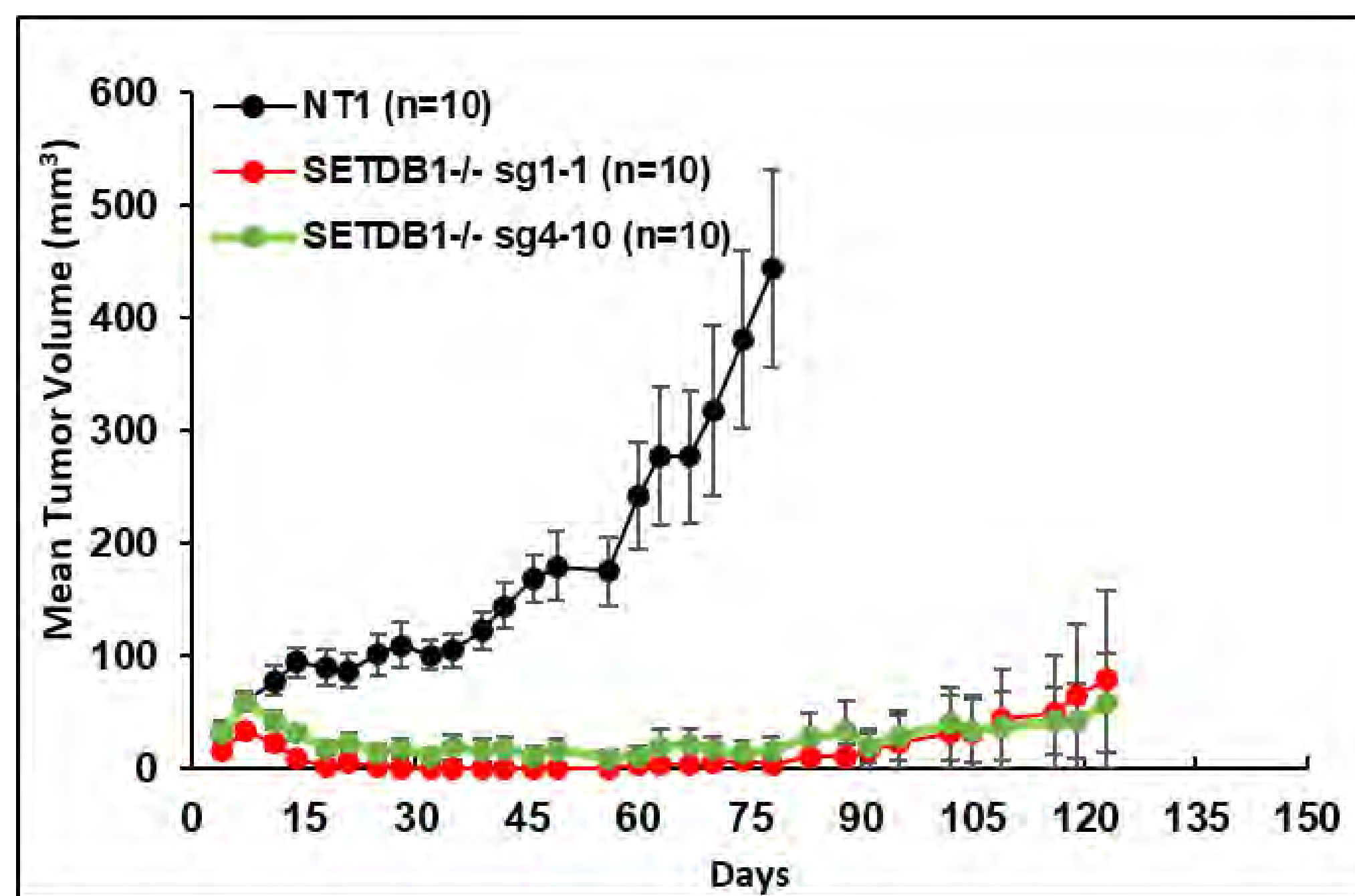
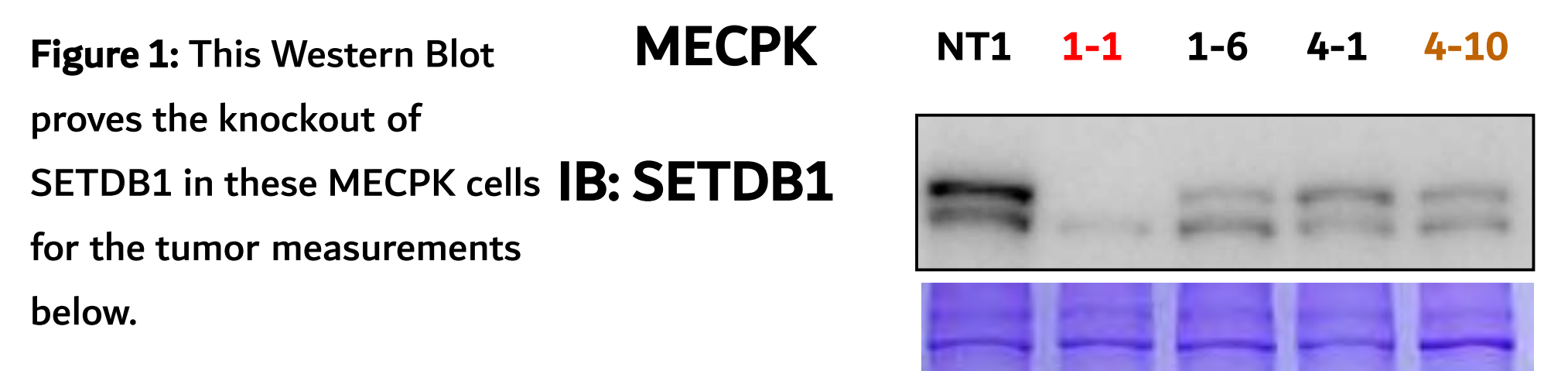


Figure 1.1: Preliminary data measuring tumor growth of knockout SETDB1 tumors and wild type SETDB1 tumors. Tumor volume was recorded across 75 to 120 days.

This preliminary data shows that the knockout of SETDB1 in MECPK cells majorly decreases the growth of tumor cells inside a mouse body, while wild type cells had a significantly higher rate of growth.

However, even though evidence points that SETDB1 is a potential factor in progressing EC; over 70 percent of EC patients are overweight/obese (Gao et. al., 2018)- a variable that may also influence the growth or impact of SETDB1 in the progression of cancer. To explore this potential extra factor in the progression of EC, we ask:

**RESEARCH QUESTION:** How does SETDB1 progress EC differently from Obese or Lean cell models? What will happen when we inject MECPK cells inside lean or obese mice?

Why does the KO tumor shrink when it is injected into the healthy immune mouse? We could potentially attribute this behavior to the immune cytokines inside the mouse body acting against the tumor's growth.

## Research Goals

The goal of this project is to further explore the roles that the gene SETDB1 plays in the progression of endometrial cancer through immune regulation, and how it influences growth in both lean and obese cell models.

## Methodology Continued

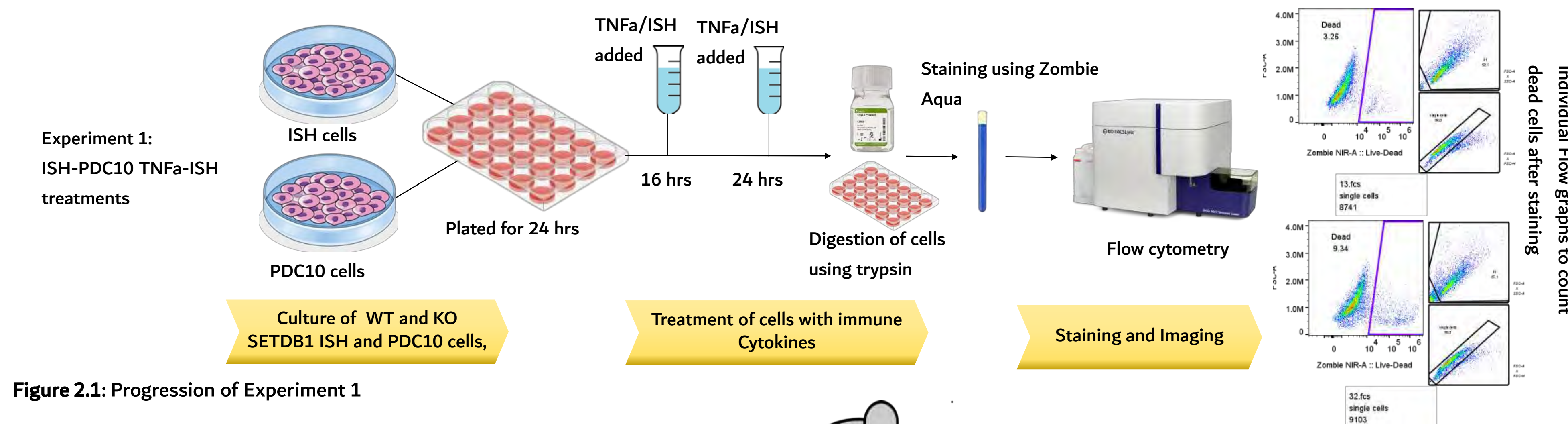


Figure 2.1: Progression of Experiment 1

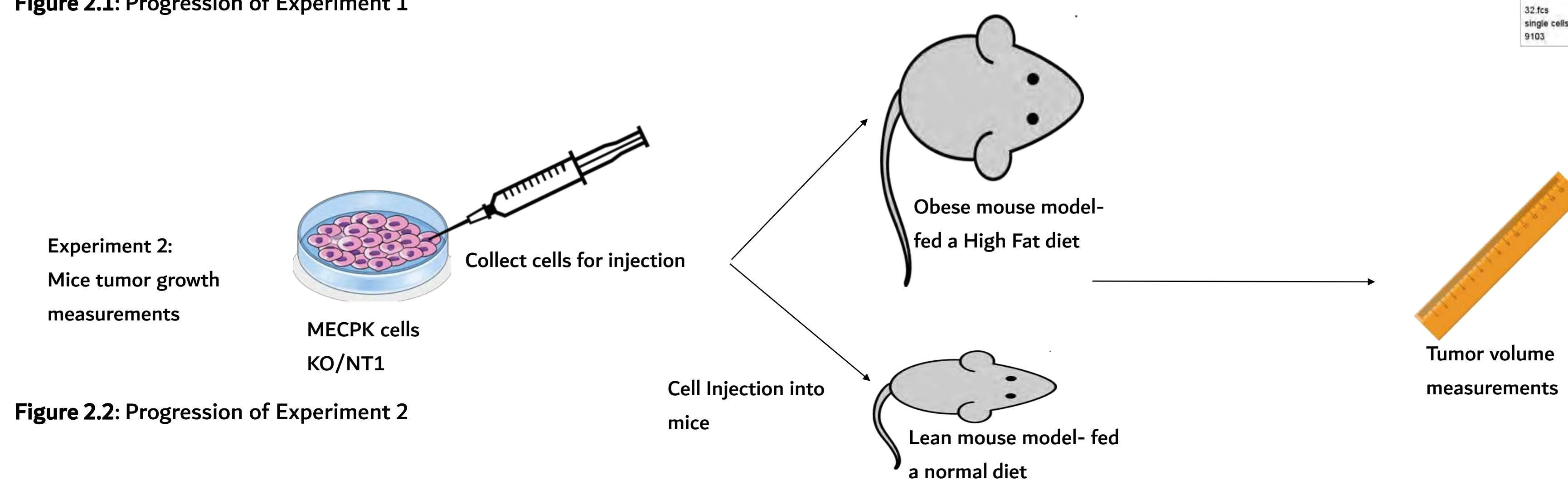


Figure 2.2: Progression of Experiment 2

## Results

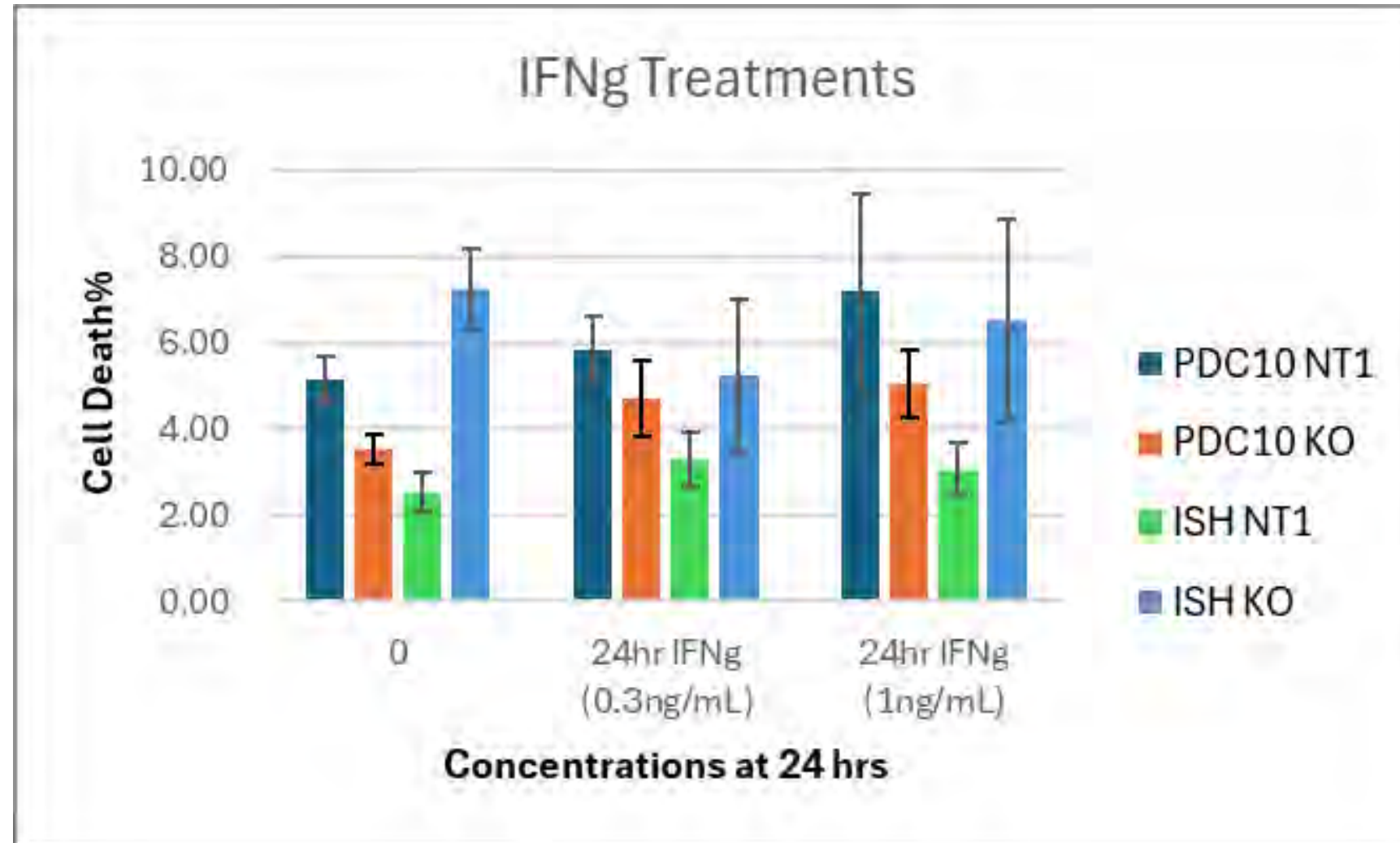
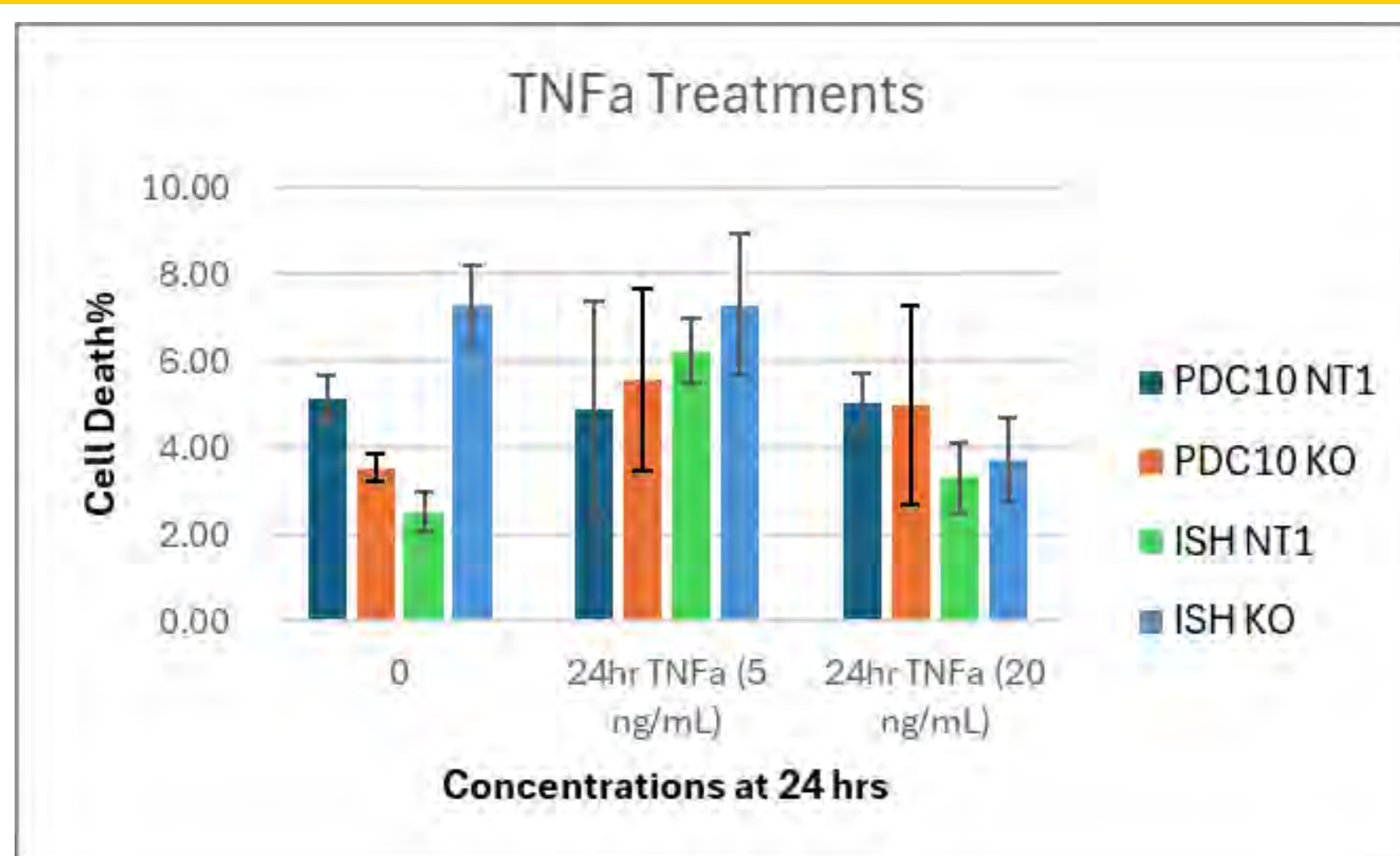


Figure 3.1: Bar graph of cell death percentage means at 24 hours

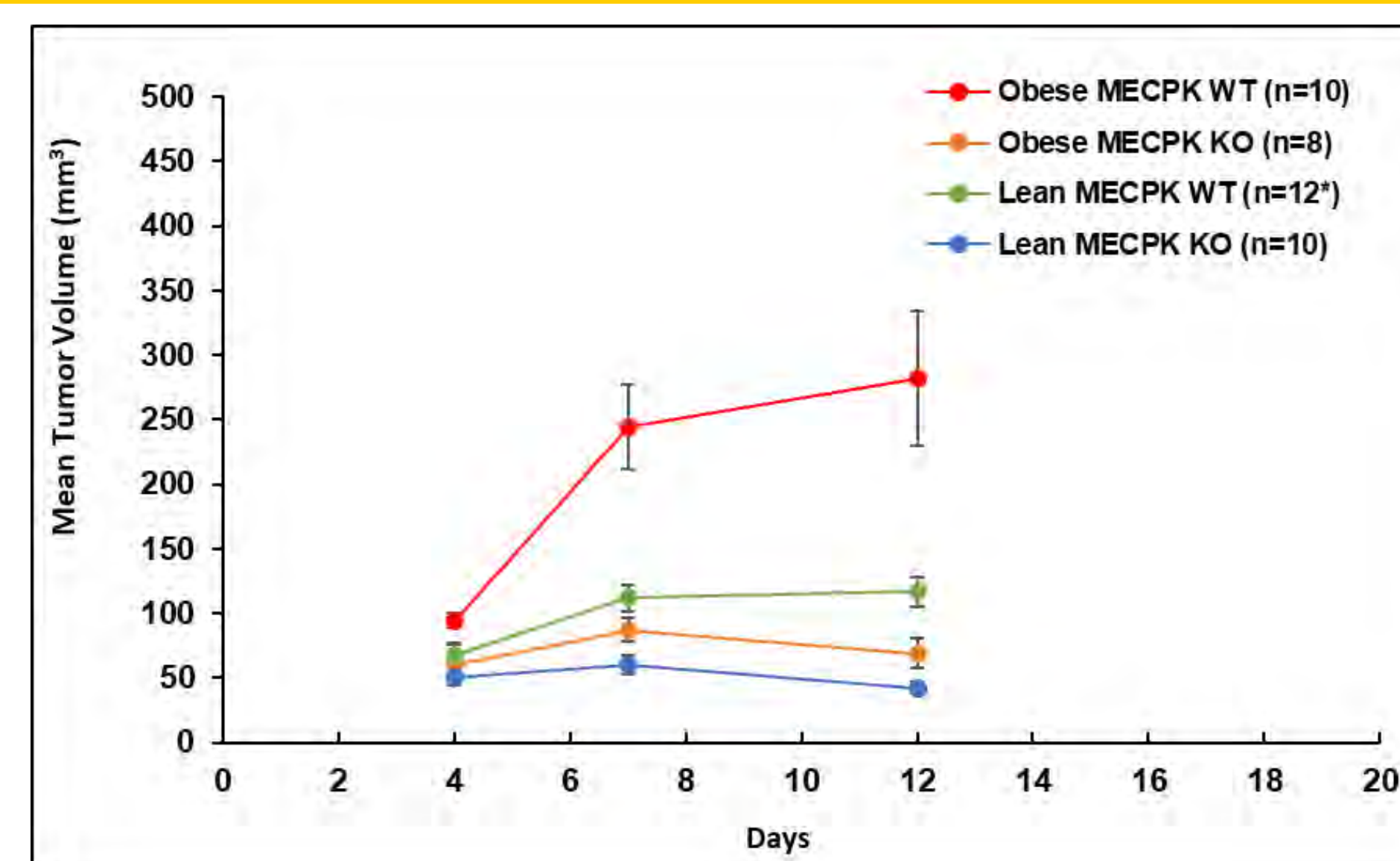
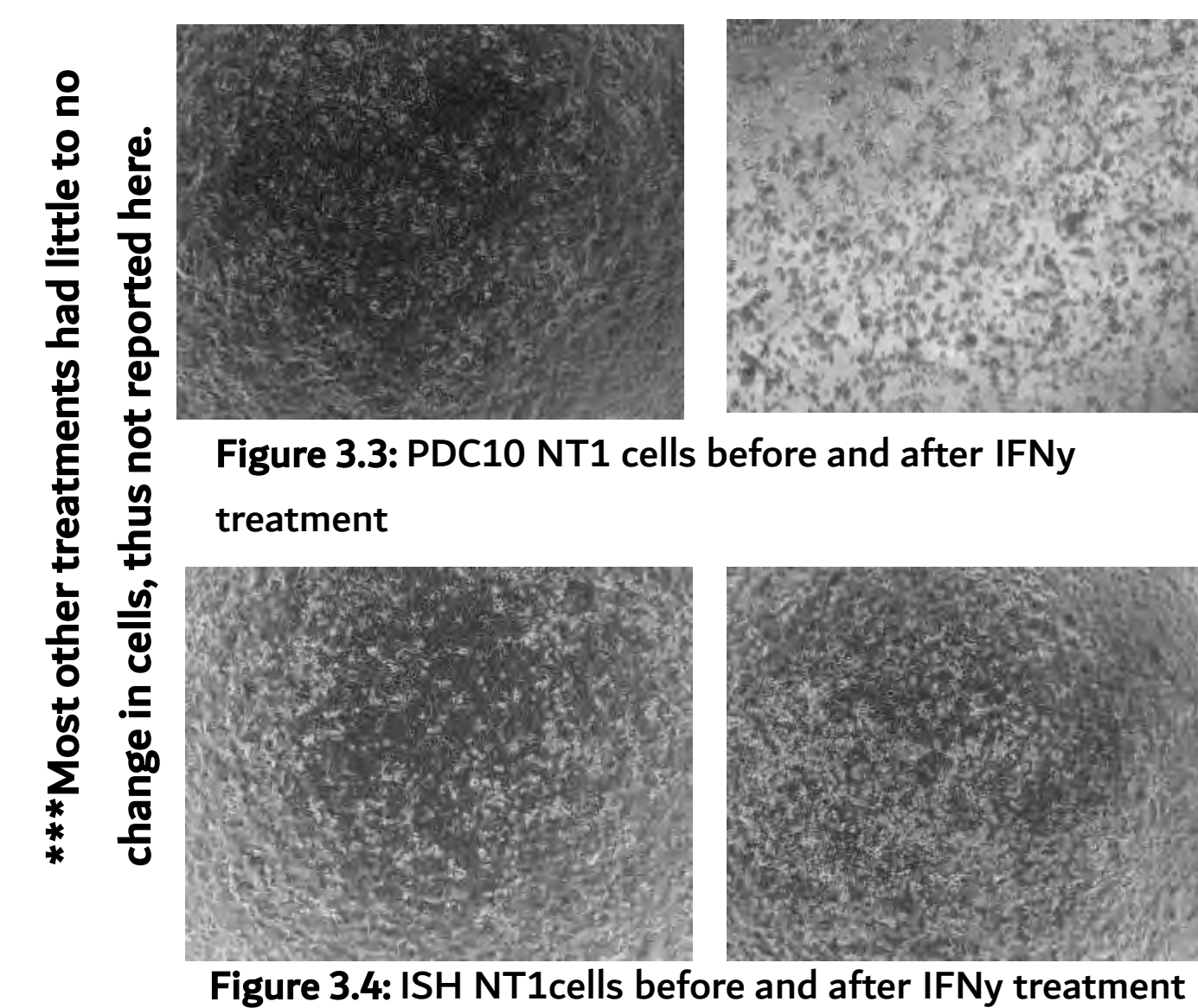


Figure 3.2: Mouse tumor growth measurements after injection



\*\*\*Most other treatments had little to no change in cells, thus not reported here.

Figure 3.4: ISH NT1cells before and after IFNy treatment

## Discussion

For the mice tumor volumes, the following differences were found significant: Obese WT vs Obese KO ( $p = 0.002$ ) Lean WT vs Lean KO: ( $p < 0.001$ ) Lean WT vs Obese WT: ( $p = 0.01$ ) Lean KO vs Obese KO was not significant ( $p = 0.053$ ). SETDB1 can thus be correlated to an increased rate of growth within these groups, where Obese WT grows at a significantly faster pace than Lean WT and Obese KO, and that Lean WT grows at a faster pace than Lean KO. It is also shown here that obesity is positively correlated with EC growth, with obese WT growing faster than Lean WT, but not shown to grow significantly faster than Lean KO.

The percentage of cell death counted and averaged per tube is not significant- little difference between groups. There is very little difference between mean dead cell percentage between concentrations for each cell line, knockout and wild type. No significant differences were observed between any cells for TNFa treatments, however, in IFNy, major differences in cell death were observed between ISH NT1 and ISH KO at an approx. ~5% difference at 24 hrs 1 ng/mL. Another difference in IFNy treatments are PDC10 KO and PDC10 NT1 at 24 hrs 1ng/mL. These results could be attributed to a potential flaw in methods, where we did not refresh cell medium or keep treating with more cytokines.

## Future Direction

Verify the function of SETDB1 in regulating immune response to allow cells to grow further.

Study downstream genes and other factors to uncover SETDB1's pathway or mechanism in regulating immune response.

Study new models of SETDB1 in lean or obese models to discover differences in the progression of EC.

## References

- Johnson, E., Salari, K., & Yang, S. (2023). SETDB1: A perspective into immune cell function and cancer immunotherapy. *Immunology*, 169(1), 3–12. <https://doi.org/10.1111/imm.13619>
- Mullins, M. A., & Cote, M. L. (2019). Beyond Obesity: The Rising Incidence and Mortality Rates of Uterine Corpus Cancer. *Journal of Clinical Oncology*, 37(22), 1851–1853. <https://doi.org/10.1200/JCO.19.01240>
- Strepkos, D., Markouli, M., Klonou, A., Papavassiliou, A. G., & Piperi, C. (2021). Histone Methyltransferase SETDB1: A Common Denominator of Tumorigenesis with Therapeutic Potential. *Cancer Research*, 81(3), 525–534. <https://doi.org/10.1158/0008-5472.CAN-20-2906>
- Yang, H., Sui, L., Cai, C., Chu, H., & Diao, Y. (2024). SETDB1 promotes progression through upregulation of SF3B4 expression and regulates the immunity in ovarian cancer. *Journal of Ovarian Research*, 17(1), 34. <https://doi.org/10.1186/s13048-024-01358-8>
- Gao, Y., Dai, X., Lee, A. C., Wise, M. R., Shen, F., & Chen, Q. (2018). Body Mass Index is Negatively Associated with Endometrial Cancer Stage, Regardless of Subtype and Menopausal Status. *Journal of Cancer*, 9(24), 4756–4761. <https://doi.org/10.7150/jca.21137>

## Acknowledgements

A huge thank you to Dr. Yang and Dr. Salari for the inspiration, support, and mentorship throughout this project. This project was supported by NIH R37-CA238274(SY) and the Department of Pathology Start-Up Fund(SY).



# Separation of Corn Oil, C18 Fatty Acids, and C18 Fatty Acid Methyl Esters with Polydimethylsiloxane (PDMS) Membranes

Xiyuan (Carol) Gong<sup>1</sup>, Keshin Huang<sup>2</sup>, Saurav Katuwal<sup>3</sup>, MS, Jett Tjaden<sup>3</sup>, BS, Ned B. Bowden<sup>3</sup>, PhD

<sup>1</sup>Interlake High School, WA, <sup>2</sup>Great Neck North High School, NY, <sup>3</sup>Department of Chemistry, University of Iowa, IA

## Introduction

Corn oil is a valuable commodity used to produce consumable products as well as industrial chemicals.<sup>1</sup> Conventional methods to separate fatty acids (e.g. mechanical pressing, fractional distillation, and crystallization) suffer from flaws such as large energy consumption, while membrane separation is popular for its relatively low energy consumption and facile upscaling.<sup>2</sup> Various studies have aimed to separate fatty acids and fatty acid methyl esters with different membranes.<sup>3,4</sup>

PDMS (Figure 1) is a hydrophobic polymer and one of the most used silicon-based polymers in industry due to its chemical stability and ease of fabrication, making it a suitable membrane for large-scale organic chemical separation.<sup>5</sup> It also exhibits swelling behavior when in contact with nonpolar solvents, allowing for transfer of absorbed chemicals.

Corn oil is generally composed of a glycerol backbone connected to three fatty acids, most commonly linoleic and oleic acid.<sup>6</sup> We investigated primarily oleic acid (Figure 2) and its methyl ester methyl oleate, as well as its salt lithium oleate.

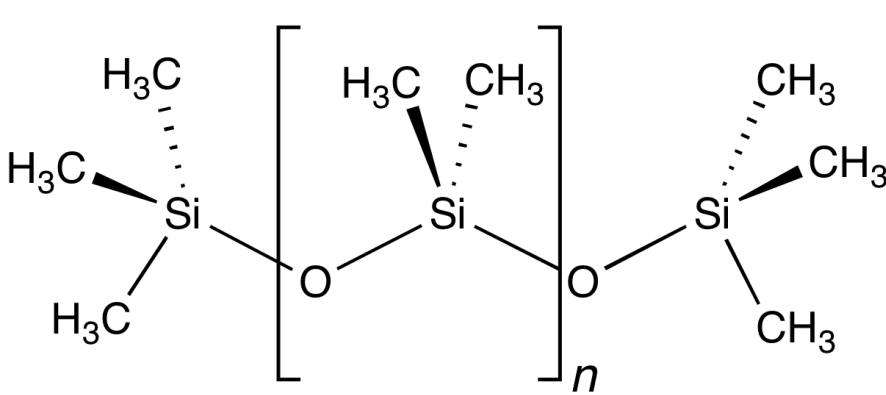


Figure 1. PDMS  
Image source: Wikipedia

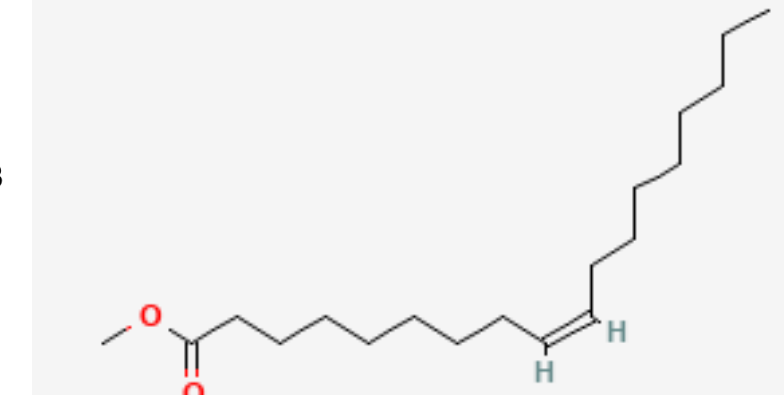


Figure 2. Methyl Oleate  
Image source: PubChem

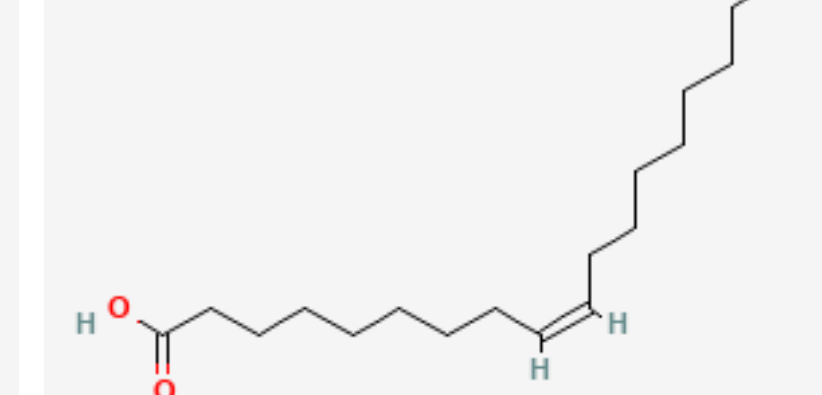


Figure 3. Oleic Acid  
Image source: PubChem

### Research Question

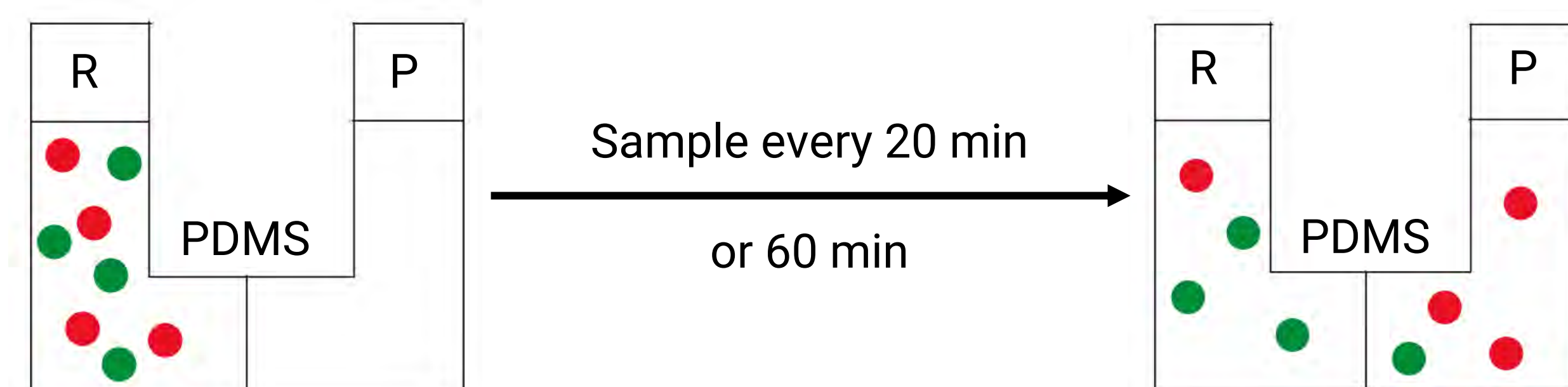
How does polydimethylsiloxane (PDMS) membrane perform in separation of organic compounds such as oils, fatty acids, and fatty acid methyl esters?

## Methodology

PDMS membranes were synthesized by combining base and curing agent in a 10:1 ratio and cured at 60°C overnight. Selected membranes were measured to be approximately 80-100  $\mu\text{m}$  thick. Membranes were cut into circular discs of radius approximately 2 cm.

Two bulbs were affixed together by an O-ring and clamp, separated by the membrane. 1:1 or 4:1 ratios of the components were prepared as the retentate. The retentate was dissolved in 30 mL hexane (in the case of the highly polar lithium oleate, it was dissolved in methanol) and placed in one bulb, while the permeate side contained only 30 mL hexane.

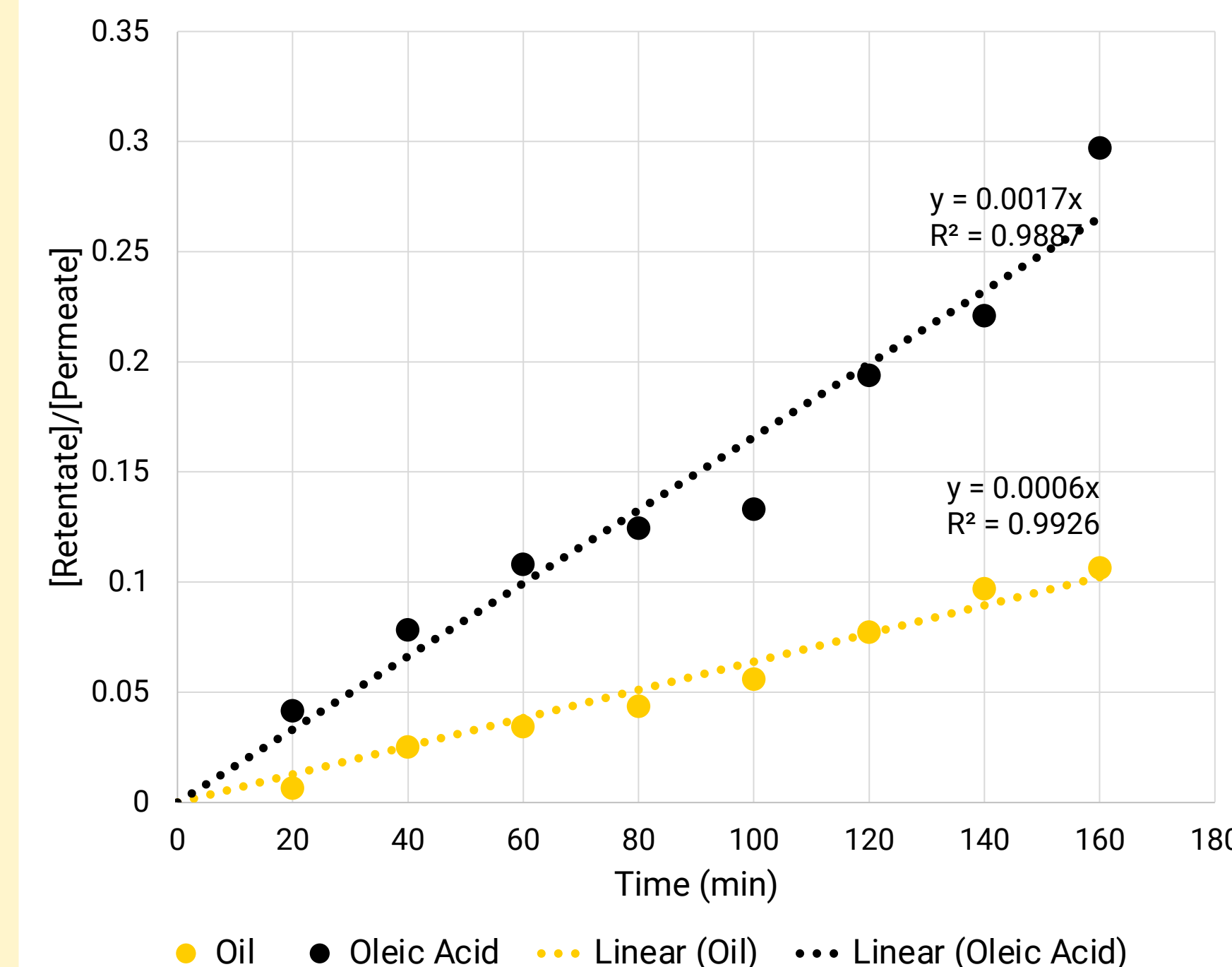
1-ml samples were taken every 20 minutes across 140 to 160 minutes. For longer trials, samples were taken every hour for 6 hours. Samples were analyzed using <sup>1</sup>H NMR spectroscopy with paranitrobenzaldehyde standard.



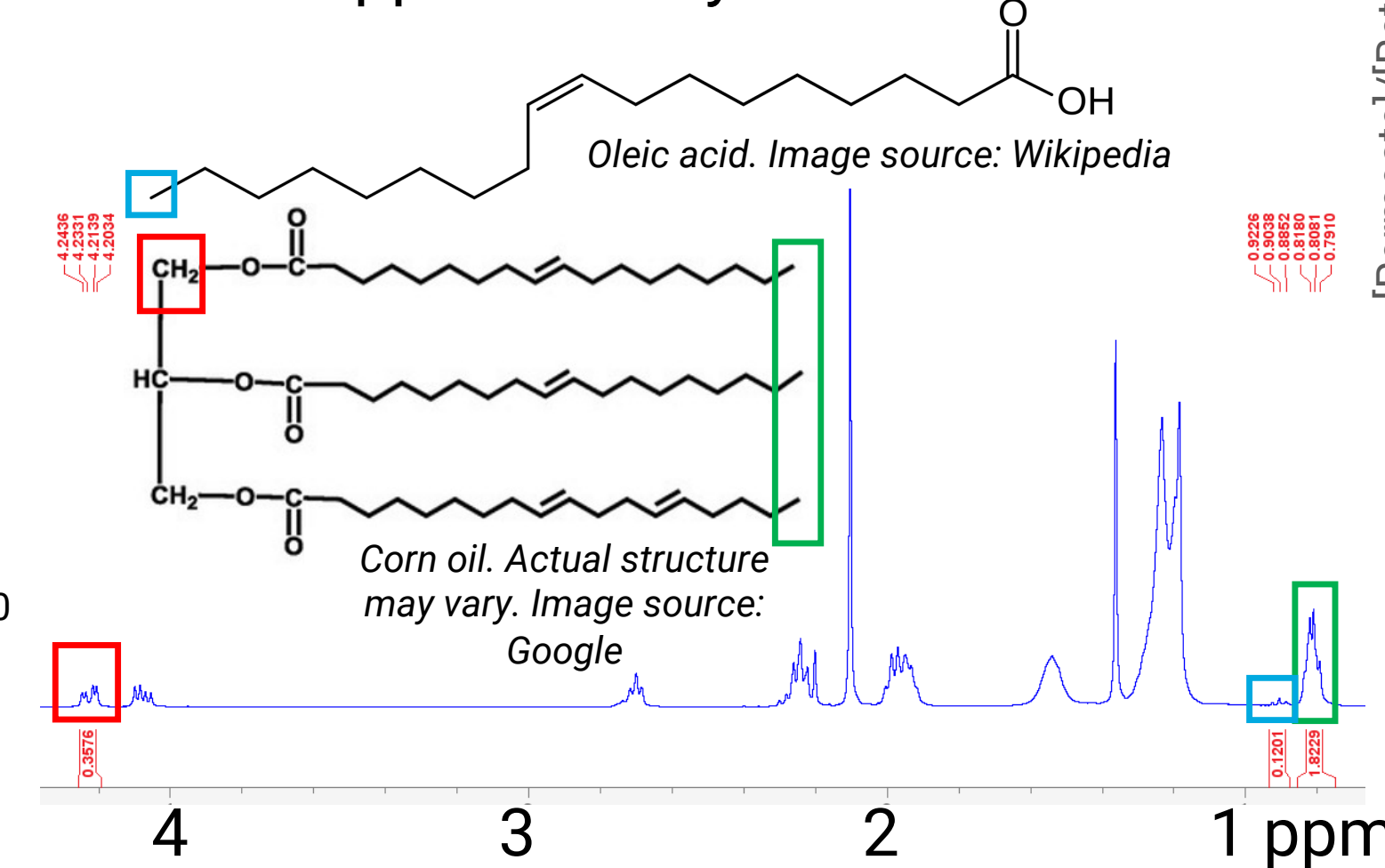
## Results & Discussion

### 1 : 1 Corn Oil vs. Oleic Acid

Flux of Corn Oil and Oleic Acid vs. Time

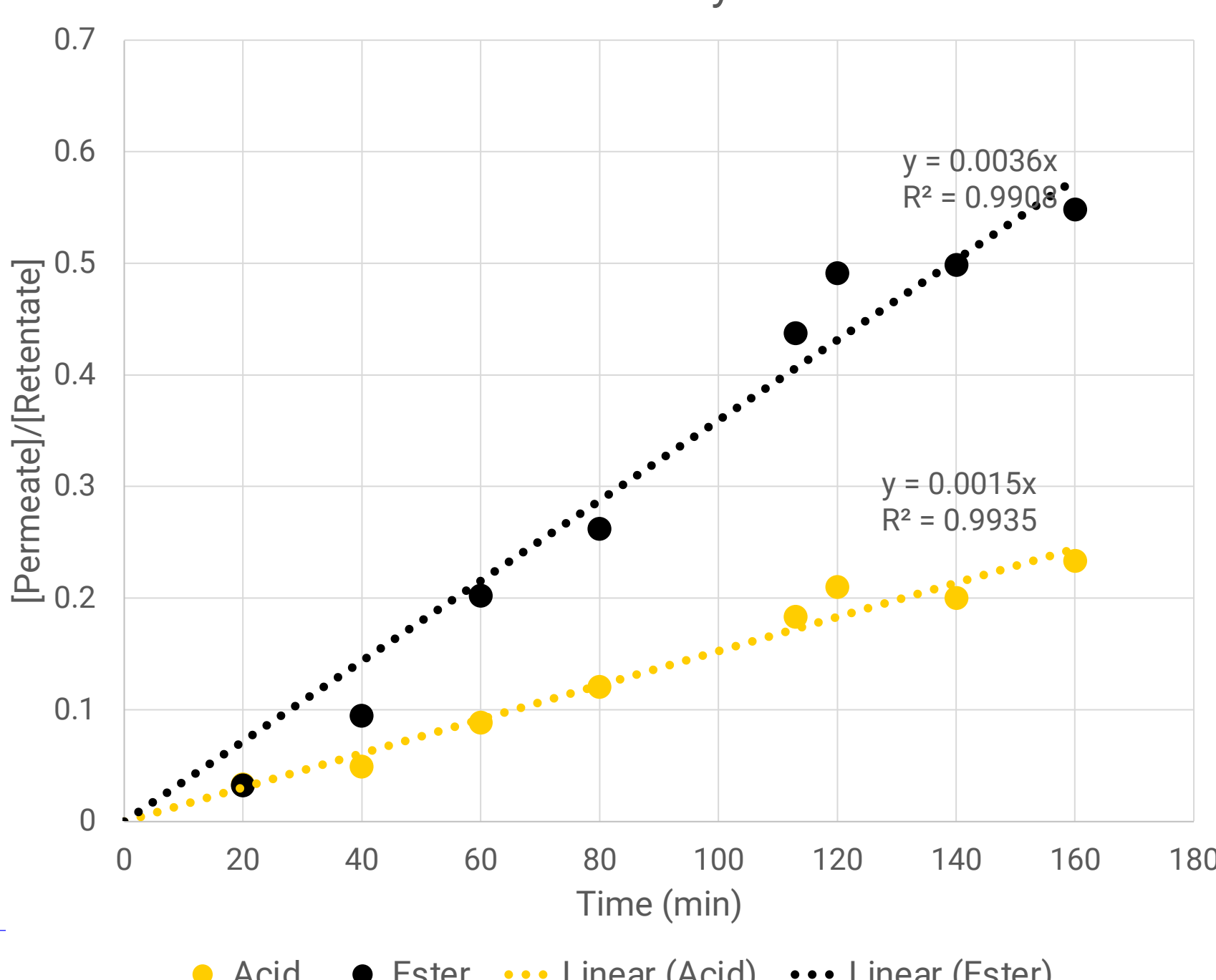


The 6-hour and 4 : 1 trials showed little correlation and inconclusive results likely due to procedural error. However, we can expect the trend to continue until equilibrium. Extension of this project will involve repeating these experiments. Flux ratio of corn oil : oleic acid was approximately 1 : 2.8.



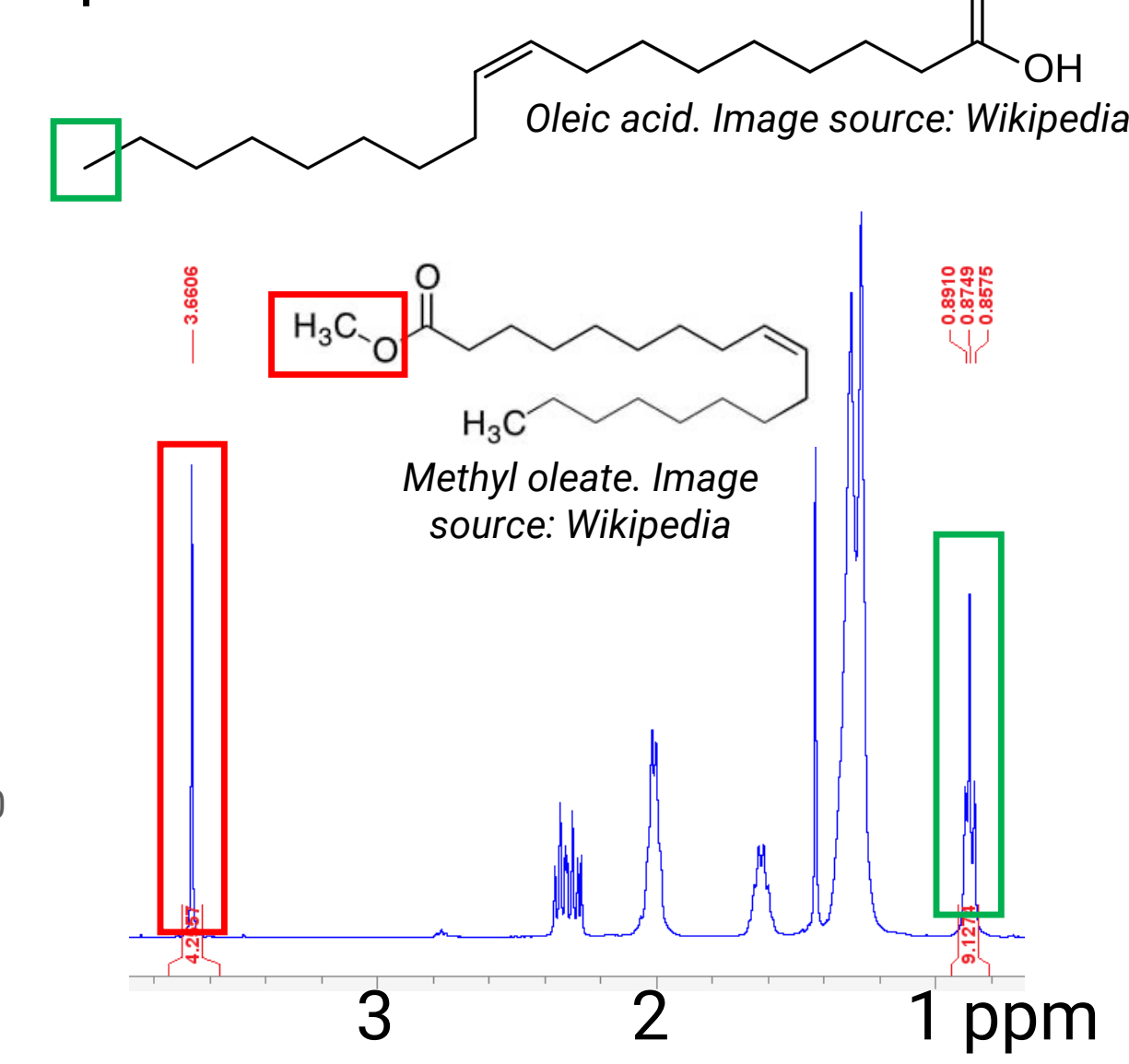
### 1 : 1 Oleic Acid vs. Methyl Oleate

Flux of Oleic Acid and Methyl Oleate vs. Time



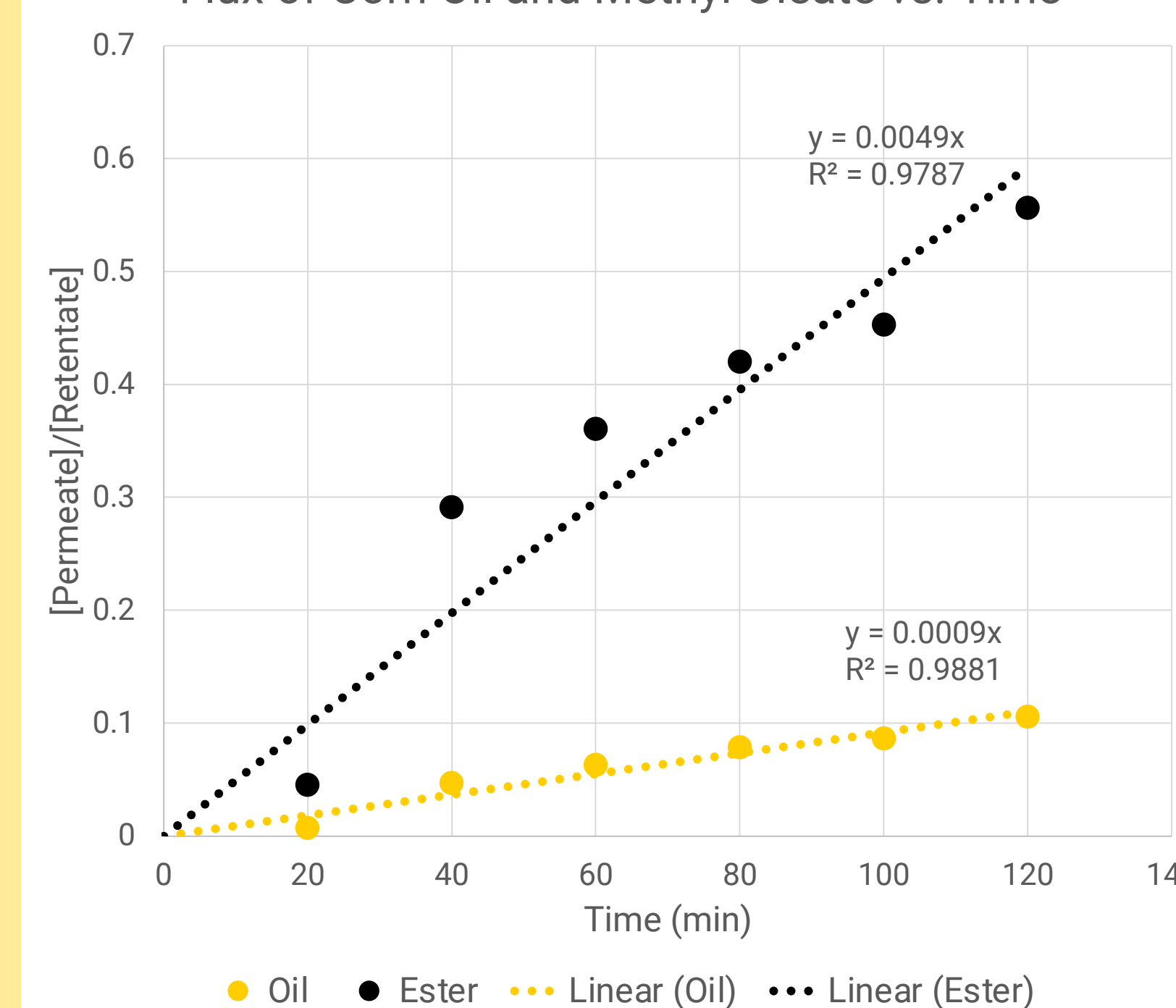
Flux ratio of oleic acid : methyl oleate was approximately 1 : 2.4.

The low difference can be explained by the similarity of the species' structures.

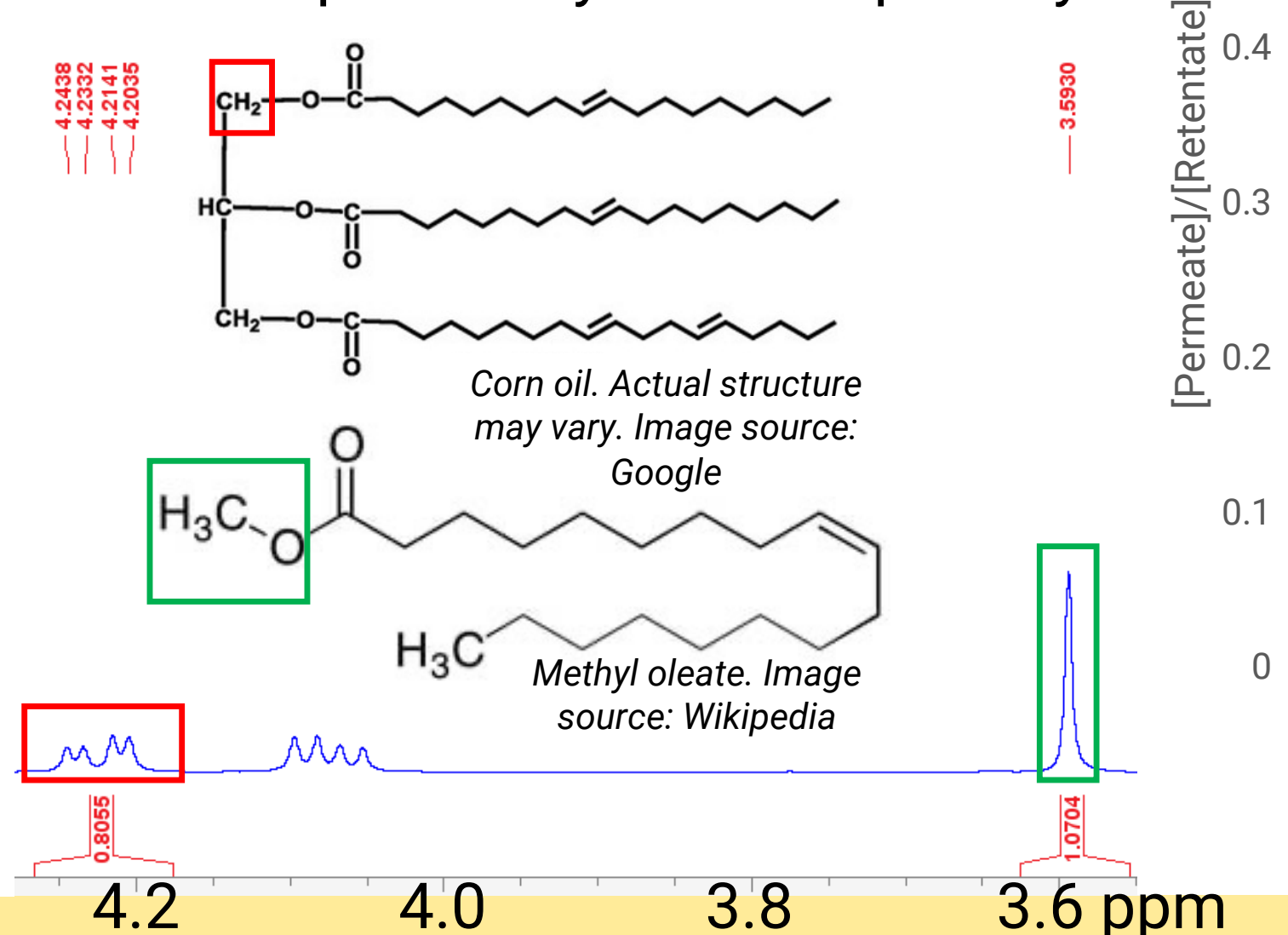


### 1 : 1 Corn Oil vs. Methyl Oleate\*

Flux of Corn Oil and Methyl Oleate vs. Time



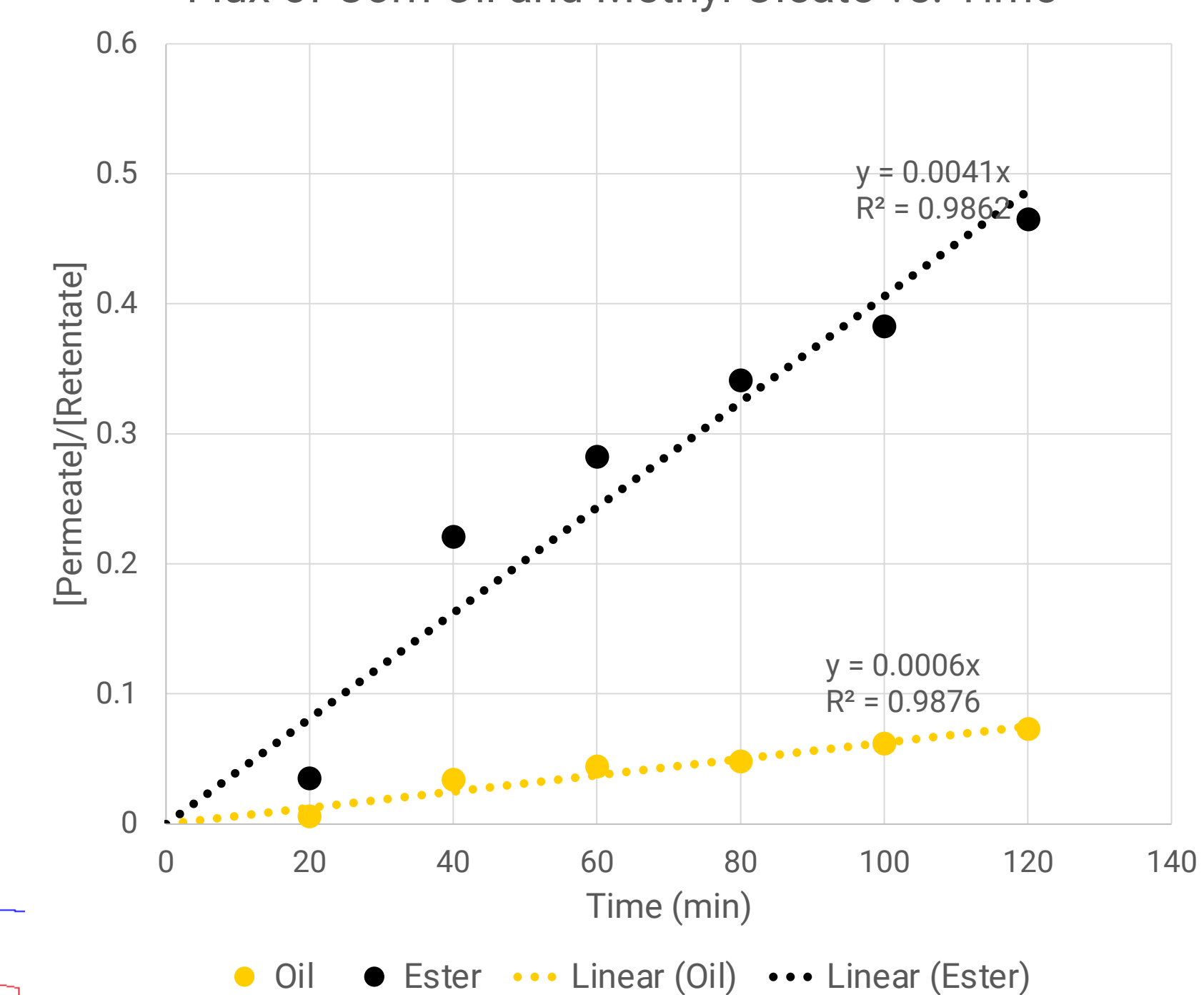
Flux ratio of corn oil : methyl oleate was approximately 1 : 5.4 for the 1 : 1 trial and 1 : 6.8 for the 4 : 1 trial. The higher permeation of methyl oleate can be explained by its lower polarity.



\*Note: Spectroscopic data show that the samples for the 40-minute retentate were originally mistakenly switched between the 1:1 and 4:1 trials. The data presented are corrected, although original data are available upon request.

### 4 : 1 Corn Oil vs. Methyl Oleate\*

Flux of Corn Oil and Methyl Oleate vs. Time



### 1 : 1 Oleic Acid vs Lithium Oleate

Results are unavailable due to the similarities between the compounds' structures preventing any effective NMR analysis. Additionally, exchange effects between oleic acid molecules prevented viewing of <sup>1</sup>H NMR spectra.

Future research will focus on comparing the permeation of lithium oleate with chemicals of a different structure such as methyl oleate or corn oil. Due to lithium oleate's high polarity, we expect it to diffuse slower across the nonpolar PDMS membrane.

## Conclusion

It was demonstrated that PDMS membranes could serve to separate C18 fatty acids and methyl esters from corn oil. Corn oil permeated slower than oleic acid and methyl oleate through the membrane likely due to its larger size hindering it from passing through the membrane cavities. Polarity of the component may influence permeation rate due to nonpolar components interacting better with the hydrophobic PDMS.

## Future Works

Investigating the effect of solvent on the permeation of various organic compounds through PDMS or other membranes. Possible solvents include methanol, ethanol, DMSO, and DCM. Possible membranes include cellulose acetate.

## Acknowledgements

Thank you to Saurav Katuwal, Keshin Huang, Jett Tjaden, and Professor Bowden for your valuable support throughout this program and for inspiring my learning in chemistry.

## References

- (1) Boukid, F.; Rosentrater, K. A. Edible Corn Oil: A Holistic Exploration from Processing to Market Dynamics. *European Journal of Lipid Science and Technology* 2024, 126 (7). <https://doi.org/10.1002/elt.202400022>.
- (2) Lv, E.; Ding, S.; Lu, J.; Yi, W.; Ding, J. Separation and Purification of Fatty Acids by Membrane Technology: A Critical Review. *International journal of chemical reactor engineering* 2020, 18 (9). <https://doi.org/10.1515/ijcre-2019-0224>.
- (3) Ranasinghe Arachchige, N. P. R.; Xiong, N. W.; Bowden, N. B. Separation of C18 Fatty Acid Esters and Fatty Acids Derived from Vegetable Oils Using Nanometer-Sized Covalent Frameworks Incorporated in Polyepoxy Membranes. *ACS Applied Nano Materials* 2023, 6 (8), 6715–6725. <https://doi.org/10.1021/acsnm.3c00442>.
- (4) Gilmer, C.; Zvokel, C.; Vick, A.; Bowden, N. B. Separation of Saturated Fatty Acids and Fatty Acid Methyl Esters with Epoxy Nanofiltration Membranes. *RSC Advances* 2017, 7 (8), 55626–55632. <https://doi.org/10.1039/c7ra11223h>.
- (5) Miranda, I.; Souza, A.; Sousa, P.; Ribeiro, J.; Castanheira, E. M. S.; Lima, R.; Minas, G. Properties and Applications of PDMS for Biomedical Engineering: A Review. *J. Funct. Biomater.* 2022, 13, 2. <https://doi.org/10.3390/jfb13010002>.
- (6) Ferranti, P. *Sustainable Food Science*; Elsevier, 2023.



# Laser-Assisted Synthesis from Ore Reduction (LASOR) for Additive Manufacturing with Hydrogen as a Reducing Agent

Sophie Hart<sup>1</sup>, Mohammad Mohammadzadeh-Sanandaji<sup>2</sup>, Sazid Rahmate-Sobhan<sup>2</sup>, Rahat Mollick<sup>2</sup>, Hongtao Ding PhD<sup>2</sup>

Francis Parker School, San Diego, CA<sup>1</sup>; Department of Mechanical Engineering, University of Iowa, Iowa City, IA<sup>2</sup>

## Introduction

### Background

- 7-8% of the world's carbon dioxide emissions are attributed to the reduction and production process of steel and iron (Raabe)
- Hydrogen has been utilized as a reducing agent in various studies, yielding water vapor as the primary reduction byproduct (Kim)
- The main thermal source of these studies have been large blast furnaces which are lower in temperature, thus slowing down the process
- Many factors such as porosity, temperature, and external obstructions can make each reaction different, enhancing the complexity of the reaction
- Additive Manufacturing (AM), or metal 3D printing, requires high-purity metallic powders as feedstock to ensure reliability
- In-situ resource utilization (ISRU) systems on the Moon and Mars have confirmed the presence of iron ores, indicating potential for localized manufacturing (Cheng)
- The process explored in this work is currently protected under U.S. Patent No. 63/563,157, filed through University of Iowa



- Green Steel Manufacturing (GSM) is an emerging development; both the U.S. and EU have invested billions of dollars in GSM companies since 2024

## Purpose

### Research Question

How can hydrogen-based reduction of iron ores be optimized with laser and used for additive manufacturing for in-situ resource utilization systems?

### Objectives

- Develop a method to optimize hydrogen-based reduction of iron ores by controlling parameters of feedstock, temperature, hydrogen flow
- Using a CW Laser, iron oxide powder, a pressurized gas chamber with hydrogen (and nitrogen), we test and analyze the reduction process of the iron ore

## Methods

### Preparing Samples

- Iron oxide powder was manually packed into pre-fabricated cylindrical molds with a diameter of ~10mm and a height of ~7mm
- Laser was programmed using Laser Desk to perform 4 passes, each 30mm in length

### Performing the Hydrogen-Based Reduction

- Chamber is initially pressurized with hydrogen gas ( $\text{H}_2$ ) to 60-80 PSI; in future trials, nitrogen gas ( $\text{N}_2$ ) is added to aid in removing excess hydrogen
- Laser is activated along the programmed path, with power levels varied across samples
- Because of the high temperature of the laser, the iron powder melts and quickly forms into a solid iron ore pellet

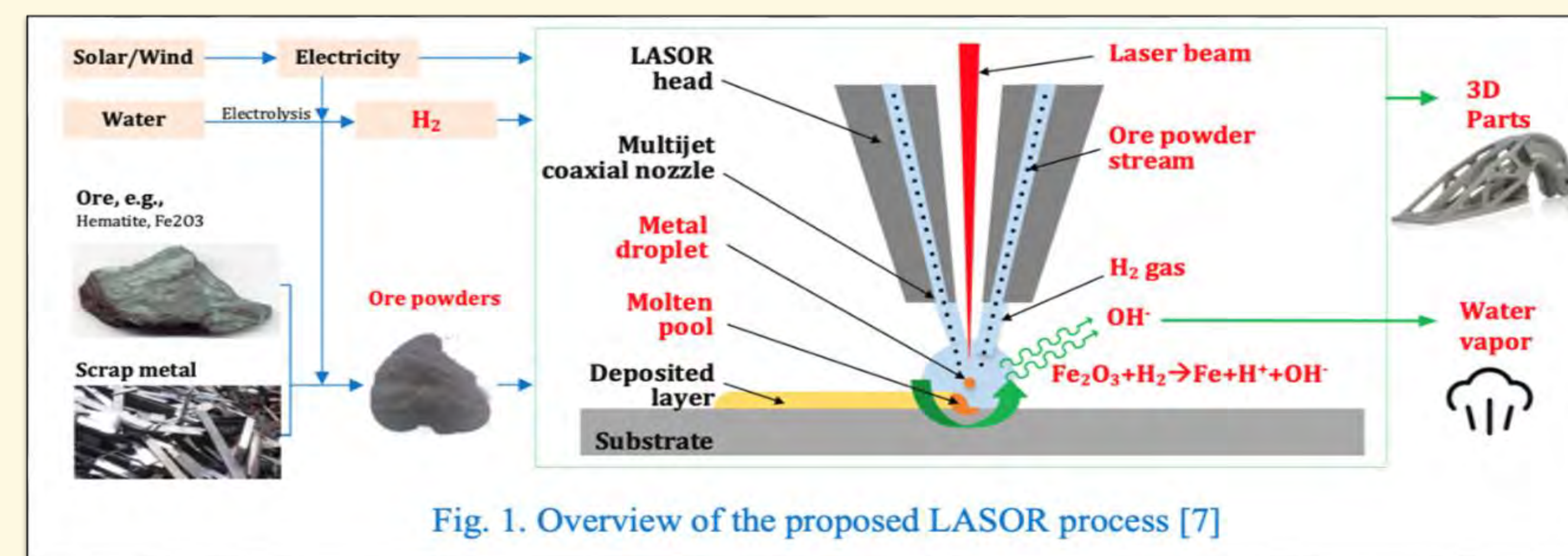
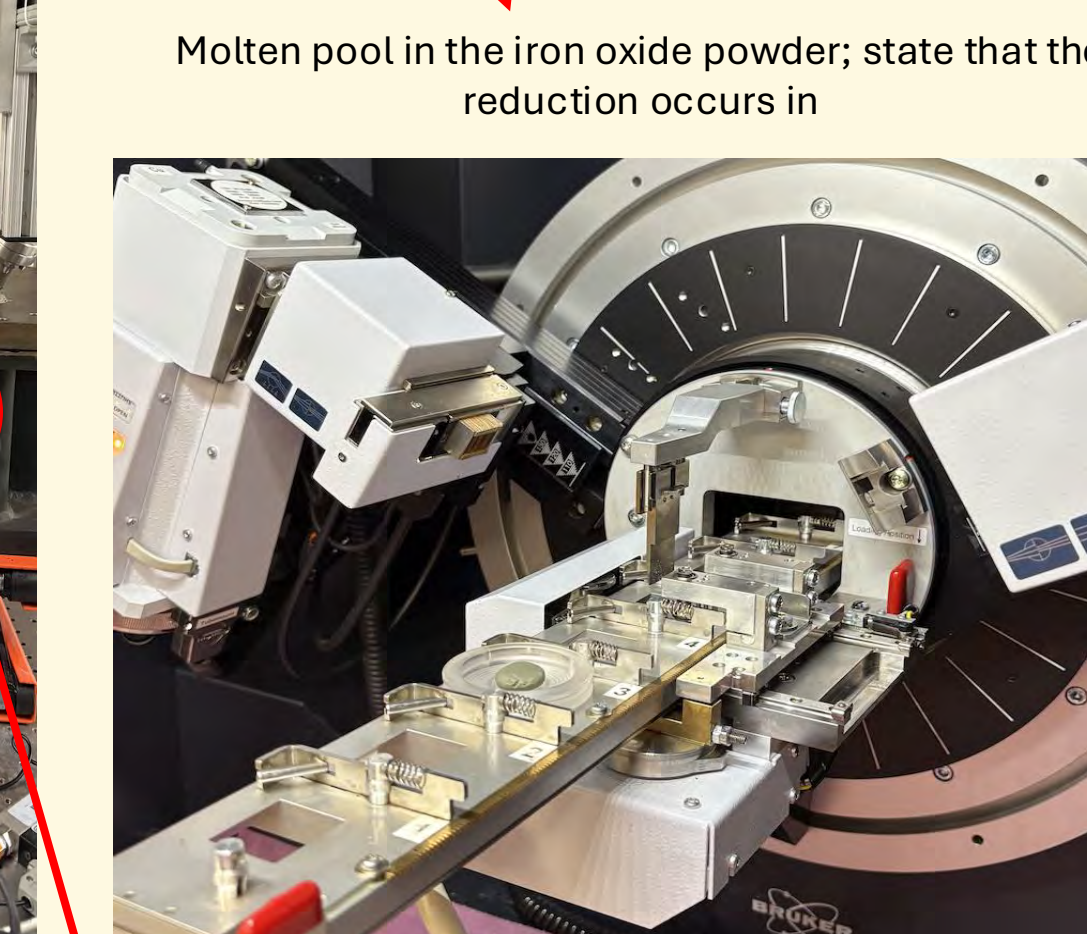
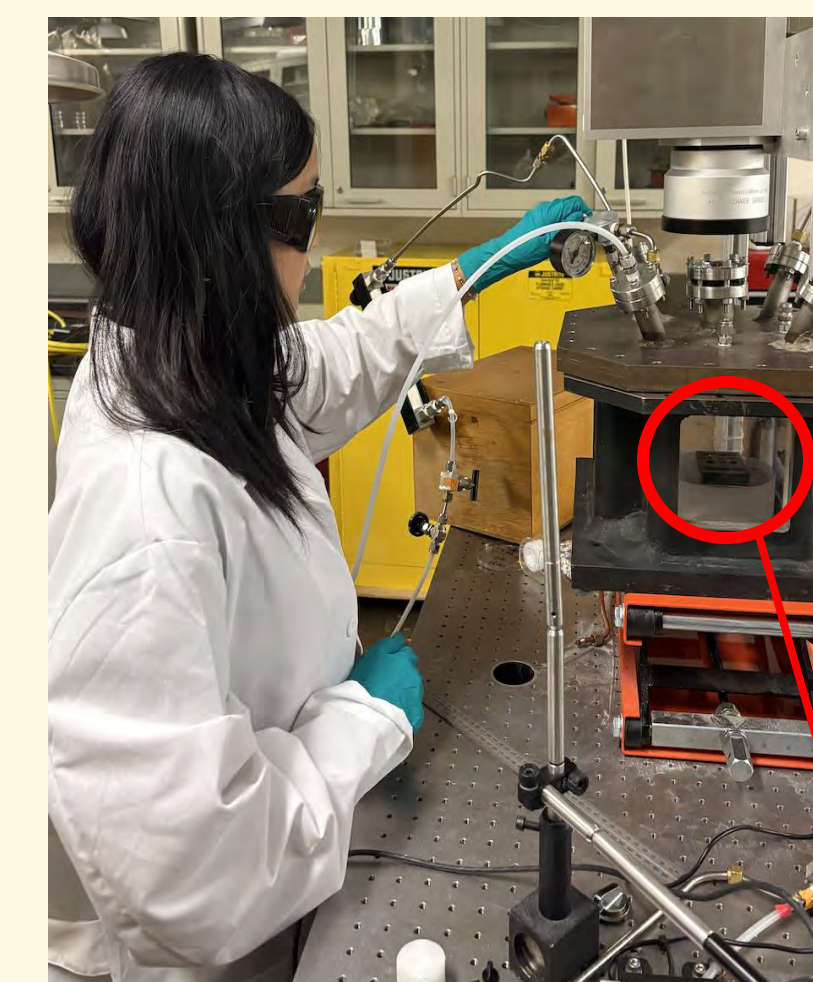


Fig. 1. Overview of the proposed LASOR process [7]

### Analyzing the Reduced Sample

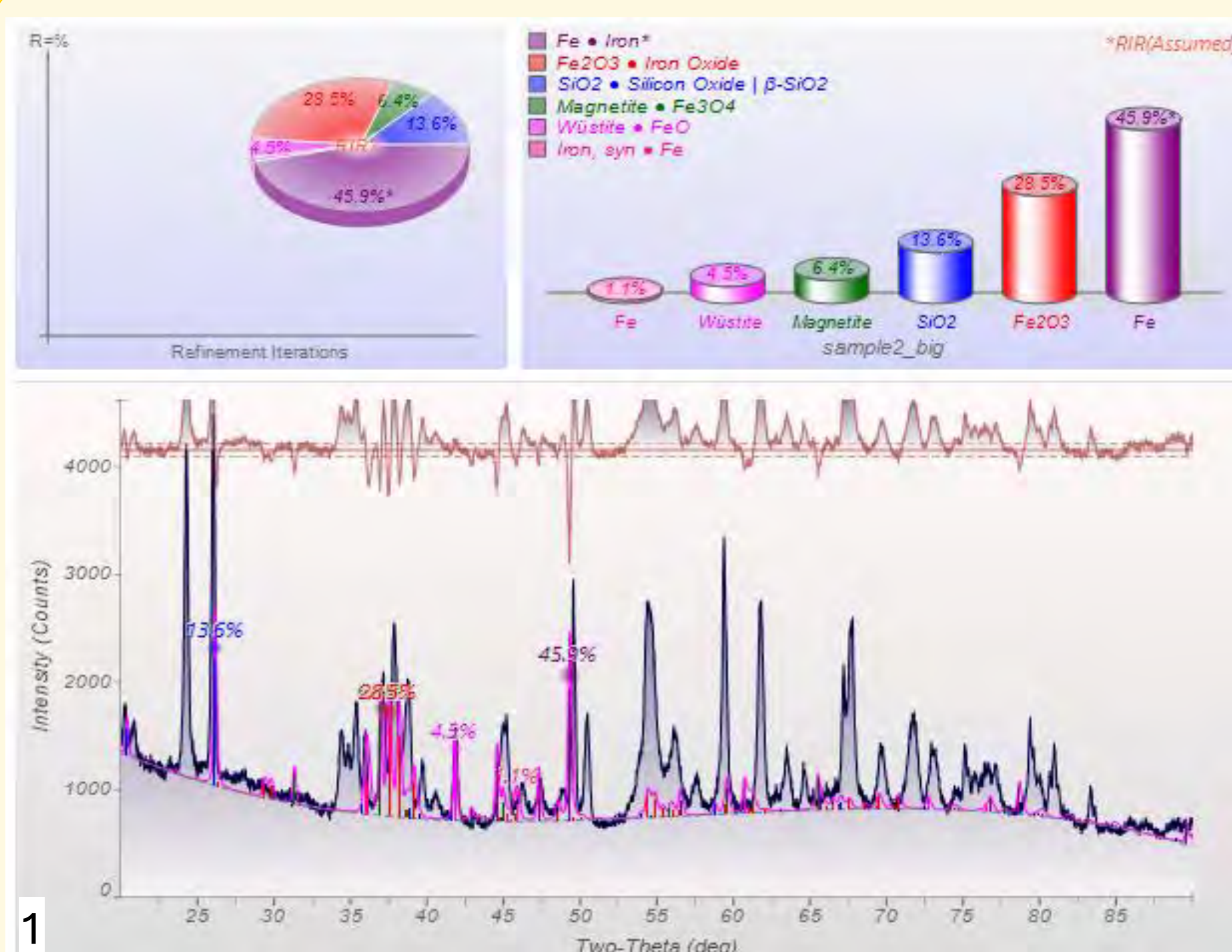
- The samples' reduction efficiency were evaluated using X-Ray Diffraction (XRD)
- The reduced sample, solidified into a pellet, is mounted on a clay base for scanning. The XRD scans over a  $2\theta$  range of 20-90 degrees
- Peaks of the graphs produced by XRD were produced and matched against International Center for Diffraction Data to identify the composition of the compound
- Energy-Dispersive X-Ray Spectroscopy (EDS) images were taken to identify and quantify the elements in the reduced compound



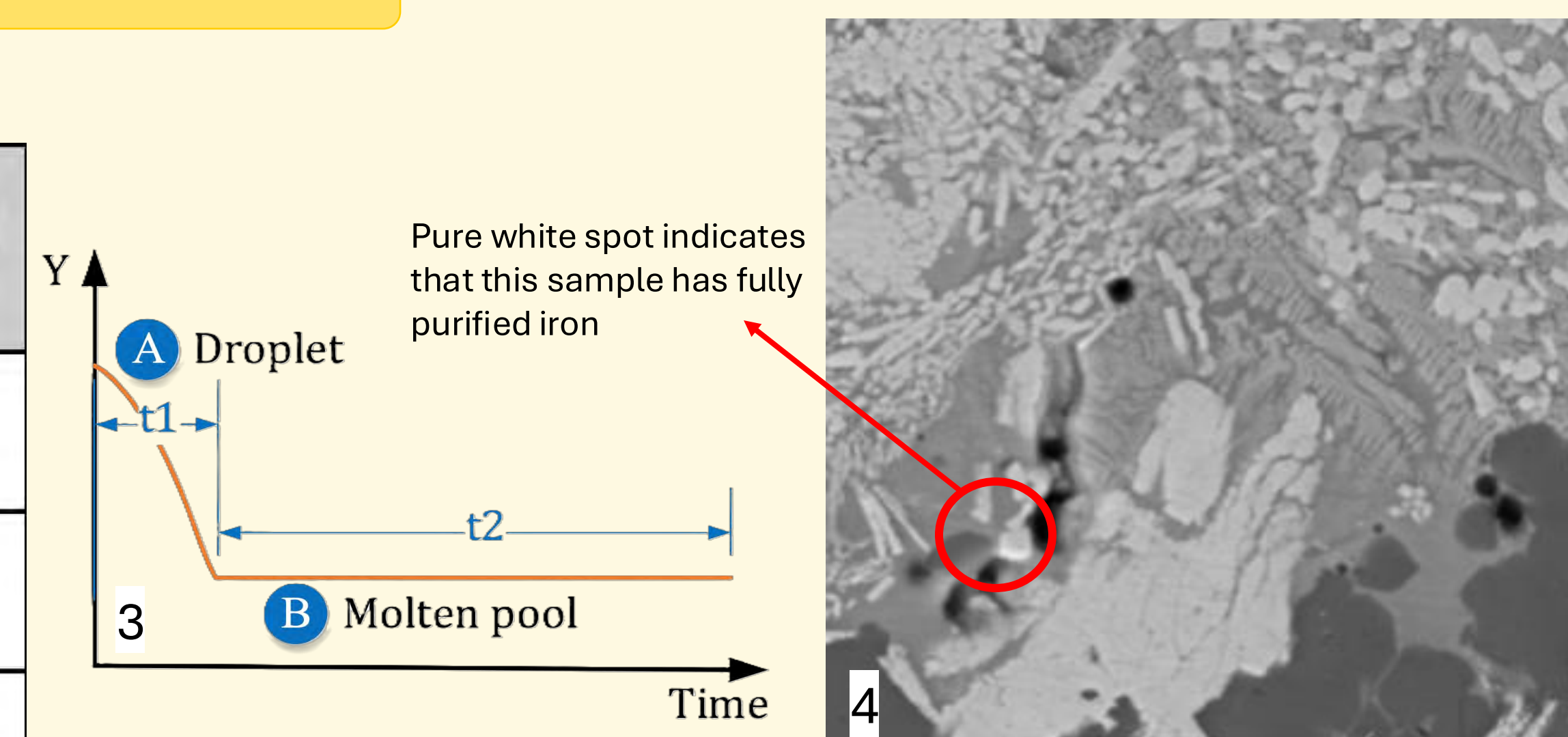
Pressurized chamber with the sample in the mold



## Results



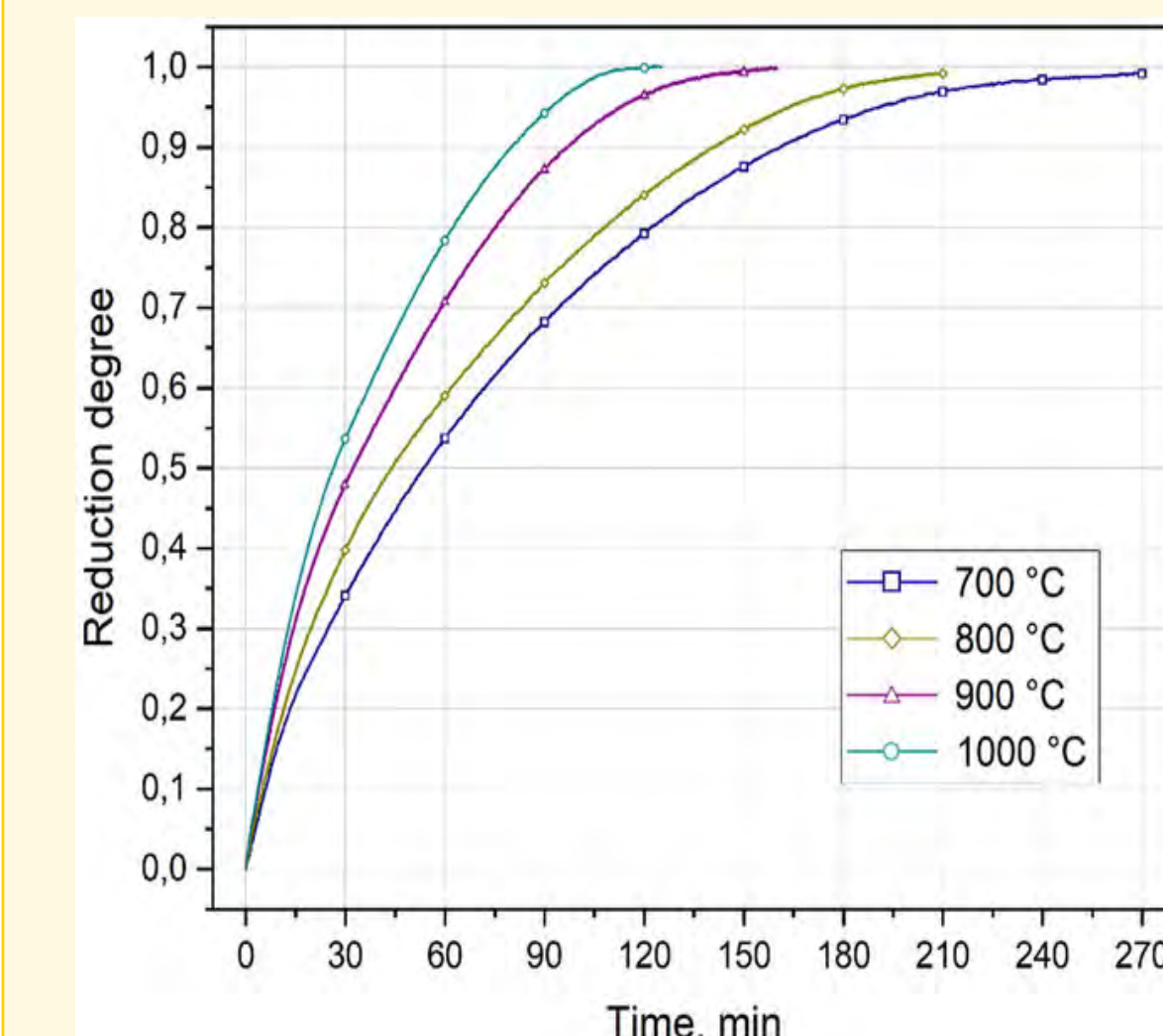
Sample	Laser Power (Watts)	Hydrogen Pressure (PSI)	Time	Size (Big or Small)	Reduction Efficiency
sample 1-s	20	50	3	small	12%
sample 2-s	20	60	5	small	12.6%
sample 3-s	25	60	5	small	42.43%
sample 1-b	25	40	5	big	39.2%
sample 2 2-b	25	40	5	big	39.52%



- Graph from the XRD analyzing the composition of the reduced ore (significant results showing ~46% pure Fe)
- Results and parameters from tests of other samples
- Graph of iron ore pellet over time; turning from a solid pellet to a molten pool
- EDS image zoomed in 5000x of the reduced ore; the lighter the shade, the more purified that spot is (white is fully purified iron)

## Conclusions & Future Research

- Although the amount of pure iron (Fe) varied between samples, XRD analysis confirmed the presence of Fe in all samples, validating the feasibility of LASOR
- Formation of  $\text{FeO}(\text{OH})$  was observed in most samples, likely due to residual hydrogen; this may be mitigated by introducing nitrogen gas during the reduction
- Large samples produced more erratic XRD graphs, so smaller samples were used to obtain clearer, more reliable data
- XRD data also showed that there was more Silicon (Si) in the feedstock than reported which affected the reduction and purity of the end material
- The relationship between temperature and reduction rate followed a known exponential trend consistent with established models
- Validates use of laser was chosen as a thermal source; laser better concentrates and focuses the heat while allowing for a greater temperature, which optimizes the reaction



- Optimization efforts focusing on adjusting parameters such as laser power, sample size, and the controlled introduction of nitrogen gas to produce more consistent and higher-purity iron
- For future samples, grinding the reduced pellets back into powder prior to XRD analysis may yield cleaner data because it would improve the X-ray penetration
- Once the reduction is optimized, future work could explore the use of the reduced iron ore powders in the context of additive manufacturing and evaluating the quality of manufactured parts

## Acknowledgements

Thank you to SSTP and all of my mentors in the Laser Materials Processing Lab: Dr. Ding, Mohammad, Sazid, and Rahat. I am so grateful for all of your support and guidance, and I have learned so much from all of you!

## References

- Cheng, Shanshan, et al. "Advances in In-Situ Resources Utilization for Extraterrestrial Construction." *Advances in Space Research*, vol. 74, no. 7, 18 June 2024, www.sciencedirect.com/science/article/pii/S0273117724005891, https://doi.org/10.1016/j.asr.2024.06.029
- Ding, H., Mohammadzadeh Sanandaji, M., Molick, R., Ratner, A., "Laser-Assisted Synthesis from Ore Reduction (LASOR) for Additive Manufacturing with Hydrogen as Reducing Agent", Invention Disclosure filed on Feb. 6, 2024; U.S. Provisional Patent Application No. 63/563,157 filed on March 8, 2024.
- Kim, Se-Ho, et al. "Influence of Microstructure and Atomic-Scale Chemistry on the Direct Reduction of Iron Ore with Hydrogen at 700°C." *Acta Materialia*, vol. 212, June 2021, p. 116933, https://doi.org/10.1016/j.actamat.2021.116933
- Raabe, Dierk. "Green Steel." *Www.dierk-raabe.com*, www.dierk-raabe.com/the-green-steel-deal/





# Benchmarking Feature Extractors, Machine Learning Models, and Large Language Models for Anxiety Detection in Text Data



Yi-Nuo Hsiao, Tippie College of Business, University of Iowa, Iowa City, IA

## Introduction

**Purpose:** Evaluate existing methods used to detect anxiety on social media → find models that are suitable for anxiety detection so that people can optimize these models later on and ultimately improve mental health monitoring on digital platforms.

**Models to Implement through Python:**

**Feature extractors** are algorithms or models that convert raw data (e.g. text, images, audio) into numerical representations (e.g. vectors) that computers can understand

**Machine learning (ML) models** are algorithms that learn patterns from past data, build functions for such patterns (in a “training” process), and use the functions to make predictions

**Large language models (LLMs)** are a subset of ML models that use deep neural networks as part of the “training” process

**Stacking** is a ML strategy where the predictions of numerous base models are used to train a meta-model (that combines and weighs base models based on their strengths) to make the final prediction

## Methods

**Data collection:** scraped (extracted) 8000 posts from r/anxiety using Reddit API (Chen et al., 2023)

**Data cleaning & labeling:** Three human annotators labeled each post as “1” (anxiety present) or “0” (anxiety absent) using a standardized annotation guideline (Shen & Rudzicz, 2017)

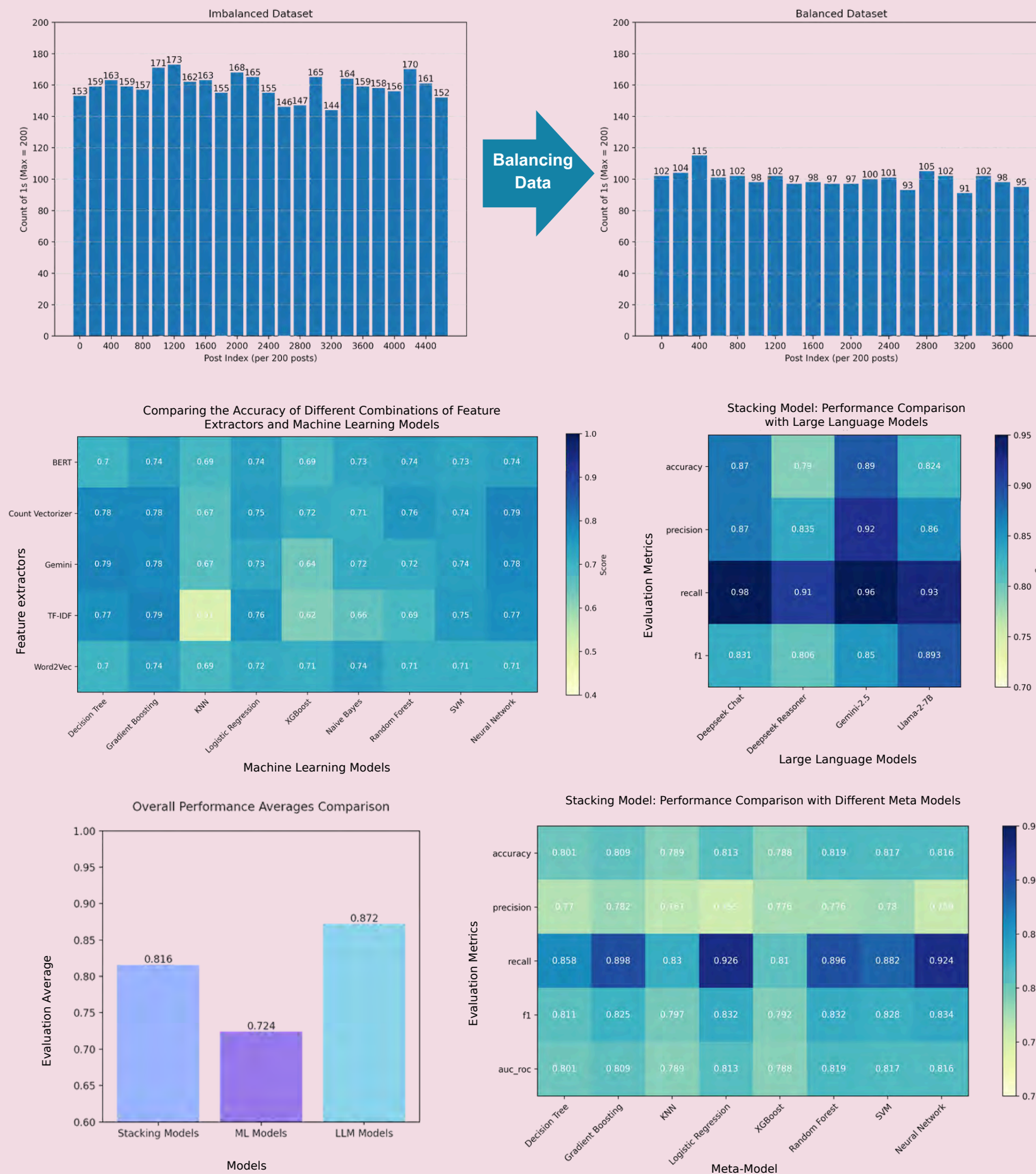
**Labeling Validation:** Calculated the Kappa score (0.764) to ensure inter-rater reliability; used the majority vote to determine the final labels (Owen et al., 2020)

**Handle Data Imbalance:** truncate excess data of 1 class by replacing them with data of the other class

**Model Implementation for ML models:** Split data into training & testing subsets; apply feature extractors on both subsets; feed the vectors into ML models; test the accuracy of each model

**Model Implementation for LLMs:** Loop through every dataset and let LLMs classify each post; calculate the accuracy of each model

## Results



## Conclusion

**Feature Extractor ranking:** Count Vectorizer, Gemini, TF-IDF (does not work well with KNN)

**ML ranking:** Gradient Boosting, Neural Network, Decision Tree

**LLM ranking:** Gemini, Deepseek Chat, Llama-2-7B

**Optimal meta-model for stacking:** outperforms single base models; similar results for different meta models; Random Forest, SVM, Neural Network

**Overall:** LLMs take a long time to run, but they are the most accurate. Meta-models are also a good choice, and ML models are the least accurate.

## Future Directions

- Optimizing embedding process by assigning weights to certain dimensions that impact the classification decision
- Optimizing LLMs by dissecting its logical reasoning process / integrating techniques like SFT to the models

## References and Acknowledgements

Owen, D., Camacho-Collados, J., & Espinosa Anke, L. (2020). Towards preemptive detection of depression and anxiety in Twitter. In *Proceedings of the Fifth Social Media Mining for Health Applications Workshop & Shared Task*, 82–89. <https://doi.org/10.18653/v1/w19-32>

Shen, J. H., & Rudzicz, F. (2017). Detecting anxiety through Reddit. In *Proceedings of the Fourth Workshop on Computational Linguistics and Clinical Psychology — From Linguistic Signal to Clinical Reality*, 58–65.

Chen, L. L., Wilson, S. R., Lohmann, S., & Negraia, D. V. (2023). What are you anxious about? Examining subjects of anxiety during the COVID-19 pandemic. In *Proceedings of the Seventeenth International AAAI Conference on Web and Social Media*, 137–148. <https://doi.org/10.36190/2023.11>

Special thanks to Sophie Zhang and Angelina Wang for labeling the Reddit dataset, Kelvin and Leo for providing valuable guidance throughout my research process, and SSTP and Belin-Blank Center for providing me with this incredible research opportunity.



# Investigating Ginkgolide A as a potential protectant against oxidative stress in BV2 microglia

Alice Hu<sup>1</sup>, Cassidy Kline<sup>2,3</sup>, Benjamin B Borrman<sup>2</sup>, Susan Q Shen MD PhD<sup>2</sup>

<sup>1</sup>Branksome Hall, Toronto, Canada; <sup>2</sup>Department of Psychiatry, Carver College of Medicine, University of Iowa,

<sup>3</sup>Human Toxicology Program, University of Iowa

# IOWA

Carver College  
of Medicine

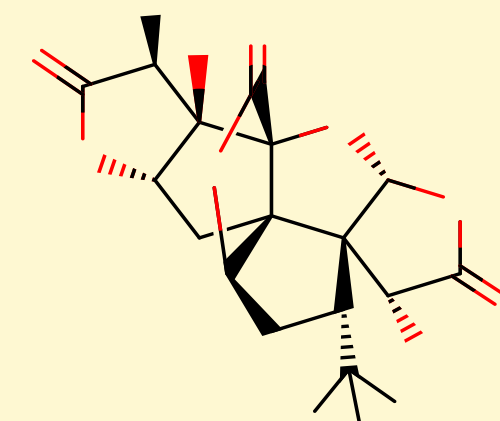
## Introduction

### Oxidative Stress

- An imbalance between reactive oxygen species and antioxidant defenses
- Involved in the pathophysiology of a large range of neuropsychiatric disorders

### Ginkgolide A (GA)

- Natural product derived from Ginkgo Biloba tree
- Known anti-inflammatory effects on microglia
- Tested in clinical trials for stroke, benefit unclear



### BV2 Cells

- Microglia are immune cells in the brain that respond to stressors
- BV2 is a widely used immortalized mouse microglial cell line amenable to scalable assays

### Hydrogen Peroxide (H<sub>2</sub>O<sub>2</sub>)

- Reactive oxygen species that induces oxidative stress
- Naturally found in human body; low levels are necessary for normal physiological function while high levels are toxic

### Significance

- Case study of a natural product with antioxidant effects that are incompletely understood and could be optimized for clinical applications

## Research Objective

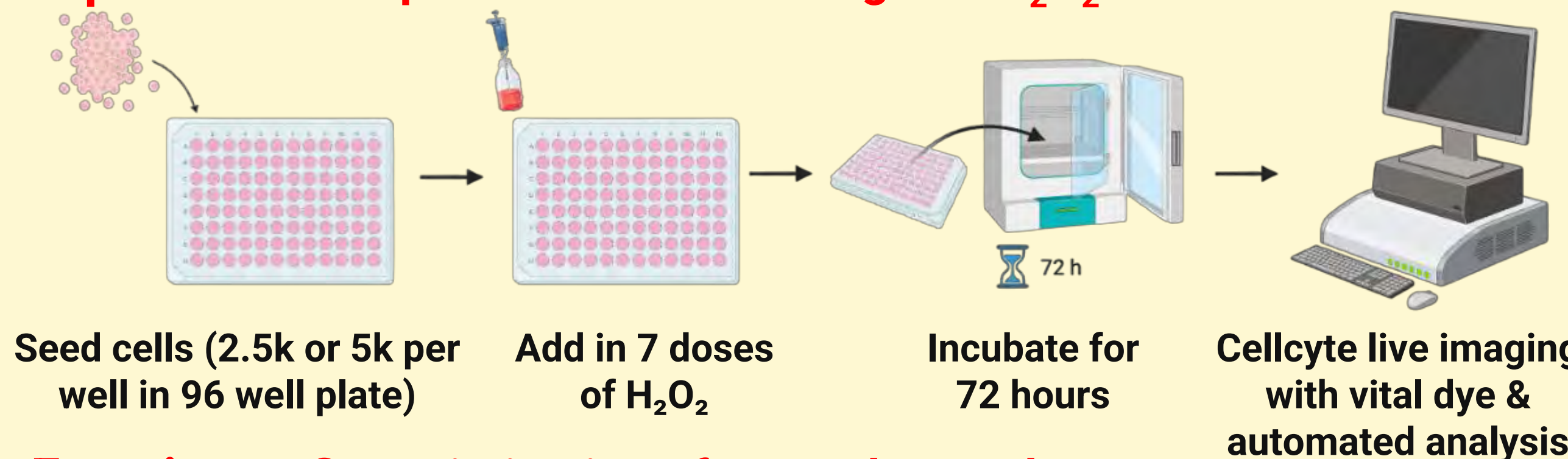
Explore the antioxidant properties of Ginkgolide A by examining how it influences cell viability under oxidative stress caused by hydrogen peroxide (H<sub>2</sub>O<sub>2</sub>) in BV2 cells.

### Hypothesis

Ginkgolide A will protect BV2 cells from H<sub>2</sub>O<sub>2</sub>-induced oxidative stress

## Methods

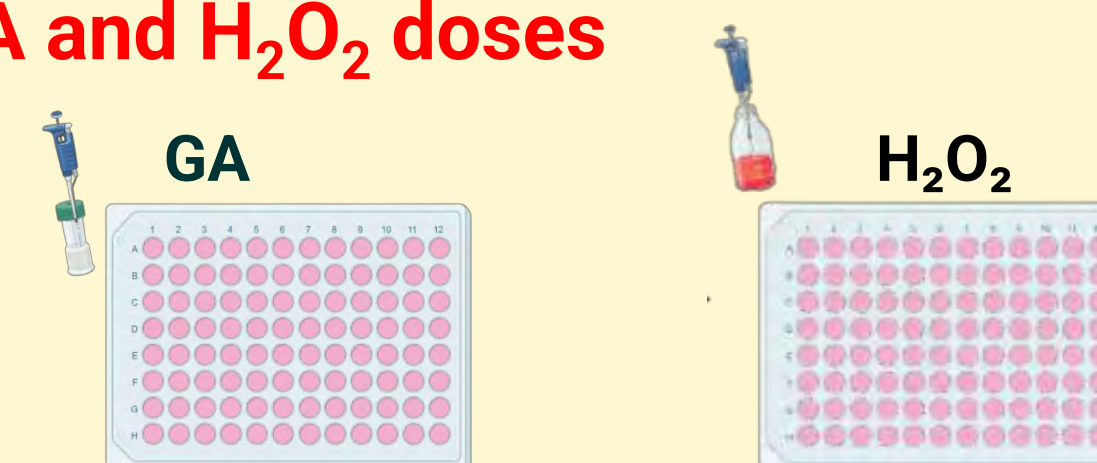
### Experiment 1: Optimization of seeding and H<sub>2</sub>O<sub>2</sub> doses



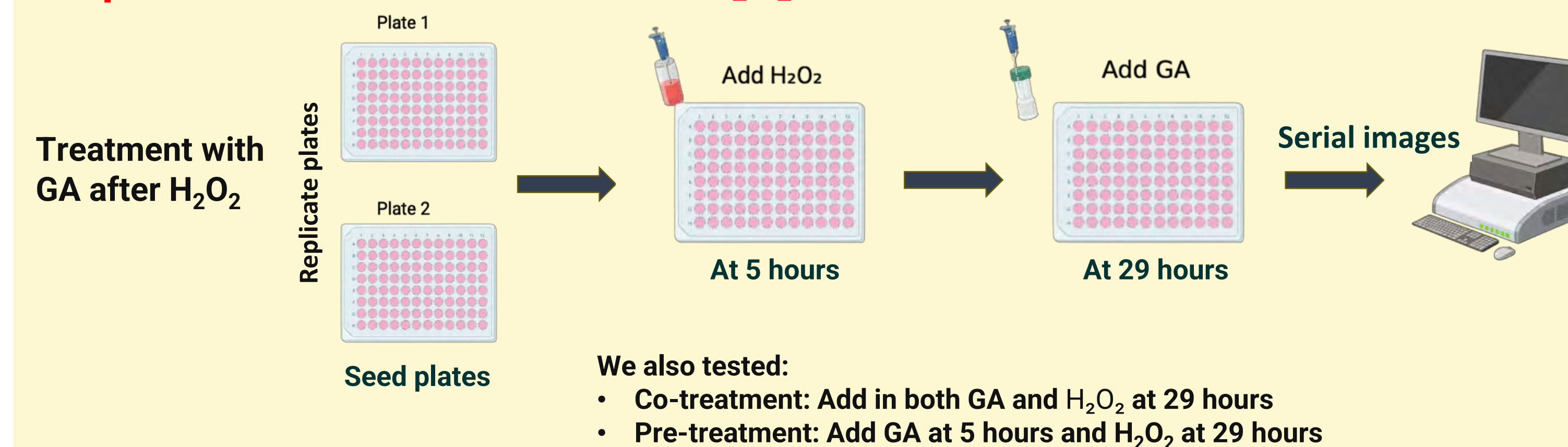
### Experiment 2: Optimization of GA and H<sub>2</sub>O<sub>2</sub> doses

Same procedure but add in 4 different doses of GA and H<sub>2</sub>O<sub>2</sub> into separate plates

Seeding density: 3k/well



### Experiment 3: Combinatorial GA+H<sub>2</sub>O<sub>2</sub> treatment



We also tested:

- Co-treatment: Add in both GA and H<sub>2</sub>O<sub>2</sub> at 29 hours
- Pre-treatment: Add GA at 5 hours and H<sub>2</sub>O<sub>2</sub> at 29 hours

## Results

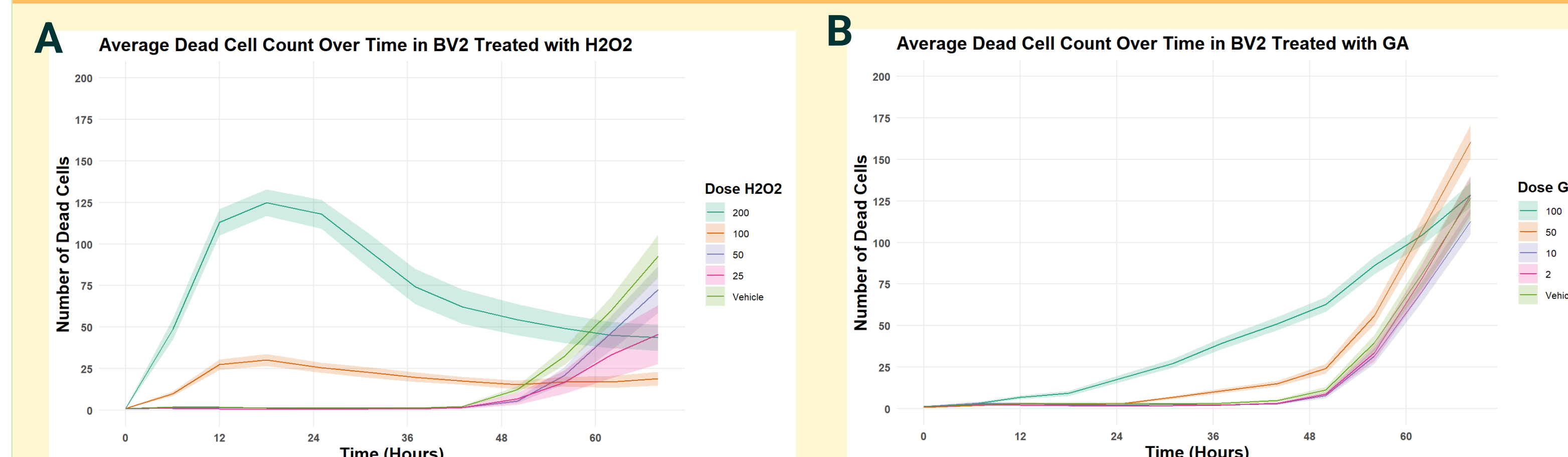


**Figure 1. Death curve results from Experiment 2.** Dead cells were quantified with Cytotox dye (fluorescent green dye) (100nM). Plates were scanned at time 0 (baseline) immediately before compound addition and then every 6 hours. Vehicle was DMSO (for GA) and water (for H<sub>2</sub>O<sub>2</sub>). Final 0.1% DMSO in all wells. (A) H<sub>2</sub>O<sub>2</sub> at 25, 50, 100, and 200μM were tested. (B) GA 2, 10, 50, and 100μM were tested. Data were averaged across wells. Error bars +/- SEM.

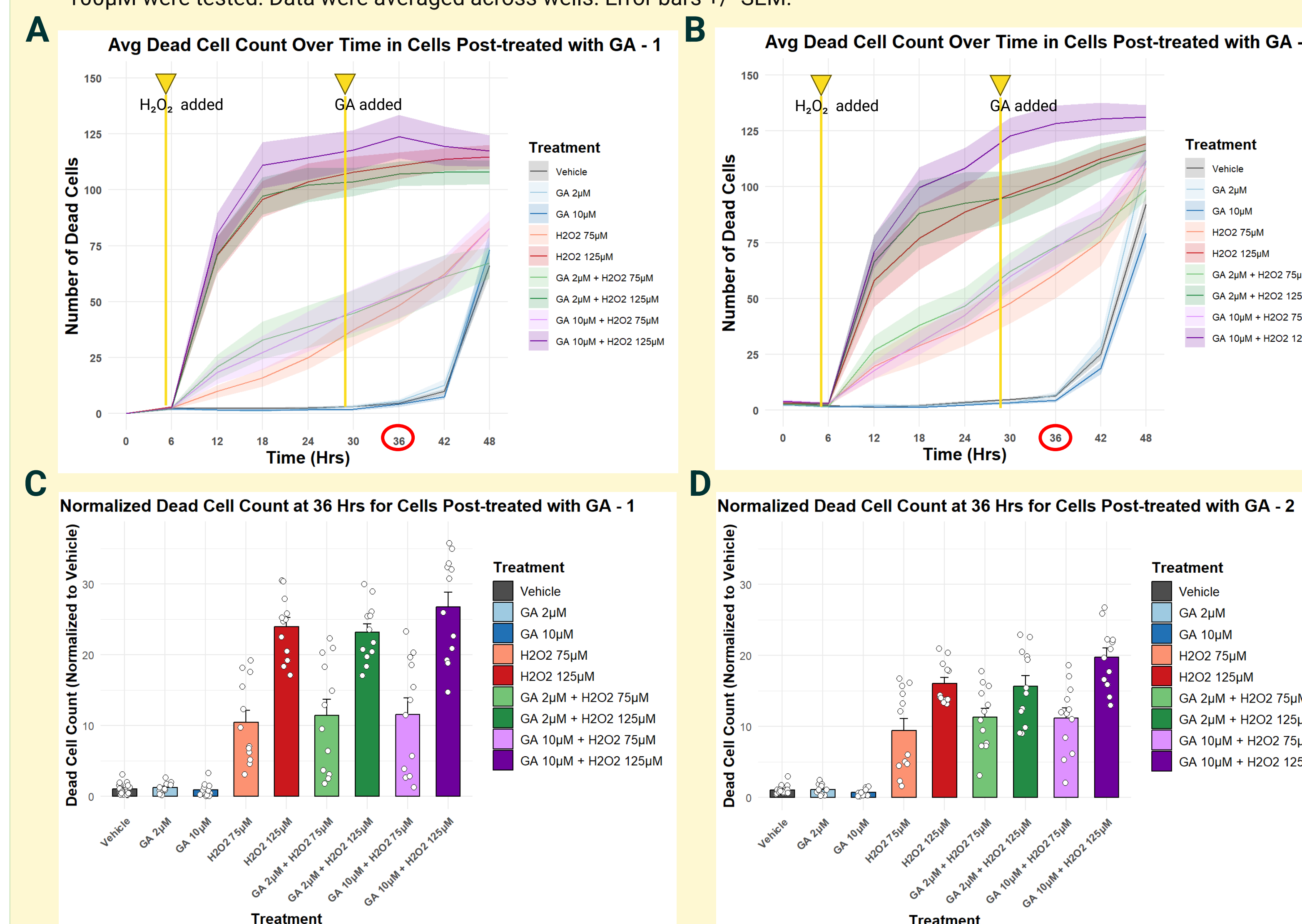


**Figure 2. Post-treatment results.** (A, B) Replicate plates 1 and 2 were imaged every 6 hours with Cytox green dye (100nM) as in Figure 1. The 5 hr timepoint (H<sub>2</sub>O<sub>2</sub> addition) and 29 hr timepoint (GA addition) are noted with yellow lines. Vehicle was DMSO (for GA) and water (for H<sub>2</sub>O<sub>2</sub>). Final 0.1% DMSO in all wells. (C, D) Bar graphs for the 36hr timepoint. Each white dot represents a single well. Error bars +/- SEM.

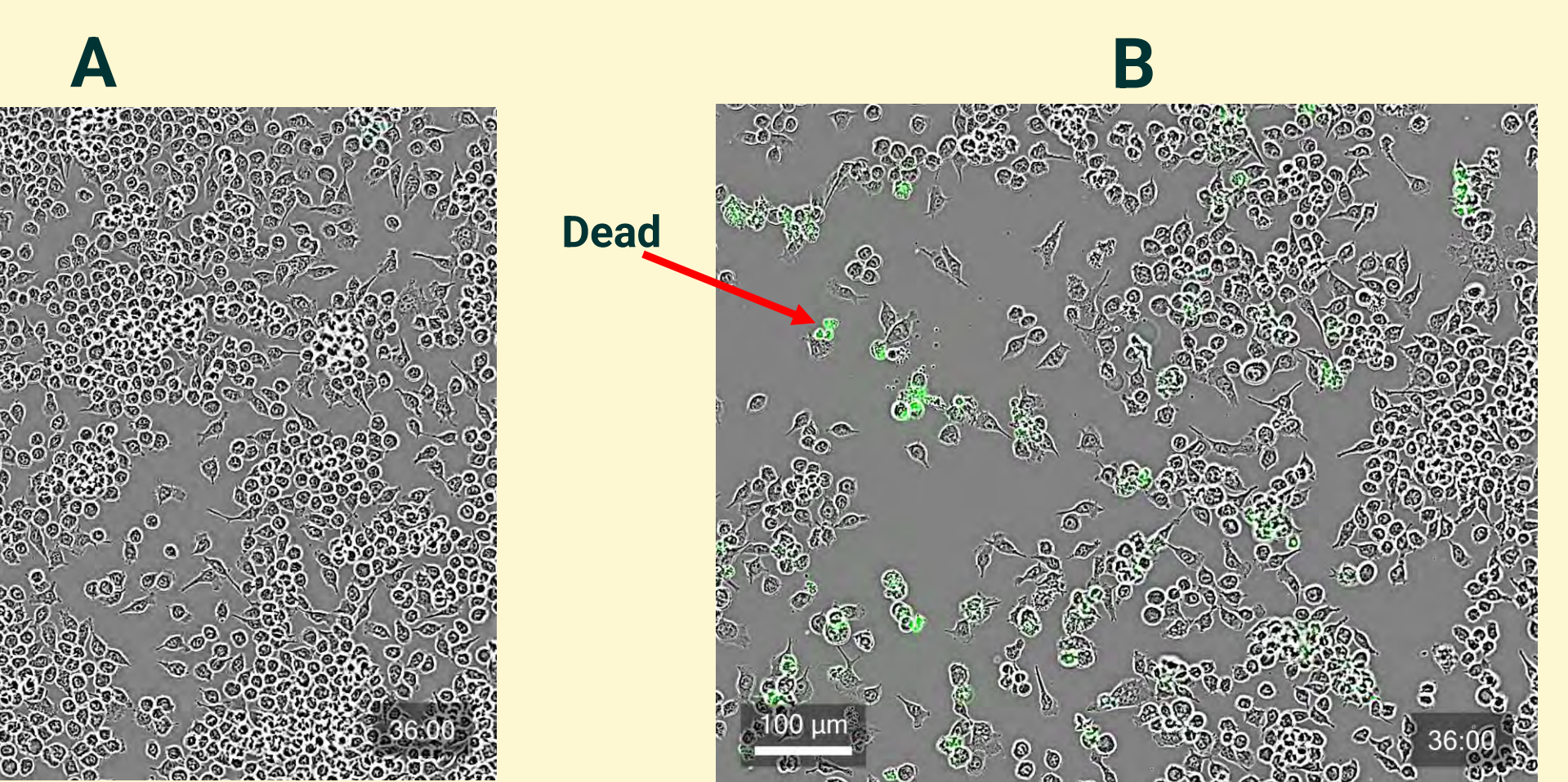


**Figure 3. Representative images at 36 hours.** Brightfield images taken on Cellcyte were overlaid with green channel (Cytotox dye showing dead cells). (A) Vehicle (no drugs added) well. (B) 125μM H<sub>2</sub>O<sub>2</sub>

## Preliminary Results

**No evidence for protective effect of GA against H<sub>2</sub>O<sub>2</sub>-induced oxidative stress in pretreatment, co-treatment, or post-treatment**

- GA 10μM + H<sub>2</sub>O<sub>2</sub> 125μM may cause greater cell death than H<sub>2</sub>O<sub>2</sub> 125μM alone
- Caveat: high confluency of cells at time of 29hr drug addition

## Future Directions

- Repeat experiments with a modified timeline with compound addition at lower confluency
- Count total number of cells with a nuclear dye to calculate % dead cells (vs. # dead cells)
- Investigate the antioxidant properties of Ginkgolide B and C
- Consider other cell types and in vivo testing

## References

- Heo, S., Kim, S., & Kang, D. (2020). The Role of Hydrogen Peroxide and Peroxiredoxins throughout the Cell Cycle. *Antioxidants*, 9(4), 280. <https://doi.org/10.3390/antiox9040280>
- Li, C., Wu, Y., Huang, M.-Y., & Song, X.-J. (2023). Characterization of Inflammatory Signals in BV-2 Microglia in Response to Wnt3a. *Biomedicines*, 11(4), 1121–1121. <https://doi.org/10.3390/biomedicines11041121>
- Pizzino, G., Irrera, N., Cucinotta, M., Pallio, G., Mannino, F., Arcoraci, V., Squadrito, F., Altavilla, D., & Bitto, A. (2017). Oxidative Stress: Harms and Benefits for Human Health. *Oxidative Medicine and Cellular Longevity*, 2017(8416763), 1–13. <https://doi.org/10.1155/2017/8416763>
- PubChem. (2025). *Ginkgolide A*. Nih.gov; PubChem. <https://pubchem.ncbi.nlm.nih.gov/compound/Ginkgolide-A>

## Acknowledgments

We thank the labs of Serena “Banu” Gumusoglu and Michael Dailey for BV2 cells.

Thank you for all the members in the Shen Lab for thorough guidance and support. Thank you Dr. Shen for always providing insightful feedbacks and guiding to build my scientific research skills, as well as advice on career plans. Thank you Benjamin B Borrman for always helping me to get familiar with protocols and lab setups. Special thanks to Cassidy Kline for detailed, thorough and careful guidance throughout the entire project and extra efforts in data analysis. Thanks also to SSTP for offering this wonderful opportunity.



# Short-term dipping method for separation of fatty acids: a study of cellulose acetate, PDMS, and molecularly imprinted polymers

Keshin Huang<sup>1</sup>, Carol Gong<sup>2</sup>, Saurav Katuwal<sup>3</sup>, Jett Tjaden<sup>3</sup>, Ned Bowden<sup>3</sup>

<sup>1</sup>Great Neck North High School, <sup>2</sup>Interlake High School, <sup>3</sup>Department of Chemistry, University of Iowa

# Introduction

## Applications of Oleochemicals

- \$20 billion industry involved in a variety of key sectors, such as food, cosmetics, household products, and biofuels
- Purification of oils into fatty acid components can lead to the invention of new materials and products
- Compared to petroleum and other oils, fatty acids are relatively safe and sustainable
- Fatty acids are notorious for being difficult to separate because of their similar size and structure

## Membrane-based Separation

- Polydimethylsiloxane (PDMS) is a silicon-based, transparent polymer with high elasticity and permeability (1)
- Cellulose acetate is a polar, biodegradable membrane material commonly used in filtration applications (2)
- Molecularly imprinted PDMS contains specific cavities that are molded into the shape of target molecules

## Research Objective

The aim of this research is to determine if PDMS, cellulose acetate, and molecularly-imprinted PDMS membranes can selectively absorb and separate structurally similar fatty acids through a short-term dipping method.

## Results

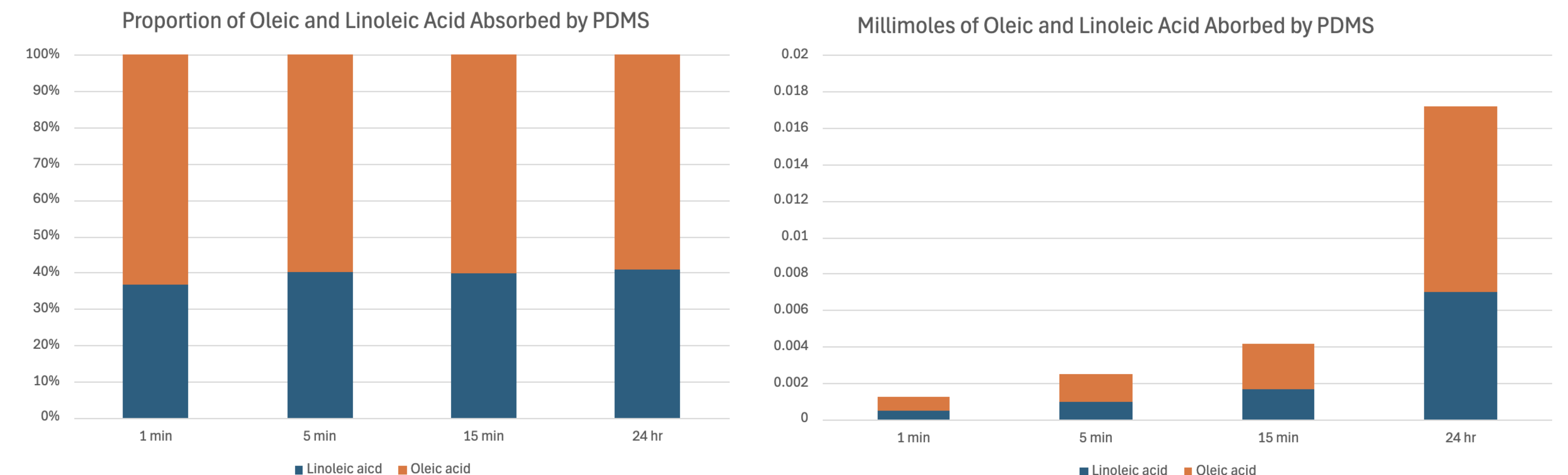
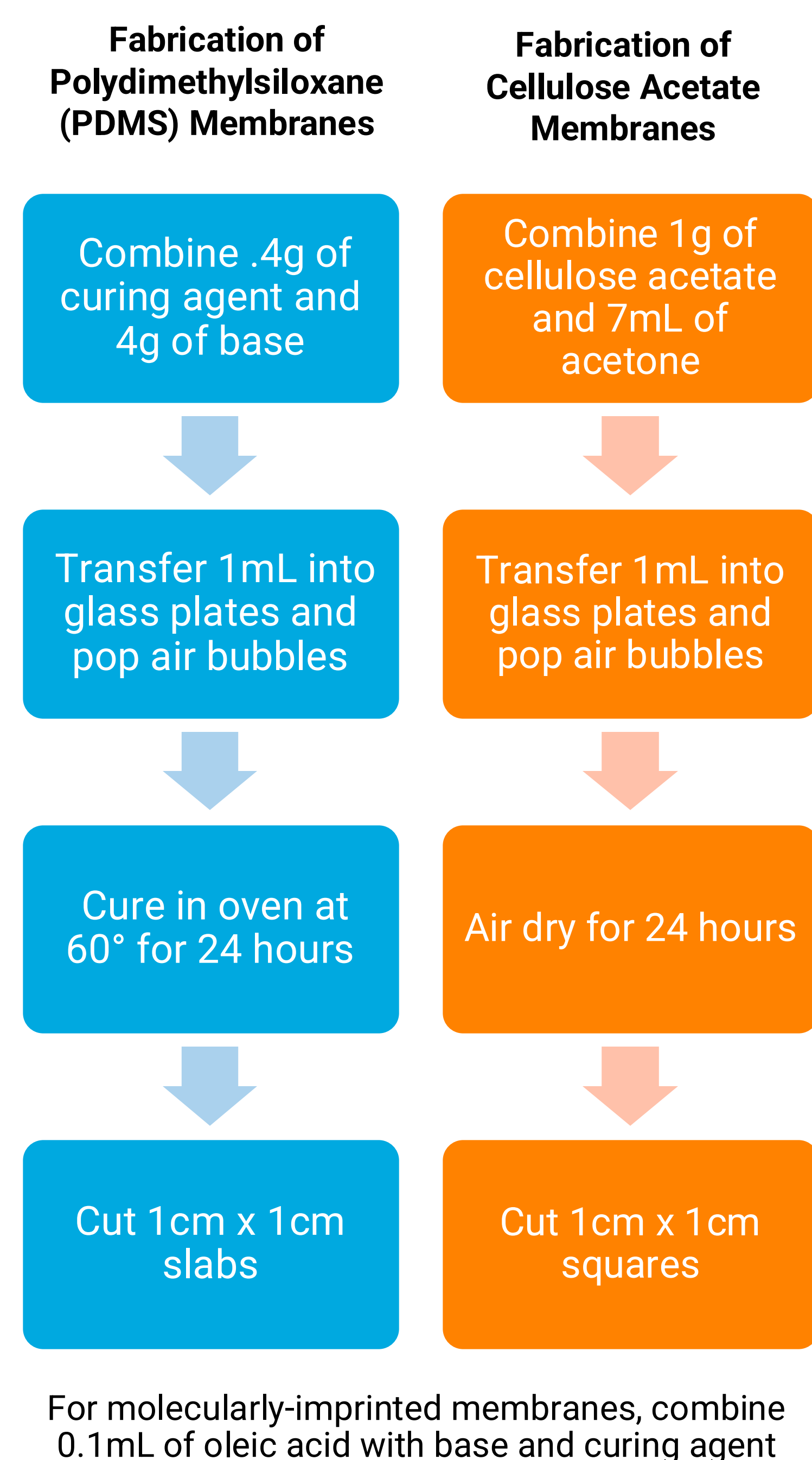


**Figure 1.** Relative proportion of oleic and linoleic acid absorbed by the PDMS membrane over various times

- Under identical conditions, the oleic acid had greater diffusion into the PDMS membrane compared to the linoleic acid
- Across the time intervals, the percentage of oleic acid is approximately 60% and the percentage of linoleic acid is approximately 40%; the rate of diffusion was constant
- For the PDMS membranes, the percentage of fatty acids absorbed is nearly consistent across 1 minute, 5 minutes, 15 minutes, and 24 hours.

**Figure 1.** Millimoles of oleic and linoleic acid absorbed by the PDMS membrane over various times

## Methodology



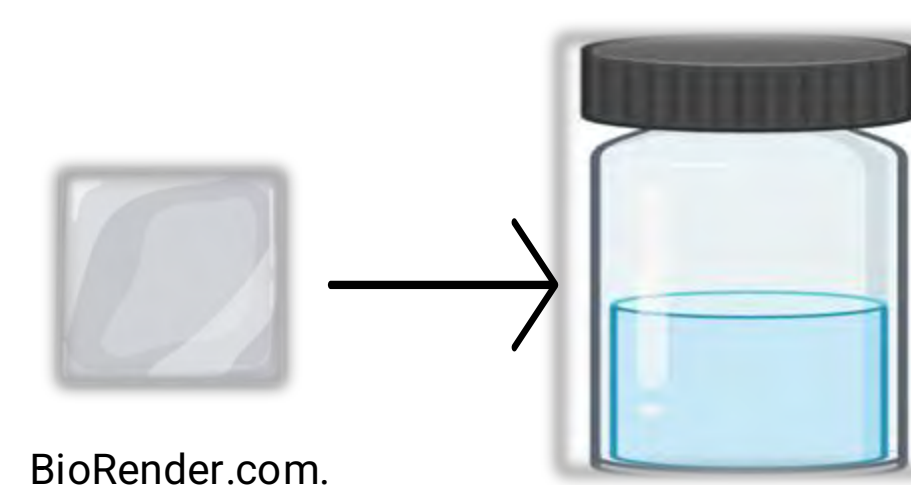
## Membrane Dipping Set-Up

**Dip membrane in fatty acid mixtures for respective times**



BioRender. *Small Glass Vial with Little Fluid [Icon]*; BioRender: Toronto, ON. (accessed July 18, 2025).

### Soak membrane in hexane



BioRender.com  
Hydrogel Film  
Icon (accessed  
July 19, 2025).

Small glass vial (half fluid) icon.  
Reproduced with permission  
from BioRender.com. Accessed  
July 19, 2025.

## Extraction of fatty acids

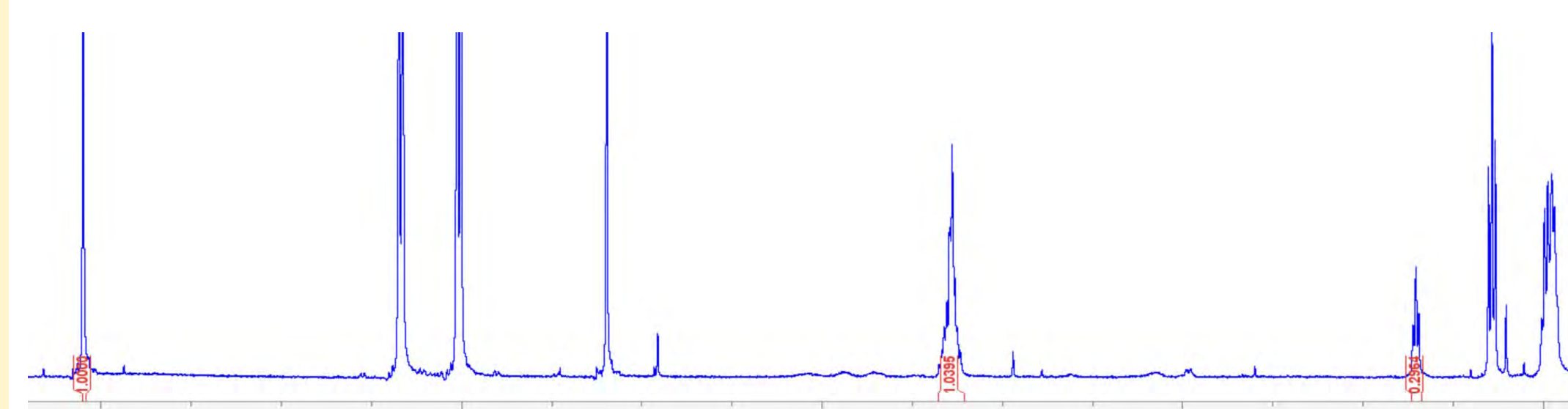


## Oleic Acid



## Linoleic Acid

Prasanta Baishya; Moon Mandal; Pankaj Gogoi; Tarun Maji. Structure of oleic acid, linoleic acid, and linolenic acid. In *Natural Polymer-Based Nanocomposites: A Greener Approach for the Future*, Chapter 5; uploaded Jul 2017; ResearchGate (accessed July 19, 2025)



### NMR of absorbed fatty acids, extracted from PDMS in hexane

## Discussion/Future Works

## Conclusions

- Structural differences between the oleic acid and the linoleic acid likely influenced how easily they were absorbed by the membranes.
- PDMS membrane is non-polar, so it prefers non-polar chemicals
- Linoleic acid is more polar and therefore less compatible with PDMS because it contains exactly one extra double bond
- The proportion of fatty acid remained consistent across time intervals
- This suggests that there is a thermodynamic factor involved rather than a kinetic factor; in other words, the system reaches equilibrium quickly– the concentration of the acids is constant
- The determining factor for the different fatty acid amounts is how compatible the acid is with the membrane, rather than how quickly they diffuse into the membrane

## Future Works

- Experimenting with different densities, thicknesses, and chemical modifications in both PDMS and cellulose acetate to enhance selectivity for specific fatty acids
- Exploring how contact time and temperature affect diffusion and absorption rates of fatty acids into the membranes

## Acknowledgements

Thank you to Dr. Bowden, Saurev, Jett, and Carol for helping me throughout my research experience. Thank you to SSTP for giving me this opportunity. I appreciate all your help and guidance throughout these past couple of weeks.

## References

1. Miranda, I.; Souza, A.; Sousa, P.; Ribeiro, J.; Castanheira, E. M. S.; Lima, R.; Minas, G. Properties and Applications of PDMS for Biomedical Engineering: A Review. *J. Funct. Biomater.* **2021**, *13* (1), 2. <https://doi.org/10.3390/jfb13010002>.
2. Vatanpour, V.; Passagolu, M. E.; Barzegar, H.; Teber, O. O.; Kaya, R.; Bastug, M.; Khataee, A.; Koyuncu, I. *Cellulose acetate in fabrication of polymeric membranes: A review.* *Chemosphere* **2022**, *295*, 133914. <https://doi.org/10.1016/j.chemosphere.2022.133914> [pubmed.ncbi.nlm.nih.gov/search.itu.edu.tr](https://pubmed.ncbi.nlm.nih.gov/search.itu.edu.tr)
3. Author(s). Title. *Journal Name* Year, Volume (Issue), pages. <https://doi.org/...>
3. BioRender Icon – Small Glass Vial  
BioRender. *Small Glass Vial with Little Fluid* [Icon]; BioRender: Toronto, ON. Accessed July 18, 2025.
4. BioRender Icon – Hydrogel Film  
BioRender.com. *Hydrogel Film Icon* [Icon]. Accessed July 19, 2025.
5. BioRender Icon with Permission Statement  
Small glass vial (half fluid) icon. Reproduced with permission from BioRender.com. Accessed July 19, 2025.
6. Figure from Book Chapter on ResearchGate  
Baishya, P.; Mandal, M.; Gogoi, P.; Maji, T. Structure of oleic acid, linoleic acid, and linolenic acid. In *Natural Polymer-Based Nanocomposites: A Greener Approach for the Future*, Chapter 5; Uploaded July 2017; ResearchGate. Accessed July 19, 2025.



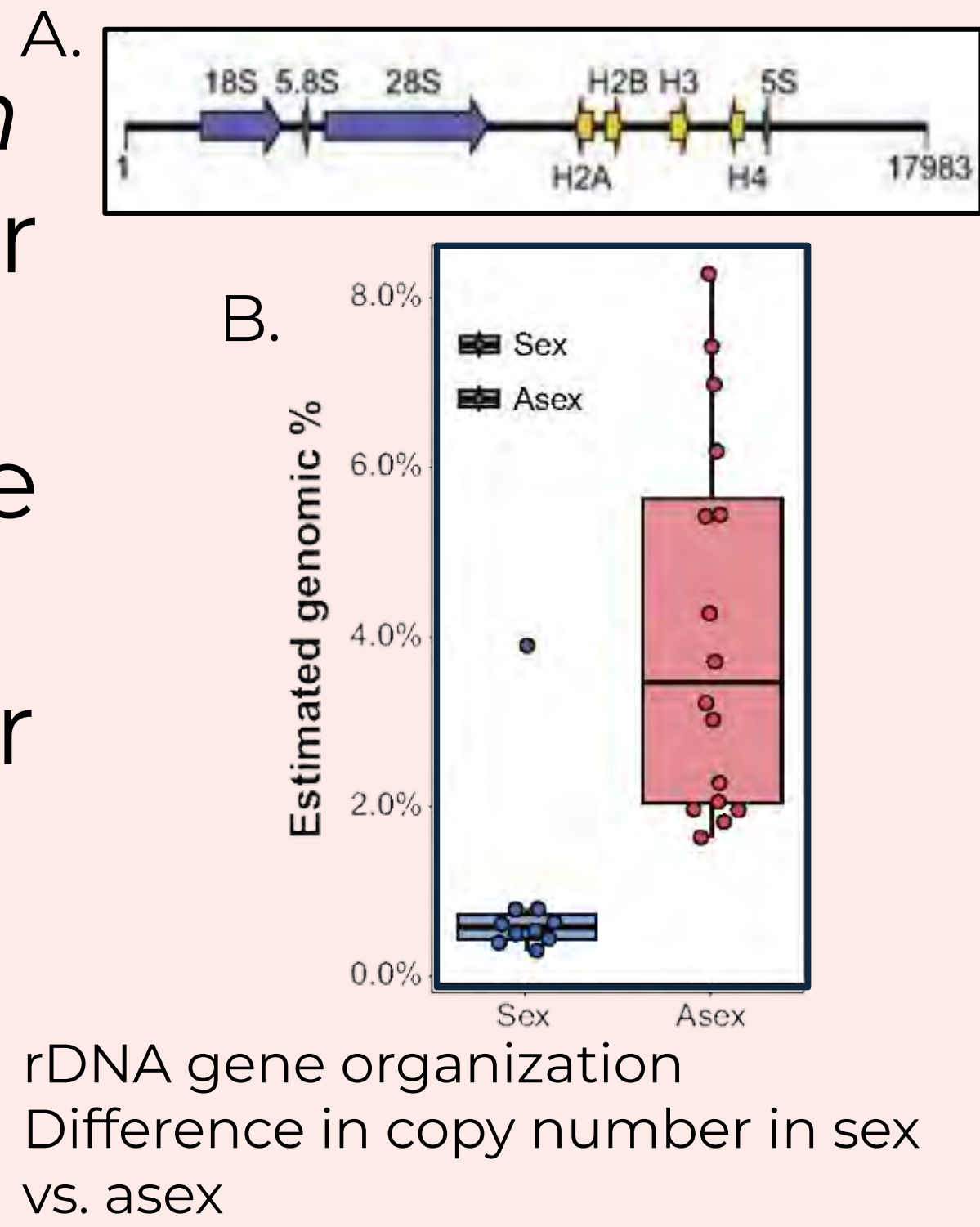
# How does genomic variation affect organismal phenotype?

- What is genomic variation?
- Insertions, deletions, copy number...
  - **Our focus: gene copy number**
- Phenotypes
- Organismal traits
  - **Our focus: growth rate**

## Does rDNA Copy Number Affect Growth Rate?

- *Potamopyrgus antipodarum*
- New Zealand snail famous for sex vs. asex
- Asexuals harbor many more rDNA copies
- Asexuals usually grow faster than sexuals

### Are growth rate and rDNA variation linked?



## Copy That: Evaluating the Relationship Between rDNA Copy Number & Growth Rate



## It's Complicated...

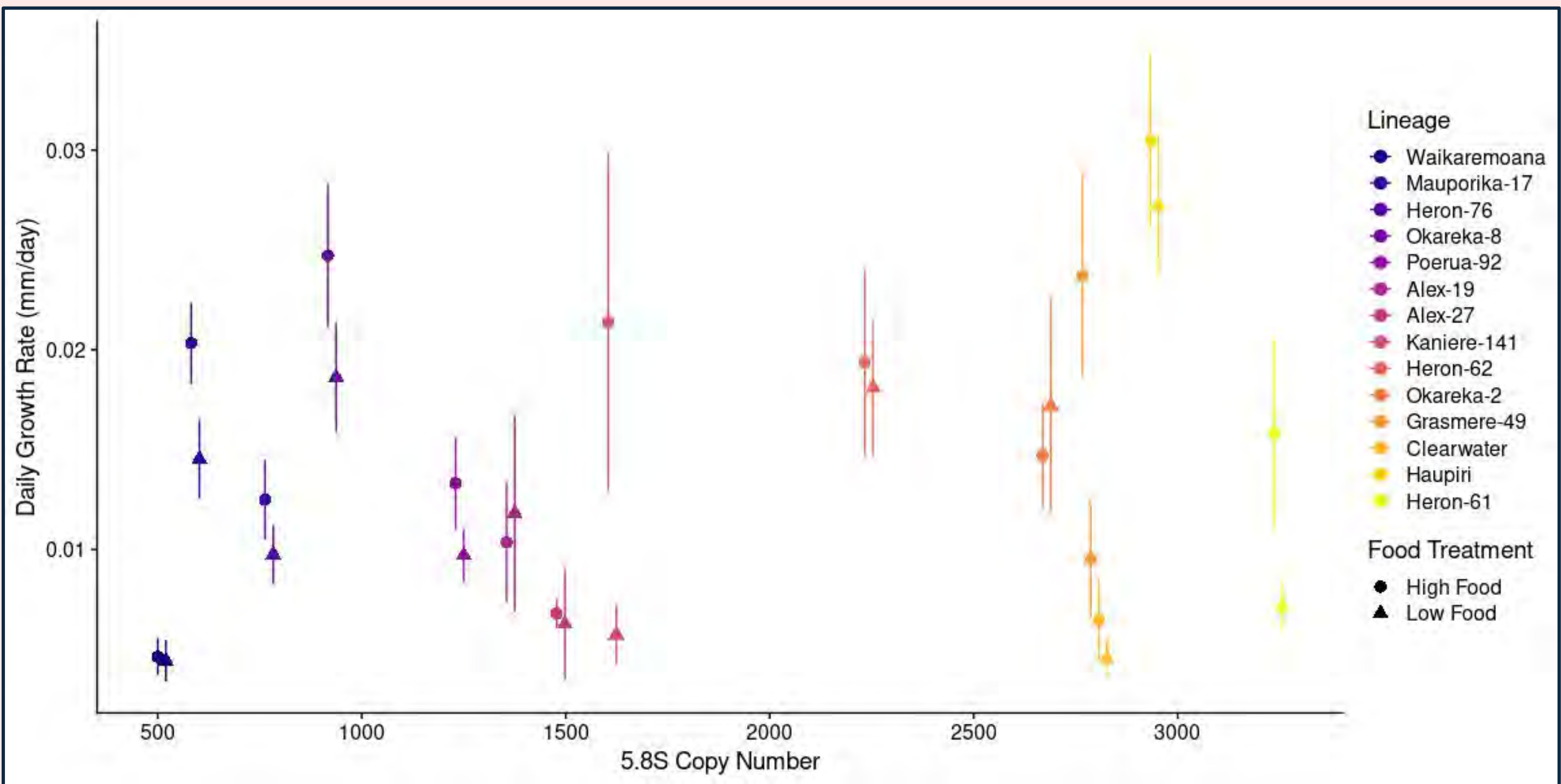


Fig 1: rDNA copy number vs. mean growth rate in high food and low-food conditions. Error bars represent +/- 1 SE.

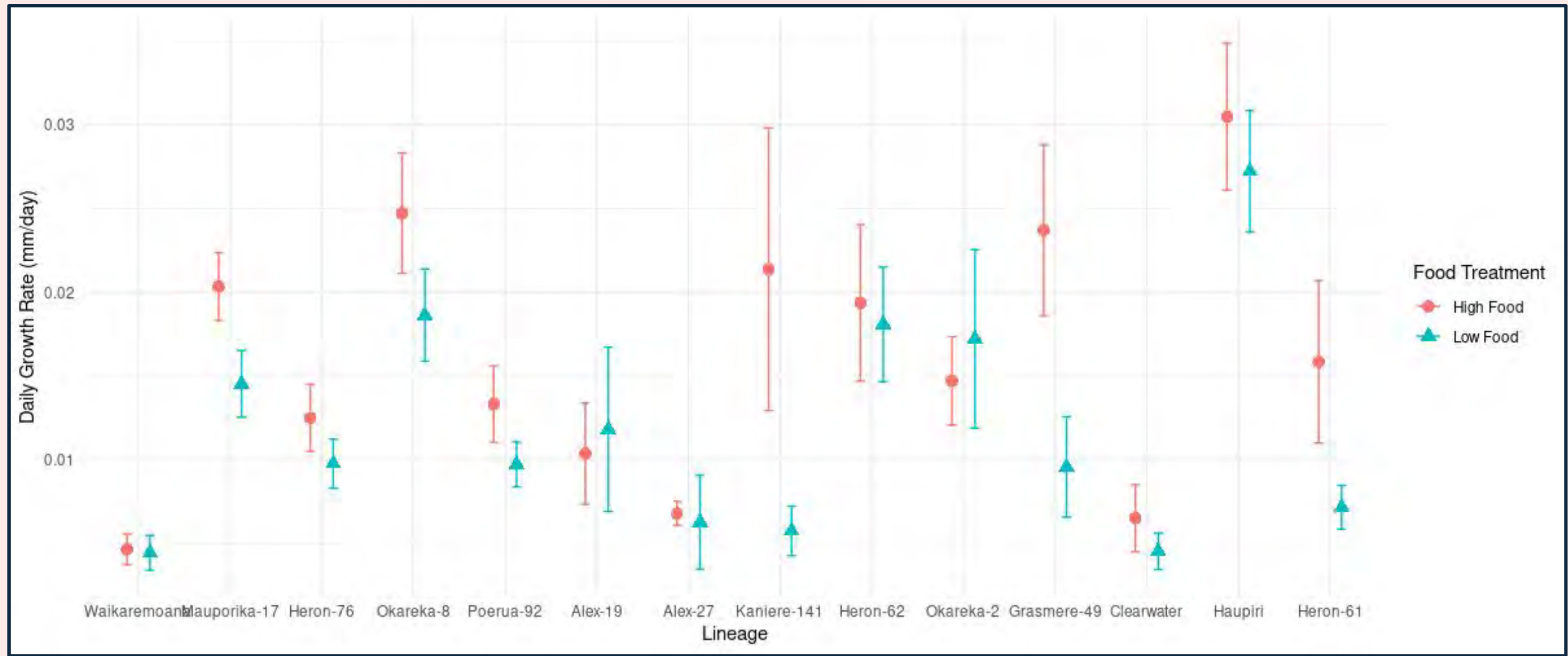
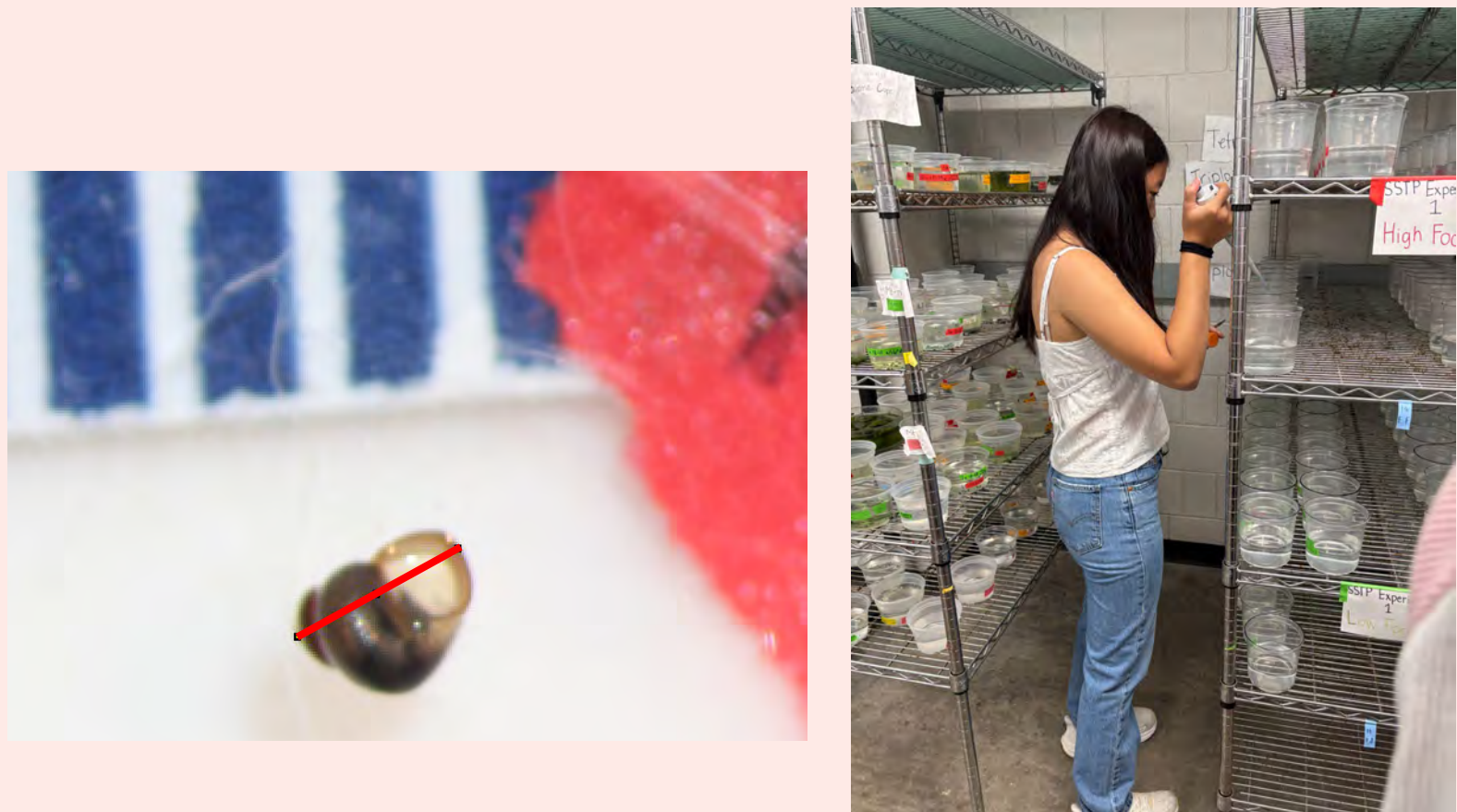


Fig 2: Lineage mean growth rate (+/- 1 SE) rank-ordered by rDNA CN

## Experimental Design

- Measured growth in 14 asexual lineages under high food & low food conditions for 4 weeks



Lineage 1		
Lineage 2		
...	...	...
Lineage 14		

**Sophia Hu<sup>1</sup>,**  
Winnie Gavin<sup>2</sup>, Helena Wu<sup>3</sup>,  
Kyle McElroy<sup>4</sup>, Maurine Neiman<sup>2</sup>,  
Varshu Saravanakumar<sup>2</sup>

<sup>1</sup>Emma Willard School, Troy, NY  
<sup>2</sup>Department of Biology, University of Iowa, IA  
<sup>3</sup>Marriotts Ridge High School, Marriottsville, MD  
<sup>4</sup>Iowa State University, Ames, IA



## Summary/Future Directions

- rDNA copy number and growth rate are not obviously correlated
  - Genomic variation does not always lead to phenotypic variation
  - Why might this be?

### Limitations

- Number of snails
- Length of experiment

### Future directions

- Are all rDNAs expressed? (qPCR)
- Asexuals vs. sexuals

### Acknowledgements & References

Donne, C., Larkin, K., Adrien-Tucci, C., Good, A., Kephart, C., & Neiman, M. (2022). Life-history trait variation in native versus invasive asexual New Zealand mud snails. *Oecologia*, 199, 785-795. <https://link.springer.com/article/10.1007/s00442-022-05222-8>

Larkin, K., Tucci, C., & Neiman, M. (2016). Effects of ploidy and reproductive mode on life history trait expression. *Ecology and Evolution*, 6(3). <https://onlinelibrary.wiley.com/doi/10.1002/ece3.1934>

McElroy, K. E., Müller, S., Lamatsch, D. K., Bankers, L., Fields, P. D., Jalinsky, J. R., Sharbrough, J., Boore, J. L., Logsdon, J. M., Jr., & Neiman, M. (2021). Asexuality associated with marked genomic expansion of tandemly repeated rRNA and histone genes. *Molecular Biology and Evolution*, 38(9). <https://academic.oup.com/mbe/article/38/9/3581/6245849>

Neiman, M., Kay, A. D., & Krist, A. C. (2013). Sensitivity to phosphorus limitation increases with ploidy level in a New Zealand snail. *Evolution*, 67(5). <https://academic.oup.com/evolution/article/67/5/1165/11651271>

Neiman, M., & Krist, A. (2016). Sensitivity to dietary phosphorus limitation in native vs. invasive lineages of a New Zealand freshwater snail. *Ecological Applications*, 26(7). <https://esajournals.onlinelibrary.wiley.com/doi/10.1002/eap.1372>

Thank you to the Neiman lab for feedback and assistance!  
Snail photo by Christian Böck, University of Innsbruck, Austria.



# Seizure Duration Patterns Captured by the Racine Scale and EEG Exhibit Propagation Dynamics

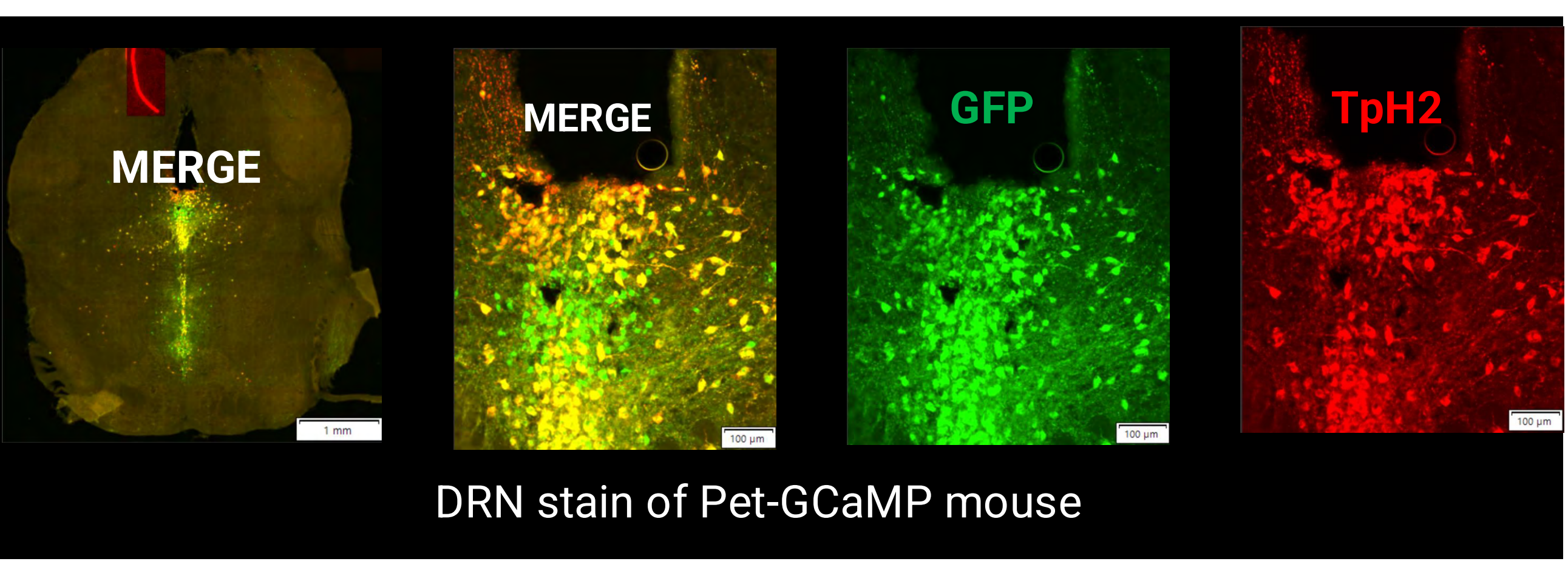
Harshil Jegan<sup>1,2</sup>, Matthew Summerfield<sup>3,5,6</sup>, Gordon Buchanan<sup>3-6</sup>

<sup>1</sup>Round Rock High School, Round Rock, TX, 78681, <sup>2</sup>Secondary Student Training, Program Belin-Blank Center, University of Iowa, Interdisciplinary Graduate Program in Neuroscience<sup>3</sup>, iDREAM Post-Baccalaureate Program in Neuroscience<sup>4</sup>, Iowa Neuroscience Institute<sup>5</sup>, Department of Neurology, University of Iowa, Iowa City, IA 52242<sup>6</sup>.

## Introduction

Epilepsy is a neurological disorder that affects more than 50 million people (Laxer et al., 2014). Approximately one-third of these people have refractory epilepsy, meaning that they cannot be treated. Sudden Unexpected Death in Epilepsy (SUDEP) is one of the most prevalent causes of fatality in epileptic patients, especially those who have refractory epilepsy (Petrucci et al, 2020).

- Dorsal Raphe Nucleus (DRN) has serotonin neurons for arousal (Smith et al, 2018)
- Suppression and removal of 5-HT neurons can lead to decreased arousal to CO2
- The increased CO2 with no response can lead to death in patients



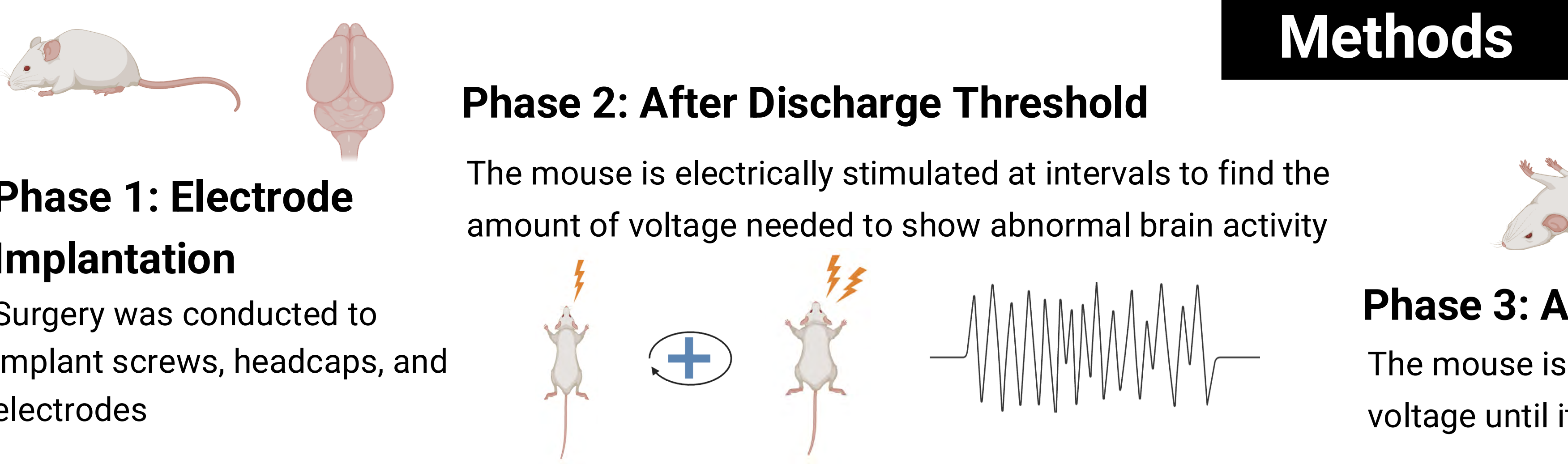
**Research Question**  
What is the correlation between the duration of a seizure and the behaviors being exhibited?

**Hypothesis**  
There is a positive correlation between behavioral seizure duration and the severity of the behavioral signs exhibited.

**Analyzing behavioral and physiological responses can help find patterns.**

- Behavioral aspects can be measured using the Racine scale, and physiological aspects can be measured using the EEG (Phelan, et al., 2015)
- Analyzing these aspects together can assist with more predictions of seizures

Stage	Behavioral Signs
1	Freezing
2	Orofacial movements and head nodding
3	Unilateral forelimb clonus
4	Bilateral forelimb clonus
5	Wild running and jumping



## Results

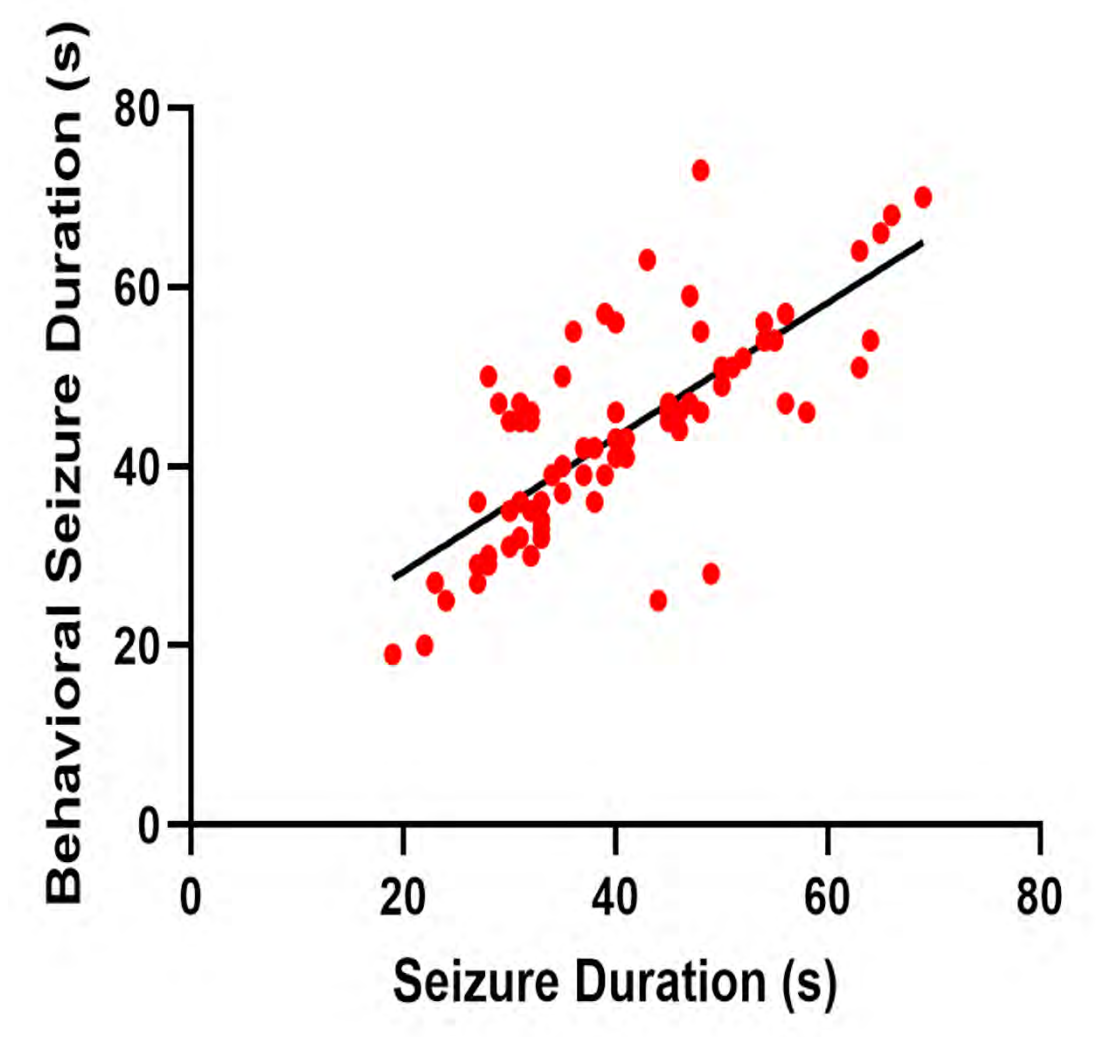


Figure 1: Correlation between behavioral seizure duration and EEG seizure duration.  $p < 0.05$ ,  $p < 0.001$ ,  $r = 0.7481$ .  $y = 0.75x + 13.26$

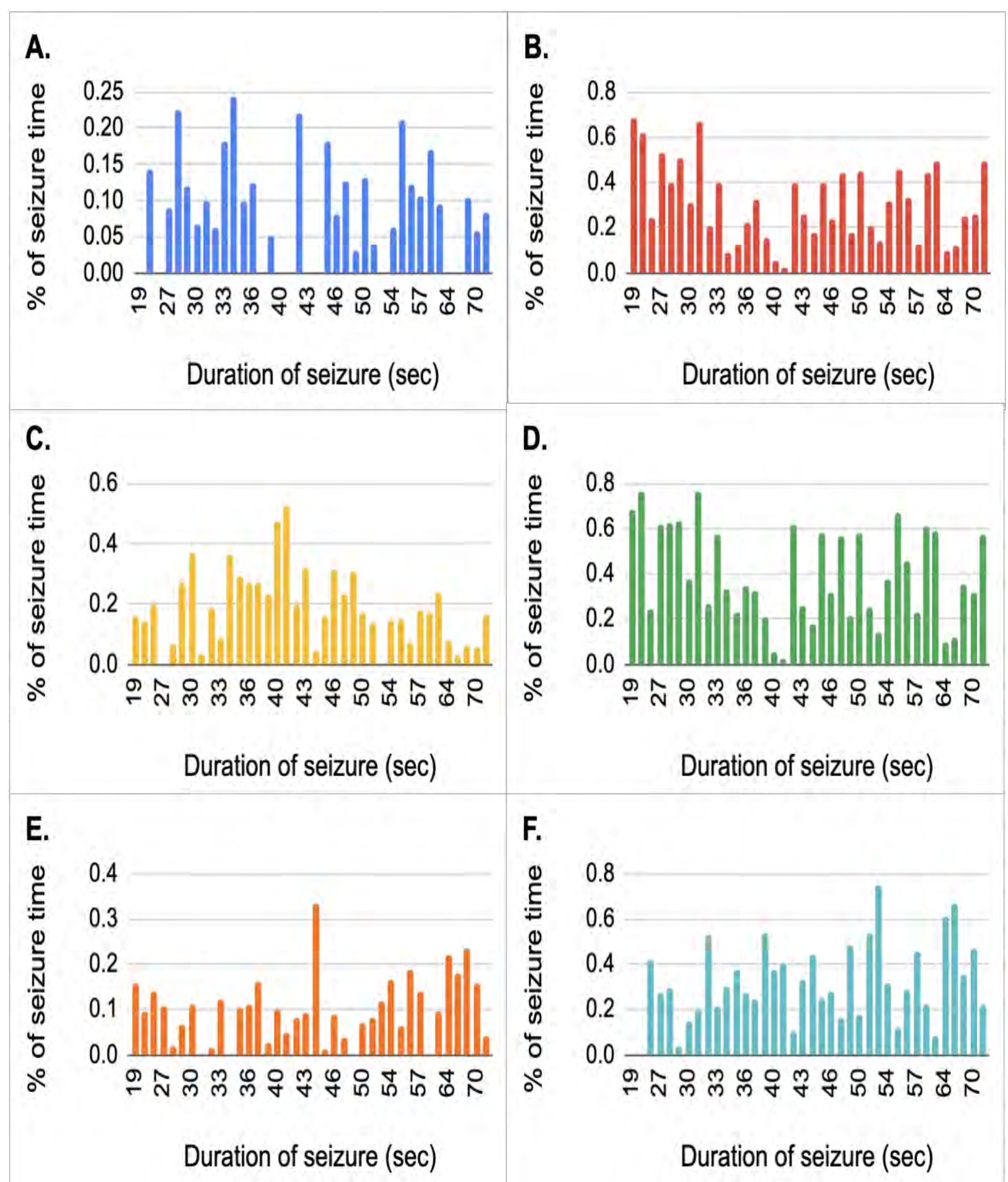


Figure 3: The percentages of (A) stage 1, (B) stage 2, (C) stage 3, (D) stage 4, (E) and stage 5 of the Racine scale during seizures.

## Methods

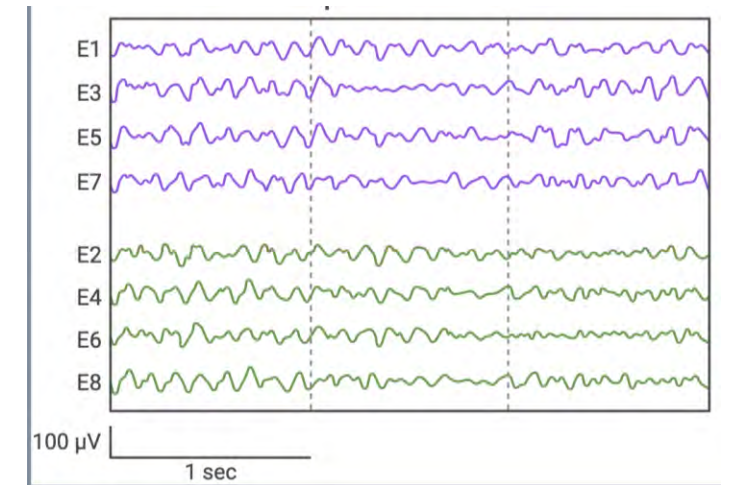


### Phase 3: Amygdala Kindling

The mouse is periodically stimulated at the ADT voltage until it has had three stage 4 seizures in a row

### Phase 4: Seizure-Inducing Trials

Once the mouse is kindled, seizure trials are conducted to study the mouse during and after



## Conclusion

- Strong positive correlation between durations
- The behavioral seizure is longer than the EEG
  - Less severe stages not yet propagated exhibit signs but show lower EEG waves
- Stages 2, 3, and 4 are the most common
  - Beginning and complete propagation of the seizure is less common
- Each mouse has its own seizure semiology
- Stage 5 does not increase with increased duration, while Stage 2 does
  - Higher duration  $\neq$  more severe seizures
- Positive correlation between stages 4 & 5
  - More severe seizures that have propagated are more likely to occur together
- Negative correlation between stages 3 & 5
  - Less severe stages will be inversely correlated with more severe ones

### Future Directions

- Looking at plethysmography data for breathing
- Observing post-ictal behavior
  - Racine scale
  - EEG data (PGES duration)
  - Breathing patterns

## Acknowledgements

The Buchanan Lab is supported by NIH/NINDS, the Beth L. Tross Epilepsy Professorship, and the Tross Epilepsy Research Fund.

## References

Buchanan G. F. (2019). Impaired CO2-Induced Arousal in SIDS and SUDEP. *Trends in Neurosciences*, 42(4), 242–250. <https://doi.org/10.1016/j.tins.2019.02.002>

Cohen, J. (1988). *Statistical Power Analysis for the Behavioral Sciences* (2nd ed.). Hillsdale, NJ: Lawrence Erlbaum Associates, Publishers.

Chi-Square Test Calculator. (2025). Retrieved from <https://www.socscistatistics.com/tests/chisquare2/default2.aspx>

Laxer, K. D., Trinka, E., Hirsch, L. J., Cendes, F., Langfitt, J., Delanty, N., Resnick, T., & Benbadis, S. R. (2014). The consequences of refractory epilepsy and its treatment. *Epilepsy & behavior : E&B*, 37, 59–70. <https://doi.org/10.1016/j.yebeh.2014.05.031>

Phelan K. D., Shwe U. T., Williams D. K., Greenfield L. J., Zheng F. (2015). Pilocarpine-induced status epilepticus in mice: A comparison of spectral analysis of electroencephalogram and behavioral grading using the Racine scale. *Epilepsy Research* 117, 90-96. <https://doi.org/10.1016/j.eplesyres.2015.09.008>

Petrucci, A. N., Joyal, K. G., Purnell, B. S., & Buchanan, G. F. (2020). Serotonin and sudden unexpected death in epilepsy. *Experimental Neurology*, 325, 113-145. <https://doi.org/10.1016/j.expneurol.2019.113145>

Petrucci, A. N., Joyal, K. G., Chou, J. W., Li, R., Vencer, K. M., & Buchanan, G. F. (2021). Post-ictal Generalized EEG Suppression is reduced by Enhancing Dorsal Raphe Serotonergic Neurotransmission. *Neuroscience*, 453, 206–221. <https://doi.org/10.1016/j.neuroscience.2020.11.029>

Smith, H. R., Leibold, N. K., Rappoport, D. A., Ginapp, C. M., Purnell, B. S., Bode, N. M., Alberico, S. L., Kim, Y. C., Audero, E., Gross, C. T., & Buchanan, G. F. (2018). Dorsal Raphe Serotonin Neurons Mediate CO2-Induced Arousal from Sleep. *The Journal of Neuroscience*, 38(8), 1915–1925. <https://doi.org/10.1523/JNEUROSCI.2182-17.2018>

All images from Biorender  
All graphs from GraphPad, Google Sheets, and Desmos





## Introduction

- The neurotransmitter dopamine (DA) is essential to motor control, learning, and motivation, and is heavily implicated in addiction and psychiatric disorders.
- Excess DA in the synaptic cleft is cleared by DAT, a transmembrane protein (Costa & Schoenbaum, 2022).
- D2 autoreceptors (D2ARs) inhibit DA transmission tonically, in a local feedback loop, by modulating dopaminergic neuron firing, DA synthesis, DA release, and DAT surface presence (Escobar et al., 2020; Ford, 2014).
- D2AR control of DAT is region specific and sex-biased (Stewart et al., 2022).

**Next step:** What other mechanisms regulate DAT?

## Preliminary Knowledge

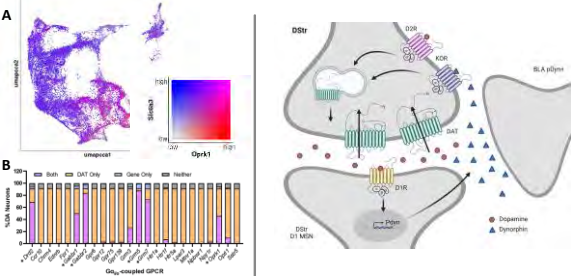


**Figure 1: KORs are consistently coexpressed with DAT.** (A) KOR presence in dopaminergic DAT positive neurons was analyzed using single cell sequencing. (B) KOR (*Oprk1*) is a GPCR with comparatively high coexpression.

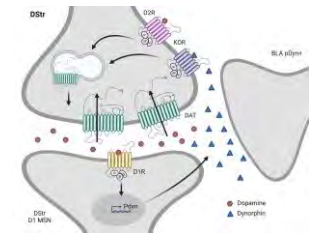


**Figure 2: KORs are expressed at the axon terminal of dopaminergic neurons.** KORs are endogenously activated by the opioid peptide dynorphin. KOR agonism promotes DAT surface trafficking and threonine 53 phosphorylation (Mayer et al., 2025).

## Research Focus

Do kappa opioid receptors (KORs) regulate DAT phosphorylation and surface trafficking across sexes and regions?

## Methodology

**Figure 3: Sample Generation.** We isolated brain slices containing DA projection regions (dorsal striatum, DStr; nucleus accumbens, NAc; and prefrontal cortex, PFC) from Wild-type (WT) C57 mice, both male and female, matured adults. Samples were immediately preserved in oxygenated artificial cerebrospinal fluid (aCSF). After recovery, slices were treated with the KOR agonist U69,593 (10  $\mu$ M, 7 min) followed by processing for surface protein biotinylation or uptake of radiolabeled [ $^3$ H]DA.

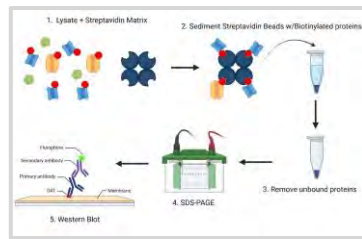
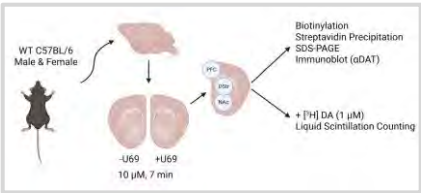


**Figure 4: Sample Processing for Biotinylation.** Streptavidin magnetic beads are added to lysed tissue samples to isolate biotinylated proteins. Beads are rinsed, so that only biotinylated proteins remain. Both pull down and total lysate samples are separated by size using SDS-PAGE. After transferring proteins to a membrane, western blotting is performed for both DAT and phosphorylated DAT (T53).

## Results

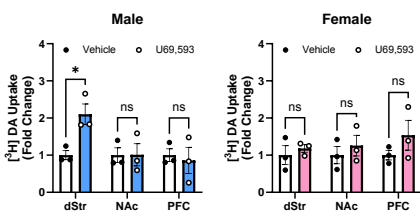


**Figure 5: KOR increases DA uptake in the dorsal striatum (dStr) of males only.** Slices isolated from WT male or female mice and containing DStr, NAc, or PFC were treated with U69,593 to activate KOR. The fold change in uptake of [ $^3$ H]DA following addition of the KOR agonist is shown. ns = not significant. \* $P$ <0.05.

## Discussion

Dorsal Striatum (dStr) dopaminergic activity is heavily linked to habit formation, and is therefore implicated in OCD's repetitive, patterned behaviors. KORs provide a new opportunity for therapeutic targeting, due to their ability to regulate dopamine transmission in the dStr. However, because the effect of KORs on DAT is only in male dStr, treatment application may be restricted in females. The regional and sex-based specificity of KOR modulation of DAT is a reminder that sex differences are prevalent in the brain, particularly in the DA system.

## Future Directions

- Process samples generated for detection of KOR-dependent DAT surface expression/phosphorylation to determine if increased DA uptake following U69 treatment is linked to DAT phosphorylation or trafficking.
- Repeat experiment on other GPCRs that are highly coexpressed with DAT in dopaminergic neurons, e.g. Grm5 or Grm7 (Figure 1B).
- Assess sex- and region-biases of other mechanisms in order to address possible treatment limitations.

## Acknowledgements

I would like to thank Dr. Adele Stewart, Jacob Bernholtz, Julia Neuharth, and Brenna Powers for welcoming me into the lab and teaching me content and lab skills. Additionally, I would like to thank the Secondary Student Training Program, the Belin-Blank Center, and the University of Iowa for this opportunity.

## References

Costa, K. M., & Schoenbaum, G. (2022). Dopamine. *Current Biology*, 32(13), R817–R824. <https://doi.org/10.1016/j.cub.2022.06.060>

Escobar, A. del F., Casanova, I. P., Andrade, M. E., & Venter, A. J. (2020). Crosslink between kappa opioid and dopamine systems in compulsive behaviors. *Frontiers in Pharmacology*, 11. <https://doi.org/10.3389/fphar.2020.00055>

Ford, C. P. (2014). The role of GPCR signaling in regulating dopamine neuron activity and transmission. *Neuroscience*, 282, 11–22. <https://doi.org/10.1016/j.neuroscience.2014.03.025>

Mayer, F. P., Stewart, A., Varman, D. R., Morris, A. E., Foster, J. D., Owens, A. W., Areal, L. B., Gowrishankar, R., Vetter, M., Wickham, K., Phelps, H., Katsanakis, R., Rabi, M., Jayatilak, L. D., Vaughan, R. A., Dawe, J. C., Biakely, A. W., & Rasmussen, S. (2020). Kappa opioid receptor antagonist restores phosphorylation, trafficking and behavior induced by a disease-associated dopamine transporter variant. *Molecular Psychiatry*. <https://doi.org/10.1038/s41380-025-0305-4>



Jaeyun(Jay) Lee<sup>1</sup>, Juliana Danesi Ruiz<sup>2,3</sup>, Casey Harwood<sup>2,3</sup>, Rachel V. Vitali<sup>3</sup>

<sup>1</sup>Western Reserve Academy (Hudson, OH); <sup>2</sup>IIHR—Hydroscience & Engineering, University of Iowa; <sup>3</sup>Department of Mechanical Engineering, University of Iowa

## Introduction

- The **Stewart Platform** (Fig. 1) is a 6 degree-of-freedom (DOF) parallel manipulator used in applications requiring precise positioning and orientation, such as flight simulators, robotics, and surgical tools.
- Achieving accurate motion control in real time requires precise coordination of all six actuators (legs) that move the platform.
- A **PID** (Proportional–Integral–Derivative) **controller** is widely used in engineering applications to regulate system outputs based on feedback.
- In the Stewart platform, **PID controllers are applied to each actuator** to control its position, ensuring smooth, stable, and accurate movement.
- The PID controller continuously adjusts actuator input by minimizing the **error** between the desired and actual position.
- Using PID control enhances the platform's ability to handle **external disturbances, non-linearities**, and maintain **stable dynamic performance**.

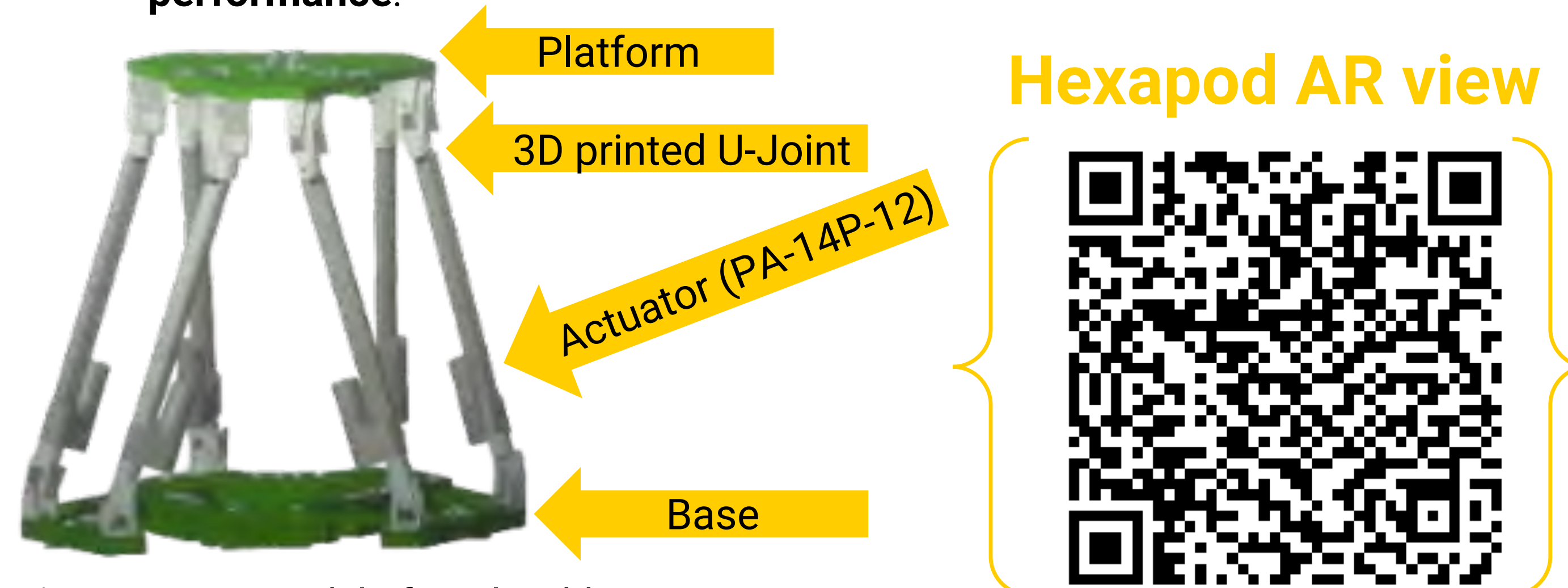


Figure 1 CAD model of Vitali Lab's Stewart Platform.

## Methods

- To test the Stewart Platform's PID controller, a ball maze (Fig. 2) serves as a practical and interactive testbed.
- Allows for observing platform's precision and responsiveness in real-time as platform maneuvers the ball (Fig. 3) through the maze.

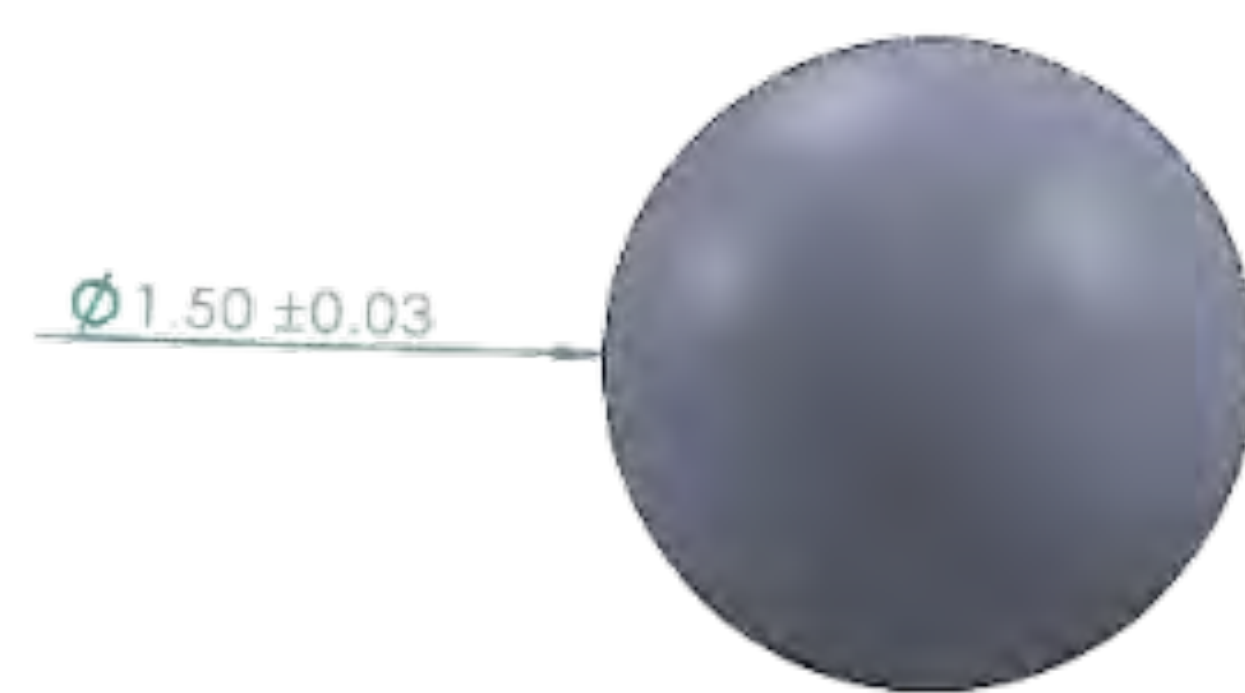
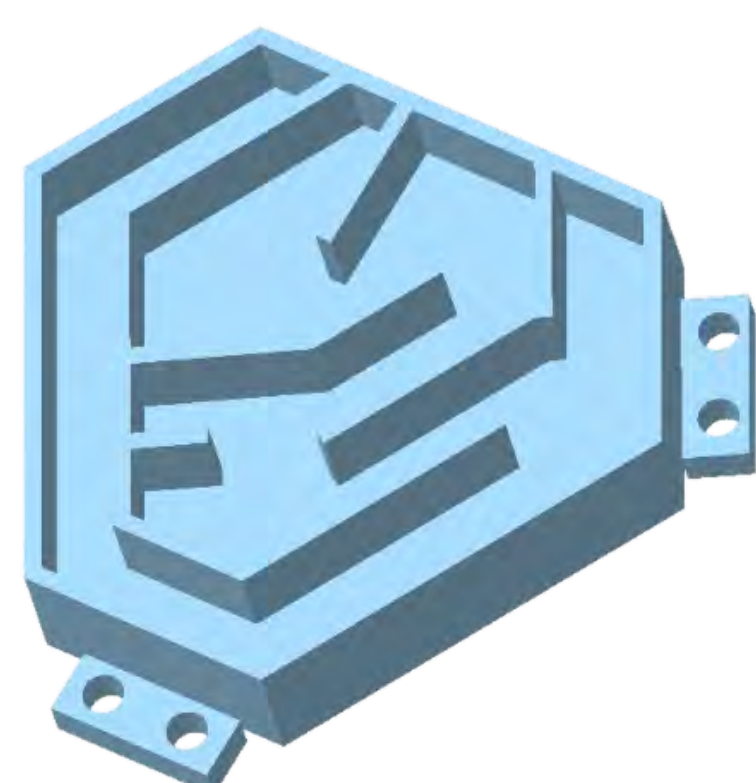


Figure 2 CAD model of ball maze attachment. Figure 3 Dimensioned CAD ball model.

- Although prior code was written in C++ through Arduino, the code was re-written in MATLAB to enable and facilitate:
  - More advanced control algorithms and matrix-based kinematic calculations for the Stewart platform.
  - More precise inverse kinematics, real-time simulation, and seamless integration with Simulink for closed-loop control and visualization.

## Methods (continued)

- Using CAD software (e.g., Onshape, SolidWorks, and Creo), all necessary components were efficiently designed to create a complete assembly file (Fig. 4) and design parts for 3D printing as needed (Fig. 5).
- One major challenging tasks was generating a .txt file that listed the actuator positions required for the Stewart Platform to reach specific poses.
  - A custom MATLAB application was designed to perform inverse kinematics calculations (Fig. 6).
  - By inputting desired platform orientations and positions, the app computed the corresponding actuator lengths for each configuration.
  - These calculated values were then compiled into a structured .txt file, which was then used to control the platform.
- This approach streamlined the process and ensured accurate positioning based on real-time motion requirements as well as leveraging the strengths of PID control.



Figure 4 Assembly model of full Stewart Platform set up with attached ball maze.



Figure 5 Improvements in 3D print

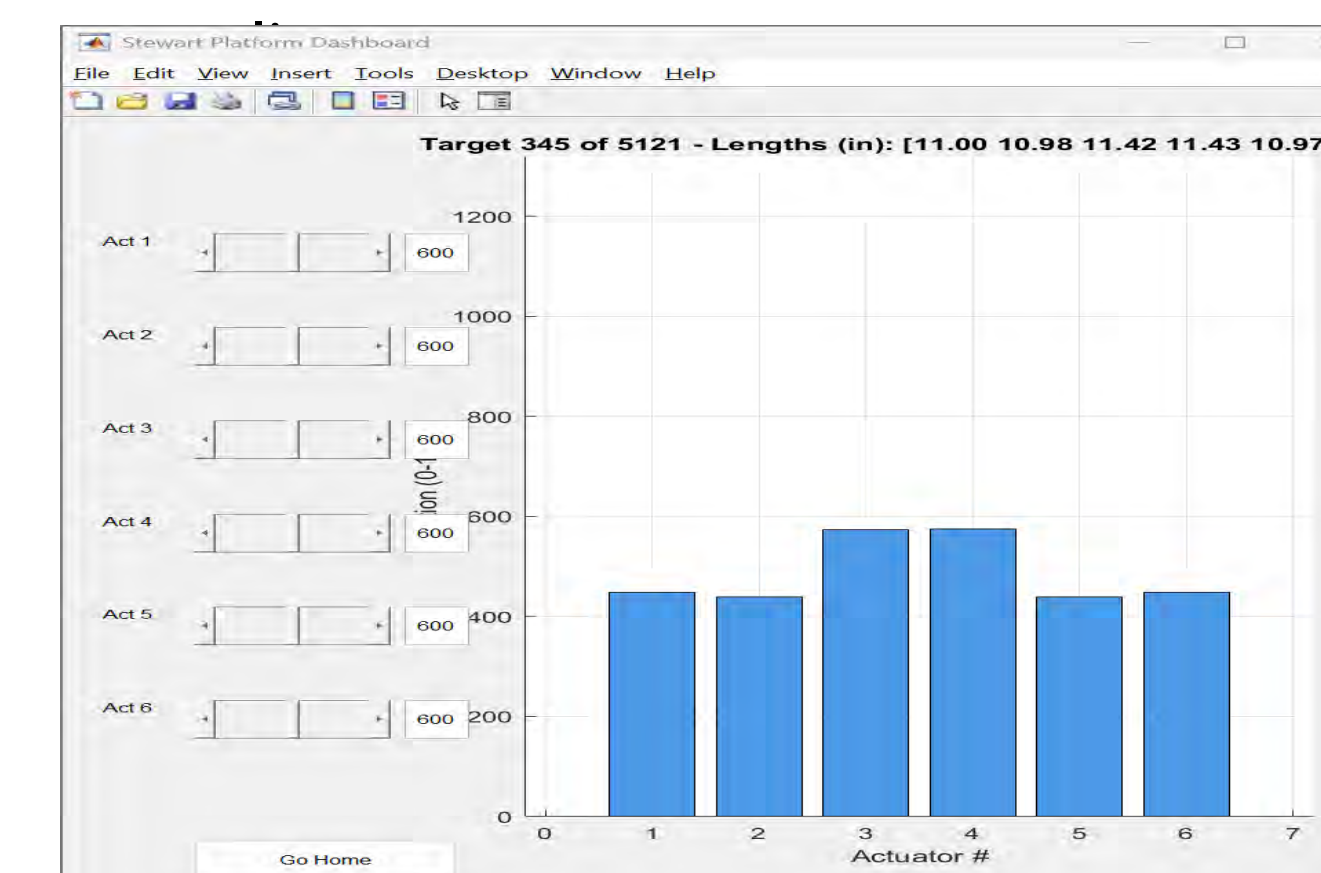


Figure 6 Screenshot of MATLAB GUI

## Video of Ball Maze



## Results

- Overall, the experiments were a clear success
  - Across repeated trials the Stewart platform smoothly guided the ball from the maze entrance to exit without any stalls or overshoot.
  - The Stewart Platform could previously only move to one hard-coded coordinate at a time and all control logic lived in an Arduino sketch that was separate from MATLAB's kinematic and visualization tool-set.
- By migrating the control loop to MATLAB and adding a text coordinate loader, the platform now reads a sequence of targets in real-time, steps through them quickly and accurately, and traces a continuous path instead of pausing between points.
- Real-time execution removes the stop-and-go constraint of the earlier system and makes the platform capable of more demanding tasks.

## Future Work

- Closed-loop vision tracking:** Integrate a top-down camera and OpenCV pipeline so the platform can locate the ball in real time, adjust its trajectory, and autonomously recover from disturbances.
- Open-source release & publication:** Package the MATLAB controller, AR model, and CAD files into a GitHub repository and submit a short paper to the ASME IDETC/Mech-Vib conference to share results with the robotics community.
- Expanded Tasks:** Develop additional end-effector attachments—e.g., a micro-pipetting arm or haptic joystick—to showcase the Stewart Platform's versatility across various applications.

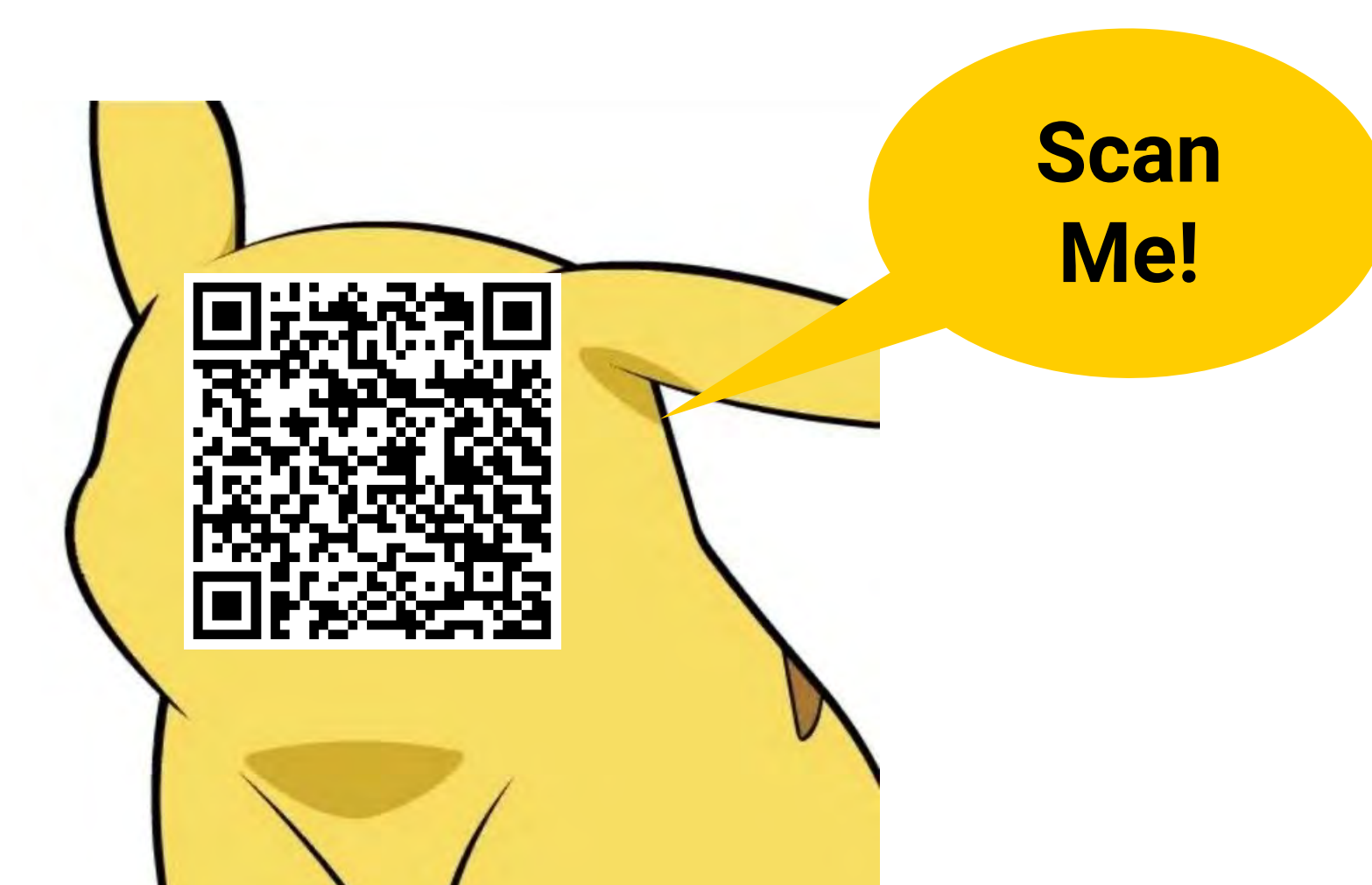
## Conclusions

- Migrating all control logic to MATLAB transformed the Stewart platform from a single-pose demonstrator into a fully dynamic testbed.
- New pipeline streams inverse-kinematic targets, follows continuous trajectories, and repeatedly guided a ball through a 3D-printed maze without stalling or overshoot—capabilities that were impossible in the original Arduino-only setup.
- Results validate the platform's real-time responsiveness and scalability, laying a solid foundation for more advanced sensing, control, and application-specific tooling in upcoming work.

## Acknowledgments

Thank you to the Belin-Blank Center, and of course, SSTP, for giving me the incredible chance to conduct college-level research and meet peers who share my interests. I'm also grateful to everyone in my lab for their support and guidance as I explored the new world of research. My success and joy wouldn't have been possible without your support, and I truly believe my experience at SSTP wouldn't have been the same without the tightly-knit community

## References





# Neuroimaging Alterations of T2-Star Relaxation Times Demonstrated in Hemophilia A Compared to Controls

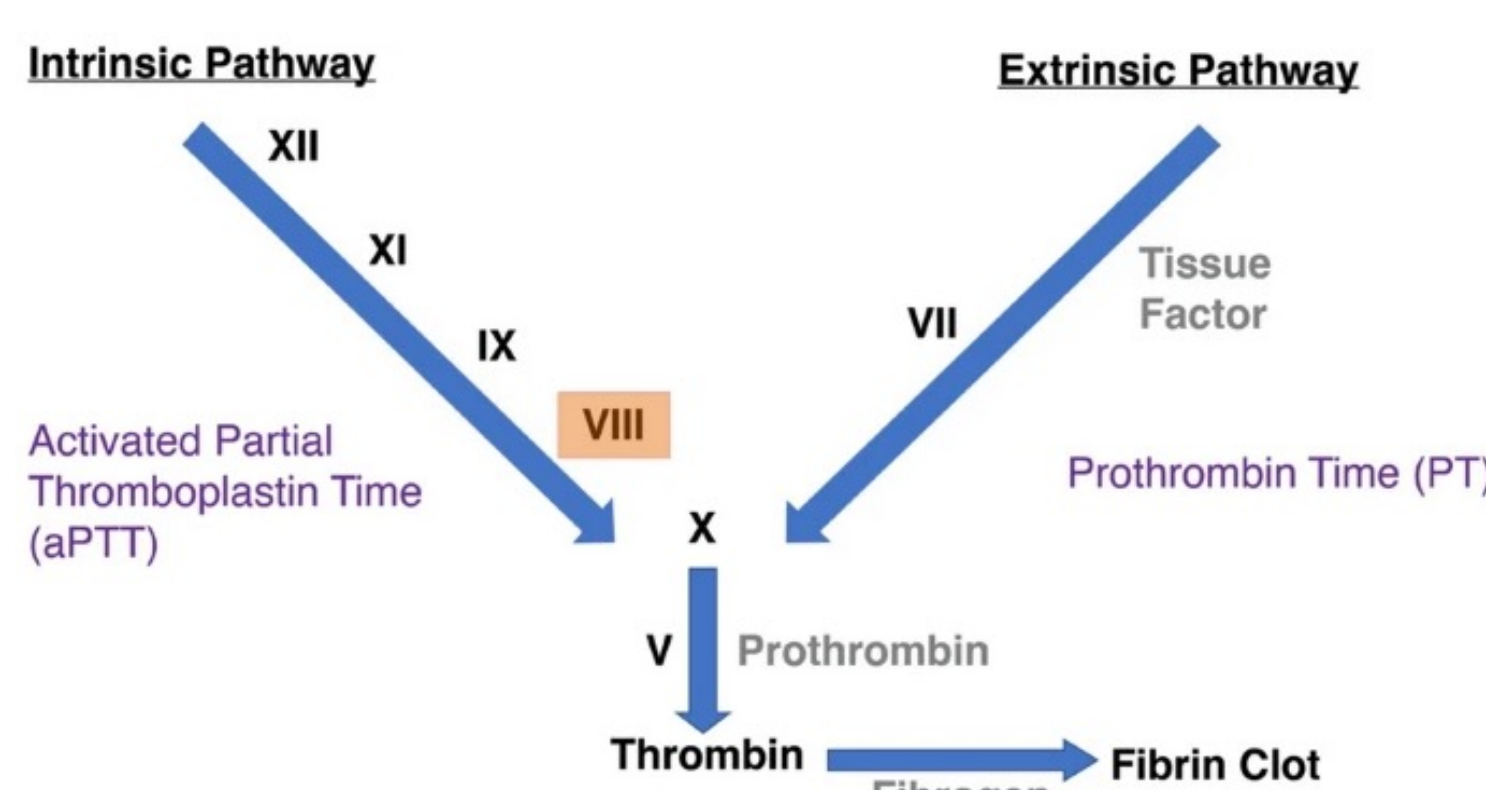
David Li<sup>1</sup>, Kevin Gubner<sup>2</sup>, Danielle York<sup>3</sup>, Lauren Hopkins<sup>3</sup>, Janice Staber<sup>3,4</sup>

<sup>1</sup>University of Chicago Laboratory Schools High School, <sup>2</sup>Carver College of Medicine, <sup>3</sup>Stead Family Department of Pediatrics, <sup>4</sup>Iowa Neuroscience Institute

## Introduction

### Hemophilia A (HA):

An X-linked genetic bleeding disorder caused by a deficiency in coagulation factor VIII (FVIII), affecting an estimated 400,000 individuals globally. FVIII enables thrombin generation, which forms fibrin clots; reduced FVIII levels lead to increased bleeding in the abdomen, joints, and brain.<sup>1</sup>



### Human Blood Clotting Cascade<sup>4</sup>

The Staber Lab previously identified that cerebellar gray matter volume is significantly decreased in children with HA compared to unaffected controls.<sup>5</sup> Previous studies associated the cerebellum with cognition and executive function and decreases in cerebellar volume is associated with poor cognitive performance.<sup>5</sup>

### Quantitative T2\* MRI:

T2-Star (T2\*) MRI: A variation of quantitative T2 MRI that reflects magnetic field inhomogeneities (i.e., iron and calcium deposition) and changes in tissue structure.<sup>2</sup>

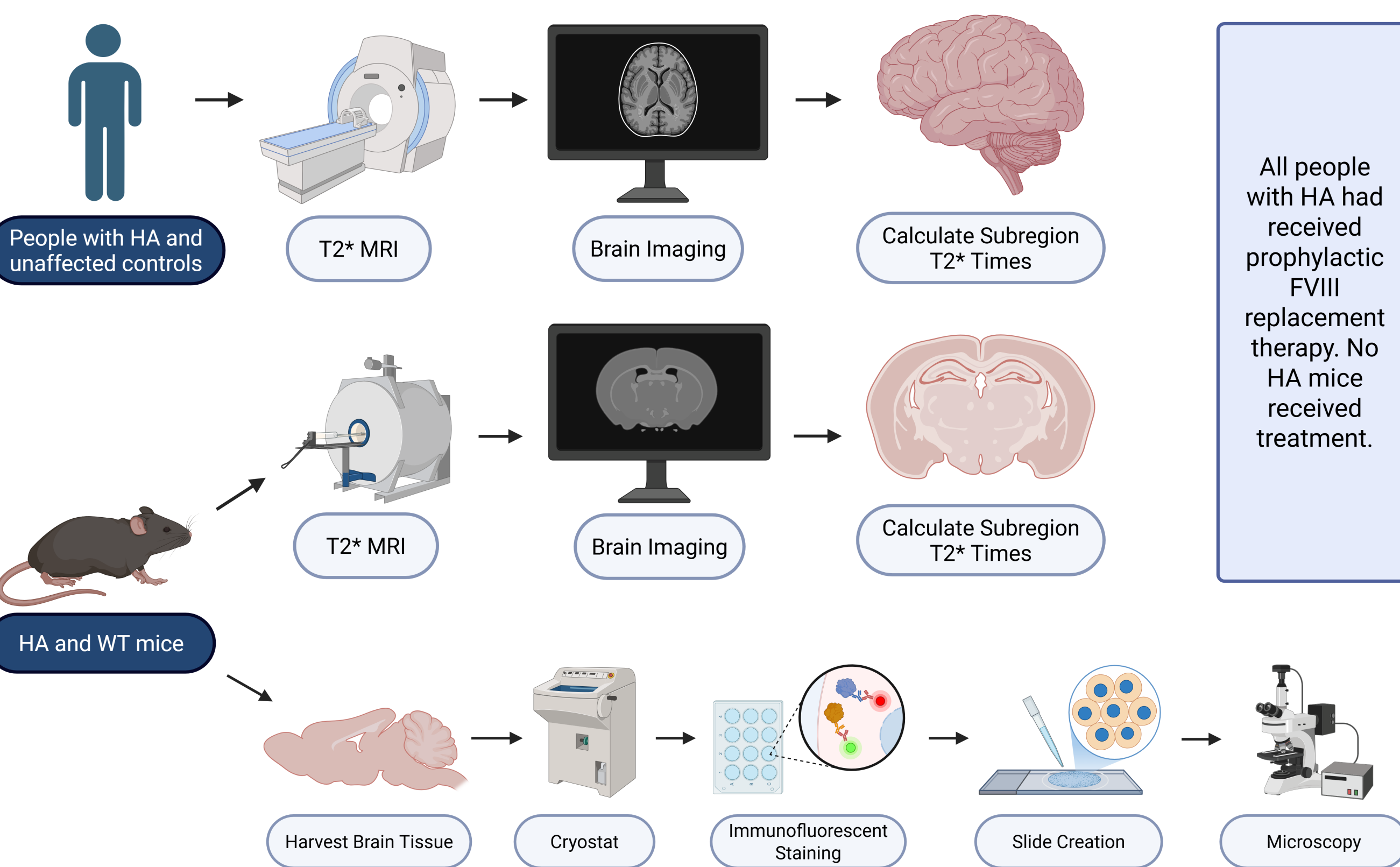
Output = relaxation times in various subregions of the brain.<sup>2</sup> Elevated relaxation times indicate increased tissue water content, often caused by neuroinflammation.<sup>3</sup>

Volumetric and T2\* imaging may be used in conjunction to investigate neuroinflammation.<sup>3</sup>

## Research Objectives

- Quantify T2\* relaxation times in HA compared to controls in regions of interest (ROIs) in human subjects and a preclinical model
- Correlate volumetric structural outcomes with T2\* relaxation times in HA compared to controls

## Methodology



Graphs and statistical analyses done using RStudio. Graphics created using BioRender.

## Results

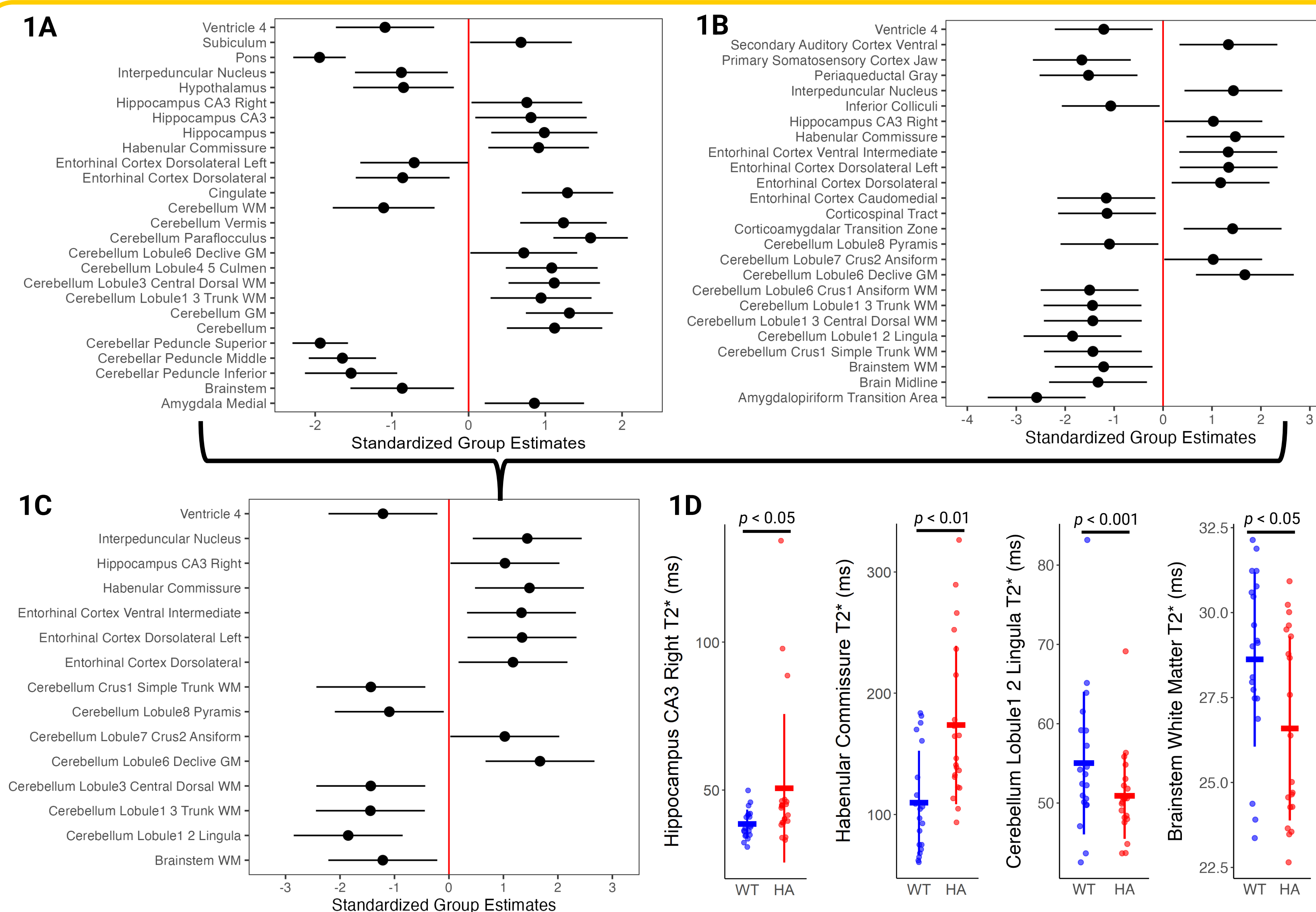


**Figure 1. Representative forest plots and grouped mean plots of brain volumes (A) and T2\* relaxation times (B-D) of 6-month-old mice with HA [n = 21 (11 M, 10 F)] compared to wild-type mice [n = 20 (9 M, 11 F)]. (A)** HA mice had significant brain volume differences, adjusted for intercranial volume, compared to WT mice in 146 ROIs total ( $p < 0.05$ ). **(B)** T2\* relaxation times of 25 ROIs in which T2\* relaxation times differed significantly in HA mice compared to WT mice are shown ( $p < 0.05$ ). **(C)** The T2\* relaxation times of the 15 ROIs which differed significantly in both T2\* relaxation times and volumetrics are shown ( $p < 0.05$ ). **(D)** Grouped mean plots of T2\* relaxation times for 4 of 15 ROIs. Models are adjusted for status and sex in figures A-C, but not in D. HA = Hemophilia A; WT = Wild-type; WM = white matter; GM = gray matter; ROIs = regions of interest.

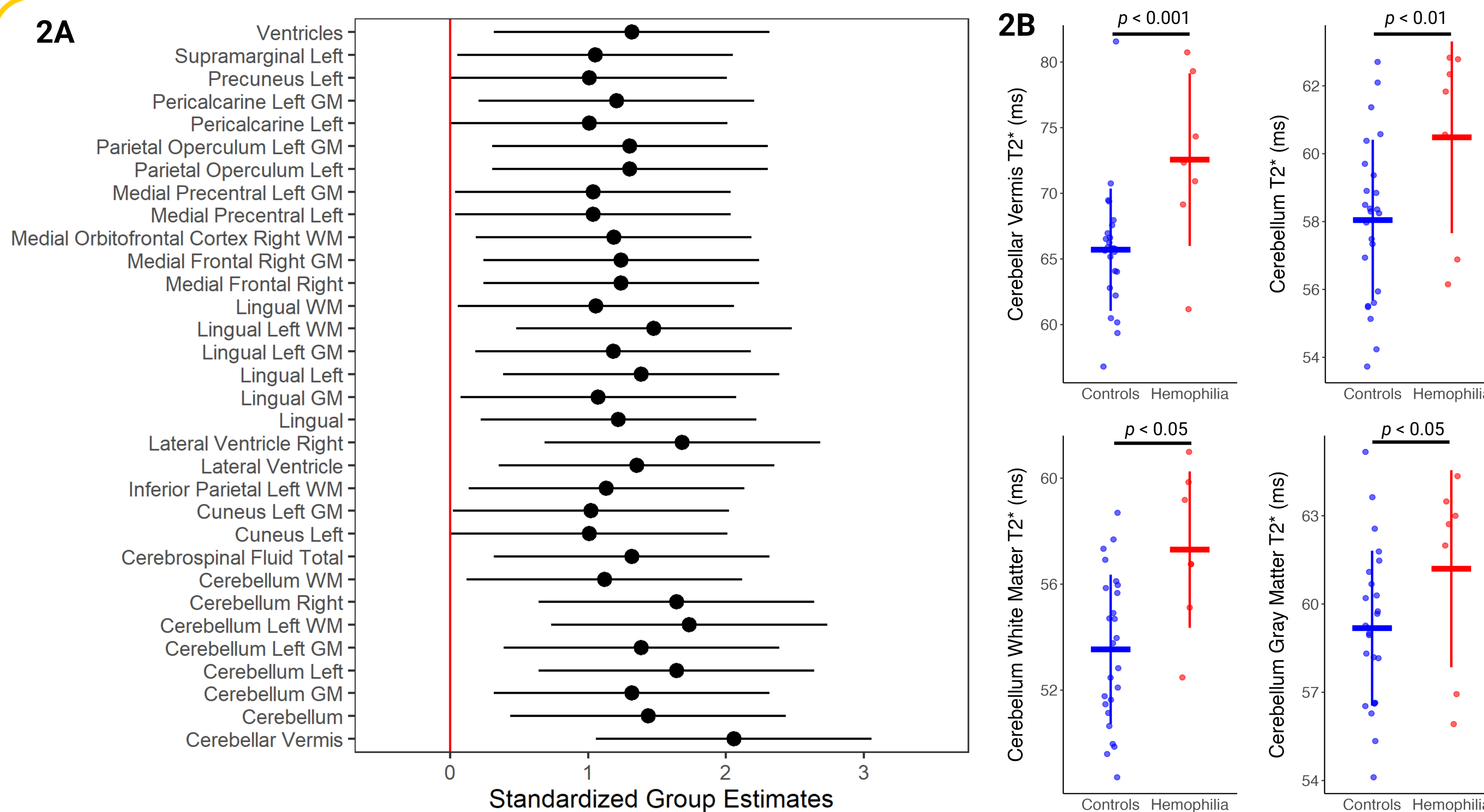


**Figure 2. Plots of T2\* relaxation times of seven humans with HA compared to 25 unaffected controls in various ROIs. All subjects were males aged 6-16. (A)** Forest plot of 33 ROIs in which T2\* times, adjusted for status, age, height, and weight, differed significantly ( $p < 0.05$ ). **(B)** Grouped mean plots showing unadjusted T2\* times in four cerebellar regions. The cerebellum was the only global ROI that had significantly different T2\* times ( $p < 0.05$ ). WM = white matter; GM = gray matter; ROIs = regions of interest.

## Conclusions

T2\* relaxation times in brain subregions including the hippocampus CA3, habenular commissure, entorhinal cortex subregions, cerebellum and brainstem white matter differed significantly in HA compared to WT mice (**Figure 1B**). Some of these regions also revealed significant differences in the volumetric data in HA compared to WT mice (**Figure 1C**).

Multiple subregions of the cerebellum had significantly different T2\* relaxation times in HA compared to controls in both humans and mice, as well as significantly higher volumes in the HA mice.

*In children with HA, all ROIs with significantly different T2\* relaxation times revealed elevation in T2\* compared to the unaffected controls (Figure 2A). This suggests neuroinflammation that is not subdued by FVIII replacement therapy.*

## Future Directions

Microglia activation, identified by the markers Iba-1 and CD68, is upregulated during inflammatory responses, making them useful markers of neuroinflammation in our HA mouse model.<sup>6</sup>

We plan to compare microglial activity in HA mice and WT mice in ROIs to identify possible differences in levels of neuroinflammation.

We plan to explore associations between T2\* relaxation times and cognitive performance in people with HA compared to unaffected controls.

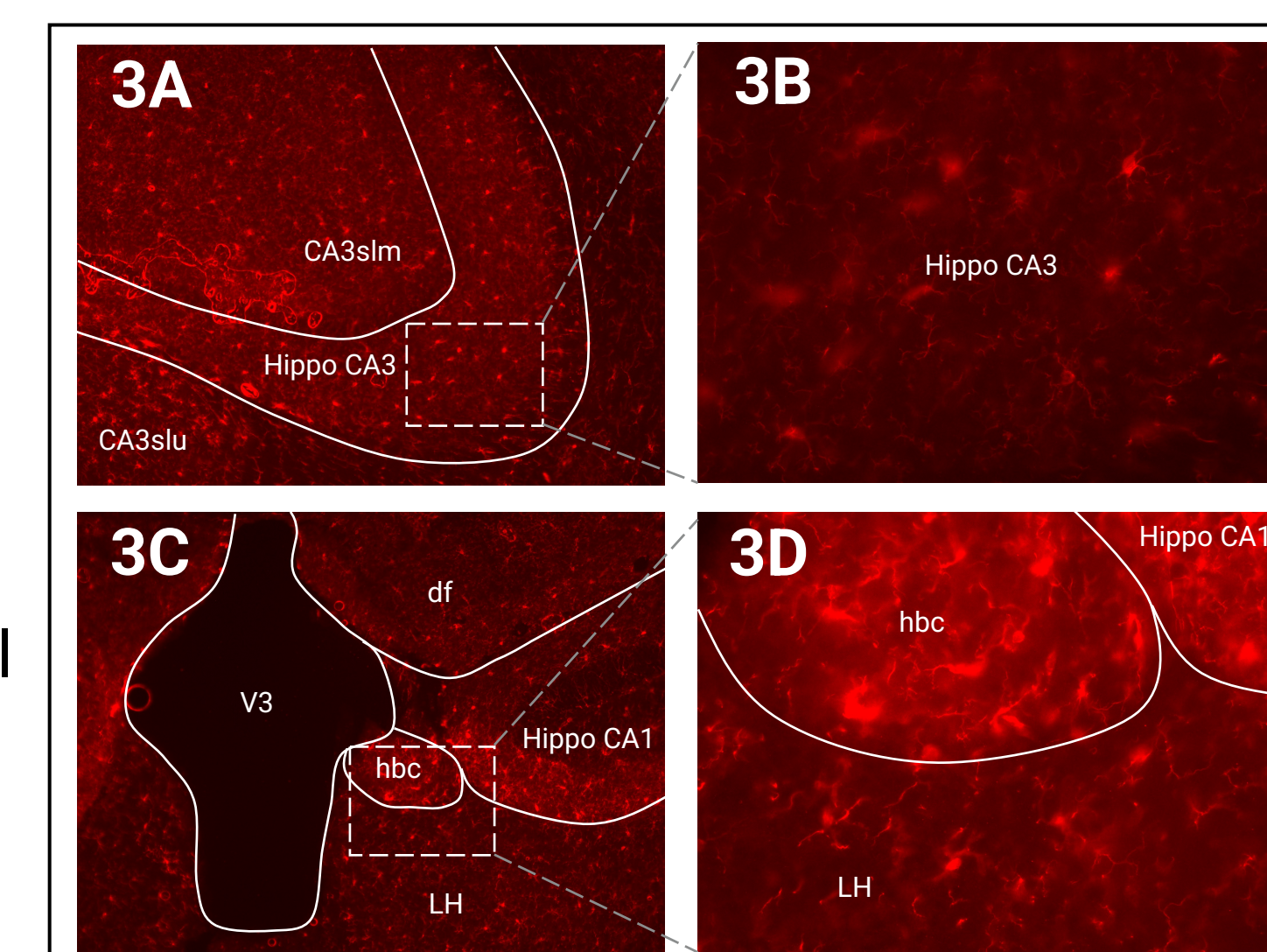


**Figure 3. Microglia in a five-month-old HA mouse stained for Iba-1 and CD68. Brain subregions labelled with abbreviations. A, B)** Microglia in the hippocampus CA3 of a HA mouse in 10x (A) and 40x (B) magnification. **C, D)** Microglia in the habenular commissure in 10x (C) and 40x (D) magnification. The microglia are more abundant in this region compared to the hippocampus CA3 and neighboring regions.

## Acknowledgements

Thank you to Dr. Staber for giving me the opportunity to learn in the Staber Lab and actively participate in research.

Special thanks to Kevin Gubner for providing R script for volumetric analysis and guidance on statistical analyses, Danielle York for her help with the neuroimaging process, and Lauren Hopkins for processing data from T2\* MRI scans.

The Small Animal Imaging Core Facility and the Magnetic Resonance Research Facility were used to obtain scans, and the authors are grateful the use of these facilities.

## References

- Mehta P, Reddivari AKR. Hemophilia. [Updated 2023 Jun 5]. In: *StatPearls [Internet]*. Treasure Island (FL): StatPearls Publishing; 2023. Available from: <https://www.ncbi.nlm.nih.gov/pmc/articles/PMC1021442/>.
- Tang MY, Chen TW, Zhang XM, Huang XH. GRE T2\*-Weighted MRI: Principles and Clinical Applications. *BioMed Res Int*. 2014;2014:312142.
- Nakamura K, Brown RA, Araujo D, Narayanan S, Arnold DL. Correlation between brain volume change and T2 relaxation time induced by dehydration and rehydration: Implications for monitoring atrophy in clinical studies. *NeuroImage Clin*. 2014;6:166-70.
- Packebush MH, Sanchez-Martinez S, Biswas S, KCS, Nguyen KH, Ramirez JF, Nicholson V, Boothby TC. Natural and engineered mediators of desiccation tolerance stabilize Human Blood Clotting Factor VIII in a dry state. *Sci Rep*. 2023;13:4542.
- Verhote S, Al-Huniti A, Novak M, Conrad AL, van der Plas E, Harshman L, Staber JM. Regional brain volumes and their relationship to neurocognitive outcomes in children with severe hemophilia A. *Blood VTH*. 2024;1(4):100021.
- Jurga AM, Paleczna M, Kuter KZ. Overview of General and Discriminating Markers of Differential Microglia Phenotypes. *Front Cell Neurosci*. 2020;14:198.





# Impact of Interferon Regulatory 6 (IRF6) on Epidermal Proliferation Throughout Embryonic Development

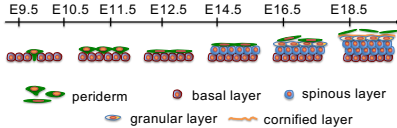
Kevin Lim<sup>1</sup>, Lindsey Rhea<sup>2</sup>, Martine Dunnwald<sup>2</sup>

<sup>1</sup>Upper Dublin High School, Fort Washington, PA; <sup>2</sup>Department of Anatomy and Cell Biology, University of Iowa, Iowa City, IA

IOWA

## Introduction

### Epidermal Embryonic Development

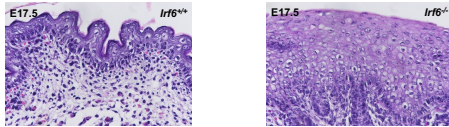


#### The periderm:

- Prevents interepithelial adhesions, for example in the oral cavity and limbs
- Transient suprabasal structure only present during embryonic development

#### Interferon Regulatory Factor 6 (IRF6):

- Transcription factor that acts as a master regulator of epidermal differentiation



- In humans, IRF6 mutations lead to cleft lip and palate
  - Interepithelial adhesions contribute to formation of CLP
- Loss of IRF6 leads to lack of or a nonfunctioning periderm in mice
- Absence of IRF6 in mice impacts orofacial, epidermal, and skeletal embryonic development



## Research Questions

- Are there differences in cell proliferation in the epithelium between wild-type and IRF6-deficient mouse embryos?
- At what stage of development are there differences in cell proliferation in the basal and suprabasal layers of the wild-type mouse embryos?

## Methods

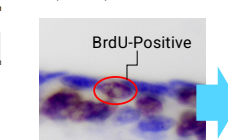
1. BrdU injected into pregnant mouse 2 hours before sacrifice



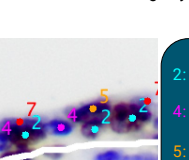
2. Take transverse sections of embryo



3. Immunohistochemistry for BrdU (brown) cells

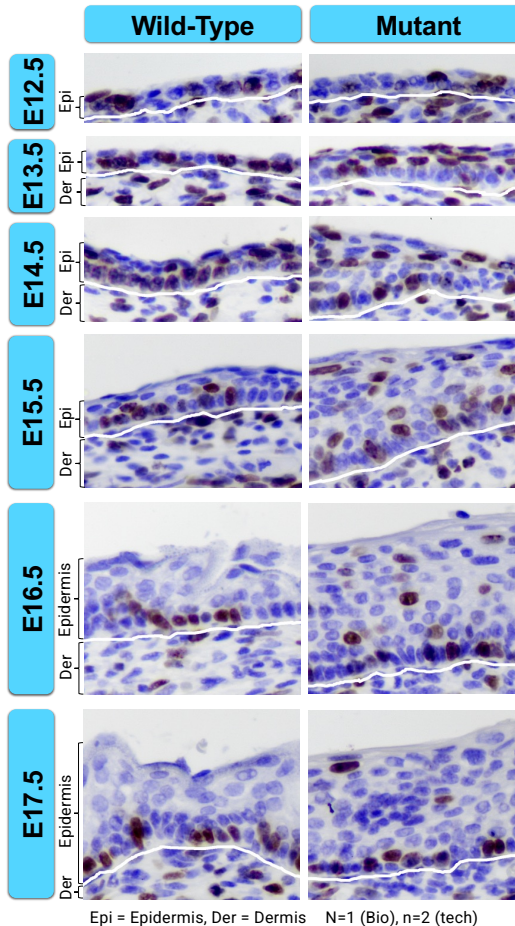


4. Count cells using key

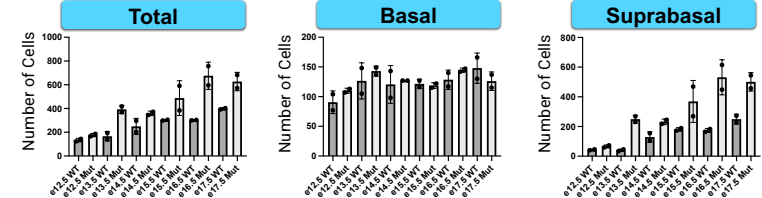


Key  
2: Basal Positive  
4: Basal Negative  
5: Suprabasal Positive  
7: Suprabasal Negative

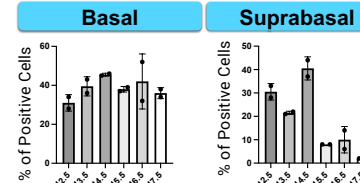
## Results



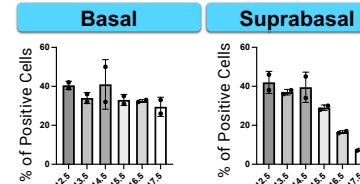
## Number of Epithelial Cells in Wild-Type and Mutant Embryonic Epidermis



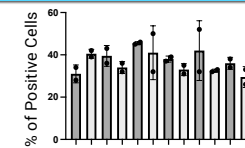
## BrdU-Positive in Wild-Type



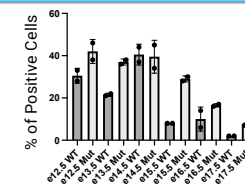
## BrdU-Positive in Mutant



## Wild-Type vs. Mutant Percentage of BrdU-Positive Basal Cells



## Wild-Type vs. Mutant Percentage of BrdU-Positive Suprabasal Cells



## Discussion and Conclusion

### Total Number of Epithelial Cells:

- Mutant had more total number of cells compared to Wild-Type at all time points
- Total number of basal cells was similar between Wild-Type and Mutant
- Mutant has more total number of suprabasal cells compared to Wild-Type
  - Greater total cells in mutant was due to thicker and denser suprabasal layers

### Percentage of Proliferating Epithelial Cells (BrdU Positive):

- Percent of proliferating basal cells similar between Wild-Type and Mutant and stayed constant at all time points
- Percent of proliferating suprabasal cells generally decreased over the course of embryonic development for both Wild-Type and Mutant
- Mutant generally had higher percentage of proliferating suprabasal cells
  - Increased suprabasal proliferation in e14.5 Wild-Type likely due to formation of stratum intermedium between the basal and periderm layers that proliferates

## Future Directions

- Repeat experiment to increase data size
- Investigate periderm development and impact of IRF6-deficiency on the proliferation of periderm cells

## Acknowledgements

Thank you so much to everyone in the Dunnwald Lab for the training, guidance, and support!

Project supported by IOS2414883 NSF Grant

Thank you to the Secondary Student Training Program and the staff for making this a great experience!

## References

- Biggs, L. C., Goudy, S. L., & Dunnwald, M. (2015). Palatogenesis and cutaneous repair: A two-headed coin. *Developmental Dynamics*, 244(3), 289–310. <https://doi.org/10.1002/dvdy.24224>
- de Lima, R. L. F., Hooper, S. A., Ghassabie, M., Cooper, M. E., Rorick, N. K., Kondo, S., Katz, L., Marasatta, M. L., Compton, J., Bels, S., Heller, U., Dixon, M. J., Daack-Hirsch, S., Borte, O., Bayat, S., Revencia, N., Venetian-Dumoulin, C., Vikkula, M., Richieri-Costa, A., & Moretti-Ferreira, D. (2009). Prevalence and nondistribution of exonic mutations in interferon regulatory factor 6 in 307 families with Van der Woude syndrome and 37 families with pustular psoriasis syndrome. *Genetics in Medicine*, 11(4), 241–247. <https://doi.org/10.1097/gim.0b013e318167a99a>
- Hixon, K., Rhea, L., Standley, J., Canady, F. J., Canady, J. W., & Dunnwald, M. (2016). Interferon regulatory factor 6 controls proliferation of keratinocytes from children with Van der Woude syndrome. *The Cleft Palate-Craniofacial Journal*, 54(3), 281–286. <https://doi.org/10.1597/15-275>
- Ingraham, C. R., Kivohita, A., Kondo, S., Yang, B., Sajen, S., Trout, K. J., Malik, M. I., Dunnwald, M., Goudy, S. L., Lovett, M., Murray, J. C., & Schutte, B. C. (2006). Abnormal skin, limb and craniofacial and morphogenesis in mice deficient for interferon regulatory factor 6 (Irf6). *Nature Genetics*, 38(11), 1335–1340. <https://doi.org/10.1038/ng1909>
- Richardson, R. J., Hammond, N. L., Coulombe, P. A., Salomata, C., Noustainen, H. O., Salonen, R., Berry, A., Hanley, N., Headon, D., Karkoski, R., & Dixon, M. J. (2014). Periderm prevents pathological epithelial adhesions during embryogenesis. *Journal of Clinical Investigation*, 124(9), 3891–3900. <https://doi.org/10.1172/JCI71946>
- Taniguchi, T., Ogasawara, K., Takaoka, A., & Tanaka, N. (2001). IRF family of transcription factors as regulators of host defense. *Annual Review of Immunology*, 19(1), 623–655. <https://doi.org/10.1146/annurev.immunol.19.1.623>
- Zuercher, T. M., Cooper, M. E., Maher, B. S., Daack-Hirsch, S., Negoskovic, B., Ribeiro, L., Capreau, D., Christensen, K., Suzuki, Y., Machida, J., Natsume, N., Yoshida, K., Viera, A. R., Orioli, L. M., Castilla, E. E., Moreno, L., Arcos-Burgos, M., Lidal, A. C., Field, L. L., & Liu, Y. (2004). Interferon regulatory factor 6 (IRF6) gene variants and the risk of isolated cleft lip or palate. *New England Journal of Medicine*, 351(8), 769–780. <https://doi.org/10.1056/nejmoa032609>

BrdU: Thymidine analog incorporated into DNA of cell during replication



# Reevaluating Host-Virus Codivergence in *Polyomaviridae* by Estimating Evolutionary Rates

JENNIFER LIN<sup>1</sup> and ANDREW KITCHEN<sup>2</sup>

<sup>1</sup> St. John's Highschool, Houston, TX <sup>2</sup> Department of Anthropology, University of Iowa

## PURPOSE STATEMENT

The purpose of this study is to explore the validity of the codivergence hypothesis, which assumes viruses have similar evolutionary rates as their hosts, explains the evolution of species in the family *Polyomaviridae*. We estimated the evolutionary rates of polyomavirus species using phylogenetic methods and Bayesian Evolutionary Analysis Sampling Trees (BEAST) software.

## INTRODUCTION

Viruses can serve as genetic markers for both recent and ancient population histories. Polyomaviruses, members of a family of double-stranded DNA viruses, are often thought to evolve through long term codivergence with their host, a process typically associated with low evolutionary rates (Kitchen, 2008). Subsequently, most evolutionary rates for polyomaviruses have been estimated with the use of the codivergence hypothesis. However, research conducted over the past two decades has yielded conflicting results on the validity of the codivergence hypothesis. While studies tracking the Bayesian phylogeography and cophylogenetic signals find strong support for host-virus coevolution (Forni 2020), others find that the evolutionary rates and comparisons of host-virus phylogenies provide no support for codivergence (Shackleton 2006). If polyomaviruses do evolve slowly, as suggested by the codivergence hypothesis, it should be impossible to estimate the evolutionary rate over short sampling times because substitutions would accumulate too slowly. In this study, we aim to estimate the evolutionary rate of Betapolyomavirus Hominis (BKV) and Betapolyomavirus Secuhominis (JCV) independent of the codivergence hypothesis.

## METHODOLOGY

### 1 GATHERING AND ALIGNING GENOMES

Viral genome sequences were downloaded from the National Library of Medicine (i.e., GenBank). Sequences were imported into Jalview and manually aligned to ensure accurate homology. Regulatory sequences, which tend to evolve at different rates than the coding sequences, were cut out to avoid biasing datasets.

### 2 DETERMINING BEST FITTING PRIORS WITH BEAST

We used Bayesian Markov chain Monte Carlo methods in BEAST to estimate evolutionary rates of Betapolyomavirus Hominis (BKV) and JCV. We tested different models with varying complexity by combining strict versus relaxed molecular clocks with either a constant or varying population size to assess the conditions that returned the highest likelihood and effective sample size scores for the Markov chain Monte Carlo. Each analysis used a HKY nucleotide substitution model, a gamma site heterogeneity model, and a Markov chain length of 100 million generations.

### 3 TESTING THE SIGNIFICANCE OF DATA

We used tip-date randomization ( $n = 20$ ) to test the strength of the estimated evolutionary rates (Firth 2011). We then compared the estimated mean evolutionary rate with 95% HPD estimated from twenty data sets with randomized dates. We also used IQ-TREE and TEMPEST to analyze the correlation between root-to-tip distances and sampling time from the phylogenetic tree.

## RESULTS

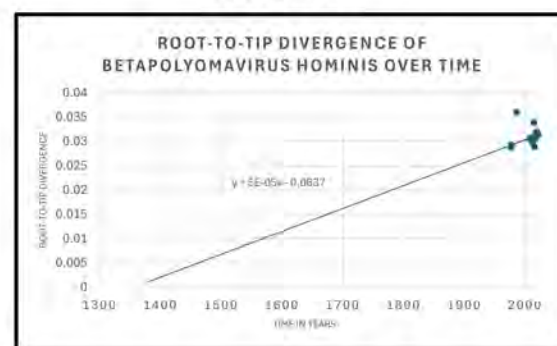


Fig 1. Time informed graph of root-to-tip distance of samples from the phylogenetic tree derived from an IQ-TREE analysis.

We assessed the degree of clock-like evolution by comparing the year to the root-to-tip genetic divergence of each sample, derived from a maximum likelihood tree. The calculated regression shows a weak presence of a molecular clock-like structure in BKV.



Fig 2. Posterior mean (red data point) and the highest posterior density (HPD), which is the shortest interval that contains 95% of all sampled values, and the 20 tip-date randomizations for BKV (blue data points). The mean rate estimated from BKV was significantly different from the randomized sets.

The null hypothesis (of no time structuring of diversity) was rejected when the mean evolutionary rate estimated from the real data did not fall within the 95% HPD of the twenty randomizations. Comparison of the empirical and randomized estimates revealed support for the temporal structure of the estimated evolutionary rate of BKV.

\*Our results for the JCV returned support for the evolutionary rate in comparison to randomizations but a lack of clock like evolution by the root-tip divergence graph found by IQ-TREE.

## CONCLUSIONS

Together, the root-to-tip regression model and randomization tests suggest the presence of a relatively high evolutionary rate in BKV. Our BEAST analysis returned a mean rate of  $1.25 \times 10^{-3}$ , significantly larger than the rates estimated with the codivergence hypothesis at around  $10^{-7}$  -  $10^{-8}$ .

Unlike BKV, JCV returned contrasting results. The randomization tests suggested a strong temporal signal from our empirical rate. However, the IQ-TREE root-tip divergence analysis displayed a negative evolutionary rate in which JCV is displaying regressive evolution. Our results are inconsistent with previous studies, suggesting that there may have been sequencing errors within our downloaded genomes or that a larger dataset of 205 sequences does not demonstrate the same evolutionary trends.

Though polyomavirus evolutionary rates have been tested outside the codivergence hypothesis before, our research contributes further evidence that polyomavirus evolution may be much more complex than the co-divergence hypothesis suggests. These findings present several questions for further research: Could variation in sampling methods, geographic representation, or data quality be influencing the conflicting evolutionary signals observed in JCV? What factors could be driving the relatively high evolutionary rate observed in BKV, and does this reflect genuine biological processes or potential methodological limitations?

## REFERENCES

- Diego Forni, Rachele Cagliani, Mario Clerici, Umberto Pozzoli, Manuela Sironi, You will never walk alone: Codispersal of JC polyomavirus with human populations. *Molecular Biology and Evolution*, 37(2), February 2020, Pages 442–454, <https://doi.org/10.1093/molbev/mz227>
- Kitchen, A., Miyamoto, M. M., & Mulligan, C. J. (2008). Utility of DNA viruses for studying human host history: case study of JC virus. *Molecular phylogenetics and evolution*, 46(2), 673–682. <https://doi.org/10.1016/j.ympev.2007.09.005>
- Codrina Firth, Andrew Kitchen, Beth Shapiro, Marc A. Suchard, Edward C. Holmes, Andrew Rambaut. Using time-structured data to estimate evolutionary rates of double-stranded DNA viruses. *Molecular Biology and Evolution*, 27(9), September 2010, Pages 2038–2051. <https://doi.org/10.1093/molbev/mq088>
- Larsen, B. B., Cole, K. L., & Worobey, M. (2018). Ancient DNA provides evidence of 27,000-year-old papillomavirus infection and long-term codivergence with rodents. *Virus evolution*, 4(1), vey014. <https://doi.org/10.1093/ve/vey014>
- Shackleton, L. A., Rambaut, A., Pybus, O. G., & Holmes, E. C. (2006). JC virus evolution and its association with human populations. *Journal of virology*, 80(20), 9926–9933. <https://doi.org/10.1128/JVI.00441-06>



# Effectiveness of Rimonabant to Induce Weight Loss in Mice

## Foundation to Evaluate a Safer Version of Rimonabant

Siegfried Liu, Aviva Fraer, Yi Chu, Mohammad Mokadem

### Introduction

Rimonabant is a class of Cannabinoid Receptor-1 (CB1) Blocker (Henness et al., 2006). Its properties give the drug a way to bind to the nervous system and regulate glucose and lipid metabolism. This allows it to have the potential to become a weight loss medication.

In 2006, Europe gave licensing to rimonabant. However, it quickly rescinded due to concerns around serious psychiatric side effects (Henness et al., 2006).

A new revised version of the drug limits its binding ability only to the peripheral nervous system to mitigate the adverse effects (Fulp et al., 2016). The new drug's efficacy in inducing weight loss is still being researched.

### Objective

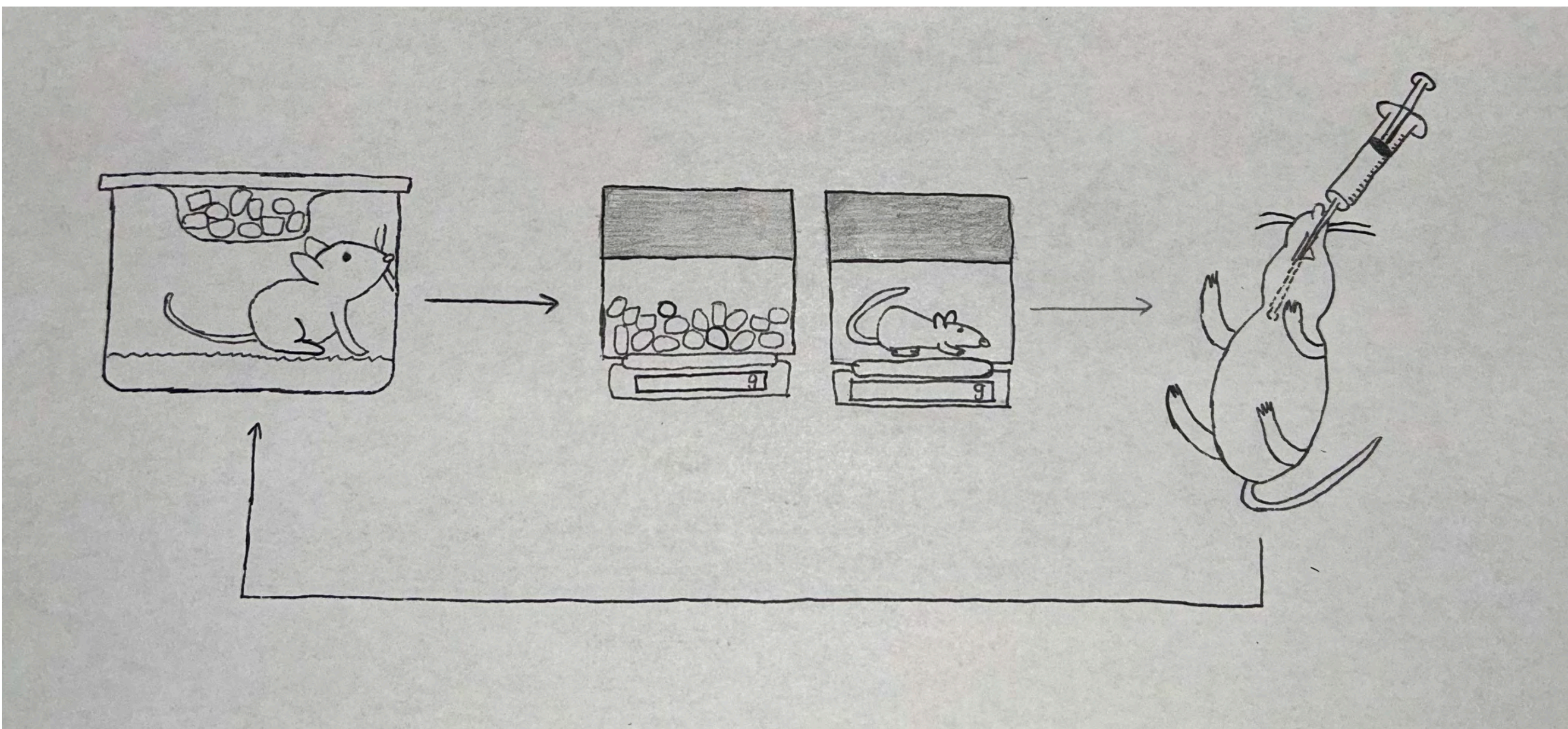
This study aims to confirm rimonabant's ability to induce weight loss in mice and explore how male/female wild type/knock out mice reacts to the medication differently. The results would be the foundation to compare the revised weight loss medication in follow up experiments.

### Methods

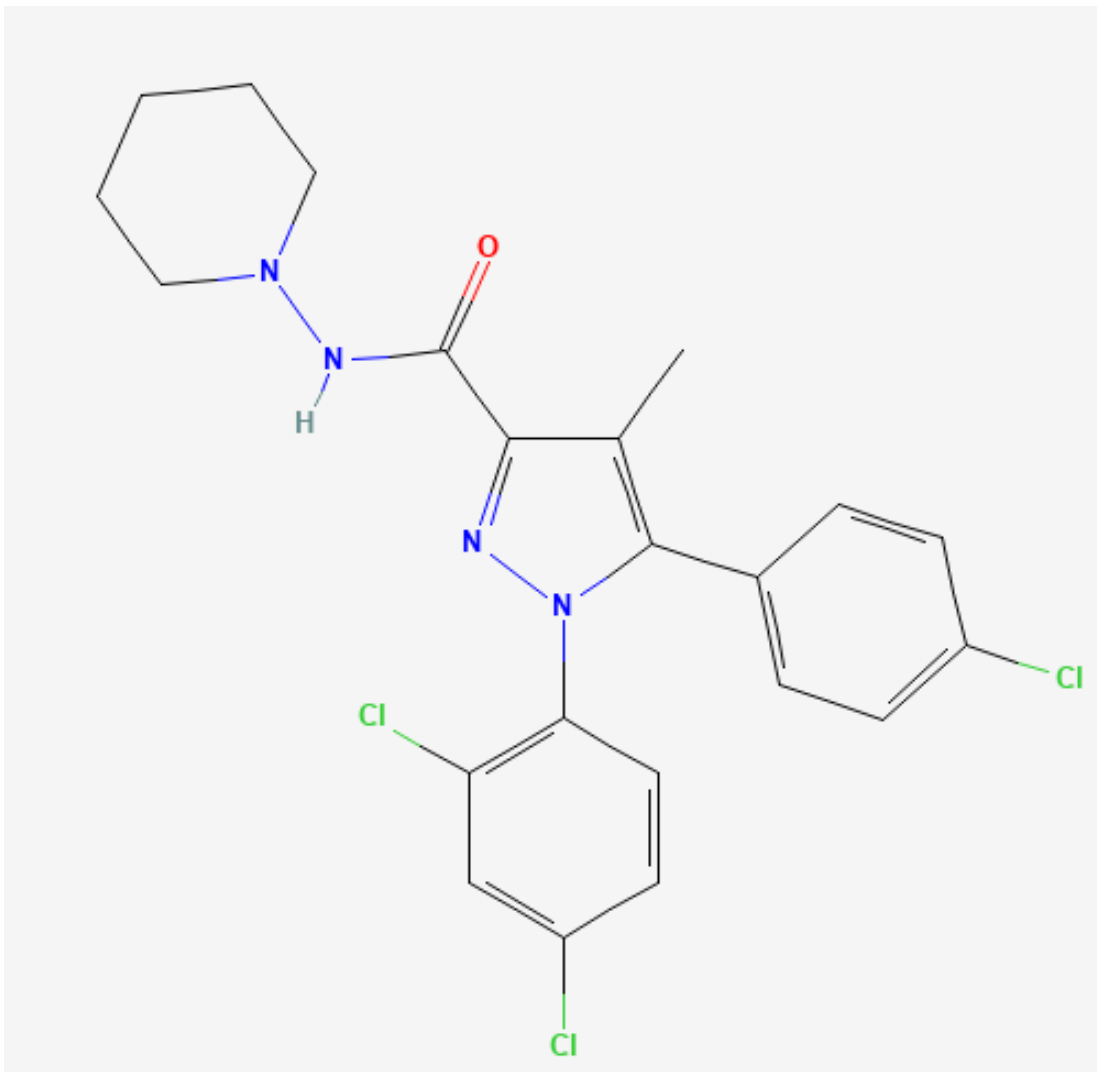
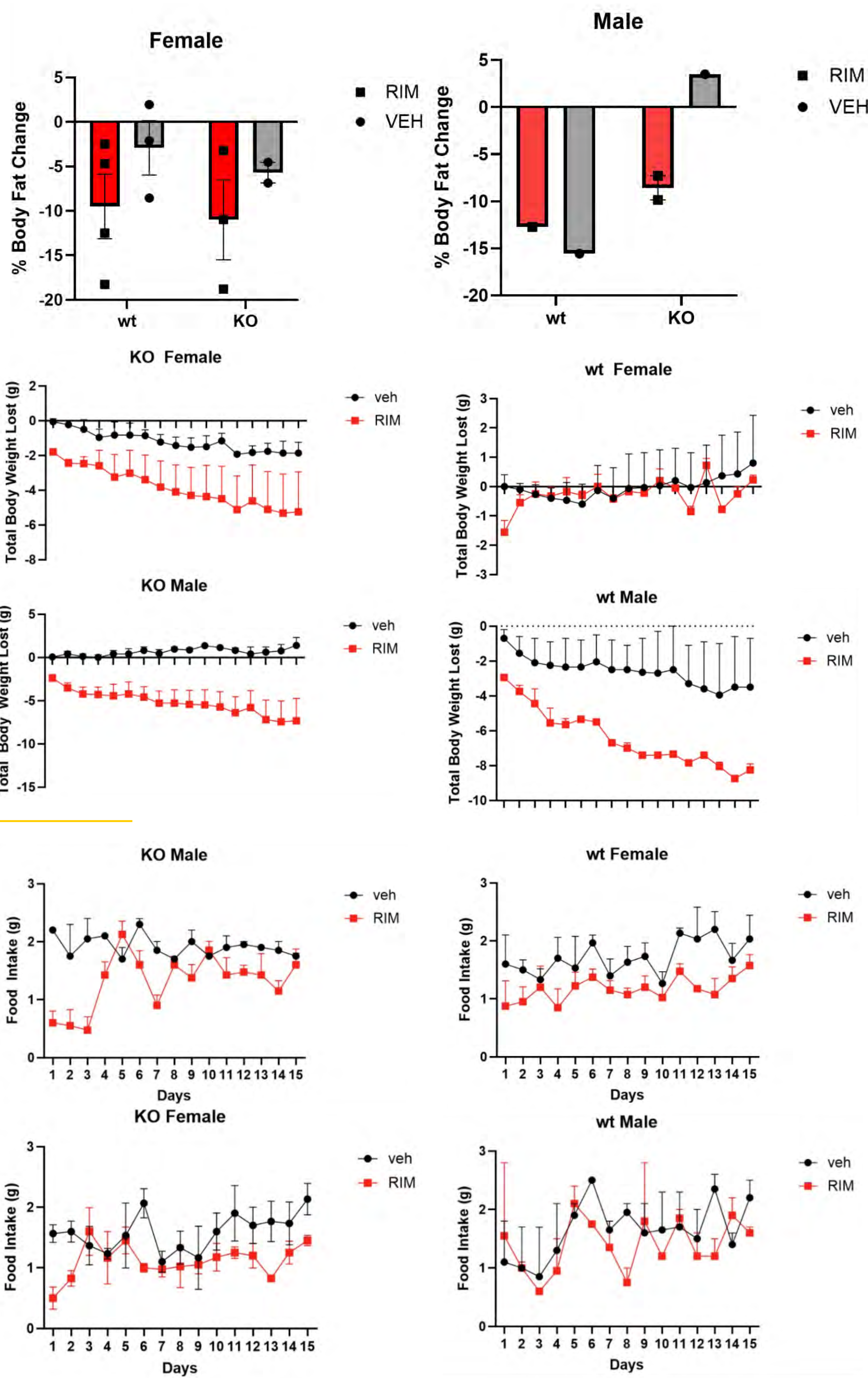
24 C57BL/6J mice, 7 wild type female, 7 knock out female, 5 wild type male, and 5 knock out male, were distributed into control group with 10 mice, and experimental group with 14 mice.

The control mice and experimental mice were both gavaged 1ml/g body weight of vehicle (corn oil) and rimonabant respectively over the span of 20 days.

Their body weight and food weight were measured daily.



### Results



### Conclusion

The results confirms rimonabant's ability to induce weight loss in mice. Knock Out/wild type and male/female are elements that influence mice's response to high fat diet and rimonabant. The primary weight loss in mice is fat composition in both male and female mice

### Discussion

Rimonabant's ability to induce weight loss in mice is shown. Since it is the same version of the medication that was approved in 2006, and later a revised version of the drug reduced psychiatric side effects, the next step is to gavage mice with the new medication and compare the results to the results of this study

### Acknowledgments

I want to thank Dr. Mohamad Mokadem for being my mentor and guiding me throughout the program. Thank you to Aviva Fraer for demonstrating lab techniques and how to analyze statistics for the research project. Finally, a thank you to Dr. Yi Chu for being always in the lab and supporting me through various lab assignments.

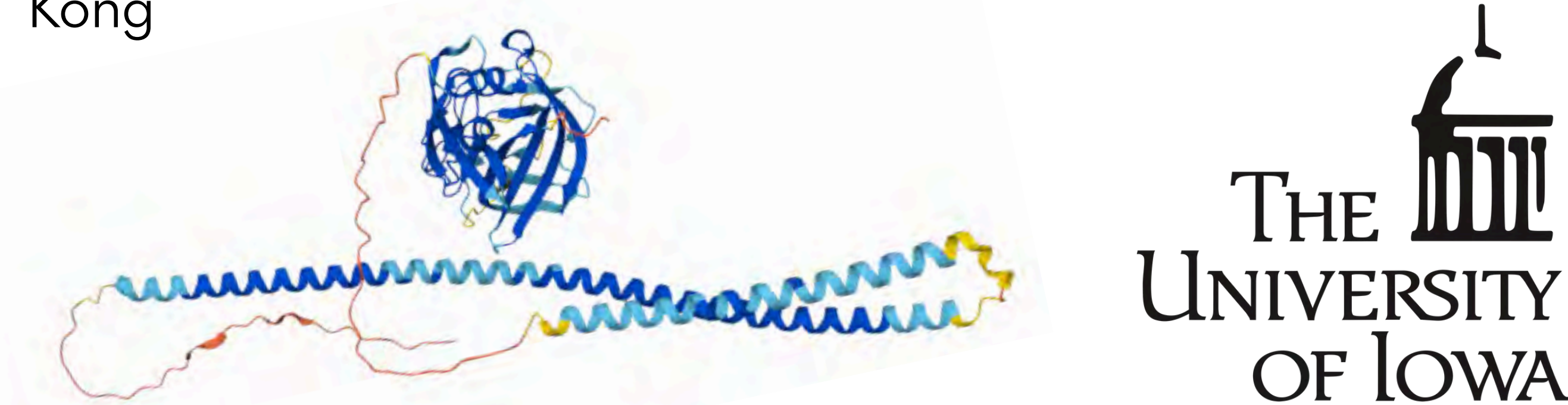
### References

- Fulp, A., Zhang, Y., Bortoff, K., Seltzman, H., Synder, R., Wiethe, R., Amato, G., Maitra, R. (2016). Pyrazole antagonists of the CB1 receptor with reduced brain penetration. *Bioorganic & Medicinal Chemistry*, 24(5), 1063-1070. <http://doi.org/10.1016/j.bmc.2016.01.033>
- Henness, S., Robinson, D.M. & Lyseng-Williamson, K.A. (2006). Rimonabant. *Drugs* 66, 2109-2119 <https://doi.org/10.2165/00003495-200666160-00006>
- National Center for Biotechnology Information (2025). PubChem Compound Summary for CID 104850, Rimonabant. Retrieved July 18, 2025 from <https://pubchem.ncbi.nlm.nih.gov/compound/Rimonabant>



# Identify Functional Consequences of Human Variants in ANGPTL3

Jiashu Luan<sup>2</sup>, Sonja Smith<sup>1</sup>, Sydney Walker<sup>1</sup>, Hattie Ruhland<sup>1</sup>, Samara Goltz<sup>1</sup>, Grace Early<sup>1</sup>, Alex Dumas<sup>1</sup>, Max Mercer<sup>1</sup>, Brandon Davies<sup>1</sup>  
<sup>1</sup>University of Iowa, Department of Biochemistry and Molecular Biology, <sup>2</sup>The Independent Schools Foundation Academy, Hong Kong



## Background

- **High-density lipoprotein (HDL)**, known as “the good cholesterol”, removes cholesterol from the bloodstream.
- **Very-low-density lipoprotein (VLDL)** and **chylomicrons** transport **triglycerides** in the bloodstream.
- **Endothelial lipase (EL)** hydrolyzes HDL.
- **Lipoprotein lipase (LPL)** hydrolyzes triglyceride-rich lipoproteins.
- **Angiopietin-like 3 (ANGPTL3 or A3)** forms a **homotrimer** to **inhibit LPL** activity, increasing plasma triglyceride levels.
- **A3** forms a **heterotrimer** with **A8** to **inhibit EL** activity.<sup>1</sup>
- **A3 deficiency** is associated with a **lower cardiovascular disease risk (CDR)**.<sup>2</sup>

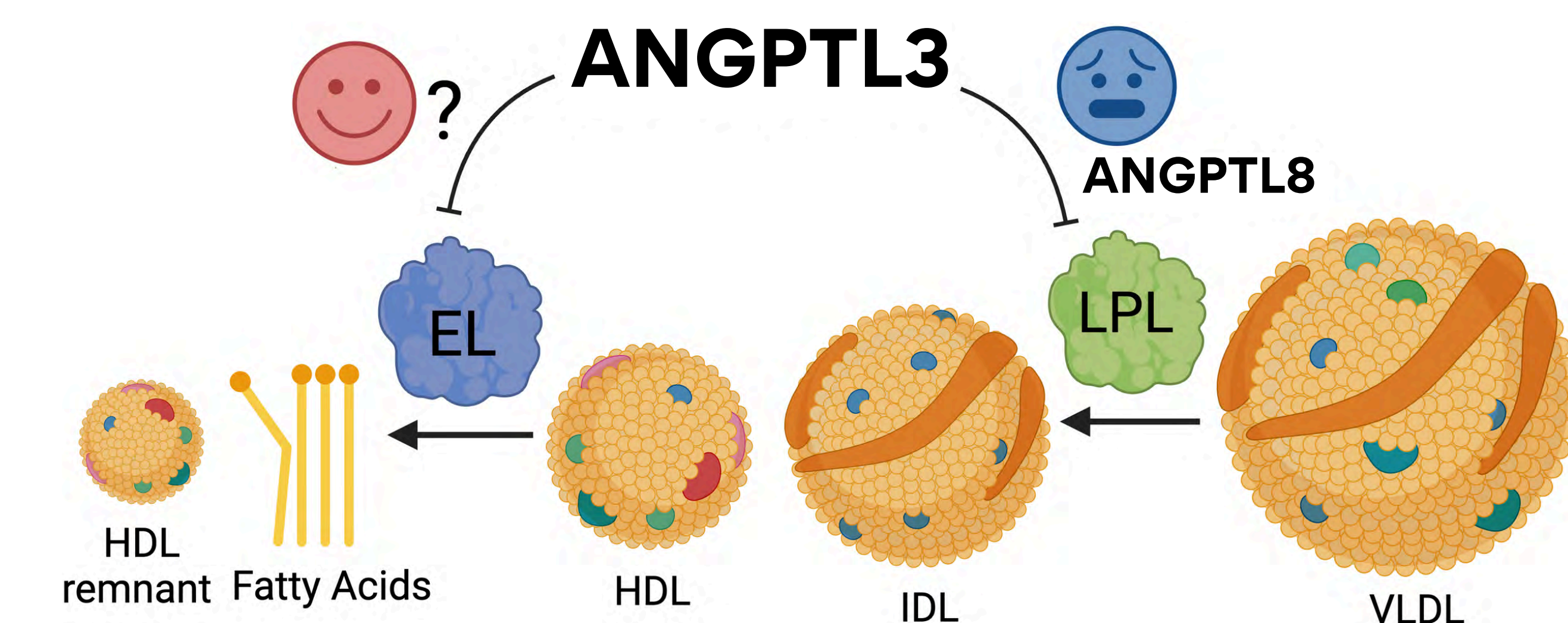
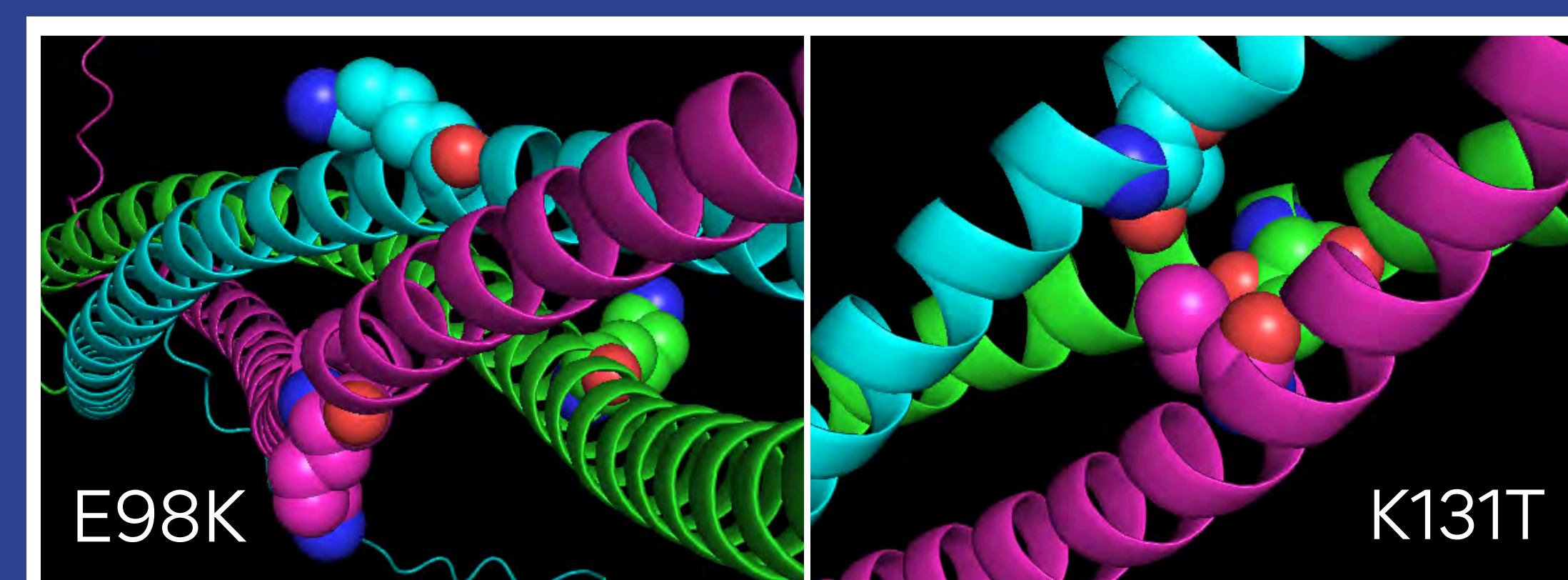


Figure 1. ANGPTL3 inhibits EL and LPL

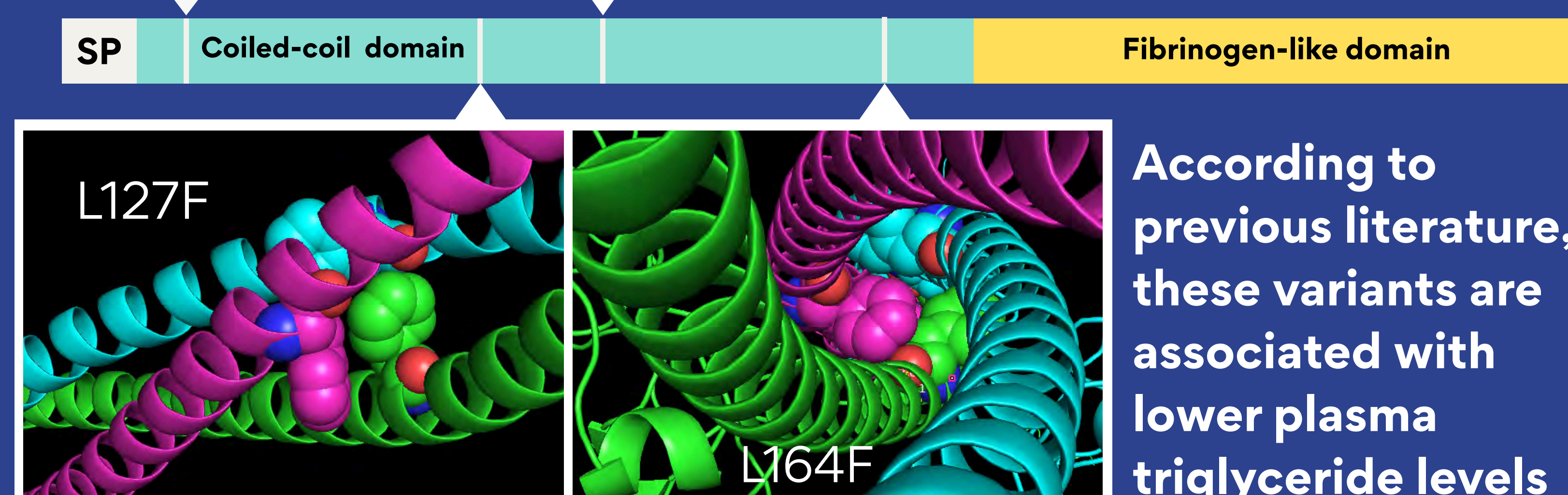
## Acknowledgements

Special thanks to Dr. Davies, Sonia, Sydney, Hattie, Samara, Grace, Alex, and Max for their guidance and encouragement! Thank you for explaining and demonstrating all the experiments until I understood, and for inspiring me to be a researcher. Special thanks to the University of Iowa and the Belin-Blank Center for this valuable opportunity.

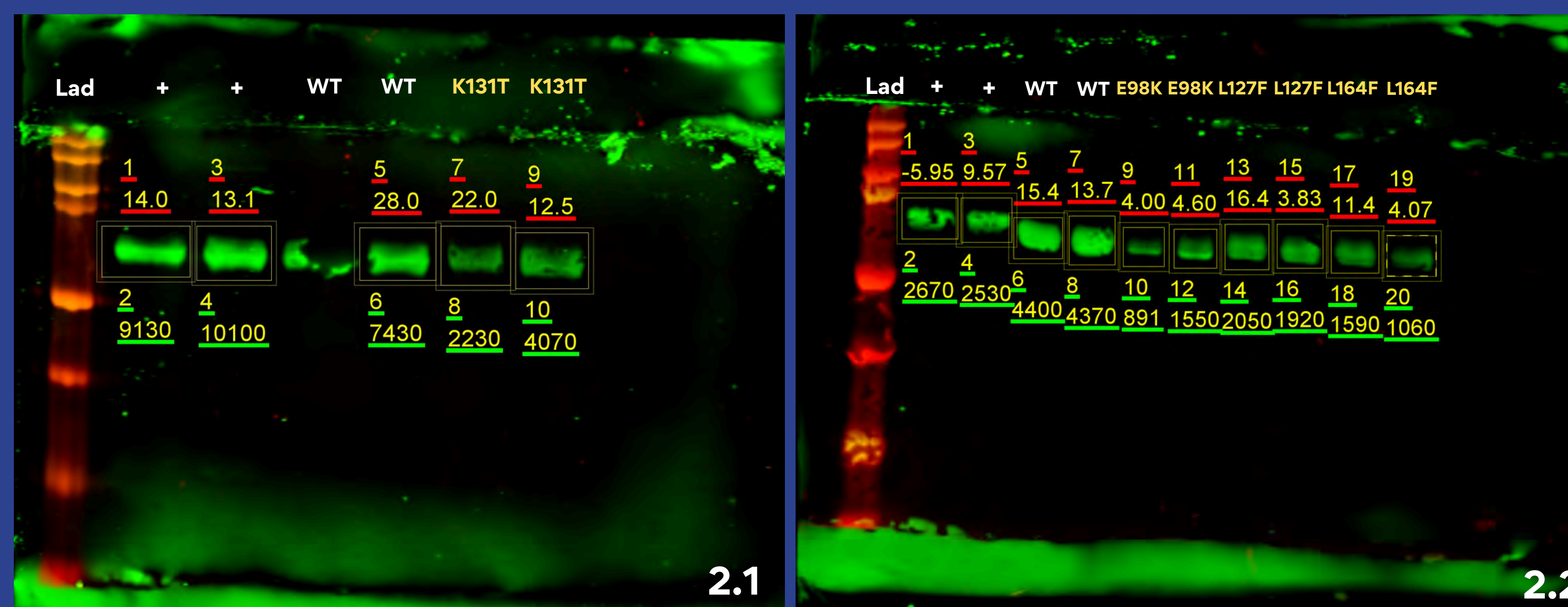
# The human variants E98K, L127F, and L164F exhibit significantly reduced EL inhibition activity compared to wild-type ANGPTL3



Four human variants located in the N-terminal coiled-coil domain of ANGPTL3 were selected for this project



According to previous literature, these variants are associated with lower plasma triglyceride levels



Figures 2.1 and 2.2 Western blot analysis of the human variants: all ANGPTL3 variants were expressed and secreted

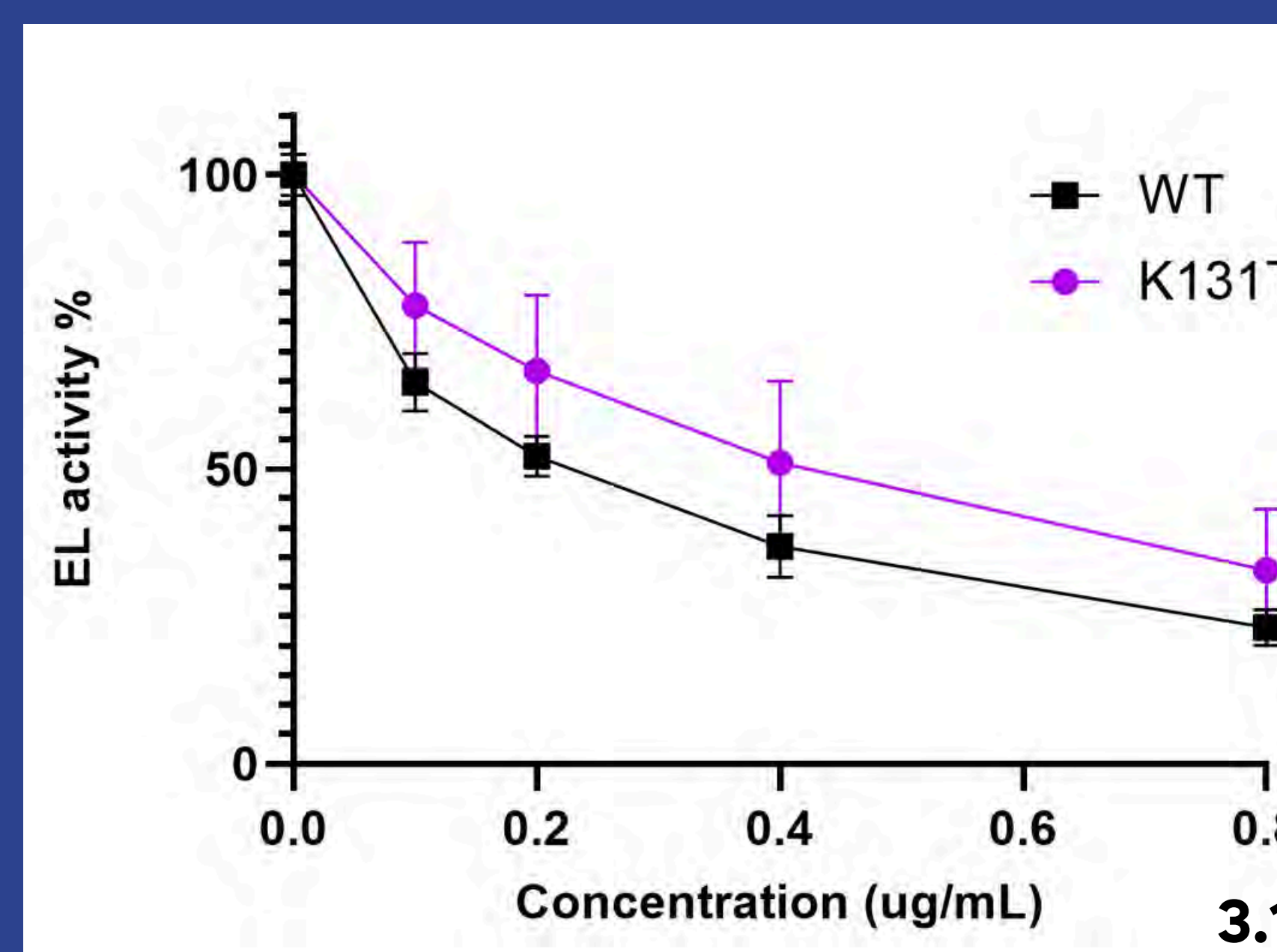


Figure 3.1 Comparison of EL inhibition activities between K131T and wild type (WT)

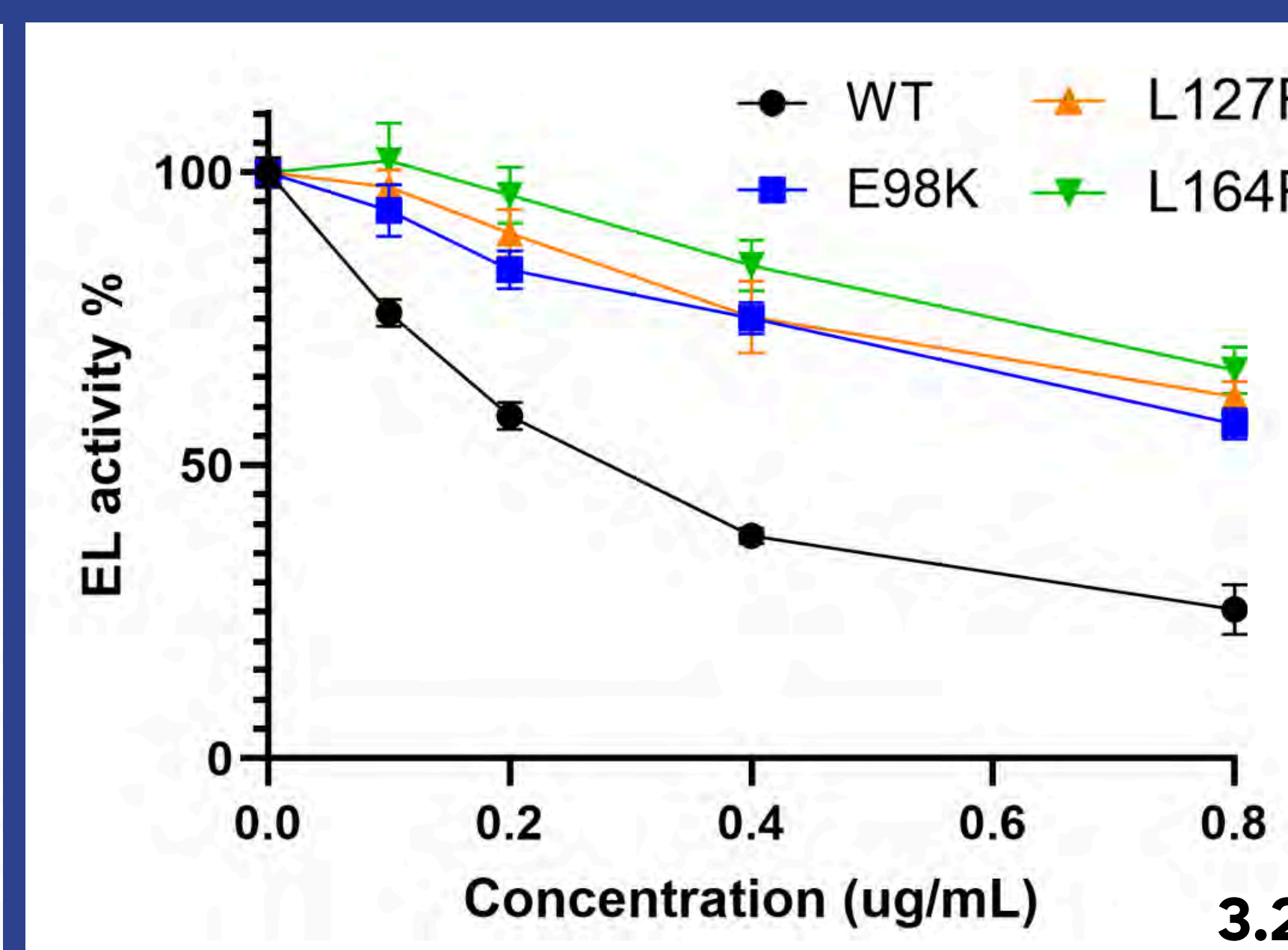
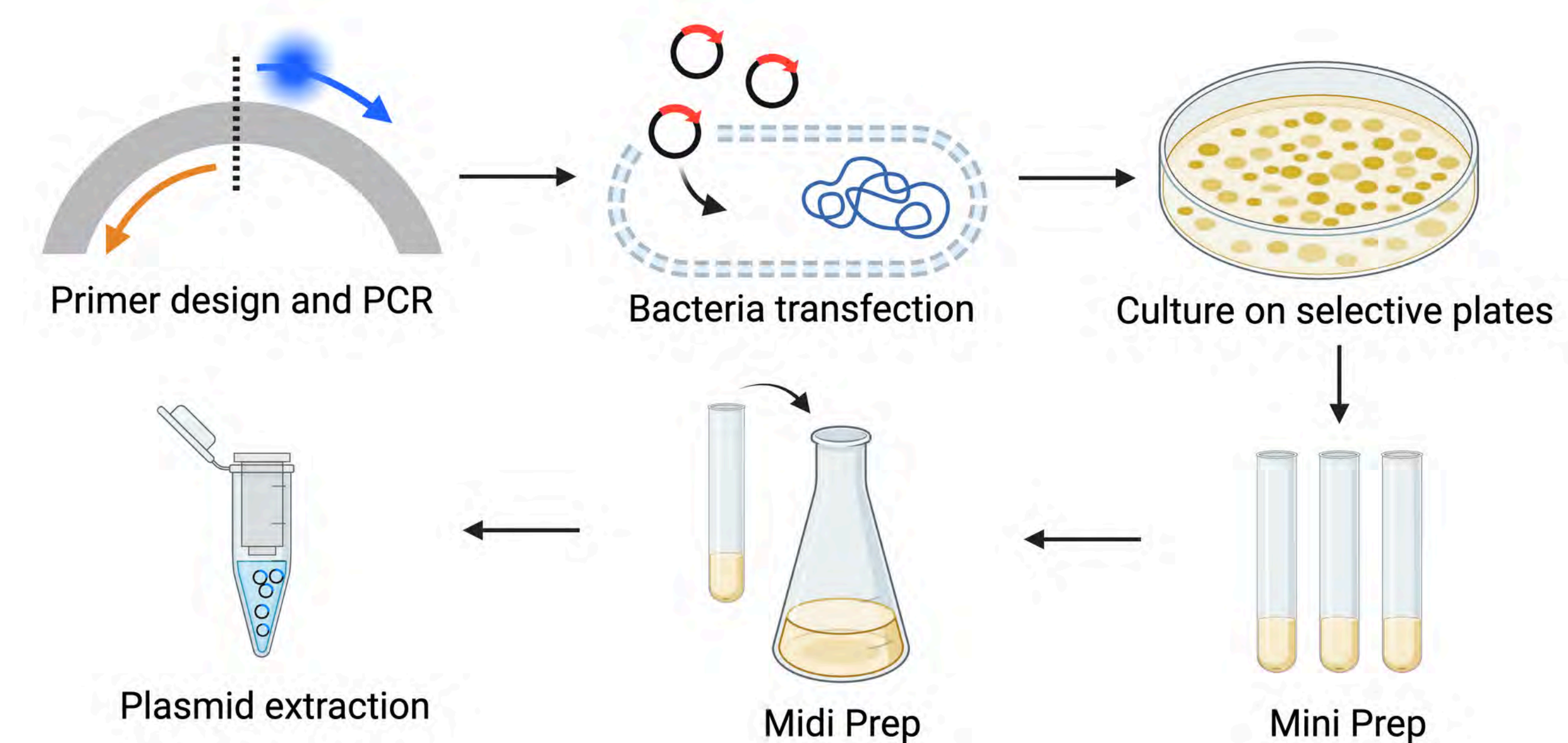


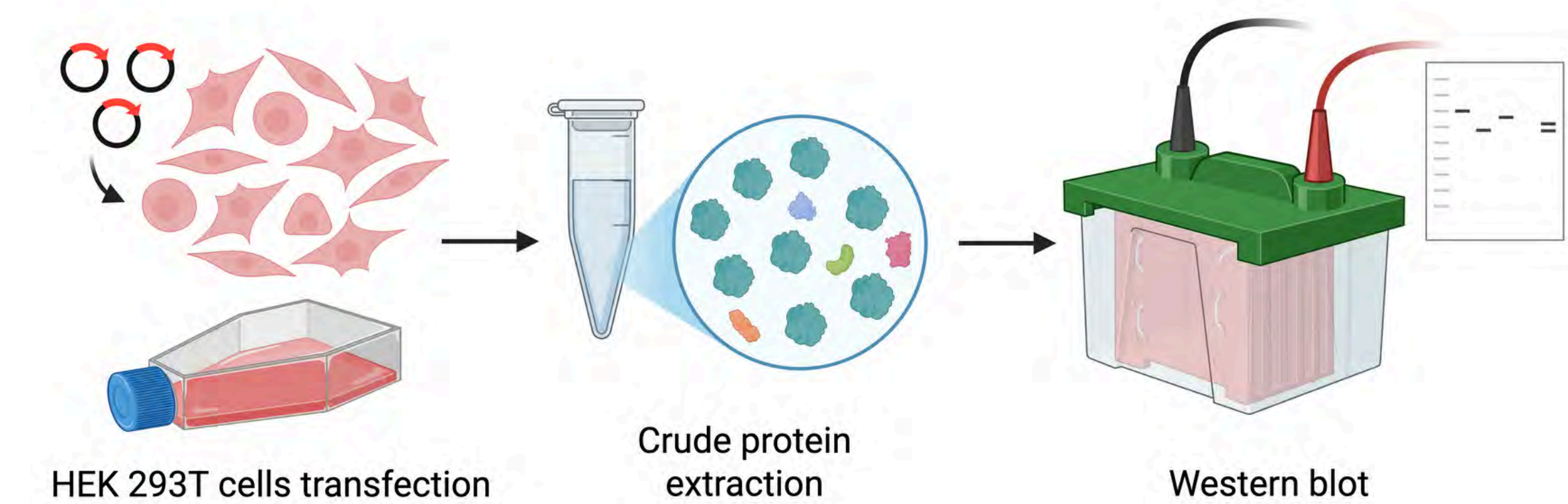
Figure 3.2 Comparison of EL inhibition activities between E98K, L127F, L164F and WT

## Methodology

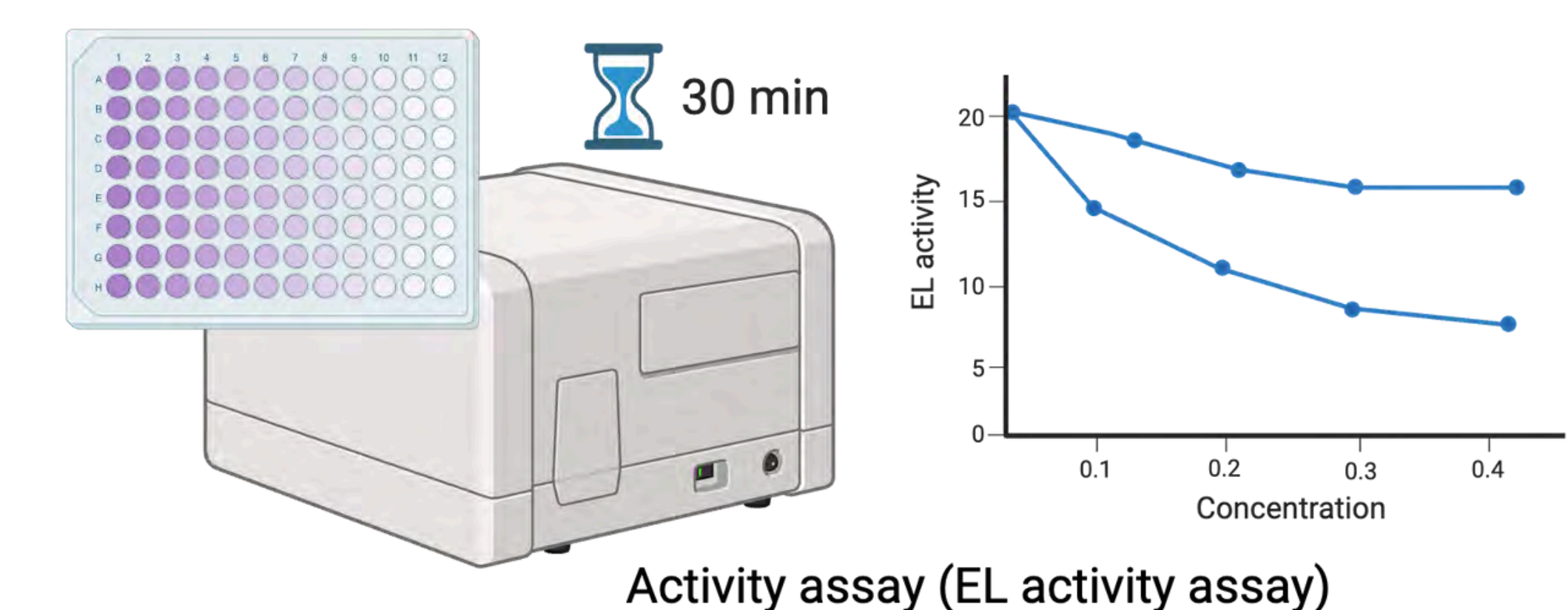
### Site-directed mutagenesis



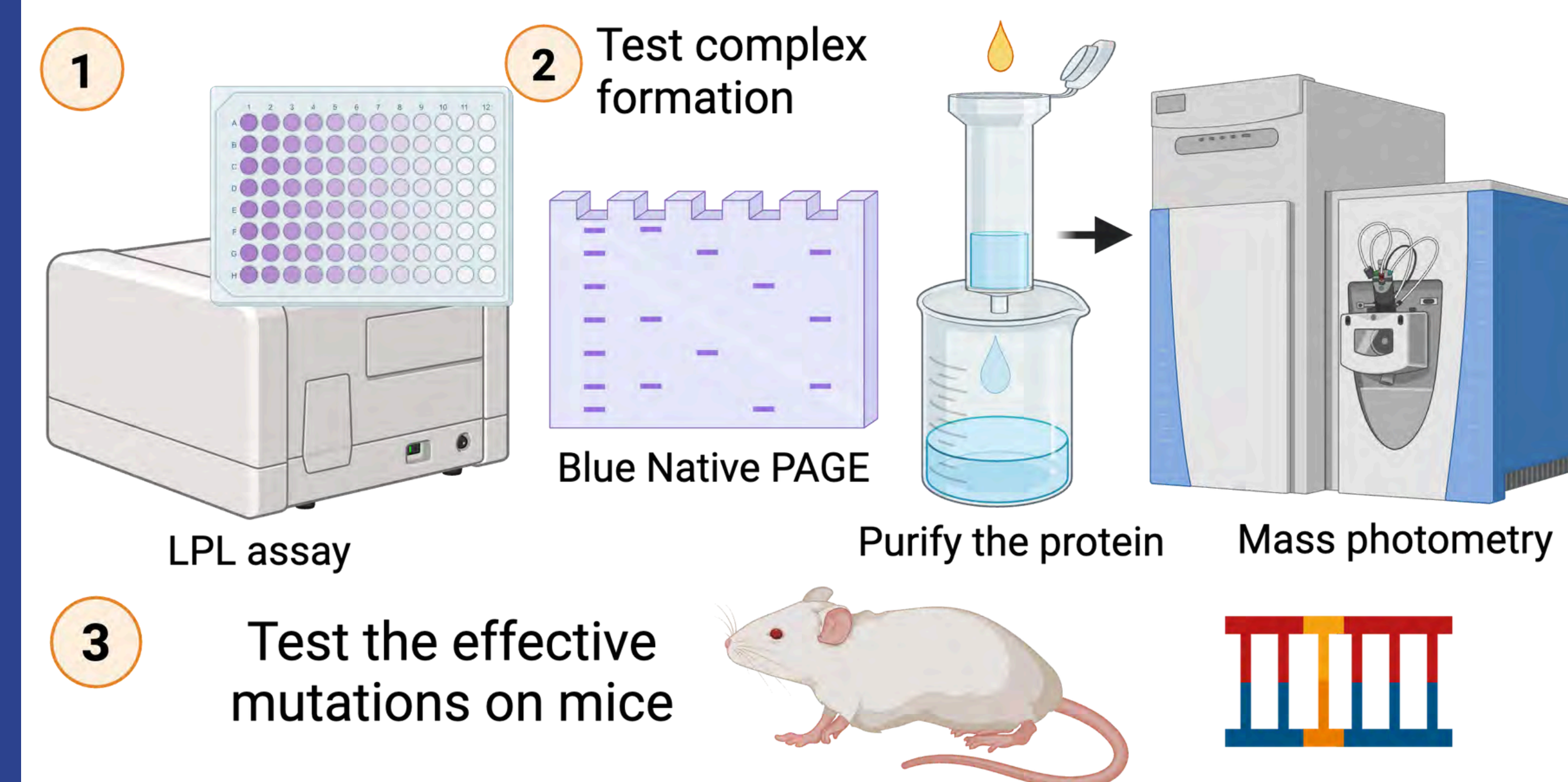
### Collect the ANGPTL3 variants



### ANGPTL3 activity assay



## Future Direction



## Reference

1. Sylvers-Davie, K.L. and Brandon (2021). Regulation of lipoprotein metabolism by ANGPTL3, ANGPTL4, and ANGPTL8. *AJP Endocrinology and Metabolism*, 321(4), pp.E493–E508. <https://doi.org/10.1152/ajpendo.00195.2021>.
2. Dewey, F.E., Viktoria Gusarova, Dunbar, R.L., Colm O'Dushlaine, Schurmann, C., Gottesman, O., McCarthy, S., Van, C.V., Bruse, S., Dansky, H.M., Leader, J.B., Murray, M.F., Ritchie, M.D., Kirchner, H.L., Habegger, L., Lopez, A., Penn, J., Zhao, A., Shao, W. and Stahl, N. (2017). Genetic and Pharmacologic Inactivation of ANGPTL3 and Cardiovascular Disease. *New England Journal of Medicine*, 377(3), pp.211–221. <https://doi.org/10.1056/nejmoa1612790>.



# Developing a Graphical User Interface for Accessible Measurement of Ankle-Foot Orthosis Stiffness

Mark Menaker<sup>1</sup>, Katherine Vaiciulis MS<sup>2</sup>, Deema Totah PhD<sup>2</sup>

<sup>1</sup>University High School, Irvine CA, <sup>2</sup>Mechanical Engineering, University of Iowa, Iowa City IA



## Introduction

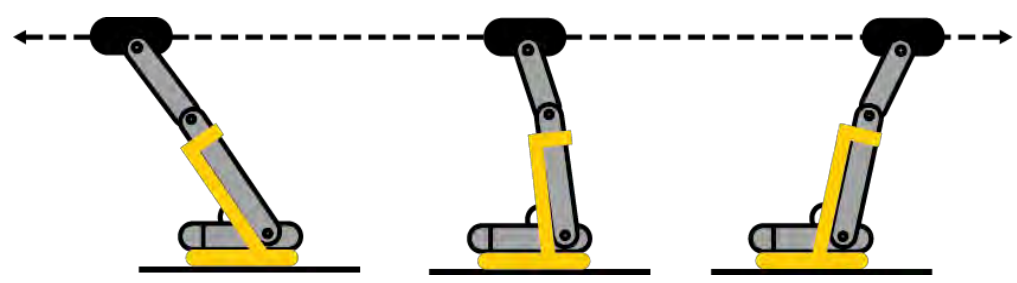
Ankle-foot orthoses (AFOs) are prescribed to individuals with gait impairments to support the ankle while walking.

### Stiffness Testing

- Stiffness is a key factor in determining the support an AFO provides, but universal testing and reporting standards do not exist, complicating research on inter-method reliability<sup>1</sup> and the effect that AFO stiffness has on gait<sup>2</sup>
- Devices such as the Stiffness Measurement Apparatus (SMAp)<sup>3</sup> can measure stiffness but are mainly limited to research settings
- A graphical user interface (GUI) can improve the accessibility of testing methods, allowing for further research on measuring AFO stiffness and use in clinical environments



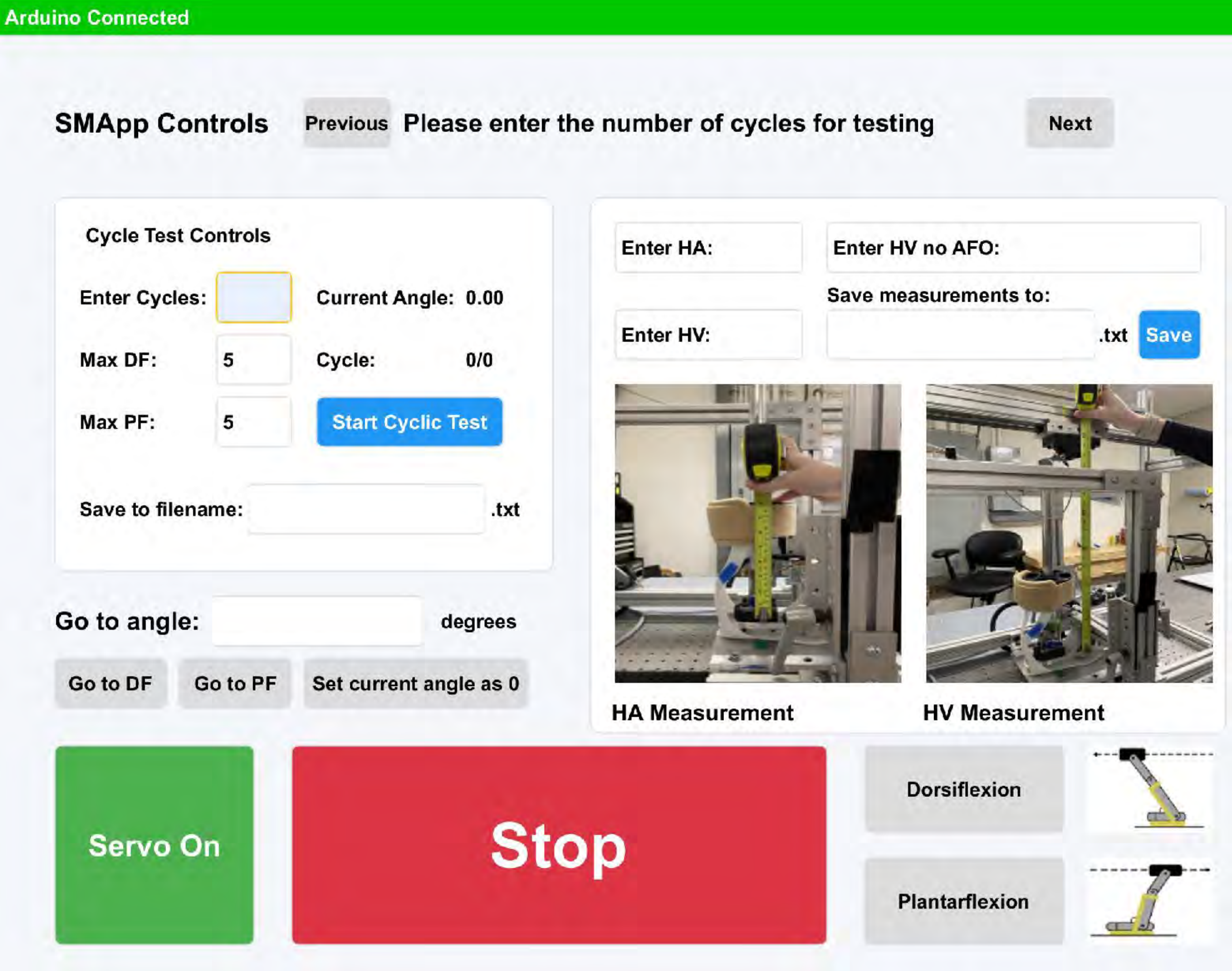
A sample thermoplastic AFO



Schematic of the SMAp measuring AFO stiffness

## Required Functionality

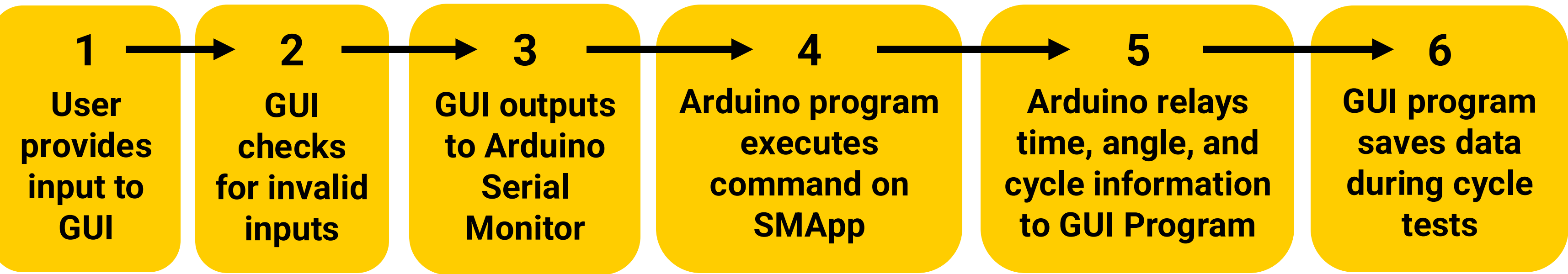
- Conduct AFO stiffness testing – user input for number of cycles and angle boundaries
- Save cyclic test data and AFO dimension data to text files
- Move the SMAp to a user-specified ankle angle
- Recalibrate and set current angle to zero
- Move the SMAp in PF (leg angled backward) or DF (leg angled forward)
- Turn on and turn off the servo motor



## Additional Features

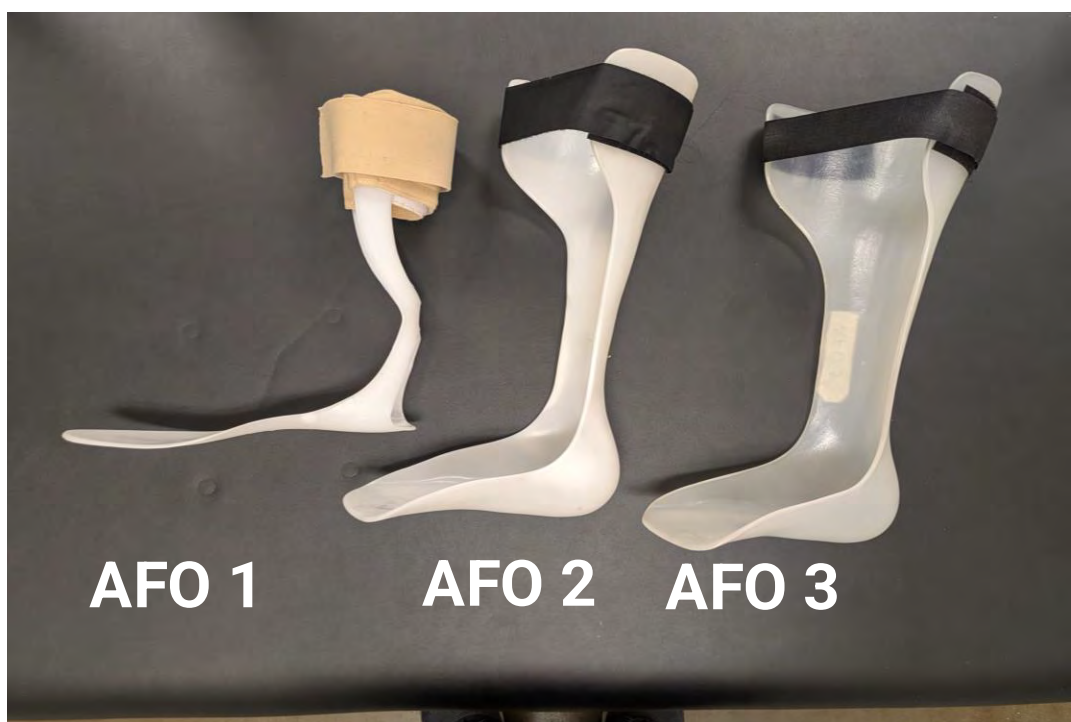
- Instructions to guide unfamiliar users through device loading and operation
- Minimal modifications to the code for device operation
- Implement safeguards to prevent incorrect commands being sent to the device operation program and display informative error messages through the GUI

## Control Flow



## Reliability Testing

Due to various updates to the SMAp since its original design<sup>3</sup>, it was tested with three different AFOs to ensure consistency of results between multiple operators.



	$\Delta$ Stiffness [Nm/deg]	
	DF	PF
AFO1	0.00	-0.02
AFO2	0.17	-0.20
AFO3	0.09	-0.08

Differences ( $\Delta$ ) in dorsiflexion and plantarflexion stiffness between two operators were below 0.2 Nm/Deg

Quantified: Intraclass Correlation Coefficient (ICC), Standard Error of Measurement (SEM), Minimum Detectable Difference (MDD)<sup>3</sup>

	DF	PF
ICC values [95% confidence intervals]	1.00 [0.87-1.00]	1.00 [0.94-1.00]
SEM [Nm/deg]	0.10	0.11
MDD [Nm/deg]	0.27	0.30

- An ICC > 0.9 is considered good for clinical measures<sup>3</sup>

## Conclusion and Impact

The GUI successfully implements all functions of the SMAp, **obtains the same results as the original command-line interface**, and makes it easier and quicker to operate the device.

- Greater Access:** The intuitive nature of the GUI makes it possible for non-engineers like doctors and physiotherapists to measure stiffness of the AFOs they research or prescribe
- Impact:** Greater access to stiffness measurement can lead to standardized testing and reporting procedures, allowing for a consensus when designing and prescribing AFOs, which currently does not exist
- Reliability:** The SMAp demonstrated excellent between-operator reliability

## Acknowledgments

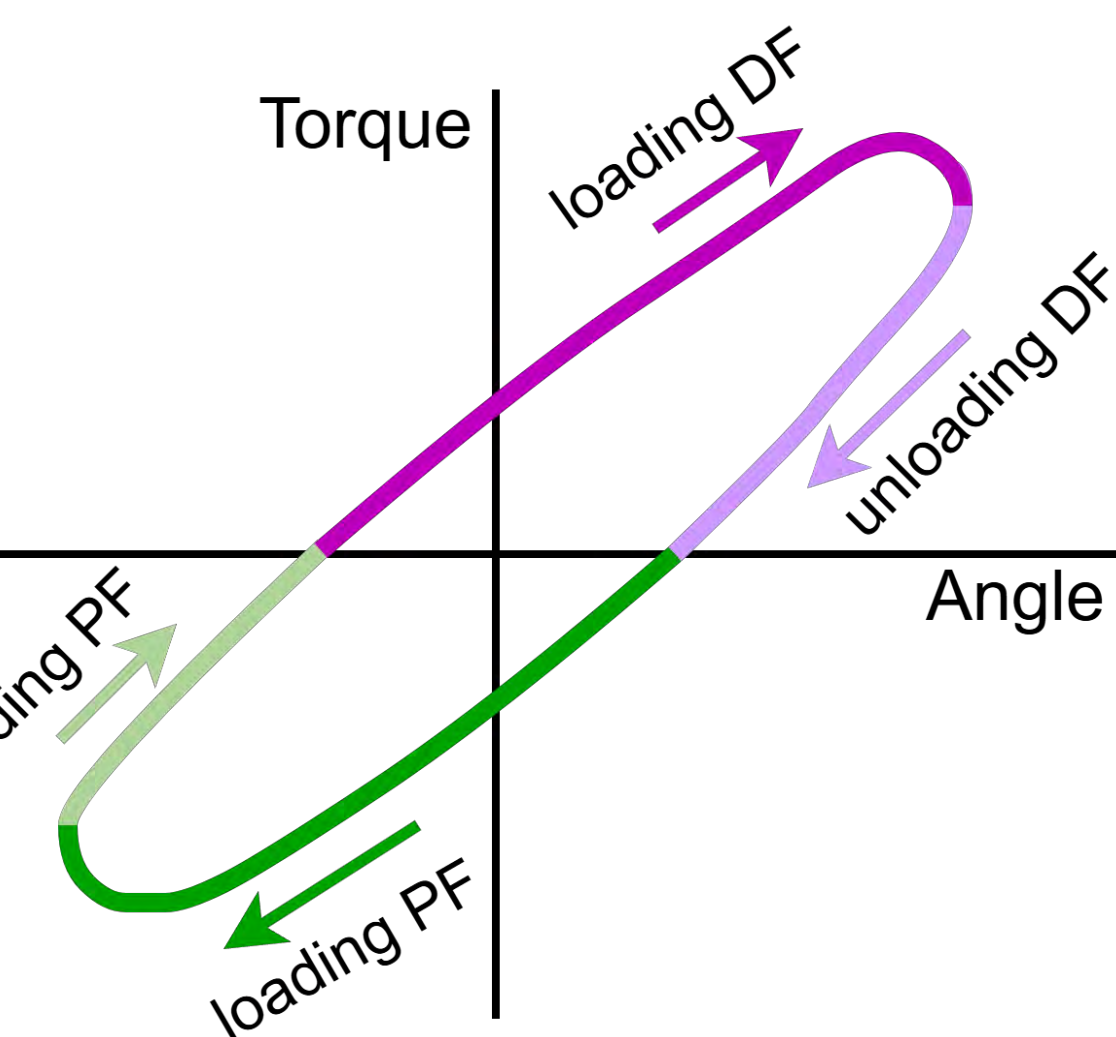
I would like to express my gratitude to my mentors for their valuable advice. This project was partially supported by start-up funds from the University of Iowa, and the Belin-Blank Center's Secondary Student Training Program.

## References

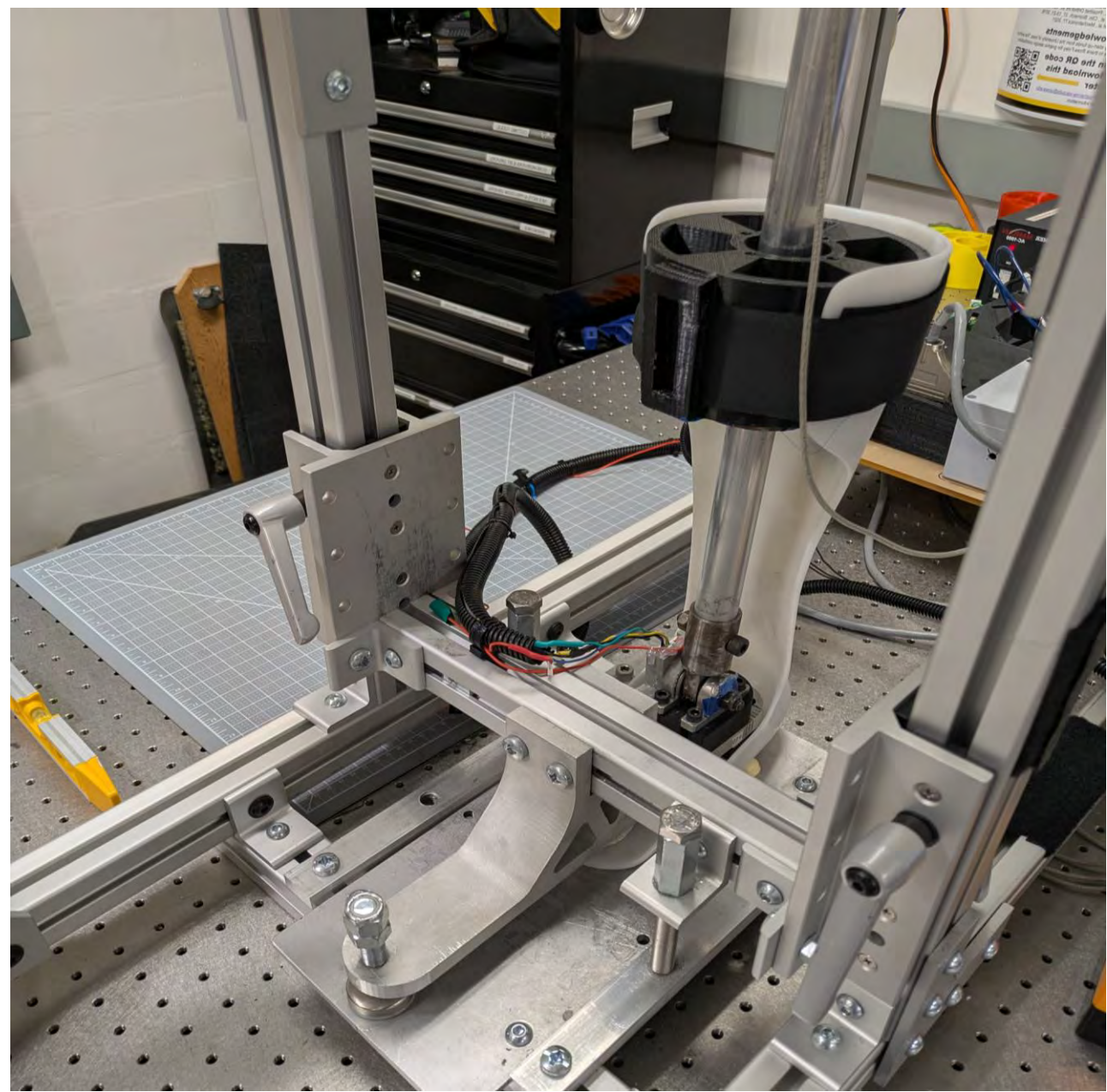
- Shuman, B.R., Totah, D., Gates, D.H. et al. Comparison of five different methodologies for evaluating ankle-foot orthosis stiffness. Journal of Neuroengineering and Rehabilitation, 20(1), 11–11 - <https://doi.org/10.1186/s12984-023-01126-7>
- Totah, D., Menon, M., Jones-Hershinow, C., Barton, K., & Gates, D. H. (2019). The impact of ankle-foot orthosis stiffness on gait: a systematic literature review. Gait & Posture, 69, 101-111. - <https://doi.org/10.1016/j.gaitpost.2019.01.020>
- Totah, D., Menon, M., Gates, D. H., & Barton, K. (2021). Design and evaluation of the SMAp: a stiffness measurement apparatus for ankle-foot orthoses. Mechatronics, 77, 102572. - <https://doi.org/10.1016/j.mechatronics.2021.102572>

## Research Objectives

The purpose of this project is to develop a **graphical user interface** to improve the usability of the SMAp for testing ankle-foot orthoses. Using code in Arduino and Processing, the interface is designed to **improve accessibility** to this tool for non-engineers, such as doctors and physiotherapists. Additionally, the SMAp will be evaluated by multiple operators in the lab to ensure **inter-operator reliability**.



Schematic of the torque-angle curve measured by the SMAp. DF and PF stiffness are calculated as the slope of the loading portions.



An AFO loaded in the SMAp. The SMAp cycles the AFO through dorsiflexion (DF) and plantarflexion (PF) while collecting force and ankle angle data.





# Using Synthetic Biology and Metabolic Engineering Techniques to Produce Polyhydroxybutyrate Bioplastic in *Escherichia coli*

Harshavardhan Narayan<sup>a</sup>, Hyeongmin Seo, PhD<sup>b</sup>

a. Detroit Country Day School, Beverly Hills, MI

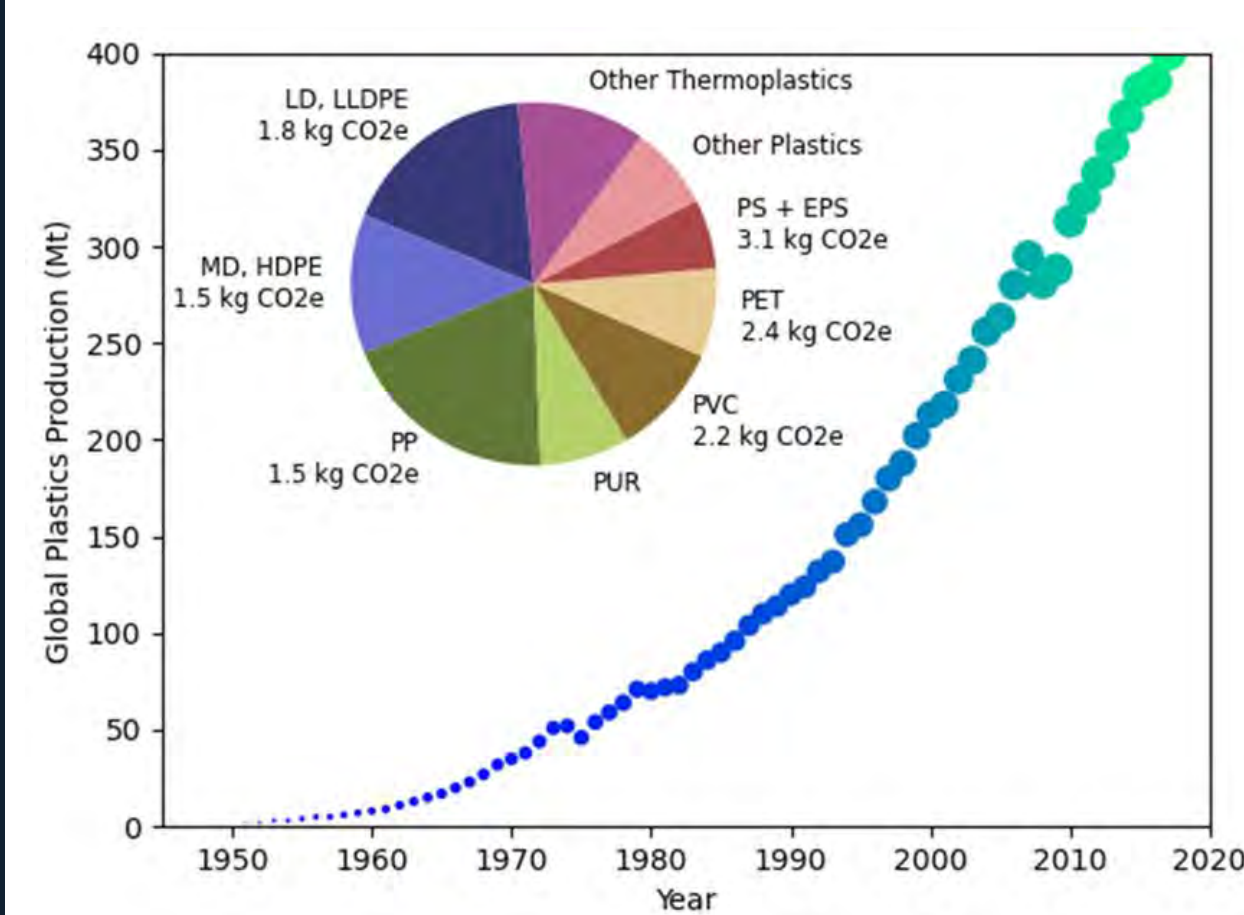
b. Department of Chemical and Biochemical Engineering, University of Iowa



## Abstract

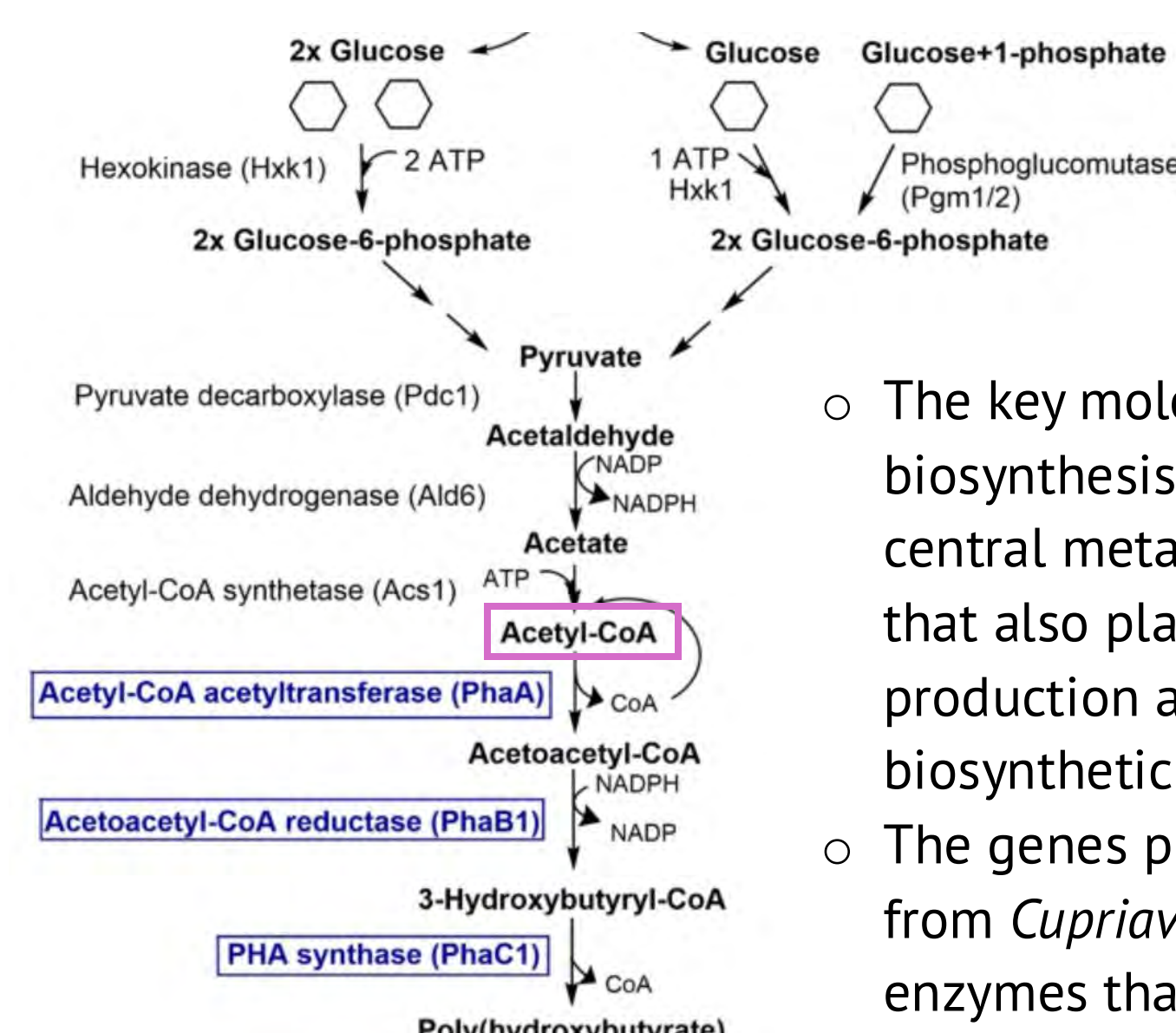
Polyhydroxybutyrate (PHB) is a biodegradable plastic with potential to replace petroleum-based materials (Sun Mi Lee et al., 2021). This project aimed to engineer *E. coli* to produce PHB by introducing the phaA, phaB, and phaC genes from *Cupriavidus necator* into the pACYCDuet plasmid (Ylinen et al., 2022). Gene fragments were assembled using Gibson Assembly with overlap PCR and DpnI digestion to improve accuracy. Colony PCR and gel electrophoresis confirmed correct insertion, and transformation into *E. coli* was successful. Expression was induced, and preliminary visual differences suggested PHB production.

## Introduction

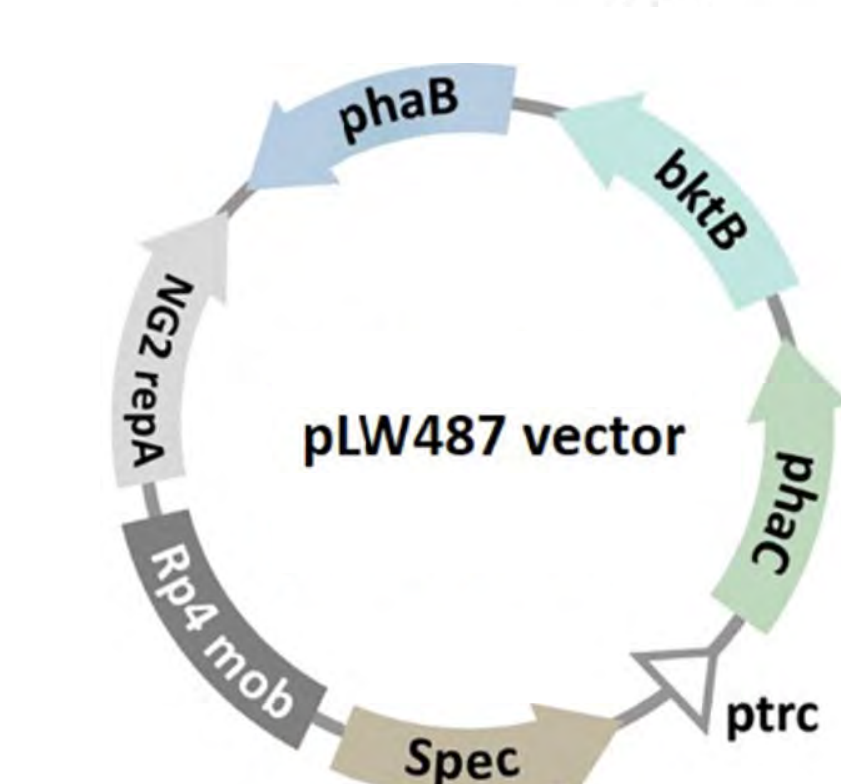


- Global plastic production has been increasing ever since it was invented, heavily polluting the environment
- Solving this issue will require multiple innovative approaches from many different fields

- Polyhydroxybutyrate (PHB) is a biodegradable bioplastic naturally produced by some bacteria as an energy storage compound



- The key molecule for PHB biosynthesis is acetyl-CoA, a central metabolic intermediate that also plays a role in energy production and other biosynthetic pathways
- The genes phaA, phaB, and phaC from *Cupriavidus necator* code for enzymes that convert acetyl-CoA into PHB (Ylinen et al., 2022)

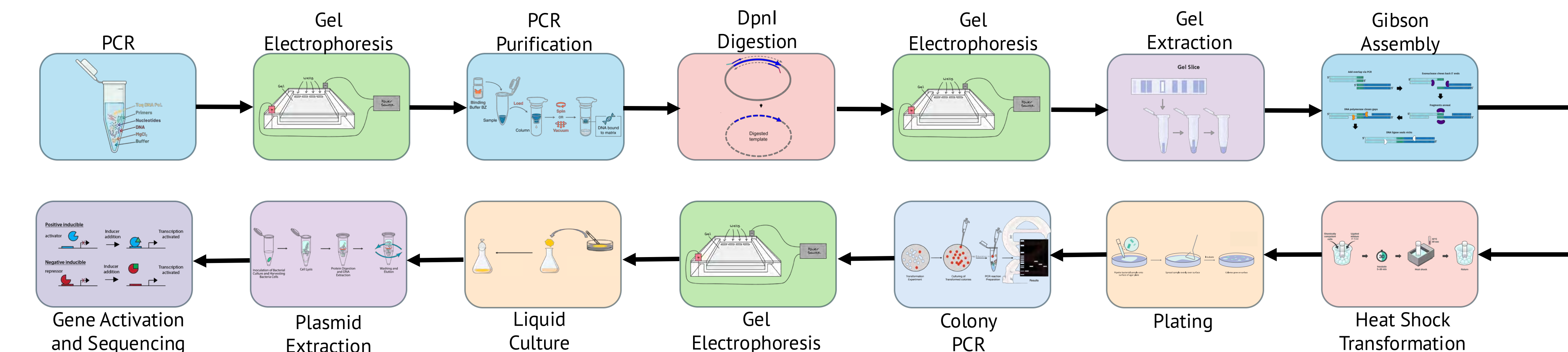
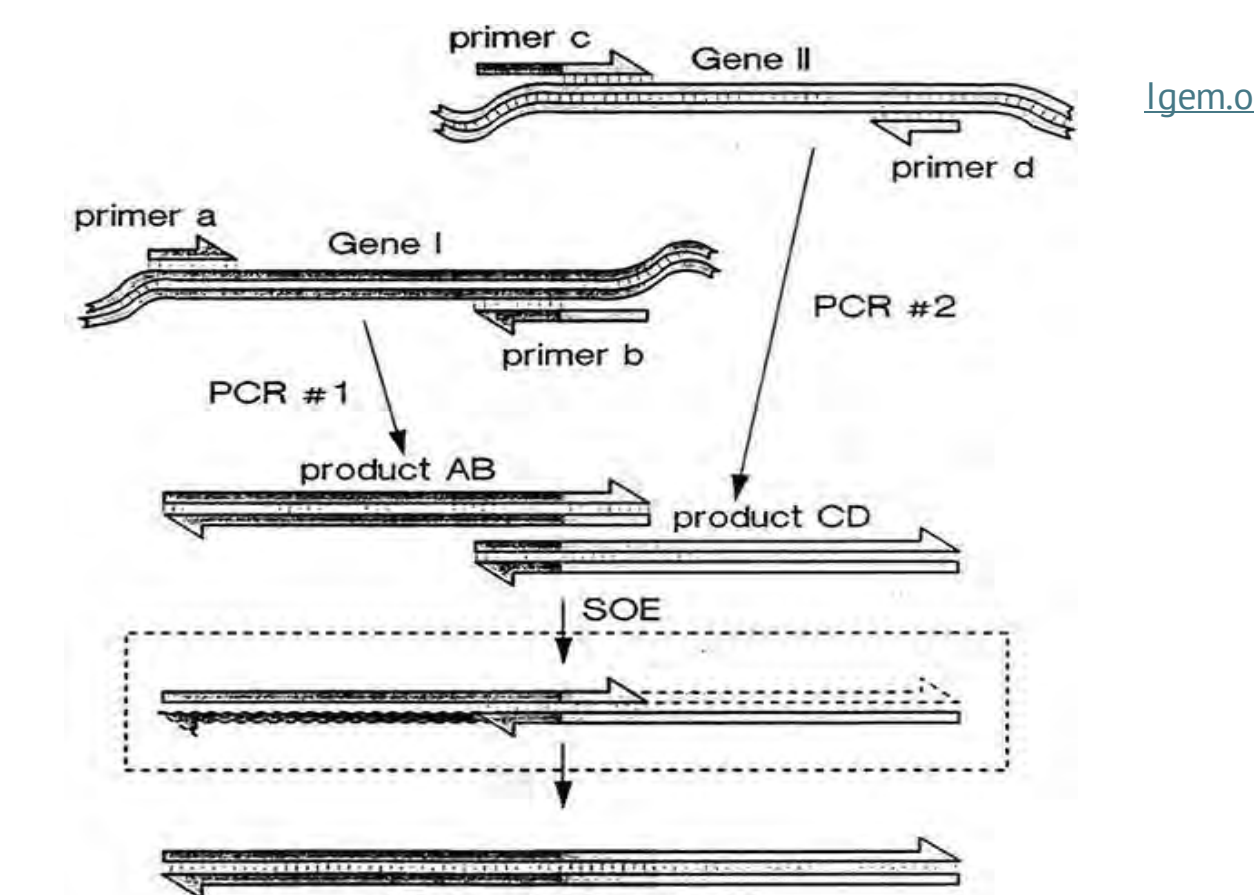


- This project aimed to clone the pha genes into the pACYCDuet plasmid backbone and transform it into *E. coli* to create a new system for PHB biosynthesis

## Methodology

- Primer design considering Gibson Assembly**
  - Primers designed with overhangs for adjacent segments
  - Designing forwards vs. reverse primers
  - Primer length and melting temperatures

**Back Bone Forward Primer:** TTGTACACGCCGATAATC  
**phaC Forward Primer:** GTTAACTTTAATAAGGAGAT  
ATACATGGCGACCGCAAAG  
**phaA Forward Primer:** CAAGGCATGACCTCATG  
GAGACAAATCATG  
**phaB Forward Primer:** GCGTATCTGAAATCAAG  
GAGTGGACATGAC  
**Back Bone Reverse Primer:** GTATATCTCTTATTAAGTT  
AAACAAATTATTTCTAC  
**phaC Reverse Primer:** TTTGTCTCCATGAGGTCATG  
CCTTGGCTTTGACGTATCG  
**phaA Reverse Primer:** CACTCTTGATTTCAGA  
TACGCTCGAAGATGG  
**phaB Reverse Primer:** GATTATGGGCGCTGTACAA  
TCAGCCCATATGCAGGCCG



## Results & Discussion

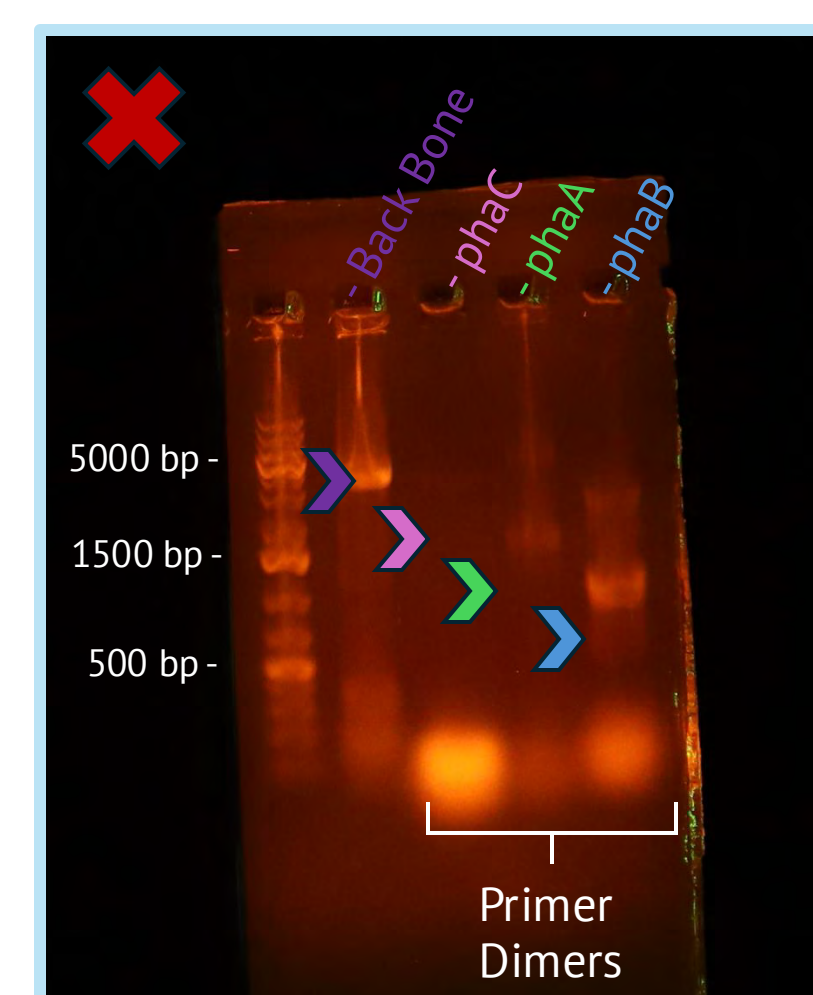


**Figure 1: Initial PCR Gel**  
Initial PCR ran using Phusion polymerase at 55°C. Backbone replicated correctly. phaCAB genes were not replicated properly, resulting in primer dimers.

Indicates expected band location

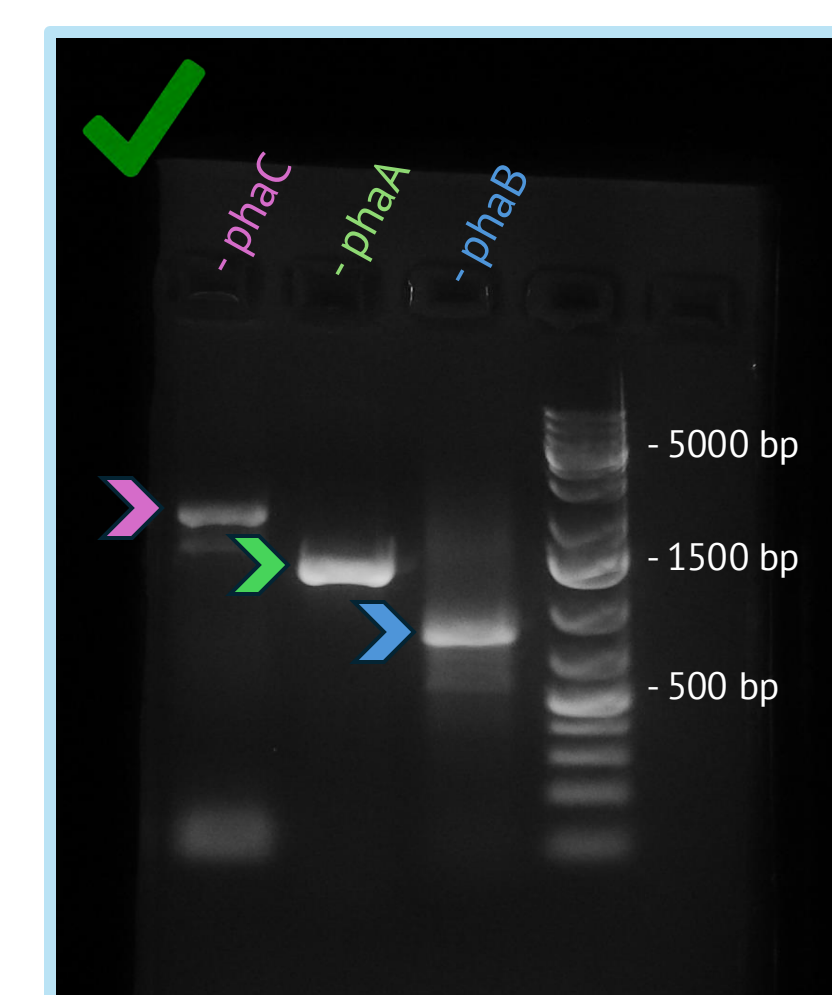


**Figure 2: Second PCR Gel**  
Second PCR ran using Q5 HiFi polymerase at 60°C. phaC, phaA, and phaB all were correctly replicated, and their bands matched the base pair length expected.

Indicates expected band location



**Figure 3: Overlap PCR (C-A & A-B) Gel**  
This PCR ran with Q5 HiFi polymerase at 55°C. The C-A overlap was successful while the A-B overlap was not.

Indicates expected band location

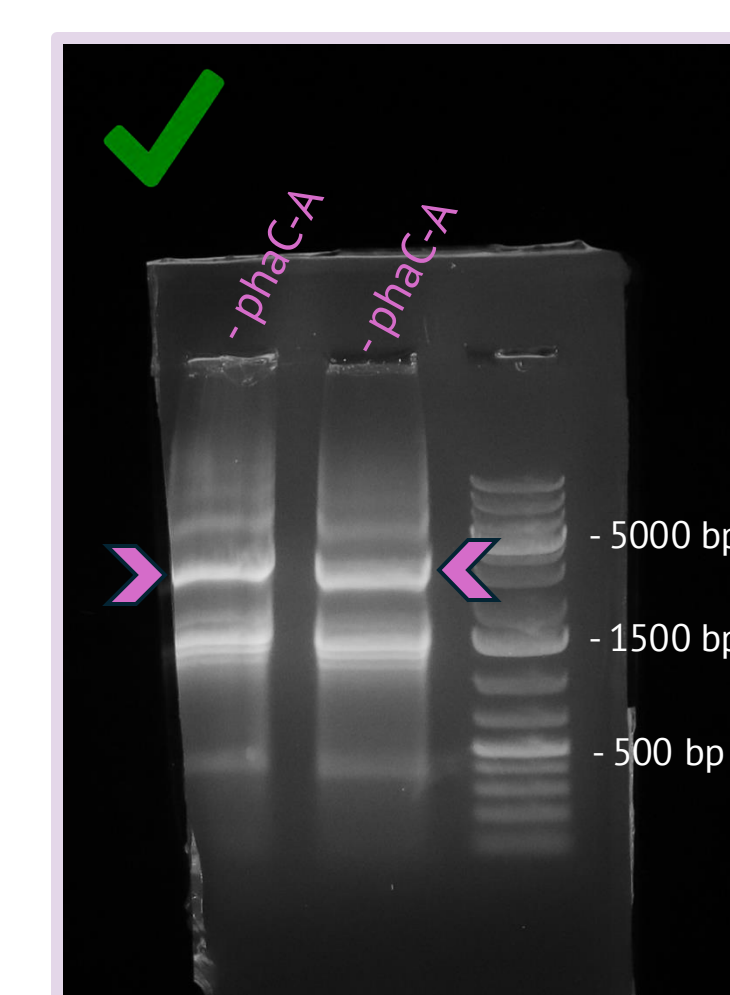


**Figure 4: phaC-A for Gel Extraction**  
This gel confirmed the correct joining of phaC and phaA in overlap PCR. The large wells were used for all the PCR product to be tested.

Indicates expected band location



**Figure 5: Plating of Transformed G.A. Product**  
The resulting plasmids were transformed into competent *E. coli* via heat shock. After recovery, cells were centrifuged and plated on chloramphenicol. Random colonies were selected and numbered.



**Figure 6: Colony PCR Gel**  
Colony PCR was performed on randomly selected colonies and gel was done. Strongest bands (2 & 10) were selected to make liquid culture

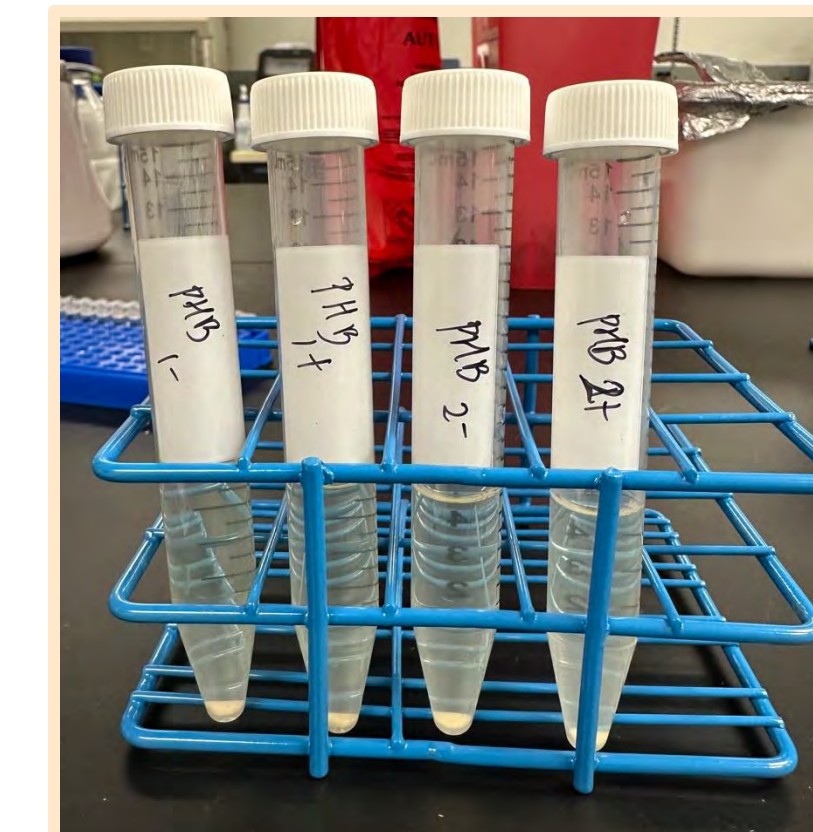


**Figure 7: Liquid Culture of transformed BL21 *E. coli***  
Strongest bands in colony PCR were cultured, transformed into BL21 competent *E. coli*, and liquid cultured with IPTG over a couple days

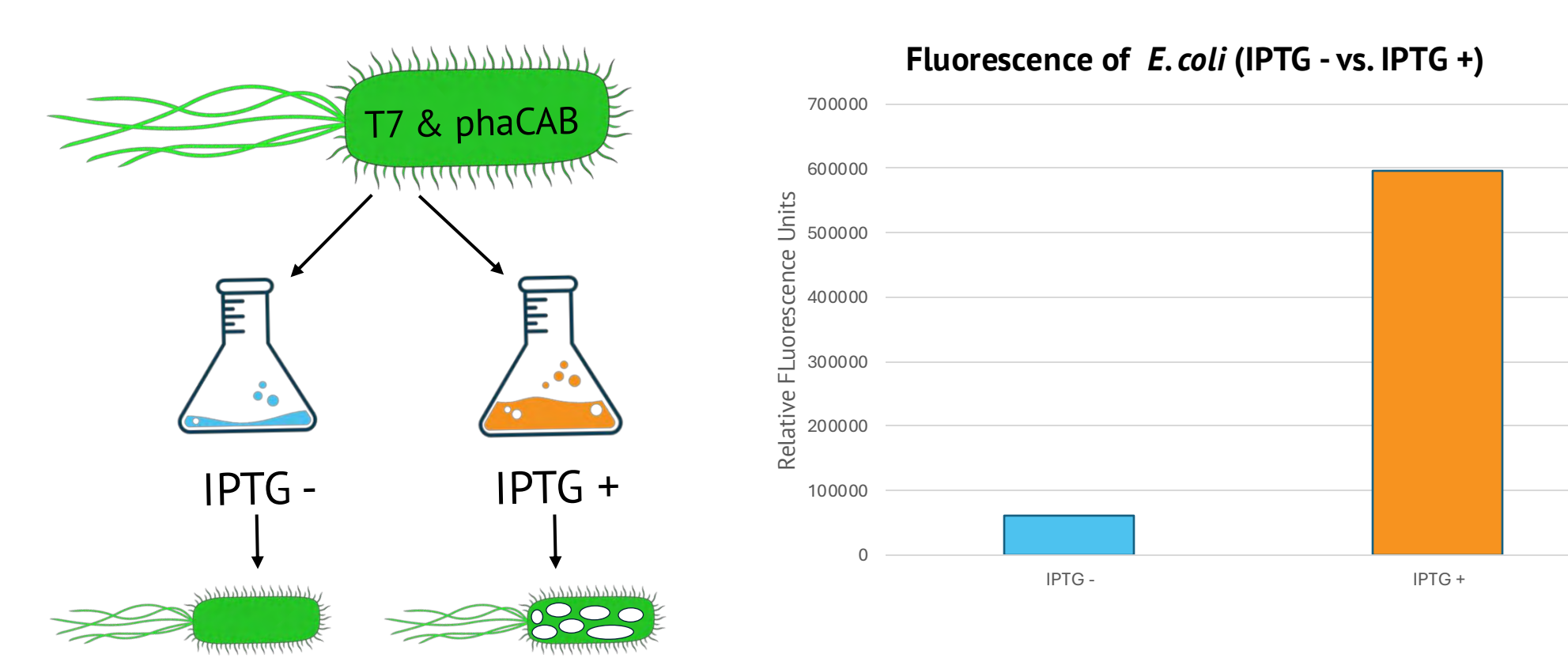
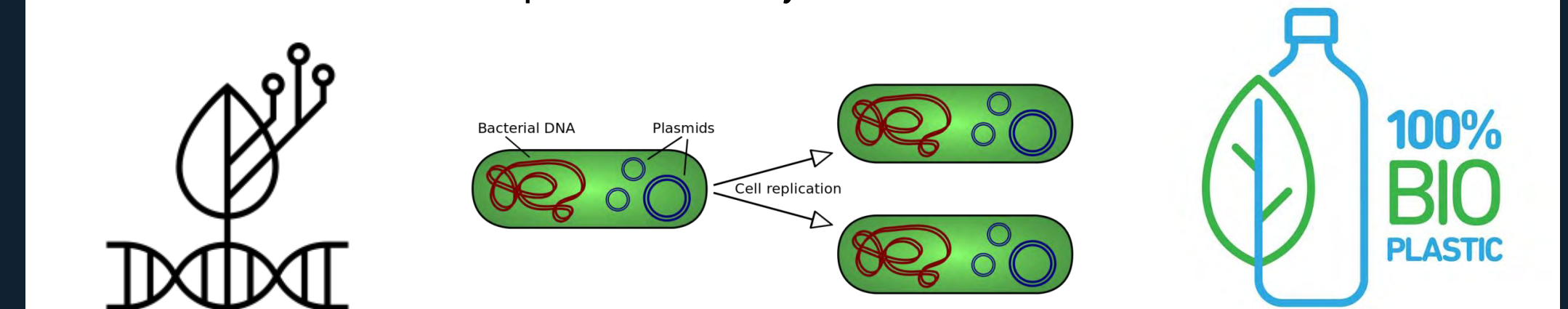


**Figure 8: IPTG + vs. IPTG - Fluorescence**  
Microplate reader was used to determine relative fluorescence based on IPTG presence. IPTG + was ~ 10 times more fluorescent than IPTG -.

## Conclusion

- This project successfully engineered *E. coli* to produce PHB by introducing the phaA, phaB, and phaC genes from *Cupriavidus necator* using gene cloning techniques
- The goal was to create a more scalable, efficient, and controllable system for PHB production in laboratory strains of *E. coli*, which are easier to grow, modify, and optimize than natural PHB-producing bacteria
- By following a gene cloning pipeline and incorporating modifications such as overlap PCR and parameter optimization, we assembled the plasmid construct and confirmed PHB biosynthesis
- This project demonstrates how synthetic biology can be used to reprogram microbial metabolism toward the production of sustainable, bio-based materials
- As the world faces increasing challenges related to plastic pollution and fossil fuel dependency, PHB offers a promising biodegradable alternative to conventional plastics
  - Engineering common lab strains to produce PHB may help make bioplastics more accessible and economically viable**
- Future directions include improving expression levels of each gene, enhancing PHB yield through additional metabolic engineering techniques, and testing different promoters, carbon sources, or host strains to further optimize the system



## Acknowledgements

Special thanks to Dr. Hyeongmin Seo for his exceptional mentorship and guidance throughout every stage of this project. I am also grateful to Elizabeth Walker, Alex Rohm, Rhea Fisch, and Antonio Galisteo for their generous help in the lab, for answering my questions, and for making the lab an enjoyable and supportive environment. Finally, I would like to thank the SSTP program and its administrators for this incredible opportunity.

## References

- Balzer, S., Kuchanova, V., Megerle, J., Lale, R., Brautaset, T., & Valla, S. (2013). A comparative analysis of the properties of regulated promoter systems commonly used for recombinant gene expression in *Escherichia coli*. *Microbial Cell Factories*, 12(1), 1–14. <https://doi.org/10.1186/1475-2859-12-26>
- Lee, H.-J., Jung, H.-J., Kim, B., Cho, D.-H., Kim, S. H., Bhatia, S. K., Ranjit Gurav, Kim, Y.-G., Jung, S.-W., Park, H. J., & Yang, Y.-H. (2022). Enhancement of polyhydroxybutyrate production by introduction of heterologous phasin combination in *Escherichia coli*. *International Journal of Biological Macromolecules*, 225(1), 757–766. <https://doi.org/10.1016/j.ijbiomac.2022.11.138>
- Lee, S. Y., & Lee, Y. (2003). Metabolic engineering of *Escherichia coli* for production of enantiomerically pure (R)-(-)-hydroxycarboxylic acids. *Applied and Environmental Microbiology*, 69(6), 3421–3426. <https://doi.org/10.1128/aem.69.6.3421-3426.2003>
- Sun Mi Lee, Lee, H.-J., Sang Hyun Kim, Min Ju Suh, Jang Yeon Cho, Ham, S., Song, H.-S., Shashi Kant Bhatia, Ranjit Gurav, Jeon, J.-M., Yoon, J.-J., Choi, K.-Y., Kim, J.-S., Sang Ho Lee, & Yang, Y.-H. (2021). Engineering of *Shewanella marisflavi* BBL25 for biomass-based polyhydroxybutyrate production and evaluation of its performance in electricity production. *International Journal of Biological Macromolecules*, 183(1), 1669–1675. <https://doi.org/10.1016/j.ijbiomac.2021.05.105>
- Yang, Y.-H., Brigham, C., Willis, L., Rha, C., & Sinskey, A. (2011). Improved detergent-based recovery of polyhydroxyalkanoates (PHAs). *Biotechnology Letters*, 33(5), 937–942. <https://doi.org/10.1007/s10529-010-0513-4>
- Ylinen, A., de Ruijter, J. C., Jouhten, P., & Penttilä, M. (2022). PHB production from cellobiose with *Saccharomyces cerevisiae*. *Microbial Cell Factories*, 21(1), 1–13. <https://doi.org/10.1186/s12934-022-01845-x>





# Salt Ions Can Modulate the Viscoelasticity of Silk Fibroin

Maya Ostermann<sup>1</sup>, Reza Amouzandeh<sup>2</sup>, Robert Groos<sup>2</sup>, Kyra Howieson<sup>2</sup>, Xuan Mu<sup>2\*</sup>

<sup>1</sup>York Community High School, IL; <sup>2</sup>Roy J. Carver Department of Biomedical Engineering, University of Iowa; Email: xuan-mu@uiowa.edu

## Introduction

- Silk fibroin is a structural protein with excellent mechanical properties, low immunogenicity, and high biocompatibility, making it a promising alternative to other natural or synthetic biomaterials for biomedical applications.
- Conventional methods used to induce the solution-to-gel (sol-gel) transition in silk often rely on organic solvents, high temperature, or high pH levels, which deviate from the natural spinning process and may compromise biofunctional properties.
- Inspired by natural silk spinning, we plan to use salt ions to induce a controlled sol-gel transition of silk fibroin, beneficial for a sustainable and biocompatible fabrication of silk-based constructs.
- Aim:** Determine the salt ion effect on the viscoelastic behavior and gelation of silk fibroin.

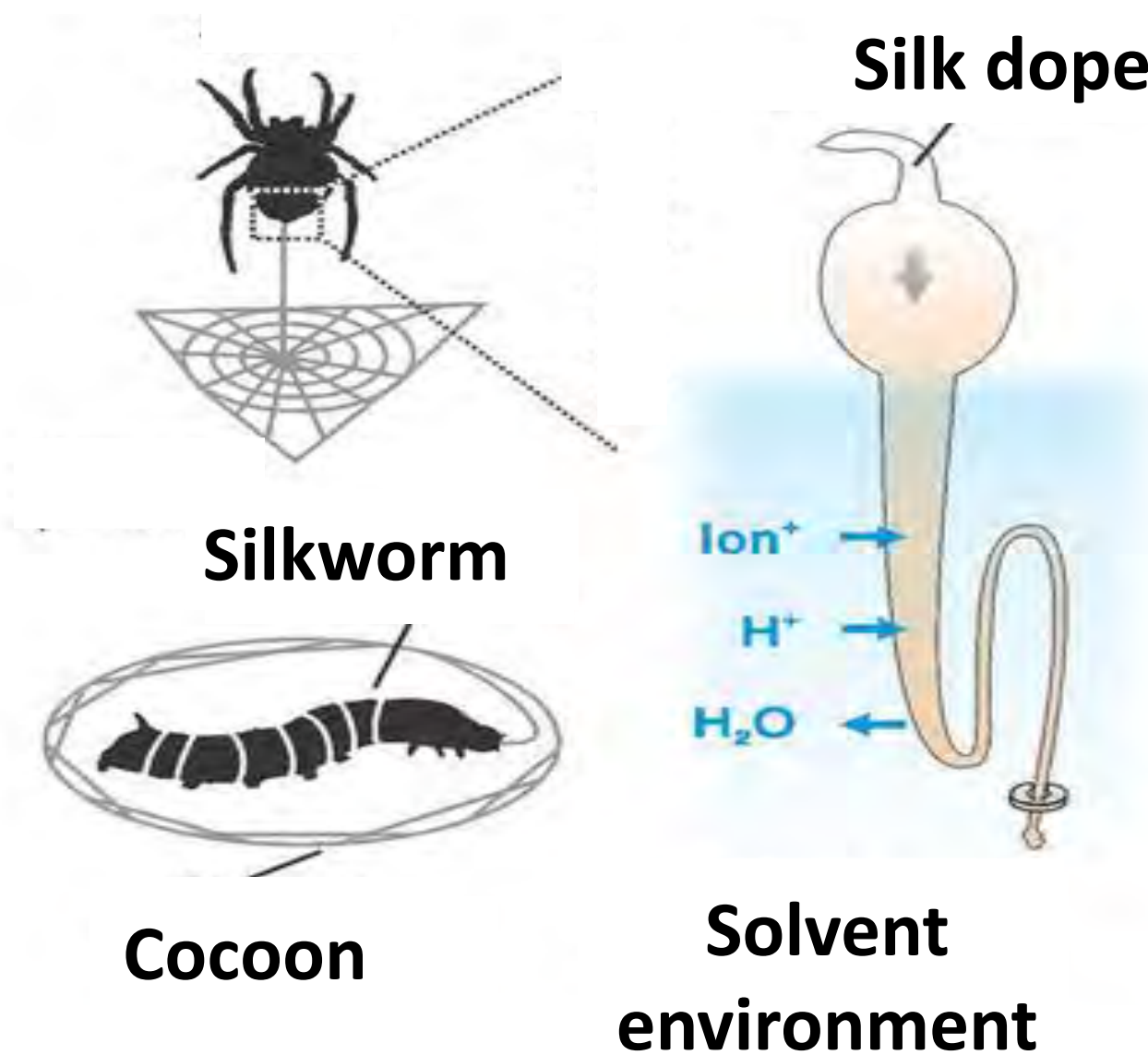


**Figure 1.** Salt ions are one of the primary regulating factors in the natural silk spinning process in spiders and silkworms.

## Methods

- 25 wt.% silk solution was prepared from silkworm cocoons according to a previously established protocol.
- We evaluated the viscoelastic behavior of silk fibroin solution in contact with different salts using a rheometer.
- Oscillatory time sweeps were conducted in the linear viscoelastic range (strain: 0.5%, frequency: 1 Hz) at room temperature.
- Salts were added at around 90 s to observe the effect of salt ions on the storage modulus ( $G'$ ), loss modulus ( $G''$ ), and complex viscosity over time.

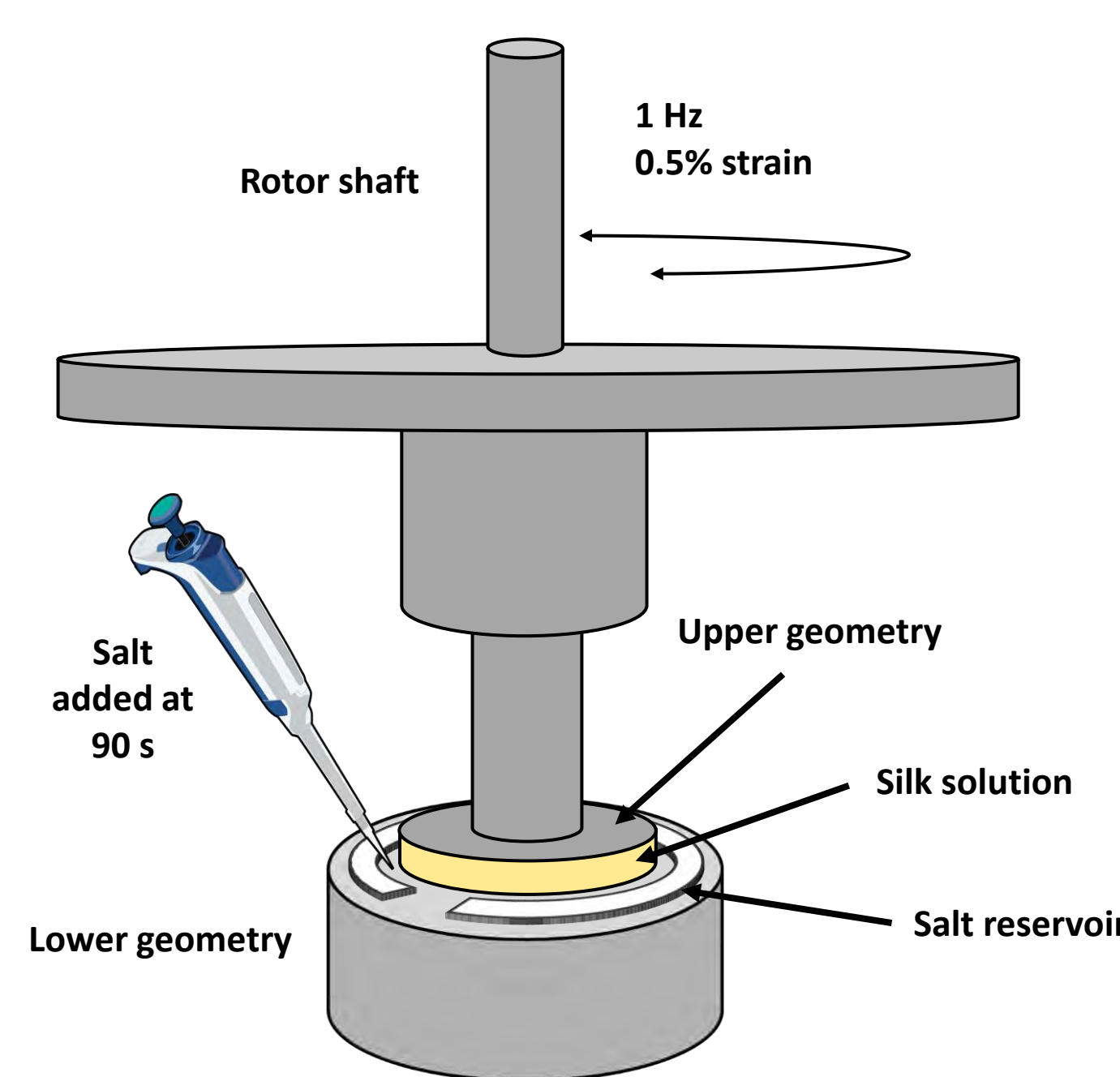


**Figure 2.** Schematic of the experimental setup for measuring the viscoelastic properties of silk fibroin solution using a rheometer.

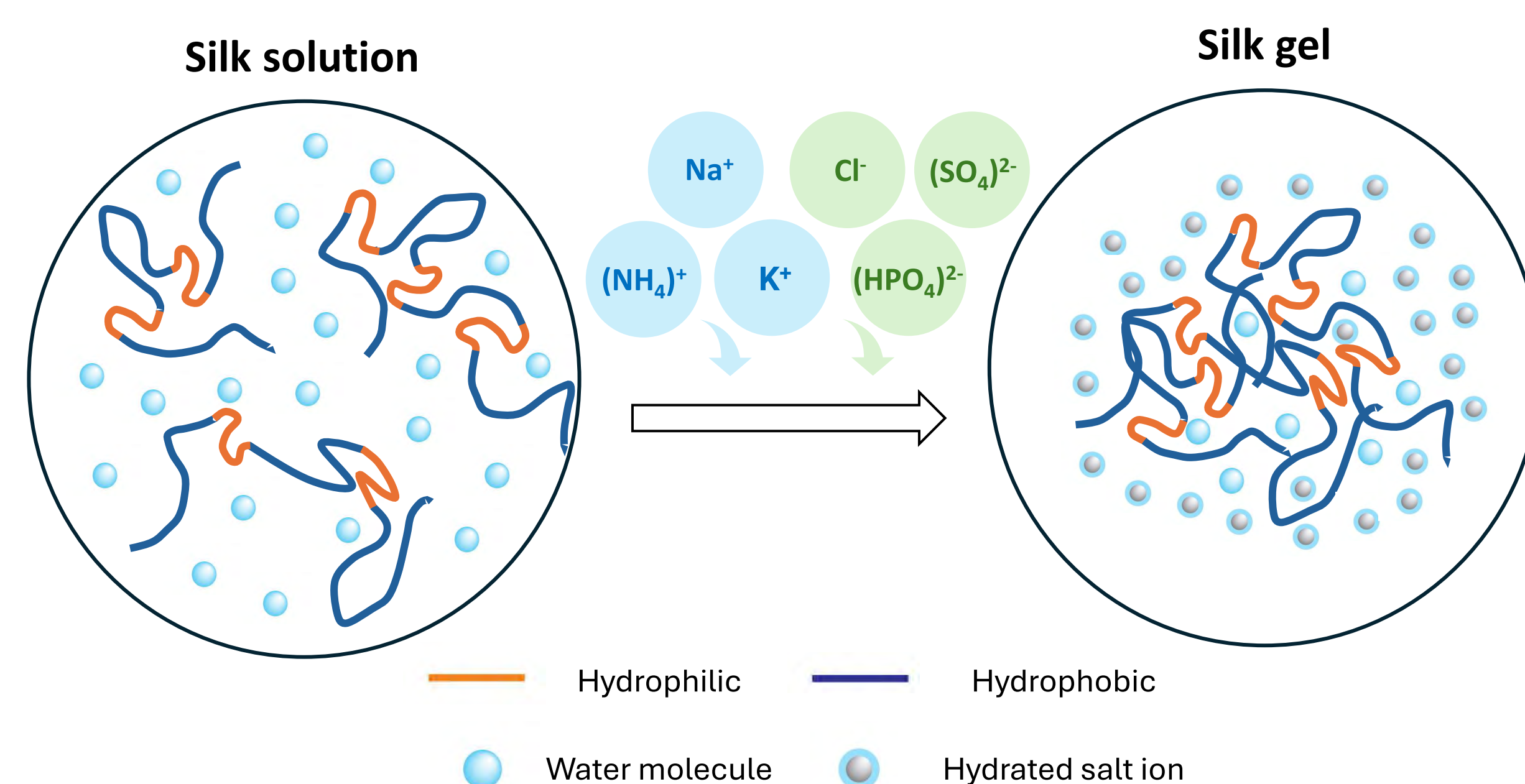


**Figure 3.** Schematics of macromolecular crowding in silk fibroin induced by salt ions.

## Results

### Salt Ion Effect

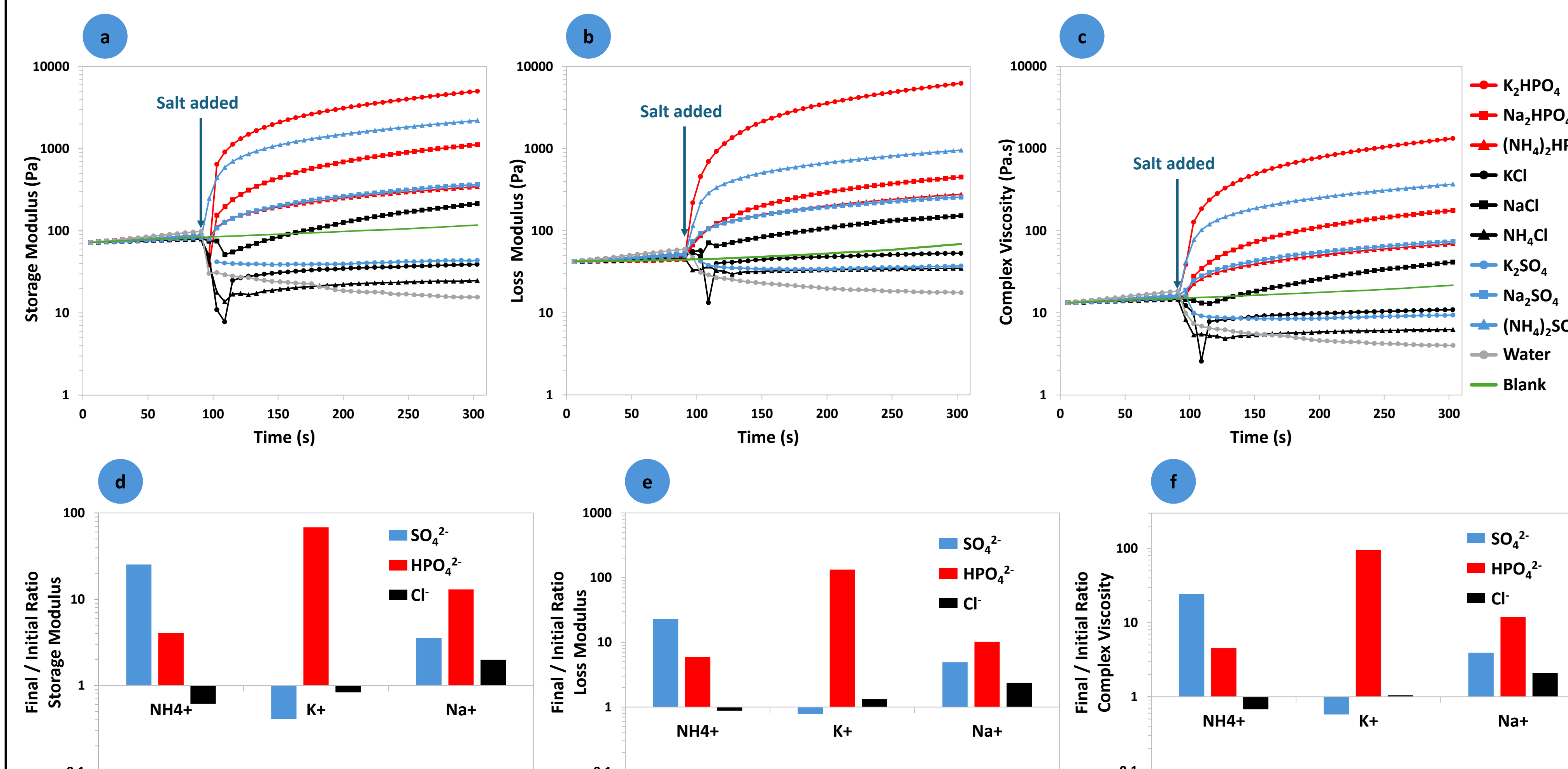


**Figure 4.** Salts that contain  $\text{HPO}_4^{2-}$  as the anion and  $\text{Na}^+$  as the cation generally induce a higher gelation degree in silk fibroin. Representative normalized time sweeps of storage modulus (a), loss modulus (b), and complex viscosity (c) reveal that, after adding the highest concentration of listed salts at 90 s, each salt composition induces a distinct trend in gelation behavior. Storage modulus ratio (d), loss modulus ratio (e), and complex viscosity ratio (f) confirm that adding salts that contain  $\text{HPO}_4^{2-}$  as the anion and  $\text{Na}^+$  as the cation around the silk fibroin generally results in a higher increase in these properties.

### $\text{K}_2\text{HPO}_4$ Concentration Effect

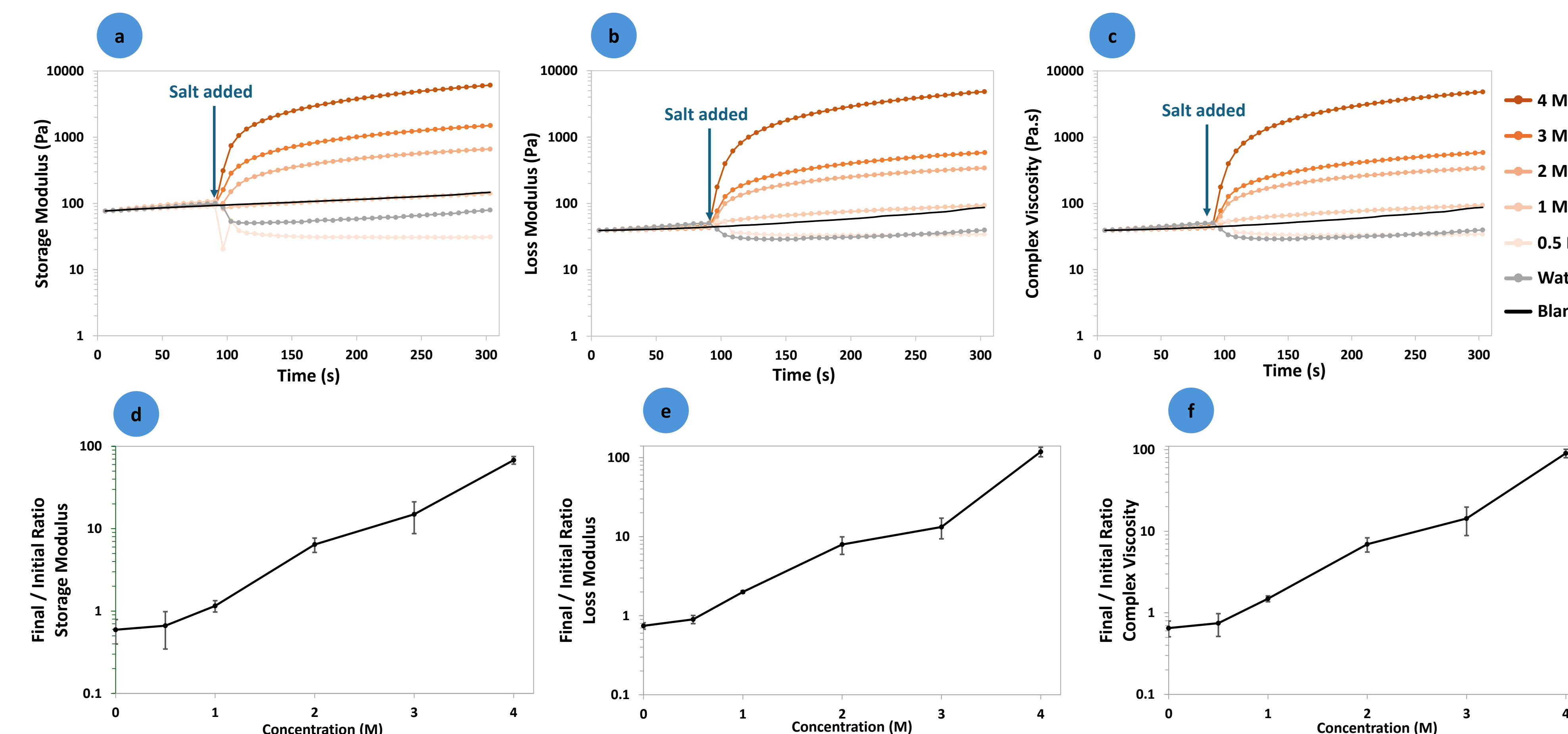


**Figure 5.** The gelation degree of silk fibroin solution is directly correlated with  $\text{K}_2\text{HPO}_4$  concentration. Representative normalized time sweeps of the storage modulus (a), loss modulus (b), and complex viscosity (c) show a gradual change after 90 s, when salt was added around the silk solution, and a more significant increase is observed as the salt concentration increases. The logarithm of the storage modulus ratio (d), loss modulus ratio (e), and complex viscosity ratio (f) versus salt concentration show a linear trend, revealing an exponential dependence on concentration.

## Conclusions and Implications

- Salt composition and concentration can be exploited to modulate the sol-gel transition of silk fibroin.
- Salts with  $\text{HPO}_4^{2-}$  anions and  $\text{Na}^+$  cations produce higher gelation degrees in silk fibroin.
- The gelation degree of the silk fibroin solution increases linearly with  $\text{K}_2\text{HPO}_4$  concentration.
- Changes in rheological properties correlate with hydration layer thickness of the cation or anion at comparable salt concentrations, with anion identity showing a more notable influence.
- These results form a strong basis for further studies on the effects of salt ions on silk fibroin, not only in sol-gel transition, but also in controlling the macroscopic properties of silk fibroin structures.
- In conclusion, salt ions offer a sustainable, aqueous, and ambient approach without harsh treatments for fabricating silk-based tissue scaffolds and drug delivery vehicles.

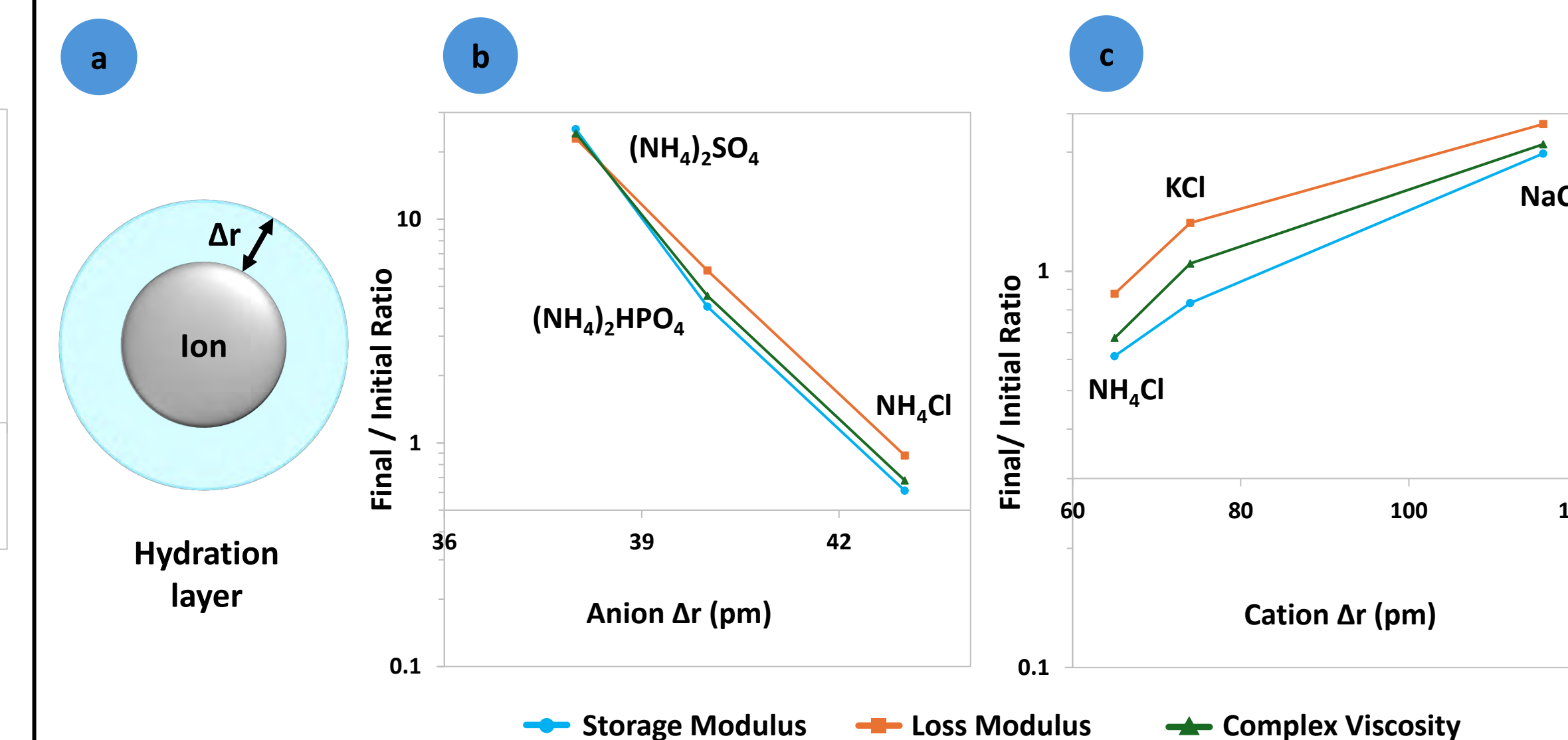


**Figure 6.** Final-to-initial ratios of rheological properties correlate with hydration layer thickness ( $\Delta r$ ) for salts that have comparable concentrations. (a) Schematic of the hydration layer around ions. The thickness of this immobilized, electrostricted hydration layer varies for each cation and anion and is an inherent property of the ion. (b) The final-to-initial ratios of storage modulus, loss modulus, and complex viscosity are inversely correlated with the anion  $\Delta r$  for salts containing  $\text{NH}_4^+$ . (c) The final-to-initial ratios of storage modulus, loss modulus, and complex viscosity are directly correlated with the cation  $\Delta r$  for salts containing  $\text{Cl}^-$ . No trend was found in other salts, which might be because of the differences in concentrations. More experiments should be performed to confirm these findings.

## Acknowledgements

We thank the Carver Charitable Trust, the Cystic Fibrosis Foundation, and the University of Iowa Jumpstarting Tomorrow Program for supporting this research project. We also appreciate Ashlee Donithan from the Belin-Blank Center for her support.

## References

- [1] Koeppel, Andreas, et al. "The Influence of Metal Ions on Native Silk Rheology." *Acta Biomaterialia*, vol. 117, 2020, pp. 204–12, <https://doi.org/10.1016/j.actbio.2020.09.045>.
- [2] Mu, Xuan, et al. "A Brief Review on the Mechanisms and Approaches of Silk Spinning-Inspired Biofabrication." *Frontiers in Bioengineering and Biotechnology*, vol. 11, 2023, pp. 1252499–99, <https://doi.org/10.3389/fbioe.2023.1252499>.
- [3] Mu, Xuan, et al. "Conformation-Driven Strategy for Resilient and Functional Protein Materials." *Proceedings of the National Academy of Sciences*, vol. 119, no. 4, 2022, <https://doi.org/10.1073/pnas.2115523119>.
- [4] Mu, Xuan, et al. "From Silk Spinning to 3D Printing: Polymer Manufacturing Using Directed Hierarchical Molecular Assembly." *Advanced Healthcare Materials*, vol. 9, no. 15, 2020, p. 1901552, <https://doi.org/10.1002/adhm.201901552>.
- [5] Mu, Xuan, et al. "Recent Advances in 3D Printing with Protein-Based Inks." *Progress in Polymer Science*, vol. 115, 2021, p. 101375, <https://doi.org/10.1016/j.progpolymsci.2021.101375>.
- [6] Mu, Xuan, et al. "3D Printing of Silk Protein Structures by Aqueous Solvent-Directed Molecular Assembly." *Macromolecular Bioscience*, vol. 20, no. 1, Wiley, 2020, pp. 1900191–91, <https://doi.org/10.1002/mabi.201900191>.
- [7] Rockwood, Danielle N., et al. "Materials Fabrication from Bombyx Mori Silk Fibroin." *Nature Protocols*, vol. 6, no. 10, 2011, pp. 1612–31, <https://doi.org/10.1038/nprot.2011.379>.



# Mitigating Clickbait Bias in News Recommendation System via Counterfactual Inference

Jaeyun Park<sup>1</sup>, Xin Zan<sup>2</sup>, PhD

<sup>1</sup>Cheshire Academy, Cheshire, CT; <sup>2</sup>Department of Industrial and Systems Engineering, University of Iowa, Iowa City, IA

IOWA



## Introduction

### Background

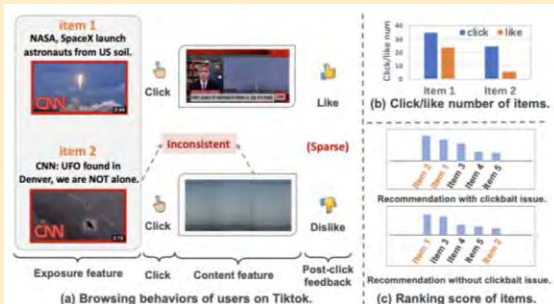
- A recommendation system is a tool that predicts user preferences and provides personalized content.
- Clickbait headlines distort user preferences, leading to biased recommendations.

### Data

- We use a filtered version of the **Adressa dataset**, consisting of **1,882 users**, **3,179 news articles**, and approximately **300,000 interactions**.
- Each interaction includes click timestamp along with article and user metadata.

## Problem Statement

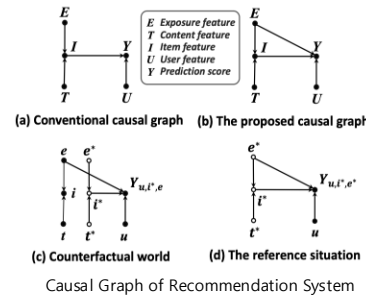
- Since it is hard to get **direct feedback** in the real world, we utilize **implicit data**—click and dwell time—as proxies for user satisfaction.
- Model the recommendation process with a causal graph that separates **pre-click exposure** features (e.g., titles) and **post-click content** features to distinguish clickbait articles.



- (a) Illustration of inconsistency between clicks and likes. (b) Number of clicks/likes on the two items where few clicks on item 2 end with likes. (c) Two recommendation lists with and without the clickbait issue, respectively.

## Method

### Counterfactual Inference



- It estimates how a user would have responded to an article **had it been presented differently**.
- Therefore, it shows how **exposure features** affect user behavior and recommendation bias.

### CI Equation

**Predicted Click Probability  $Y(u, i, e)$ :**  
Predicted score for click behavior under  $(u, i, e)$

$$Y_{u, i, e} = f_Y(U = u, I = i, E = e), \text{ where } i = f_I(E = e, T = t)$$

#### Natural Direct Effect (NDE)

$$NDE = Y_{u, i^*, e} - Y_{u, i^*, e^*}$$

$$= f_Y(U = u, I = i^*, E = e) - f_Y(U = u, I = i^*, E = e^*)$$

#### Total Effect (TE)

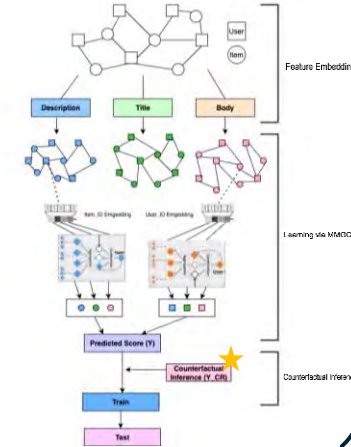
$$TE = Y_{u, i, e} - Y_{u, i^*, e}$$

#### Total Indirect Effect (TIE)

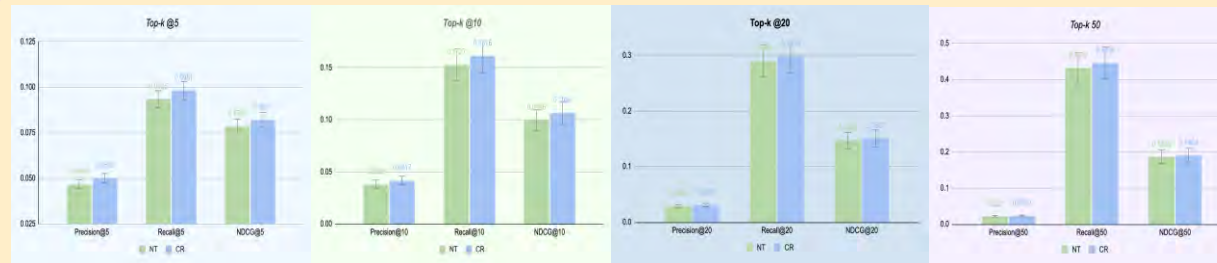
$$TIE = TE - NDE$$

$$\rightarrow Y_{CR} = Y_{u, i, e} - Y_{u, i^*, e}$$

### Flow Chart



## Result



NT – Normal Training CR – Counterfactual Recommendation

Metric	P@5	R@5	N@5	P@10	R@10	N@10	P@20	R@20	N@20	P@50	R@50	N@50
NT	0.0468	0.0935	0.0785	0.0383	0.1527	0.0996	0.0285	0.2898	0.1469	0.0221	0.4312	0.1865
CR	0.0502	0.0981	0.0821	0.0417	0.1616	0.1064	0.0309	0.2979	0.1507	0.0232	0.4458	0.1904
%Improve	7.26%	4.92%	4.59%	8.88%	5.83%	6.83%	8.42%	2.80%	2.58%	4.97%	3.39%	2.10%

P – Precision R – Recall N – NDCG # – Top-k

## Conclusion

- The **CR(Counterfactual Recommendation)** model consistently outperforms the **NT(Normal Training)**, achieving notable improvements in Precision@10 and Precision@20—specifically, **8.88%** and **8.42%** higher than NT, respectively.
- Results highlight the effectiveness of the proposed method, which utilizes a counterfactual inference to reduce the direct effect of exposure features. Overall, **CR leads to more satisfying recommendations**, enhancing user engagement and generating greater economic value.
- This research is particularly meaningful lies in its simplicity and practicality: **the model relies solely on click data, without incorporating additional feedback** such as dwell time or ratings. This makes the method highly adaptable and easy to apply in real-world settings where only implicit feedback is available.

## Future Work

**Problem Statement:** Using click data alone to detect clickbait may lead to over-interpretation.

**Proposed Solution:** Dwell time can serve as a more reliable signal of user interest while being easier to obtain than explicit feedback.

**Expected Effect:** Integrating dwell time into counterfactual inference could improve both recommendation performance and clickbait detection accuracy.

**Related Work:** The paper "Reweighting Clicks with Dwell Time in Recommendation" proposes sigmoid-based normalization and debiasing assumptions to model dwell time.

**Proposed Method:** Dwell time can be incorporated as weighting parameter in the counterfactual framework to enhance model robustness.

## References

- Wang, W., Feng, F., He, X., Zhang, H., & Chua, T. S. (2021, July). *Clicks can be cheating: Counterfactual recommendation for mitigating clickbait issue*.
- Wei, Y., Wang, X., Nie, L., He, X., Hong, R., & Chua, T. S. (2019, October). *MG-CNN: Multi-modal graph convolutional network for personalized recommendation of micro-video*.
- Xie, R., Ma, L., Zhang, S., Xia, F., & Lin, L. (2023, April). *Reweighting clicks with dwell time in recommendation*.
- Wang, W., Feng, F., He, X., Nie, L., & Chua, T. S. (2021, March). *Denosing implicit feedback for recommendation*.
- Zan, X., Semenov, A., Wang, C., Xian, X., & Gremew, W. (2024). *Causality-aware social recommender system with network homophily informed multi-treatment confounders*.



Hayan Raffi<sup>1,2</sup>, Tamara Busch<sup>3</sup>, Nina Mba<sup>3</sup>, Rishitha Gadde<sup>3</sup>, Oluwafunmilayo Ajala<sup>3</sup>, Miskiyat Sanni<sup>3</sup>, Mojisola Olujitan<sup>3</sup>, Emmanuel Aladenika<sup>3</sup>, Lord JJ Gowans<sup>3</sup>, PhD, Azeez Butali<sup>3</sup>, PhD

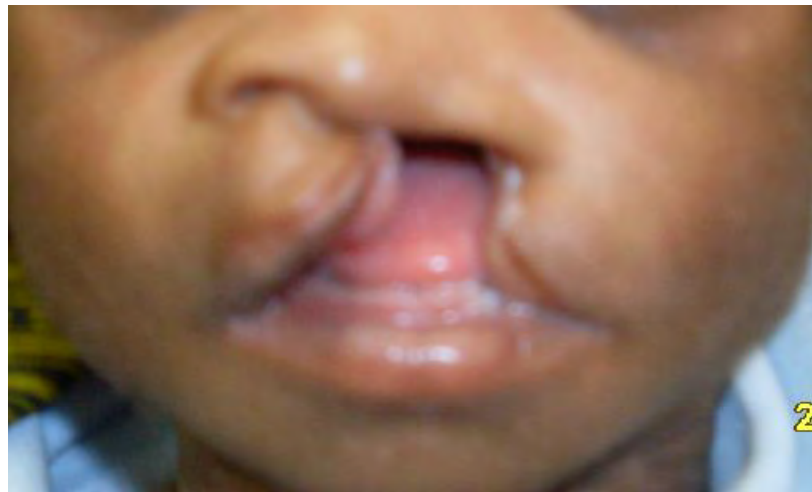
<sup>1</sup>Wichita Collegiate School, <sup>2</sup>Secondary Student Training Program, <sup>3</sup>Department of Oral Pathology, Radiology, and Medicine

## Introduction

Orofacial cleft disorders are among the most commonly found craniofacial anomalies in the world today (Shivlani et al., 2022).

A case occurs every **1 in 700** live births (Putri et al., 2024).

- Cleft lip/palate (CLP) is a congenital craniofacial disorder where an individual's lip and/or roof of the mouth do not fuse properly (Leslie & Marazita, 2013).
- CLP can be further classified into syndromic (SCLP) or nonsyndromic (NCLP) forms and as unilateral or bilateral. SCLP is inherited as part of a larger disorder, while NCLP appears in individuals as an isolated disorder (Leslie & Marazita, 2013).
- While there is a significant genetic component of CLP's heritability, it is a multifactorial condition. Environmentally linked factors include smoking and/or drinking during pregnancy and folic acid deficiency (National Institute of Dental and Craniofacial Research).
- Several studies using whole-genome and exome sequencing have identified variants in genes associated with CLP.
- The appearance of CLP in individuals can be linked to multiple genes, so identifying those variants can reveal potential causes of CLP.



Cleft Lip



Cleft Palate

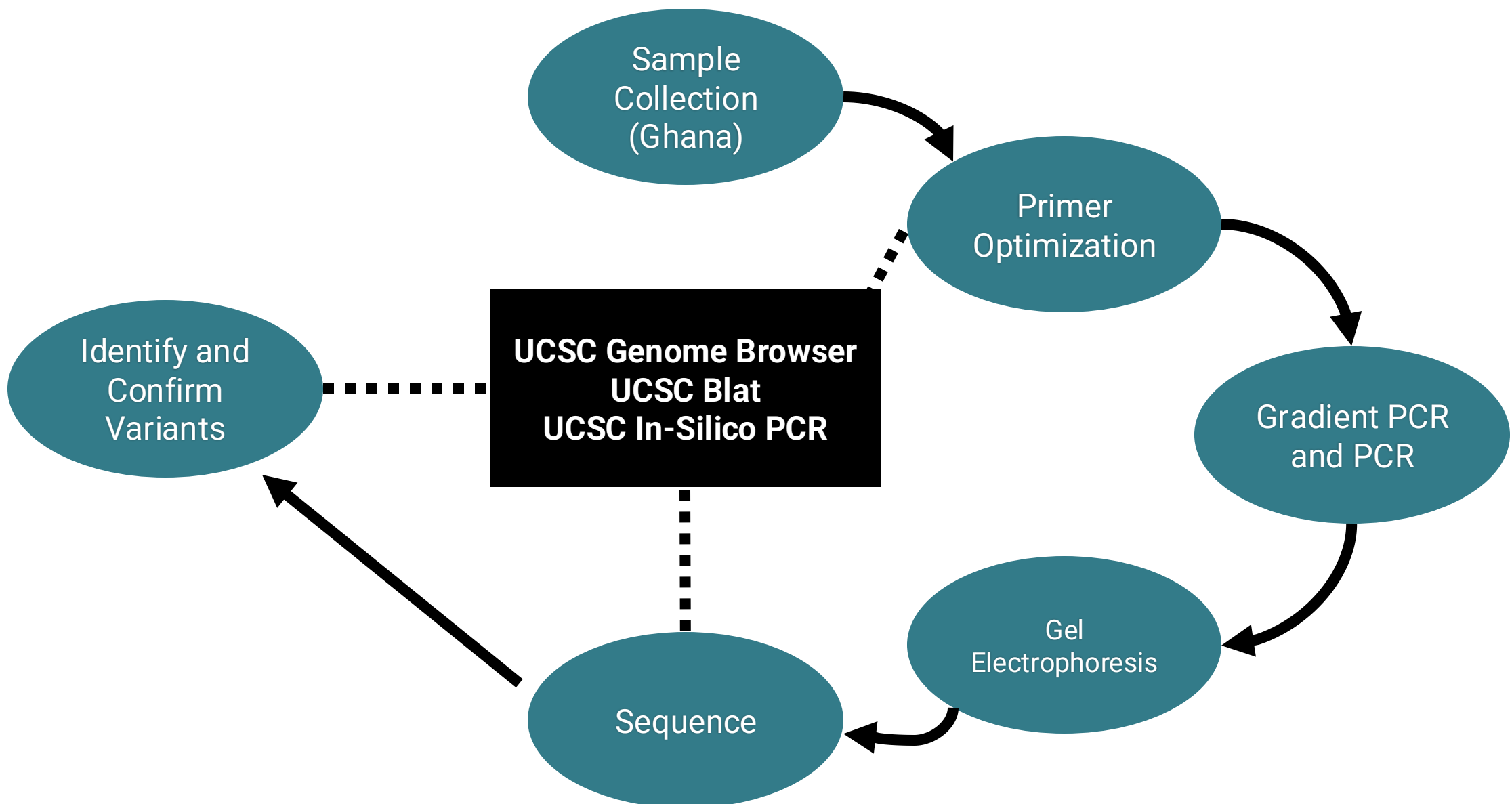
## Research Question and Aim

Are there variants in the form of genetic mutations that contribute to the syndrome's appearance in Ghanaian patients?

Using Sanger sequencing, identify, confirm, and investigate variants found in Ghanaian individuals affected by cleft lip/palate.

## Methodology

Researchers in Ghana collected samples from cleft-affected families and used a technique called exome sequencing to identify genetic variants. They identified several target genes where there was a variant that could be linked to the appearance of clefts in these individuals. I used a process called Sanger sequencing for this research to confirm the variants.



## Results

### Example Sanger Sequence Analysis of Gene MYH3

Consed	Individual	Phenotype	Genomic Coordinate	Nucleotide Present	Result Codon	Predicted Amino Acid
	Proband	Freeman-Sheldon's Syndrome (CL)	Chr17: 10641317	CT*	GTA	Histidine
	Father	Unaffected	Chr17: 10641317	CC	GCA	Arginine
	Mother	Unaffected	Chr17: 10641317	CC	GCA	Arginine

\* de novo mutation

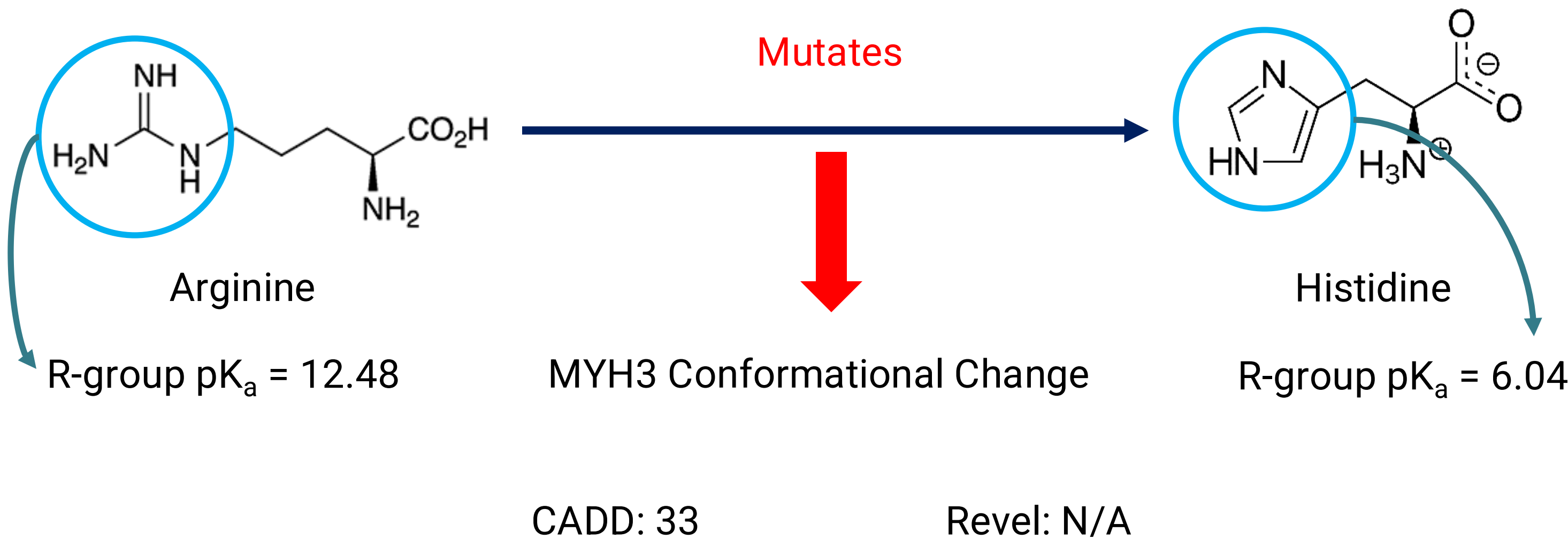


**Figure 1:** The CT allele causes a mutation from arginine to histidine that induces a conformational change in the MYH3 protein. This leads to a dysfunctional myosin-3 protein integral to cell differentiation, proliferation, and apoptosis for craniofacial development in the early stages of pregnancy.

Phenotype	Gene	Genomic Coordinate	Codon Change	Protein Change	Damage
BCLP	FBN2	Chr5:128357278	(TAA) > (TGA)	Ile>Thr	CADD: 23.7 Revel: 0.478
UCL	ZFYVE21	Chr 14: 103728964	(CGT)>(TGT)	Arg>Cys	CADD: 33 Revel: 0.629
UCL	PAX6	Chr11:31793530	(TAC) -> (CAC)	Met>Val	CADD: 24.1 Revel: 0.454
BCLP	STAB2	Chr12:103638076	(CCA)>(CAA)	Pro>Gln	CADD: 25.5 Revel: 0.318
No CLP*	TJP2	Chr9: 69212557	(ATG)-(GTG)	Met>Val	CADD: 23.3 Revel: 0.358

\* Craniosynostosis with no clefting

## Discussion & Conclusion

**The variants we identified LIKELY contribute to the development of cleft lip/palate in the individuals tested.**

To assess the potential impact of these mutations, we used predictive tools CADD and Revel. CADD score is a tool we can use to predict the severity of the consequences that a mutation may confer. Revel Score is another instrument used to predict the pathogenicity of a mutation.

CADD score percentiles in severity of damage:

- 20 < CADD < 30 – 99.9<sup>th</sup>
  - CADD > 30 – 99.99<sup>th</sup>
- For Revel scores:
- Revel ≈ <0.5% - likely a benign/non-pathogenic mutation
  - Revel ≈ >0.5% – likely a pathogenic/damage-causing mutation

Of the seventeen genes sequenced, ten had relevant CADD and Revel Scores. All had CADD scores greater than 20 (some even exceeding 30). All had Revel scores that fall into the “somewhat” or “likely” pathogenic range. Although these are predictive tools, results indicate that the mutations we investigated are extremely dangerous and likely disease-causing.

An example analysis of the MYH3 gene mutation is depicted in figure 1.

- Histidine is much more likely to deprotonate in the physiological pH of the body compared to arginine (lower pK<sub>a</sub>) → different tertiary structures
- Results in dysfunctional myosin-3 due (Khemais et al., 2011).
- Linked to Freeman-Sheldon's Syndrome, a condition that confers cleft lip and palate on the individual (Toydemir et al, 2006).
- Individual sampled with this mutation was diagnosed with Freeman-Sheldon Syndrome → further confirmation of study
- Similar protein analyses of other mutations in different genes further corroborate our study, validating the association of variants in these genes to the development of CLP in the individuals sampled.

## Acknowledgements

I would like to thank Dr. Butali, the University of Iowa, and the Secondary Student Training Program for giving me an opportunity to research here. I would also like to thank my lab manager Tamara and the four undergraduate students (Nina, Rishitha, Funmi, and Misky) for guiding and helping me during my time in the lab.

## References

- Al-Namankany, A., & Alhubaishi, A. (2018). Effects of cleft lip and palate on children's psychological health: A systematic review. *Journal of Taibah University Medical Sciences*, 13(4), 311–318.
- Khemais Oukhai, Maricic, N., Schneider, M., Winfried Harzer, & Tausche, E. (2011). Developmental myosin heavy chain mRNA in masseter after orthognathic surgery: A preliminary study. *Journal of Cranio-Maxillofacial Surgery*, 39(6), 401–406.
- Leslie, E. J., & Marazita, M. L. (2013a). Genetics of cleft lip and cleft palate. *American Journal of Medical Genetics Part C: Seminars in Medical Genetics*, 163(4), 246–258.
- National Institute of Dental and Craniofacial Research. (2021). *Cleft Lip & Palate*. [www.nidcr.nih.gov](http://www.nidcr.nih.gov).
- Shivlani, V., Niranjane P., Kamble, R., & Lakhe, P. (2022). Syndromes Associated to Cleft Lip and Palate: A Review. *Journal of Research in Medical and Dental Science*, 10(10), 224–229.
- Toydemir, R. M., Rutherford, A., Whitby, F. G., Jorde, L. B., Carey, J. C., & Bamshad, M. J. (2006). Mutations in embryonic myosin heavy chain (MYH3) cause Freeman-Sheldon syndrome and Sheldon-Hall syndrome. *Nature Genetics*, 38(5), 561–565.



# Improving the diagnosis and treatment of human choroideremia

Aashni Sahai; Jeaneen Andorf; Louisa Affatigato; Narendra Pandala, PhD; Nicholas Stone, PhD; Edwin Stone, MD, PhD

Institute for Vision Research, Department of Ophthalmology and Visual Sciences, Carver College of Medicine, University of Iowa, Iowa City, IA

## Introduction

Choroideremia is an inherited eye disease which causes progressive vision loss and blindness. It is typically passed down with an X-linked recessive inheritance pattern, caused by a mutation in the CHM gene encoding the protein REP-1. REP-1 is vital in intracellular trafficking throughout the choroid, a vascular layer in the eye which provides oxygen and nutrients to the photoreceptors in the retina. The sclera, the ‘white’ of the eye, sits just below the choroid and can become increasingly visible in fundus photos of choroideremia as the aforementioned layers degrade.

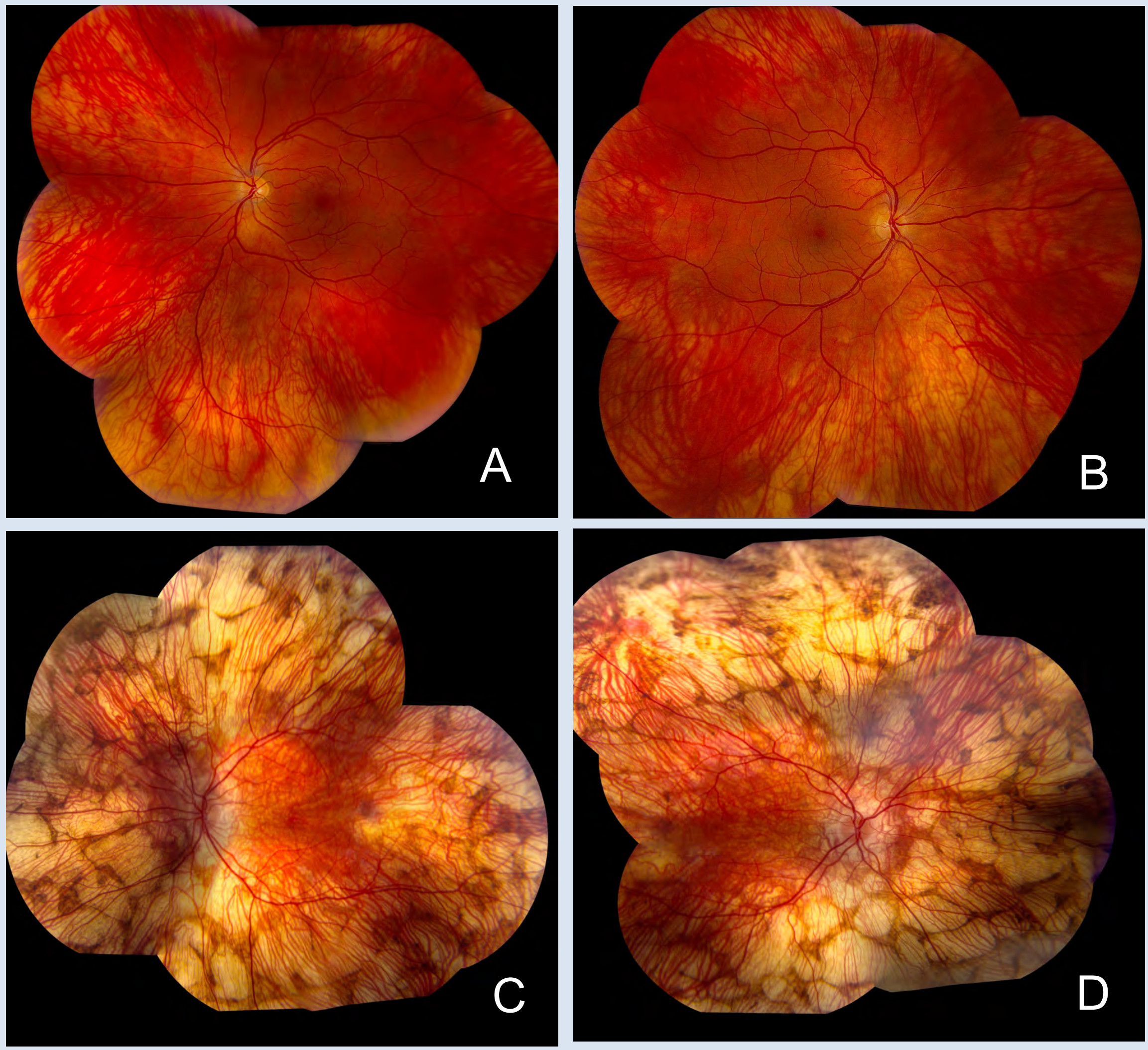


**Figure 1:** Images A and B are fundus photos of the retinas of a normally-sighted individual with 20/20 visual acuity. C and D depict an individual with late-stage choroideremia.

10 members of a 4-generation family exhibited a dominant form of choroideremia for which the causative gene is unknown. Six of these affected individuals and two of their unaffected relatives are the subjects of this study.

## Study Aims

1. Find the gene responsible for this non-CHM variety of choroideremia
2. Investigate the physiological mechanisms driving choroidal disease
3. Quantify the partial dissociation of photoreceptors from human organoids

## Acknowledgements

Special thanks to Jeaneen Andorf, Louisa Affatigato, Dr. Narendra Pandala, Dr. Edwin Stone, Dr. Nicholas Stone, and the Institute for Vision Research for their unwavering kindness and support. Their guidance has been nothing short of invaluable.

Coussa, R. G., & Traboulsi, E. I. (2011). Choroideremia: A review of general findings and pathogenesis. *Ophthalmic Genetics*, 33(2), 57–65. <https://doi.org/10.3109/13816810.2011.620056>

Im, K., Mareninov, S., Diaz, M. F., & Yong, W. H. (2018). An introduction to performing immunofluorescence staining. *Methods in Molecular Biology*, 299–311. [https://doi.org/10.1007/978-1-4939-8935-5\\_26](https://doi.org/10.1007/978-1-4939-8935-5_26)

Stone, E. (n.d.). Home. <https://www.stonerounds.org/>

Stone, E. M., Andorf, J. L., Whitmore, S. S., DeLuca, A. P., Giacalone, J. C., Streb, L. M., Braun, T. A., Mullins, R. F., Scheetz, T. E., Sheffield, V. C., & Tucker, B. A. (2017). Clinically focused molecular investigation of 1000 consecutive families with inherited retinal disease. *Ophthalmology*, 124(9), 1314–1331. <https://doi.org/10.1016/j.ophtha.2017.04.008>

Stone, N. E., Bohrer, L. R., Mullin, N. K., Berthold, A., Wright, A. T., Han, I. C., Stone, E. M., Mullins, R. F., & Tucker, B. A. (2025). Device-free isolation of photoreceptor cells from patient ipsc-derived retinal organoids. *JCI Insight*. <https://doi.org/10.1172/jci.insight.186338>

## Methods

Short Tandem Repeat Polymorphisms (STRPs) can be used to determine the inheritance of parental alleles in family members. Researchers use the Polymerase Chain Reaction (PCR) to amplify the DNA containing STRPs. The number of repeats vary within the population, and because humans are diploid, they will have no more than two different alleles of a given polymorphism. Using gel electrophoresis, the repeats of different lengths can be separated, revealing the genotype of an individual. In this study, STRPs were used to identify regions of chromosomes that could contain the disease-causing gene in this 4-generation family.

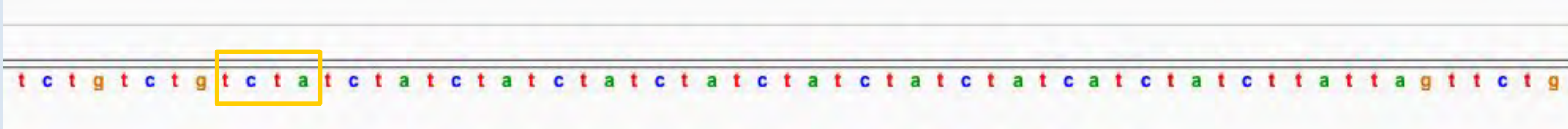


**Figure 2:** This figure shows a short tandem repeat on chromosome 5. Highlighted in yellow are the four nucleotides of the first repeat (tcta).

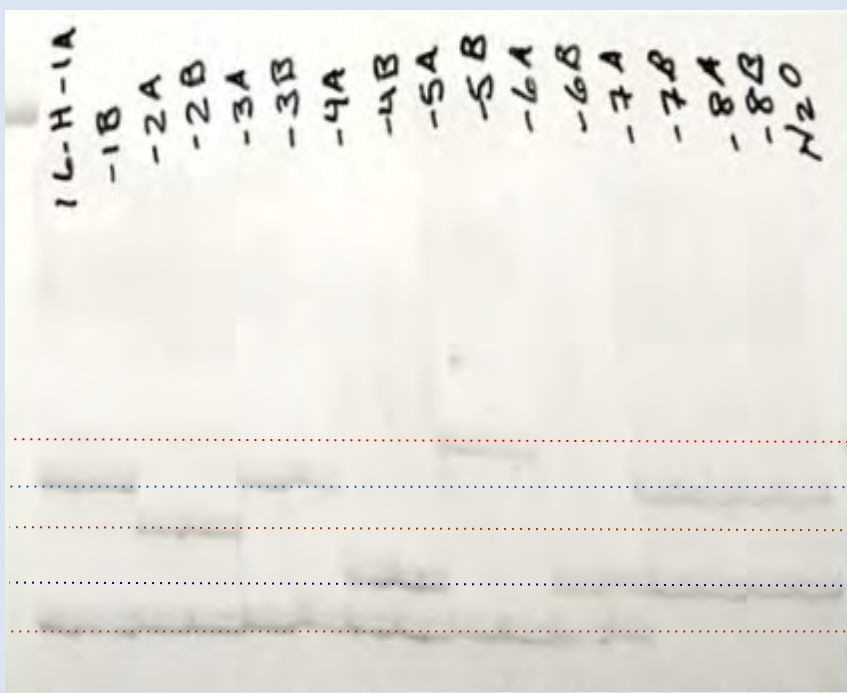


**Figure 3:** This figure reveals the result of gel electrophoresis for marker D5S2848 on chromosome 5 in 8 family members. The bands are representative of different alleles. Vertical position determines the allele number.

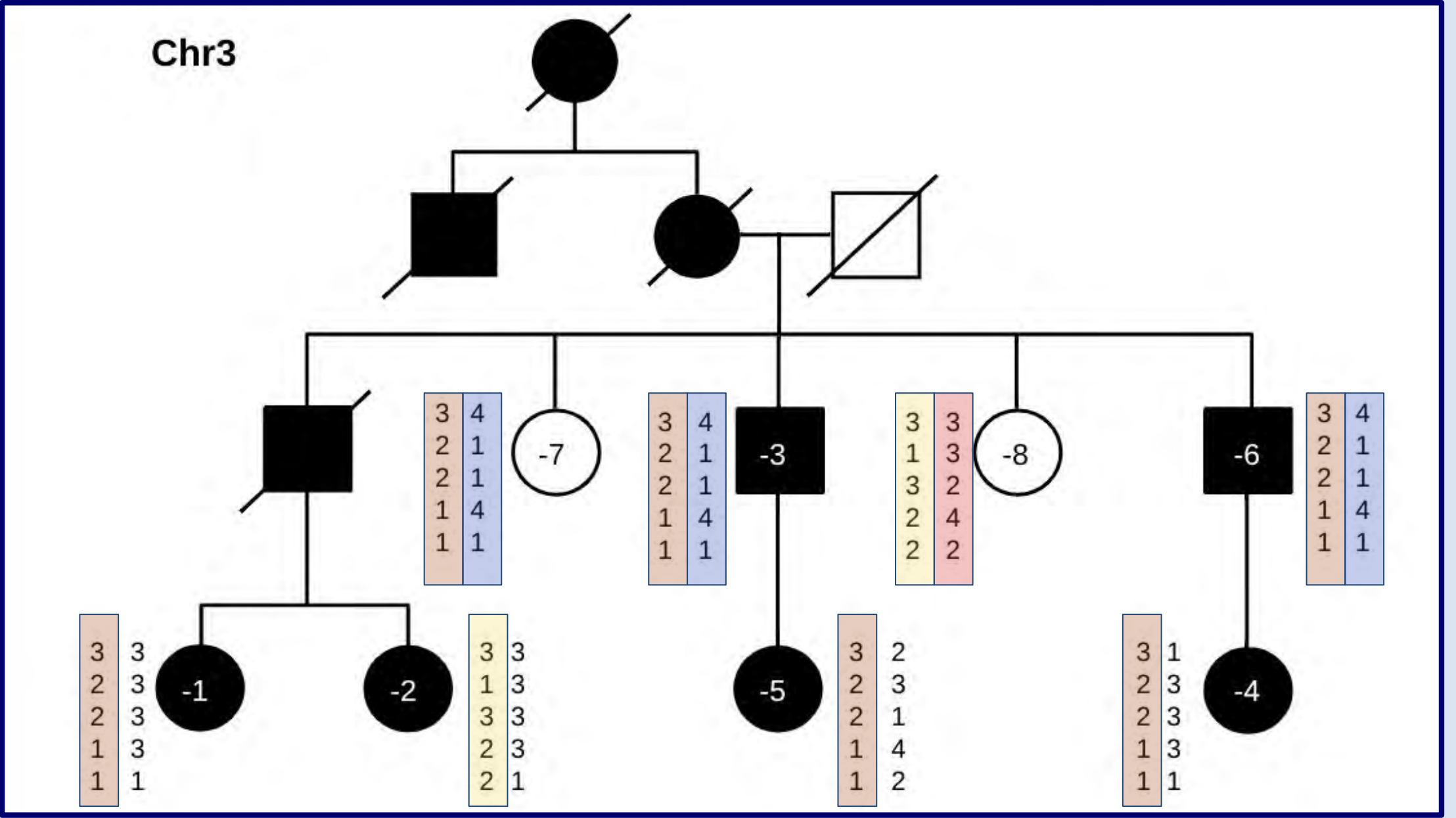


**Figure 4:** This pedigree shows that chromosome 3 cannot be the location of the causative mutation in this family. Notice that individuals 1 and 2 don’t share an allele.

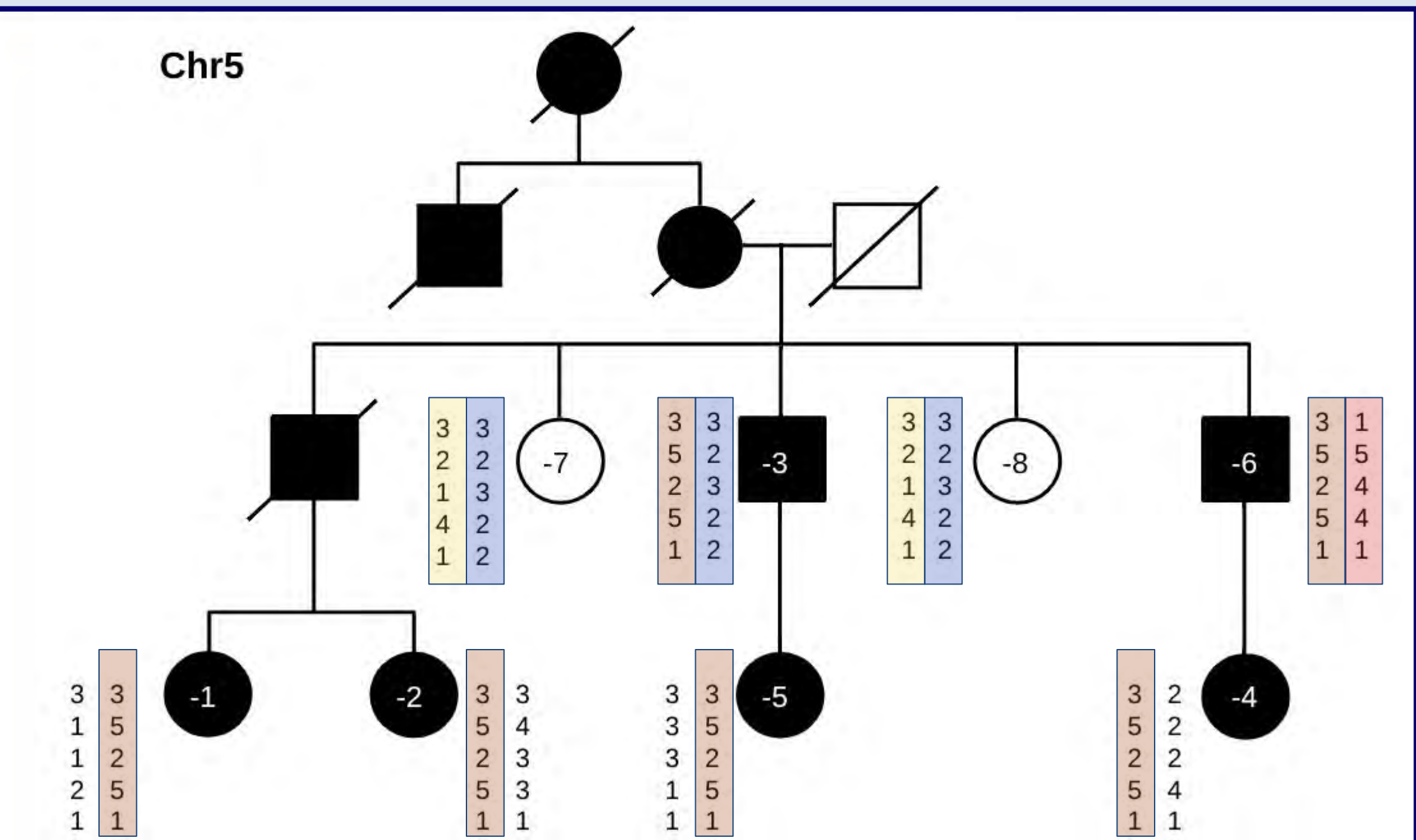


**Figure 5:** This pedigree shows that chromosome 5 could be the location of the causative mutation for this family’s disease. Notice that the “35251” allele is carried by all of the affected members and not carried by the unaffected family members.

## Physiological Effects of Choroid Disease

Tissue from a rat eye with a choroidal disease was sectioned and stained using antibodies tagged with immunofluorescent labels. The results were imaged using a microscope.

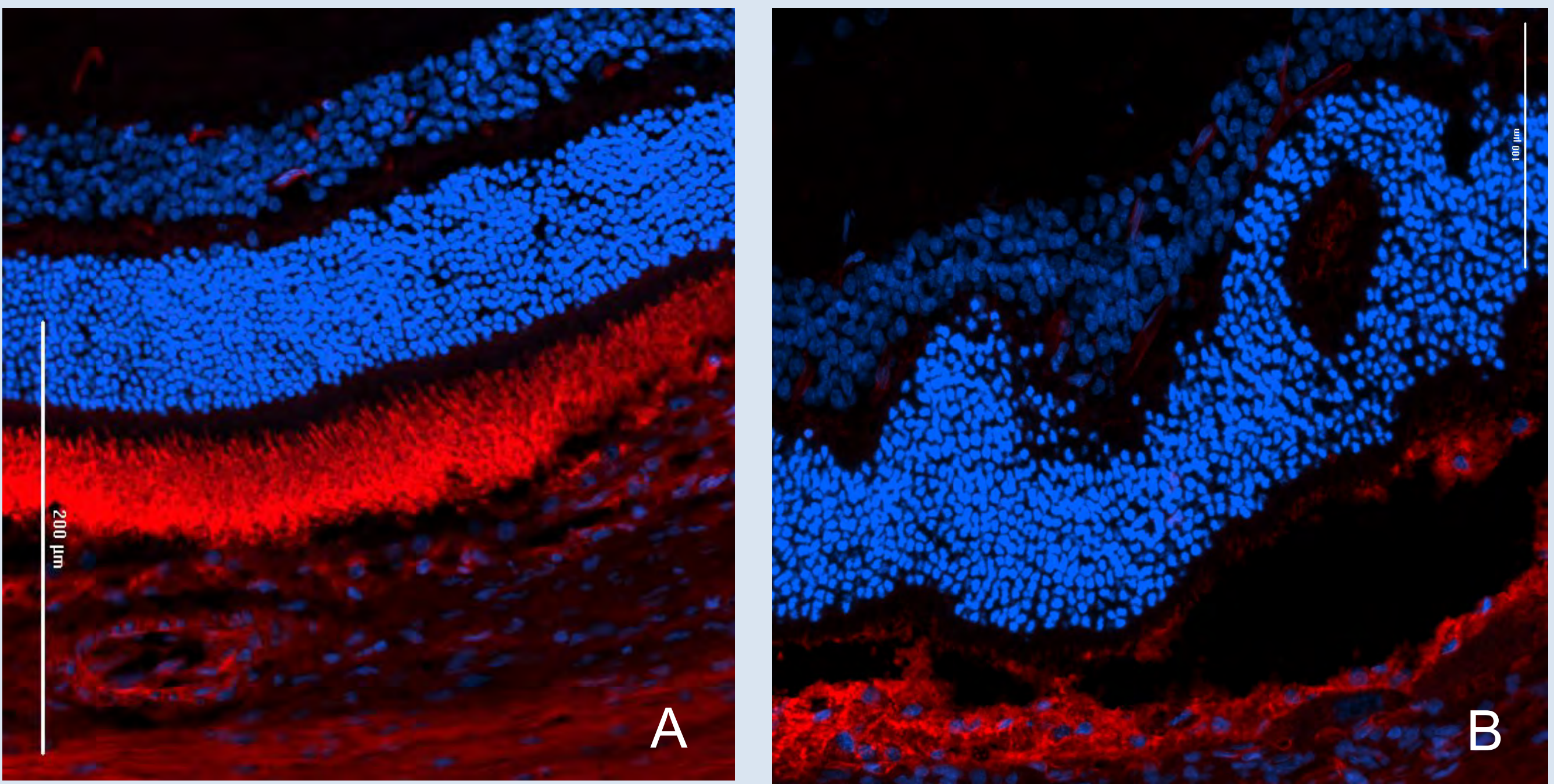


**Figure 6:** Image A depicts the retina of a normal mouse, while Image B depicts that of one genetically modified to have a choroidal disease. The prominent bands of blue stained nuclei correspond to the photoreceptor cells and bipolar cells of the retina while the bright red stain reveals the position of TL lectin on the endothelial cells of the choroid.

## Future Treatments

Stem cell transplantation shows great promise to be an effective treatment of choroideremia (as well as other inherited retinal diseases). For such a treatment, it is often desirable to select specific cell types from a differentiated “organoid.” This technique involves dissociating photoreceptor precursors from the surface of the organoid into the transparent medium surrounding them. By measuring the change in turbidity of the medium, researchers hope to identify the point at which the dissociated cells are of optimal purity for transplantation to patients.

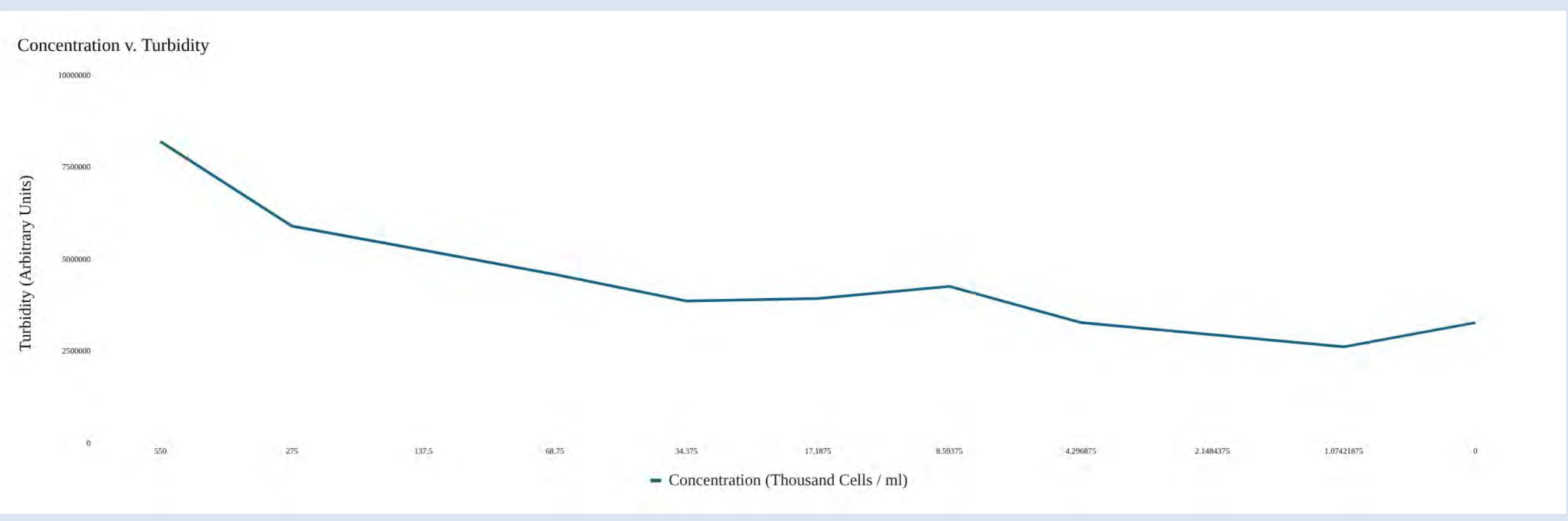


**Figure 7:** This graph shows the relationship between turbidity and cell concentration during a dissociation experiment.

## Conclusions

This study used linkage analysis to pursue the causative gene of a rare form of choroideremia. We also investigated the histopathological features of a murine model of a choroidal disease, and a method for selecting specific cell types for therapeutic transplantation. Gradual enzymatic dissociation shows great future potential to treat choroideremia and a variety of other inherited eye diseases. The studies described here span the entire spectrum of molecular ophthalmology from clinical diagnosis, through molecular diagnosis and pathophysiologic investigation to therapeutic stem cell transplantation.



# Correlations Between Wada and Standard Memory Assessments in Epilepsy Surgery Candidates

Shen, Annie<sup>1,3</sup>, Diah, Kimberly<sup>1</sup>, Martin, Ashby<sup>1</sup>, Bowren, Mark<sup>1</sup>, Thomas, Amber<sup>1,2</sup>, Tranel, Daniel<sup>1,2</sup>

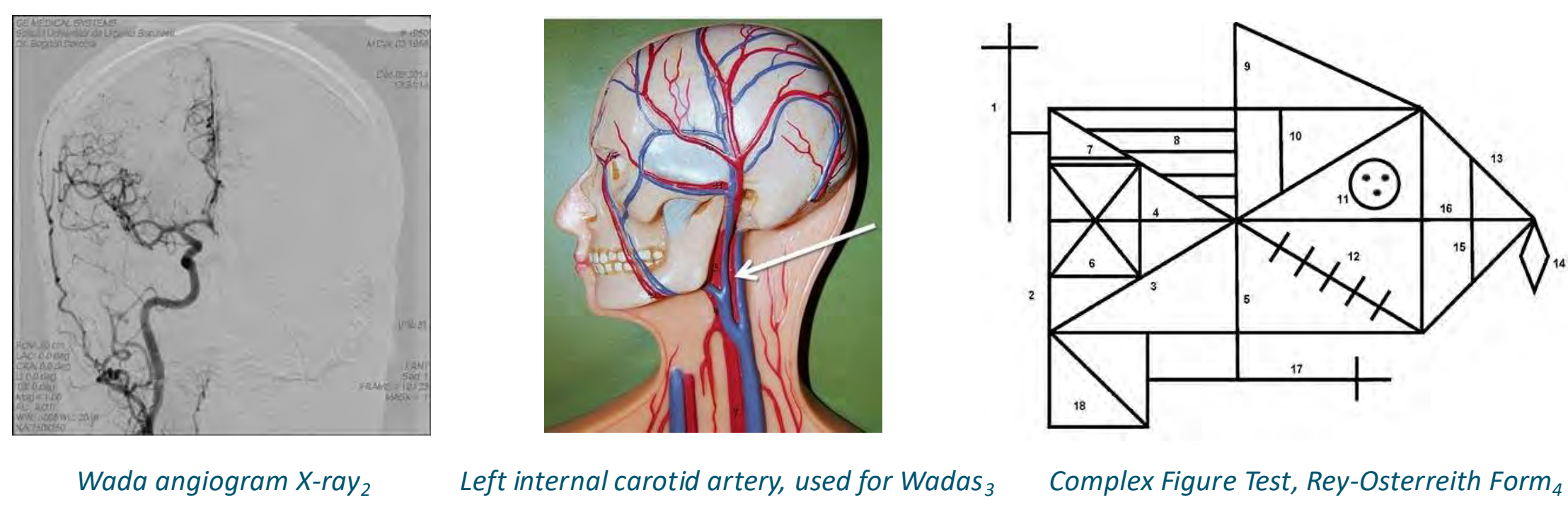
<sup>1</sup>Department of Neurology, <sup>2</sup>Department of Psychological and Brain Sciences, University of Iowa, Iowa City, IA, <sup>3</sup>The Wellington School, Columbus, OH

## Introduction

Patients with refractory epilepsy considering surgery undergo pre-operational cognitive testing and a Wada procedure to detail language and baseline memory lateralization.

- ❖ The Wada is invasive: Left/right carotid artery angiogram occurs where a local anesthetic and dye are applied to the brain via catheter. Wadas help visualize language lateralization and cognitive state (John Hopkins Medicine, 2024)
- ❖ Neuropsychological assessments clinically test memory performance (among other brain functions) and behavioral state

In this study, we evaluated memory correlations between neuropsychological assessment performance and left/right hemisphere Wada performances, assisting in developing efficient test batteries

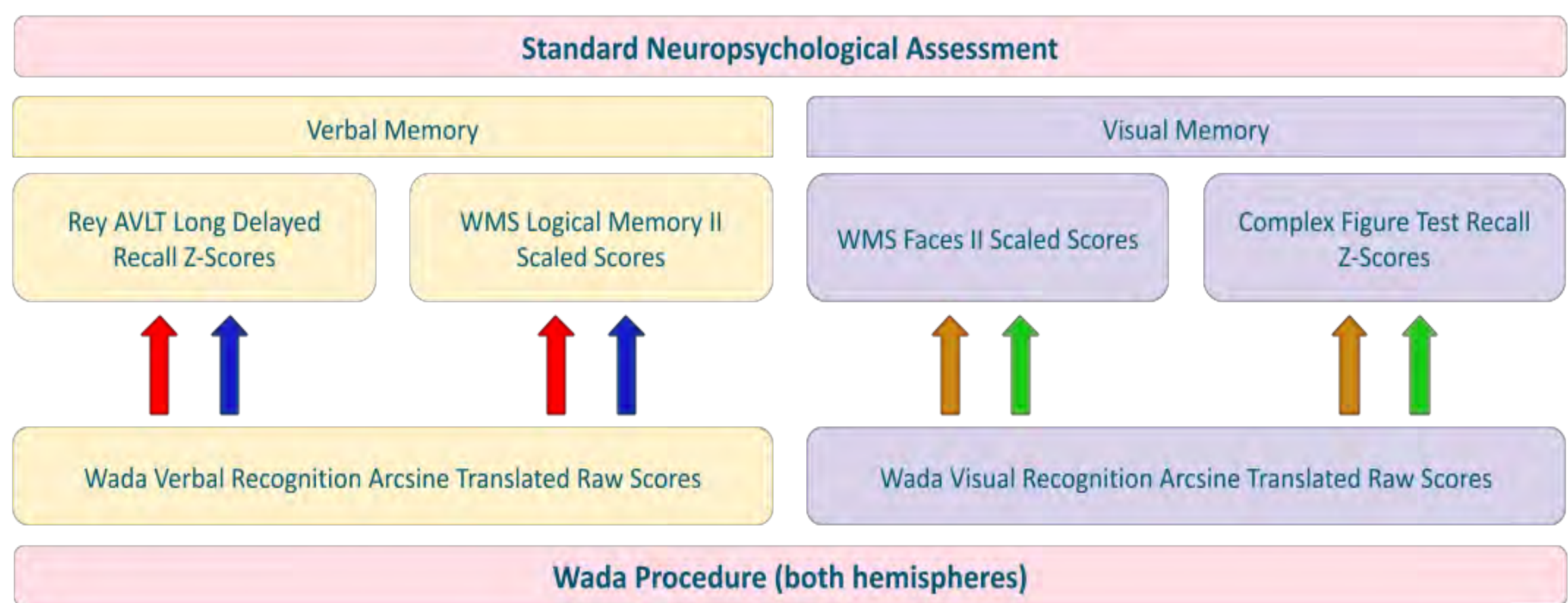


## Research Question

How do left and right hemisphere performances on verbal and visual memory portions of the Wada test correlate to performance on verbal and visual memory portions of neuropsychological assessments?

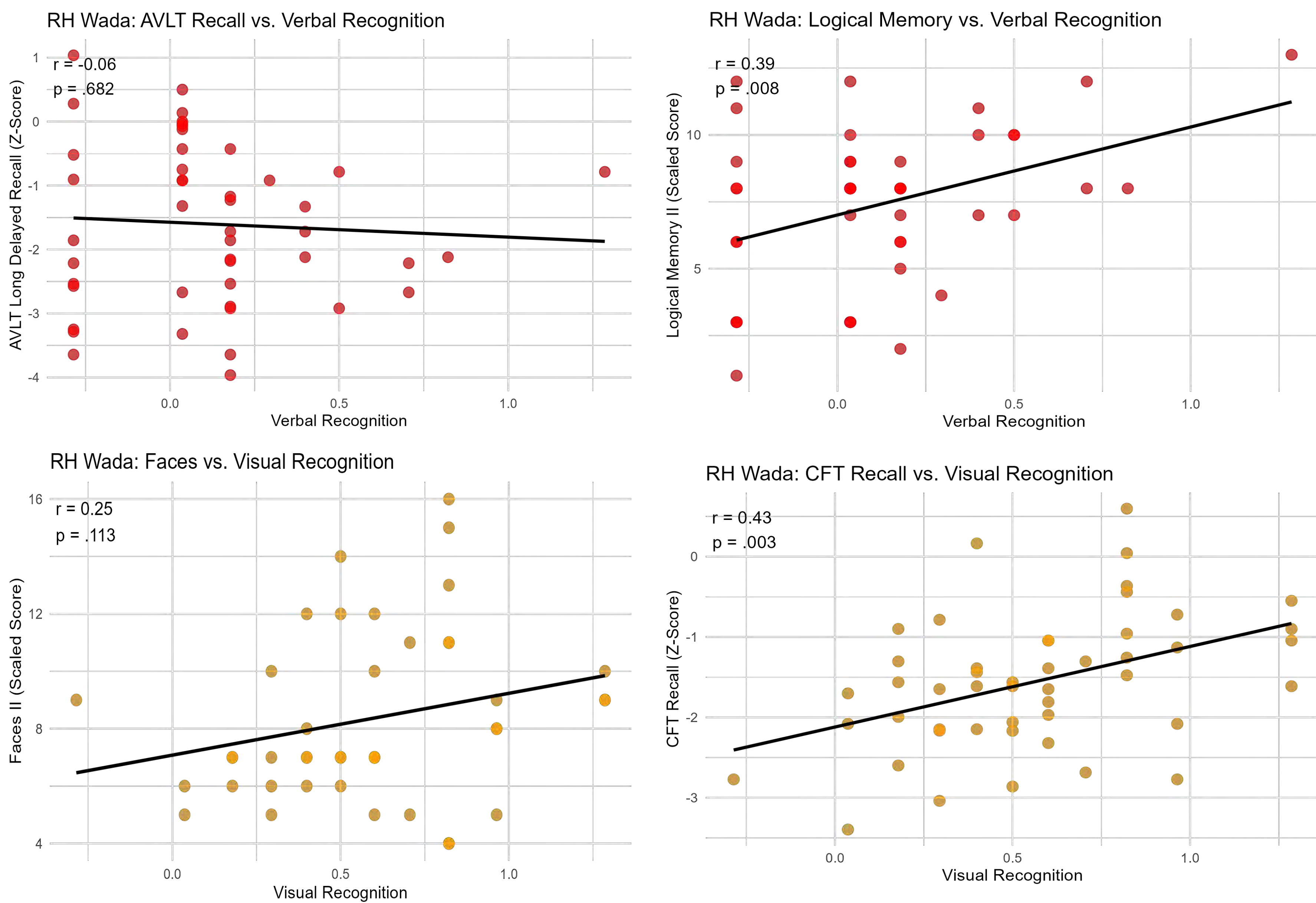
## Methods

- n = 49 UIHC patients who completed Wada procedure and Phase I Protocol neuropsychological testing selected & retrospectively studied (age = 13 years, 7 months to 67 years, 1 month)
- ❖ Wada: Raw scores for Verbal Recognition and Visual Recognition (both hemispheres), then converted with arcsine transformation for analysis
  - ❖ Standard neuropsychological assessment: Z-scores for Rey AVLT Long Delayed Recall & Complex Figure Test recall, scaled scores for WMS Logical Memory II & WMS Faces II

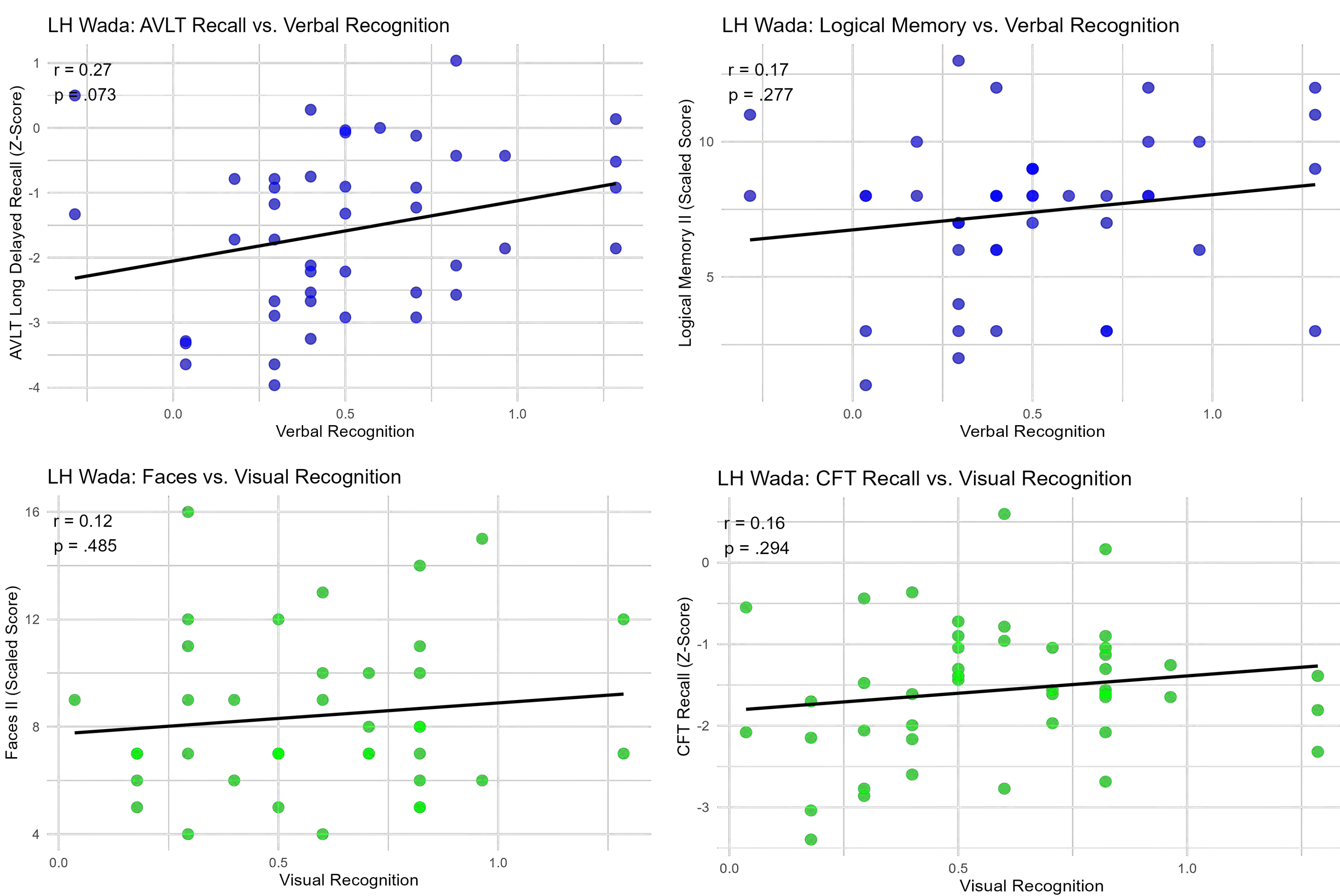


## Results

### Right Hemisphere Wada vs. Standard Neuropsychological Assessment Results



### Left Hemisphere Wada vs. Standard Neuropsychological Assessment Results



## Discussion

- ❖ Right hemisphere Verbal Recognition Wada performance is positively correlated with Logical Memory II on standard neuropsychological assessment (r = 0.39, p < 0.05)
- ❖ Right hemisphere Visual Recognition Wada performance is positively correlated with CFT Recall on standard neuropsychological assessment (r = 0.43, p = 0.003)
- ❖ Although not statistically significant, all tests except right hemisphere Verbal Recognition vs. AVLT Recall has positive r (positive correlation)

## Conclusion

- ❖ Verbal and visual memory portions of Wada tests for both hemispheres generally have positive correlations with verbal & visual memory portions on standard neuropsychological assessments
  - RH Wada Verbal Recognition vs. AVLT Recall was negatively correlated
- ❖ Limitations: small sample size (may lower statistical significance), stringent selection criteria, and localization of seizure activity not considered
- ❖ This study offers initial insight into how correlated Wada and standard neuropsychological assessment performance is regarding verbal & visual memory for each hemisphere
  - May be used by clinicians and future research to develop efficient test batteries for epilepsy surgery candidates

## Acknowledgments

I would like to thank my mentor, Dr. Tranel, for allowing me to work in his lab and ensuring that I am on track for success. I am also thankful for Ashby Martin, Amber Thomas, Dr. Diah, and Dr. Bowren for helping me work through the logistics and giving me everything I need to thrive. In addition, I would like to thank the Benton Neurology Clinic for being such a supportive community and providing me with shadowing opportunities. Lastly, I am eternally grateful for my family and the friends that I have made at SSTP for creating an unforgettable experience this summer.

## References

- John Hopkins Medicine. (2024). Wada Testing. [Hopkinsmedicine.org](https://www.hopkinsmedicine.org/health/conditions-and-diseases/epilepsy/wada-testing).
- Mahmoud Zaki el-Dine, H. (2021). Anteroposterior and lateral views for DAS carotid system [Photograph]. Ain Shams University. <https://doi.org/10.4236/nm.2021.121002>
- (2023). Internal Carotid Artery Model [Photograph]. Mavink.com. <https://mavink.com/explore/Internal-Carotid-Artery-Model>
- Zhang, X. (2021, August). The 18 scoring units of the Rey-Osterrieth Complex Figure [Digital Image]. First Hospital of Shanxi Medical University. <https://doi.org/10.3389/fneur.2021.680474>





# Ion-induced changes in regenerated *B. Mori* silk self-assembly

David Shi<sup>1</sup>, Alvis Chen<sup>2</sup>, Xuan Mu<sup>2\*</sup>

<sup>1</sup> Johnston High School, IA; <sup>2</sup> Roy J. Carver Department of Biomedical Engineering, University of Iowa; Email: xuan-mu@uiowa.edu

## Introduction

- Silk fibroin (SF) is a **sustainable** and **proteinaceous** biomaterial characterized by high tensile strength, toughness, and extensibility, making it an attractive **alternative** to conventional polymers.<sup>1,2</sup>
- This strength derives from a **hierarchical** self-assembly process, particularly the transition from random coils into  $\beta$ -sheet nanostructure.<sup>2,3</sup>
- The natural silk spinning process requires both a **pH gradient** and shear force, where low pH and **kosmotropic ions** on the **Hofmeister Series** trigger **liquid-liquid phase separation (LLPS)** from liquid droplets into aligned nanofibrils.<sup>3</sup>
- The lyotropic properties of different salts enable the SF self-assembly process to be tailored to specific applications, such as tissue scaffolding and **targeted drug delivery** for chronic diseases like cancer.<sup>1,4</sup>
- The desired structure is manufactured in a process designed to replicate the natural silk spinning process through **regenerated silk fibroin**, **3D printing**, and **salt baths**, employing kosmotropic ions to promote gelation and  $\beta$ -sheet nanostructure.<sup>2-4</sup>
- The gelation behavior of silk can be finely tuned using kosmotropic salts, shear stress, pH, or functional additives, allowing precise control of material stiffness and structure, including **porosity**.<sup>1-3</sup>
- While both pH and Hofmeister series salts are known to influence silk assembly, their **separate effects** and **interactions** are poorly understood.
- The goal of this study is to **isolate and compare** the effects of pH and ion concentration by **decoupling** via adjustable buffers.

## Methodology

### Silk Fibroin Regeneration

- Silk is degummed in 8.48g Na<sub>2</sub>CO<sub>3</sub>, dissolved in 9.3M LiBr, and dialyzed to achieve the desired concentration (10% w/v).

### Salt & Buffer Preparation

- Salts of various lyotropic qualities and increasing concentrations are dissolved and diluted.
- pH of all salts are measured and replicated
- MES + NaOH buffer is prepared to match the pH of the salts

### Silk treatment

- 10% Silk Fibroin is mixed with increasing concentrations of salts in a 2:1 ratio.
- MES + NaOH buffer and water are added in the same ratio

### Absorbance Assay

- Absorbance of 550 nm 10% SF + Salt is measured in 96-well microplate reader
- Readings are taken at 5, 10, 15, 20, 25, and 30 minutes
- Each Salt is triplicated to account for variability and reduce error

### Data Processing

- Absorbance data is gathered and compiled with pH readings.
- Processed data was plotted in a 3D surface plot, turbidity vs. salt concentration, and turbidity vs. time for ease of analysis
- Statistical analysis was performed for correlations between turbidity and pH and concentrations

### Sample imaging

- IgG-Texas Red fluorescence 3D confocal imaging is conducted on samples to view microstructure.

## Results

### Turbidity (OD) vs Salt Concentration

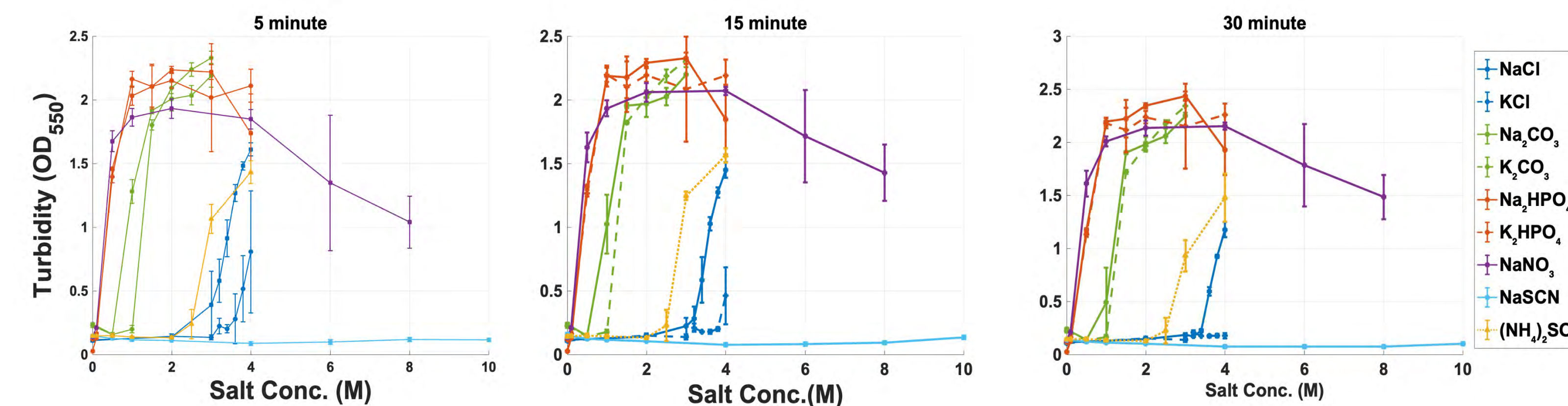


**Figure 1:** Turbidity at 550nm of 10% silk fibroin (SF) solutions measured 5, 15, and 25 minutes after the addition of various salts at increasing concentrations. Salts of similar composition (same anion) are marked in similar colors.

### Turbidity vs. pH of NaCl, KCl & MES + NaOH / TMAH

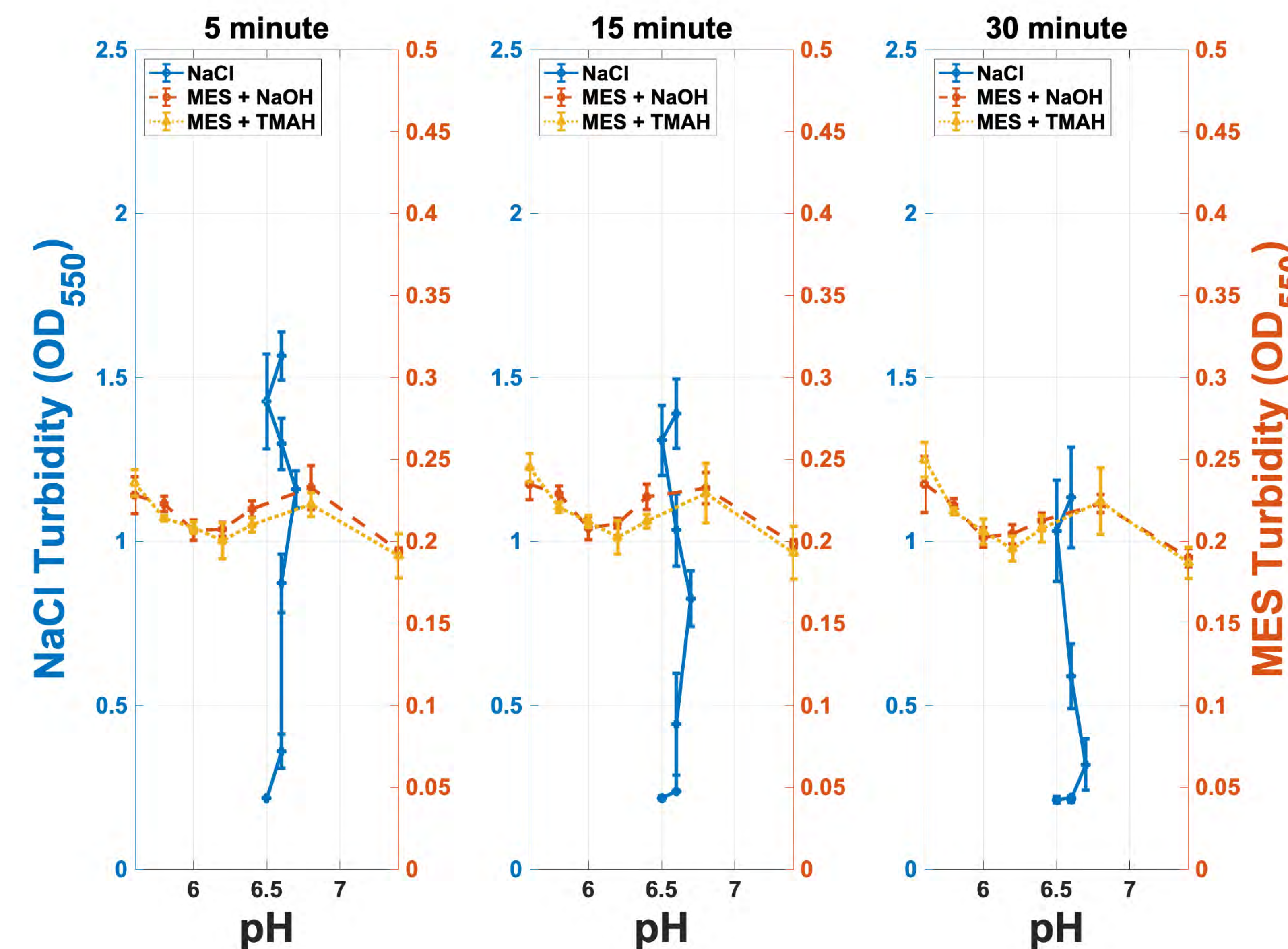
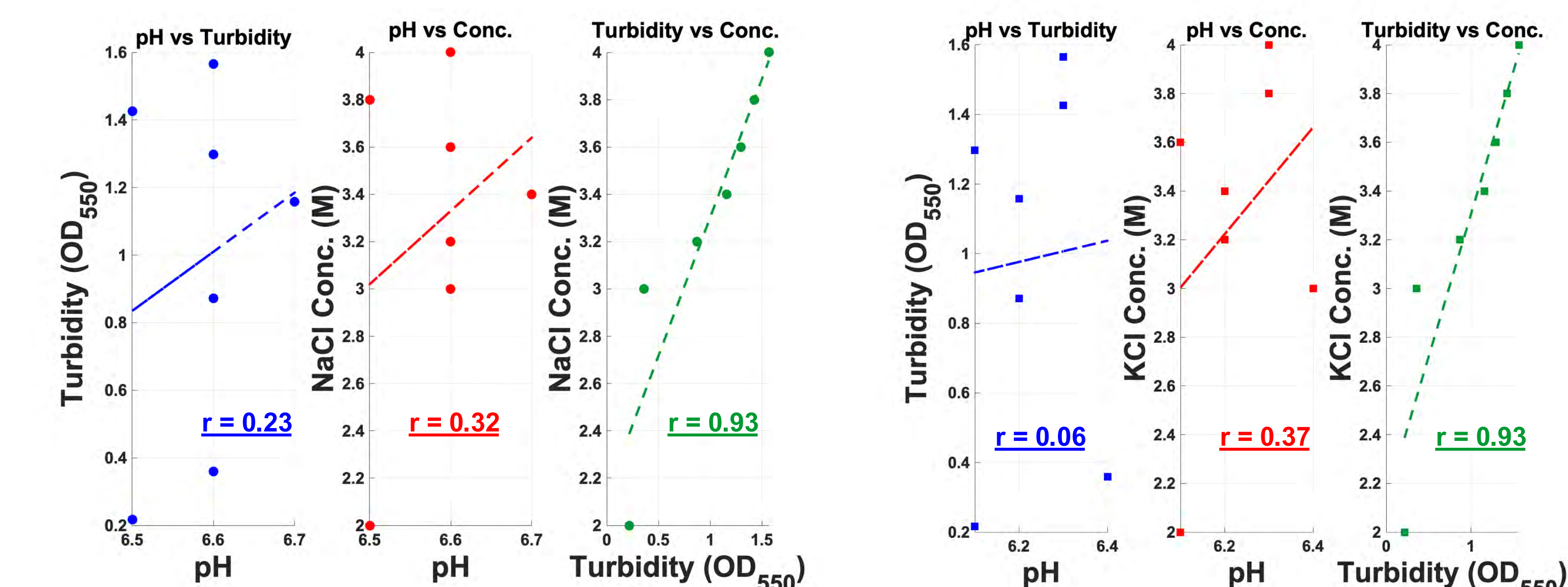


**Figure 2:** Turbidity at 550nm of 10% silk fibroin solutions measured 5, 15, and 30 minutes after the addition NaCl and MES buffers.

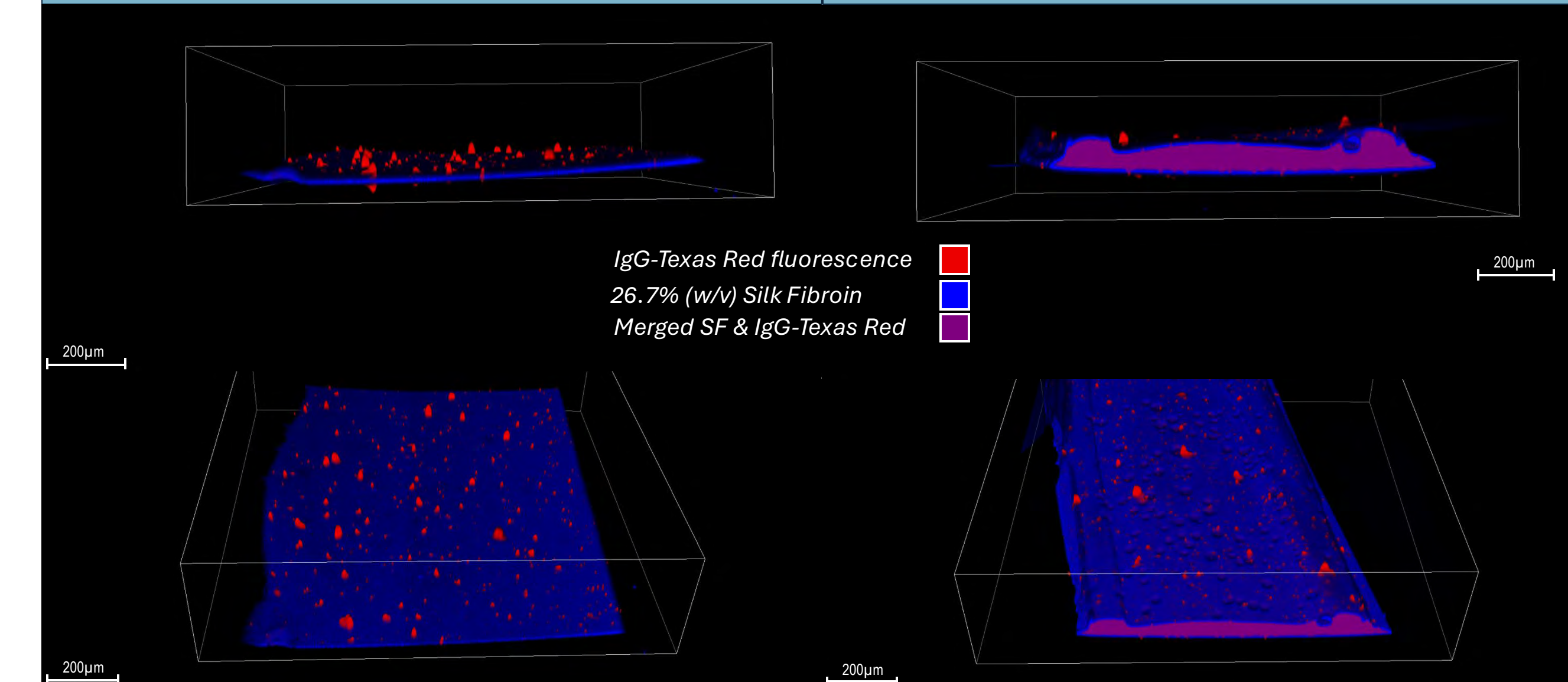
### Pairwise Correlation Plots



**Figures 3 & 4:** Correlation between 3 different parameters – pH, turbidity, and salt concentration – is shown for 10% silk fibroin 5 minutes after the addition of salts. No significant association exists between pH vs. turbidity nor pH vs. concentration. Strong correlation exists between turbidity and concentration.

### Confocal Imaging ((NH<sub>4</sub>)<sub>2</sub>SO<sub>4</sub>)

### Confocal Imaging (NaH<sub>2</sub>PO<sub>4</sub>)



**Figures 5-8:** Confocal imaging of SF sample after the addition of (NH<sub>4</sub>)<sub>2</sub>SO<sub>4</sub> (Fig. 4) and NaH<sub>2</sub>PO<sub>4</sub> (Fig. 5) ions.

## Discussions

- Salt ions can **regulate the assembly behavior of silk fibroins** to form new phases (e.g., LLPS), which may be related to the formation of  **$\beta$ -sheets-rich nanostructures**.
- Kosmotropic** cations and anions (NH<sub>4</sub><sup>+</sup>, PO<sub>4</sub><sup>3-</sup>, SO<sub>4</sub><sup>2-</sup>, CO<sub>3</sub><sup>2-</sup>) promoted **assembly behavior**, and those with **greater chaotropic strength** (SCN<sup>-</sup>, NO<sub>3</sub><sup>-</sup>) **decreased turbidity**.
- For most salts tested (KCl, H<sub>2</sub>PO<sub>4</sub><sup>-</sup>, SCN<sup>-</sup>, NO<sub>3</sub><sup>-</sup>), there is **no significant association** between pH and turbidity at high concentrations ( $p < 0.05$ ).
- There is a **very strong association** ( $p < 0.01$ ) between concentration and turbidity and concentration and pH.
- Some salts (NaCl, KCl) were **buffered with MES + NaOH / TMAH** solutions. pH **did not** have a **significant correlation** with observed turbidity at the 550nm level.
- Additionally, the turbidity of SF solutions with NaCl and KCl was **significantly higher** ( $p < 0.05$ ) than that of MES with similar pH for **high concentrations** ( $> 3.0$ ) and for earlier times ( $< 15$  min).
- Comparative analysis of confocal imaging using **IgG-Texas Red fluorescence** shows SF's filament **microstructure** is **highly tunable**.

## Future Work

- Additional buffers can be utilized to **decouple pH** from **ion concentration** for other pH ranges (e.g., Citrate for pH 3-7 and CAPS for pH 9-12).
- Perform **statistical analysis** of decoupled salt and buffer solutions
- Other **concentrations of silk fibroin** (8.5%, 20%, 25%) could be tested
- We tested kosmotropic, intermediate, and chaotropic anions, but only tested kosmotropic and intermediate cations. A chaotropic anion like Ca<sup>2+</sup> could be tested to ensure comprehensiveness
- Testing of **salt-bath assisted** 3D printing structures

## References & Acknowledgements

I would like to thank Professor Xuan Mu, Alvis Yu-Wei Chen, and the rest of the Mu lab for their mentorship and the opportunity to work in this lab. Additionally, I would like to thank the Ashlee Donithan of the Belin Blank Center, and everyone else involved with SSTP for this amazing opportunity.

- [1] Lin, Xiang, et al. "Stimuli-responsive silk fibroin for on-demand drug delivery." *Smart Medicine*, vol. 2, no. 2, 16 Feb. 2023, <https://doi.org/10.1002/smm.20220019>.
- [2] Mu, Xuan, et al. "3D printing of silk protein structures by aqueous solvent-directed Molecular Assembly." *Macromolecular Bioscience*, vol. 20, no. 1, 21 Aug. 2019, <https://doi.org/10.1002/mabi.201900191>.
- [3] Mu, Xuan, et al. "A brief review on the mechanisms and approaches of silk spinning-inspired biofabrication." *Frontiers in Bioengineering and Biotechnology*, vol. 11, 6 Sept. 2023, <https://doi.org/10.3389/fbioe.2023.1252499>.
- [4] Mu, Xuan, et al. "3D printing of monolithic proteinaceous cantilevers using regenerated silk fibroin." *Molecules*, vol. 27, no. 7, 26 Mar. 2022, p. 2148, <https://doi.org/10.3390/molecules27072148>.



# Impacts of High Strain on Particulate Structures of Various Subdivisions

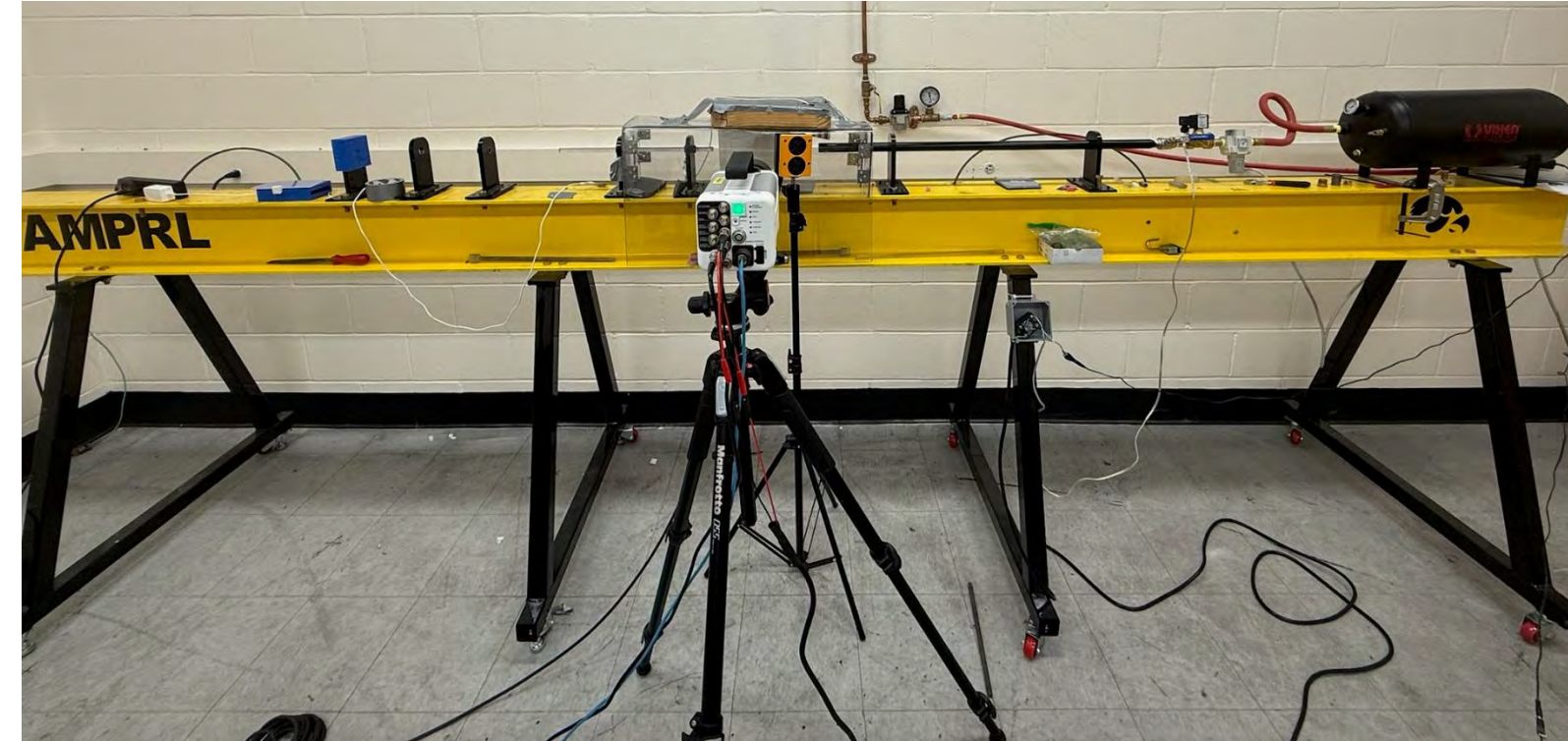
Malick Sogur, Yi-Wei, Arnold Bangel PHD, Nazanin Tabatabaei, Helen Chang, Jack Berlage, Xuan Song PHD  
Department of Industrial and Systems Engineering, University of Iowa

## Research Purpose

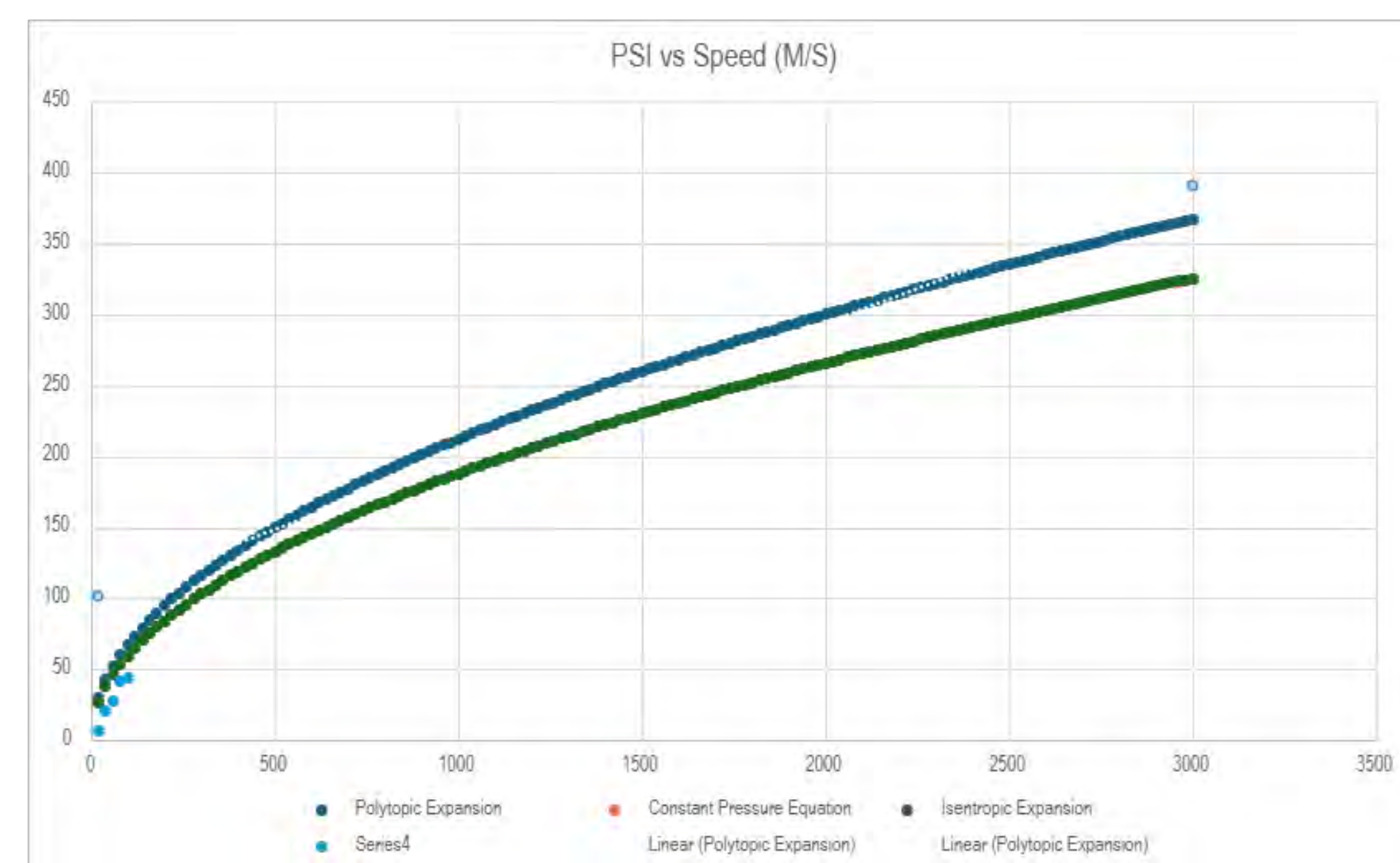
- **Research Objective:** The purpose of this study is to investigate how different patterns of particulate matter deform under high strain This enables understanding of how other particulate materials with similar structures may react under strain.
- **Real World Application:** Increases understanding of real-world deformation of energetic materials, and how brittle materials in defense, aviation, or automotive systems may react to sudden strain.

## Methods

- **Main Equipment Used:**
  - **Direct Impact Hopkinson Bar:** Similar to a gas gun, utilizes pressure to shoot a carbon-fiber rod at high speeds to inflict high strain onto directly onto objects in this case a sugar cube.



- **Hopkinson Bar Calibration:** In order to make sure speeds surpassing 40-50m/s were reached the bar was shot numerous times with calculated results. With max speeds of 60 m/s at 100 psi. Below showcases theoretical models for psi vs speed in m/s.



- **Sugar Cubes as Particulate Matter:**
  - **Visual Clarity:** Differences between the larger blue sugar molecules and smaller pink ones make analyzing easier.
  - **Energetic Materials:** Sugar has a similar molecular structure to many energetic materials that would not be safe to test in the lab, for example pentaerythritol tetranitrate.
  - **Moldable Structure:** Easier to work with compared to other materials to shape.

## Methods Cont...

- **Molding Sugar Cube:**
  - Binder made with 10:1 ratio of silicone elastomer base and silicone curing agent which is PDMS
  - Each Cube is 20\$ Binder and 80% Sugar
  - Pink Powder passed through size 200 sieve and blue powders don't fit through size 80 sieve causing more density in pink areas and less density in blue parts.



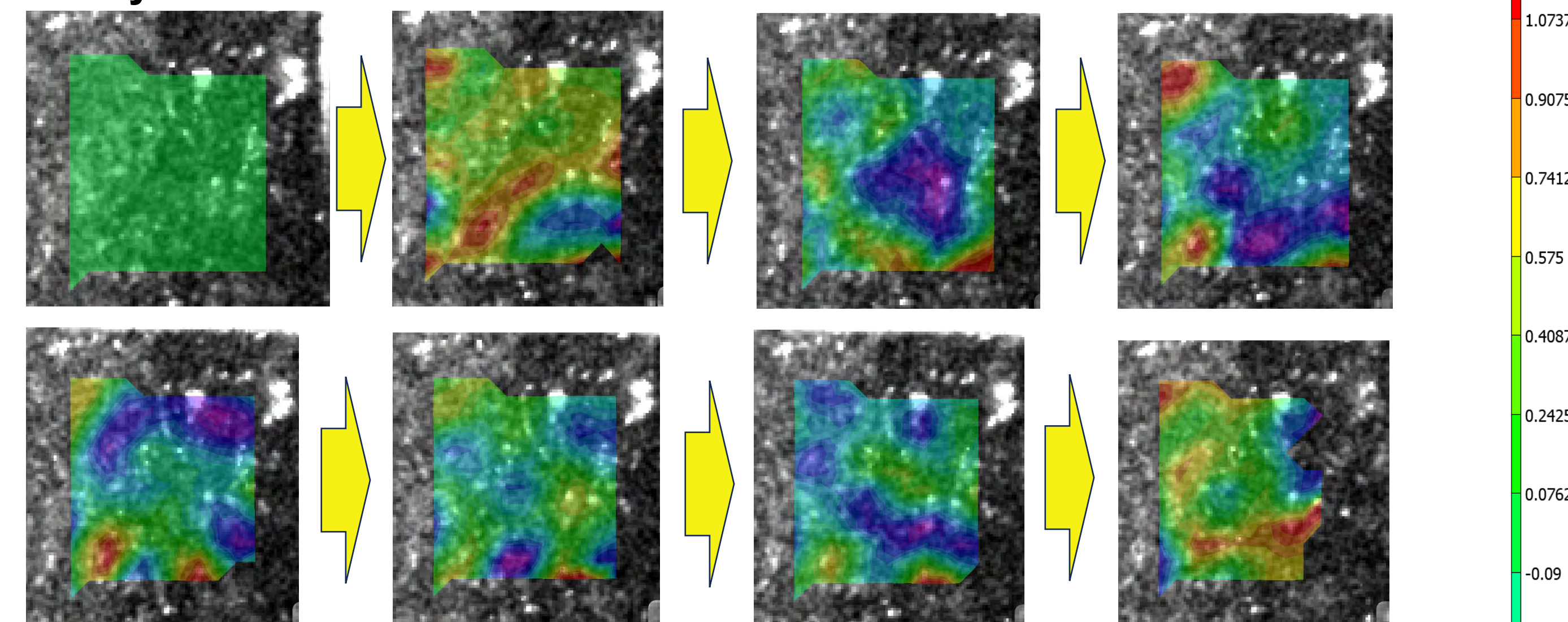
- **Utilizing Hopkinson Bar**
  - Each Shot of bar done at 100psi ~50-60m/s
  - Camera recorded at 160kFPS
  - Three half cut cubes, and two 2x2s and 3x3s were tested

- **VIC 2D**
  - Videos from launches were uploaded into VIC-2D for image analysis
  - Through the software is where data on strain impacts could be found

## Results

Although Image Analysis for half-half cubes was successful, once cubes became more divided due to camera quality and software struggles it became difficult for the software to pick up accurate strain results.

**Half by Half Cube:** Over first 8 frames of deformation

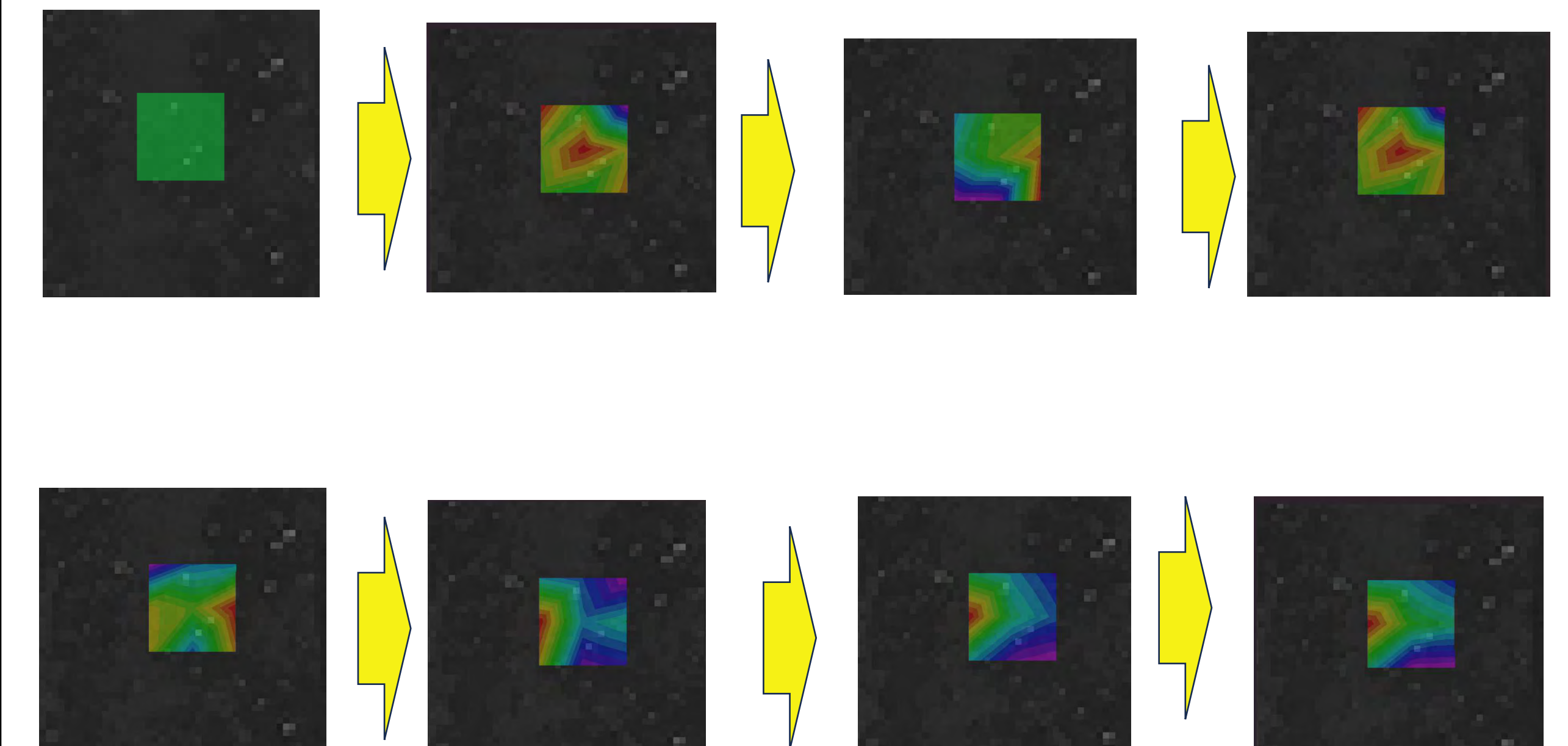


**2x2 Cubes:**



## Results Cont...

**3x3 Cube did not product accurate strain results:**  
The following images came after when capabilities increased to 500k frame rate, first 8 frames.



## Future Work

- Take Additional Time to Analyze Strain Results to Draw Conclusions
- In order to make experimentation more effective
  - Use a light of higher lumen count
  - Use higher detail high speed camera
  - Lower area of interest so resolution does not affect imaging

## Acknowledgments

Thank you to the Belin blank center for hosting UIOWA SSTP and allowing the opportunity for me and many other students to get involved in research. Additionally, thank you to Dr.Song for allowing me to work in his lab this summer through the SSTP at UIOWA. Additional thanks to the grad students in the lab for helping guide through the project.

## References

1. Narayan, D., Bhatnagar, N. (2024). Design and Fabrication of a Single-Stage Gas Gun. In: Velmurugan, R., Balaganesan, G., Kakur, N., Kanny, K. (eds) Dynamic Behavior of Soft and Hard Materials Volume 1. IMPLAST 2022. Springer Proceedings in Materials, vol 34. Springer, Singapore. [https://doi.org/10.1007/978-981-99-6030-9\\_46](https://doi.org/10.1007/978-981-99-6030-9_46)
2. Ravindran, S., Tessema, A., Kidane, A., & Jordan, J. (2019). Weak-shock wave propagation in polymer-based particulate composites. *Journal of Applied Physics*, 125(14). <https://doi.org/10.1063/1.5081035>
3. Shin, H., & Kim, J.-B. (2019). Evolution of specimen strain rate in split Hopkinson bar test. *Proceedings of the Institution of Mechanical Engineers. Part C, Journal of Mechanical Engineering Science*, 233(13), 4667–4687. <https://doi.org/10.1177/0954406218813386>
4. Spulak, N., Seidt, J., Ruggeri, C., Revilock, D., & Gilat, A. (2025). Direct impact Hopkinson compression bar experiment for testing at a strain rate of 50,000 s<sup>-1</sup>. *International Journal of Impact Engineering*, 201, 105277. <https://doi.org/10.1016/j.ijimpeng.2025.105277>



# Investigating the behavioral and molecular effects of excess neonatal testosterone on the hippocampus of wild-type mice

Jonathan Szeto<sup>1</sup>, Pravda Quiñones-Labernik<sup>2,3</sup>, Emily Hagan<sup>2,4</sup>, Ted Abel<sup>2,3</sup>, Sarah Ferri<sup>3,4</sup>

<sup>1</sup>The Harker School, San Jose, CA

<sup>2</sup>Department of Neuroscience and Pharmacology, Carver College of Medicine, IA

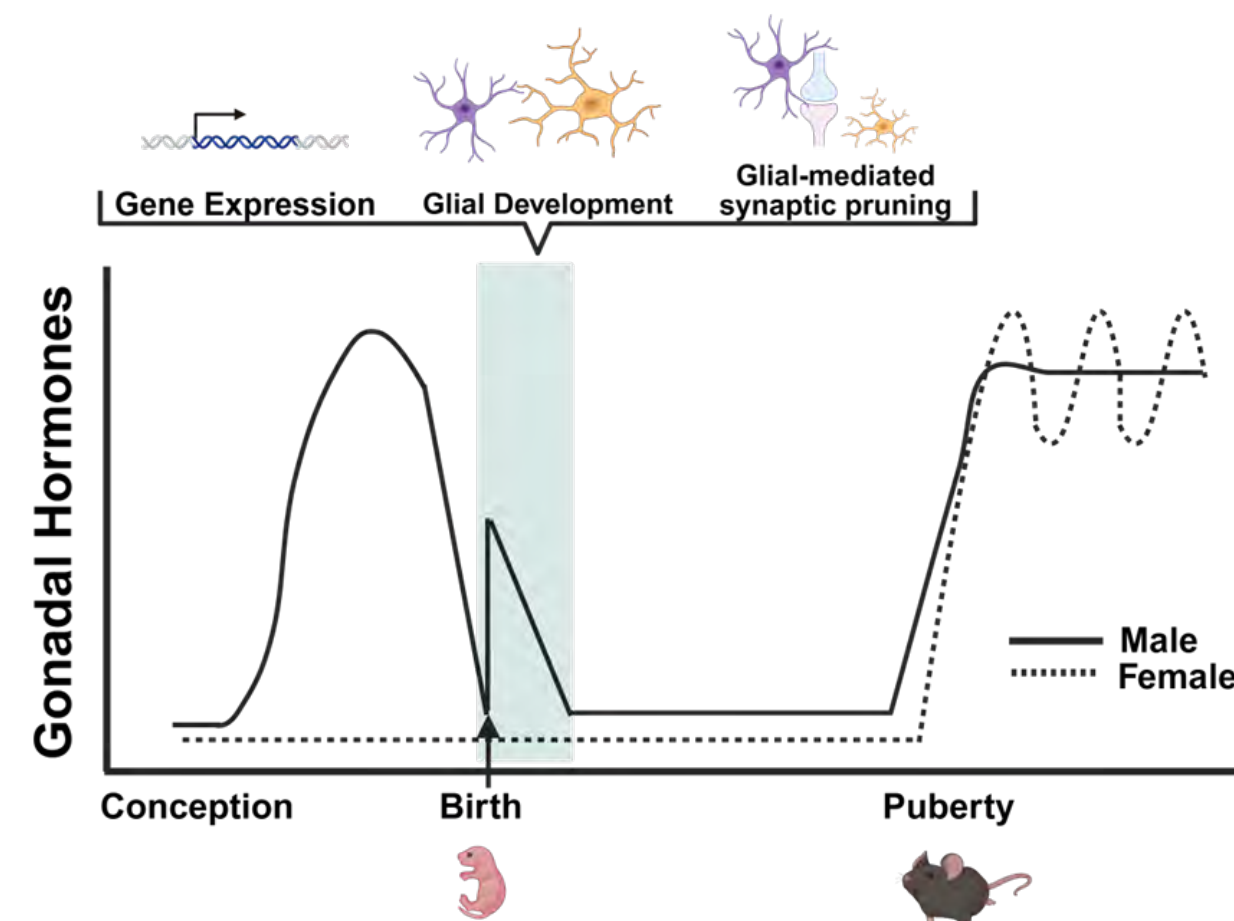
<sup>3</sup>Iowa Neuroscience Institute, University of Iowa, IA

<sup>4</sup>Stead Family Department of Pediatrics, Carver College of Medicine, IA

**IOWA**

Carver College  
of Medicine

## One of the earliest developmental differences between males and females is a perinatal testosterone surge



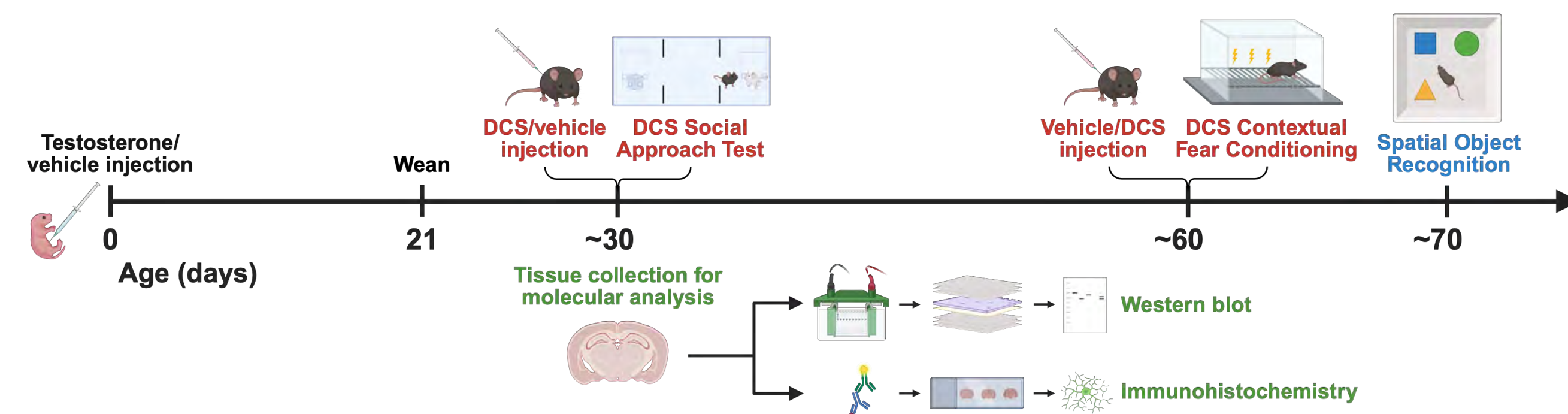
- Neurodevelopmental disorders (NDDs) are associated with social and cognitive deficits and exhibit male bias.
- Testosterone surge masculinizes brain and influences sex-dependent maturational trajectories of glial cells.
- Rodents are useful models for hormone manipulation as their neonatal period mirrors human late fetal development.

## Sex hormone dysregulation at birth has been linked to NDDs and NDD-associated behaviors

- Pregnancy complications involving androgen dysregulation, including gestational diabetes and pre-eclampsia, increase NDD risk in offspring.
- Excess testosterone at P0 but not P18 causes male-specific deficits in social behavior and fear memory, dependent on the amygdala and the hippocampus.
- Amygdala-dependent cued fear conditioning is unaffected by excess neonatal testosterone, prompting further investigation into its effects on the hippocampus.

## Experimental design of neonatal testosterone and D-cycloserine administration in wild-type mice

- D-cycloserine (DCS) is a cognitive enhancer shown to improve social behaviors in animal models of ASD as a partial agonist at the NMDA receptor glycine site.



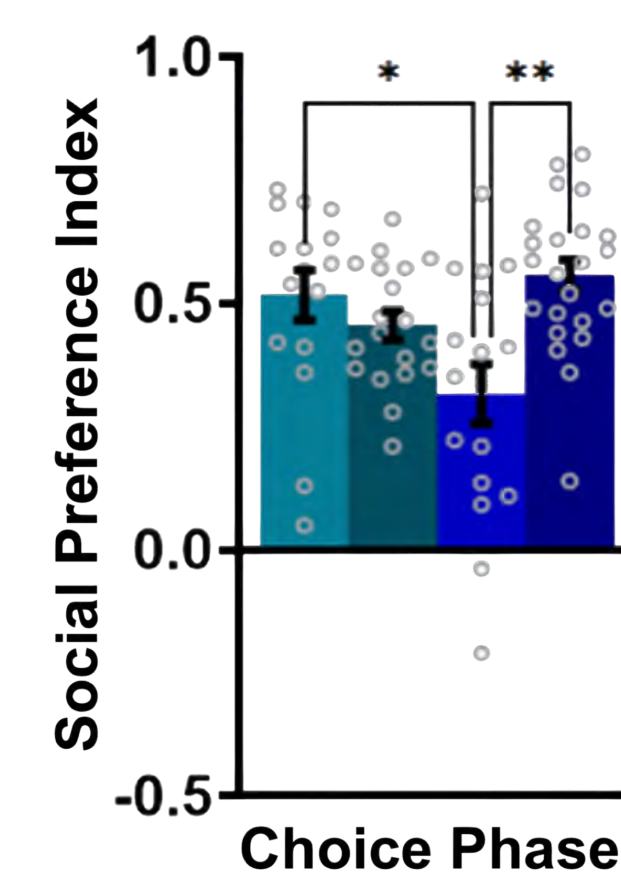
**Testosterone treatment:** 100 µg testosterone propionate in vehicle (sesame oil) or sesame oil was injected subcutaneously within 12 h of birth.

**DCS treatment:** 32 mg/kg DCS in vehicle (saline) or saline was injected subcutaneously 30 min before tests.

## DCS, a partial NMDAR agonist, may rescue testosterone-induced male deficits in social and fear memory

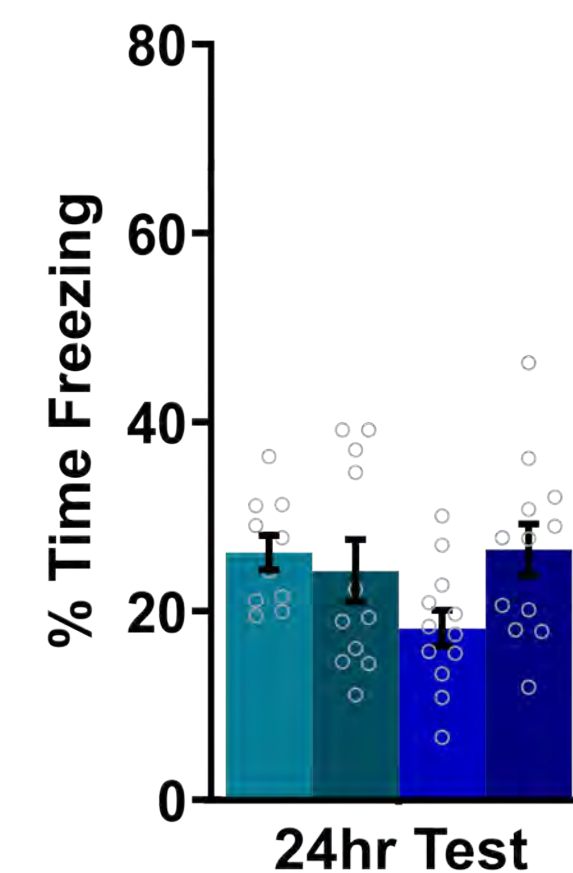
### Three-Chamber Social Assay

- Males + veh (PN0) + veh (PN 30) (16)
- Males + veh (PN0) + DCS (PN30) (19)
- Males + T (PN0) + veh (PN30) (17)
- Males + T (PN0) + DCS (PN30) (23)



### Contextual Fear Conditioning

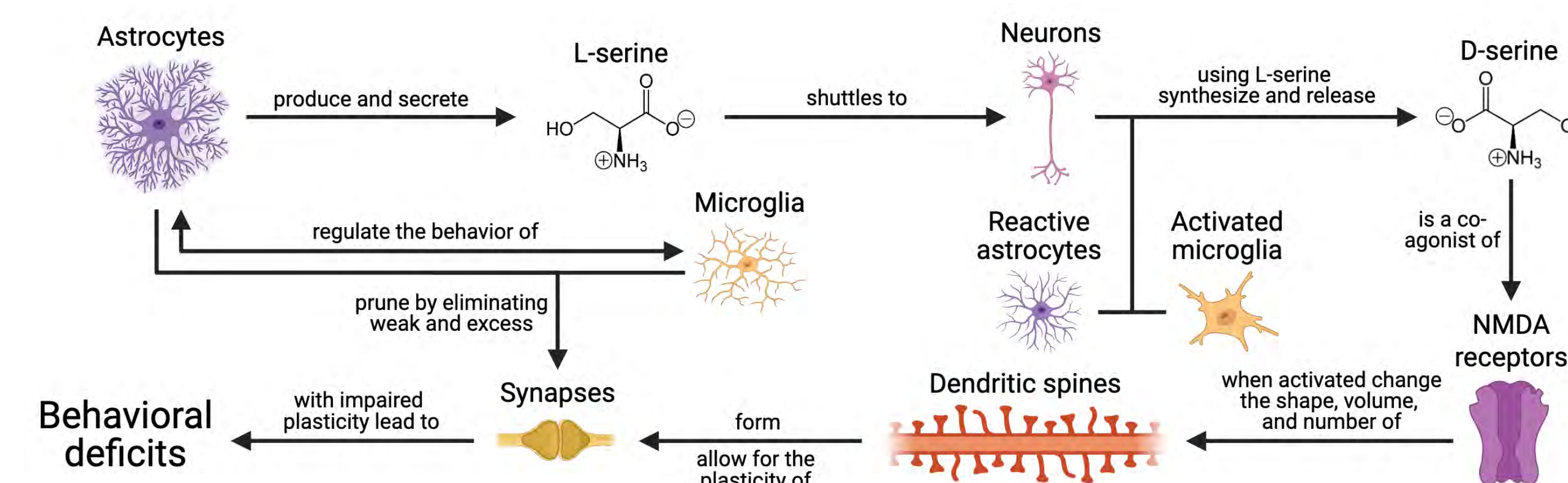
- Males + veh (PN0) + veh (PN30) (10)
- Males + veh (PN0) + DCS (PN30) (11)
- Males + T (PN0) + veh (PN30) (12)
- Males + T (PN0) + DCS (PN30) (12)



**Social Approach Test:** Mice were placed in an arena with clear cylinders for 10-min habituation, followed by 10-min choice phase with novel object (Duplo block) in one and novel social stimulus (age- and sex-matched gonadectomized mouse) in the other. Duration of sniffing of each cylinder was quantified with Noldus EthoVision XT software. Social Preference Index is calculated as (time sniffing social cylinder – time sniffing nonsocial cylinder) / (total sniffing time).

**Contextual Fear Conditioning:** After mice spent 2 min 28 s in chamber freely exploring, 1.5 mA footshock was delivered for 2 s through electrified metal grid flooring, and mice were removed 30 s afterward. Following 24 h, mice were placed back in chamber for 5 min, and duration of freezing was quantified with Cleversys Freezescan software.

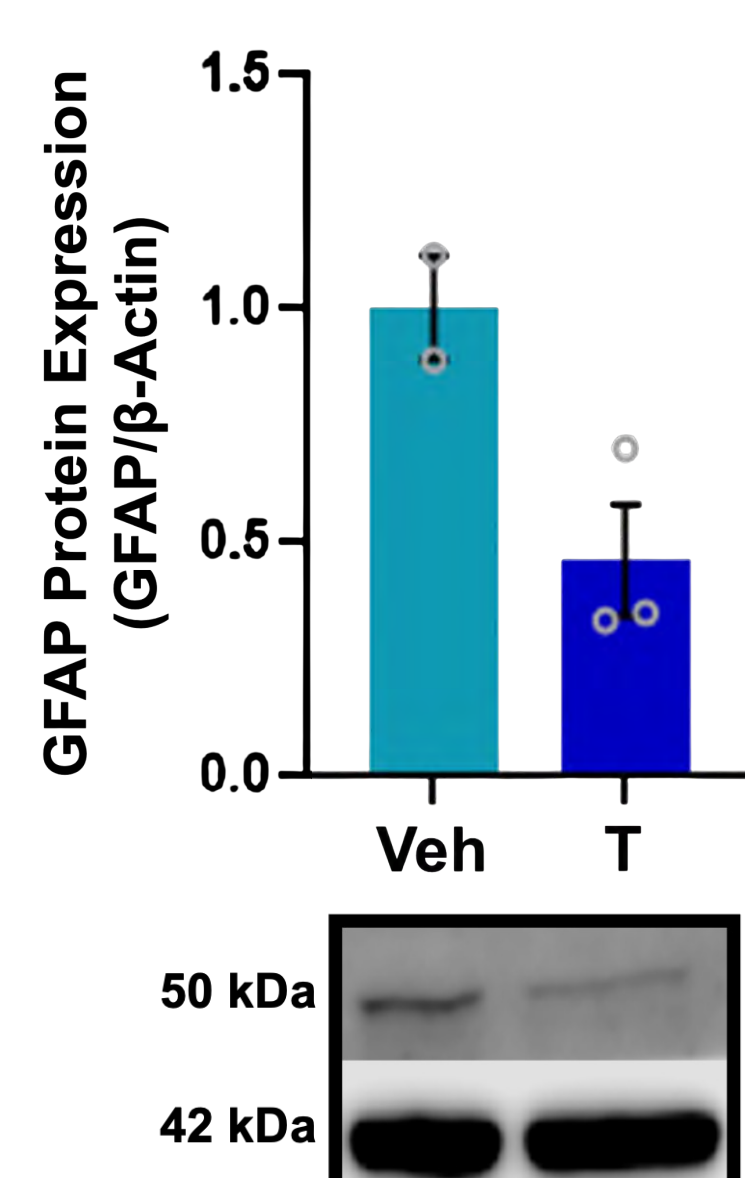
## Glia regulate refinement of synaptic neuronal networks via serine-shuttling pathway and synaptic pruning



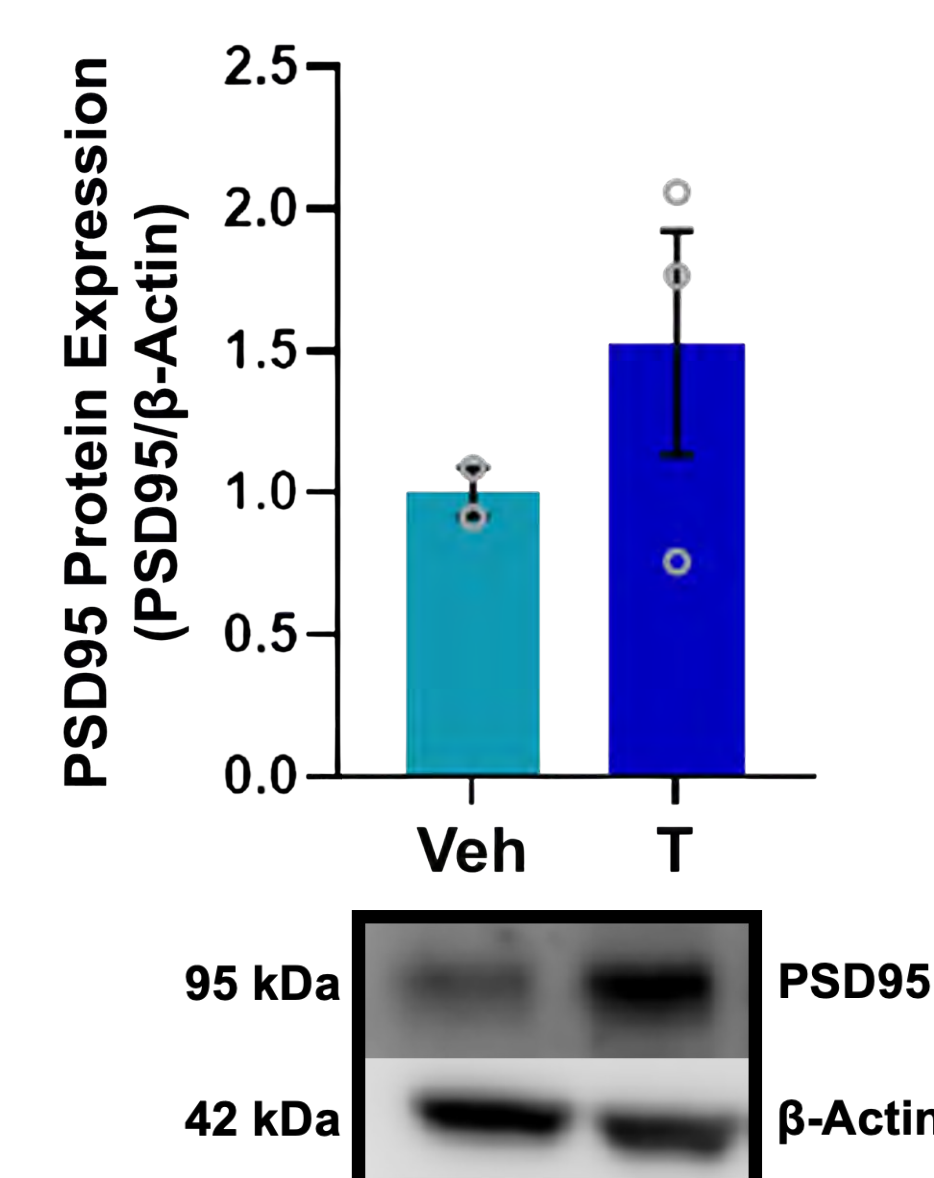
- Astrocytes and microglia play key roles in regulating synaptic plasticity through their involvement in D-serine production and glia-mediated synaptic pruning.
- NMDAR activation induces long-term synaptic plasticity via the remodeling of dendritic spines, and NDD-associated deficits may arise when such plasticity is impaired.

## Excess neonatal testosterone affects expression of astrocyte- and dendritic spine-specific proteins in the hippocampus

### GFAP Western Blot



### PSD95 Western Blot

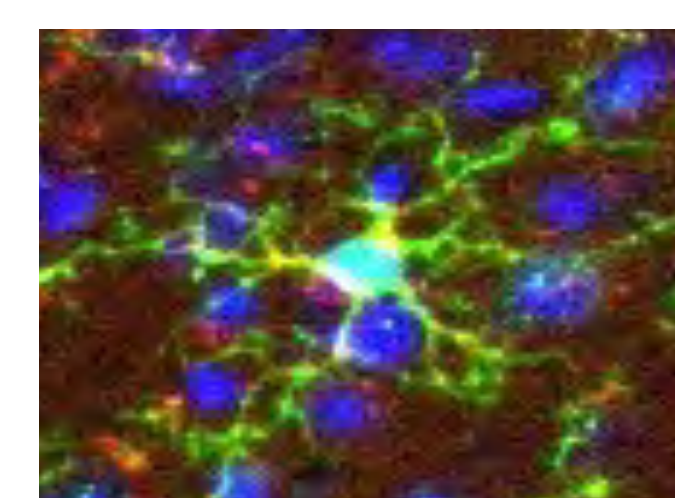


Hippocampi were dissected and homogenized for protein extraction. 25 µg protein was loaded in each well of SDS-PAGE gel and separated via electrophoresis. Proteins were transferred to PVDF blotting membrane and incubated in blocking buffer, primary antibodies (anti-PSD95, anti-GFAP), and secondary (HRP-conjugated). Images were acquired with LI-COR Odyssey<sup>®</sup> Fc. Protein expression was normalized to β-Actin control. Representative bands are shown.

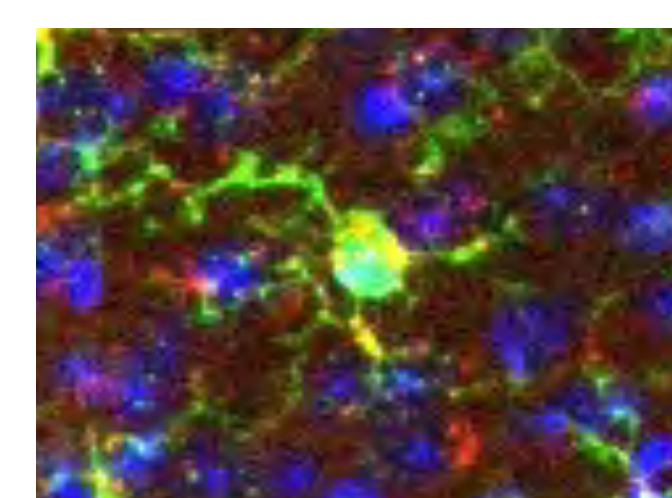
## Double staining IHC protocol allows for investigation of effect of excess neonatal testosterone on hippocampal microglia

**IBA1** was used as a general marker for microglia providing clear visualization of cell morphology, **CD68** as a marker of neuroinflammation and microglial activation, and **DAPI** as a counterstain. In the activated microglia stain (right) yellow is visible where both proteins are expressed, and the cell takes on an amoeboid shape in contrast to the ramified morphology seen on the left.

### Ramified



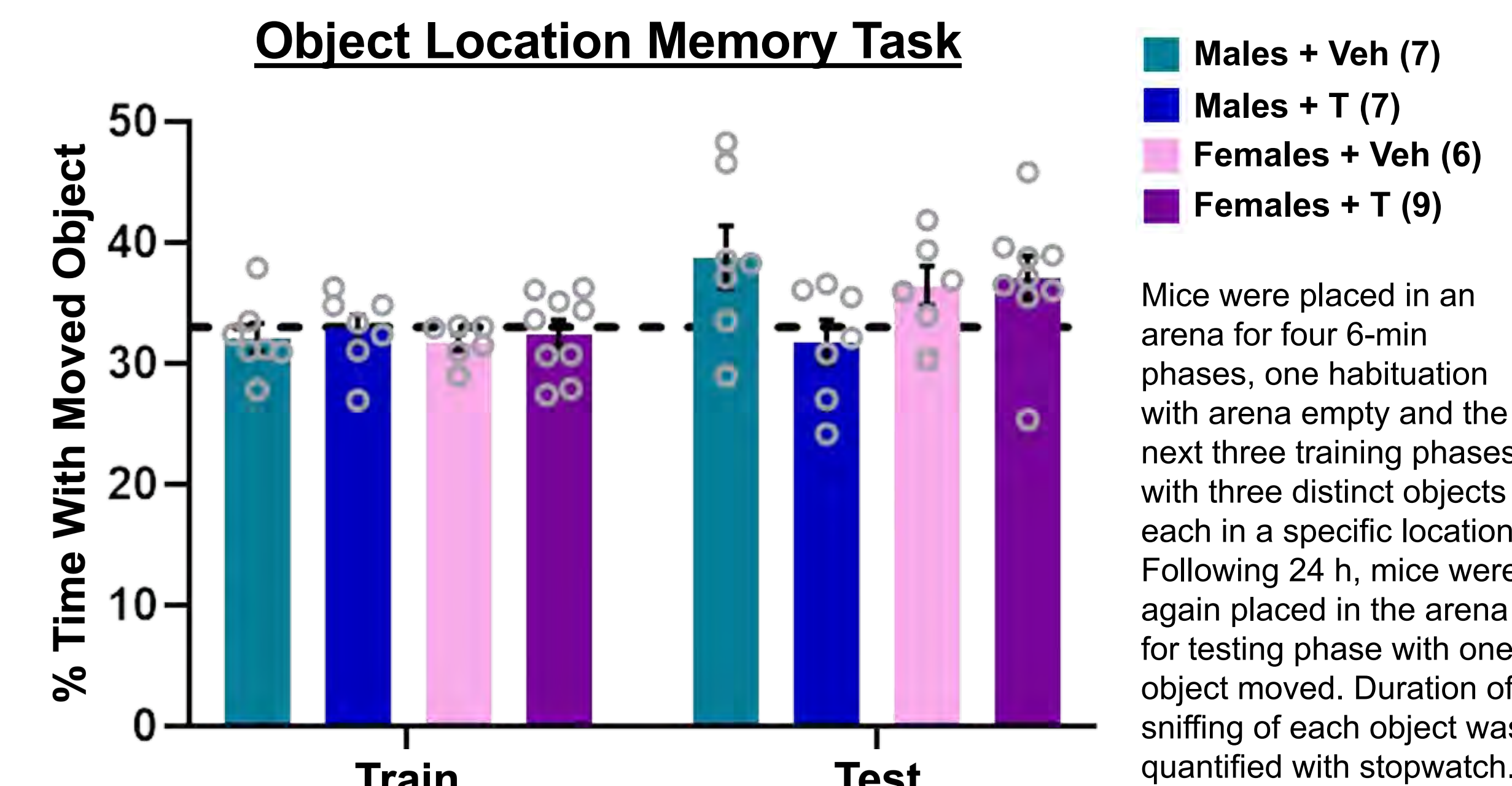
### Activated



Coronal brain sections were incubated in blocking solution, primary antibodies (anti-IBA1, anti-CD68), secondary (anti-rabbit IgG), and DAPI, with 1X TBS washes in between, then mounted and imaged with Leica TCS SPE confocal.

## Excess neonatal testosterone in wild-type mice may cause male-specific spatial object recognition deficits

### Object Location Memory Task



## Conclusions

- DCS may alleviate testosterone-induced deficits through the serine-shuttling pathway by enhancing NMDA receptor function in the hippocampus.
- Excess neonatal testosterone may reduce the abundance of astrocytes, exporters of the D-serine precursor L-serine, but increase the number of dendritic spines, which are fundamental units of synaptic plasticity.
- Brief periods of hormonal dysregulation can lead to long-term effects on hippocampus-dependent behavior and memory, such as spatial object recognition, and on the molecular interactions between glia and neurons.

## Future Directions

- Compare the abundance and morphology of ramified and activated microglia in the hippocampus of testosterone- versus vehicle-treated mice using the developed IBA1/CD68 IHC protocol.
- Investigate the excess of dendritic spines in the hippocampus of testosterone-treated mice by assessing spinal maturity.
- Investigate the effects of excess neonatal testosterone on glia-mediated synaptic pruning and synaptogenesis in the hippocampus.

## Acknowledgements

- K01 MH119540
- Hawk-IDDRC Pilot Grant (P50 HD103556)
- NIH T32GM144636
- University of Iowa Neural Circuits and Behavior Core
- Iowa Neuroscience Institute
- Secondary Student Training Program, Belin-Blank Center

## References

- Gumusoglu, Serena B., et al. "Neurodevelopmental outcomes of prenatal preeclampsia exposure." *Trends in Neurosciences*, vol. 43, no. 4, Apr. 2020, pp. 253–268, 10.1016/j.tins.2020.02.003.
- Ivanov, Andrei D., and Jean-Pierre Mothet. "The plastic D-serine signaling pathway: Sliding from neurons to glia and vice-versa." *Neuroscience Letters*, vol. 689, Jan. 2019, pp. 21–25, 10.1016/j.neulet.2018.05.039.
- Modi, Meera E., and Larry J. Young. "D-cycloserine facilitates socially reinforced learning in an animal model relevant to autism spectrum disorders." *Biological Psychiatry*, vol. 70, no. 3, Aug. 2011, pp. 298–304, 10.1016/j.biopsych.2011.01.026.
- Quiñones-Labernik, Pravda, et al. "Excess neonatal testosterone causes male-specific social and fear memory deficits in wild-type mice." *eNeuro*, 7 July 2025, 10.1523/eneuro.0020-25.2025.
- Rowland, Jennifer, and Claire A. Wilson. "The association between gestational diabetes and ASD and ADHD: A systematic review and meta-analysis." *Scientific Reports*, vol. 11, no. 1, 4 Mar. 2021, 10.1038/s41598-021-84573-3.
- Vivi, Eugenia, and Barbara Di Benedetto. "Brain stars take the lead during critical periods of early postnatal brain development: Relevance of astrocytes in health and mental disorders." *Molecular Psychiatry*, vol. 29, no. 9, 29 Mar. 2024, pp. 2821–2833, 10.1038/s41380-024-02534-4.



## Introduction

### Background

- Population-scale crowdsourced family tree datasets extract information from publicly available genealogy websites and can offer advanced insights into human evolution, population dynamics, and migration (Wohns et al., 2022)
- Current family tree datasets are skewed to overrepresent certain groups and are can contain a range of errors such as duplicates and missing data (Koylu et al., 2025)

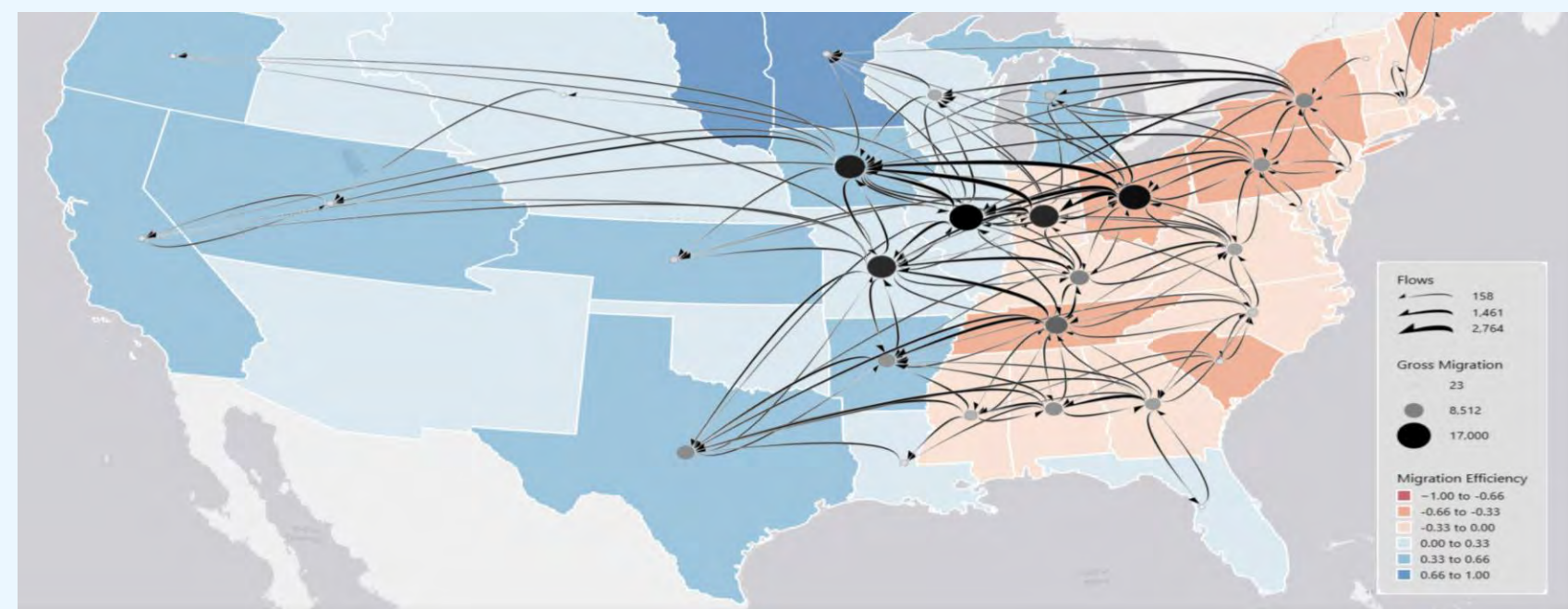


Figure 1. Migration Flow Map Developed with Family Tree Data. Koylu et al. (2024) created a plot of migration flows from 1830-1857 using only family tree data

### Existing Literature

- Currently, the largest visualization for a single pedigree of a family tree population dataset displays approximately 6,000 individuals.

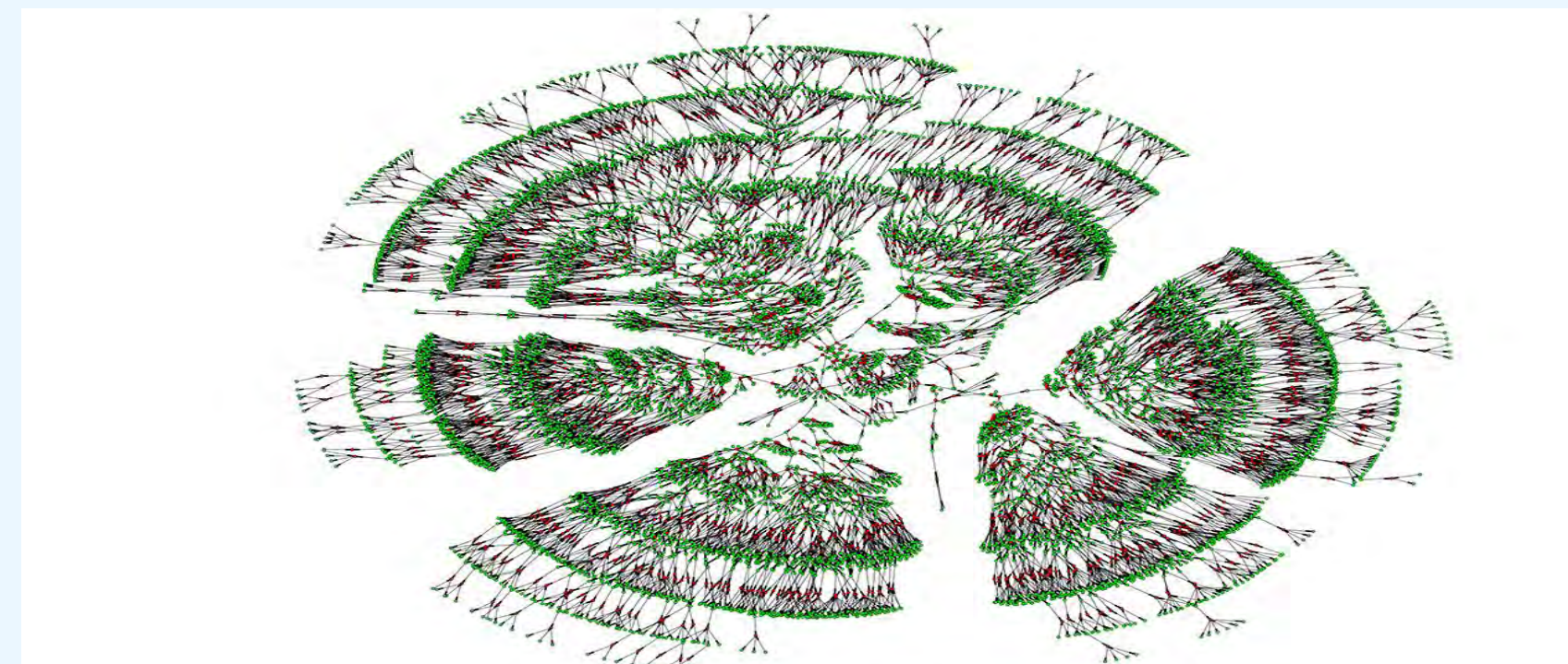


Figure 2. Seven Generation Visualization. Visualization by Kaplanis et al. (2018) that represents the connections between seven generations of over 6,000 individuals

## Objectives

### Purpose Statement

- In this study, we develop a framework for visualizing population-scale genealogical networks using a compilation of crowdsourced family tree datasets, highlighting direct lineages and spousal connections within the population

### Research Questions

- How can we create an effective visualization of population-scale family tree data that can display spatiotemporal changes in kinship and population dynamics?
- How can visualizing population-scale family tree data reveal inconsistencies and biases in the genealogical network data that are otherwise difficult to notice?

## Methodology

### Data Summary

- The data used was compiled by Koylu et al. (2021), who created a family tree dataset using crowdsourced genealogical profiles from rootsweb.com
- The dataset contains multigenerational pedigrees representing over 40 million individuals, spanning many centuries

### Visualization Workflow

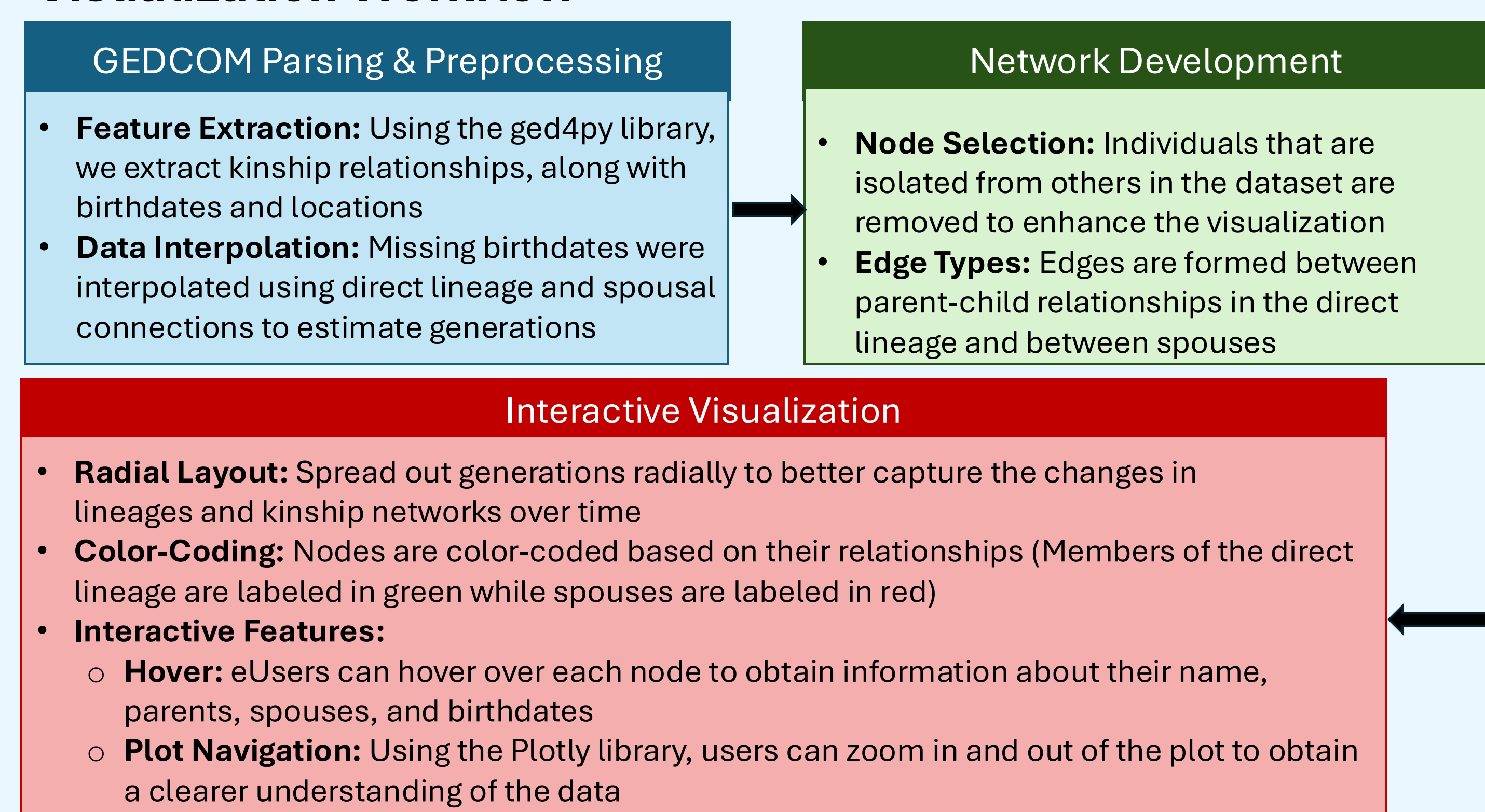


Figure 3. Visualization Creation Workflow. The key steps in the process of interconnecting individuals in the dataset and developing the visualization are processing the GEDCOM files, constructing the network, and interactively visualizing the connections between each node

## Results

### Framework

- Developed a framework for visualizing large-scale genealogical networks, to better understand their structure and identify issues in data quality

### Structures of Multigenerational Family Trees

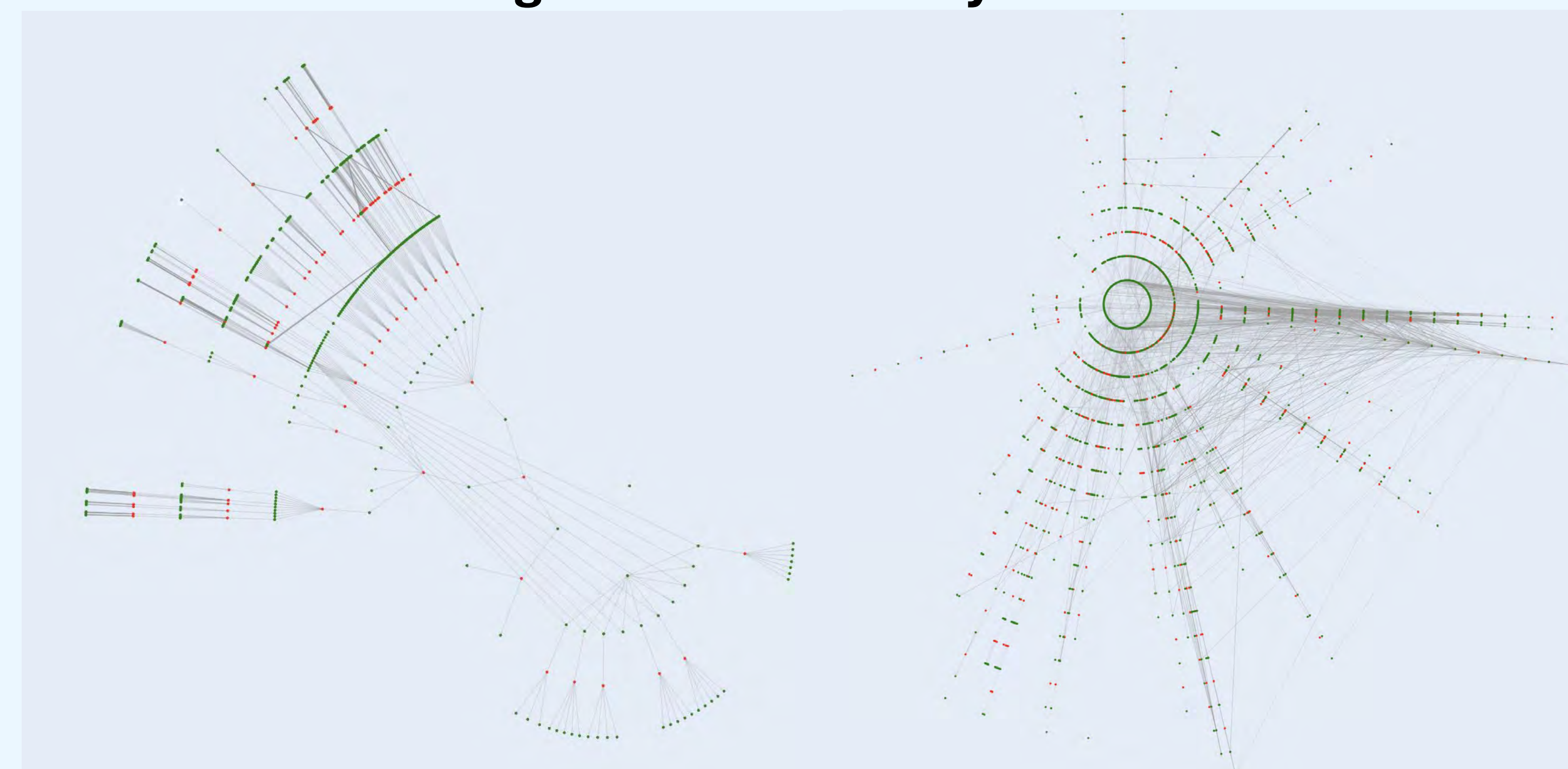


Figure 4. Plotly and NetworkX Visualizations of Two Sets of Individuals. Two sample visualizations of a set of GEDCOM files representing over 700 and 26,000 individuals, respectively. Nodes are color-coded based on type of connection to the lineage and are spread out radially by generation.

## Conclusions

### Discussion

- Created the largest visualization to-date of a large-scale genealogical network, consisting of over 26 thousand individuals
- Enables in-depth analysis of the anatomy of family tree datasets, along with the impact of historical events on population dynamics across space and time

### Limitations

- The data that comprised the visualizations contains bias towards the underrepresentation of specific minorities (Koylu et al. 2022)

### Future Work

- Utilizing this visualization framework onto more diverse and representative datasets, to get a better understanding of how populations as a whole respond to historical events
- Implement geocoding into the visualization to not only see changes in kinship ties, but also in spatiotemporal migration patterns in response to various evolutionary events

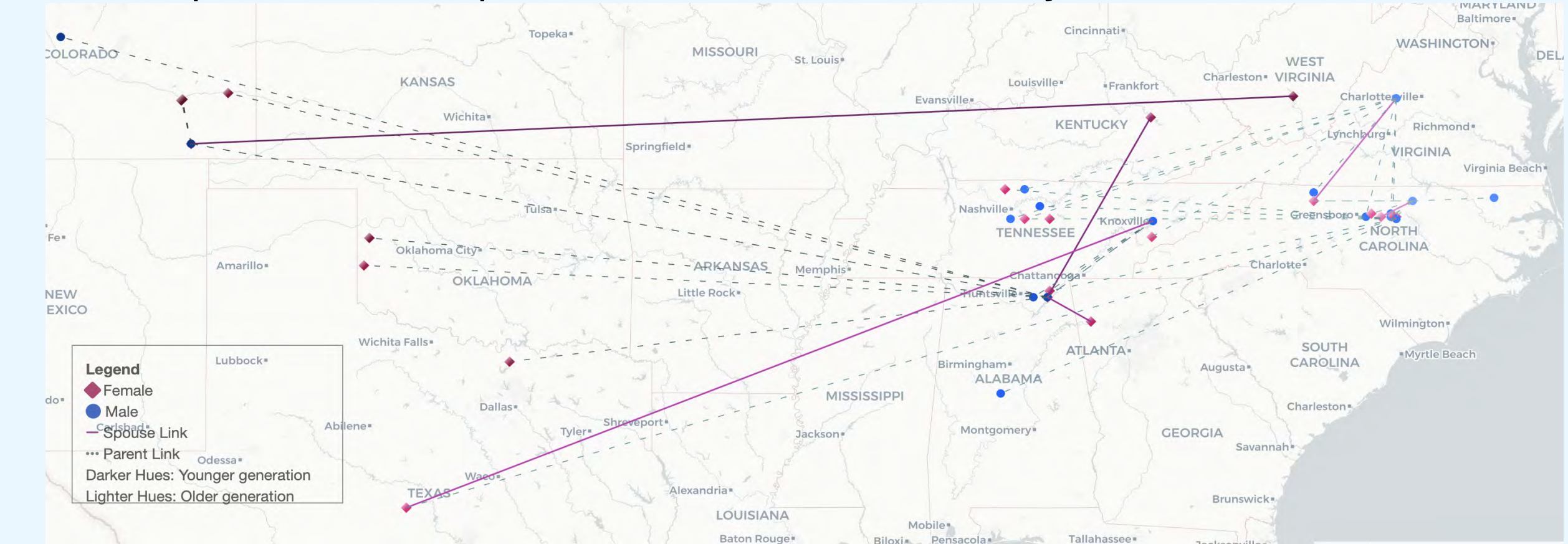


Figure 5. Visualization of Geocoded Family Tree Data. In the study conducted by Clio et al. (under review), family tree data is plotted geographically to observe spatiotemporal variations

## Acknowledgements

I would like to acknowledge the support from my mentors and fellow researchers at the Geo-Social Lab. Namely, I want to thank Dr. Koylu, Loretta, Maryam, and Jinyi for their guidance throughout this study.

## References

- Kaplanis, J., Gordon, A., Shor, T., Weissbrod, O., Geiger, D., Wahl, M., Gershovits, M., Markus, A., Sheikh, M., Gymrek, M., Bhatia, G., MacArthur, D. G., Erlich, Y., & Carmel, L. (2018). Quantitative analysis of population-scale family trees with millions of relatives. *Science*, 360(6385), 171–175. <https://doi.org/10.1126/science.aam9309>
- Koylu, C., Guo, D., Huang, Y., Kasakoff, A. B., & Grieve, J. (2021). Connecting family trees to construct a population-scale and longitudinal geo-social network for the U.S. *International Journal of Geographical Information Science*, 35(12), 2380–2423. <https://doi.org/10.1080/13658816.2020.1821885>
- Koylu, C., & Kasakoff, A. B. (2022). Measuring and mapping long-term changes in migration flows using population-scale family trees. *Cartography and Geographic Information Science*, 46(1), 57–71. <https://doi.org/10.1080/15230406.2021.2011419>
- Koylu, C., & Kasakoff, A. B. (2025). Ethical challenges in analyzing and mapping historical demographic changes and migration using population-scale family trees. *Cartographic Perspectives*, 105, 55–62. <https://doi.org/10.14714/CP105.1945>
- Wohns, A. W., Wong, Y., Jeffery, B., Akbari, A., Mallick, S., Pinhasi, R., Patterson, N., Reich, D., Kelleher, J., & McVean, G. (2022). A unified genealogy of modern and ancient genomes. *Science*, 375(6583), eabi8264. <https://doi.org/10.1126/science.abi8264>



# The Language of Anxiety: A Lexicon-Based Approach for Online Anxiety Detection

Jingxuan Wang<sup>1</sup>, Jiyuan Yu<sup>2</sup>, Yikang Wang<sup>2</sup>, Weiguo Fan, PhD<sup>2</sup>

<sup>1</sup>Great Valley High School, Malvern, PA; <sup>2</sup>Department of Business Analytics, University of Iowa, Iowa City, IA

## Introduction

About 10.9% of people experience subclinical anxiety—mild symptoms that can impair quality of life just as much as clinical anxiety (Haller et al., 2014).

- Traditional mental health **surveys** often **fail** to capture subtle signs of anxiety, especially when the survey-takers choose to **self-censor** due to stigma (Chen et al., 2023)
- On the other hand, **Reddit** allows users to share personal thoughts anonymously, which enhances the expression of **spontaneous emotions** (Shen & Rudzicz, 2017)
- Most machine learning models using social media for mental health detection had employed **black-box algorithms** that **provide little insight** as to how predictions are being made (Owen et al., 2020)
- Lexicon-based approach changes this trend by explicitly identifying linguistic features related to anxiety
- A lexicon geared towards mental health detection also assists clinical screening tools (Fan et al., 2025)

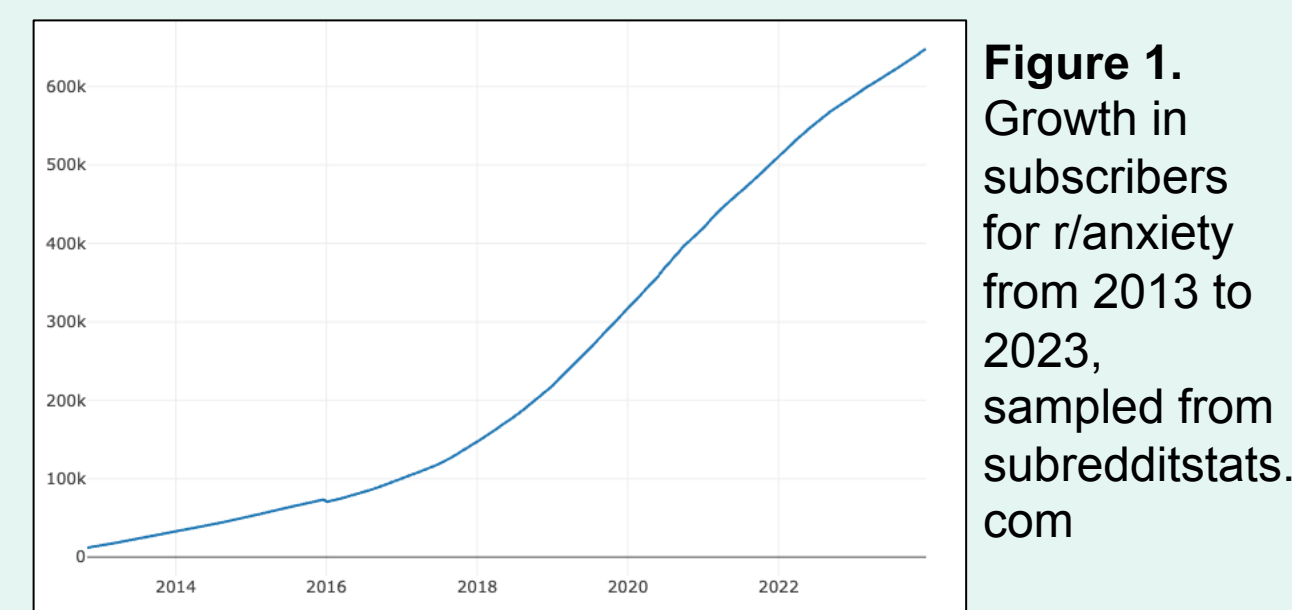


Figure 1. Growth in subscribers for r/anxiety from 2013 to 2023, sampled from subreddits.com

## Purpose

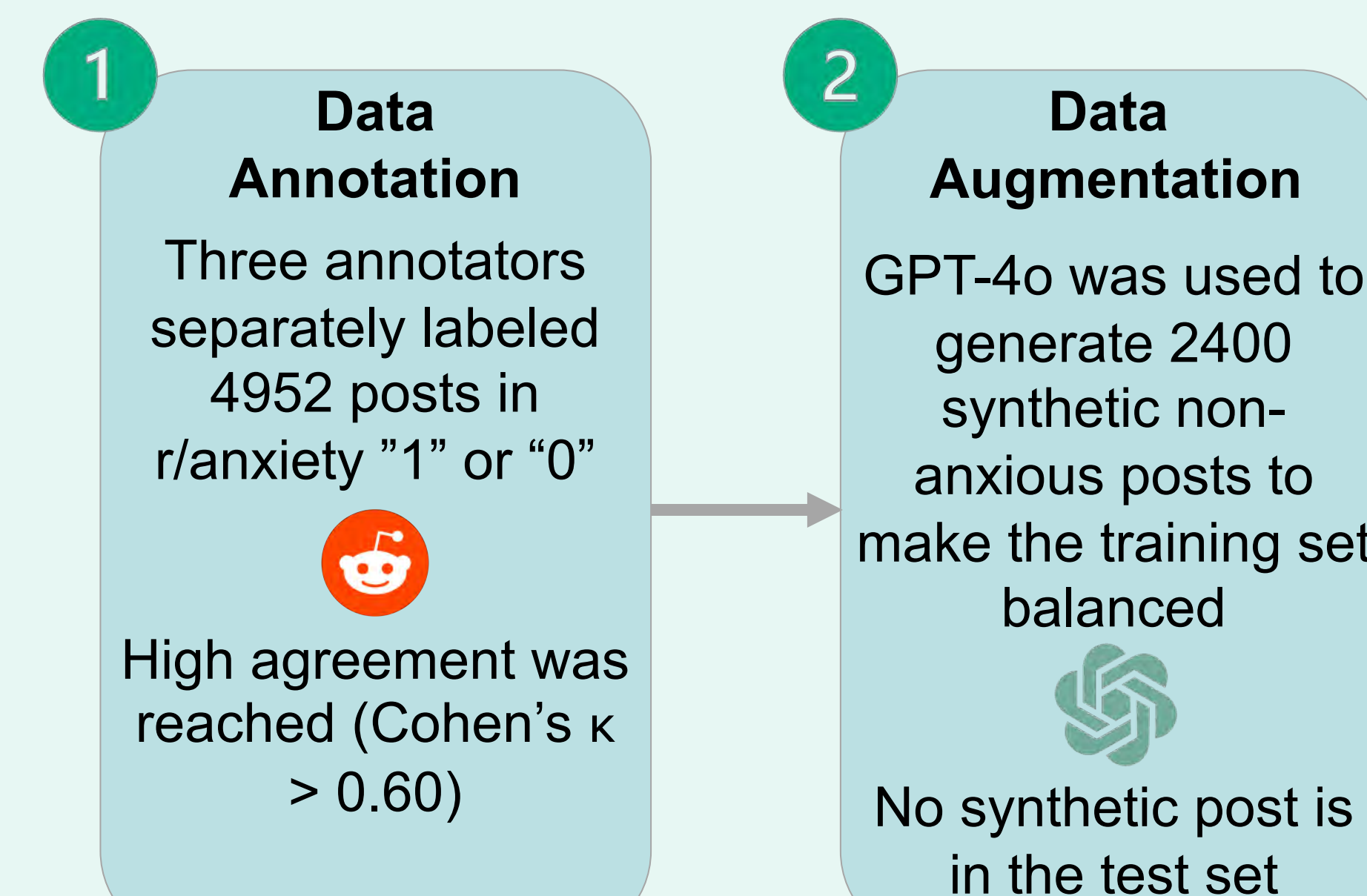
### Research Question

How can lexicon-based approaches improve anxiety detection in social media?

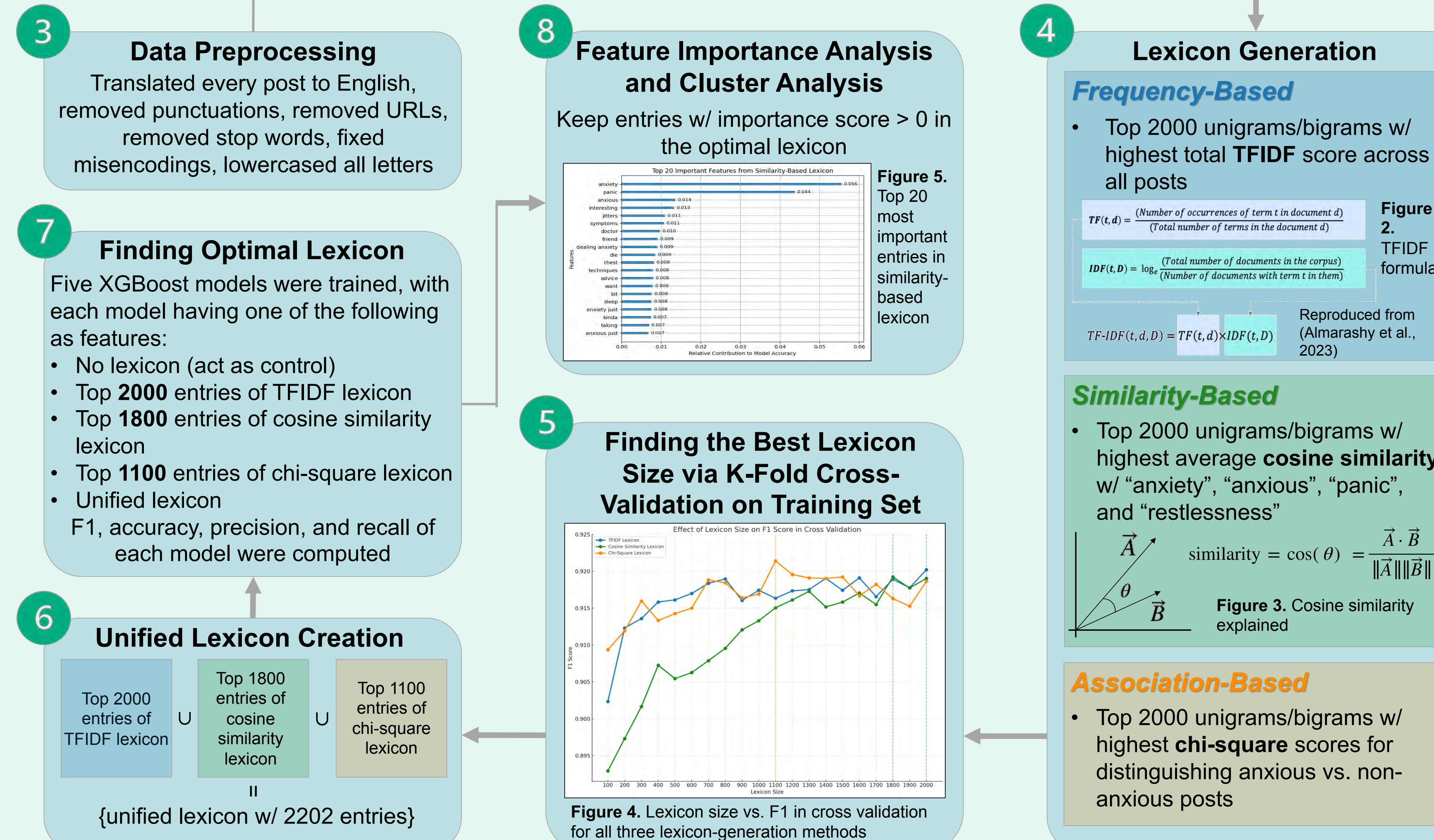
### Objectives

- Develop a **lexicon** for **anxiety detection** using frequency-based, similarity-based, and association-based methods
- Lay groundwork for AI-driven mental health interventions

## Methodology



## Methodology



## Results



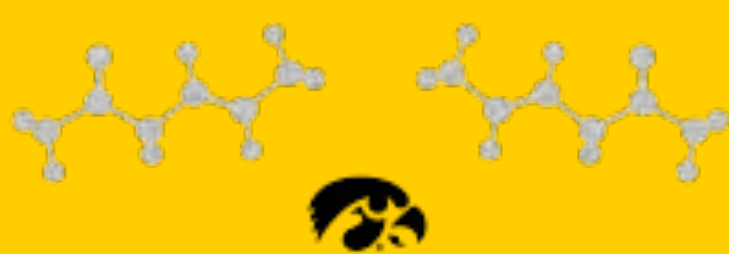
## Acknowledgements

Special thanks to Jiyuan Yu, Yikang Wang, and Dr. Fan for their invaluable support and mentorship. I would also like to thank Enos Hsiao and Sophie Zhang for their help during the data annotation process. Finally, thank you to the Secondary Student Training Program for providing me with this wonderful opportunity.

## References

- Almarashi, A. H. J., Feizi-Derakhshi, M.-R., & Salehpour, P. (2023). Enhancing fake news detection by multi-feature classification. *IEEE Access*, 11. <https://doi.org/10.1109/ACCESS.2023.3339621>
- Chen, L. L., Wilson, S. R., Lohmann, S., & Negraia, D. V. (2023). What Are You Anxious About? Examining Subjects of Anxiety during the COVID-19 Pandemic. *Proceedings of the International AAAI Conference on Web and Social Media*, 17, 137-148. <https://doi.org/10.1609/icwsm.v17i1.22133>
- Fan, W., Fan, J., Yu, J., Zhang, M., Du, Q., Tong, L., & Fan, W. (2025). Loneliness Detection from Social Media: A Text Analytics Approach. *Hawaii International Conference on System Sciences*, 3772-3779. <https://hdl.handle.net/10125/109298>
- Haller, H., Cramer, H., Lauche, R., Gass, F., & Dobos, G. J. (2014). The prevalence and burden of subthreshold generalized anxiety disorder: A systematic review. *BMC Psychiatry*, 14(1). <https://doi.org/10.1186/1471-244x-14-128>
- Owen, D., Camacho-Collados, J., & Espinosa Anke, L. (2020). Towards Preemptive Detection of Depression and Anxiety in Twitter. *Proceedings of the Fifth Social Media Mining for Health Applications Workshop & Shared Task*, 82-89. <https://aclanthology.org/2020.smmh-1.12.pdf>
- Shen, J. H., & Rudzicz, F. (2017). Detecting Anxiety through Reddit. *Association for Computational Linguistics, Proceedings of the Fourth Workshop on Computational Linguistics and Clinical Psychology? From Linguistic Signal to Clinical Reality*, 58-65. <https://doi.org/10.18653/v1/W17-3107>





# Electrochemical Behavior of Pyridine and 1-Aminopyridinium on Glassy Carbon and Platinum Electrodes: Insight for CO<sub>2</sub> Recycling

Yubo Wang<sup>1</sup>, Darby H. Duffy<sup>2</sup>, Setayesh Parsapour<sup>2</sup>, Scott. K. Shaw, PhD<sup>2</sup>

<sup>1</sup>St. Margaret's Episcopal School, <sup>2</sup>Department of Chemistry, University of Iowa



## Introduction

### Carbon Dioxide in our Air

- CO<sub>2</sub> is one of the main pollutants in Earth's atmosphere
- Previous work has done to maximize atmospheric CO<sub>2</sub> capture and conversion<sup>(5)</sup>
- Using electrochemistry to convert CO<sub>2</sub> into useful materials is an advanced and novel approach

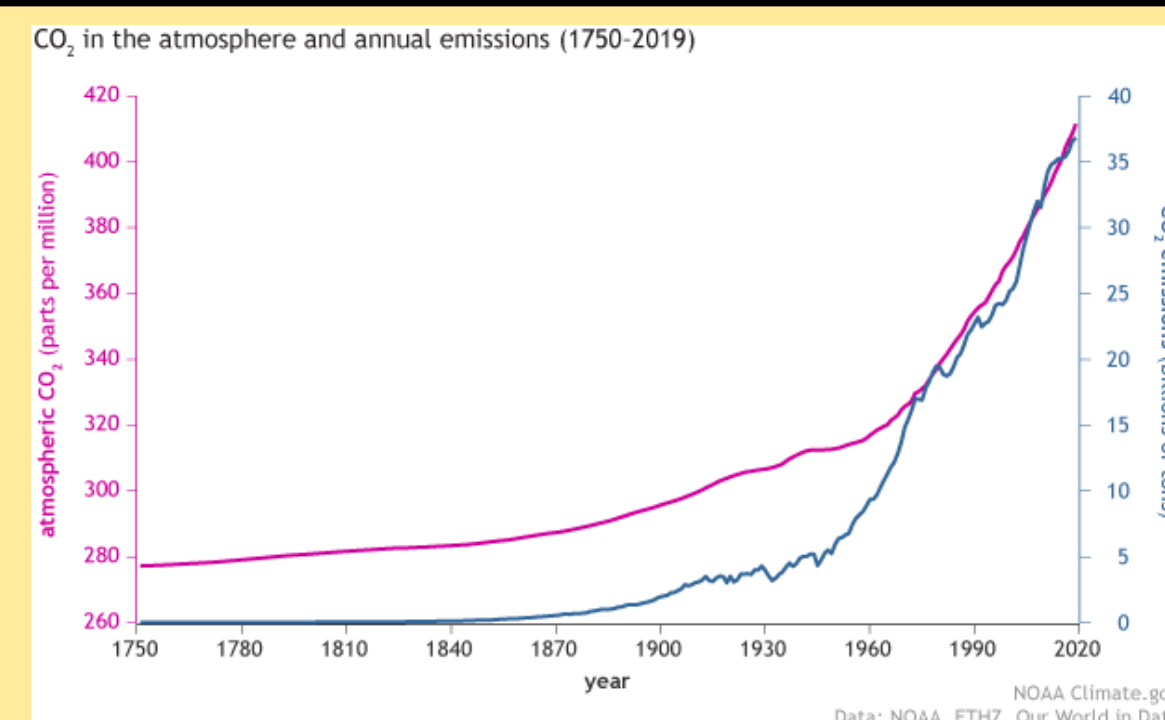


Fig 1: Global CO<sub>2</sub> emissions and atmospheric levels

### There are many experimental variables:

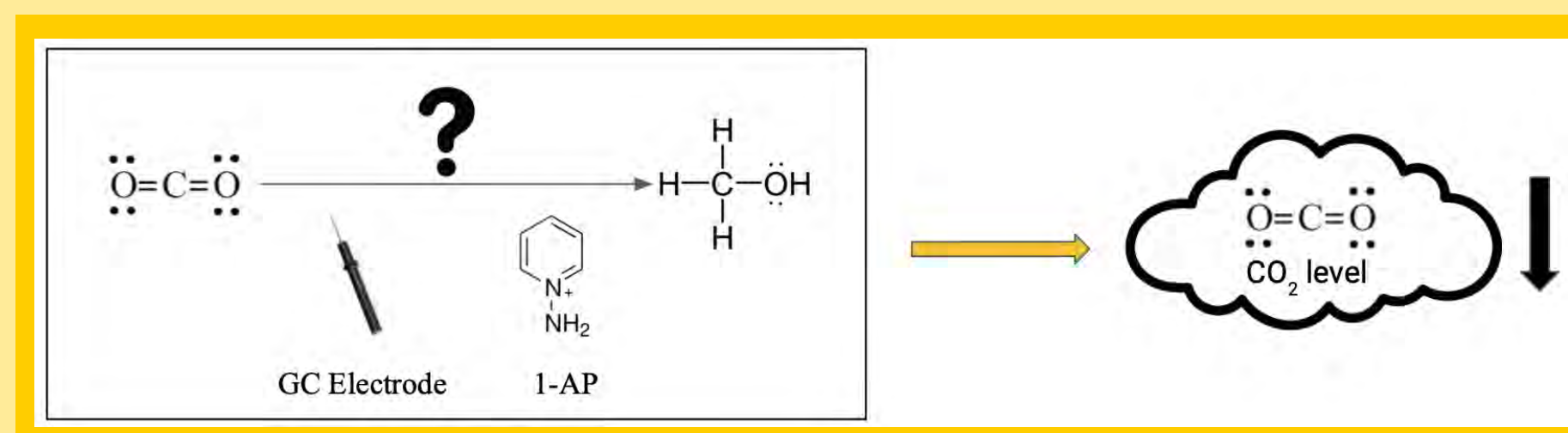
- Working electrodes (WE) offer different reactivity, sensitivity, and efficiency
  - Platinum (Pt)<sup>(1,5,6)</sup>, photochemical<sup>(3)</sup>, gold<sup>(4)</sup>, and glassy carbon (GC)
- Electrolyte conditions can be tuned to TBAPF<sub>6</sub>, KNO<sub>3</sub><sup>(3)</sup>, KCl, etc.

### Weak acid catalysis:

- Prior research used pyridine (or its alternate forms like 1-aminopyridinium nitrate 1-AP) as a homogenous catalyst in aqueous systems<sup>(3)</sup>.
- Pt electrode was previously used and showed to have unexpected redox activities. Previously thought reduction at -0.6 V vs SCE with pyridine.

### Research Question:

- Can weak acids, such as pyridine, catalyze the reduction of carbon dioxide on glassy carbon electrodes?



### Hypothesis:

- If glassy carbon working electrode and pyridine is used, an irreversible reduction peak will be observed at around -1.6V vs. SCE, indicating the reduction of pyridine or 1-AP

## Method

### 1. Reagents Preparation:

**Solutions:** 0.5 M KCl in 50 mL of Milli-Q water in 50 mL volumetric flask

**Catalysts:** 10-20 mM of 1-AP, pyridine, and citric acid added as catalysts

**Gas Pumps:** Argon and CO<sub>2</sub> tanks provided via low pressure gas lines

### 2. Electrochemical Cell:

- Working Electrode (WE): Pt/ Glassy carbon electrodes, polished with 1 and 0.3 μm Al<sub>2</sub>O<sub>3</sub>
- Reference Electrode (RE): Ag wire (MeCN) or Ag/AgCl<sub>(Aq)</sub>
- Counter Electrode (CE): Platinum coil, polished in H<sub>2</sub> flame

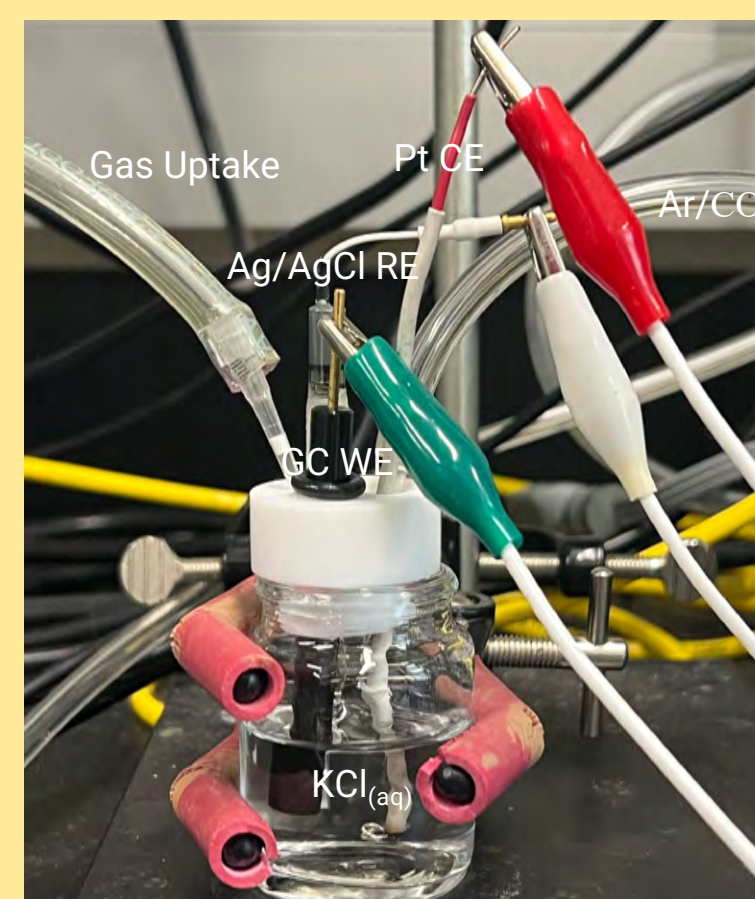


Fig 2: Full Apparatus

### 3. Cyclic Voltammetry Measurements:

- Record background data (Argon and salt)
- Record added redox active compound data
- Record added redox active compound and CO<sub>2</sub>
  - six scan rates were recorded: 25, 50, 100, 175, 250, 500 mV/s
- Record added redox active compound, CO<sub>2</sub>, and ferrocene methanol (internal standard)

## Results

### Comparison Between Glassy Carbon and Pt Electrodes

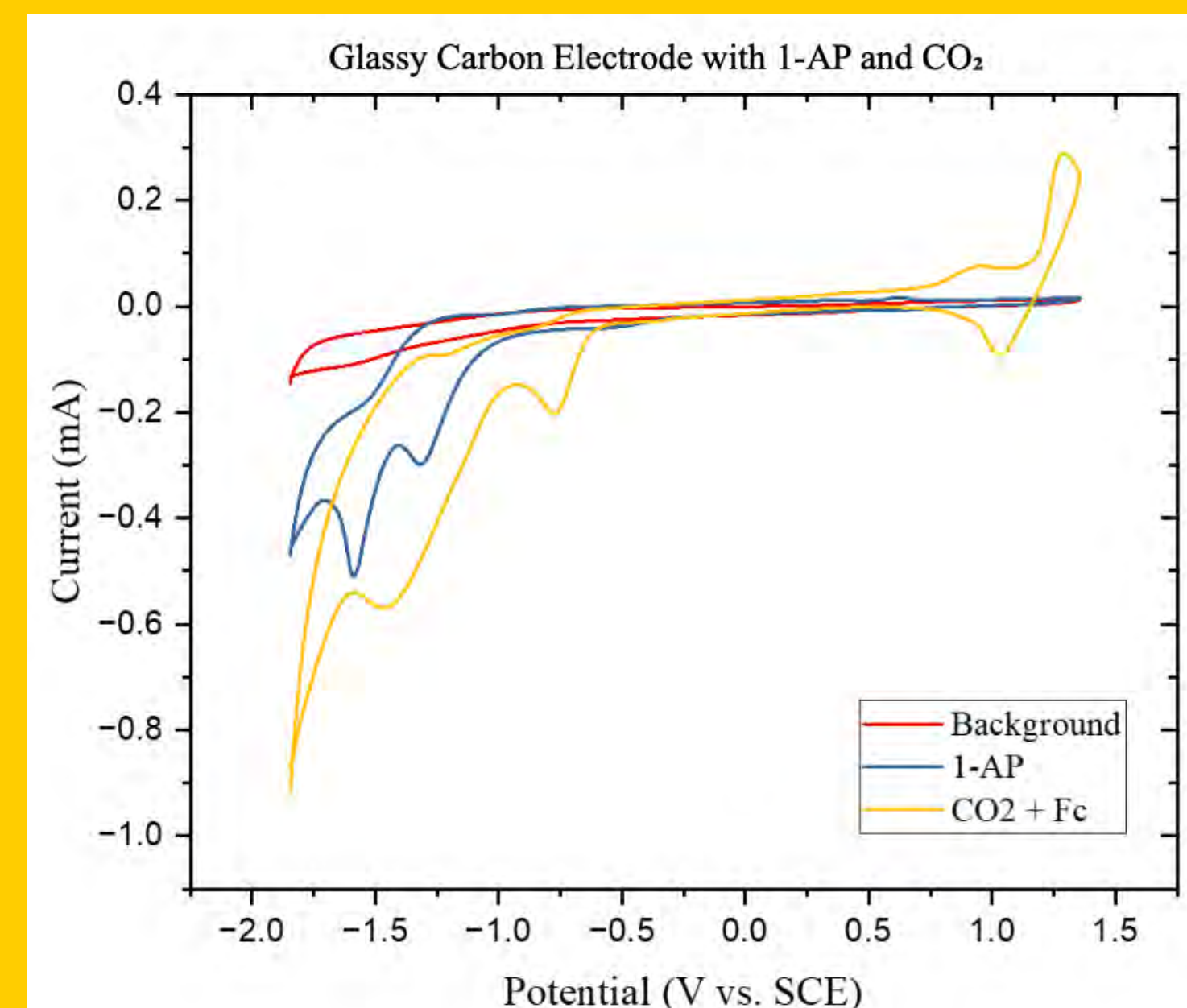


Fig 3: CO<sub>2</sub> and 1-AP on Glassy Carbon Electrode at 250mV/s; Two irreversible reduction peak are found with 1-AP. When CO<sub>2</sub> is added, reduction peaks shifted right.

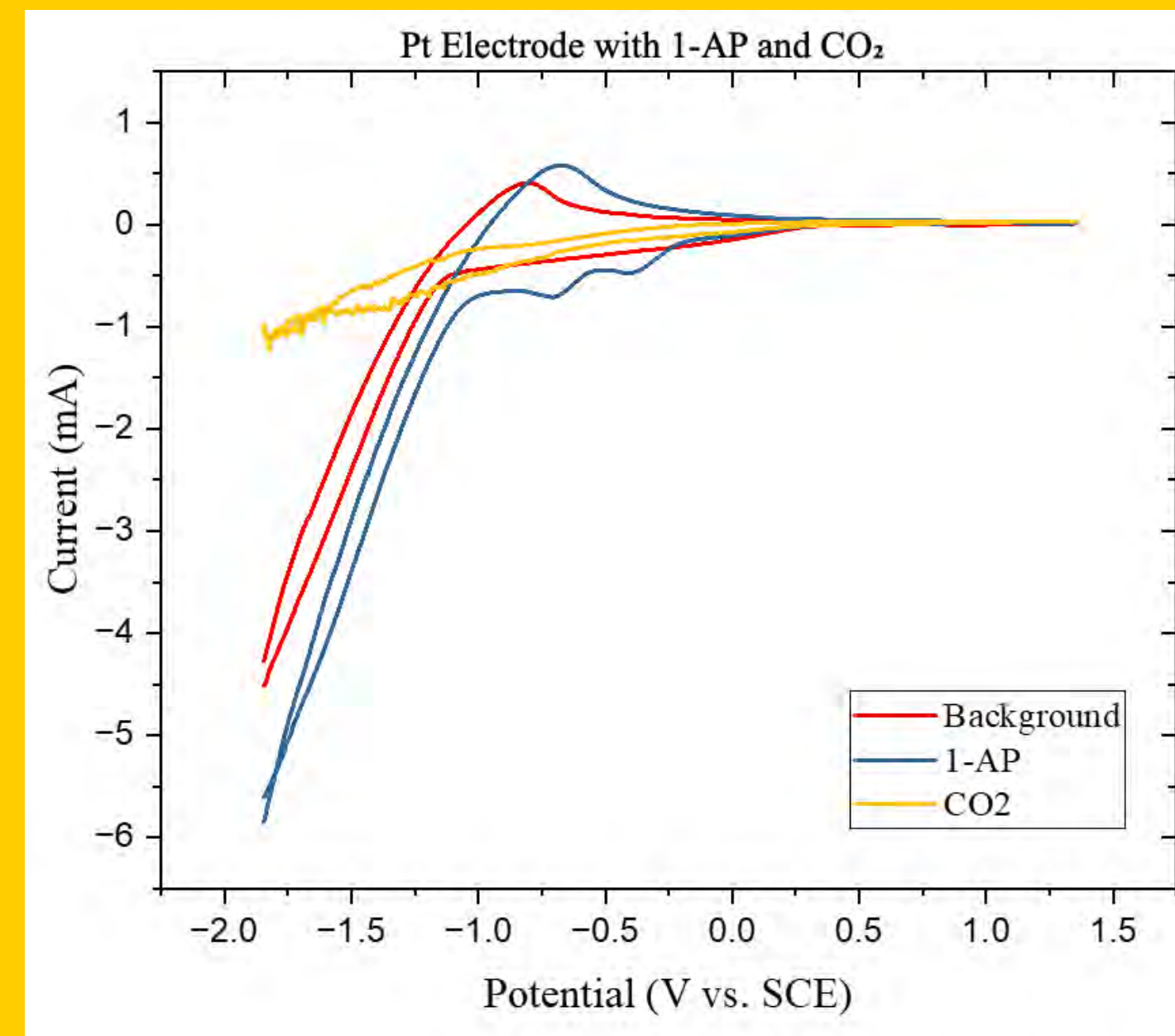


Fig 4: CO<sub>2</sub> and 1-AP on Platinum Electrode at 250mV/s; Reduction of water is observed at -1.8V vs. SCE. No detectable redox activity for CO<sub>2</sub>

### Scan Rate Differences' Effects on 1-AP Reduction

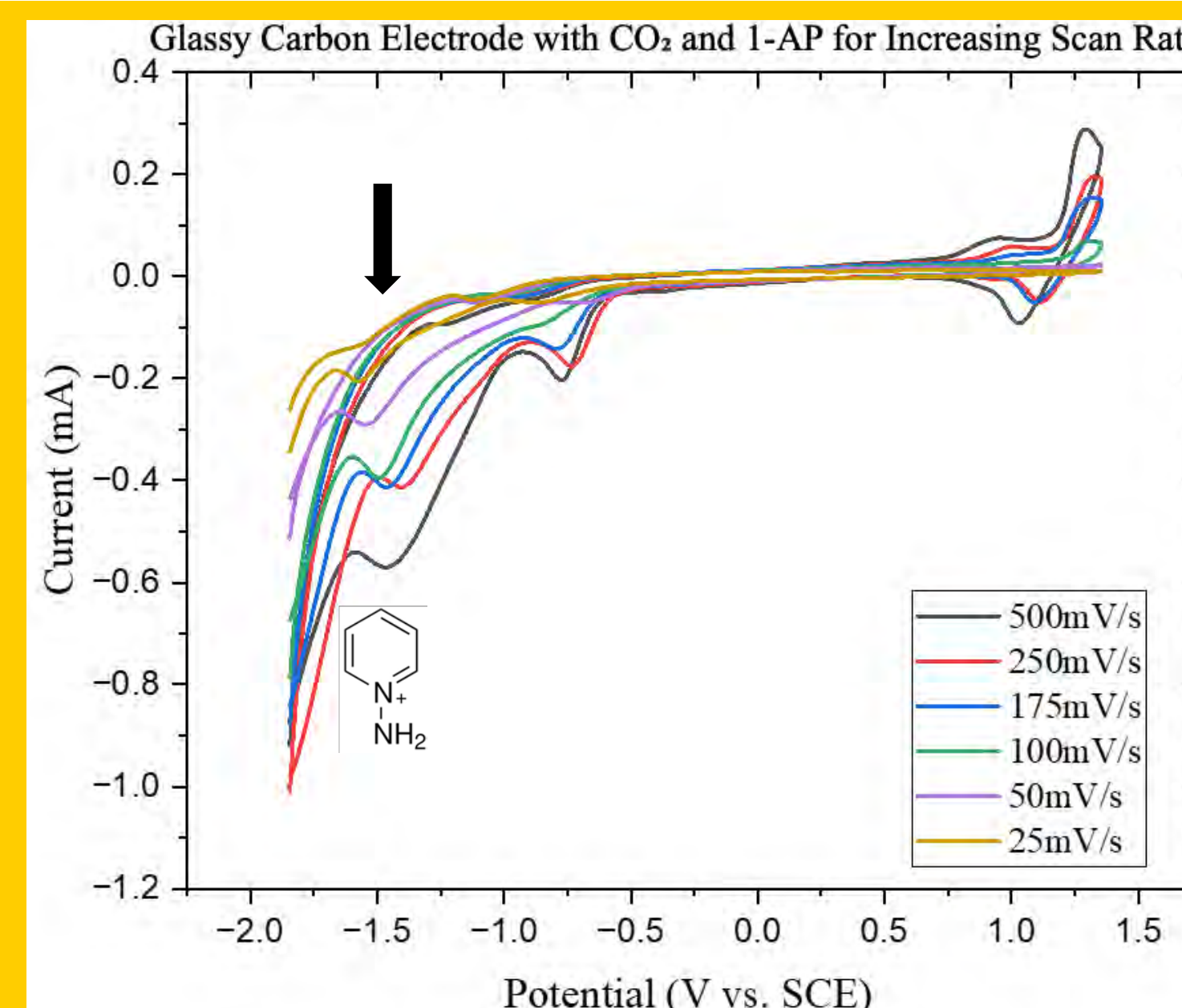


Fig 5: CO<sub>2</sub> and 1-AP on Glassy Carbon Electrode at 25, 50, 100, 175, 250, 500 mV/s. Two irreversible reduction peaks and one reversible reduction peak are observed

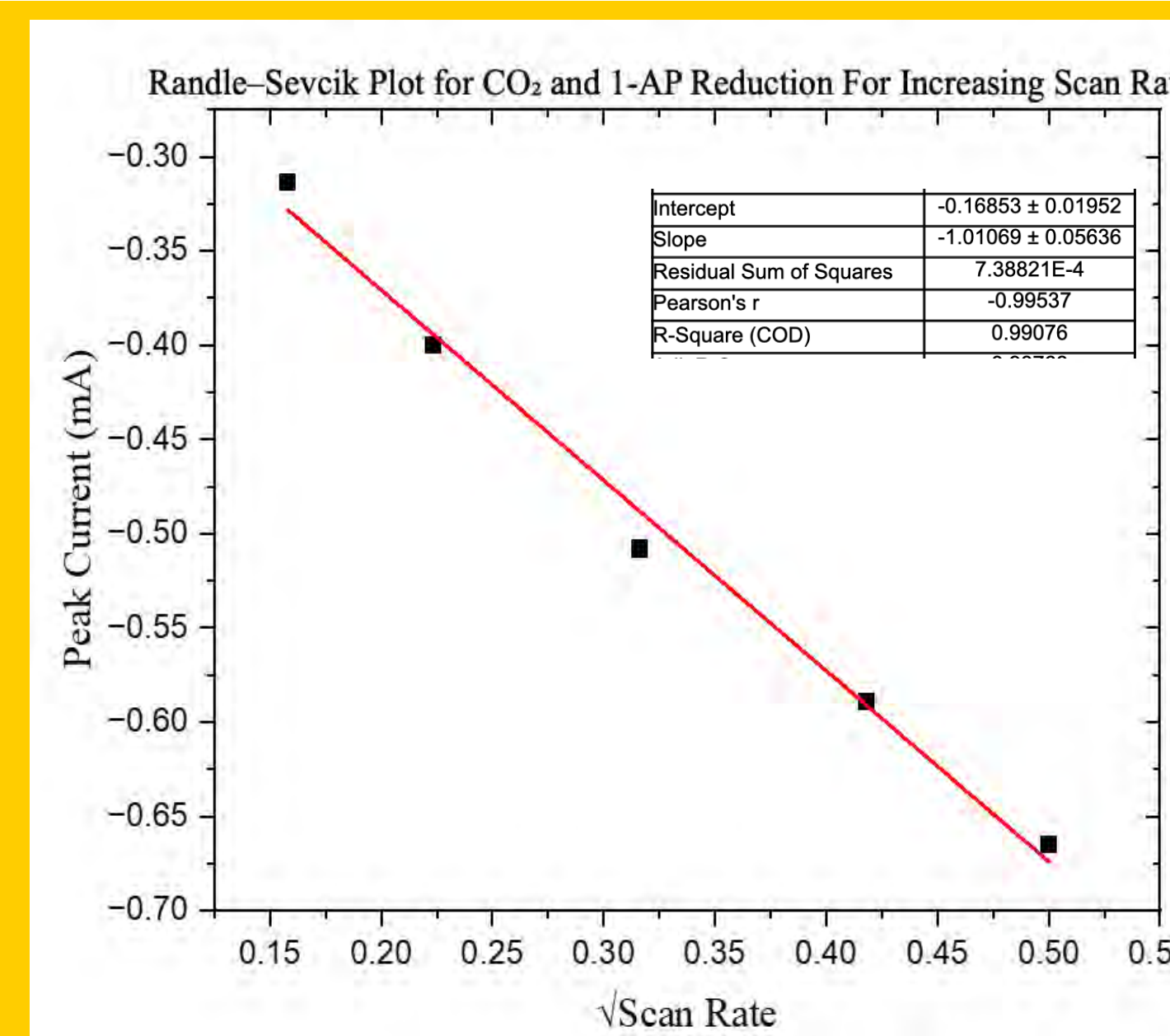


Fig 6: CO<sub>2</sub> and 1-AP on Glassy Carbon Electrode Randle Sevcik Plot on the reduction of pyridine (-1.5V vs. SCE). Data are average of two runs

### Different Catalyst and Electrode Comparisons

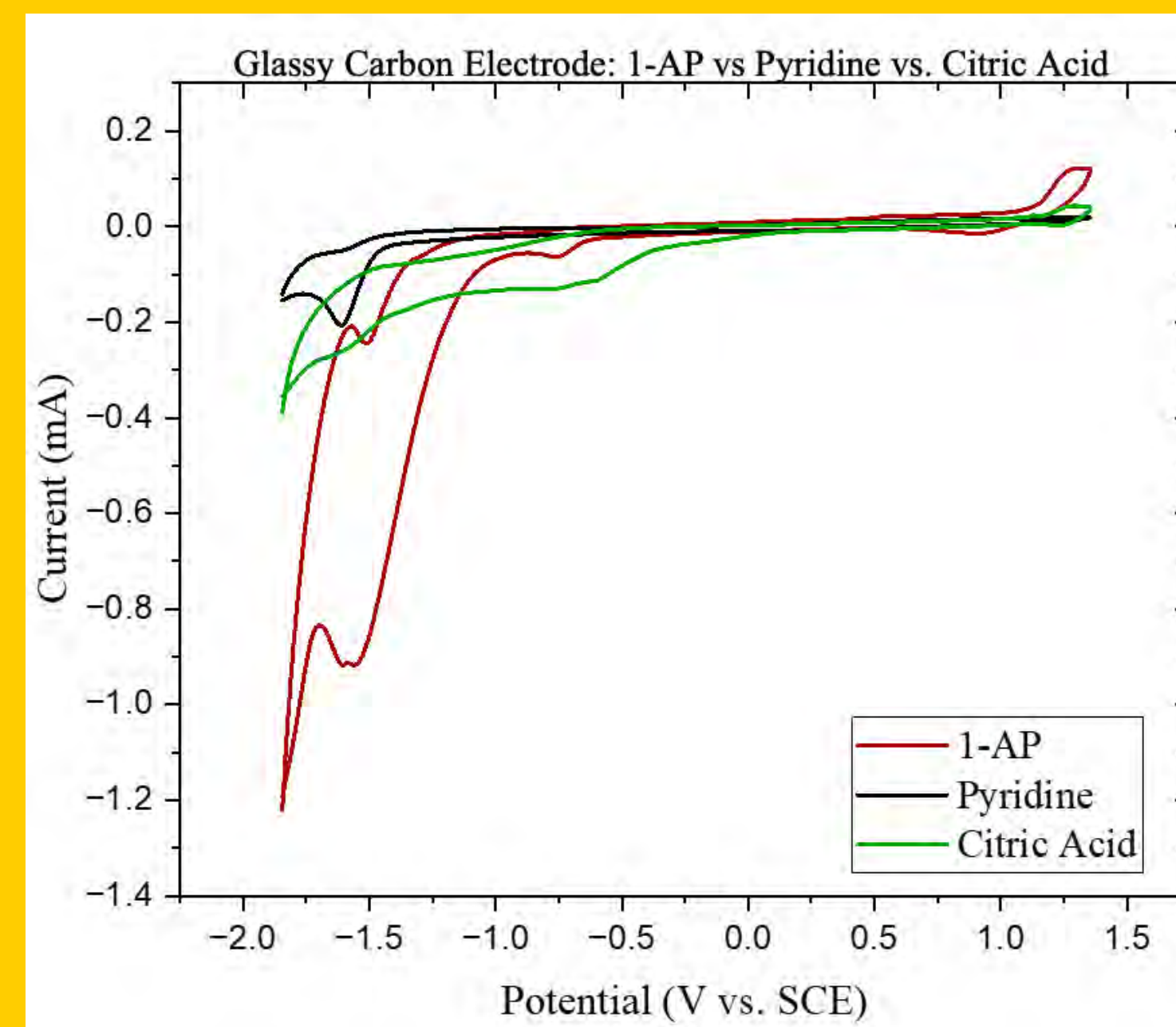


Fig 7: CO<sub>2</sub> and different redox active compounds (1-AP, pyridine, citric acid) on Platinum Electrode at 250mV/s. Greatest reduction peak observed with 1-AP.

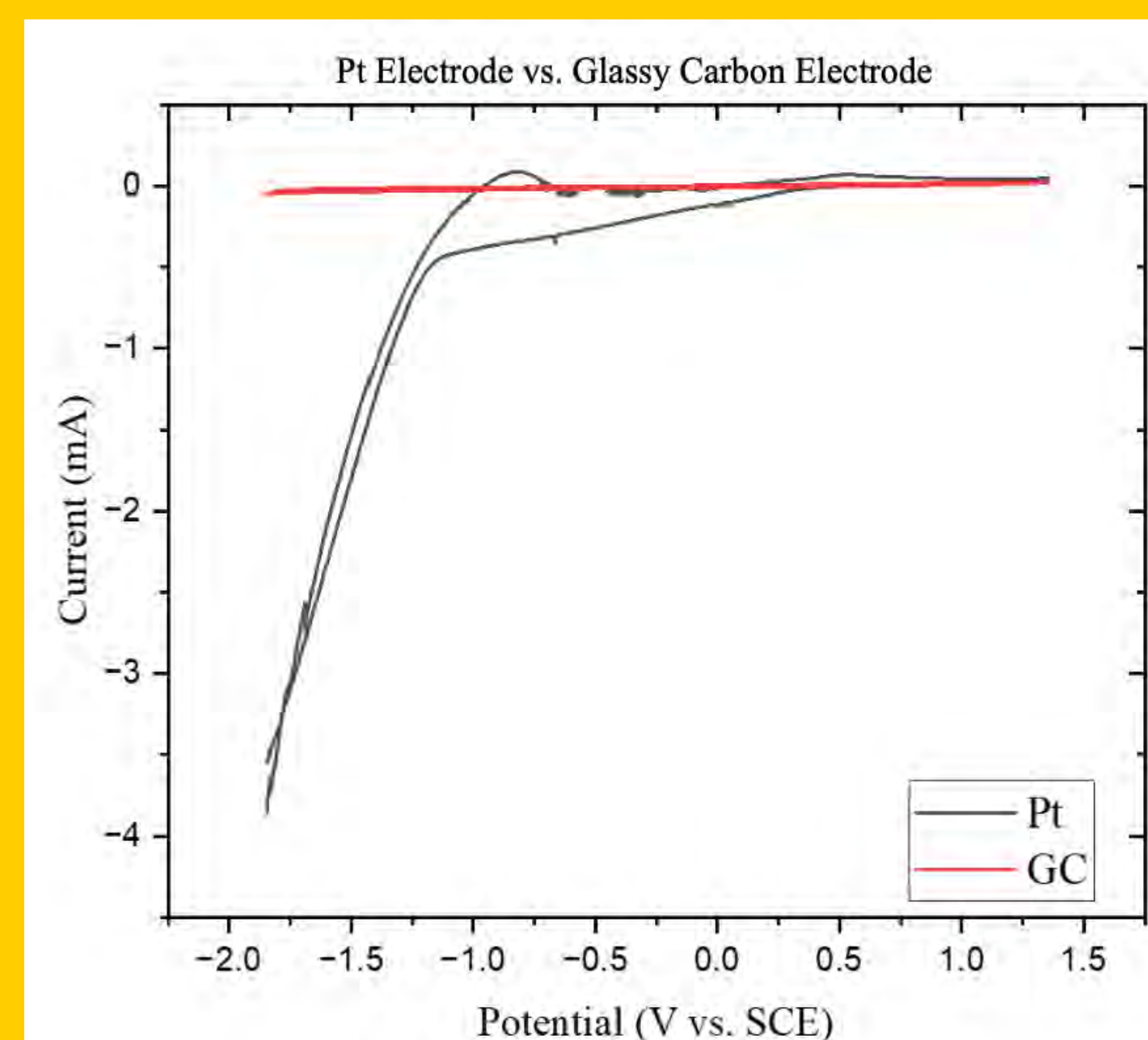


Fig 8: Ar gas purged in aqueous solution on Glassy Carbon vs Pt Electrode at 100mV/s. Pt electrode showed more redox data compared to GC electrode.

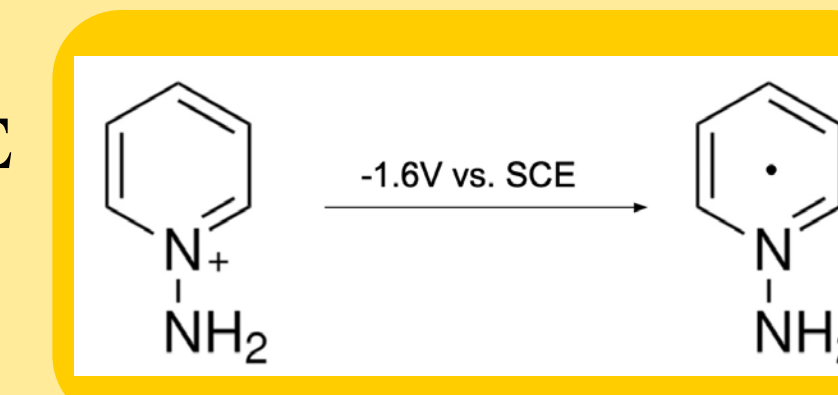
## Discussion

- Our data suggests that there are two reduction peaks for 1-AP on glassy carbon electrode. The one at -1.6 V is the actual 1-AP reduction, and the one at -0.5 V is the commonly mistaken weak acid reduction. (Fig 3 & 5)
- Comparing added CO<sub>2</sub> and 1-AP vs only 1-AP added, there is minimal redox activity for CO<sub>2</sub> and 1-AP on Platinum electrode. This data suggests that platinum should not be used as a working electrode for CO<sub>2</sub> reduction. (Fig 4)
- Looking at the Randle-Sevcik graph, square root of scan rate and peak current has a linear relationship, indicating that the reaction is diffusion controlled, electron transfer is fast, and 1-AP reduction is stable. (Fig 6)
- Compared to other weak acids, 1-AP exhibits the most redox activity under CO<sub>2</sub>, as indicated by the sharp increase in cathodic current near -1.8 V vs SCE. This suggests 1-AP is the best candidate for electrochemical CO<sub>2</sub> reduction. (Fig 7)
- Platinum electrode is not inert. Looking at Fig 4 & 8, Pt electrode reduces water at the potential before 1-AP gets reduced.

## Conclusions

### Key Findings:

- 1-AP gets irreversibly reduced at **-1.6V vs. SCE** at glassy carbon electrode: Not the previously understood -0.5V vs. SCE<sup>(3)</sup>.



- Platinum electrode is **not purely inert**. It reduces water and other weak acids in the solution that may cause misunderstandings.

- Instead, **glassy carbon** is an inert electrode that should be used for CO<sub>2</sub> recycling in electrochemistry, better than the previously used photochemical<sup>(3)</sup>, Pt<sup>(1,5,6)</sup>, and gold<sup>(4)</sup>.

- 1-AP** is the most redox active compound out of the three tested in this research (1-AP, pyridine, and citric acid), giving it the best potential for CO<sub>2</sub> recycling electrochemically.

### Next Steps:

- We can keep trying 1-AP reduction on Pt electrode to see if it can be reduced. (i.e. going more negative on the potential axis.)
- Using chemicals like pyridine and NH<sub>3</sub> to determine whether the reduced radical of pyridine and 1-AP are actually formed during reduction, given they are unstable.

## Acknowledgments

**Thank you:** Dr. Shaw, Shaw research group (Darby, Setayesh, Grace, Chamini, Colleen, YeJun, and more.), Dr. Grice, Belin- Blank center, Chemistry Dept., and SSTP staff!

## References

- Barton Cole, E.; Lakkaraju, P. S.; Rampulla, D. M.; Morris, A. J.; Abelev, E.; Bocarsly, A. B. Using a One-Electron Shuttle for the Multielectron 2. Reduction of CO<sub>2</sub> to Methanol: Kinetic, Mechanistic, and Structural Insights. *Journal of the American Chemical Society* **2010**, *132* (33), 11539–11551.
- Barton, E. E.; Rampulla, D. M.; Bocarsly, A. B. Selective Solar-Driven Reduction of CO<sub>2</sub> to Methanol Using a Catalyzed P-Gap Based Photoelectrochemical Cell. *Journal of the American Chemical Society* **2008**, *130* (20), 6342–6344.
- Le Saux, E.; Georgiou, E.; Dmitriev, I. A.; Hartley, W. C.; Melchiorre, P. Photochemical Organocatalytic Functionalization of Pyridines via Pyridinyl Radicals. *J. Am. Chem. Soc.* **2022**, *145*, 47–52.
- Lucio, A. J.; Shaw, S. K. Pyridine and Pyridinium Electrochemistry on Polycrystalline Gold Electrodes and Implications for CO<sub>2</sub> Reduction. *The Journal of Physical Chemistry C* **2015**, *119* (22), 12523–12530.
- Seo, H.; Rahimi, M.; Hutton, T. A. Electrochemical Carbon Dioxide Capture and Release with a Redox-Active Amine. *Journal of the American Chemical Society* **2022**, *144* (5), 2164–2170.
- Yan, Y.; Zeitler, E. L.; Gu, J.; Hu, Y.; Bocarsly, A. B. Electrochemistry of Aqueous Pyridinium: Exploration of a Key Aspect of Electrocatalytic Reduction of CO<sub>2</sub> to Methanol. *Journal of the American Chemical Society* **2013**, *135* (38), 14020–14023.



# Chronic Intermittent Hypoxia Reshapes Erythroid Island Macrophages in the Bone Marrow

Yuchen Wang<sup>1</sup>, Zishan Zhang<sup>2,5</sup>, Mackenzie Berschel<sup>3</sup>, Derick Delloro<sup>4</sup>, Matthew Delzell<sup>4</sup>, Carter Lane<sup>4</sup>, Charles Jedlicka<sup>4</sup>, Mikhail Vasilyev<sup>5</sup>, Anastasiia Vasileva<sup>4</sup>, Michael H. Tomasson<sup>2,3,5\*</sup>, and Melissa L. Bates<sup>2,3,4,5,6\*</sup>

<sup>1</sup>St. Mark's School, Southborough, MA, <sup>2</sup>Department of Internal Medicine, <sup>3</sup>The Interdisciplinary Graduate Program in Molecular Medicine, Hematology, Oncology, and Bone Marrow Transplant, Department of Health, <sup>4</sup>Health and Human Physiology, and <sup>5</sup>Stead Family Department of Pediatrics, <sup>6</sup>Holden Comprehensive Cancer Center, University of Iowa, Iowa City, IA, 52242

IOWA

## Introduction

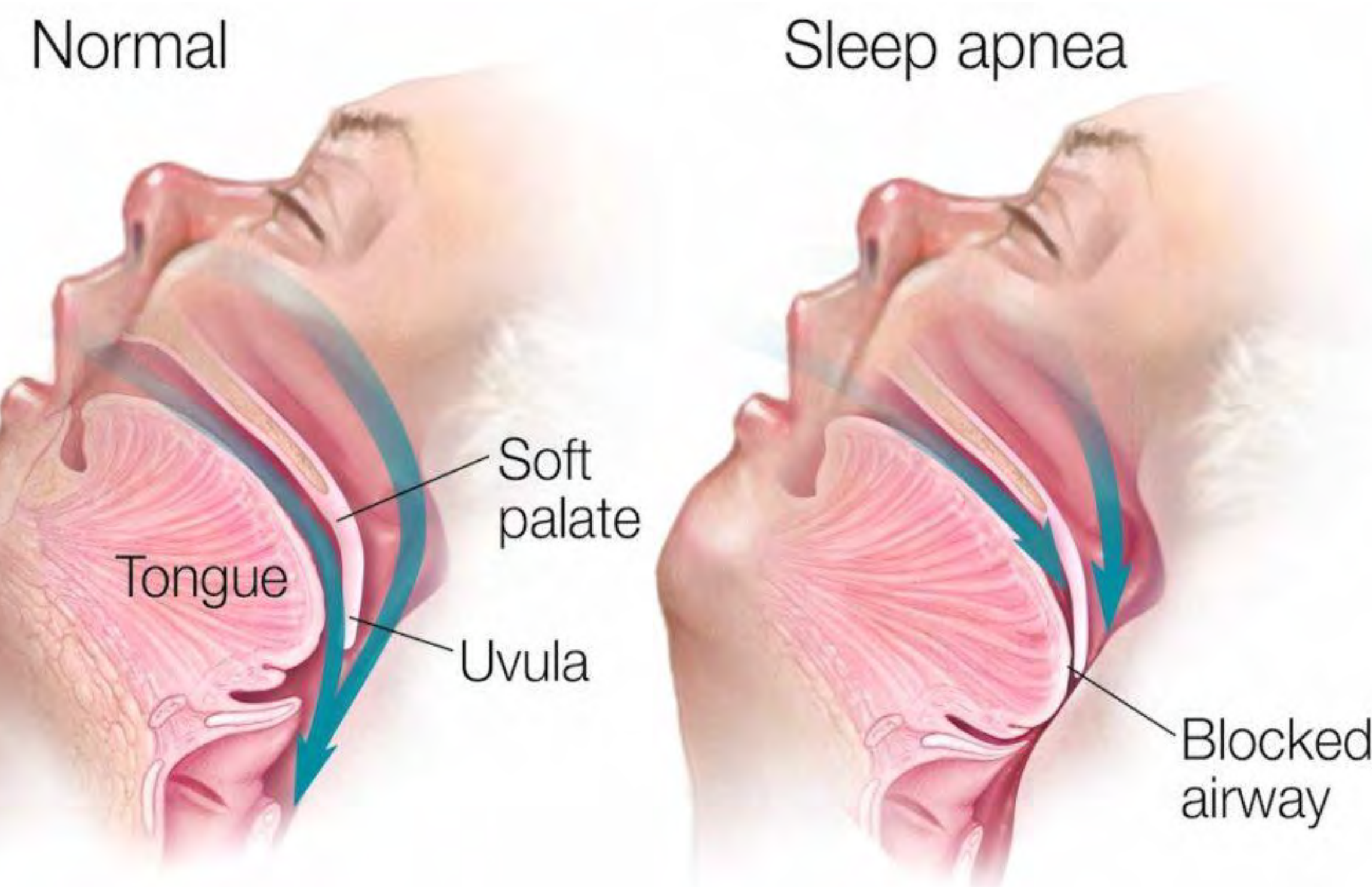


**Figure 1.** Sleep apnea patients' airway in comparison to a normal persons [7].

- CIH is a feature of sleep apnea (interrupted breathing due to airway blockage), characterized by periodic drops in oxygen levels during sleep at least 5 times per hour [1].
- Increases MM progression, a cancer that arises from plasma cells (a type of immune cell) in the bone marrow [2].
  - Key gap: CIH's impact on the bone marrow microenvironment remains unclear.
- CIH upregulates genes (Timd4, Mrap, Mrc1, etc.) in MM-resistant mice, mirroring changes in MM-susceptible mice.
  - These genes are phagocytosis/erythropoiesis-related, possibly belonging to erythroid island macrophages (EIMs) – support erythropoiesis (removes nuclei from developing RBC) [3].
  - EIM's behavior in disease conditions is poorly understood
- Understanding how CIH reprograms the EIM in the bone marrow could:
  - Reveal effects of CIH on the cellular level.
  - Help develop cell targets for therapy for cancer.

## Objectives

### Does CIH affect EIM population?

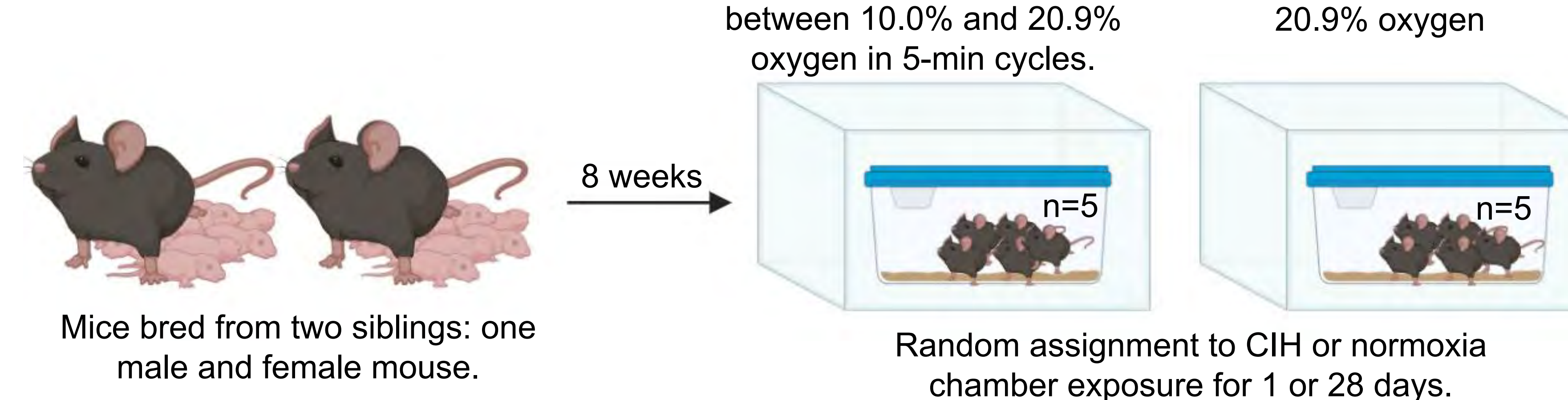
The purpose of this study is investigate CIH's effect on the bone marrow microenvironment. **We hypothesized** that CIH increases EIM population in comparison to normoxic conditions.

### Why not just study gene transcription?

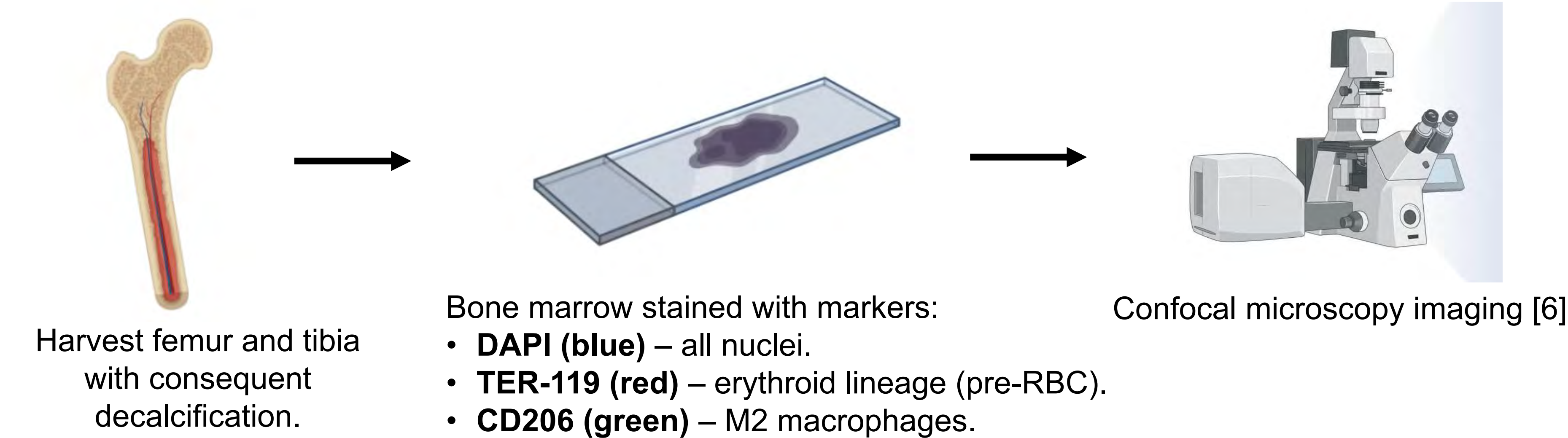
- Though CIH upregulates genes functionally similar to EIMs, it is unclear if these genes are specific to EIMs.
- Increased upstream gene expression does not confirm changes in EIM abundance, making downstream cellular validation critical.

## Methods

### Step 1: Introduce CIH/Normoxia to mice



### Step 2: Immunohistochemistry and Confocal Microscopy



### Step 3: EIM analysis with ImageJ

- Bone marrow tissue was analyzed (4 mice per group; 2 images per mouse were used for analysis).
- The analysis process was blinded to prevent bias.

### Criteria for EIM identification:

- Contain green CD206 marker
- Surrounded by < 5 erythroblasts, stained with TER-119 (red) and containing a nucleus (blue DAPI).

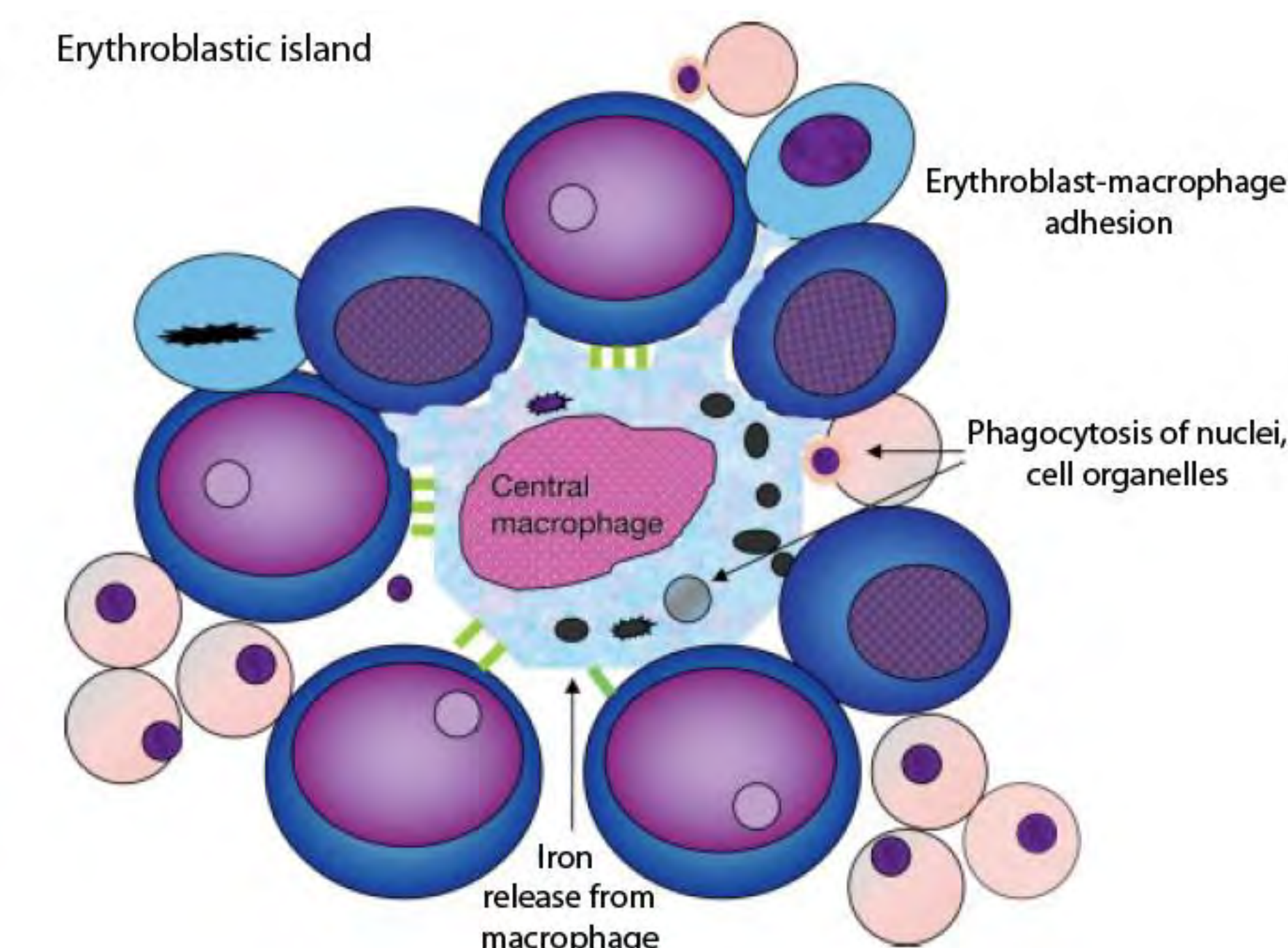


**Figure 2.** An illustration of EIM [5].

## Results

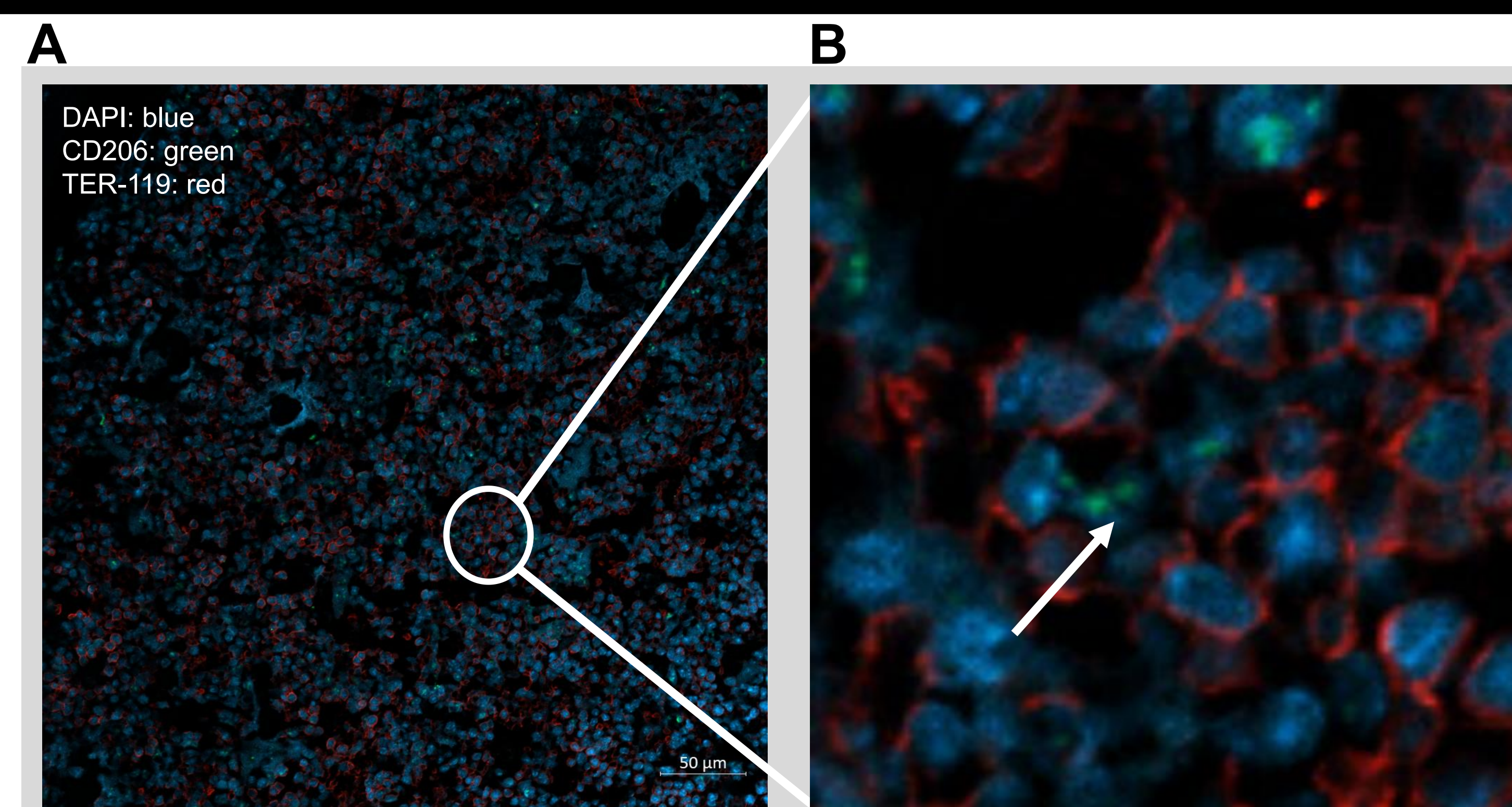


**Figure 3. Confocal Microscopy Imaging.** (A) An image of mouse femur bone marrow with the staining of DAPI, CD206, and TER-119 (B) An example of EIM in the bone marrow.

### Erythroid Island Macrophages

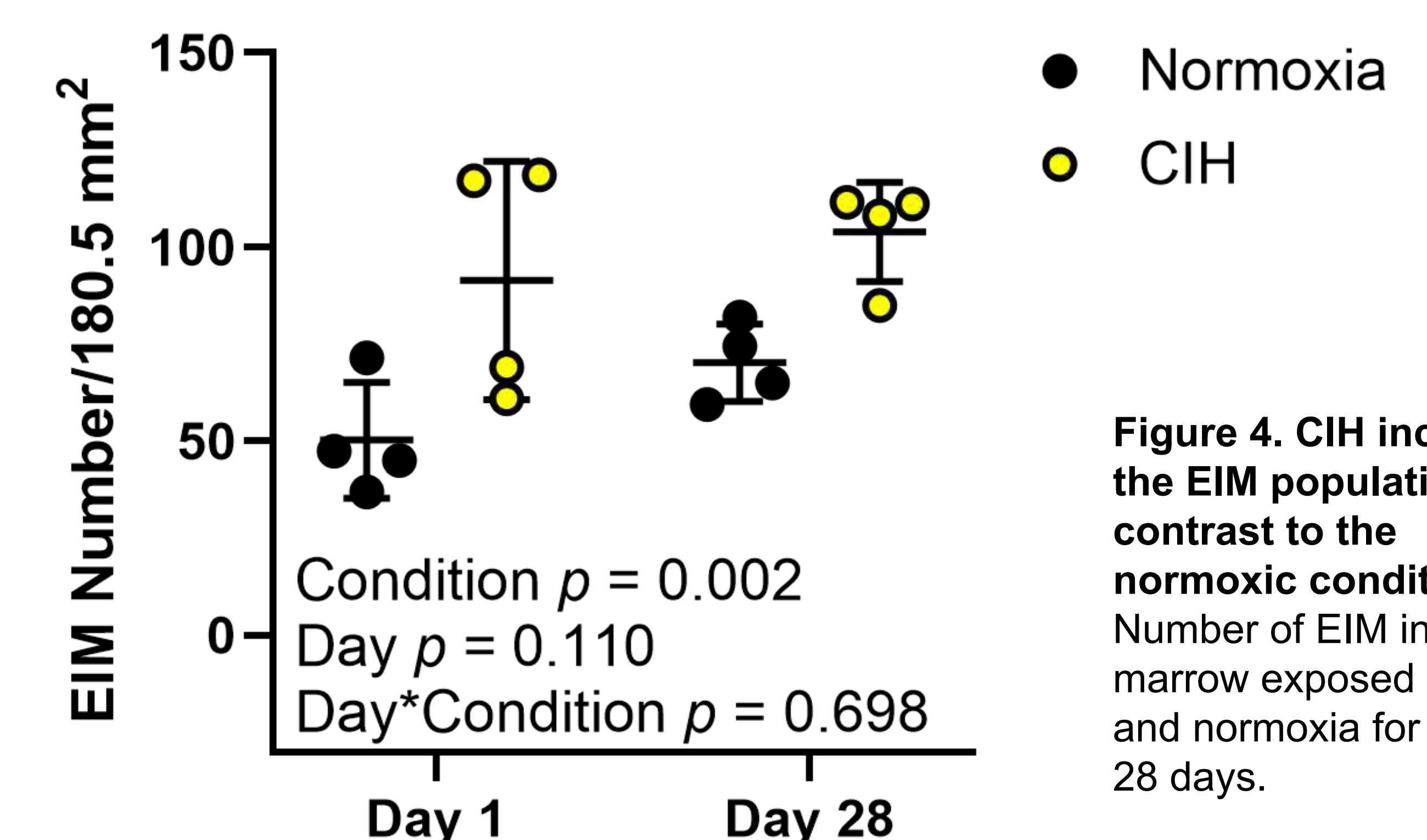


**Figure 4. CIH increased the EIM population in contrast to the normoxic condition.** Number of EIM in bone marrow exposed to CIH and normoxia for 1 and 28 days.

## Discussion

- The impact of CIH on EIM population is time-independent.
  - 24 hours may be enough for EIM proliferation – immediate HIF-1a stabilization (transcription factor that regulates cellular responses to hypoxia) may reprogram EIM within hours [8].
- CIH increased EIM population, possibly shaping a favorable bone marrow microenvironment for MM progression.
  - May promote angiogenesis and tumor progression [4].
  - May suppress anti-tumor immunity – erythroblastic islands inhibited dendritic cell function and weakened T cell responses in hepatoblastoma [4].

## Future Directions

- Test if CIH-induced EIMs promote vascular growth and immune suppression.
- Identify CIH-induced pathways in EIM.
- Examine how EIMs affect MM cell survival and proliferation.

## Acknowledgements

I am very grateful for working in the IPG lab and having this research opportunity provided by the Belin-Blank Center and the organizers of SSTP.

## References





# ANPRE: An End-to-End Neuroinformatics Toolkit for Digitizing Clinical Neuropsychological Data

Wang, Lucas<sup>1,4</sup>, Brzus, Michal, Ph.D.<sup>2</sup>, Martin, Ashby<sup>1</sup>, Tranel, Daniel, Ph.D.<sup>1,3</sup>

<sup>1</sup>Department of Neurology, <sup>2</sup>Department of Pediatrics, <sup>3</sup>Department of Psychological and Brain Sciences, University of Iowa, Iowa City, IA, <sup>4</sup>Los Gatos High School, Los Gatos, CA

## Introduction

### Current Landscape

- Cataloguing of neuropsychological assessment performance is analog and clinic-specific
- Little documentation exists on the best practices for extracting score data
- Clinical neuropsychologists are not commonly trained on data automation technology

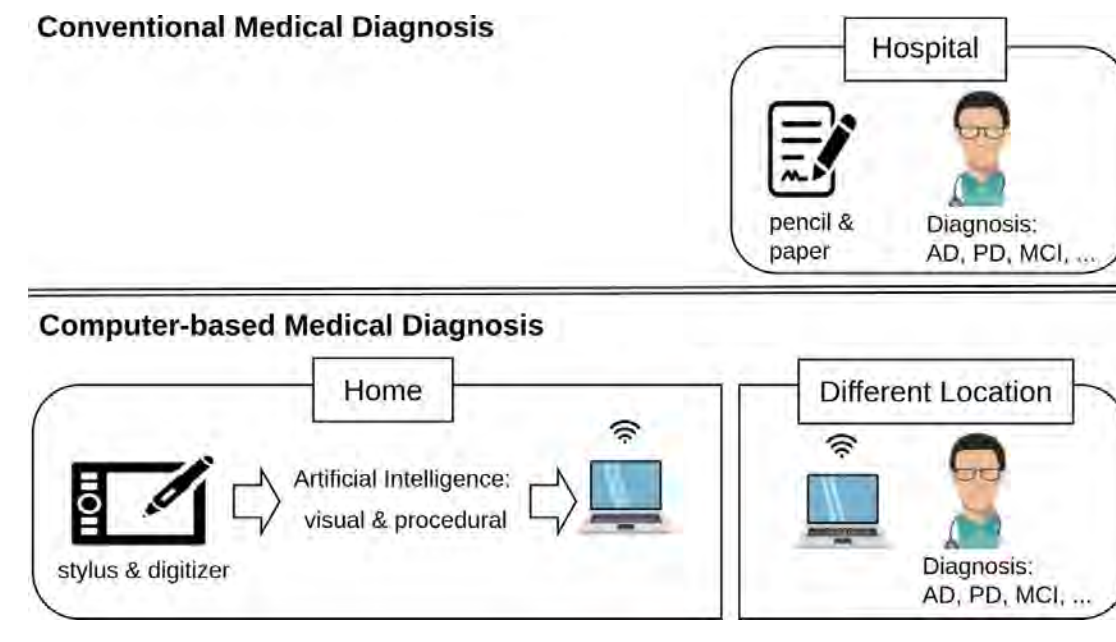


Figure 1 Example of traditional vs. computer led clinic protocol for neuropsychology (Moetesum et al., 2022)

- Biomedical informatics, which has undergone rapid horizontal research development<sup>[3]</sup>, has established the foundation for how to implement data automation in clinical neuropsychology<sup>[2]</sup>
- Inherent difficulties in managing sensitive patient data while maintaining privacy protections<sup>[1], [4]</sup>

## Research Aims

- Develop a **computer vision-based neuroinformatic pipeline** to process neuropsychological assessments at scale.
- Maintain **toolkit organization** to allow both inference-level and development-level adaptation as a proof-of-concept

## Data and Methods

The Benton Neuropsychology Clinic's clinical datasheets (BNCSS) contains most quantitative data from the battery for evaluating a patient.

- Patient Information Block:** such as name, DOB, referral information, handedness, education
  - De-identification would usually remove this section
- Field Labels:** each row, representing tests (e.g. WAIS-IV), test categories (MEMORY), or subtests (Rey-Osterrieth: Copy)
- Data Groups:** each of 3 main columns, resp.
  - Test Information:** test parameters, patient time taken, errors made
  - Raw Score**
  - Clinician Comments:** percentiles, confidence intervals, norms

### Constraints of Input:

- BNCSS can be found within the **first ~10 pages** of case files → faster runtimes
- Patient info is in **metadata**, accessible without processing

- Scan sheet **need not be straight**
- Handwriting quality can be **poor**
- Handwriting can lie **outside** or **between** the the frame

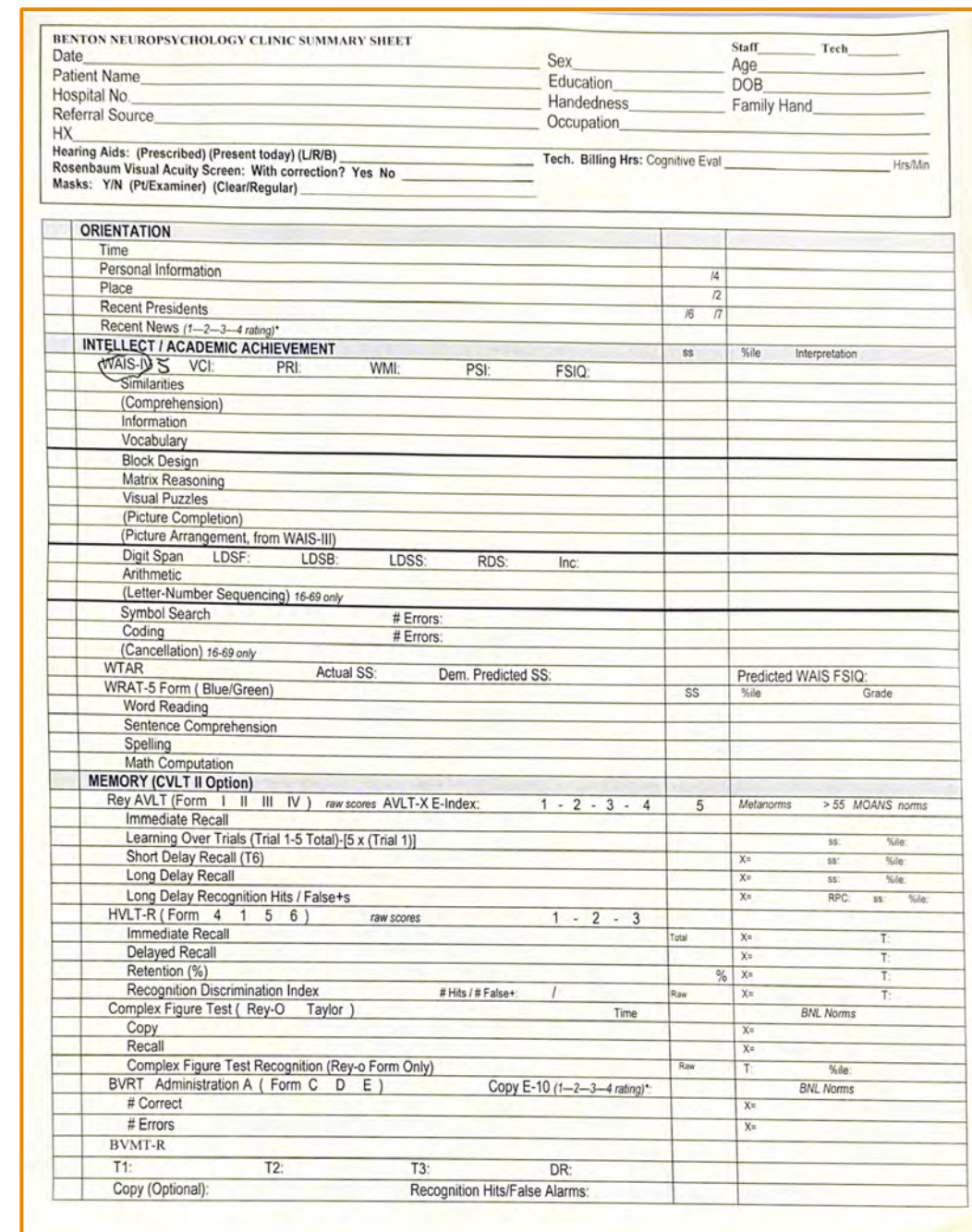


Figure 2 Empty BNCSS sample. As seen, the scan is misaligned (rotated and skewed), which may affect text quality. This type of error is corrected for in 2. Segmentation.

## ANPRE Multi-Modular Framework Development

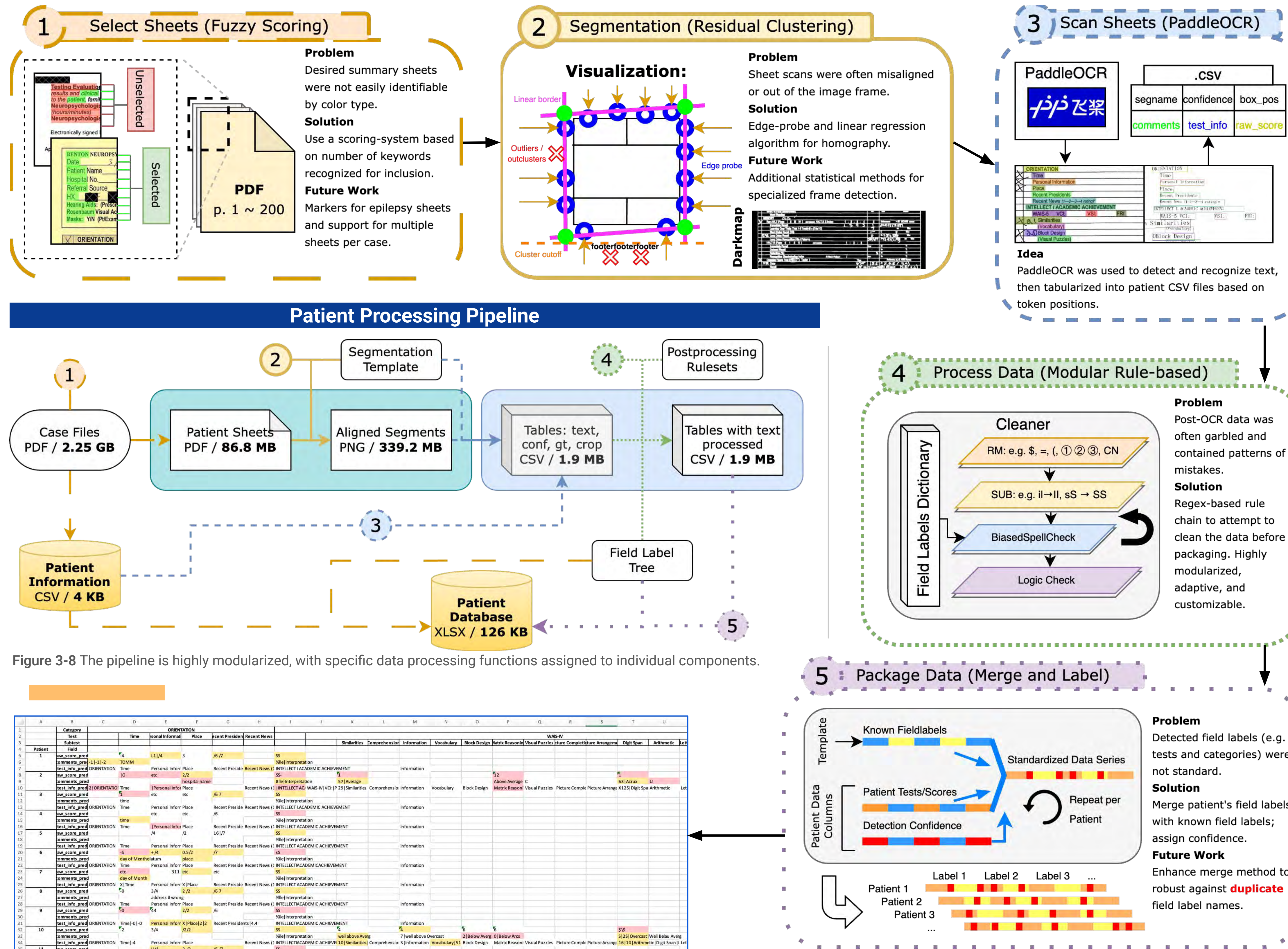


Figure 3-8 The pipeline is highly modularized, with specific data processing functions assigned to individual components.

Figure 9 Instance of patient data spreadsheet. Rows: patients. Subrows: data groups. Columns: categories, tests, and subtests. Red and yellow indicates low-confidence. Data was jumbled for demonstration.

## Results → Quantitative Performance Analysis

### Engineering Experiment Design

- Dataset Overview:** Random sample of n=30 from patient cases conducted in 2025
- Implementation:**
  - Computer Cases:** Implement in Python (~2200 lines)
  - Human Cases:** Token crops (groundtruth) lined up along detect text, holistically scored by me as Wrong, Recoverable, or Correct for data capture acc. (DCA).
- Explanatory data groups:**
  - Field Labels:** either all field labels or only Orientation+WAIS were included
  - Handwriting:** Handwriting (HW) and no-HW groups were measured separately. No-HW usually indicates no data / the test wasn't performed

Table 1 Comparison of performance times for manual data entry, automated entry with Computer A (Macbook CPU), and data entry with Computer B (Windows GPU)

Pipeline	Human	Average Time per Patient (s)	Computer A (CPU)	Computer B (GPU)
Selection	~30	0.705	1.90%	~0.705
Segmentation		0.506	1.40%	~0.506
Text Detection	~420	34.796	96.20%	2.524
Processing	~180	0.361	1.00%	0.392
Synthesis		0.037	0.10%	0.035
Time / patient	10.5 min	36.405 s		4.162 s

### Score Capture Performance

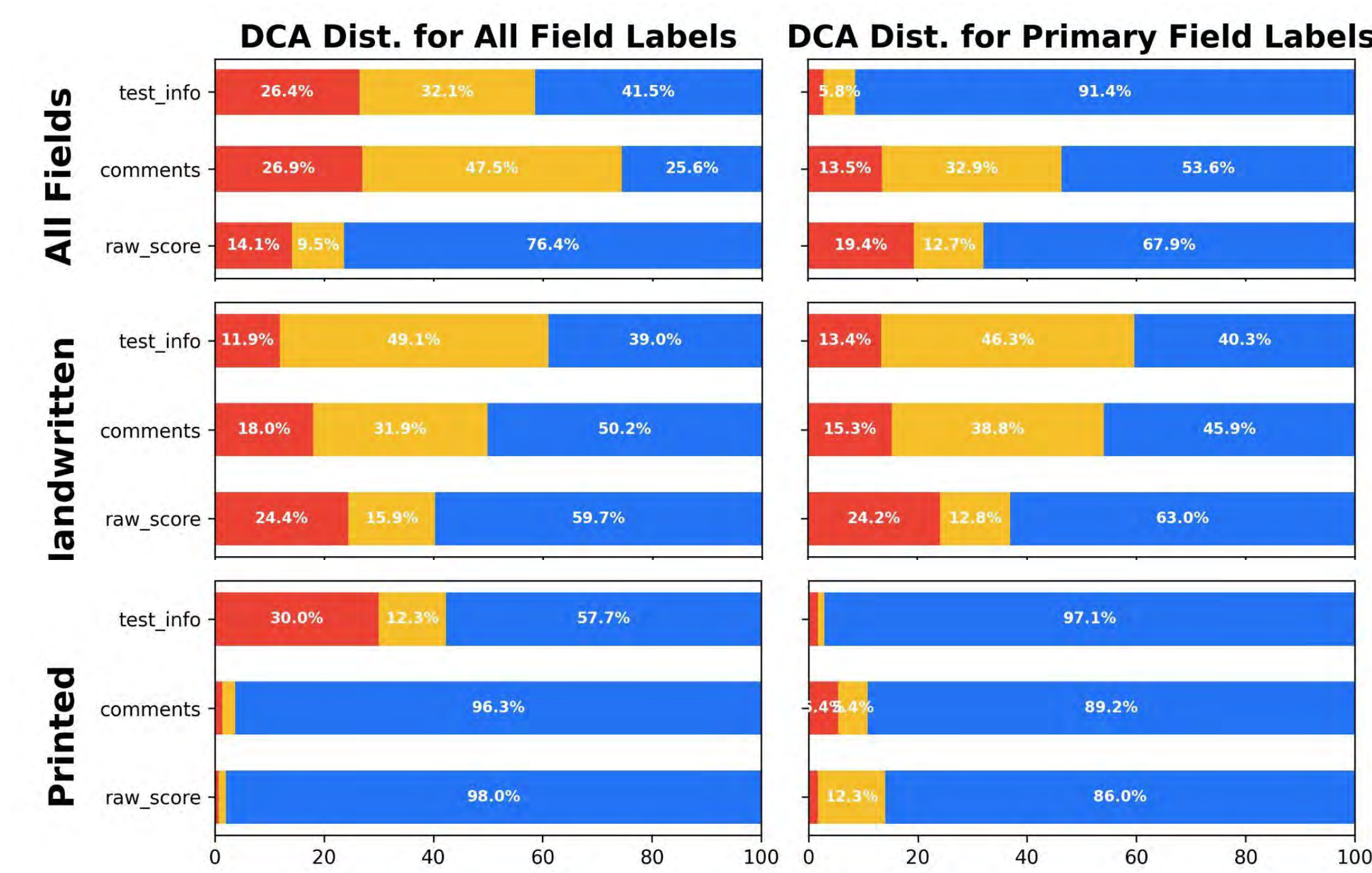


Figure 10 The left column represents data capture accuracy (DCA) distribution for all field labels (categories, tests, subtests), while the right column represents DCA for only Orientation and WAIS (Intellect), which can be applied the most generally. The first row represents both HW and no-HW data; the second row includes with-HW data; and the third row includes only no-HW data.

## Results → Metrics

For 100 patients...

- (S1) Accuracy of selecting BNCSS: **99%**
- (S2) Accuracy of segmenting BNCSS: **97.25%**
- If accurate, potential improvements include
  - Reduction in data collection time: **10 minutes → 4 seconds . 99.333% time and work saved**
  - Reduction in amount of data to be analyzed: **2.25 GB → 141 KB . 99.997% processing data saved**

### Sheet Selection Performance

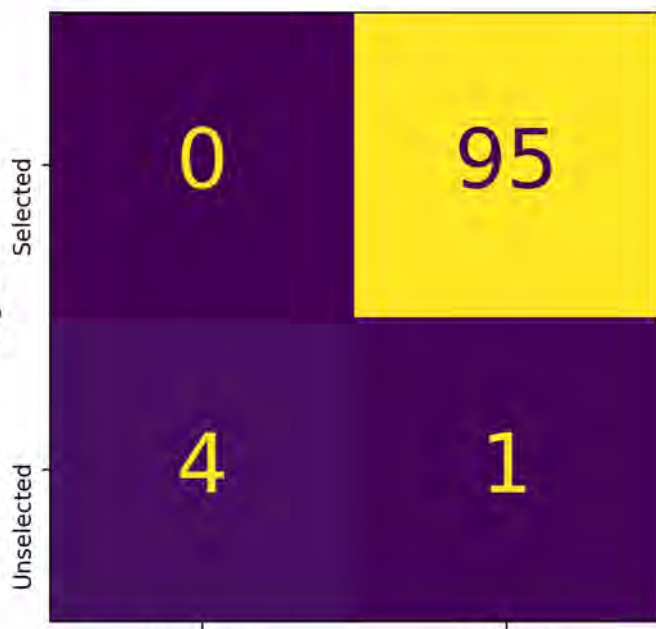


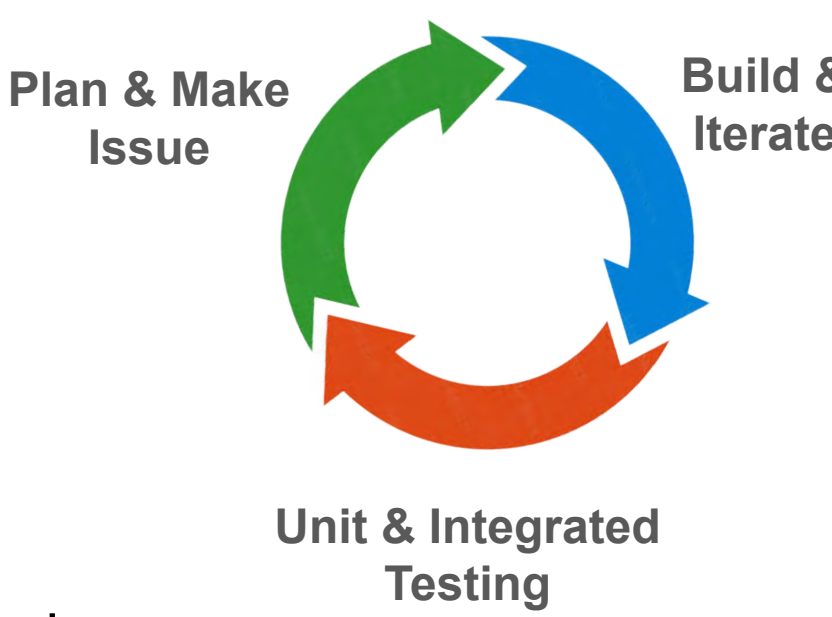
Figure 11 Confusion matrix of accuracy of sheet selection. One epilepsy sheet was incorrectly selected, making a false positive.

## Discussion

- Convert raw patient casefiles → **standardized** .xlsx database in format prepared for analysis and research
- Confidence-level** labeling for clinical feasibility
- The ANPRE toolkit serves as a **starting point** for digitizing neuropsychological data with minimal interference to clinical procedure
- Multimodular framework enables continued development and accuracy optimization for ANPRE

### Skill Development

- Designed algorithms **from scratch**, using concepts from well-known techniques: fuzzy-logic, coordinate clustering, regex, rulesets, feature-extraction
- Built a software and programming workflow
  - Developed a **multi-module** project with interacting components, which helped significantly with debugging and reworking previous code
  - Improved Github usage autonomy: trees, pre-commits, etc.
- Interacted with toolkits: PaddleOCR, PyTesseract



### Future Directions and Continued Pipeline Development

- Develop textual groundtruth dataset to increase sample size and facilitate future development and testing
- Develop a **data labelling GUI** to adapt new tests, templates, and field label corrections for broader clinical applications
- Detect single data cells for strictly-aligned text detection
- Explore alternatives to PaddleOCR, with consideration of data confidentiality in mind
- Conduct integration testing and a lesion-mapping case using this data

## Acknowledgements

I would like thank my mentors Michal, Ashby, and Dr. Tranel. Thank you all for being so incredibly supportive and helpful throughout this process! I would also like to express my gratitude for everyone in the Tranel Lab and Benton Neuropsychology Clinic for providing us with a variety of opportunities, from shadowing to research paths. Thanks to the Belin-Blank Center for granting me this research opportunity. Finally, I want to thank all my friends in the lab for having a great time together!

## References

- [1] Bellazzini, R. (2014). Big data and biomedical informatics: a challenging opportunity. Yearbook of medical informatics, 23(01), 08-13.
- [2] Miller, J. B. (2019). Big data and biomedical informatics: Preparing for the modernization of clinical neuropsychology. The Clinical Neuropsychologist, 33(2), 287-304. <https://doi.org/10.1080/13854046.2018.1523466> (MedNexus)
- [3] Moetesum, M., Diaz, M., Masroor, U., Siddiqui, I., & Vessio, G. (2022). A survey of visual and procedural handwriting analysis for neuropsychological assessment. Neural Computing and Applications, 34(3), 9561-9578. <https://doi.org/10.1007/s00521-022-07185-6> (ResearchGate)
- [4] Parsons, T. D., McMahon, T., & Kane, R. (2018). Practice parameters facilitating adoption of advanced technologies for enhancing neuropsychological assessment. The Clinical Neuropsychologist, 32(1), 16-41. <https://doi.org/10.1080/13854046.2017.1337932> (PubMed)
- [5] PaddlePaddle. (2023). PaddleOCR [Computer software]. GitHub repository. Retrieved July 14, 2025, from <https://github.com/PaddlePaddle/PaddleOCR> (GitHub)
- [6] Shaharun, N. A., Ahmad Zamzuri, M. A. I., Ariffin, A. A., Azman, A. Z. F., & Mohd Ali, N. K. (2023). Digitalisation medical records: Improving efficiency and reducing burnout in healthcare. International Journal of Environmental Research and Public Health, 20(4), 3441. <https://doi.org/10.3390/ijerph20043441> (PubMed)



# Seizure-prone *prickle*-mutant flies exhibit the clinical features of Autism Spectrum Disorder

Avery Yu<sup>1</sup>; Meher Garg<sup>2</sup>; Brady Williquett<sup>3</sup>; Bridget C. Lear<sup>3</sup>; G. Gregory Neely<sup>4</sup>; J. Robert Manak, PhD<sup>3,5</sup>

<sup>1</sup>Oak Park High School, <sup>2</sup>Springfield High School, <sup>3</sup>Department of Biology, University of Iowa, <sup>4</sup>School of Life and Environmental Sciences, University of Sydney, <sup>5</sup>Department of Pediatrics, Carver College of Medicine, University of Iowa

## INTRODUCTION

Approximately 30% of individuals with Autism Spectrum Disorder (ASD) have epilepsy.<sup>1</sup> Interestingly, there is an enrichment of pathogenic DNA sequence variants in *PRICKLE* genes found in individuals with epilepsy as well as ASD.<sup>2,3</sup> In *Drosophila*, homozygous loss-of-function (LOF) mutations of the *prickle-spiny-legs* (*pk<sup>sple</sup>*) isoform of *prickle* trigger seizures and ataxia similar to those seen in humans.<sup>4-7</sup> Here we now show that seizure-prone *prickle* mutants have increased sensitivity to pain, altered sleep patterns, learning deficiencies, and social isolation, all characteristics of individuals with ASD.

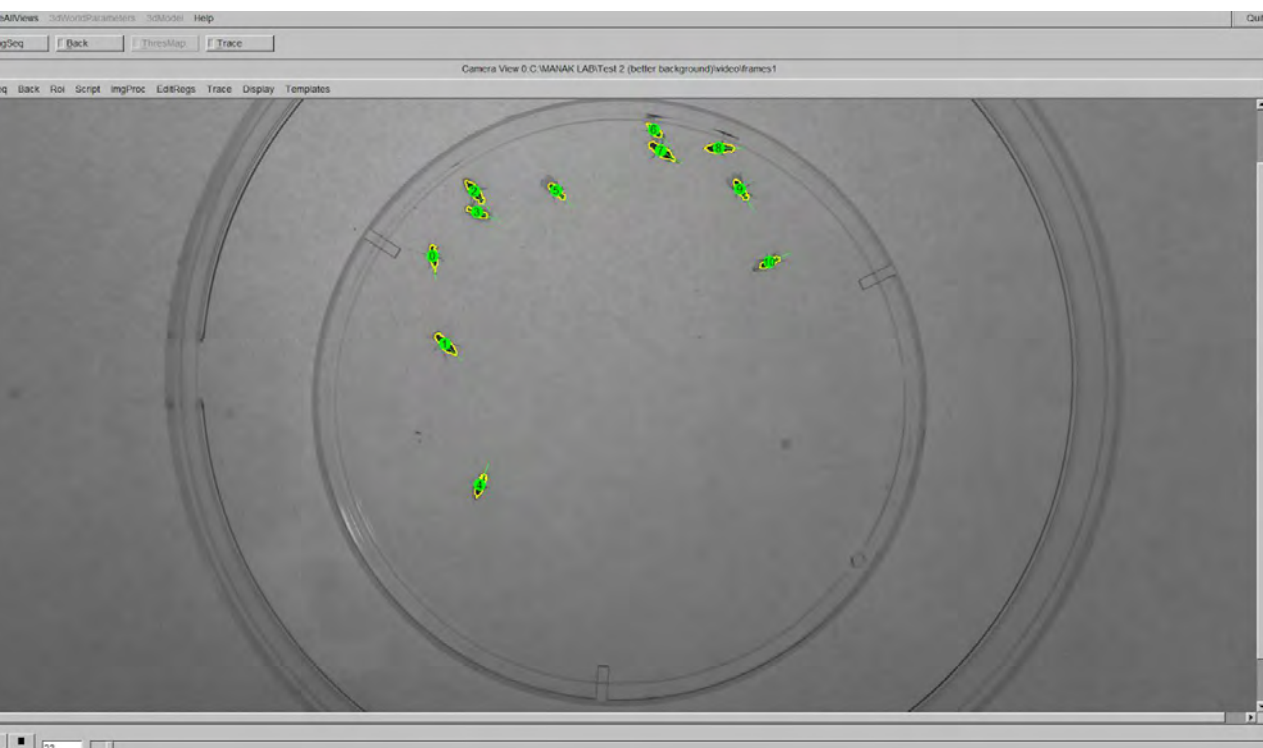
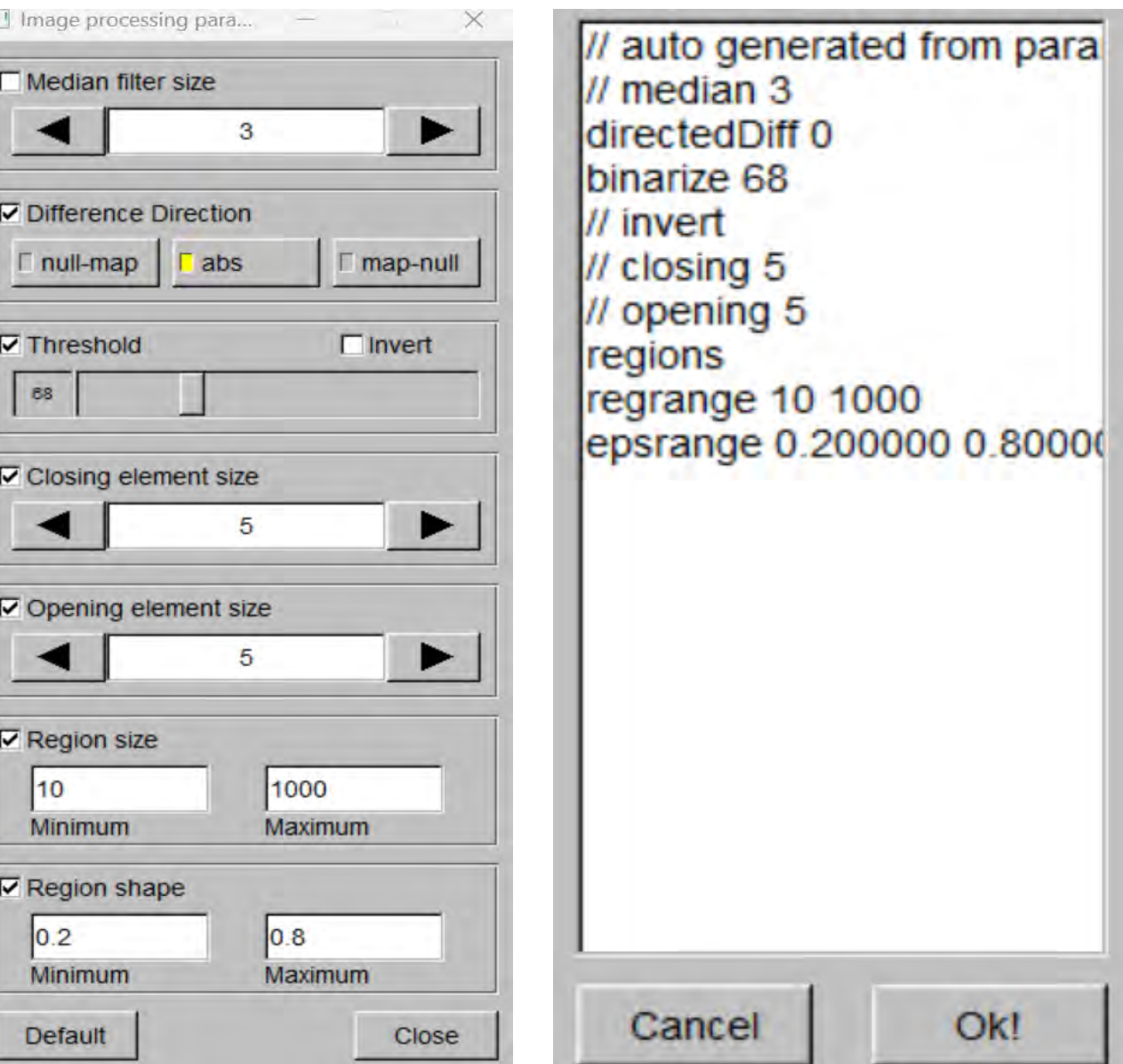
## MATERIALS AND METHODS

### *Drosophila* stocks and genetics:

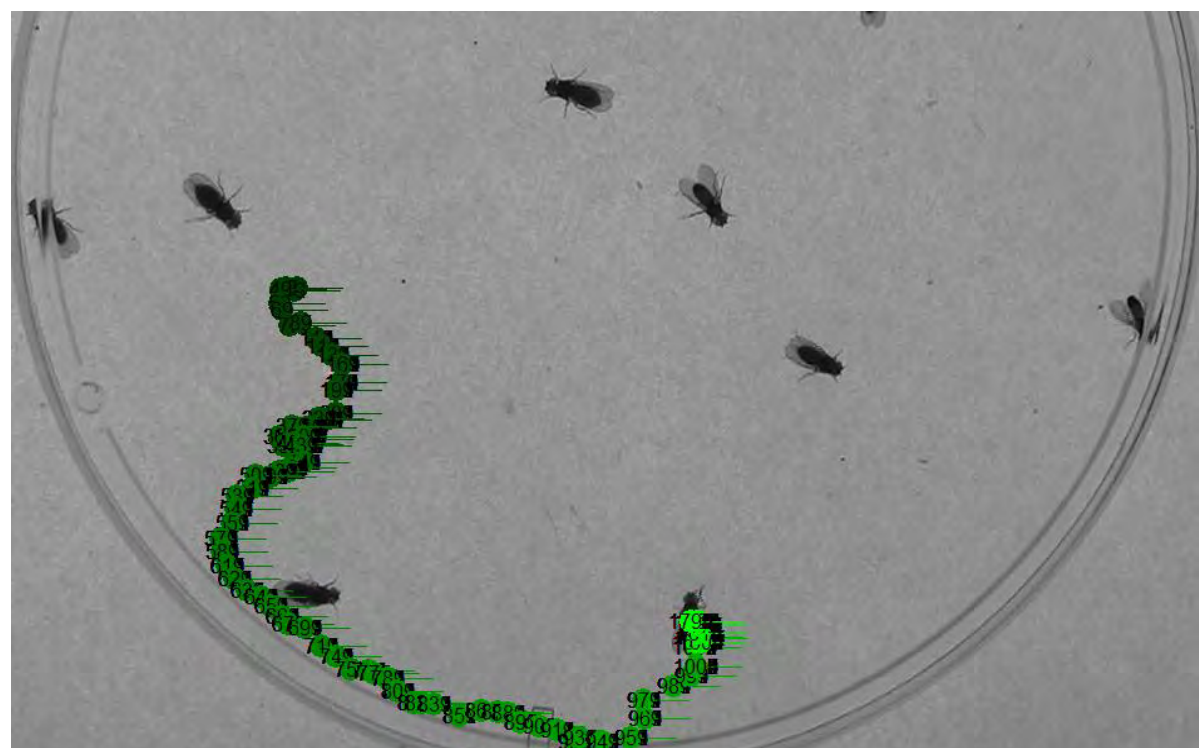
- Drosophila melanogaster* *w<sup>1118</sup>*, *pk<sup>pk</sup>* and *pk<sup>sple</sup>* fly lines were used for all experiments
- Flies were reared at 25°C and aged to 7-10 days post-eclosion (dpe)

### Recording:

- 10 flies (5 male, 5 female) were placed into a 95 mm shallow round chamber in the recording room (55-60% relative humidity, 25 °C).
- To assist with secure transfer of all ten flies, the flies were cold shocked at 0°C. Flies were transferred in a cold room to an empty, pre-cooled vial with a Flug pushed to the bottom to absorb moisture from condensation and transported to a 25°C video room in the ice bucket during the cold shock. After 1 min 10 sec, flies were taken out of the ice and transferred onto a large petri dish and covered with the 95 mm chamber. The flies were recorded on a light box after 5 minutes for recovery from the cold shock and acclimation to the light box.
- Flies were recorded from minutes 5-6 and 8-9.
- ivTools (an opensource software suite developed by Lindemann and Bertrand) was used to find the coordinates of each fly every 10 frames. Matlab was used to compute distances of each fly to every other fly. Statistical and graphical analyses were conducted using Prism and GraphPad, respectively.



ivTools successfully processing an image and correctly identifying flies as regions



ivTools showing the path of a fly over one minute

### Troubleshooting ivTools:

- ivTools is a software that takes frames of a video and processes each frame to determine “region objects” which it then maps.
- Coordinates of each fly were assessed.
- The parameters and script indicated on the left were used in image processing.

## RESULTS

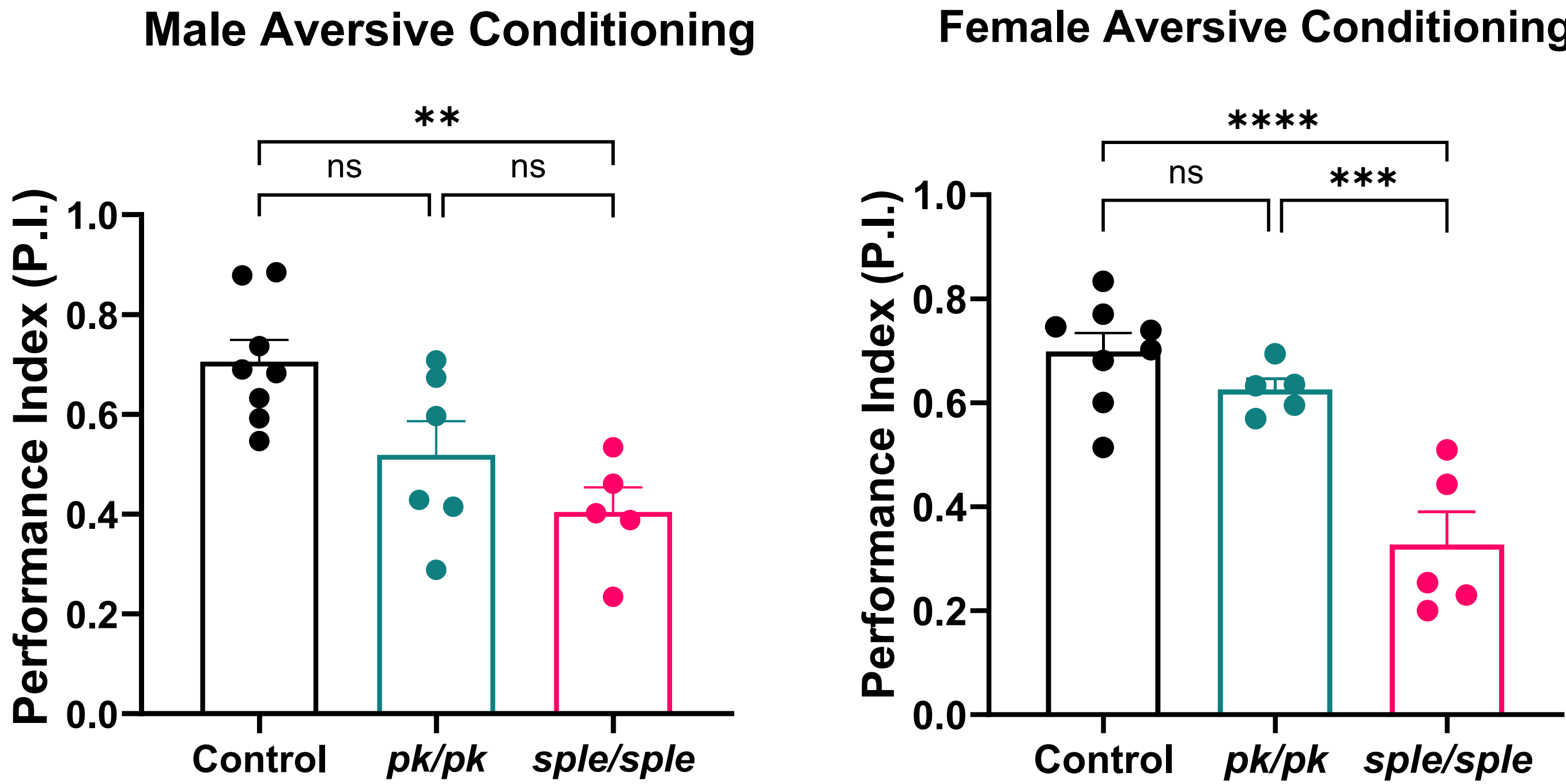


**Figure 1A:** *sple/sple* but not *pk/pk* mutant males show a significant decrease in learning using a T-maze apparatus and Pavlovian conditioning procedure

**Figure 1B:** *sple/sple* but not *pk/pk* mutant females show a significant decrease in learning using a T-maze apparatus and Pavlovian conditioning procedure

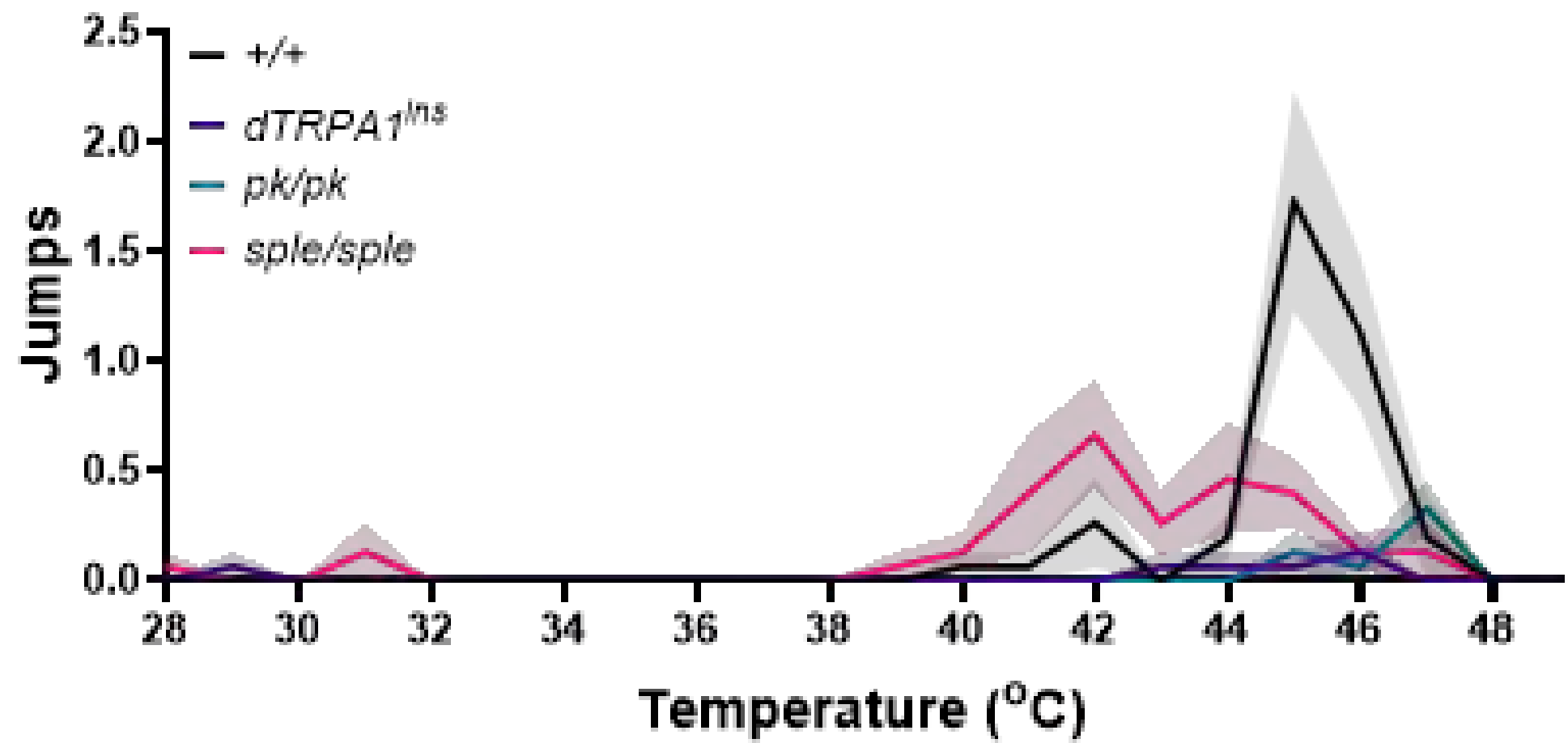


**Figure 2:** 7-9 days old *sple/sple* but not *pk/pk* male flies show increased pain susceptibility using a nociceptive heat response assay.

	Period ± SEM	Power ± SEM	% Rhythmicity ± SEM
+/+	23.8 ± 0.1	45.5 ± 7.2	82 ± 3
<i>sple/sple</i>	23.4 ± 0.3	18.5 ± 3.7	52 ± 9 *
<i>pk/pk</i>	23.9 ± 0.1	14.6 ± 4.4	43 ± 9 *

**Figure 3:** Both *sple/sple* and *pk/pk* flies show reductions in rhythmicity during dark-dark cycle, demonstrating alterations in circadian rhythm.

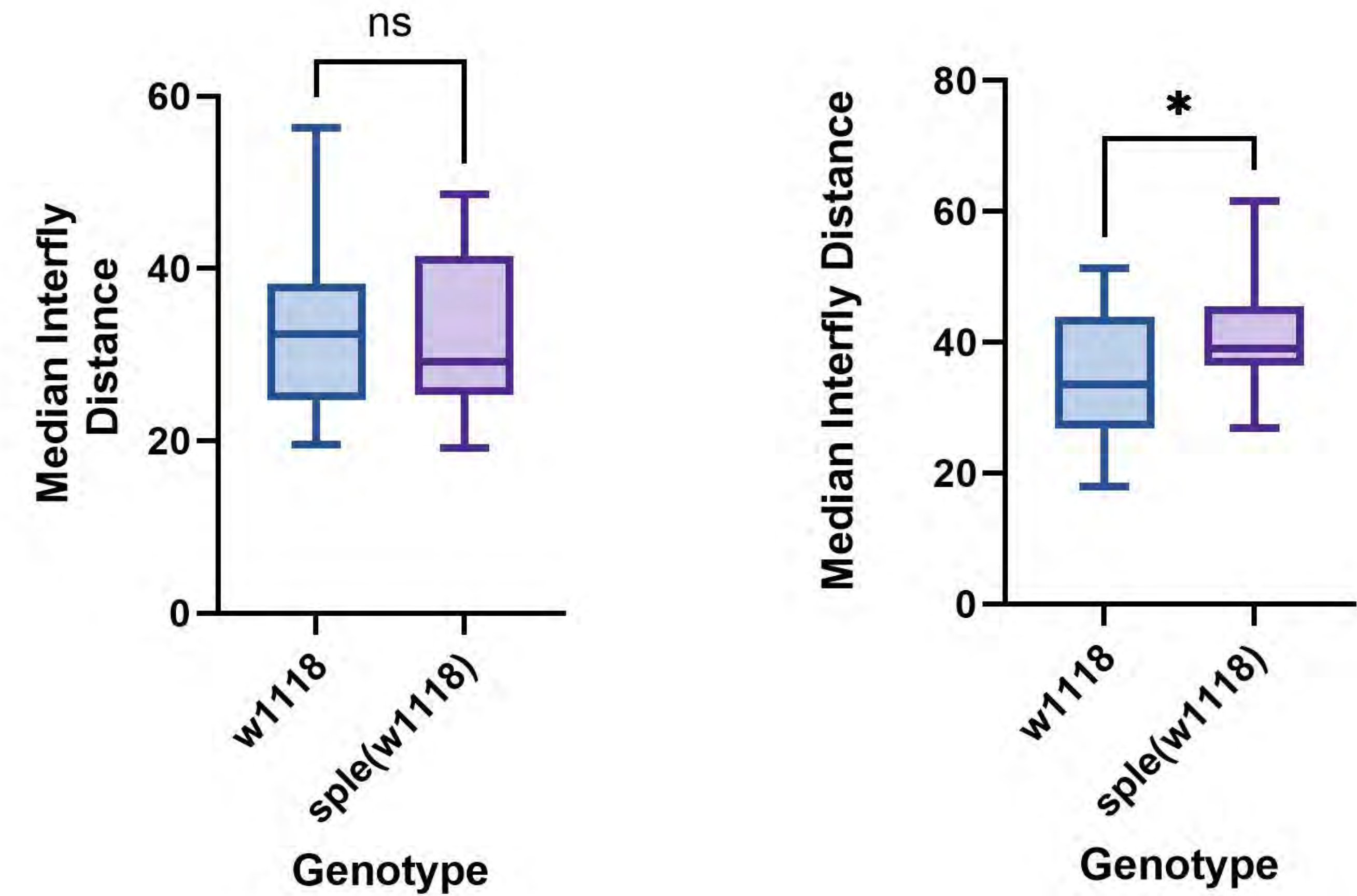
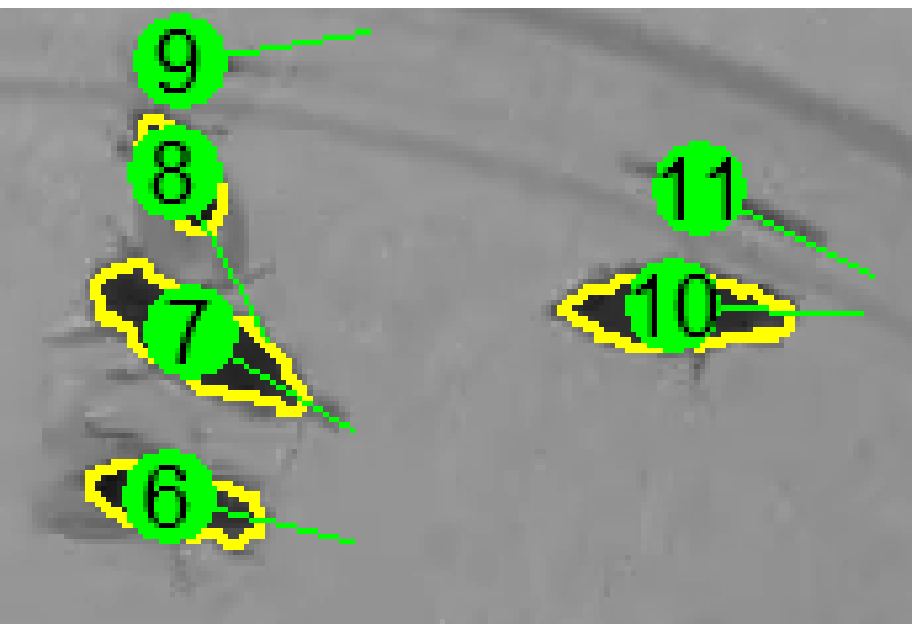


**Figure 4A:** From 5-6 minutes, both control and *sple/sple* flies showed comparable inter-fly distances. Mann Whitney statistical test, 20 flies total (10 male, 10 female).

**Figure 4B:** From 8-9 minutes, *sple/sple* flies showed greater inter-fly distances, demonstrating a higher degree of social isolation. Mann Whitney statistical test, 20 flies total (10 male, 10 female).

## SOFTWARE ADAPTATIONS



Error: regions 9 and 11 are not flies

- Due to outdated software issues, mistakes in fly calling oftentimes occurred (i.e. non-flies were mis-identified as flies, flies were not properly identified). In these cases, the frames were manually corrected. Due to the switching of region indices, the computer failed to correctly re-sort the indices, resulting in manual sorting.
- Only the first in every 10 frames were manually corrected and used for Matlab analysis.

## CONCLUSIONS

### Inter-fly distances

- sple/sple* mutants showed a statistically significant increase in inter-fly distances in comparison to control flies (e.g., social isolation), a key characteristic of ASD.
- Differences were only significant at the 8-9 minute mark, possibly because the *sple/sple* flies needed more time to disperse. Additionally, the cold shock may have slowed the flies' movements, further contributing to the delayed dispersal.

### Circadian rhythm

- sple/sple* flies also show significantly less rhythmicity in circadian rhythm.
  - Could be manifested as sleep disorders in humans with ASD.

### Learning ability

- Both male and female *sple/sple* flies exhibited learning deficits, similar to what is observed in ASD individuals.

### Sensitivity to thermal pain

- sple/sple* flies showed hypersensitivity to heat pain, another characteristic of ASD.

## FUTURE DIRECTIONS

- More advanced software could be used to track fly positions. One such software is DeepLabCut, a machine learning application that accurately tracks positions and poses of multiple animals.
- A larger chamber could be used to provide flies more space to spread out.
- Social networks could be analyzed using FlyTracker or similar software.
- More biological replicates could be analyzed to increase statistical power.
- Courtship behavior could be analyzed to assess inter-fly communication issues.

## REFERENCES

- Viscidi EW, Triche EW, Pescosolido MF, et al. Clinical characteristics of children with autism spectrum disorder and co-occurring epilepsy. *PLoS One*. 2013;8(7):e67797. doi:10.1371/journal.pone.0067797
- Paemka L, Mahajan VB, Skeie JM, et al. PRICKLE1 interaction with SYNAPSIN I reveals a role in autism spectrum disorders. *PLoS One*. 2013;8(12):e80737. doi:10.1371/journal.pone.0080737
- Sowers LP, Loo L, Wu Y, et al. Disruption of the non-canonical Wnt gene PRICKLE2 leads to autism-like behaviors with evidence for hippocampal synaptic dysfunction [published correction appears in *Mol Psychiatry*. 2014 Jun;19(6):742. Manak, R J [corrected to Manak, J RJ]. *Mol Psychiatry*. 2013;18(10):1077-1089. doi:10.1038/mp.2013.71
- Bassuk AG, Wallace RH, Buhr A, et al. A homozygous mutation in human PRICKLE1 causes an autosomal-recessive progressive myoclonus epilepsy-ataxia syndrome. *Am J Hum Genet*. 2008;83(5):572-581. doi:10.1016/j.ajhg.2008.10.003
- Tao H, Manak JR, Sowers L, et al. Mutations in prickle orthologs cause seizures in flies, mice, and humans. *Am J Hum Genet*. 2011;88(2):138-149. doi:10.1016/j.ajhg.2010.12.012
- Ehaideb SN, Wignall EA, Kasuya J, et al. Mutation of orthologous prickle genes causes a similar epilepsy syndrome in flies and humans. *Ann Clin Transl Neurol*. 2016;3(9):695-707. doi:10.1002/acn3.334
- Nukala KM, Lilienthal AJ, Lye SH, Bassuk AG, Chtarbanova S, Manak JR. Downregulation of oxidative stress-mediated glial innate immune response suppresses seizures in a fly epilepsy model. *Cell Rep*. 2023;42(1):112004. doi:10.1016/j.celrep.2023.112004

## ACKNOWLEDGEMENTS

We would like to thank Dr. Manak, Brady Williquett, and the Manak Lab for their invaluable guidance and mentorship. We thank the Manak Lab, University of Iowa, and Belin-Blank Center for providing us this opportunity.



# Xuanzang and the Materiality of Buddhist Scriptures: Tracing Manuscript Production and Transmission in Pre-Medieval Asia



Aaron Widjaja<sup>1</sup>, Paul Dilley, PhD<sup>2</sup>

<sup>1</sup> Menlo School, Atherton, CA; <sup>2</sup> Department of Religious Studies, Erling B. "Jack" Holtsmark Associate Professor in the Classics, University of Iowa



## Introduction

Xuanzang (602-664 CE) is a seventh century Buddhist monk who traveled to India in search of authentic Buddhist scriptures for accurate translation.<sup>1</sup>

**Xuanzang's Travelog highlights detailed accounts of:**

- People, landscapes, and cultures he encountered.
- Geography, topography, and political-social structures of visited regions.
- Religious practices, institutions, and doctrinal views.
- Cultural observations and translation-related concerns.

He notes the types, formats, and doctrinal significance of the texts Xuanzang observed and brought back to China.

His travelogue notes his thought process, motivations, and scholarly approach to scripture collection.<sup>2</sup>

Xuanzang's role as an important translator shaped the Chinese Buddhist canon.<sup>3</sup>



**Figure 1.** *Heart Sutra*, stone rubbing, 672. Monument erected by Emperor Gaozong (r. 650-683 CE) at Gaofu Monastery, Chang'an, with Xuanzang's version of the text. In *The Heart Sutra: A Comprehensive Guide to the Classic of Mahayana Buddhism*, by Kazuaki Tanahashi, 96. Boston: Shambhala, 2014. Public domain.

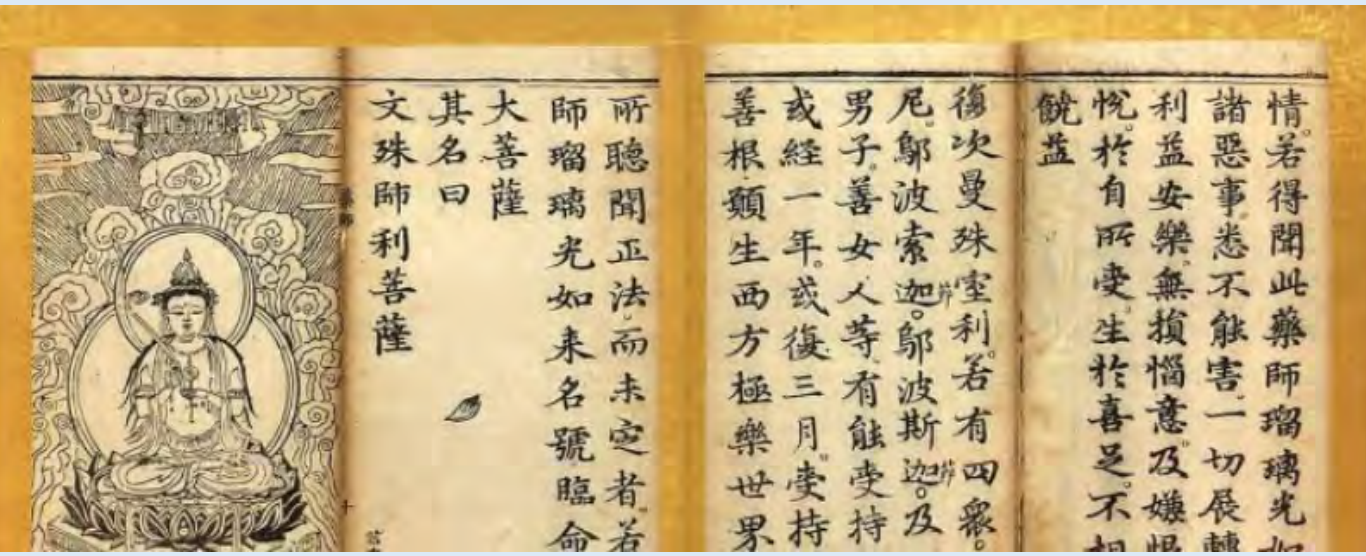


**Figure 2.** *Sutra of the Merits of the Fundamental Vows of the Master of Healing, the Lapis Lazuli Radiance Tathagata (Yaoshi liuli guang rulai benyuan gongde jing)*, woodblock print, 31.2 x 26.0 cm. Jingnan Huguo Chanlin edition, n.d. Illustrated with the twelve great vows, with inscriptions by Zhang Yiting (1872). Library of Congress.

## Purpose

**Research Question:** How did Xuanzang describe the material and physical characteristics of the scriptures he observed and collected during his journey to and from India?

**Objectives:**

- 1) Compile a detailed itinerary of the Buddhist pilgrim's travels, highlighting key locations visited.
- 2) Identify and document the scriptures he encountered during his journey.
- 3) Catalog the scriptures he collected and brought back, contributing the information to the existing database.

**\*\*Data Wrangling: Transferring spreadsheet scripture data into an interactive database, including Xuanzang's Chinese translations of Sanskrit texts like the Diamond Sutra.\*\***

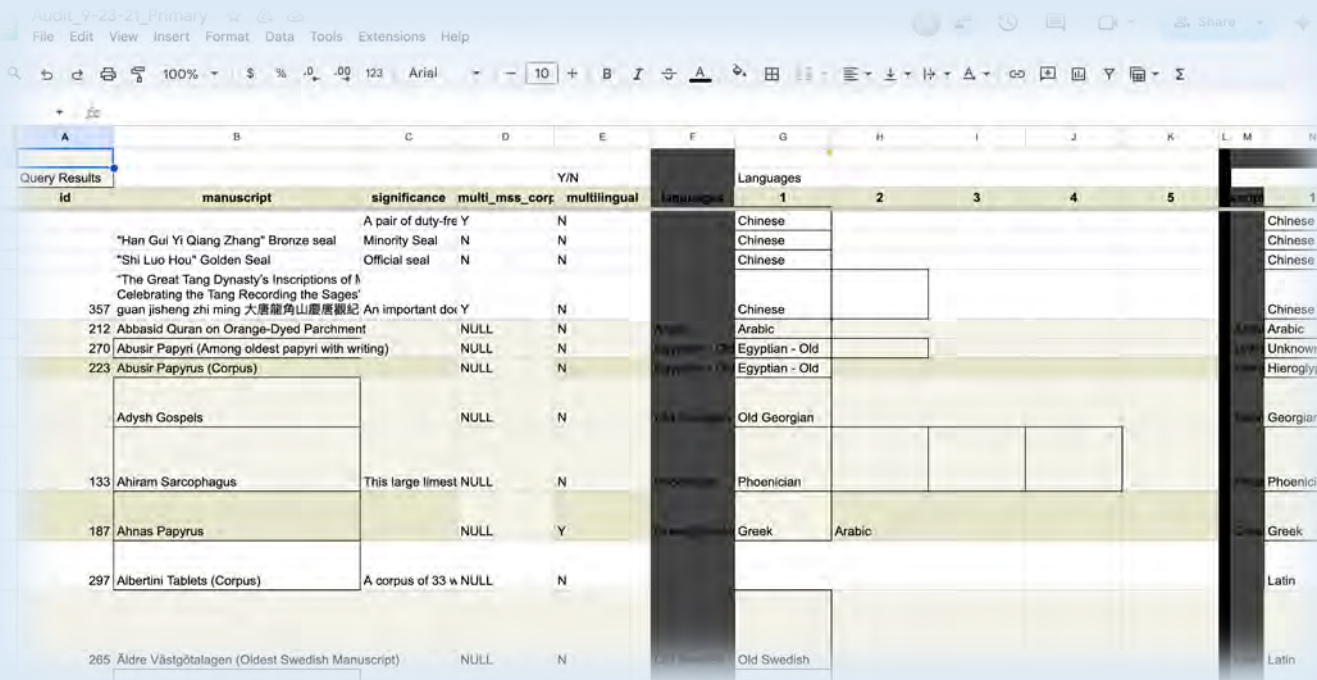


**Figure 3.** *The original spreadsheet of a wide range of scriptures that I imported into Core DataCloud for data wrangling.*

## Method

**Step 1:** Review journal articles on Xuanzang's life, translation standards, and the geopolitical context to provide background for his journey.

**Step 2:** Read an English translation of *The Great Tang Dynasty Record of the Western Regions*; document every scripture he mentions. The primary keywords I searched for were 'sutra' and 'śāstra,' terms used to describe scriptural works in Hinduism and, more prominently, in Buddhism.

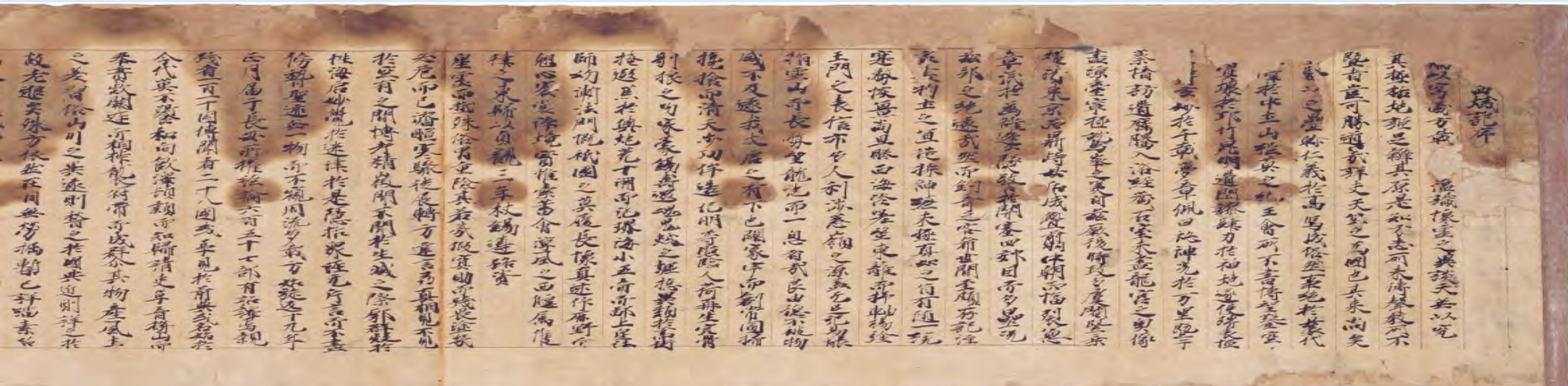


**Figure 4.** *The Great Tang Dynasty Record of the Western Regions (Datang xiyu ji)*, handscroll, ink on paper, 25.6 x 884 cm, Heian period, 12th century. Kyoto National Museum, B甲96. Completed in 1102 (Kowa 4), the oldest extant copy of Xuanzang's travelogue of his journey to India.

**Step 3:** Research each scripture's material, format, location, and other specific information for database input.

**Step 4:** Enter all collected details into the Core DataCloud database.

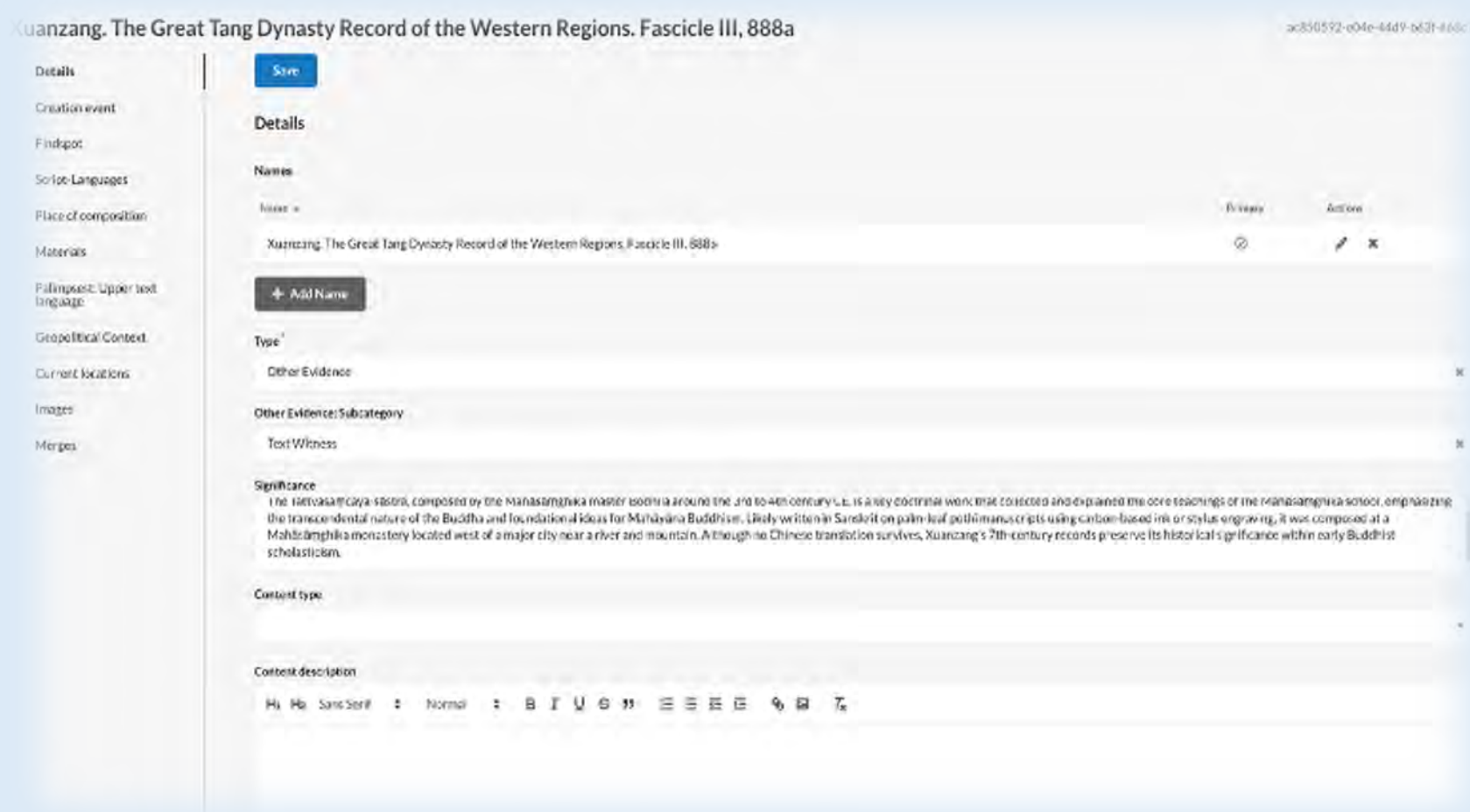


**Figure 5.** *Inputting data and specific details into Core DataCloud.*

## Results

### Material and Physical Characteristics of Scriptures

- **Materials:** Primarily palm-leaf manuscripts (*pothī*); birch bark in regions like Kashmir and Gandhāra.
- **Format:** Long, narrow pothī-style folios, ink or stylus-written, strung with a cord through a central hole, protected by wooden covers or cloth.
- **Scripts:** Brāhmī-derived scripts (Gupta, early Nāgarī, Kharoṣṭhī) in India/Central Asia; Chinese translations on paper scrolls or stitched volumes.
- **Storage:** Monastery libraries; revered texts kept in special chests or dedicated rooms.

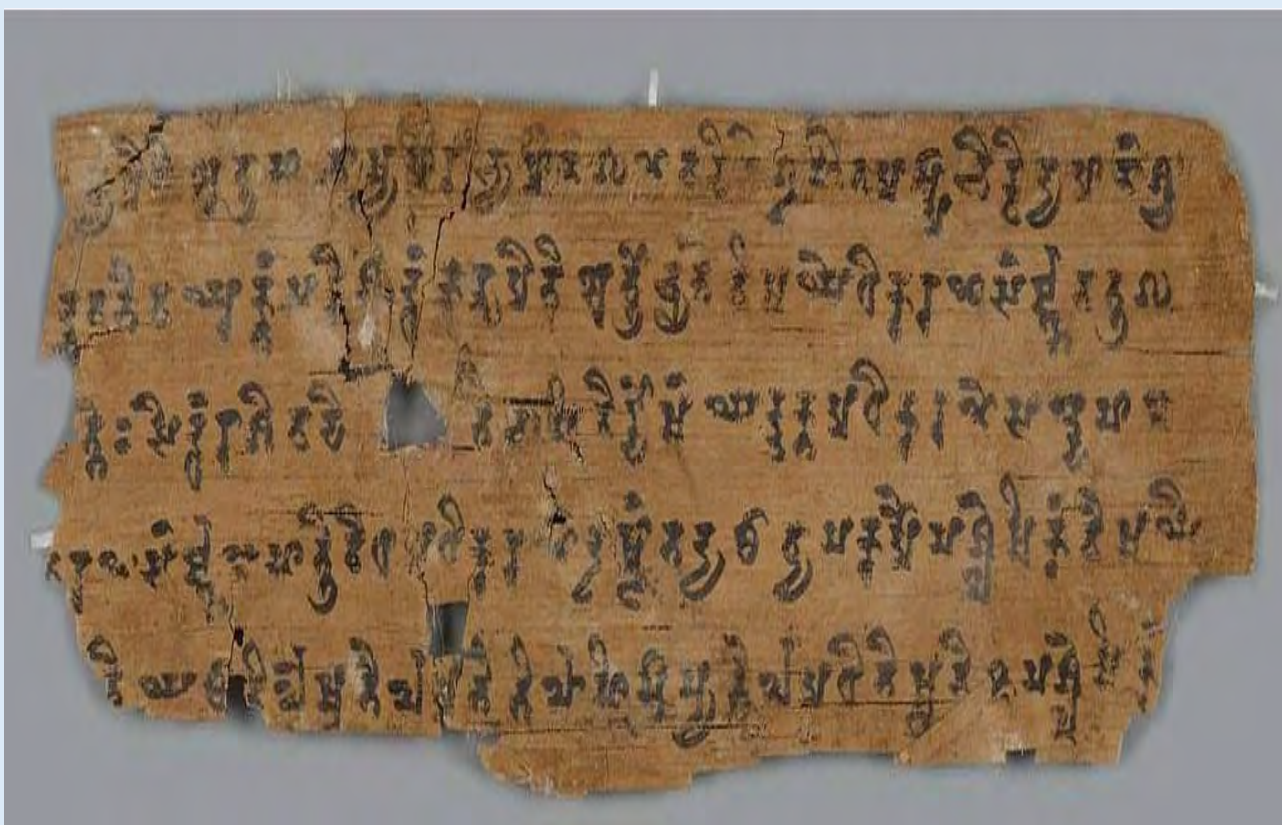
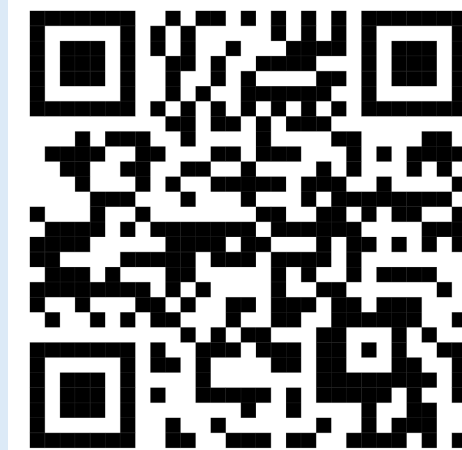


**Figure 5.** *Palm-leaf Sanskrit manuscript in Brahmi script, Miran, northwest China, 1200-1500. Ink on palm leaf, M.II.0011. International Dunhuang Project. Public domain.*

## Results Continued

### Travel Itinerary

- Traveled from Chang'an (China) across the Gobi Desert, passing key Central Asian cities (Liangzhou, Kucha, Samarkand) into India via Bactria.
- Stayed at major Buddhist centers: Nalanda, Kashmir, Lumbini, Bodh Gaya, Sarnath, Kushinagar, Rajagriha.
- Returned via Khotan, Kucha, and Dunhuang.



### Scriptures Encountered & Collected

- Documented diverse Buddhist texts: Abhidharma treatises, foundational sūtras, grammatical and logic texts.
- Detailed the physical and regional features of key scriptures in monastic libraries.
- Returned to China with 657 Sanskrit manuscripts, statues, reliquaries, and oral teaching notes.

### Database Contribution

- Xuanzang's records enhance cataloguing of scripture type, origin, and format.
- Database improves research on Buddhist textual culture and doctrinal transmission.

## Conclusion

### Conclusion

- Xuanzang's journey highlights the enduring impact of cross-cultural knowledge transmission.
- His work guides both historical research and modern approaches to preserving and translating important texts.

### Next Steps

- Deepen analysis of Xuanzang's translations and compare them with archaeological evidence.
- Apply his methods to improve current translation and preservation practices.

## References

- <sup>1</sup> He, Jiachuan. (2023). "A brief introduction to Xuanzang's view of translation." *International Journal of Education and Humanities* 8, no. 2, 145-149. <https://doi.org/10.54097/ijeh.v8i2.7793>.
- <sup>2</sup> Sen, Tensen. (2006). "The travel records of Chinese pilgrims Faxian, Xuanzang, and Yijing: Sources for cross-cultural encounters between ancient China and India." *Education About Asia*, 11, no. 3, 24-33.
- <sup>3</sup> Xuanzang. *The Great Tang Dynasty Record of the Western Regions*. Translated by Li Rongxi. BDK English Tripiṭaka Series. Taishō Volume 51, Number 2087. Berkeley, CA: Bukkyo Dendo Kyokai America, Inc., 1996.

## Acknowledgements

The knowledge and work required to carry out this research have been generously supported by Professor Paul Dilley. This project would not have been possible without his guidance. I am deeply grateful to Professor Dilley for his invaluable advice and support!



# Organisms vs. Climate Change

Climate change affects environmental stressors





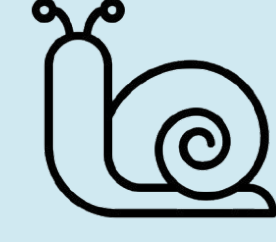


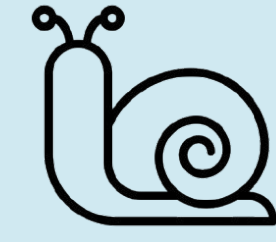
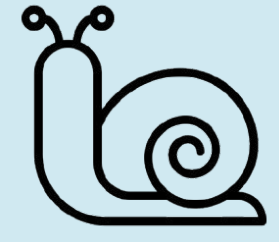
- **Temperature & nutrient availability** are main stressors for aquatic organisms
- **Temperature** affects growth rate by altering cell function
- **Phosphorus** needed to synthesize DNA/RNA

What happens to aquatic life under environmental stress imposed by climate change?

## Why *P. antipodarum*?

- *Potamopyrgus antipodarum*: New Zealand freshwater snail species
- Invasive worldwide; ecotoxicology model; observable life-history traits
- Investigate the interactive effects of temperature and phosphorus level on growth rate in a diverse group of *P. antipodarum*

## Experimental Design: Temperature x Phosphorus

 x192		
 16°C/60.8°F	 x48	 x48
 24°C/75.2°F	 x48	 x48

# Double Trouble: How Do Multiple Environmental Stressors Interact to Influence Key Life-History Traits?



Worldwide distribution of *P. antipodarum*

**Helena Wu<sup>1</sup>,**  
Winnie Gavin<sup>2</sup>, Sophia Hu<sup>3</sup>, Maurine Neiman<sup>2</sup>, Briante Najev<sup>2</sup>  
<sup>1</sup>Marriotts Ridge High School, Marriottsville, MD  
<sup>2</sup>Department of Biology, University of Iowa  
<sup>3</sup>Emma Willard School, Troy, NY



# Science in Action



Figure 1:  
Snails in 24C were housed in a growth chamber; Helena changing cups



Figure 2:  
Algae culture set-up; left and middle flasks: high phosphorus; right flask: low phosphorus

## Results

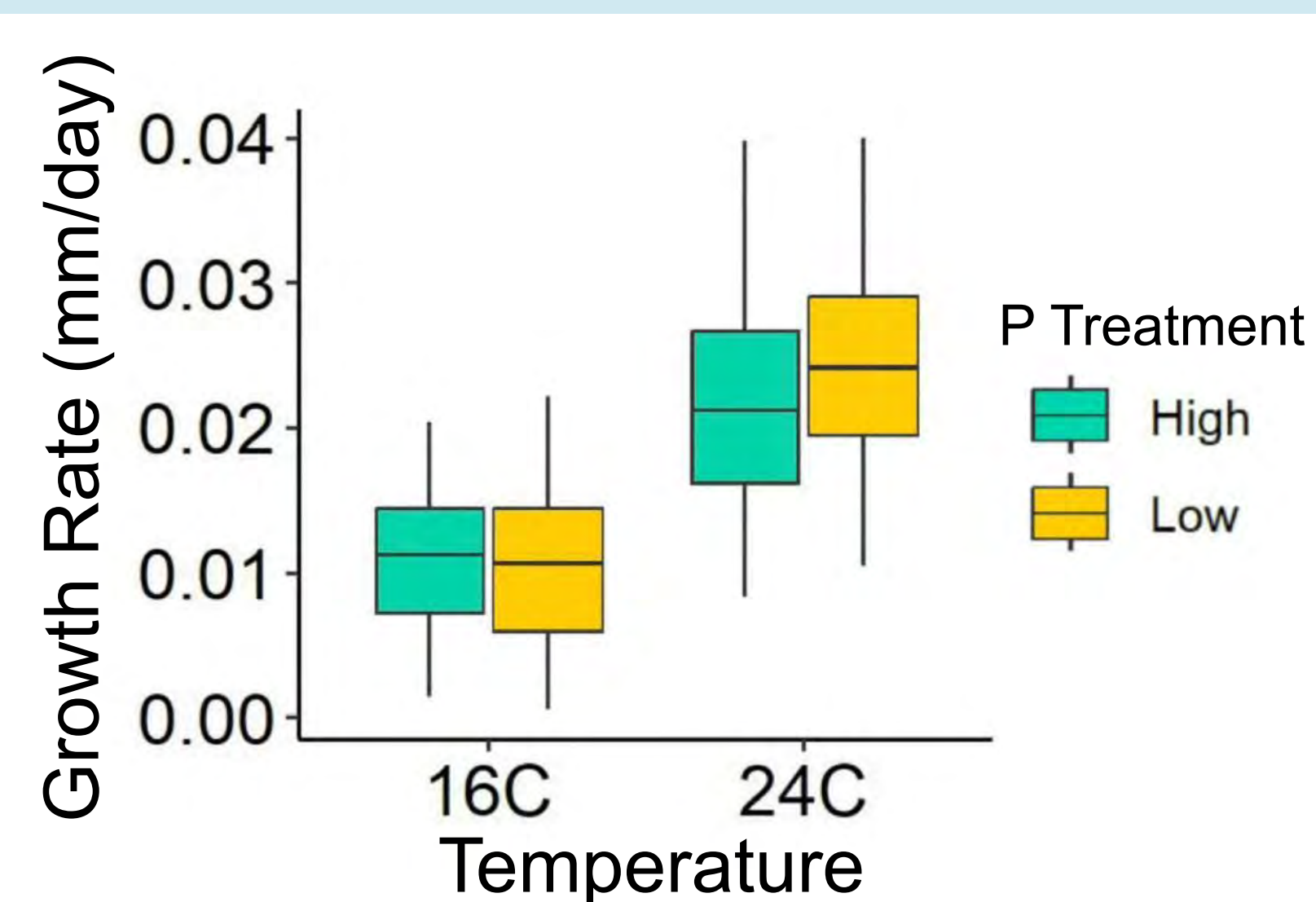


Figure 3:  
Growth rate across temperature and P conditions

Kruskal-Wallis analyses revealed that growth was significantly faster at high temperatures, but there was not a significant relationship with P treatment conditions

## Conclusions & Next Steps

- *P. antipodarum* raised at high temperature grew more rapidly; no major effect of P
- Limitations: only 4 weeks; 192 snails; asexual 3x lineages; freshwater lake habitats
- Future: How do these stressors affect growth of sexual vs. asexual lineages? Invasive vs. noninvasive lineages?

## References & Acknowledgments:

Böck, C. (n.d.) photo of *P. antipodarum* [Unpublished photograph]. University of Innsbruck.  
Ries, C. & M. Pfeiffenschneider (Eds.), 2025. *Potamopyrgus antipodarum* (Gray, 1843). In: neobiota.lu - Invasive Alien Species in Luxembourg. National Museum of Natural History, Luxembourg.  
Dybdahl, M. F., & Kane, S. L. (2005). Adaptation vs. phenotypic plasticity in the success of a clonal invader. *Ecology*, 86(6), 1592–1601. <https://doi.org/10.1890/04-0898>  
Krist, A. C., Kay, A. D., Larkin, K., & Neiman, M. (2014). Response to phosphorus limitation varies among lake populations of the freshwater snail *Potamopyrgus antipodarum*. *PLoS ONE*, 9(1). <https://doi.org/10.1371/journal.pone.0085845>  
Neiman, M., Kay, A. D., & Krist, A. C. (2012). Sensitivity to phosphorus limitation increases with ploidy level in a New Zealand snail. *Evolution*. <https://doi.org/10.1111/evo.12026>  
Persson, J., Wojewodzic, M. W., Hessen, D. O., & Andersen, T. (2010). Increased risk of phosphorus limitation at higher temperatures for *Daphnia magna*. *Oecologia*, 165(1), 123–129. <https://doi.org/10.1007/s00442-010-1756-4>  
Starke, C. W., Jones, C. L., Burr, W. S., & Frost, P. C. (2020). Interactive effects of water temperature and stoichiometric food quality on *daphnia pulex*. *Freshwater Biology*, 69(2), 256–265. <https://doi.org/10.1111/rwb.13633>

Special thanks to all Neiman lab members for their guidance on this study. Thank you SSTP, Belin-Blank Center, and the University of Iowa for this wonderful research opportunity.



# Investigating the Effects of Zatolmilast on the Behavior of Mice with Houge-Janssens Syndrome 1

Alice Xie<sup>1</sup>, Chian Ju Jong<sup>2</sup>, PhD, Anthony Papadatos<sup>2</sup>, Chunling Chen<sup>2</sup>, PhD, Stefan Strack<sup>2</sup>, PhD

<sup>1</sup>The Lawrenceville School, Lawrenceville, NJ, <sup>2</sup>Department of Neuroscience and Pharmacology, Carver College of Medicine, University of Iowa

## Introduction

- Protein Phosphatase 2A (PP2A/PPP2) is a heterotrimeric Ser/Thr phosphatase composed of scaffolding A, catalytic C and one of twelve regulatory B subunits (Figure 1).
- Houge-Janssens Syndrome 1 (HJS1) is a rare neurodevelopmental disorder caused by de novo mutations in the PPP2R5D gene (Figure 1) (Shang et al., 2016).
- Symptoms include macrocephaly, hypotonia, autism spectrum disorder (ASD) and developmental and cognitive delays (Levine et al., 2023).
- Both E198K and E420K mutations are the most severe form of mutation, while E200K mutation has a milder phenotype (Shang et al., 2016).
- Restricted interests is one of the common autistic features (Lung et al., 2024).
- The marble burying test is used as an indirect measure of restricted interests in several mouse models of ASD (Sonzogni et al., 2018, Qin et al., 2022).
- Zatolmilast is a selective phosphodiesterase-4D (PDE4D) inhibitor that prevents cyclic AMP (cAMP) degradation and enhances downstream PKA signaling (Figure 2). PKA plays a crucial role in learning and memory (Gurney et al., 2019).
- Zatolmilast is used to treat fragile X syndrome and other brain disorders (Shionogi, 2024). Currently, it is in a phase 3 clinical trial for fragile X syndrome and about to enter in a phase 1/2 clinical trial for HJS1.

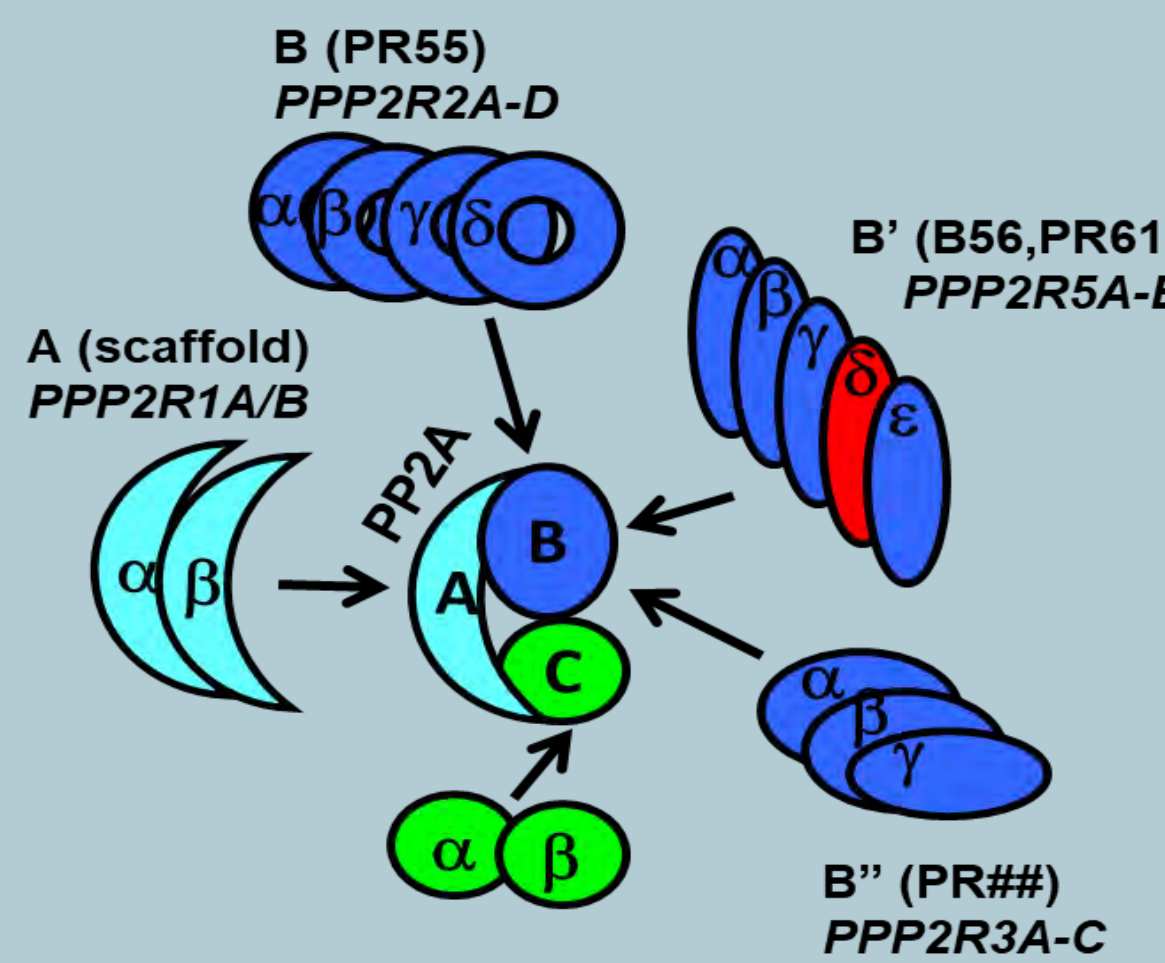


Figure 1. PP2A enzyme structure

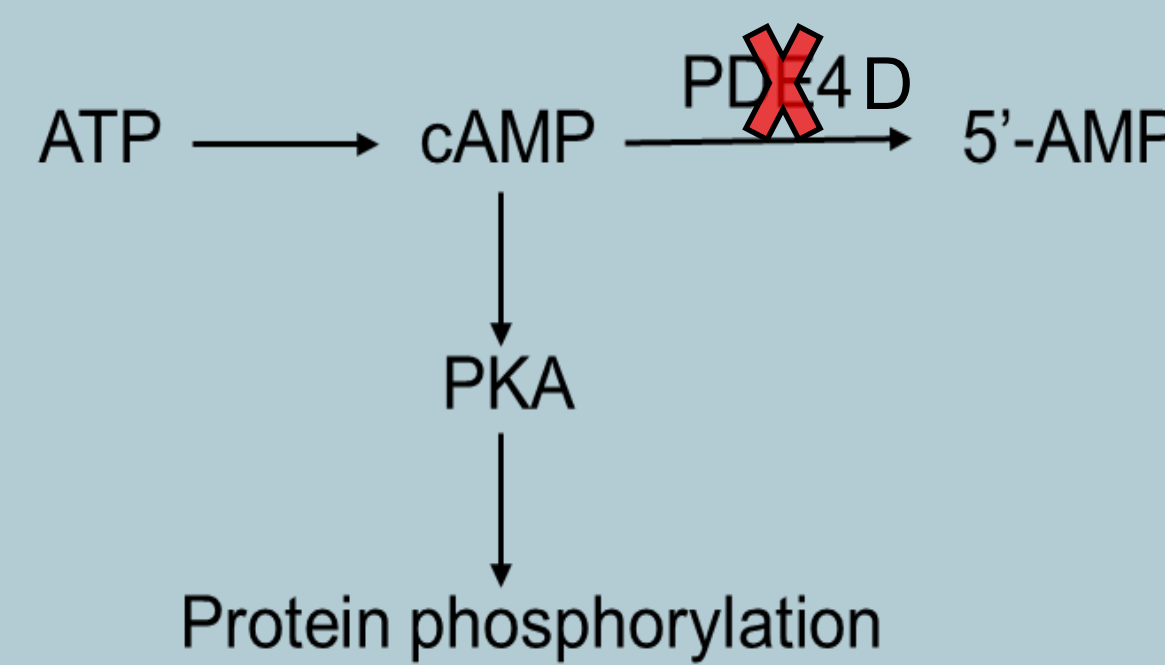


Figure 2. Zatolmilast inhibits PDE4D to boost PKA signaling

## Objective

Determine if mice with the E198K, E200K, and E420K mutations exhibit restricted interest and if zatolmilast can reverse behavior deficits in mouse models of the E198K mutation.

## Methodology

- Marble burying test:** WT, E198K, E200K and E420K mice (Figure 3) were habituated in corncob bedding for thirty minutes. Mice were then returned to home cage and twelve marbles were placed on the corncob bedding. Mice were placed back on the corncob bedding with marbles. After thirty minutes, mice were returned to home cage. Three independent experimenters, blinded to the genotype of the mice, scored the number of marbles that were at least two-thirds buried (Figure 4).
- Zatolmilast treatment:** E198K mice were subcutaneously injected with five mg/kg zatolmilast and habituated in corncob bedding for thirty minutes prior to the marble burying test. As a control, WT and E198K mice were subcutaneously injected with PBS.

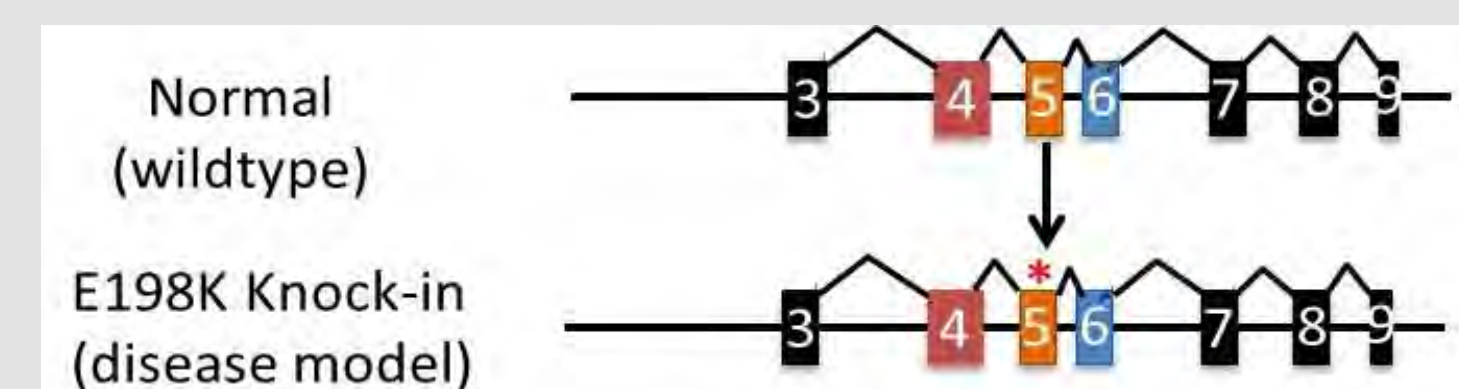
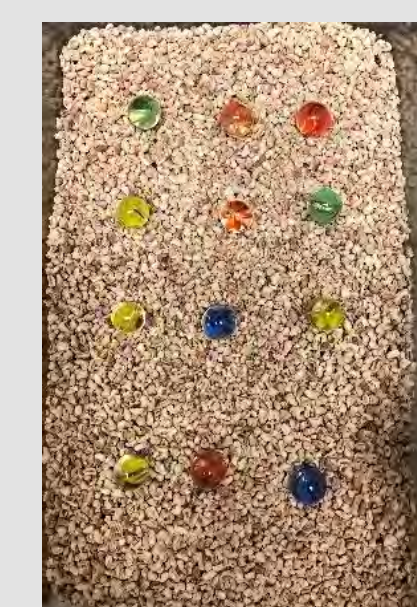


Figure 3. The constitutive E198K, E200K and E420K knock-in mouse model of HJS1 was generated at University of Iowa Genome Editing Core Facility using the CRISPR/Cas9-mediated gene editing to introduce the E198K mutation into the murine Ppp2r5d locus.

Figure 4. Twelve marbles were placed on the corncob bedding and the number of marbles that were at least 2/3 buried during the 30-minute test was scored.



## Results

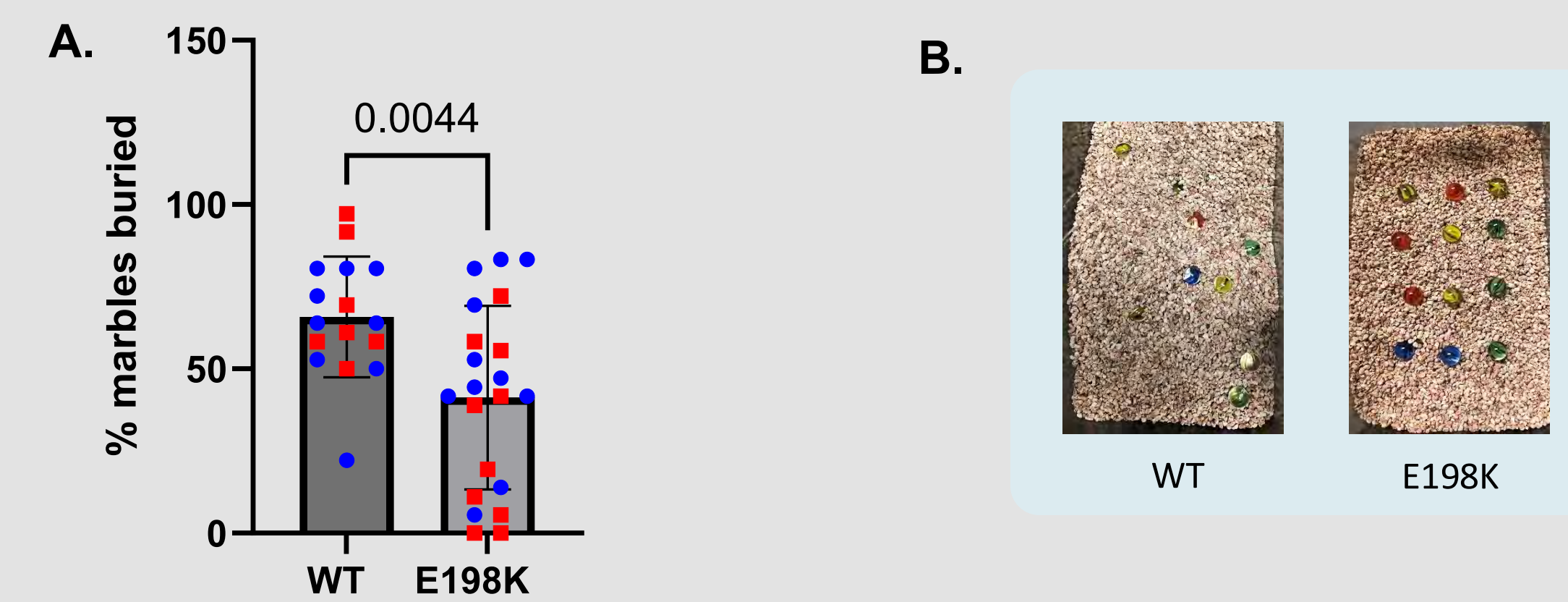


Figure 5. (A) E198K mice buried significantly less marbles than the WT mice. (B) Representative images of marbles buried by WT and E198K mice.

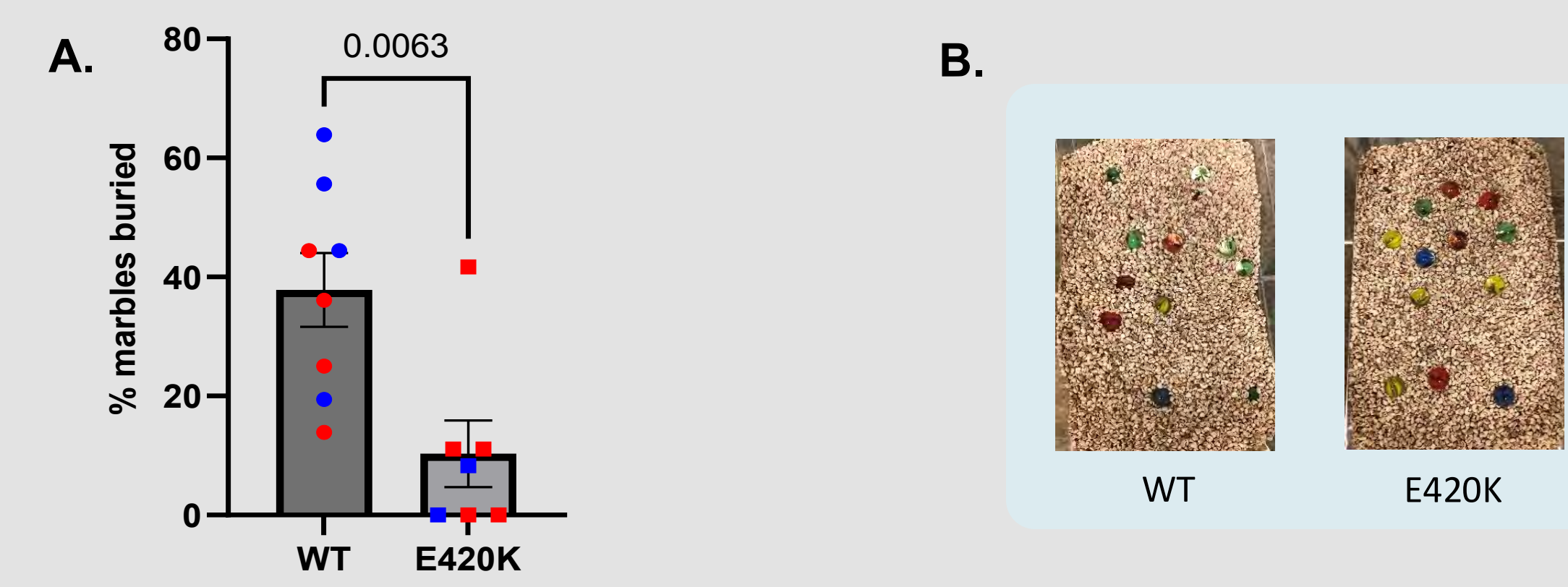


Figure 6. (A) E420K mice buried significantly less marbles than the WT mice. (B) Representative images of marbles buried by WT and E420K mice.

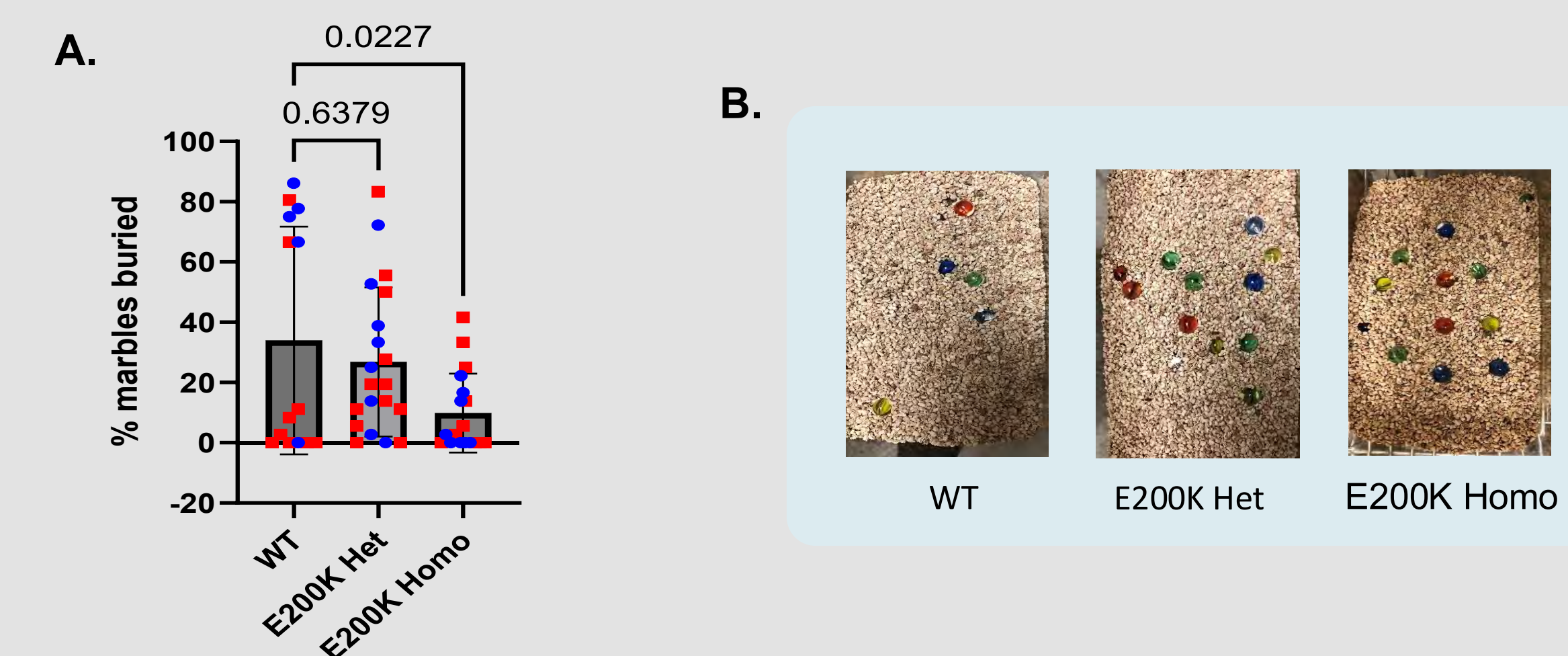


Figure 7. (A) While there is no significant difference in the percentage of marbles buried between E200K het mice and WT mice, the E200K homo mice buried significantly less marbles than the WT mice. (B) Representative images of marbles buried by WT, E200K het and E200K homo mice.

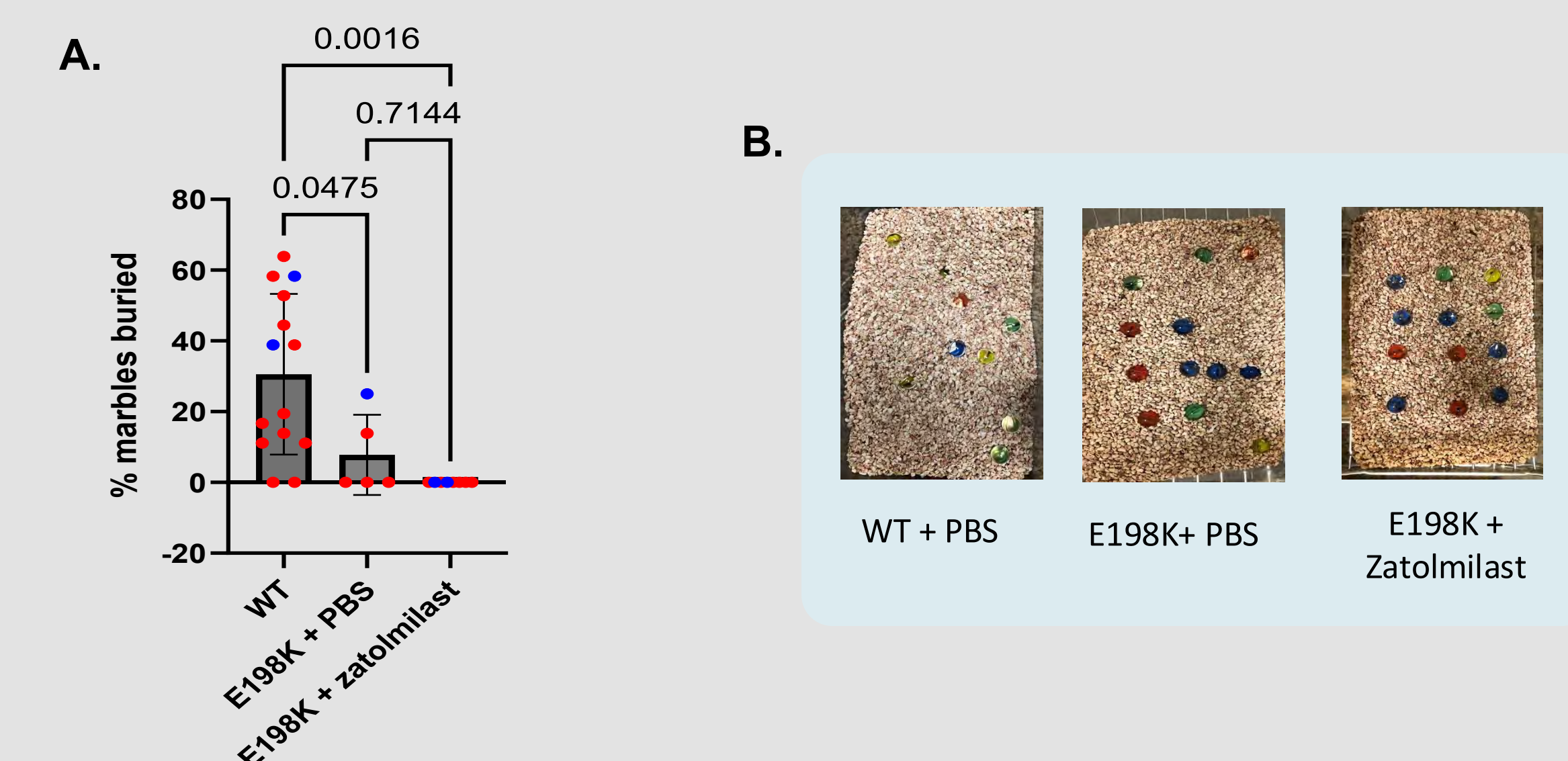


Figure 8. (A) Zatolmilast treatment did not restore the marble burying behavior in E198K mice. (B) Representative images of marbles buried by WT+PBS-, E198K+PBS- and E198K+zatolmilast-treated mice.

## Conclusion and Discussion

- Both the E198K and E420K mice showed a significantly lower proportion of marbles buried compared to the WT mice, suggesting restricted interests in these mice.
- The E200K homo but not the E200K het mice show a significant decrease in the percentage of marbles buried compared to the WT mice, suggesting the possibility of an autistic feature in the E200K homo but not the E200K het. However, more than 80% of the female WT mice (red symbols) buried few to no marbles, a confounding factor that lowers the average of the percent of marbles buried in these WT mice.
- The E198K mice treated with PBS also showed a significant decrease in the percentage of marbles buried compared to the WT mice. Similarly, the E198K mice treated with zatolmilast showed a significant decrease in the percentage of marbles buried compared to the WT+PBS mice, suggesting that the inhibition of PDE4D by zatolmilast to enhance PKA signaling did not restore the marble burying behavior in E198K.
- The E198K, E420K, and E200K mice all exhibit some sort of restricted interest in marble burying compared to the wild type mice. The zatolmilast treatment does not restore the marble burying behavior in E198K mice.

### Future Directions:

- We would like to assess the efficacy of zatolmilast on other behaviors in mouse models of HJS1 such as hyperactivity and cognition.
- We would also like to assess the efficacy of other drugs such as baclofen (GABA receptor agonist), rapamycin (mTOR inhibitor) or rolipram (PDE4 inhibitor) in treating restricted interests behavior in mouse models of HJS1.

## Acknowledgements

I would like to thank Dr. Jong, Dr. Strack, and the rest of the Strack lab for all their help this summer. I would also like to thank William Paradee of the Genome Editing Core.

## Fundings

PPP2R5D support by State of California/JGA (#A19-3376-S004)  
PPP2R5D support by State of California/JGA  
PPP2R5D support by Simons Foundation Autism Research Initiative (#877875)

## References

- Angoa-Pérez, M., Kane, M. J., Briggs, D. I., Francescutti, D. M., & Kuhn, D. M. (2013). Marble burying and nestlet shredding as tests of repetitive, compulsive-like behaviors in mice. *Journal of Visualized Experiments*, (82), 50978. <https://doi.org/10.3791/50978>
- Gurney, M. E., Nugent, R. A., Mo, X., Sindac, J. A., Hagen, T. J., Fox, D., O'Donnell, J. M., Zhang, C., Xu, Y., Zhang, H.-T., Groppi, V. E., Baile, M., White, R. E., Romero, D. L., Vellekoop, A. S., Walker, J. R., Surman, M. D., Zhu, L., & Campbell, R. F. (2019). Design and synthesis of selective phosphodiesterase 4D (PDE4D) allosteric inhibitors for the treatment of fragile X syndrome and other brain disorders. *Journal of Medicinal Chemistry*, 62(10), 4884-4901. <https://doi.org/10.1021/acs.jmedchem.9b00193>
- S., Walker, J. R., Surman, M. D., Zhu, L., & Campbell, R. F. (2019). Design and synthesis of selective phosphodiesterase 4D (PDE4D) allosteric inhibitors for the treatment of fragile X syndrome and other brain disorders. *Journal of Medicinal Chemistry*, 62(10), 4884-4901. <https://doi.org/10.1021/acs.jmedchem.9b00193>
- Hamilton, J. (2024, September 23). Fragile X held him back. An experimental drug is helping him break free. *NPR*. <https://www.npr.org/sections/shots-health-news/2024/09/22/nx-s1-5076913/fragile-x-experimental-drug-helping-autism-adhd-intellectual-disability>
- Levine, A. D., & Chung, W. K. (2023). Clinical features of PPP2 syndrome type R5D (Jordan's syndrome) to support standardization of care. *Cold Spring Harbor Molecular Case Studies*, 9(3), a006285. <https://doi.org/10.1101/mcs.a006285>
- Lung, S. L. M., Picard, E., Soulieres, I., & Bertone, A. (2024). Identifying the functions of restricted and repetitive behaviors and interests in autism: A scoping review. *Research in Autism Spectrum Disorders*, 117, 102458. <https://doi.org/10.1016/j.rasd.2024.102458>
- Qin, Y., Du, Y., Chen, L., Liu, Y., Xu, W., Liu, Y., Li, Y., Leng, J., Wang, Y., Zhang, X. Y., Feng, J., Zhang, F., Jin, L., Qiu, Z., Gong, X., & Wang, H. (2022). A recurrent SHANK1 mutation implicated in autism spectrum disorder causes autistic-like core behaviors in mice via downregulation of mGluR1-IP3R1-calcium signaling. *Molecular Psychiatry*, 27(7), 2985-2998. <https://doi.org/10.1038/s41380-022-01539-1>
- Shang, L., Henderson, L. B., Cho, M. T., Petrey, D. S., Fong, C. T., Haude, K. M., Shur, N., Lundberg, J., Hauser, N., Carmichael, J., Innis, J., Schuette, J., Wu, Y. W., Asaika, S., Pearson, M., Folk, L., Retterer, K., Monaghan, K. G., & Chung, W. K. (2016). De novo missense variants in PPP2R5D are associated with intellectual disability, macrocephaly, hypotonia, and autism. *Neurogenetics*, 17(1), 43-49. <https://doi.org/10.1007/s10048-015-0466-9>
- Shionogi Provides Updates on Zatolmilast, an Investigational Drug for Fragile X Syndrome, Including Recent Changes to Study Protocol to Increase Access for Participants and Families. (2024, July 18). *Shionogi*. <https://www.shionogi.com/us/en/news/2024/07/shionogi-provides-updates-on-zatolmilast-an-investigational-drug-for-fragile-x-syndrome-including-recent-changes-to-study-protocol-to-increase-access-for-participants-and-families.html>
- Sonzogni, M., Wallaard, I., Santos, S. S., Kingma, J., du Mee, D., van Woerden, G. M., & Elgersma, Y. (2018). A behavioral test battery for mouse models of Angelman syndrome: a powerful tool for testing drugs and novel Ube3a mutants. *Molecular Autism*, 9, 47. <https://doi.org/10.1186/s13229-018-0231-7>



## Introduction

- In addition to increasing the likelihood of a behavior, some have posited that consistent reinforcement also reduces its variability.
- Although behavioral variability decreases in tasks involving one response, attempts to generalize that result to more complex response sequences have been less conclusive [1-2].
- Sequential-response tasks have 1) reinforced only a subset of possible sequences, and 2) allowed for repeated responses to the same stimulus, potentially engendering less variable behavior.

**We explored whether the variability in behavioral sequences performed by pigeons would decrease in an environment that doesn't demand it.**

## Method

Eight pigeons underwent daily 120-trial sessions. On each trial, pigeons pecked a start stimulus and then pecked four visually distinct stimuli, with each peck removing the corresponding stimulus from the screen. Reinforcement was given after all four stimuli were pecked. Half of the subjects received a fixed reinforcement of 2 pellets; the other half received reinforcement that varied from 1 to 3 pellets.

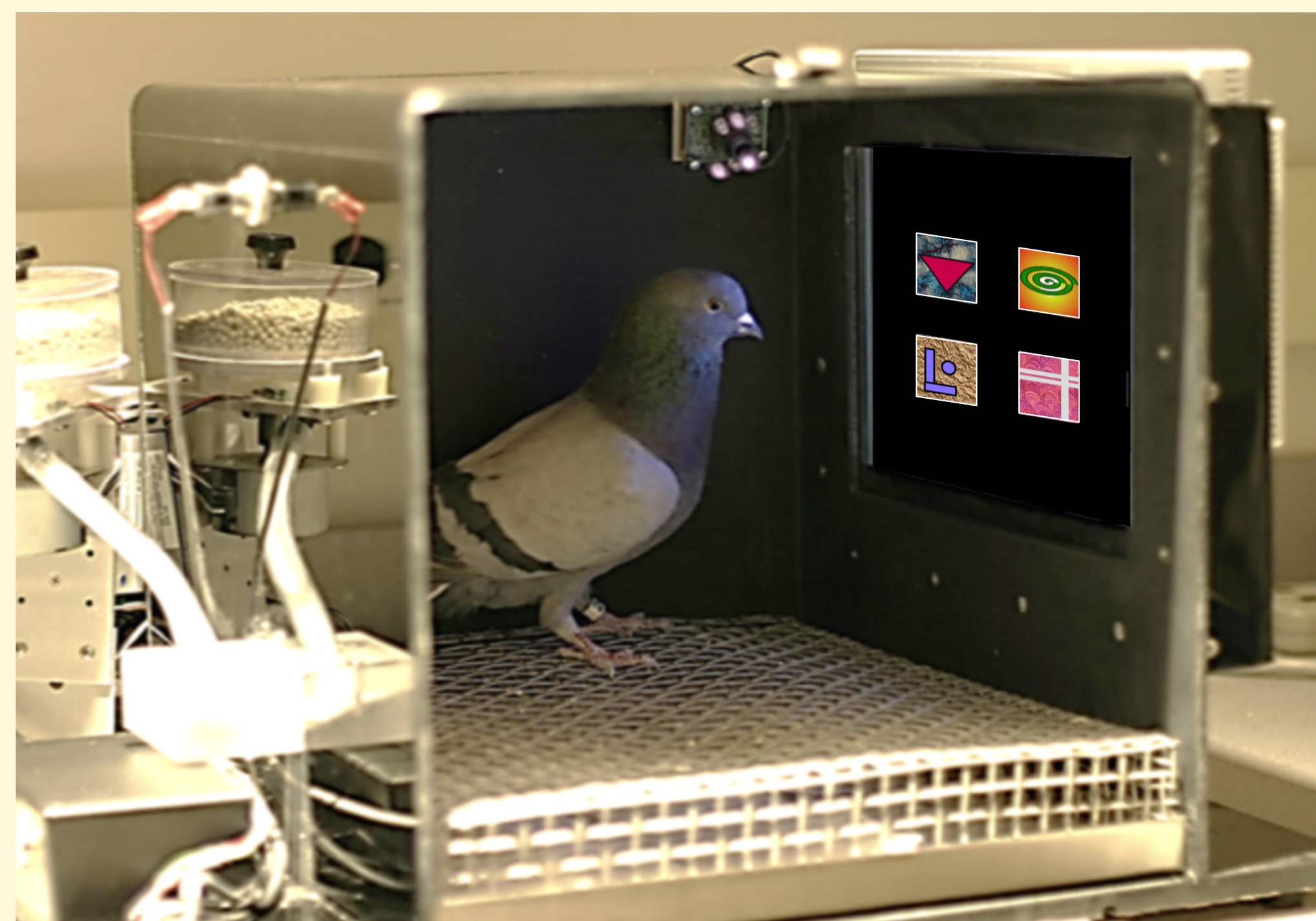


**Figure 1.** Experimental apparatus with the 4 stimuli shown

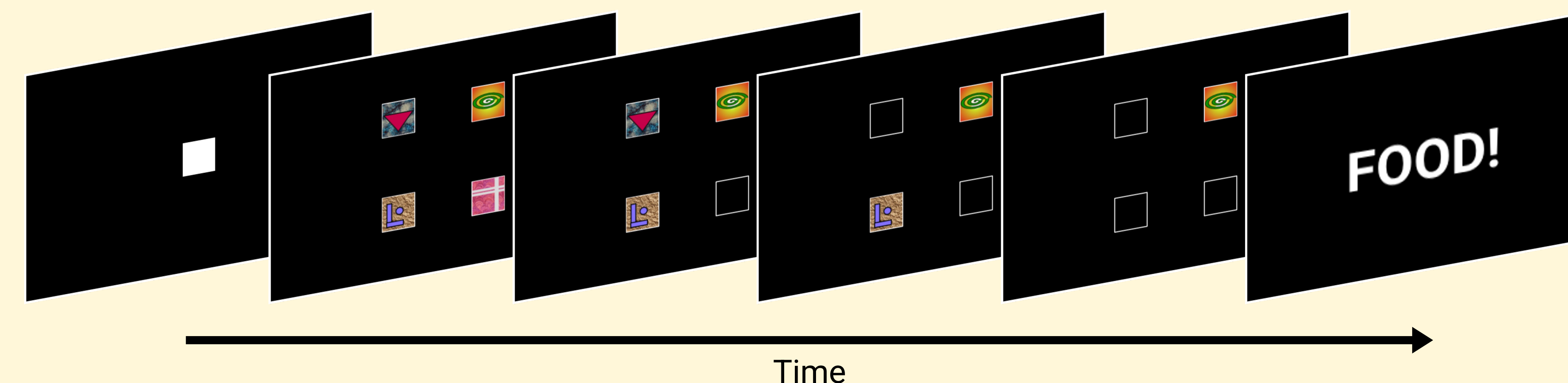


**Figure 2.** Trial sequence; reinforcement is given after all 4 buttons have been pecked

## Results

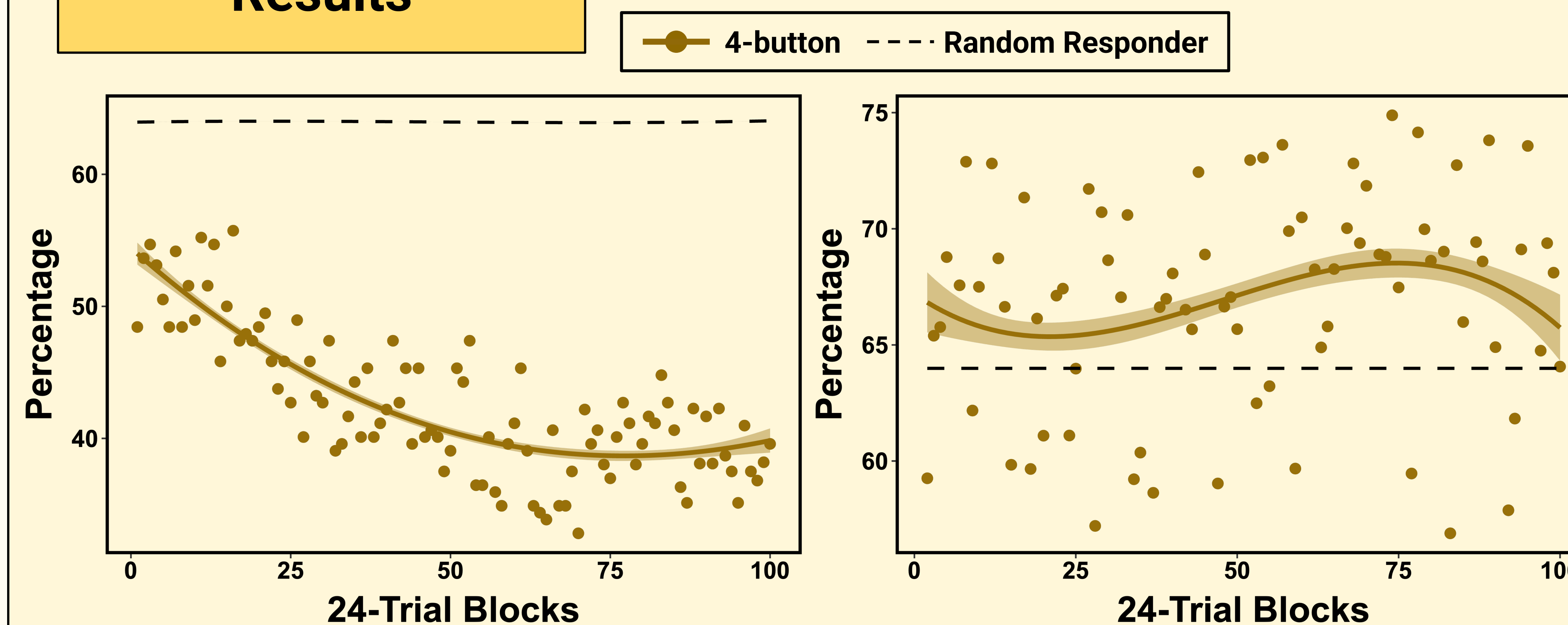


**Figure 3.** Mean percentage of sequences performed (out of the 24 possible) in each 24-trial block. **Figure 4.** Mean percentage of sequences repeated from the prior block, excluding the first block of each session.

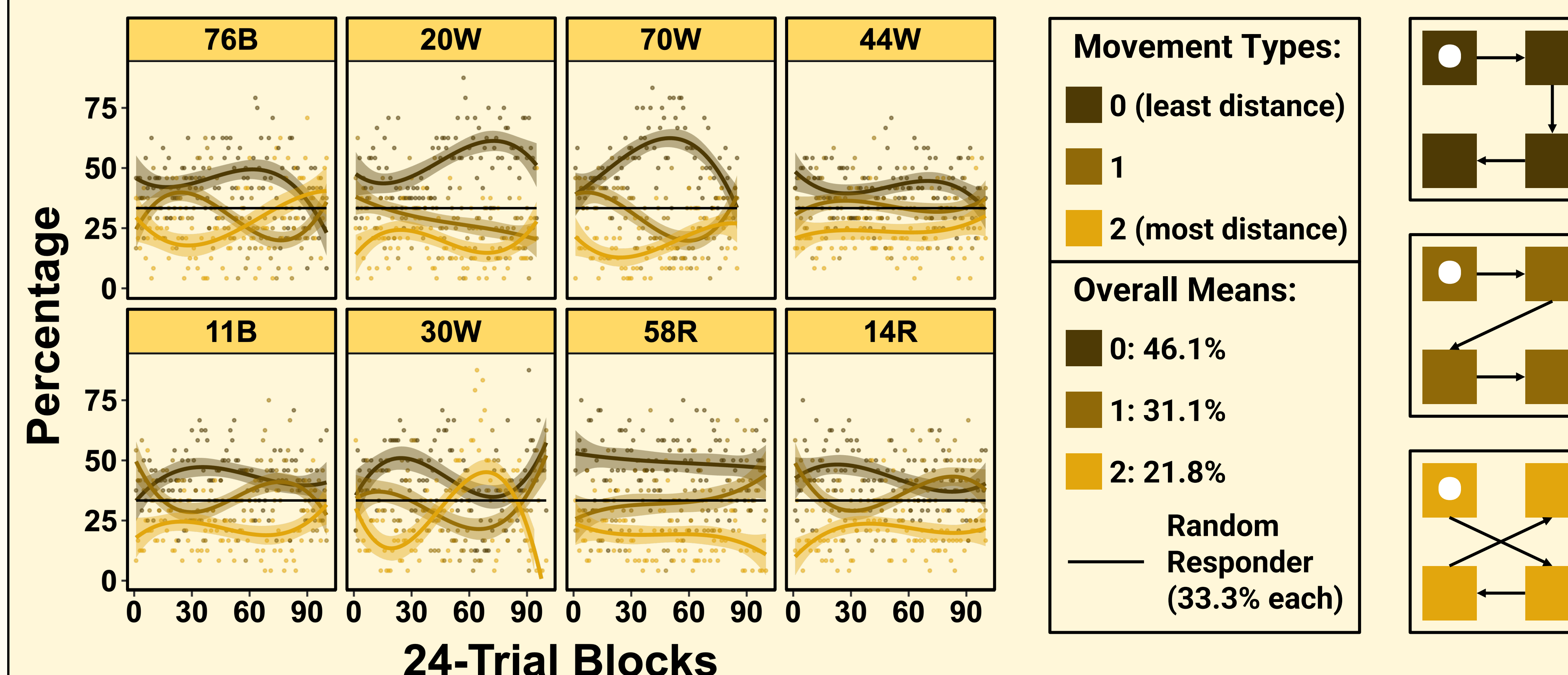


**Figure 5.** Percentage of sequences from the three movement types. 1<sup>st</sup> row: fixed reinforcement; 2<sup>nd</sup> row: variable

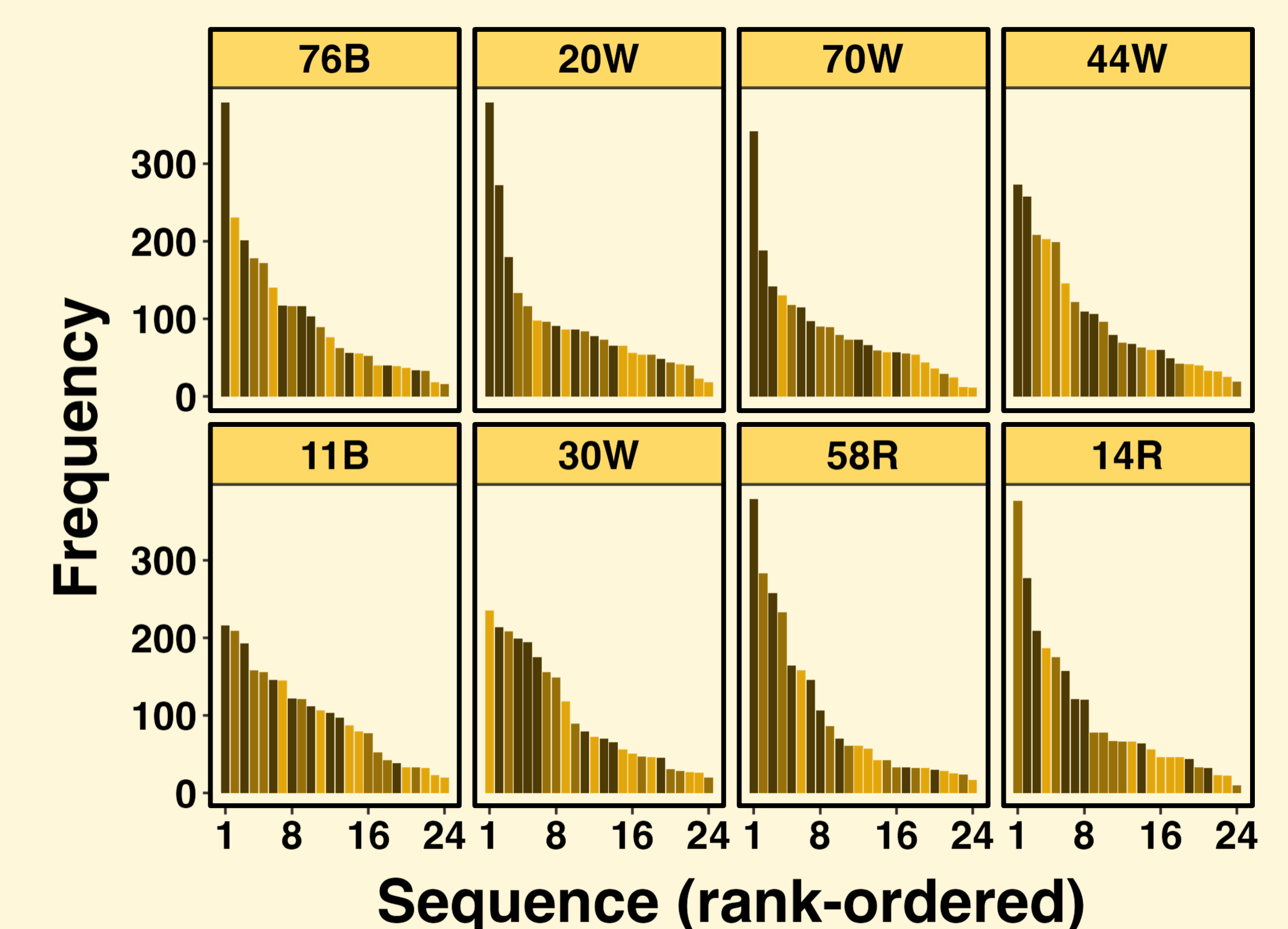


**Figure 6.** The frequency of each sequence performed by each pigeon, rank-ordered and split by movement type.

## Conclusions

- The variability of pigeons' behavior decreased.
- The pigeons were biased towards sequences involving smaller distances.
- Despite these trends, the pigeons continue to dynamically vary their behavior.

## Future Directions

Assess the extent to which results differ from...

- a previous study that used 5 buttons,
- humans, including clinical populations (e.g., autistic children or people with depression).

## Acknowledgements

I would like to thank Professor Wasserman and Odysseus Orr for mentoring me. I would also like to acknowledge the Belin-Blank Center for providing me with this opportunity to learn and conduct research in a professional setting.

## References

1. Eckerman, D. A., & Lanson, R. N. (1969). Variability of response location for pigeons responding under continuous reinforcement, intermittent reinforcement, and extinction. *Journal of the Experimental Analysis of Behavior*, 12(1), 73-80. <https://doi.org/10.1901/jeab.1969.12-73>
2. Vogel, R., & Annau, Z. (1973). An operant discrimination task allowing variability of reinforced response patterning. *Journal of the Experimental Analysis of Behavior*, 20(1), 1-6. <https://doi.org/10.1901/jeab.1973.20-1>



# Microscopic Characterization of Outdoor Environmental Films

Eric Zang<sup>1</sup>, Arman Chowdhury<sup>2</sup>, Ruwini Weerasinghe<sup>2</sup>, Alexei Tivanski, Ph.D.<sup>2</sup>

<sup>1</sup>William P. Clements High School, <sup>2</sup>Department of Chemistry, University of Iowa

## Introduction

**Outdoor environmental films** are thin layers of chemical and biological species that accumulate on surfaces exposed to the environment over time, such as solar panels, buildings, and other infrastructure. Despite their prevalence, the mechanisms behind their growth and the influence of environmental factors such as relative humidity and sources of deposited particles remain poorly understood. This study investigates how different environmental conditions in Hawaii, Iowa, and Texas affect the film formation and morphology after one month of exposure. We utilize **atomic force microscopy (AFM)** and **optical microscopy (OM)** for complementary nanoscale and microscale observations, respectively. We show that all three films display film morphology consisting of particles of varying sizes, and that the particle number density, sizes, and surface coverage differ by outdoor exposure conditions.

**Atomic force microscopy (AFM)** offers high-resolution, three-dimensional topographical imaging at the nanoscale. It operates by measuring interatomic forces between a sharp probe ( $<10$  nm) and the sample surface at distances of 0.2–10 nm. We use AFM to analyze particles ranging from 1 nm up to  $\sim 10$   $\mu$ m.

**Optical microscopy (OM)** provides rapid visualization of sample morphology under visible light. OM is effective at the microscale and is used here to analyze particles larger than  $\sim 10$   $\mu$ m.

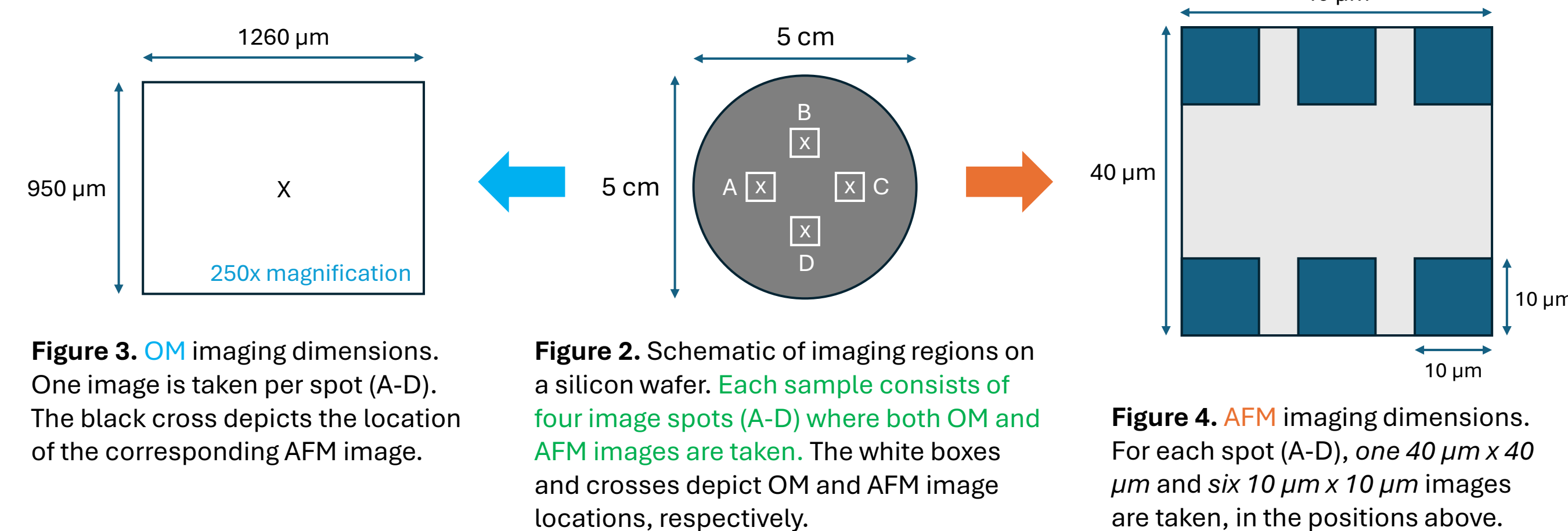
## Materials and Methods

The surfaces that we used for our experiments were silicon wafers. Silicon wafers are smooth even at the nanoscale (Figure 1) and work well with both AFM and OM.

Silicon wafers were placed in the following three locations:

- Honolulu, **Hawaii**: tropical, humid and hot, sea spray
- Coralville, **Iowa**: temperate, humid and warm, agriculture
- Lubbock, **Texas**: arid, dry and windy, dusty

Deposited film samples were collected after 1 month of exposure, imaged with AFM and OM, and analyzed with **Igor Pro** and **ImageJ**, respectively. Figures 2–4 show the imaging process below.



Using both Igor Pro and ImageJ software, the following variables were collected:

- Particle Length (L,  $\mu$ m)**: the largest distance between two points on a particle's perimeter
- Particle Number Density (PND, #Particles/ $\mu$ m<sup>2</sup>)**: the ratio of the number of identified particles (N) to the total studied surface area (SA) 
$$PND = \frac{N}{SA}$$
- Surface Coverage (SC, %)**: the ratio of the sum of all (n) identified particle surface areas (SA<sub>i</sub>) to the total studied surface area (SA) 
$$SC = \frac{\sum_{i=1}^n SA_i}{SA} \cdot 100$$

**AFM**: For each spot (A–D) within samples, **supermicron** particles ( $L > 1$   $\mu$ m) were analyzed from 40  $\mu$ m  $\times$  40  $\mu$ m AFM images, and **submicron** particles ( $L < 1$   $\mu$ m) were analyzed from 10  $\mu$ m  $\times$  10  $\mu$ m AFM images. For each spot, distributions of particle lengths were determined and fit to a Gaussian function, yielding the mean ( $\mu$ ) and standard deviation ( $\sigma$ ).

**OM**: For each spot (A–D) within samples, particles were analyzed from 1260  $\mu$ m  $\times$  950  $\mu$ m images.

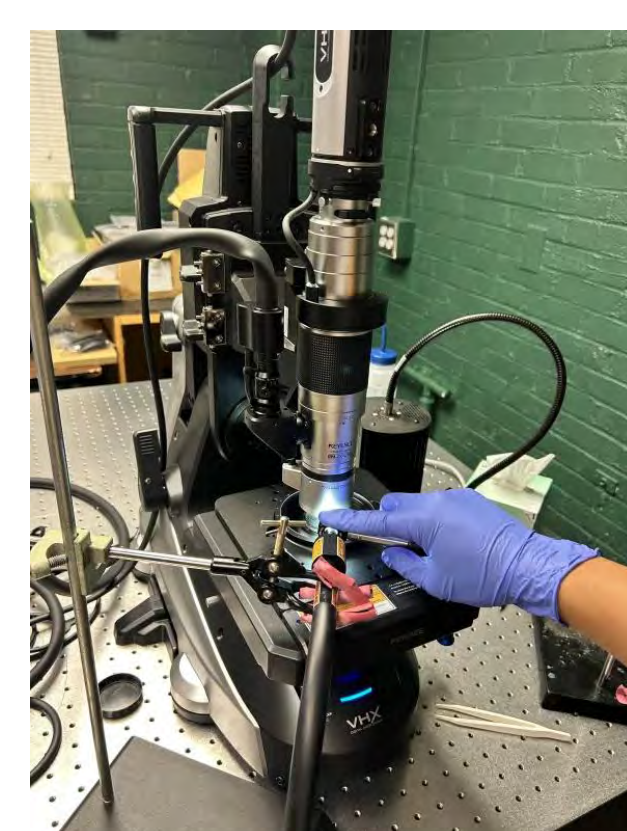


**Figure 5.** OM apparatus. A polarizer was used to darken images for ImageJ analysis.

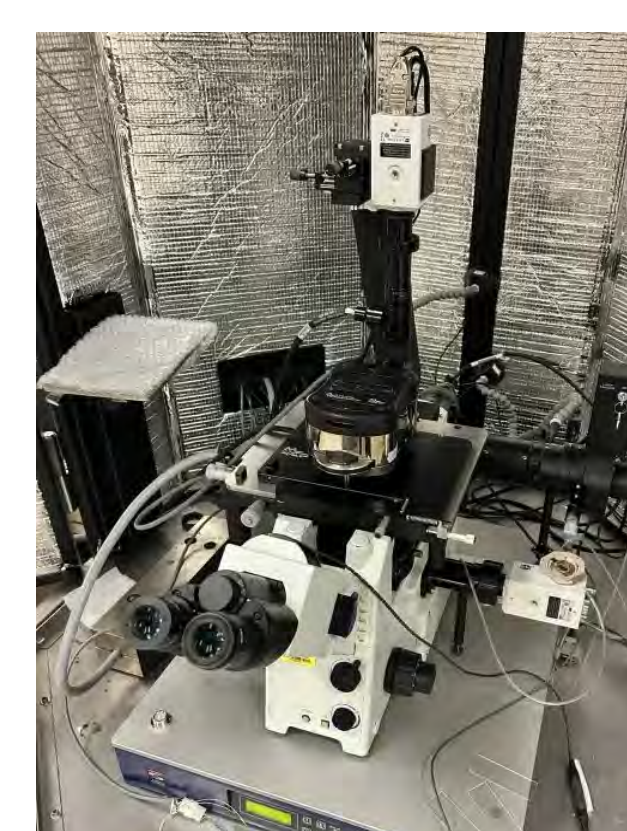


**Figure 6.** AFM apparatus. Tapping mode was used for imaging; the minimum studied particle height was 1 nm.

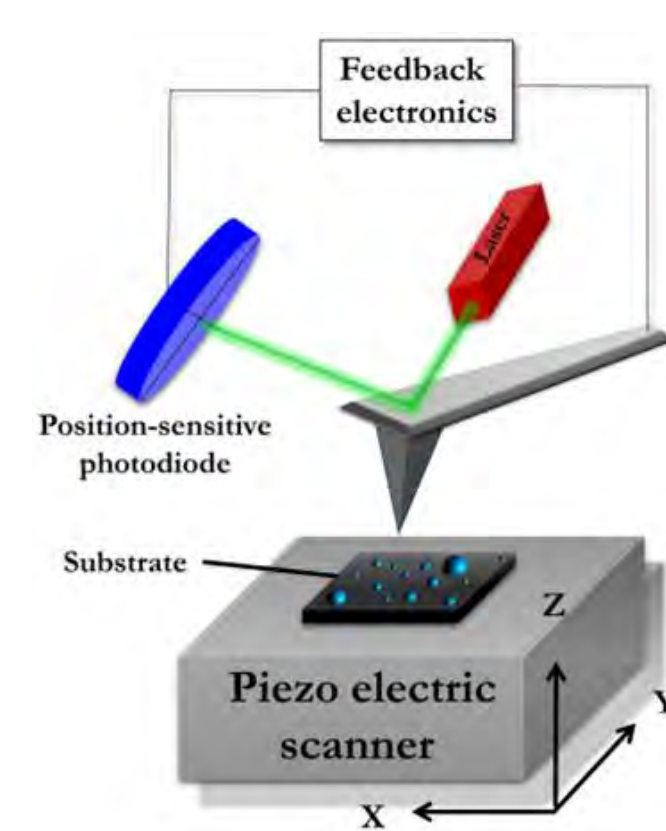
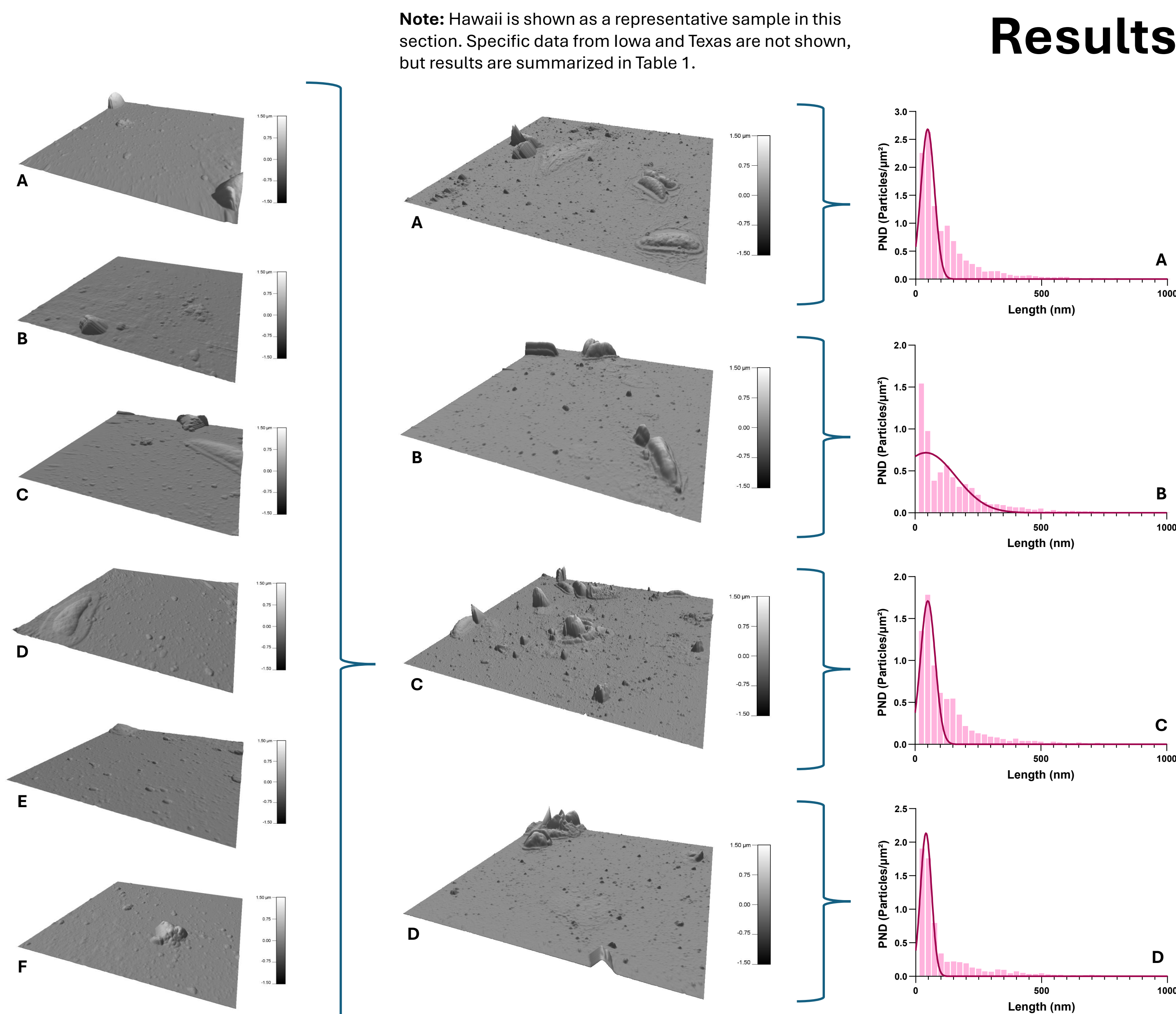


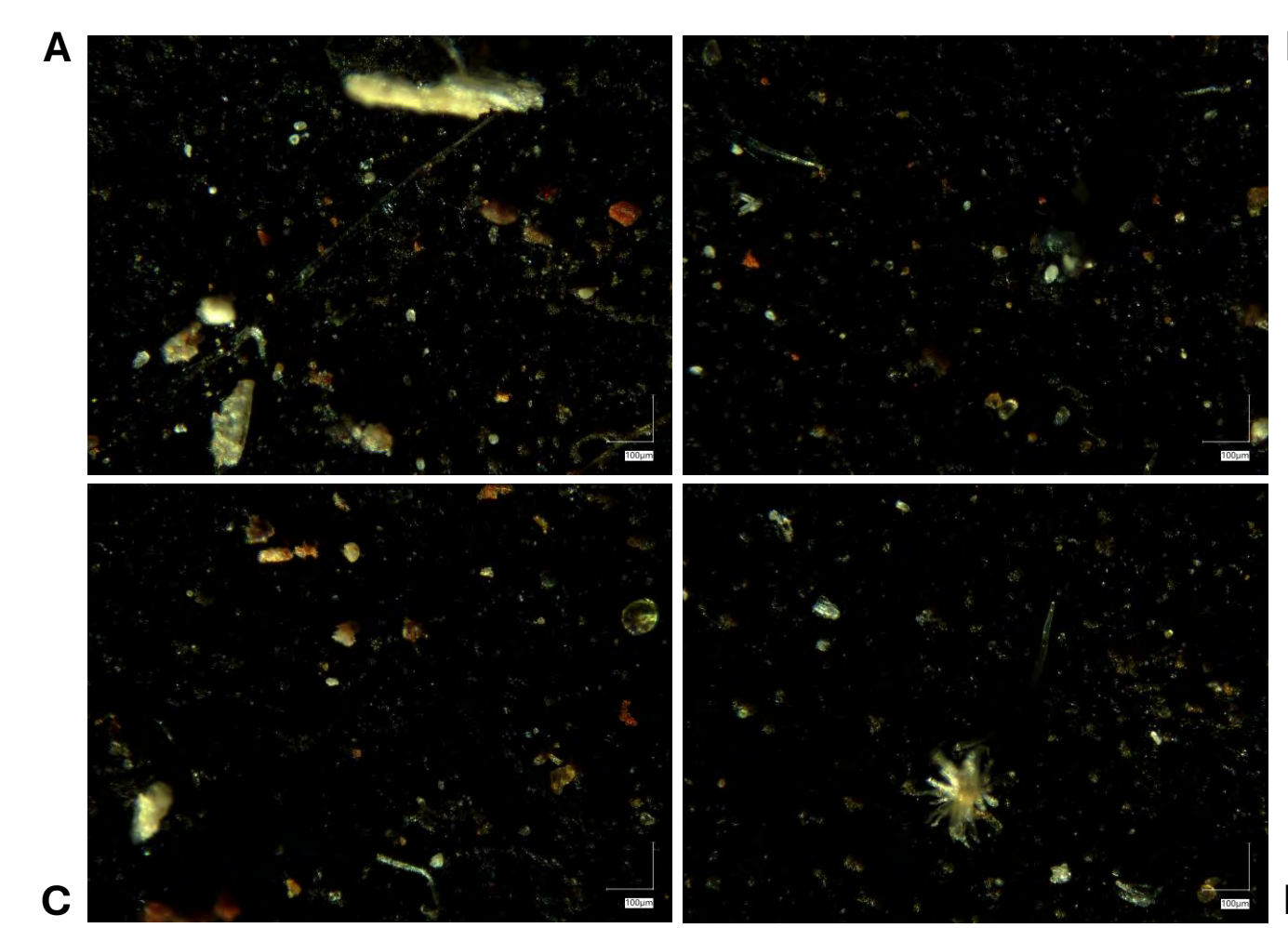
**Figure 7.** Schematic of AFM imaging. A sharp cantilever tip is used for measurements.



**Figures 8A–F.** Six 10  $\mu$ m  $\times$  10  $\mu$ m AFM height images from Hawaii Spot C contained within Figure 9C. These images were used to analyze AFM submicron particles.

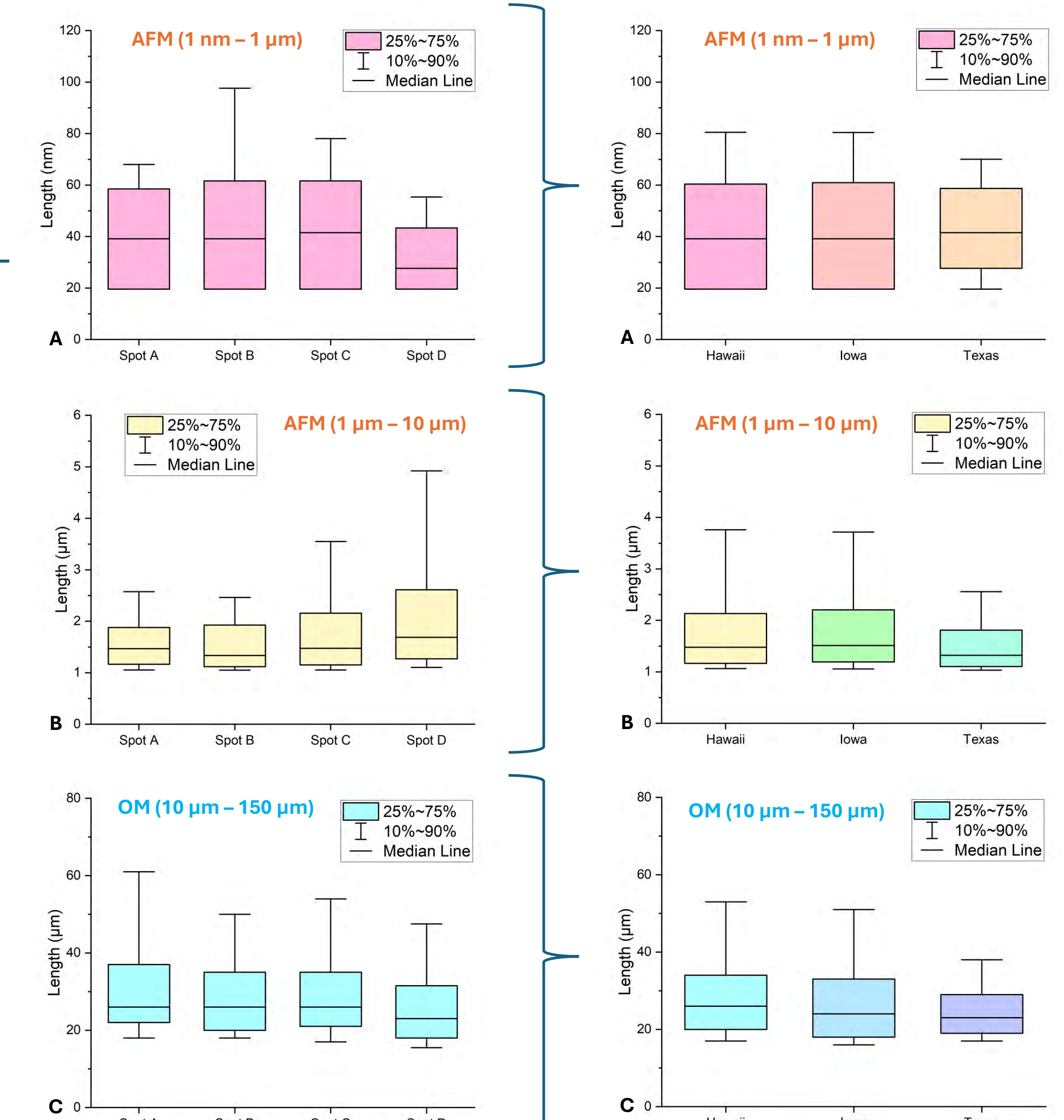
**Figures 9A–D.** Four 40  $\mu$ m  $\times$  40  $\mu$ m AFM height images from Hawaii spots A–D that were used to analyze AFM supermicron particles.

**Figures 10A–D.** Four histograms (with bin sizes of 25 nm) and Gaussian fits of AFM submicron particle lengths from their corresponding Hawaii spots A–D.



**Figures 13A–D.** Four 1260  $\mu$ m  $\times$  950  $\mu$ m OM images from the four spots A–D of the Hawaii sample. The scale is 100  $\mu$ m.

## Results



**Figures 11A–C.** Three box plots of particle length distributions for each spot of the Hawaii sample. In Figure 11A, only particles with lengths within  $\mu \pm \sigma$  of their corresponding Gaussian fit were included.

**Figures 12A–C.** Three box plots of particle length distributions combining all spots (A–D) for each location.

Sample Location	AFM Total Percent (%) SC [Sub- $\mu$ m, Super- $\mu$ m]	OM Total Percent (%) SC	Combined Total Percent (%) SC (AFM + OM)	AFM Sub- $\mu$ m PND (#Particles/ $\mu$ m <sup>2</sup> )	AFM Super- $\mu$ m PND (#Particles/ $\mu$ m <sup>2</sup> )	OM PND (#Particles/ $\mu$ m <sup>2</sup> )	AFM Total Median Length [Total SD] (nm)	AFM Most Probable Sub- $\mu$ m Length $\pm$ SD (nm)	OM Total Median Length [Total SD] ( $\mu$ m)
Hawaii	40 [32, 8]	3	43	1.9	3.7E-02	6.8E-05	80 [410]	50 $\pm$ 30	26 [23]
Iowa	33 [21, 12]	4	37	0.8	4.6E-02	9.1E-05	80 [530]	50 $\pm$ 20	24 [20]
Texas	16 [11, 5]	2	18	1.3	4.2E-02	6.7E-05	70 [280]	50 $\pm$ 10	23 [18]

**Table 1.** Combined table for several selected variables identified for three sample locations from AFM and OM data.

## Conclusions

### 1. Surface Coverage and Particle Number Density

- Hawaii had the highest surface coverage, followed by Iowa, and then Texas.
- Likely due to Hawaii's elevated humidity and sea/forest particles sources in contrast to Texas's low humidity and dust particles sources.
- Submicron particles provided the dominant contribution to both surface coverage and particle number density.

### 2. Particle Dimensions and Variability

- Texas had the smallest median particle length, likely due to its dusty and windy environment.
- The most probable submicron particle length was similar across all locations.
- Iowa had the greatest heterogeneity in particle length, followed by Hawaii, with Texas having the lowest.

## Future Directions

Besides silicon wafers, we also analyzed two other host surfaces (aluminum and polymer-coated aluminum) and samples with longer exposure times. In addition to continuing our analyses of current and incoming samples, multiple experimental extensions could be investigated:

- Improve ImageJ and Igor Pro software to identify particles more accurately
- Record trends of multilayer deposition film thicknesses over time
- Determine the elemental and chemical composition of deposited particles

## References

- Nanoscience Instruments. *Atomic Force Microscopy*. <https://www.nanoscience.com/techniques/atomic-force-microscopy/>
- Grant, J.S.; Zhu, Z.; Anderton, C.R.; Shaw, S.K. Physical and Chemical Morphology of Passively Sampled Environmental Films. *ACS Earth and Space Chemistry* **2019**, *3* (2), 305–313.
- Or, V. W.; Alves, M. R.; Wade, M.; Schwab, S.; Corsi, R. L.; Grassian, V. H. Crystal Clear? Microspectroscopic Imaging and Physicochemical Characterization of Indoor Depositions on Window Glass. *Environmental Science & Technology Letters* **2018**, *5* (8), 514–519.

## Acknowledgements

I would like to thank Professor Alexei Tivanski along with graduate students Arman Chowdhury and Ruwini Weerasinghe for their help and support regarding this project. Thank you also to all those who made SSTP an amazing experience this year!



# Causal Analysis of Chain-of-Thought Reasoning in LLM-Based Anxiety Detection

Sophie Zhang<sup>1</sup>; Weiguo Fan, PhD<sup>2</sup>; Yikang Wang<sup>2</sup>; Jiyuan Yu<sup>2</sup>

<sup>1</sup>Secondary Student Training Program; <sup>2</sup>Department of Business Analytics, University of Iowa

## Introduction

### Background:

- Large learning models (LLMs) are strong in detecting mental health conditions using online text (Patil & Gedhu, 2025)
- Chain-of-thought (CoT) prompting has improved performance and interpretability in various tasks, particularly for larger models (Wei et al., 2022)
- However, CoT outputs are unstable and sensitive to small changes in prompts (Chatziveroglou et al., 2025)
- This instability challenges the safe use of LLMs in mental health, where interpretability is critical

### Research Question:

Which steps in Deepseek-V3's CoT reasoning process can be causally linked to changes in its anxiety classification outcomes?

### Terminology:

**CoT prompting:** a technique where models generate intermediate reasoning steps before making a prediction

**Interpretability:** The degree to which a human can understand the reasoning behind a model's prediction (McGrath & Jonker, 2024)

## Methodology

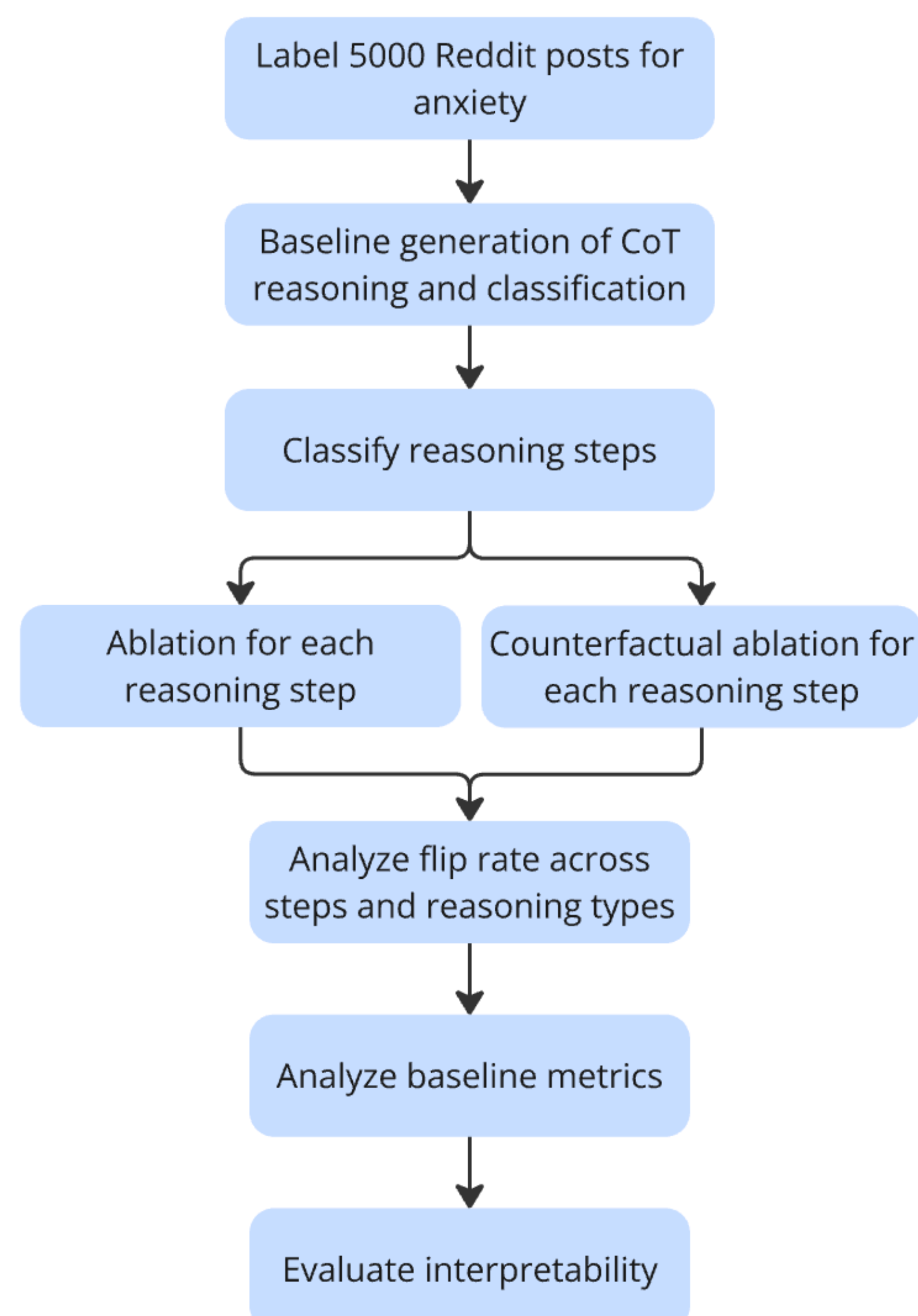


Figure 1: Visualization of Methodology

## Results

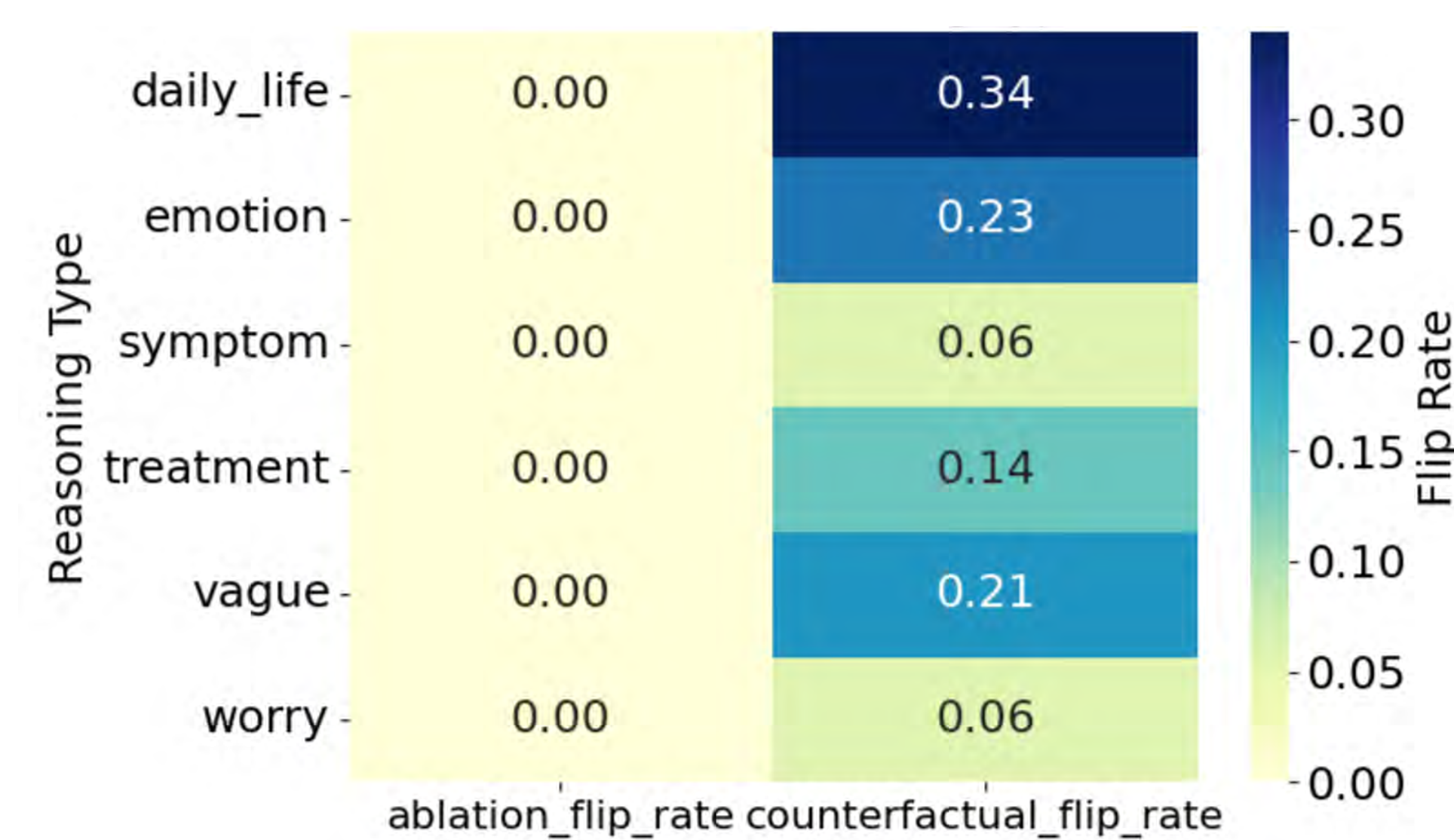


Figure 2: Flip Rate by Reasoning Type

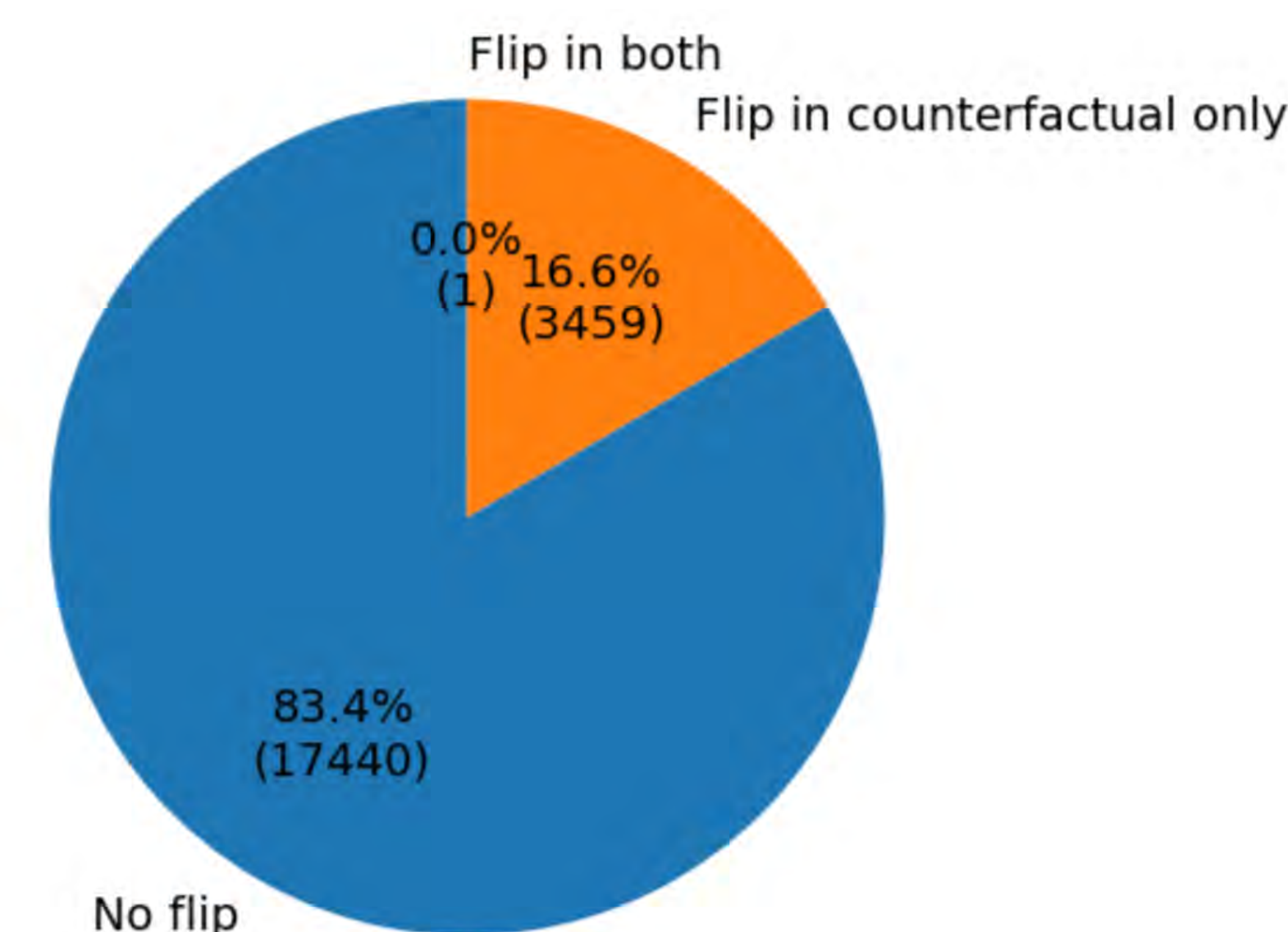


Figure 4: Causal Flip Overlap

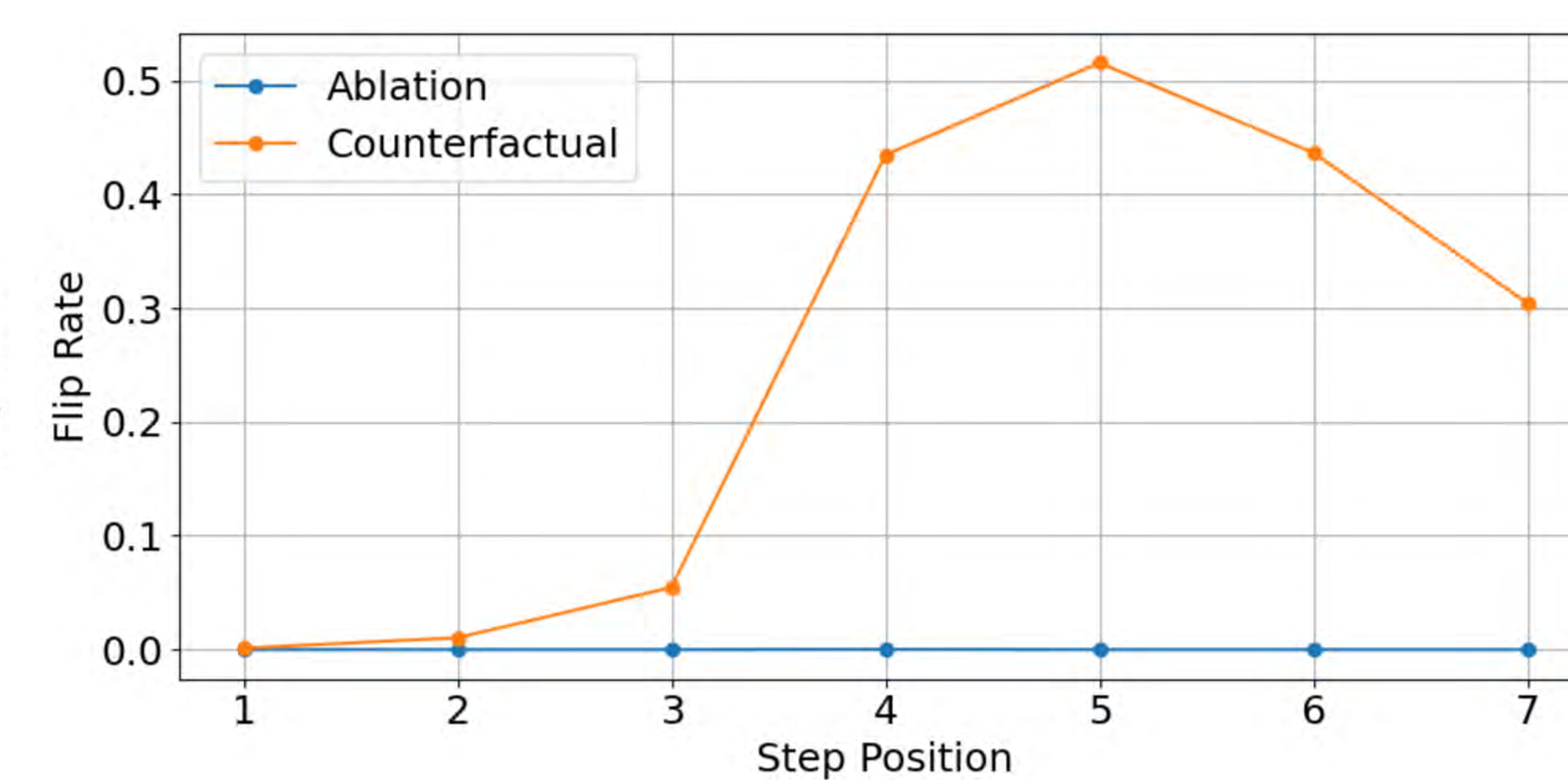


Figure 3: Flip Rate per Step Index

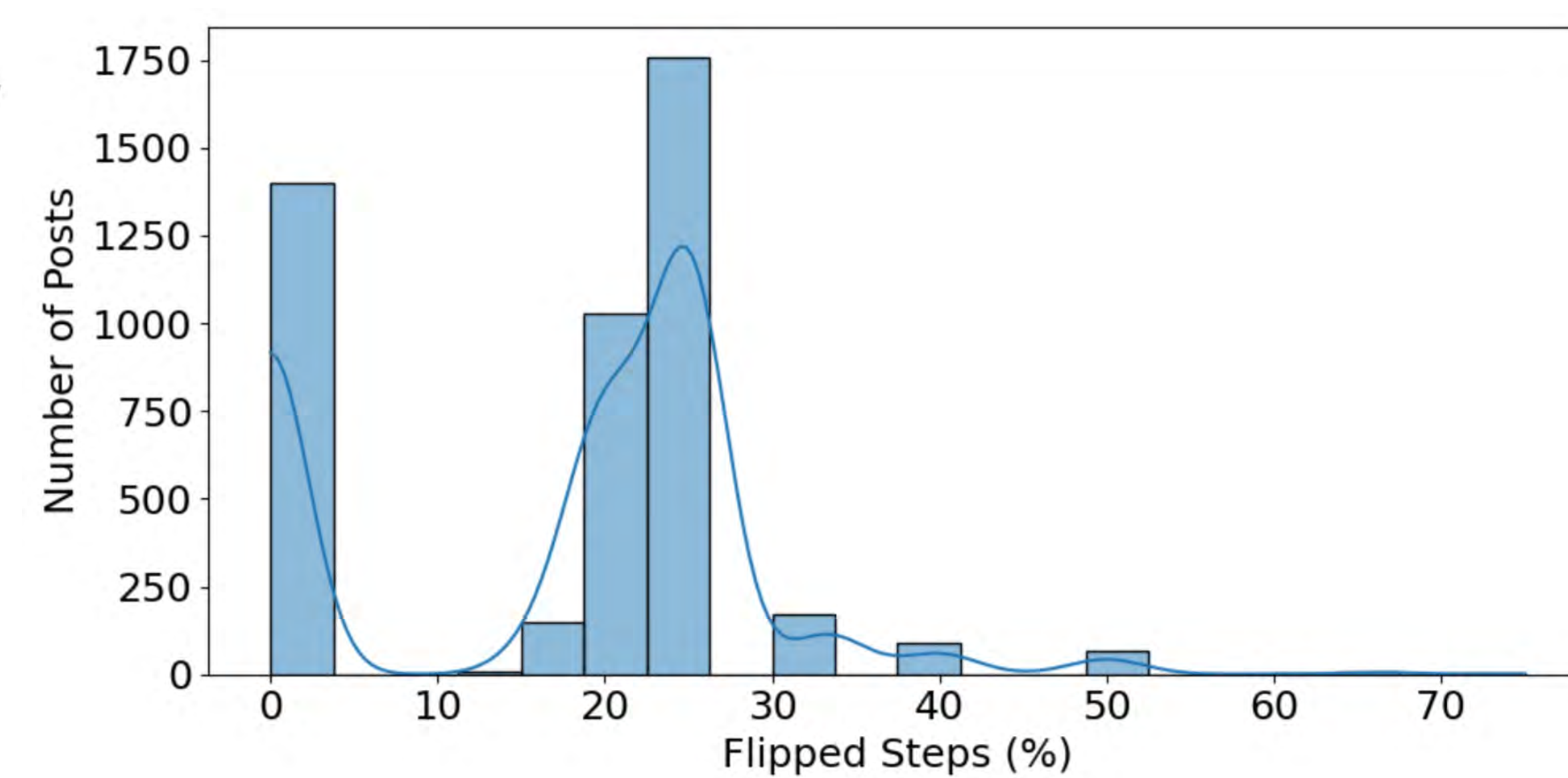


Figure 5: Percentage of Flipped Steps per Post

reasoning_type	count	accuracy	precision	recall	f1_score
daily_life	822	0.0705596	0	0	0
emotion	1405	0.178648	0.666667	0.0017316	0.00345423
symptom	238	0.147059	0	0	0
treatment	134	0.0895522	0	0	0
vague	451	0.172949	0.150685	0.0341615	0.0556962
worry	223	0.2287	0	0	0

Figure 6: Counterfactual Ablation Flip Metrics

reasoning_type	helpful_flip_rate
daily_life	0.0705596
emotion	0.178648
symptom	0.147059
treatment	0.0895522
vague	0.172949
worry	0.2287

Figure 7: Helpful Flip Rate

## Discussion

- Model is locally interpretable, with late steps in CoT being most influential
- Model is robust to removal but sensitive to replacement

Reasoning Type	Flip Rate	Precision	F1 Score	Helpful Flip Rate	Interpretation
daily_life	0.34 (highest)	0.00	0.00	0.07	<b>Non-causal influence.</b> Influential in producing flips, but flips are rarely accurate or helpful, suggesting shallow reliance.
emotion	0.23	0.67 (highest)	0.0035	0.18	<b>Causally relevant.</b> When this step changes the prediction, it's usually correct, showing targeted reliance.
vague	0.21	0.15	0.0557 (highest)	0.17	<b>Partial causal sensitivity.</b> Model sometimes relies on vague reasoning, although not always accurate.
treatment	0.14	0.00	0.00	0.09	<b>Non-causal.</b> Weak influence and rarely correct when flipped. Possibly ignored or used heuristically.
symptom	0.06	0.00	0.00	0.15	<b>Non-causal.</b> Rarely influences prediction. Even when changed, it doesn't impact model outcome, suggesting minimal reliance.
worry	0.06	0.00	0.00	0.23 (highest)	<b>Strong latent causal role.</b> Few flips occur, but when they do, they align with the true label, suggesting precision in rare use.

Figure 8: Interpretation of Data by Reasoning Type

## Conclusion

### Findings:

- Reasoning types vary in robustness to perturbation
- *Emotion*- and *Worry*-related reasoning are most causal reasoning types
- Reasoning related to *Symptoms* and *Treatment* are least causal
- Overall, reasoning types related to affect and ambiguity are most causal
- Reasoning is distributed across multiple types
- Influence is concentrated in later steps
- Flip behavior reveals model fragility

### Implications:

- LLM predictions are unstable when handling contradictions
- Poor symptom and treatment reasoning limits clinical utility
- Models should combine multiple reasoning types
- LLMs used in mental health context should be built for emotional sensitivity

## Limitations & Future Work

### Limitations:

- Low flip counts limit statistical power
- Single-model focus limits generalizability
- No distinction in step importance

### Future Directions:

- Causal finetuning by reasoning type
- Counterfactual robustness training
- Human-in-the-loop interpretability tools

## Acknowledgements

I would like to thank the SSTP Program and the Belin-Blank Center for providing me with this invaluable research opportunity. I am especially grateful to Dr. Fan and the Business Analytics Lab for their support and for granting access to the Reddit dataset used in this study. Finally, I would like to thank Enos Hsiao and Angelina Wang for their assistance in annotating the original dataset.

## References

- Chatziveroglou, G., Yun, R., & Kelleher, M. (2025). Exploring llm reasoning through controlled prompt variations. ArXiv. <https://doi.org/10.48550/arxiv.2504.02111>
- McGrath, A., & Jonker, A. (2024, October 8). What is AI interpretability?. IBM. <https://www.ibm.com/think/topics/interpretability>
- Patil, A., & Gedhu, A. K. (2025). Cognitive-mental-llm: Evaluating reasoning in large language models for mental health prediction via online text. ArXiv. <https://arxiv.org/abs/2503.10095>
- Wei, J., Wang, X., Schuurmans, D., Bosma, M., Chi, E. H., Le, Q. V., & Zhou, D. (2022). Chain-of-thought prompting elicits reasoning in large language models. NIPS'22: Proceedings of the 36th International Conference on Neural Information Processing Systems, USA, 24824–24837. <https://doi.org/10.48550/arxiv.2201.11903>